FACULTE DES SCIENCES
Center for Education and Research on Macromolecules (CERM)

Advancing the use of CO_2-sourced activated cyclic carbonates for the synthesis and recycling of heteroatom-rich polymers

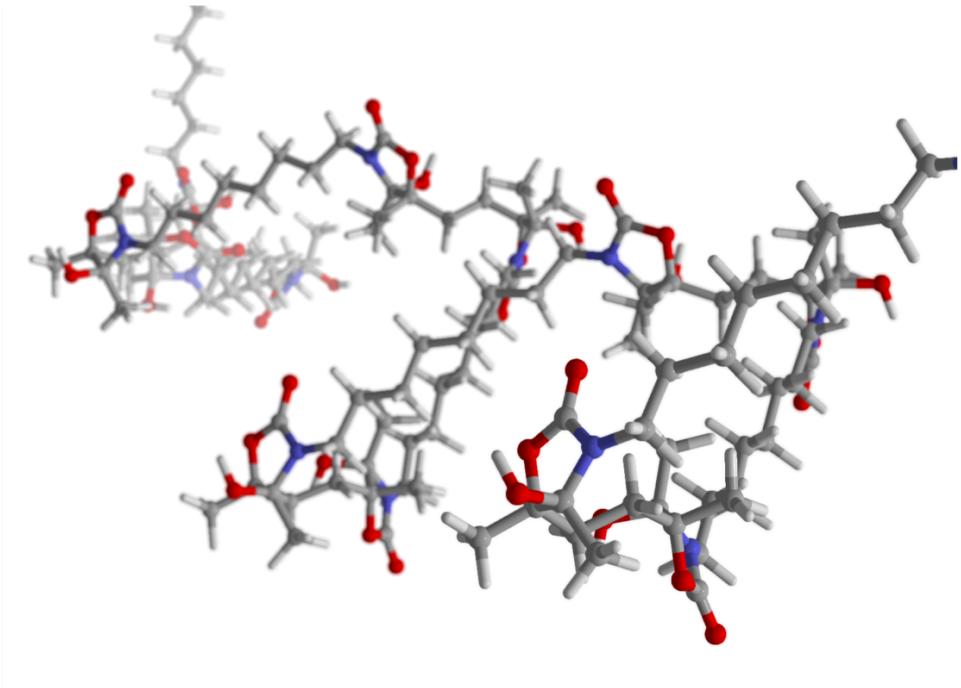

Année académique 2024-2025

Dissertation présentée par
Thomas HABETS
en vue de l'obtention du grade de
Doctorat en Sciences

Thesis jury

Prof. Christophe DETREMBLEUR	University of Liege (Supervisor)
Dr. Antoine DEBUIGNE	University of Liege (Secretary)
Prof. Jean-Christophe MONBALIU	University of Liege (President)
Prof. Jean-François GOHY	University of Louvain
Prof. Maarten SMULDERS	University of Wageningen
Prof. Charlotte WILLIAMS	University of Oxford

SUMMARY

The remarkable diversity of plastics, offering immense versatility in properties across numerous applications, positions them as fundamental materials in the worldwide everyone's daily life. However, their substantial growing production from fossil sources has led to resources depletion and accumulation of plastic waste in landfills and oceans. Moreover, the unique and versatile properties of plastics, combined with their low production cost, position them as irreplaceable with a yearly growing demand.

There is therefore an urgent need for our society to re-think the plastics design through the valorization of wastes such as carbon dioxide (CO_2) while considering their recyclability.

Among the conventional plastics, heteroatom-rich polymers hold significant market importance due to their high tunability, which makes them ideal candidates for a wide range of applications. The most well-known families of these polymers include polyurethanes (PUs), polycarbonates (PCs), polyesters, and polyamides. PUs are typically synthesized from toxic isocyanates – hazardous compounds for both the human health and the environment. Current regulations are however pushing toward a drastic limitation on the usage of these substances.

The global long-term challenge is to develop sustainable and safe production of polymers under mild conditions from non-hazardous reagents and to offer recycling options for these materials.

The aim of this PhD thesis is to advance the fundamental chemistry of α-alkylidene cyclic carbonates as CO_2-derived building blocks toward unique macromolecular heteroatom-rich structures. Although our group has previously demonstrated a proof-of-concept for the synthesis of various polymer families from this technology, the thermal, mechanical, and chemical properties of the polymers remain largely unexplored. This thesis provides an in-depth study into the synthesis and characterization of novel polymers derived from α-alkylidene cyclic carbonates, expanding the library of polymers that can be obtained from this versatile building block. Importantly, the work considers the end-of-life options for these polymers, ensuring they align with current environmental sustainability goals. Through this work, I aim to contribute to the global effort of finding sustainable alternatives to traditional plastics.

This work was financed by the Fonds National de la Recherche Scientifique (F.R.S-FNRS) in the frame of the CO_2Switch project under grant T.0075.20.

RÉSUMÉ

La remarquable diversité des matières plastiques, offrant une immense polyvalence dans leurs propriétés à travers de nombreuses applications, les positionne comme des matériaux fondamentaux dans la vie quotidienne de chaque personne dans le monde. Cependant, leur production croissante à partir de sources fossiles conduit à l'épuisement des ressources et à l'accumulation des déchets plastiques dans les décharges et les océans. De plus, les propriétés uniques et polyvalentes des plastiques, combinées à leur faible coût de production, les rendent irremplaçables avec une demande annuelle croissante.

Il y a donc un besoin urgent pour notre société de repenser la conception des plastiques à travers la valorisation des déchets tels que le dioxyde de carbonate (CO_2) tout en considérant leur recyclabilité.

Parmi les plastiques conventionnels, les polymères riches en hétéroatomes occupent une place importante sur le marché en raison de leur grande capacité d'adaptation, ce qui en fait des candidats idéaux pour une large gamme d'applications. Les familles de polymères les plus connues incluent les polyuréthanes (PUs), les polycarbonates (PCs), les polyesters et les polyamides. Les PUs sont typiquement synthétisés à partir d'isocyanates toxiques – des composés dangereux tant pour la santé humaine que pour l'environnement. Les réglementations actuelles poussent cependant vers une limitation drastique de l'utilisation de ces substances.

Le défi à long terme, à l'échelle mondiale, est de développer une production de polymères durable et sûre dans des conditions douces à partir de réactifs non dangereux, ainsi que d'offrir des options de recyclage pour ces matériaux.

L'objectif de cette thèse de doctorat est de faire avancer la chimie fondamentale des carbonates cycliques α-alkylidène dérivés du CO_2 comme blocs de construction vers des structures macromoléculaires uniques riches en hétéroatomes. Bien que notre groupe ait déjà démontré la preuve de concept pour la synthèse de diverse familles de polymères à partir de cette technologie, les propriétés thermiques, mécaniques, et chimiques des polymères restent largement inexplorées. Cette thèse propose une étude approfondie sur la synthèse et la caractérisation de nouveaux polymères dérivés des carbonates cycliques α-alkylidène, élargissant la bibliothèque de polymères qui peuvent être obtenus à partir de ce bloc de construction polyvalent. De manière importante, le travail prend en compte les options de fin de vie de ces polymères, s'assurant qu'ils s'alignent sur les objectifs actuels en faveur de l'environnement. Á travers ce travail, je vise à contribuer à l'effort mondial de trouver des alternatives durables aux plastiques traditionnels.

Ce travail a été financé par Le Fonds de la Recherche Scientifique (F.R.S-FNRS) dans le cadre du projet CO_2Switch sous la subvention T.0075.20.

ACKNOWLEDGEMENTS

The journey of pursuing a PhD has been an immensely enriching experience, unveiling a genuine passion for fundamental research in chemistry. It has also shown me the multifaceted nature of being a researcher, requiring patience, and resilience through many failures before achieving a small success. The satisfaction of seeing a simple idea evolve into completed and published research is immense. I had the chance to learn new things every day, in an environment filled with competent individuals, where you can meet enriching people and create new friendships.

Firstly, I would like to express my deepest gratitude to my thesis jury: Prof. Christophe Detrembleur, Dr. Antoine Debuigne, Prof. Jean-Christophe Monbaliu, Prof. Jean-François Gohy, Prof. Maarten Smulders, and Prof. Charlotte Williams for their precious time spent reading and evaluating my thesis, and for their participation in my thesis defense.

I am deeply grateful to my supervisor, Christophe, for the trust placed in me by signing my PhD contract on the day of my master's graduation, and for granting me the freedom to research throughout my thesis. This freedom allowed me to explore many of my own ideas and learn a lot about myself and my work methodology. I also appreciate the trust given in mentoring many PhD students from the very beginning of my own thesis, reflecting the high level of confidence you had in me. I have always tried my best to prove that this trust was well-placed. Our almost collegial relationship, filled with laughs around beers and filter-free open discussions, has been truly rewarding. This is the beauty of fundamental research.

I warmly thank Bruno. You always work behind the scenes but contribute significantly to most of the works in the lab with your valuable many ideas. Your always show a great dedication to chemistry and to the greater good of the lab. You are a model for many people in the lab, including me. For these reasons, you always have filled the role of co-supervisor since my master thesis. It was a pleasure to share unplanned brainstorming sessions in our offices, but also to create a friendship beyond professional boundaries.

I wish to express my gratitude to Christine Jerome. After my first year of master, I was uncertain about which direction to take and in which lab I would like to make my master thesis. After passing the exam of macromolecular chemistry, you encouraged me to visit the lab and meet researchers (Bruno especially) and this is what has led me to join the group. I found there a passion for research that I might not have discovered somewhere else. Thank you so much for that!

Looking back further, I want to deeply thank my teachers in secondary schools who always supported my scientific curiosity, and who were given a gift for teaching these disciplines. I especially thank Sabine Lenartz and Vincent Portzenheim, whose guidance and motivation were pivotal in my decision to pursue studies in chemistry.

ACKNOWLEDGEMENTS

I warmly thank my collaborators on various projects throughout my thesis: Prof. David Mecerreyes, Prof. Filip du Prez, Prof. Alejandro Müller, Prof. Jean-Marie Raquez, Dr. Raphaël Méreau, Dr. Haritz Sardon, and the students involved: Fabiana, Guillem, Stephan, Jorge, Marco.

I would also like to thank the CERM family for all the good times we shared, with special thanks to the technical stuff at the heart of the smooth running of the lab: Greg, Val, Martine, Charlotte, Sophie. Special thanks to Val and Greg, from whom I learned so much. A special mention to Val, who has become a close friend. I am grateful to all group members, especially Pierre, Fabiana, Max le cycliste, Bruno, Jeremie, Raph, Manas, François, Zoe, Charlene, Lilas, Sara, Florent, Anna, Sofia, Oscar, Zinnia, Laéticia, Pascal, Maude, Luca, Maxime Houbben, Antoine, Philippe, Lionel, Maliheh, Victor, and Maksimov. Engaging in constructive discussions with some of the best researchers I know – Pierre, Max, Fabiana, Bruno – was a real pleasure.

I want to thank the department staff who support the university's activities. My deepest gratitude goes to the late Alice, whose talent as a glass blower was invaluable and whose kindness and helpfulness was greatly appreciated. Special thanks to Enza for her exceptional professionalism and help. Thanks also to Christian Damblon for his assistance with the NMR and the many hours we've spent together troubleshooting the instrument.

I also want to thank my friends who supported me throughout this journey, each in their own way. My friends from Liège during my studies and PhD: Thomas, Axelle, Damien, Steph, Meriem, Amandine, Florian, Laurence, Théo, Max, François. My hard core from high school: Sam, Fritze, Magrin, Tox, Max Pincky. My friends from Bilstain: Thibaut Mager, Thibault Bastin, Camille, Chloé, Giano, Dech, Mathieu, Cheminot, Tom. And many more !

Au-delà de tout cela, je souhaite remercier ma famille. Votre soutien indéfectible et vos encouragements ont été le fondement de mon parcours, m'aidant au jour le jour à combattre mon perpétuel manque de confiance en moi. Merci d'avoir été toujours là pour moi et de m'avoir toujours poussé à donner le meilleur de moi-même dans ce que je pouvais réaliser. Tout mon parcours, je vous le dois.

Last but not least, I thank my girlfriend Fabiana. During our shared moments in the lab, I have professionally learned so much from you and, more personally, ultimately fell in love with you. Not only were we the *dream team* as Christophe said for our collaborative work in the lab, but we are also a dream team in life. Your love and support have been my constant source of strength and motivation. You have always cared about me since we met and have been there for me through the highs and lows. You not only made this journey possible but also gave me inspiration for all the work I accomplished in these last years. I love you.

Infine, desidero ringraziare la mia nuova famiglia italiana, Caterina, Enrico, Bruno, Clara, Pietro per il loro sostegno e ammirazione per il mio lavoro, che mi ha dato ulteriore motivazione per

questa fase finale. Li ringrazio calorosamente per avermi accolto nella loro famiglia e per avermi fatto sentire uno di loro.

TABLE OF CONTENTS

Chapter I

Room temperature synthesis of non-isocyanate polyurethanes

1. Introduction

Polyurethanes (PUs) are among the most widely utilized polymers globally, with an annual production of about 30 million metric tons in 2022—a testament to their critical role in numerous industries. Their applications span high-performance thermoplastics elastomers[1], foams for comfort and insulation[2,3], as well as adhesives and coatings[4]. This widespread usage stems from the ability to finely tune their unique properties to target specific applications, distinguishing them from other polymer classes[5–7].

Conventional PUs are synthesized by the step-growth polymerization of polyisocyanates with polyols (**Scheme 1**). This reaction is often conducted at room temperature using catalysts such as dibutyltin dilaurate (DBTL) or an organobase like 1,4-Diazabicyclo[2.2.2]octane (DABCO). However, isocyanates are toxic and hazardous compounds, posing significant health and environmental issues. In response to this hazard, European REACH regulations have imposed drastic restrictions on isocyanate usage. This intensified research for safer non-isocyanate alternatives, named non-isocyanate or isocyanate-free polyurethanes (NIPUs).

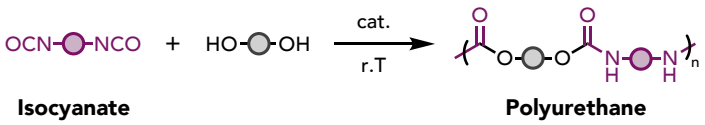

Scheme 1 – Conventional PU synthesis from isocyanates.

The 12 principles of Green Chemistry[8] state that chemistry should be achieved at room temperature (r.T) for energy efficiency[9,10]. This not only reduces the energy footprint of a process, but also enhances selectivity and minimizes side reactions – commonly observed at elevated temperatures[11]. This approach also enables greater functional group tolerance, crucial in polymer chemistry where functional groups on the polymer backbone significantly influence the final material properties. Additionally, the capacity to formulate and cure these materials at ambient temperature makes polyurethanes more accessible for consumer applications without the need for specialized equipment, but also to fit in existing PU industrial facilities.

While offering significant economic and environmental benefits, the room temperature synthesis of NIPUs presents enormous challenges, primarily due to the low reactivity of the monomers compared to isocyanates. Moreover, this low reactivity complicates the formation of materials endowed with complex architectures, such as PU foams. In traditional PU foam

synthesis, water is introduced in the formulation and reacts with isocyanates, generating CO_2 as chemical blowing agent to create the foam cellular structure. Achieving similar results without isocyanates at r.T thus requires innovative approaches to replicate isocyanate-based expanded materials.

This literature review will explore the chemical strategies developed to enable room-temperature polymerizations toward NIPUs. It will critically examine the routes that have proven successful to synthesize NIPUs at r.T and highlight the strategies that have made this possible. This includes reaction optimization through molecular engineering of the monomers, the usage of specific catalysts, or solvation effects in specific reaction routes. This is generally achieved by examination of small model molecules reactivity studies, and/or directly during polymerization.

2. NIPUs by aminolysis of 5-membered cyclic carbonates

One of the most promising strategies toward NIPUs is the step-growth polyaddition between polyfunctional 5-membered cyclic carbonates (**5CC**) and polyamines to produce poly(hydroxyurethane)s (PHUs). (Poly)**5CC** can be synthesized by the well-established coupling of CO_2 onto epoxides (**Scheme 2A**), with an ever-expanding library of molecules. This approach is not only relatively inexpensive but has also been scaled up to the kilogram level[12]. The reaction between **5CC** and amines occurs *via* nucleophilic attack of the amine onto the electrophilic carbonyl function of the carbonate, followed by ring-opening to yield a hydroxyurethane product **1** (**Scheme 2A**). The bond scission can occur on both sides, yielding a mixture of two isomers: (i) an isomer containing a secondary alcohol, which is formed in larger amounts, and (ii) an isomer containing a primary alcohol.

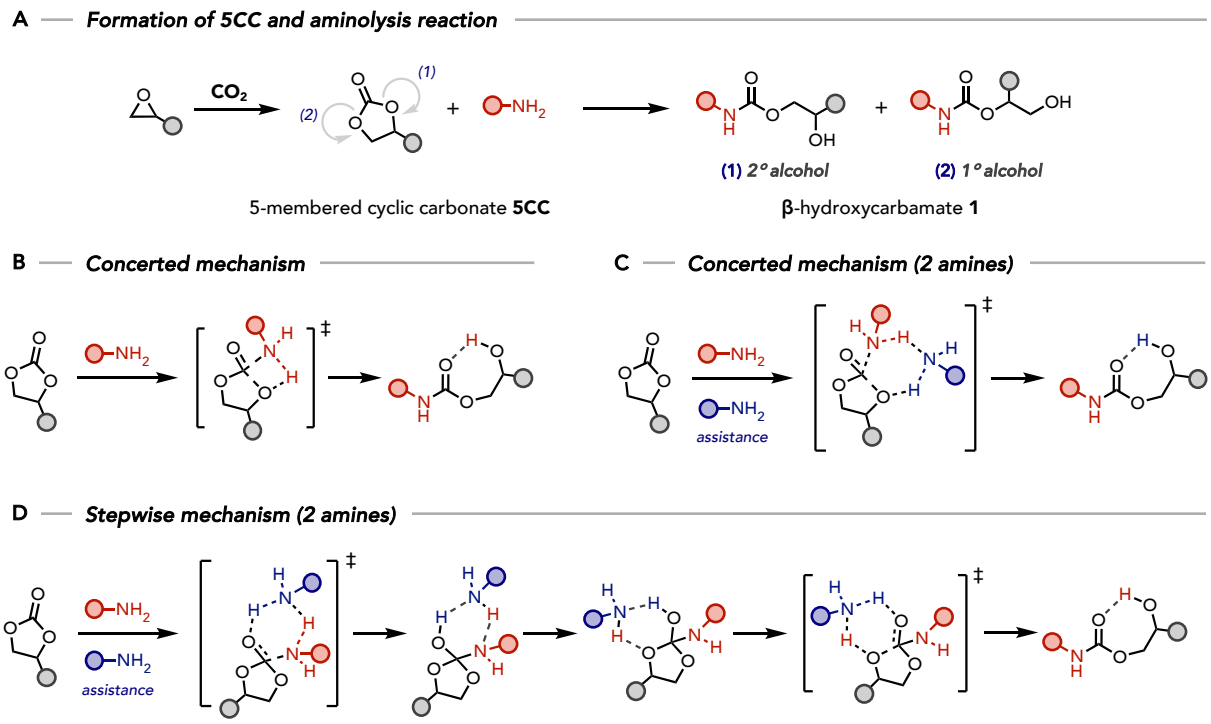

Scheme 2 – (A) CO_2 fixation on epoxide toward **5CC**, followed by its aminolysis into **1**. Several mechanisms were computationally unraveled, such as (B) a simple concerted mechanism, (C) the same concerted mechanism with the assistance of an extra amine, and (D) a stepwise mechanism with the assistance of an extra amine.

However, these **5CC** scaffolds display low reactivity toward amines at room temperature, and polymerizations are typically achieved at temperatures above 80 °C. Additionally, side

reactions are reported for this reaction at temperatures above r.T. This leads to an undesired decrease of molecular weight in thermoplastic or cross-link density in thermosets, as well as irregularities in the (macro)molecular structure. There exist only few reports of polymerizations at r.T. In this section, we will discuss (i) the mechanism of reaction and side reactions, (ii) strategies employed to achieve reaction at lower temperature, (iii) the current limitations of this chemistry, (iv) the reported polymers synthesized at r.T, and (v) a perspective to better understand and, consequently, overcome these roadblocks.

2.1. Mechanism of reaction and reported side reactions

Kinetic experiments demonstrated that the overall reaction rate is governed by two contributing pathways: noncatalytic and autocatalytic. This means that the reaction can proceed either by the reaction of **5CC** with a single amine or through a mechanism involving two amines, where one acts as catalyst[13–17]. These mechanisms were further supported by computational studies on model compounds. Zabalov suggested in 2011 that the amine attacks the cyclic carbonate following a one-step addition and ring-opening process involving either one or two amines. The presence of a second amine in the autocatalytic route significantly lowers the energy barrier of the reaction[18,19]. When a second amine is involved, it serves as a proton relay, forming a more stable 6-membered ring within the transition state (TS). It replaces the strained 4-membered ring formed when only one amine is involved, as illustrated in **Schemes 2B** and **2C**. Alternatively, an even more favorable multi-step process featuring a tetrahedral intermediate was also demonstrated when two amines are involved (**Scheme 2D**).

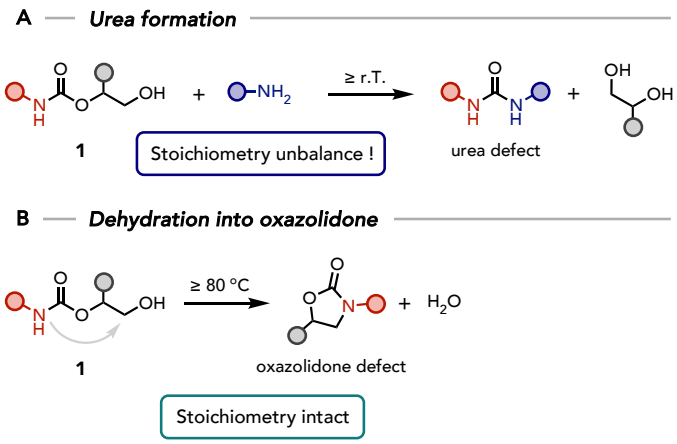

Scheme 3 – Main side reactions in PHU chemistry: (A) urea formation, and (B) oxazolidone formation.

Model reactions evidenced that side reactions occur with this chemistry. The most frequently reported is the formation of unreactive urea and diol, occurring through the reaction of a free amine with a hydroxyurethane **1**[20]. Although most studies evidence its formation in small amounts at 80 °C[21], up to 6 % of these products were observed at temperatures as low as 50 °C or even r.T[22–24]. At higher temperature (generally starting from 80 °C), a five-membered oxazolidone can be formed through dehydrative ring-closure. The formation of urea is problematic as it leads to a stoichiometry deviation in the system, consequently leading to low molecular weight polymers. The formation of oxazolidones does not hamper step-growth polymerization but is responsible for the release of water molecules, which can be troublesome if water-sensitive functionalities are present.

2.2. Strategies for increasing reactivity

Different strategies were adopted by researchers to increase the reaction rate at low temperature: by adapting the structure of **5CC** and the amine, by catalyzing the reaction, or by utilizing some solvents. Each of them will be discussed point-by-point below. As most of the works dealing with PHUs concern the preparation of thermosets for coating, adhesive or foam applications, monitoring the reactivity of the monomers is not straightforward due to the crosslinked nature, and thus insolubility, of the product. Model reactions and theoretical works on small molecules were thus carried out by many research groups in the last years to better understand the influence of each parameter on the reaction as well as to facilitate the characterization of the (by)products.

2.2.1. Increased reactivity by molecular engineering of 5CC

The most straightforward strategy to accelerate the reaction rate is to increase the reactivity of the reactants. The structure of **5CC** can be easily adjusted thanks to the broad diversity of available (poly)epoxides and synthesis pathways thereof. Cornille identified three key parameters affecting the reaction rate: (i) the presence and position of electron-withdrawing groups (EWGs), (ii) the steric hindrance around the functional group, and (iii) the ability of the group to form hydrogen bonds with free amines[17]. It was found that EWGs in the vicinity of the carbonate function significantly accelerated the reaction by pulling electrons away from the carbonate through negative inductive effect (I^-), thus making the carbonate function more electrophilic[15,17,22,23,25]. These groups also help to stabilize transition states where partial negative charges appear when the amine adds to the ring. A ranked list of **5CCs** with varying

substituents is provided in **Scheme 4** by order of reactivity. Furthermore, the proximity between the carbonate and the EWG has shown crucial for increasing the reaction rate[26].

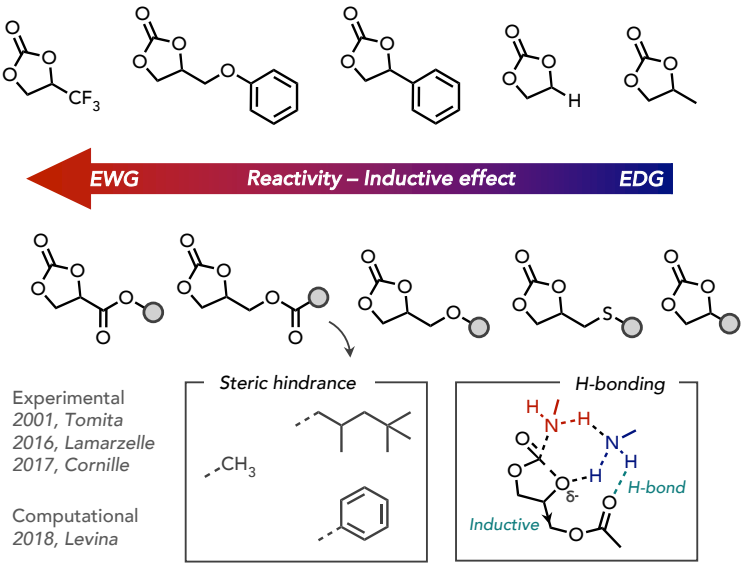

Scheme 4 – 5CCs with varying functional groups ranked by order of reactivity.

A computational study further supported the reactivity order of the cyclic carbonates and the contribution of an EWG in stabilizing transition states[27]. The study revealed that the inductive effect of an ester group contributed to stabilizing the transition state (TS) by 2 kcal·mol^{-1}, while hydrogen-bonding provided a more moderate stabilization of 1 kcal·mol^{-1}. Both contribute to the overall decrease in energy barrier, thereby accelerating the reaction rate.

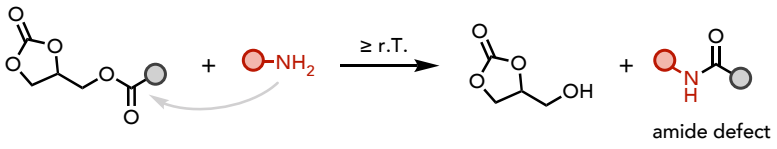

Scheme 5 – Amidation side reaction with ester-containing **5CC**.

Although ester groups are effective activating groups, they also introduce an additional potential side reaction – amidation by free amines, which results in the formation of a free alcohol and an amide bond (**Scheme 5**). This side reaction was reported to occur at temperatures as low as 50 °C or even r.T[17,22,28]. Due to the absence of extra side reactions and their easier synthesis, ether-derived **5CCs** have become the most commonly used[29]. Less explored is the impact of the ring substitution degree. However, di- and tri-functionalized **5CC** compounds were systematically reacted with amines at high temperatures[30–34], a testament for their low reactivity. Endo showed that **5CCs** fused with aliphatic cyclohexyl or cyclopentyl rings

are less reactive than ethylene carbonate, probably due to an increased substitution and a positive inductive effect stemming from the aliphatic nature of the rings. However, a **5CC** bearing the six-membered fused ring exhibited greater reactivity than the five-membered analog, matching the induced ring strain[35].

2.2.2. Increased reactivity by the choice of the amine

The reactivity of amines toward **5CC** is highly dependent on several factors identified through comparative kinetic studies: (i) the amine order, (ii) steric hindrance, (iii) electronic effects, and (iv) the molecular weight of the (poly)amine[36]. Among these, the amine order is critical – secondary amines generally show low reactivity with **5CC** at r.T, except for piperidine derivatives[37–39]. Consequently, primary amines are the obvious choice for synthesizing PHUs. Steric hindrance significantly impacts the reaction rate by reducing the spatial accessibility of the amine group. For example, cyclohexyl- and α-alkylated- amines (such as n-methylbutylamine) typically exhibit low reaction rates. In contrast, less hindered aliphatic amines (such as n-butylamine) demonstrate higher reaction rates[38,40–42].

Electronic effects near the amine group also markedly influence reactivity. EWGs such as benzyl or ethoxy groups diminish reactivity due to their negative inductive effect I^- compared to aliphatic amines. Interestingly, despite their negative inductive effect, the presence of a secondary or tertiary amine in the β position of the primary amine group significantly increases the reaction rate[37,38]. Although this has not been rationalized, this effect might potentially arise from an autocatalytic effect brought by the basic nature of amines. Aromatic amines generally exhibit no reactivity in the absence of a catalyst, as the mesomeric effect makes the amine poorly nucleophilic[38,40,41]. A ranking of amines ordered by reactivity is presented in **Scheme 6A**.

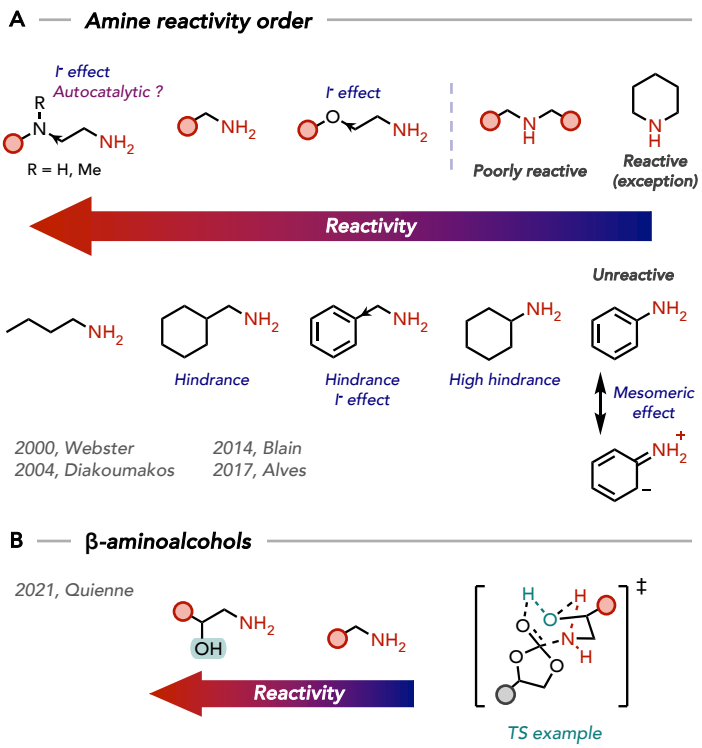

Scheme 6 – (A) Amines ranked by order of reactivity toward **5CC**. (B) Enhanced reactivity of *β*-aminoalcohols and example of a transition state for the amine addition onto **5CC**.

Interestingly, *β*-aminoalcohols have shown greater reactivity toward **5CC** than aliphatic amines despite the inductive *I*- effect of the hydroxyl group[15,37,43]. A computational study rationalized this difference through the stabilization of transition states by intramolecular hydrogen-bonding and proton relay effects[43] (**Scheme 6B**).

Finally, it was demonstrated that decreasing the molecular weight of diamines increased their reactivity[38,39]. Although this was not commented, this effect might arise from higher mobility and accessibility of the amine groups in small molecules rather than in oligomeric ones.

2.2.3. Increased reactivity through catalysis

A common strategy to lower energy barriers and consequently increase reaction rate at low temperature involves catalysts. Many catalysts were evaluated, such as inorganic salts[40,44,45] (e.g. $MgBr_2$, $FeCl_3$, LiCl), organobases[40,44,46] (e.g. TEA, DBU, TBD, MTBD, DMAP, DABCO, phosphazenes), phosphines[40], and (thio)urea derivatives[40,44,46,47]. Among these, TBD and (thio)urea-derived catalysts have demonstrated superior performance in terms of reaction rates, though they differ in their substrate activation mechanism.

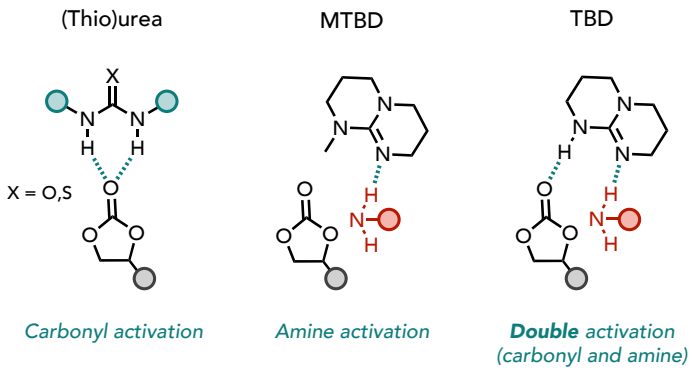

Scheme 7 – Typical catalysts and activation modes for the aminolysis of **5CC**.

(Thio)ureas enhance the carbonate electrophilicity of **5CC** through strong hydrogen bonding interactions with the carbonyl group. In contrast, MTBD acts as a strong base, interacting with the amine protons to enhance the amine nucleophilicity. TBD shows superior substrate activation compared to other organobases of similar pKa. This is due to the dual activation mechanism that involves both amine nucleophilic enhancement and carbonate activation via hydrogen bonding. The proton of TBD indeed stabilizes the tetrahedral intermediate by stabilization of the partial negative charge following amine addition on the ring. Furthermore, TBD serves as a proton transfer agent, simultaneously donating and accepting protons in concerted steps. Computational studies support this dual behavior, revealing that the bifunctional nature of TBD is crucial, particularly when compared to MTBD, for significantly lowering the energy barrier of the manifold[41,48] (**Scheme 7**).

It must be noted that the efficiency of TBD was further applied to the aminolysis of challenging substrates, including densely substituted cyclic carbonates[49,50] and to the use of aromatic amines to produce arylcarbamates[51]. Lombardo studied more complex binary systems comprising TBD and LiOTf, which has demonstrated a 3-fold decrease in reaction time compared to TBD alone[52].

2.2.4. Increased reactivity by the choice of the solvent

Solvents have a significant impact on the reaction between **5CC** and amines. It was observed that aprotic polar solvents, such as DMSO or DMF, enhance the reaction rate more effectively than solvents with lower dielectric constants, such as dioxane, toluene, or THF[15,17,20,27]. This enhancement is attributed to the proton acceptor capabilities of polar aprotic solvents (**Scheme 8A**). Computational studies align with these experimental findings through the addition of numerous explicit solvent molecules in the model (**Scheme 8B**). In the case of DMSO, they demonstrate that weak hydrogen bonds involving two solvent molecules contribute to

stabilizing the TSs and, consequently to lower energy barriers. These bonds aid in solvating the reactants and shielding the electronic density around electronegative oxygen atoms[53,54]. Studies with dioxane revealed only slight stabilization, the energy barrier being unaffected whether one or more solvent molecules are included[55,56].

Interestingly, chloroform demonstrated to be a good solvent for the reaction, reaching the rate observed in DMF[17,20]. It is hypothesized that chloroform may act as a weak proton donor, assisting the reaction process[43] (**Scheme 8C**).

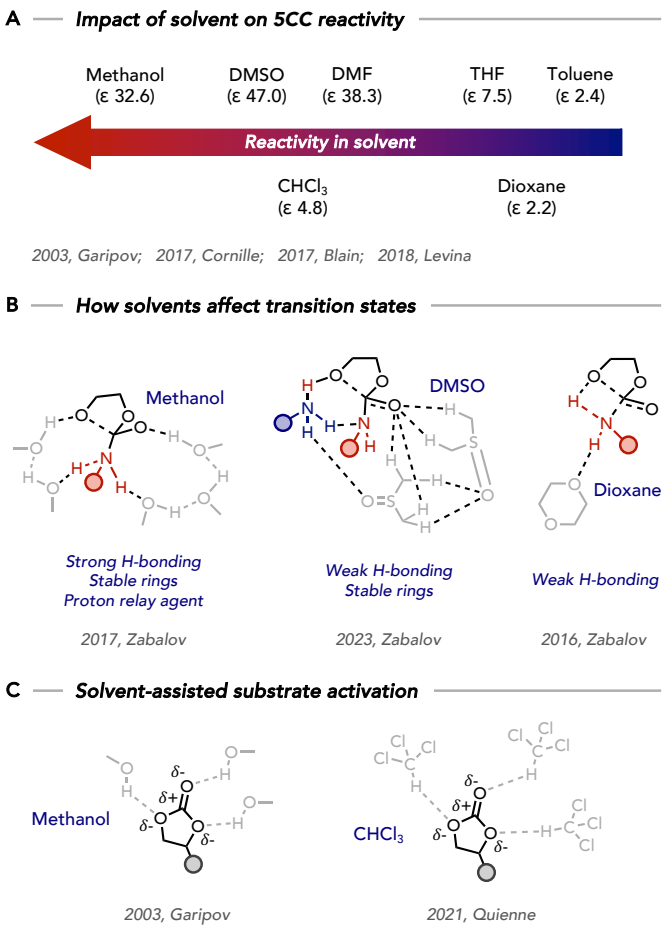

Scheme 8 – (A) Solvents ranked by order of reaction rate enhancement. (B) Transition states including explicit solvents molecules. (C) Effect of methanol and chloroform on the substrate activation.

Protic solvents have proven to be particularly effective and significantly increased the reaction rate[15–17,20,27]. It was proposed that such solvents, such as methanol (MeOH), might create hydrogen bonds with the oxygen atoms of the cyclic carbonate, thereby increasing **5CC** electrophilicity (**Scheme 8C**). Subsequent computational studies reported the solvation of transition states by explicit solvent molecules, forming stable cycles resulting in a two-fold

decrease in energy barrier compared to reactions conducted in the gas phase or including implicit solvation models[53,56] (**Scheme 8B**). Methanol thus plays a crucial dual role: (i) it stabilizes the TSs through less strained rings formations while shielding partial negative charges created on oxygen atoms, and (ii) it acts as a proton transfer agent, which is not possible with aprotic solvents such as DMSO.

2.2.5. Water as solvent

The use of protic solvents like methanol has been associated with excellent aminolysis rates. It might be expected that water would function similarly, acting as both a hydrogen bonding agent to stabilize transition states and as proton transfer agent. Nohra demonstrated the feasibility of this approach by the aminolysis of **5CC** in water at 50 °C, achieving 90 % of conversion in approximately 15 minutes[39]. However, the reaction proceeded at the cost of competitive hydrolysis of **5CC**, releasing CO_2 and a diol to provide the carbamate product along with around 15 % of the by-products (**Figure 1A**). Olsén later reported the reaction between **5CC** and unprotected amino acids in water[57], noting that the presence of a carboxylic acid group might interfere with the reaction by neutralizing the amine function and altering the reaction mechanism. It was shown that the reaction rate was dependent on the pH of the solution. If the pH is too low, the amine becomes protonated and unreactive (**Figure 1B**). The balance between aminolysis and hydrolysis is highly sensitive to the amount of base used to regulate the medium basicity, requiring careful adjustments to favor aminolysis over hydrolysis. Bourguignon further studied this tradeoff, emphasizing the importance of adjusting the pH relative to the amine pKa. Importantly, he noted that pH can fluctuate as CO_2 released from **5CC** hydrolysis leads to water acidification (**Figure 1C**). This topic will be thoroughly discussed in the polymerization section. Additionally, Bourguignon also reported no hydrolysis of **5CC** even at 100 °C in the absence of a base catalyst[58]. The hydrolysis reaction was observed in the presence of primary amines and, to a larger extent, in the presence of strong organobases such as DBU. Using water in large excess for PHU synthesis is therefore expected to yield only low molecular weight oligomers due to the competitive hydrolysis leading to a stoichiometric deviation between the two monomers.

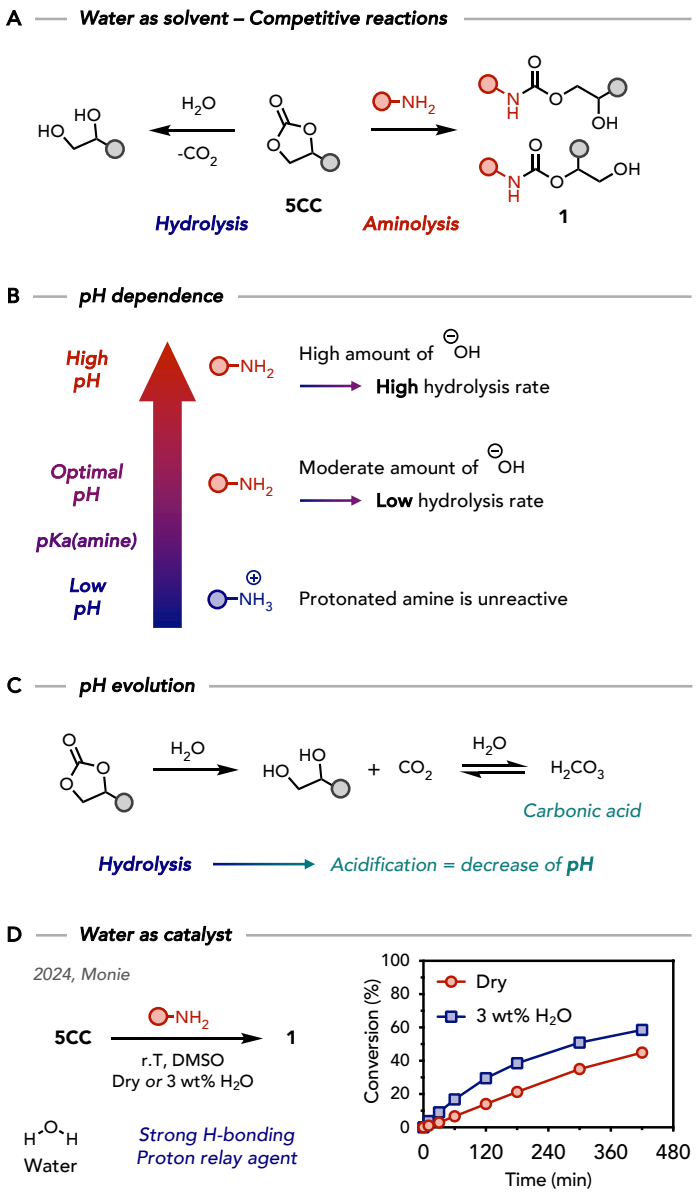

Figure 1 – (A) Competitive aminolysis and hydrolysis reactions with **5CC**. (B) pH dependence of the reactivity of **5CC** for both reactions. (C) The hydrolysis reaction releases CO_2, responsible for solution acidification through carbonic acid formation. (D) Aminolysis reaction at r.T in DMSO in the presence or not of 3 wt% of water.

Very recently, Monie demonstrated that a small amount of water (3 wt%; 62 mol%) in a diluted medium (DMSO) exhibited catalytic activity in the model reaction between **5CC** and amine at r.T[59] (**Figure 1D**). Methanol (62 mol%) had a similar effect. Water-catalyzed model reactions conducted in bulk showed that this approach significantly increased the reaction rate with only limited hydrolysis (around 3%).

2.3. Limitations of the chemistry

Careful examination of kinetic experiments on model molecules reactions indicates that the synthesis of NIPUs from this **5CC** aminolysis chemistry suffers from different drawbacks: (i) inherent side reactions, (ii) slow reactions kinetics at r.T, and (iii) incomplete **5CC** conversions in most processes.

First, irreversible side reactions pose significant issues. Although less prevalent at low temperature (r.T), even slight deviation from stoichiometry prevents to reach high molecular weight through step-growth polymerization. Despite their lower reactivity, ether-containing **5CCs** can be used instead of the more activated ester-containing **5CCs**, prone to amidation side reactions. As these reactions mostly occur at a temperature higher than 50 °C, it is underlined that maintaining r.T is critical to minimize their importance and achieve defect-free high molecular weight polymers.

Secondly, the reactivity of **5CC** is inherently low. Molecular engineering of the precursors and catalysis have proven useful to improve reactivity, but the reaction remains sluggish at r.T, particularly with industrially relevant diamines that show low reactivity such as ethoxy-containing or hindered diamines – e.g. 2,2′-(Ethylenedioxy)bis(ethylamine) (EDR-148), Jeffamine, isophorone diamine (IPDA), 4,4'-Diaminodicyclohexylmethane (PACM). Consequently, most reported PHUs have been synthesized at temperatures of 80 °C or higher, increasing energy consumption and the occurrence of side reactions.

Finally, many studies noted that aminolysis of **5CC** generally plateaus and fails to reach complete conversion, even after extended reaction time (**Figure 2A**). The team of Caillol suggested in numerous works that this may be ascribed to the formation of a dense H-bonded network of hydroxyurethanes **1**[17,20,43]. However, the incomplete reaction was also observed in diluted media and with small model molecules, where diffusion is faster than in macromolecular architectures. This feature has been overlooked by researchers and would deserve more attention to overcome this roadblock to the synthesis of high molecular weight polymers. Following Carothers equation, non-quantitative monomers consumption indeed inherently leads to polymers with low molar masses.

In the context of this literature review, we aimed to gather hints hidden in data from previous research, giving new directions for further studies that might rationalize the incomplete **5CC** conversion.

First, Fortman evidenced in 2017 that the aminolysis of **5CC** is reversible, with cyclic carbonate and amine back-formation at high temperature from **1**[60]. Similar observations have been made by other groups[61,62]. The conversion plateau may thus originate from an equilibrium state between the reactants and products, marking the end of reaction.

Secondly, reaction kinetics in the pseudo-first order regime showed that the reaction rate is governed by the combined contributions of two terms: one involving the reaction of one amine with **5CC**, and a second term involving a second amine in an autocatalytic process[13,16] (**Figure 2A**). The second term is largely predominant, meaning the rate is mainly governed by the reaction involving two amine molecules. This is in line with mechanistic studies showing the important decrease in energy of activation when several amines are involved in the process[18,19]. It can be hypothesized that this autocatalytic effect allows for fast reaction kinetics at the start of the reaction, and becomes negligible as the amine gets consumed, therefore reaching a plateau as depicted in **Figure 2B**. To support this hypothesis, it was shown that if the temperature is raised, the plateau is still observed, albeit at higher conversion[17]. Moreover, introducing additional amine molecules in the system at r.T increases the conversion. In conclusion, we hypothesized that the reaction might become unfavorable as the amine gets consumed, with the need of higher temperatures to overcome the high energy barriers where only one amine molecule is involved.

However, it is noteworthy that two exceptions exist in the literature: (i) when the reaction is catalyzed by TBD[44] (**Figure 2A**), and (ii) when the reaction is carried out in methanol[17].

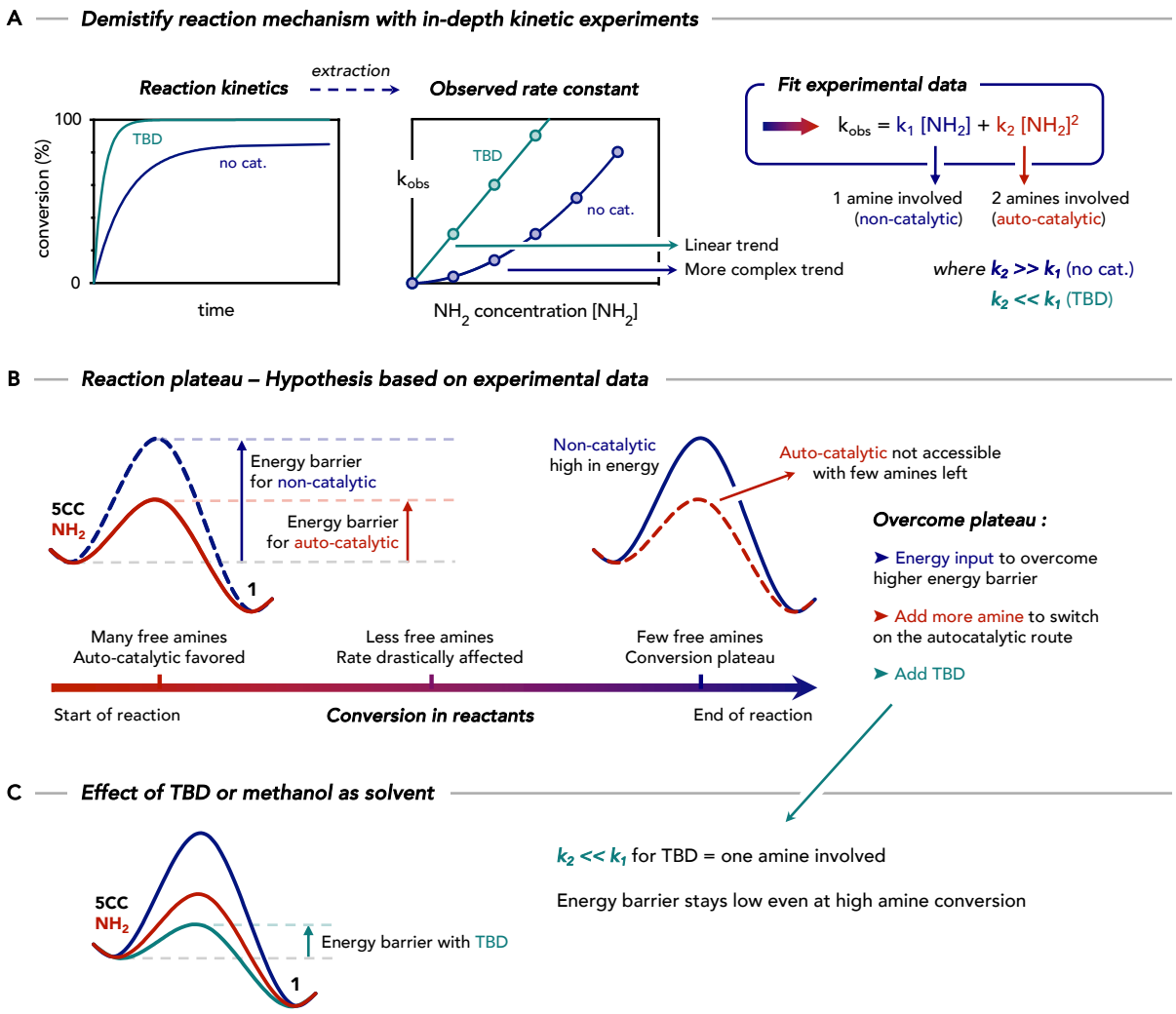

Figure 2 – (A) Schematic representation of kinetics experiments for the reaction of **5CC** and amines. From these kinetics are extracted observed reaction rates k_{obs}. This allows to rationalize the contribution of two mechanisms in the overall reaction rate. (B) Hypothesis of mechanism switch between the start and the end of the reaction as a consequence of amine consumption. (C) Hypothesis on the effect of TBD or methanol to reach quantitative conversions.

Zabalov demonstrated that the use of TBD as catalyst accelerated the reaction but also modified the importance of the two contributions to the overall reaction rate, the noncatalytic term becoming greater than the autocatalytic one[48] (**Figure 2C**). This might be rationalized by the ability of TBD to both activate the substrates and play the role of efficient proton transfer agent[63], explaining why this catalyst enables to reach complete conversion while others fail at this task.

Without catalyst, it has also been observed that performing the reaction in chloroform reached a plateau after 24 h and did not evolve 7 days later. The same reaction in methanol as solvent

allowed to reach quantitative conversion after 24 h[17]. As already discussed, the acceleration of the reaction in methanol was effective thanks to the stabilization of TSs through solvation and proton relay effect[56]. Reaction kinetics proved that the non-catalytic and the autocatalytic routes might be in close competition[16], while only the autocatalytic route is prominent in other aprotic solvents. The use of methanol as solvent could therefore have the same impact as TBD on the reaction, favoring the non-catalytic term in the reaction rate to get quantitative conversion even at high amine consumption.

This discussion shows that there is still room for fundamental research around this reaction to better understand the origin of the non-quantitative conversion in diverse conditions, and to the design of catalysts or other additives that might favor quantitative conversions.

2.4. Reported polymerizations at r.T

2.4.1. Linear polymers

Only few works reported the polymerization of poly(**5CC**)s and polyamines at room temperature. In 2000, Steblyanko reported the synthesis of PHUs by the reaction of an ester-activated bis**5CC** and several diamines in DMF at r.T for 3 days[64]. Polymers with M_n ranging from 6,300 to 13,200 g·mol^{-1} were obtained and they were characterized by T_gs ranging from 0 to 30 °C (**Figure 3A**).

In 2014, Annunziata reported the synthesis of PHUs from oligomeric PPG-derived bis**5CC** and poorly reactive diamines (Jeffamine, high steric hindrance and EWG in β position)[65] (**Figure 3B**). Only low conversions of 31 % were obtained at 25 °C after 48h. Increasing the temperature to 50 and 80 °C improved the conversion to 59 and 78 % respectively. This study highlighted the challenging polymerization of non-ideal precursors (Jeffamine – ethoxy-containing diamine with hindrance), even at higher temperature.

In 2015, another group polymerized a lignin-based bis**5CC** with two different diamines in DMSO at room temperature for 24 h[66] (**Figure 3C**). The aliphatic diamine led to a high M_n of 23,000 g·mol^{-1}, which could be increased to 30,000 g·mol^{-1} using 5 mol% of TBD as catalyst. This monomer therefore seems to show increased reactivity compared to most scaffolds, but this feature was not discussed by the authors. Using a more hindered diamine resulted in slow polymerization and low molecular weight (M_n 3,300 g·mol^{-1}, improved to 6,300 g·mol^{-1} with TBD). The polymers had high T_gs of 60 and 90 °C.

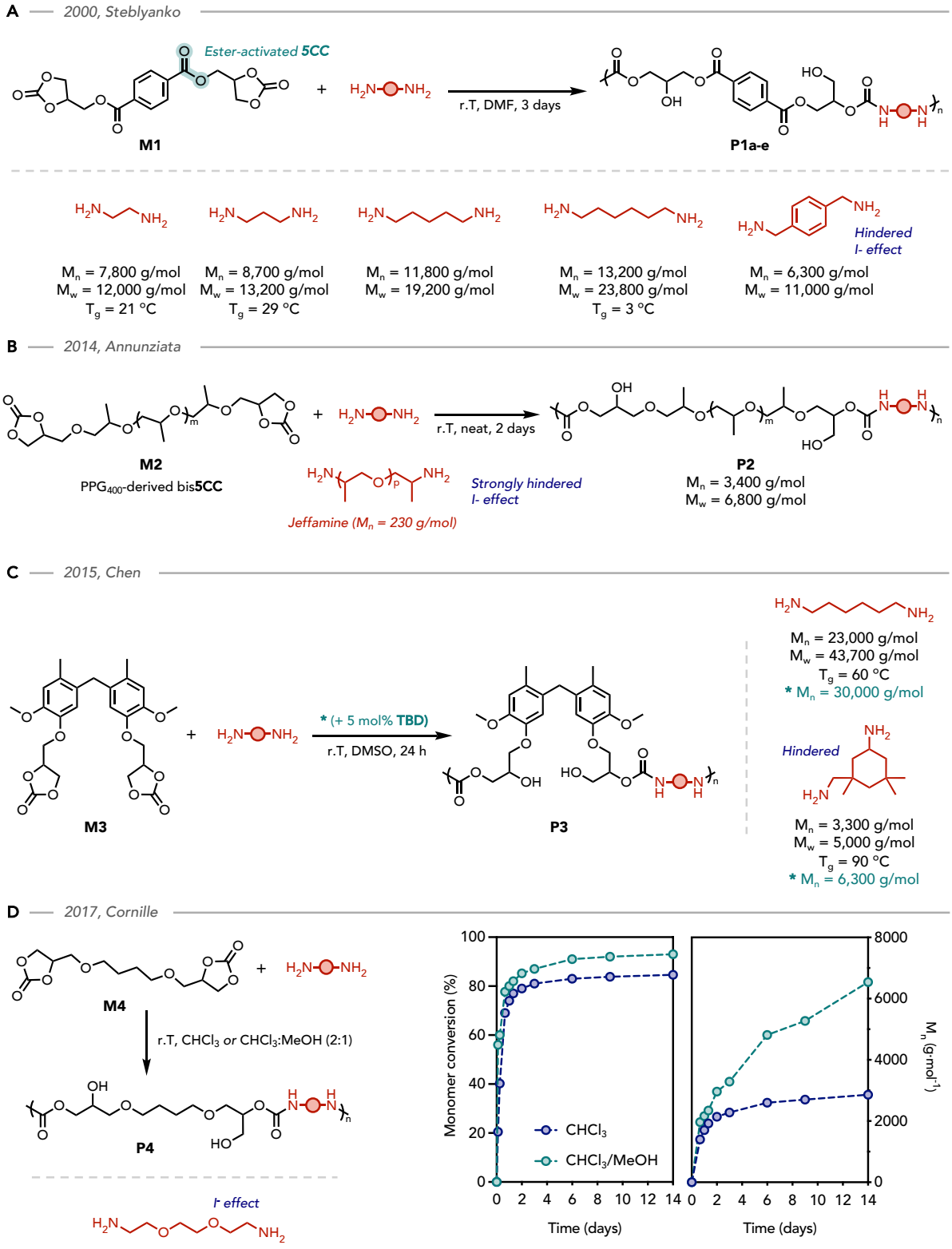

Figure 3 – Synthesis of PHUs at r.T from (A) ester-activated bis**5CC**, (B) PPG-derived bis**5CC**, and (C) lignin-derived bis**5CC**. (D) Solvent effect ($CHCl_3$ *vs* $CHCl_3$/MeOH 2/1) on PHU synthesis. Both monomer conversion and M_n were followed along time.

In 2017, Cornille compared a polymerization at r.T in chloroform or in a 2:1 mixture of chloroform and methanol as solvents[17] (**Figure 3D**). The polymerization was rather slow and low conversions of 74 and 80 % were respectively obtained after 24 h together with M_n values of 1700 and 2200 g·mol^{-1}. After 14 days, the conversion in chloroform remained limited at a plateau value of 85 % with a M_n of 2800 g·mol^{-1} but the reaction mixture containing methanol as co-solvent provided 93 % of conversion together with a higher M_n of 6600 g·mol^{-1}. In both cases, the reaction is slow, certainly due to the mild reaction conditions (r.T), the absence of catalyst, and the usage of the challenging EDR148 as diamine embedding electron-withdrawing ether groups. It is however noted that higher conversions and, therefore, higher molar masses, are obtained in the presence of methanol as co-solvent.

Synthesizing linear PHUs with high molecular weight at r.T represents a significant challenge, showcased by the limited number of examples described in the literature where long reaction times and the use of organic solvents – preventing vitrification – are generally needed. However, the synthesis of thermosets is comparatively less elusive as it does not require high monomer conversion to form a gel, and minor side reactions typically do not compromise too much the final material properties. Despite these advantages, the inherently low reactivity of **5CC** monomers still poses a challenge in achieving thermoset materials in short times as illustrated below.

2.4.2. Thermosets

Diakoumakos demonstrated that bulk polymerization of a trifunctional **5CC M5** with DETA was very slow, requiring 8 days to reach completion[38] (**Figure 4A**). The reaction time was halved by adding triethylamine as a base catalyst, with a gel time of 6.5 h. Fleischer later polymerized trifunctional **M6** and a short diamine, reaching a conversion plateau of 60 %, which could be increased to 90 % by adding DABCO (1 wt%) as a base catalyst[67] (**Figure 4B**). This plateau was the result of the polymer T_g higher than r.T (47 °C), in contrast to the previous work of Diakoumakos where the T_g of the polymer was well below r.T (-14 °C). This stresses the importance of targeted polymer T_g in the curing process at r.T: if the T_g of the resulting material is too high, vitrification quickly hampers further cross-linking (**Figure 4C**).

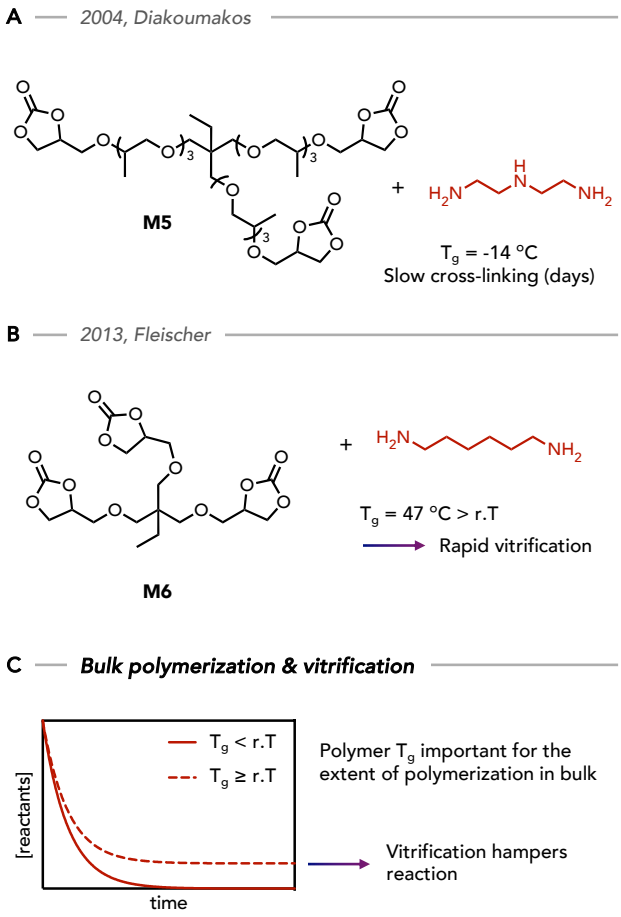

Figure 4 – Bulk polymerization of trifunctional **5CC** with diamines yielding either a (A) low T_g polymer **P5** or a (B) high T_g polymer **P6**. (C) Schematic representation of the reactants conversion in the two situations.

Most PUs formulations incorporate solvents to achieve a lower viscosity state, facilitating efficient mixing and enabling higher conversion of reactants. This is particularly useful for applications like coatings or adhesives, where reduced viscosity enhances the ease of application of the formulations onto substrates. However, regulatory measures aim to restrict the amount of volatile organic compounds (VOCs), which pose health and environmental risks.

Wu evaluated ambient-curable coating through the polymerization of pre-polymers. They first reacted an excess of bis**5CC** and a diamine at high temperature (150 °C) in DMF as solvent to yield **5CC**-terminated PHU prepolymers **M7**. These prepolymers were subsequently reacted with PEI at r.T and applied as coatings[68] (**Scheme 9**). The gel time varied between 3 and 14 h depending on the pre-polymer and PEI molecular weight, and T_gs values ranged from 35 to 50 °C. Although not highlighted by the authors, the polymers contained 50 wt% DMF, likely serving as a plasticizer to mitigate viscosity and prevent early vitrification.

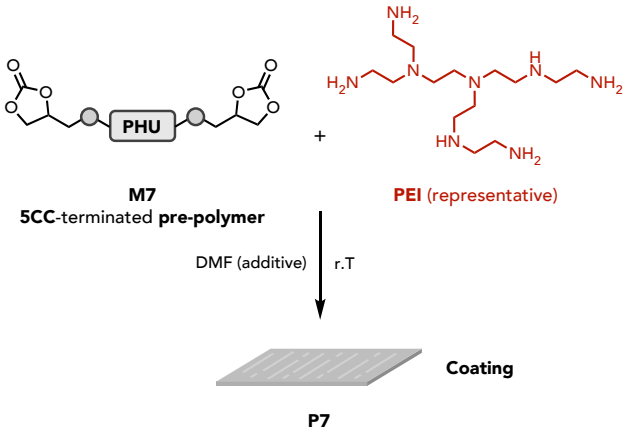

Scheme 9 – Polymerization of **5CC**-terminated PHUs with PEI (representative structure) at r.T for coating applications.

Fortman has shown that polymerization of a bis**5CC** with Tris(2-aminoethyl)amine (TREN) occurred in 1 h at r.T in DCM as solvent[60]. After 24 h, the gel was subjected to reduced pressure and elevated temperature (90 °C) to eliminate the solvent. However, the actual gel time and the extent of **5CC** consumption in the gel state were not determined, as high temperatures during gel drying might post-cure the material.

In response to the regulations on VOCs limiting the use of solvents in PU formulations, waterborne PUs were largely adopted, offering significant environmental and safety advantages. Translating the process to NIPUs is therefore of high interest.
Although the use of water as solvent is detrimental for making linear PHUs due to the competitive hydrolysis reaction, Bourguignon successfully synthesized hydrogels in short reaction times by designing water-soluble monomers. In a first work, water-soluble PEG-derived bis**5CC** was reacted with polyethyleneimine (PEI) in water[69] (**Figure 5A**). It was demonstrated that the pH of the solution has a drastic impact on the polymerization reaction – protonation of the amine at low pH (pH = 9) prevents polymerization, while a high pH (pH = 12.5) accelerates hydrolysis (30 % hydrolysis; 60 % of hydroxyurethane formation) (**Figure 5B**). The solution acidification during the reaction due to released CO_2 from hydrolysis (see **Figure 1C**) further complexifies the system. By properly selecting the solution pH (optimal conditions at pH 10.5 in this case), the hydrolysis was limited to 9 % while enhancing the aminolysis, although **5CC** consumption remained limited (60 %). A small excess of **5CC** was found beneficial for the reaction (0.8 eq. of amine for 1 eq. of **5CC**) (**Figure 5B**). This ratio is rationalized by a consumption of all amines with the presence of additional sacrificial **5CC** functions that inevitably undergo hydrolysis. In optimal conditions of pH and monomers ratio,

a gel point was rapidly obtained within 15 minutes at r.T, with complete **5CC** consumption as determined by IR. A high gel content of 85 % confirmed the cross-linked nature of the hydrogel. For comparison, the bulk polymerization of various bifunctional ether-activated **5CC** with a reactive triamine (TREN) at 40 °C resulted in gel times between 2h30 and 16 h[70]. Impressively short gel times were thus achieved when performing the crosslinking reactions in water at r.T compared to neat conditions.

The authors also investigated how additives could enhance the mechanical properties of hydrogels. Notably, by adding a small amount (2.5 wt%) of nanoclays as fillers, a 180% increase in Young's modulus and a 330% increase in stress at break were achieved. A second strategy involved the creation of a double network – (i) the synthesized covalent PHU network and (ii) a physical network made of gelatin relying on non-covalent interactions. For a 10/6 weight ratio of PHU to gelatin, an outstanding 5100 % increase in stress at break was obtained, likely due to the rearrangement of the physical cross-link nodes within gelatin upon stress application. This proof-of-concept not only demonstrated the robustness of the waterborne PHU hydrogels synthesis, but also showed the significant potential for hydrogels properties enhancement through the use of numerous additives.

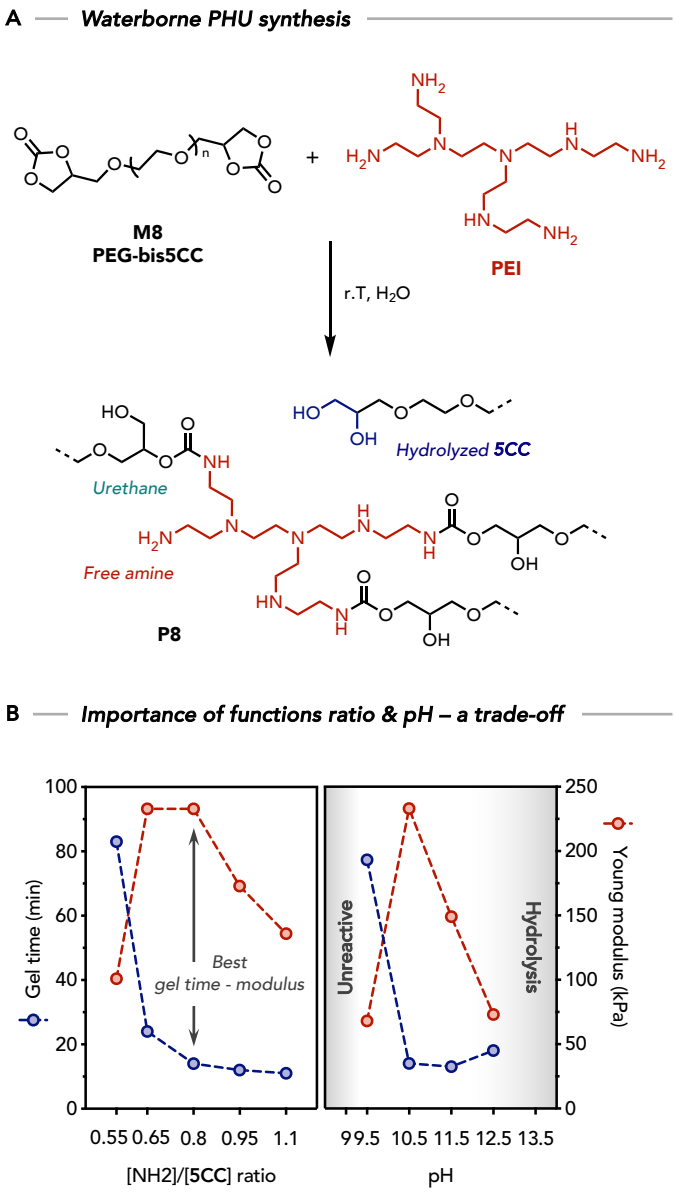

Figure 5 – (A) Waterborne PHU synthesis at r.T from water-soluble PEG-derived bis**5CC M8** and PEI to yield a hydrogel **P8**. (B) Importance of the amine to **5CC** functions ratio (left) and the pH (right) to the gel time and the Young's modulus of the material final properties.

In a second work, the scope of hydrogels was extended by developing water-soluble poly(**5CC**) that react with a broad array of diamines, of varied molecular structure and pKa[71]. A methacrylate derivative of **5CC** was synthesized and co-polymerized with hydrophilic monomers, resulting in water-soluble polymers embedded with reactive **5CC** groups and hydrophilic functional groups: neutral PEG (**M9a**), anionic sulfonate (**M9b**), and cationic ammonium groups (**M9c**) (**Figure 6A**). At pH 12, HMDA reacted with **M9a**, achieving gelation in only 1 min. The storage modulus (G') plateaued after 2 h of reaction, indicating complete conversion. The gel time of other diamines varied: a few minutes for reactive TETA, and

significantly longer for less reactive XDA and EDR148 (**Figure 6B**). This aligns with the previously reported reactivity trend of primary amines (see **Scheme 6**). Interestingly, the gel time for HMDA increased to 12 min at pH 11, with only minor changes for other diamines. At pH 10.5, HMDA was unreactive, unlike other monomers. This highlights the strong relationship between the amine pKa and the pH of the solution: amines with a higher pKa require a sufficiently high pH to prevent excessive protonation inhibiting the reaction. For amines of lower pKa, a lower pH may be chosen to minimize competitive hydrolysis (**Figure 6B**). As a general trend, a fast crosslinking with limited **5CC** hydrolysis requires a solution pH of one unit higher than the pKa value of the involved amine.

Using anionic **M9b**, gels with TETA formed within 17 min at pH 12. The authors took advantage of the anionic sulfonate functional groups to decrease gel time (5 min) and increase the cross-link density (475% increase) of the scaffold through the addition of $CaCl_2$ (25 mol% *vs* sulfonate groups), creating non-covalent ionic bonds (**Figure 6C**). The network also became opaque due to the formation of $CaCO_3$ within the hydrogel following hydrolysis-driven decarboxylation and formation of carbonate anions (**Figure 1C**). The authors hypothesized these $CaCO_3$ particles to participate in the network reinforcement.

Cationic **M9c** provided provided gels in <1 to 9 min from different diamines, and the resulting polymers exhibited thermoresponsive properties.

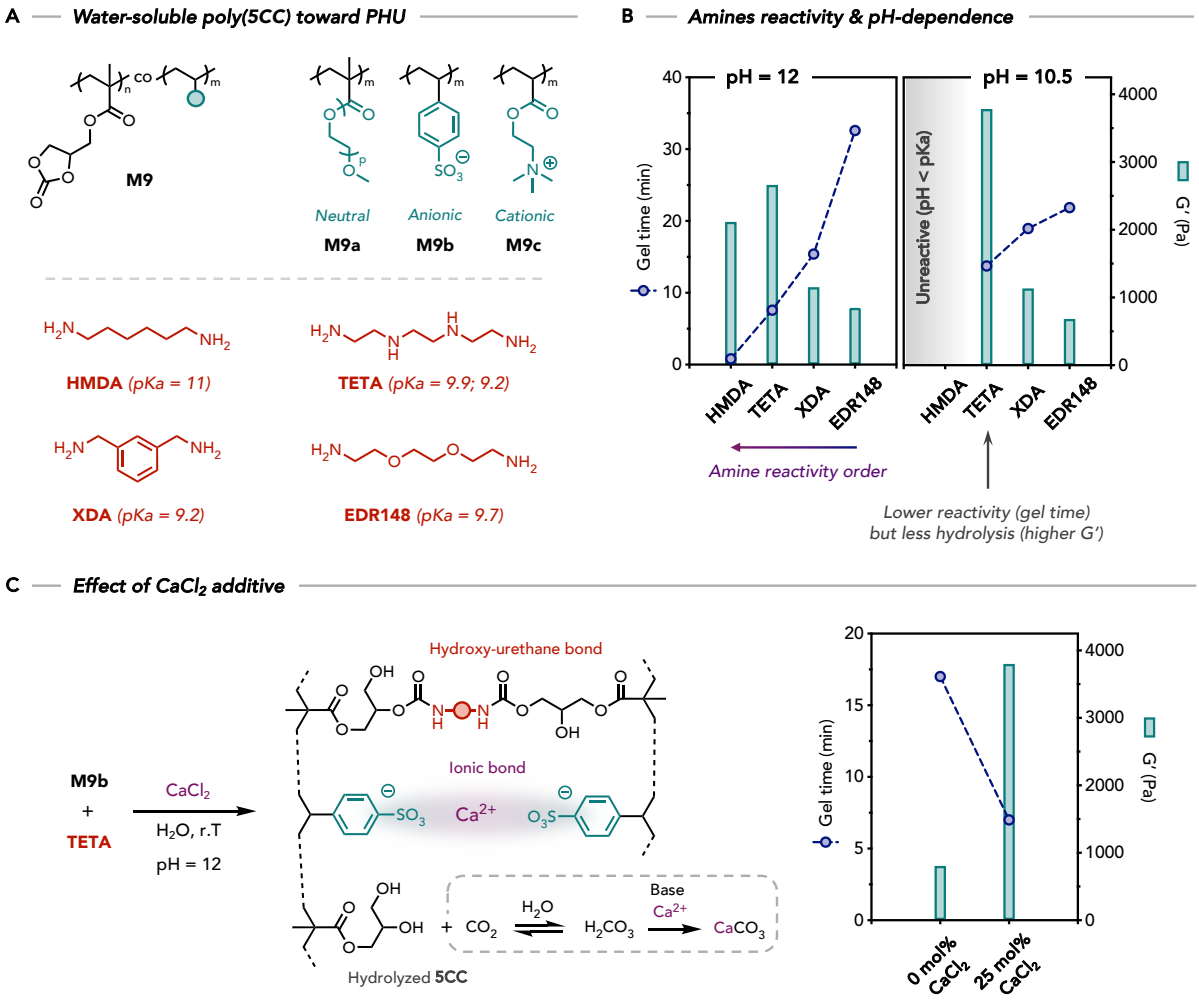

Figure 6 – (A) Synthesis of water-soluble polyfunctional **5CC** monomers **M9**. (B) pH-dependence on the amines respective reactivities using **M9a**. (C) Improvement of gel time and cross-link density in hydrogel from anionic **M9b** and TETA with the addition of $CaCl_2$ as additive, creating additional non-covalent crosslinking nodes.

In another work, poly(vinyl amine) was used with PEG-derived bis**5CC M8** at pH 10 to produce PHU coatings **P10** for indoor air purification (**Figure 7A**), particularly for formaldehyde (FA, an emblematic toxic indoor air pollutant) capture[24]. For that purpose, the coating had to contain excess amine groups that irreversibly capture FA by the formation of a six-membered ring as illustrated in **Figure 7B**. An optimal ratio of [NH_2]/[**5CC**] of 4 was therefore selected to target a high cross-link density value for a hydrogel decorated by NH_2 groups needed for FA capture. This resulted in a short gel time of 2.5 min at r.T and an end of reaction after 2 h. The gel time was also adjusted by the pH, extended from 2.5 min at pH 10 to 20 min at pH 8.5. It is important to note that poly(vinyl amine) tends to promote the formation of some urea through the formation of six-membered rings facilitated by the proximity of the neighboring amine functions

(48% of the polymer functionalization at pH 8.5; 31% at pH 10; the rest of the functionalization being carbamate linkages) (**Figure 7A**). When the coating was evaluated for gaseous **FA** capture, up to 97 % of **FA** was effectively trapped within the PHU after 1 day. Reloading the test chamber several times proved that the polymer was capable of continuously trapping more **FA**. As the pollutant is covalently trapped, no release was observed from the PHU after capture.

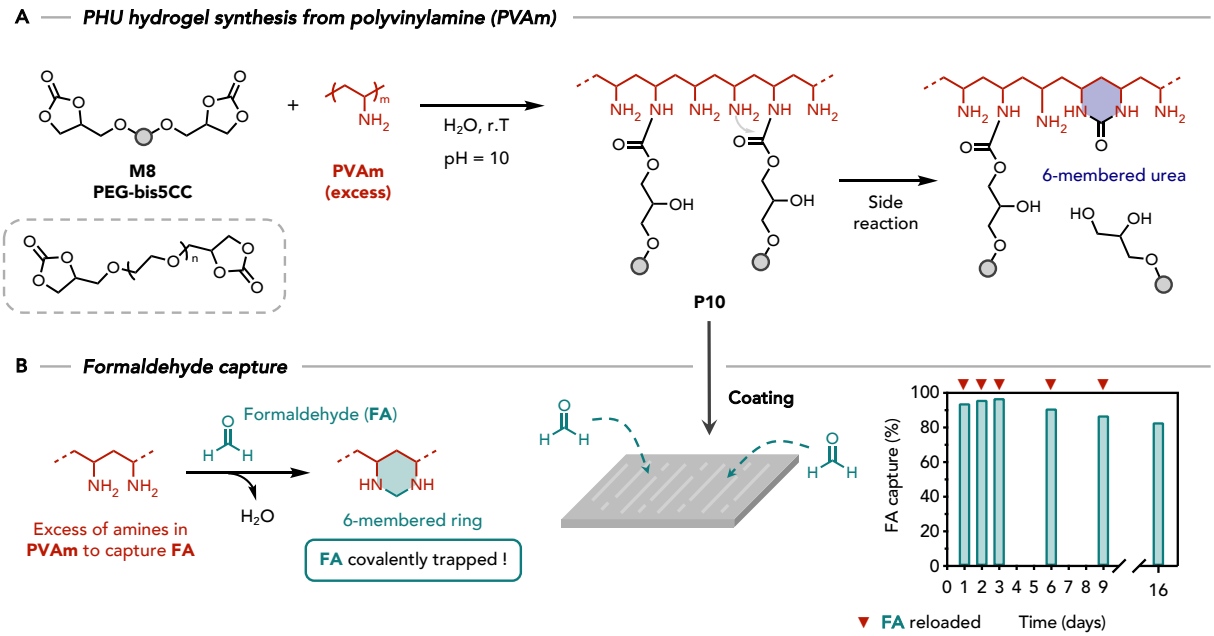

Figure 7 – (A) Amine-rich NIPU hydrogel **P10** synthesis from **M8** and an excess of poly(vinyl amine) (**PVAm**). Urea formation at r.T is facilitated by the formation of stable six-membered rings. (B) Polymer **P10** can be applied as coating to trap formaldehyde (**FA**) pollutant through chemical capture into six-membered rings and water release. The coating can consecutively capture a large quantity of **FA** as demonstrated by the day-per-day renewal of **FA** atmosphere around the material.

These developments not only represent a significant advance in the synthesis of PHU thermosets at r.T, but also emphasize the role of water in readily increasing reaction rates to reach short gel times. An explanation for this exceptional activity is detailed in the solvent effect section (see sections 2.2.4-5), where both a catalytic activity of water and a specific solvation power characteristic to protic solvents were discussed. Additionally, recent extensive rheological studies by Monie further evidenced the role of water in facilitating PHU network formation[59]. The reaction between dry reagents (bis**5CC M5**, **EDR148**) led to a gel time of 15.5 h at r.T, while adding 5wt% of water to the formulation reduced the gel time to 4 h, a 4-fold decrease. This significant reduction is attributed to the catalytic effect of water (**Figure 1D**) and to hydroplasticization of the polymer matrix that lowers the polymer T_g and delays vitrification.

This enhanced chain mobility is due to the high affinity of water for hydroxyl-containing PHUs as determined by rheological analyses. Water effectively disrupts intra- and inter-chain hydrogen bonds, thus enhancing molecular mobility and accelerating the growth of polymer chains (**Scheme 10**). This study underscores the dual role of water as catalyst and plasticizer in facilitating fast network formation. It is worth mentioning that numerous studies in PHU chemistry do not report whether reagents and catalysts were dried or used as stored. As a minimal amount of water can significantly impact reaction rates and gel times, the comparability between studies may be biased depending on the reagents grades and purities, as well as environmental humidity conditions.

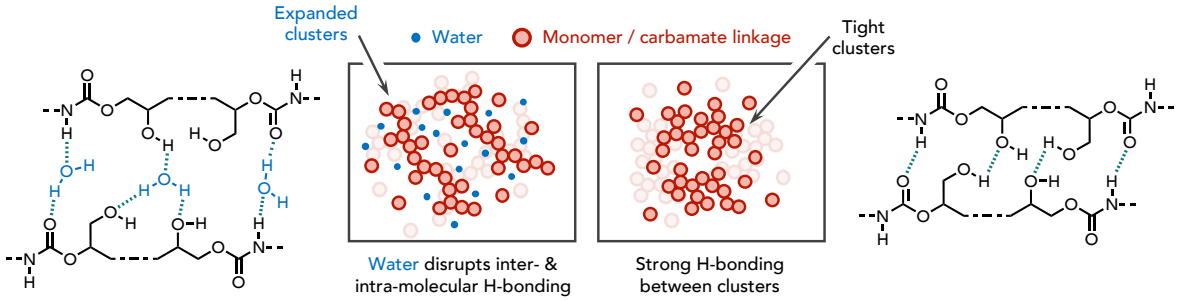

Scheme 10 – During PHU network formation, water can act as hydrogen bond donor and acceptor, thus disrupting hydrogen-bonding within and between the PHU clusters in formation. The clusters are more expanded and benefit from higher mobility. In the absence of water, the clusters are in strong interactions and are tightly grouped, restraining their diffusion power.

3. NIPUs by aminolysis of 6- to 8-membered cyclic carbonates

Increasing the cyclic carbonate ring size is an effective strategy to enhance the cyclic carbonate reactivity as compared to more stable five-membered cyclic carbonates **5CC**. Tomita demonstrated through model reactions that the reactivity of 6-membered cyclic carbonates **6CC** was over 30 times greater than that of a comparable **5CC**[72] (**Scheme 11**). Maisonneuve confirmed this finding and showed through kinetic experiments that although the reaction starts quickly, complete **6CC** conversion can take up to 4 days. Raising the temperature to 50 °C reduces the reaction time to approximately 24 h[73]. Similar to **5CC**, variation of the ring substituents through inductive effect can further increase the reaction rate[17,22,23]. A simplistic computational study demonstrated that the difference in enthalpy of formation between the carbamate products and the cyclic carbonates reactants (5CC *vs* larger rings) increases with the carbonate ring size[74]. Tomita suggested that this trend could be

attributed to increased ring strain within cyclic carbonates of larger size, thereby affecting their reactivity. However, a low level of theory (semi-empirical model) was used in the study and modern DFT methods might provide more accurate values. Moreover, these values must be corroborated by experimental data to validate the methodology used by the authors.

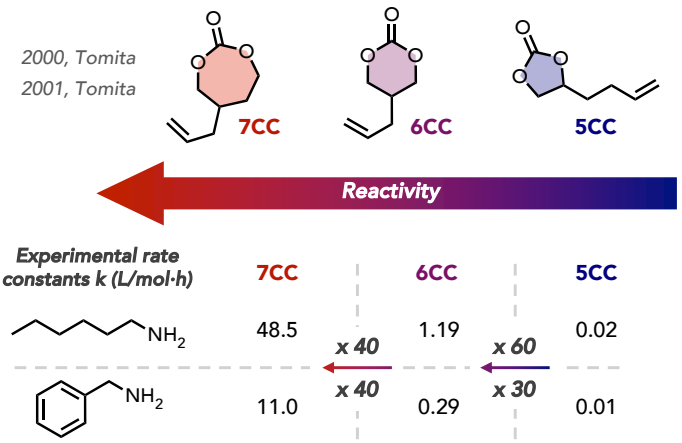

Scheme 11 – Experimental rate constants for the aminolysis reaction of **5CC** as compared to **6CC** and **7CC** in similar reaction conditions.

Tomita compared the reactivity of two representative bis**5CC** and bis**6CC** with a diamine at 50 °C using DMAc as solvent[75]. A full monomer conversion was attained with bis**6CC** after 48 h of reaction, reaching a M_n of 26,000 g·mol^{-1}. In contrast, the conversion in bis**5CC** remained incomplete after 14 days, with a M_n of 15,000 g·mol^{-1}. Maisonneuve performed similar polymerizations at various temperatures, emphasizing the significance of increasing the temperature from r.T to 50 °C to go from M_n of 14,000 to 22,000 g·mol^{-1} [73]. However, prolonged reaction at 50 °C resulted in an insoluble gel. This was ascribed to undesirable reaction of pendant alcohol functions of the **6CC**-derived hydroxyurethane product **2** with **6CC** functions to produce a carbonate linkage (**Scheme 12**). It is important to note that this side reaction was not observed with **5CC** as they are less reactive than **6CC**.

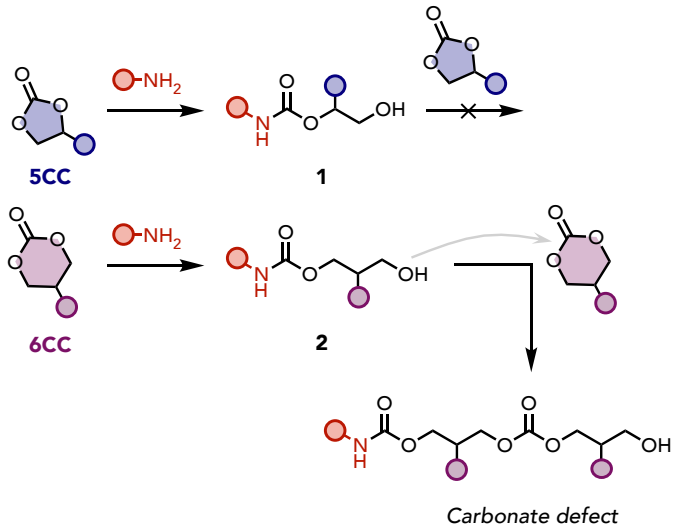

Scheme 12 – Ring-opening of **6CC** by pending alcohols on **2** to furnish carbonate defects.

Lambeth realized an in-depth study of the effect of catalysts on the course of the reaction and associated side reactions. He concluded that gelation occurs even without any catalyst at r.T due to initiated ring-opening of **6CC** by free alcohols[76]. By using thiourea as organocatalyst through activation of the carbonyl function, the M_n was increased from 10,000 to 22,000 $g \cdot mol^{-1}$ at r.T and up to 90,000 $g \cdot mol^{-1}$ at 50 °C. Using TBD as organocatalyst proved detrimental to PHU formation due to the strong activation of **6CC** toward ring-opening polymerization (ROP) from free alcohols.

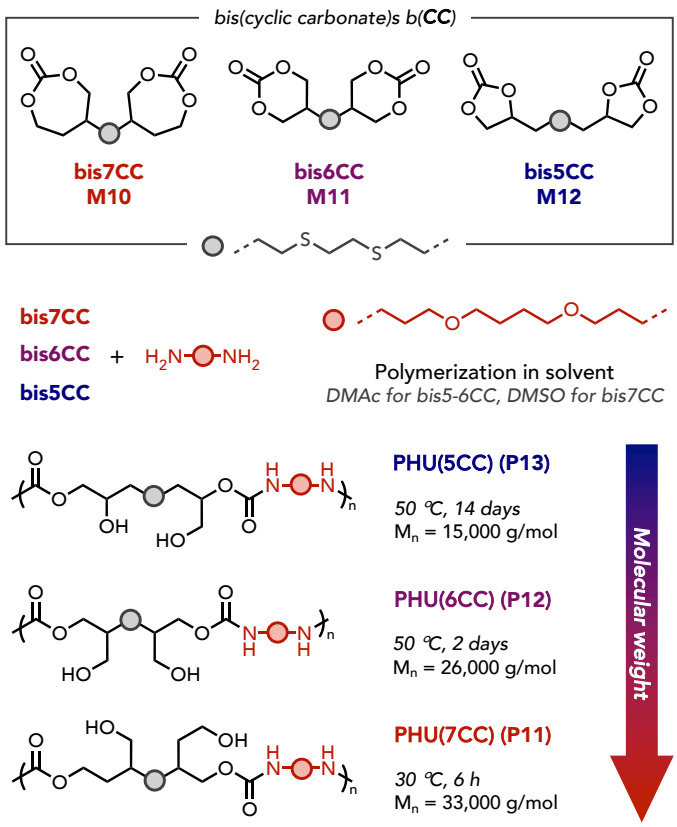

Scheme 13 – Comparative polymerization of bis**5CC M12**, bis**6CC M11**, and bis**7CC M10** analogs with the same diamine.

Tomita reported the synthesis and aminolysis of seven-membered cyclic carbonates **7CC**, hypothesizing that their reactivity might surpass that of **6CC**. Model reactions demonstrated a 40-fold increase in reactivity for **7CC** over **6CC** at r.T, with complete reactant consumption in 1 h, even with the less reactive benzylamine[74] (**Scheme 11**). The synthesis of PHUs from bifunctional monomers was successfully carried out at r.T in DMSO (**Scheme 13**), yielding polymers with a M_n of 33,000 g·mol^{-1} (M_w = 90,000 g·mol^{-1}) using a reactive aliphatic diamine after 6 h, and with a lower M_n of 11,000 g·mol^{-1} (M_w = 14,200 g·mol^{-1}) with a benzylic diamine after 24 h. This study highlighted a significant enhancement in molecular weight at r.T compared to smaller rings **6CC** and **5CC**.

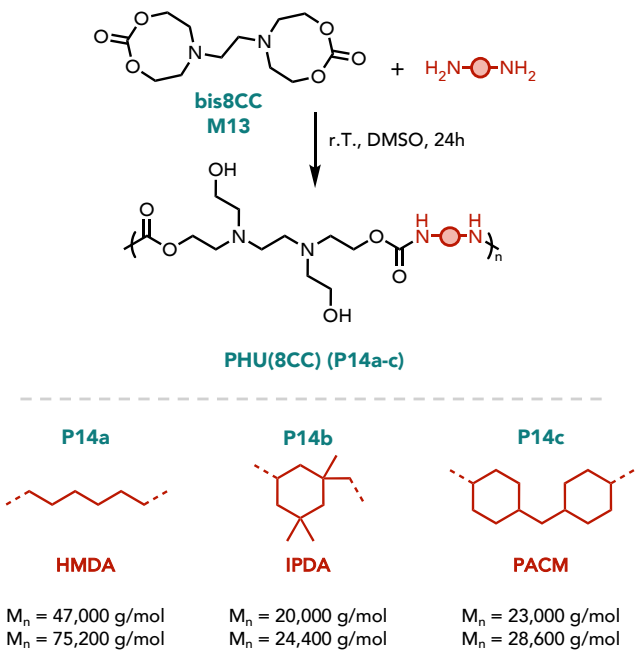

Scheme 14 – Polymerization of bis**8CC** (**M13**) with diamines at r.T into PHU **P14a-c**.

Based on the same assumption, Yuen reported the synthesis of 8-membered cyclic carbonates **8CC** as PHU precursors[77]. Comparative model reactions showed **8CC** to be significantly more reactive than **5CC** and **6CC**. Polymerizations from bis**8CC** and HMDA at r.T for 24 h in DMSO yielded polymers of high molecular weight with M_n of 47,000 g·mol^{-1} (M_w = 75,200 g·mol^{-1}). The scope was extended to challenging sterically hindered diamines, such as IPDA and PACM, resulting in polymers of decent molecular weight (M_n = 20,000 and 23,000 g.mol^{-1}, respectively) (**Scheme 14**). A secondary diamine was included in the scope but exhibited too low reactivity to form polymers.

Following excellent results obtained for **5CC** hydrogels, **8CC** precursors were evaluated for the waterborne PHU synthesis[78]. By reaction of the bis**8CC** with PEG-diamine and TREN as cross-linker (0.4 eq.), it was found that lower water content reduced gel times (50 wt% water content leaded to a gel time of 350 min; 70 wt% to a gel time of 750 min), indicating an important concentration effect. With excessive water, not only the gel was not formed after 24 h, but it also favored **8CC** hydrolysis over efficient aminolysis. Expectedly, an increase in triamine over diamine resulted in significant gel time decrease, from 30 h with 0.2 eq. of cross-linker to seconds with 1 eq. of cross-linker.

Current limitations in six- to height-membered rings and perspectives

Although cyclic carbonate rings of size higher than five are promising precursors for the synthesis of high molecular weight NIPUs, their use faces several limitations. One major issue is the side reaction of ring-opening by primary alcohols, which are prevalent in the hydroxyurethane product **2**. While this typically occurs at 50 °C or higher[73,77], Lambeth's work demonstrated that gelation can occur at r.T[76]. An in-depth investigation on the influence of various factors such as substituent or solvent effect might be needed to understand the extent of the undesired side rection over the aminolysis reaction. Moreover, the reported rather high molecular weights for the polymers prepared from bis**6CC** to **8CC** might possibly account for branched species if ring-opening by pendent alcohols occurs even at low extent.
The use of a catalyst might be essential in some scenarios, especially in the case of bis**6CC** and challenging amines. Besse reported the use of DIPEA (2 mol%) for the polymerization of bis**6CC** at r.T without observable gelation after 24 h[79]. Lambeth later studied the influence of TU and TBD catalysts as they have proven to have high catalytic activity for the aminolysis of **5CC**. While TU was beneficial for reaching high molecular weights, gelation was obtained extremely rapidly with TBD, certainly because it is an excellent activator for 6-membered[80–82] and 8-membered[83,84] cyclic carbonates ROP. There remains a need for a systematic search for catalysts that selectively promote aminolysis of cyclic carbonates over ROP by alcohols.
Finally, a limitation of these precursors is their difficult synthesis. While **5CC** is easily produced from CO_2-epoxide coupling, larger rings are more challenging to obtain due to their facile ring-opening by diverse substrates compared to less reactive **5CC**. These are most easily and commonly prepared from nasty reagents including phosgene or derivatives[85,86]. More sustainable alternatives are currently searched, notably using CO_2 as feedstock[80,87–89], but there remains much work for the scaled production of bifunctional monomers.

4. NIPUs by aminolysis of α-alkylidene cyclic carbonates

α-alkylidene cyclic carbonates (**αCC**) are five-membered cyclic carbonate derivatives featuring an exo- or endo-vinylene group. Exovinylene cyclic carbonates are commonly produced from the well-studied catalyzed CO_2 fixation onto propargyl alcohols[90–93] (**Scheme 15A**). In contrast, endo-ones are typically obtained by reaction of α-hydroxy ketones with phosgene derivatives[94,95] (**Scheme 15B**). Recent works have however demonstrated their availability from diphenyl carbonate[96], and from the rearrangement of exo-vinylene ones[97].

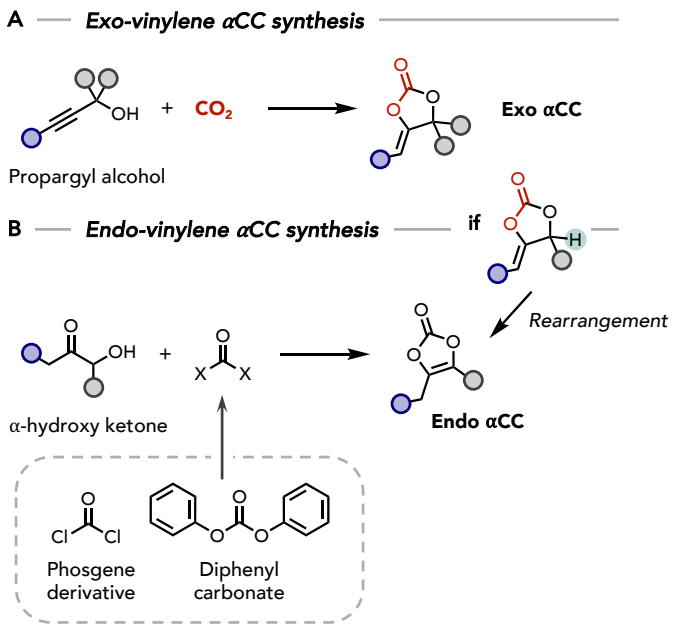

Scheme 15 – (A) Synthesis of exo-vinylene **αCC** from CO_2 and propargyl alcohol. (B) Synthesis of endo-vinylene **αCC** from α-hydroxyketone and phosgene or diphenyl carbonate. The endo- can also be obtained from an exo-analog by rearrangement if one ring substituent is an H atom.

Exovinylene **αCC** undergo smooth aminolysis with both primary amines and secondary amines to provide (a)cyclic carbamates in good to high yields at r.T[98–103] (**Figure 8A**), sometimes in one-pot starting from a mixture of the propargyl alcohol, the amine, and CO_2[104–107]. The aminolysis of **αCC** occurs through regioselective ring-opening of the carbonate on the side of the exovinylene group, followed by tautomerization of the resulting enol into a ketone to form an *oxo*-carbamate moiety **3**. If the amine is primary, the -NH- group of the carbamate can attack the ketone through intramolecular ring-closure to provide a hydroxy-oxazolidone **4**. The exceptional reactivity of **αCC** at r.T is attributed to increased ring strain provided by the exovinylene function. Once ring-opened, the tautomerization towards the *oxo*- adduct drives the equilibrium toward product formation. Although the regio-selective opening has not been rationalized yet, crystallographic structures of **αCC** derivatives indicate an increased bond length at the side of bond scission, suggesting a weaker bond strength certainly induced by the neighboring exovinylene group (**Figure 8C**).

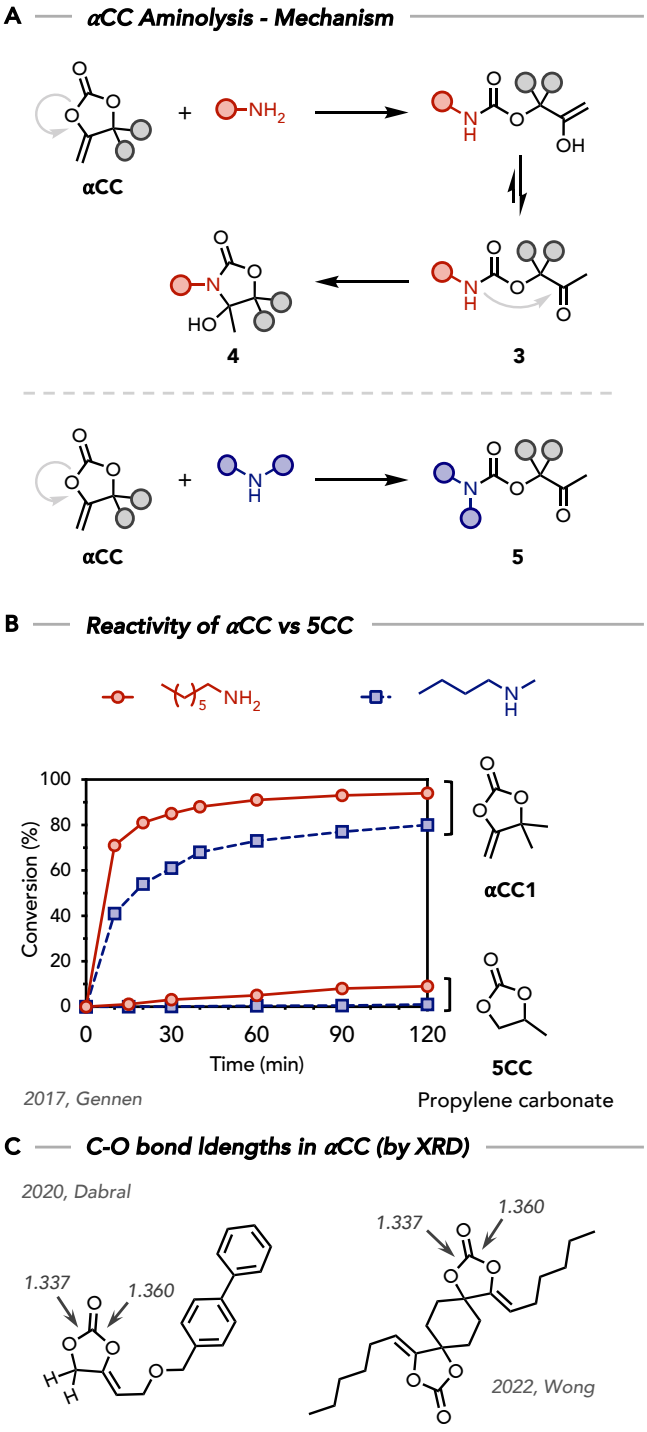

Figure 8 – (A) **αCC** aminolysis mechanism in the presence of primary and secondary amines. (B) Comparative reactivity of a substituted exovinylene **αCC** (**αCC1**) and **5CC** (propylene carbonate) toward primary and secondary amines at r.T without catalyst. (C) Molecular structure of two **αCC** compounds as determined by XRD.

4.1. Model reaction studies

4.1.1. Effect of the αCC structure

Kinetic experiments attest the substantial increase in reactivity of **αCC1** compared to **5CC** (propylene carbonate) toward primary and secondary amines at r.T (**Figure 8B**). The reaction of **αCC** with primary amines into **4a** is fast and quantitative within few hours, while the reaction with secondary amines, though slower, keeps complete in 24 h into **5**. It was also observed that adding a catalytic amount of DBU speeds up these reactions.

Following this seminal work, subsequent studies explored the reactivity of structurally divergent substrates. Dabral synthesized elusive unsubstituted exovinylene cyclic carbonates **αCC2** from primary propargyl alcohols[108]. The reaction with primary amine is fast at r.T, providing a hydroxy-oxazolidone **4b** which spontaneously dehydrates into an endo-vinylene oxazolidone **6b**[92] (**Scheme 16B**). The reaction with a secondary amine (pyrrolidone) is slower but still provides quantitative reaction at r.T in 6 h.

Chauveau assessed the reactivity of commercial disubstituted endo-vinylene cyclic carbonate **αCC3**[109]. With primary amines, the reaction is smooth at r.T and provides a hydroxyoxazolidone **4c**. When a secondary amine is used with a catalytic amount of DBU (1 mol%), the reaction quickly produced the *oxo*-carbamate **5c** in 3 h (**Scheme 16C**). However, translation of the **αCC3** aminolysis to polymer chemistry failed with low monomer conversion and side reactions.

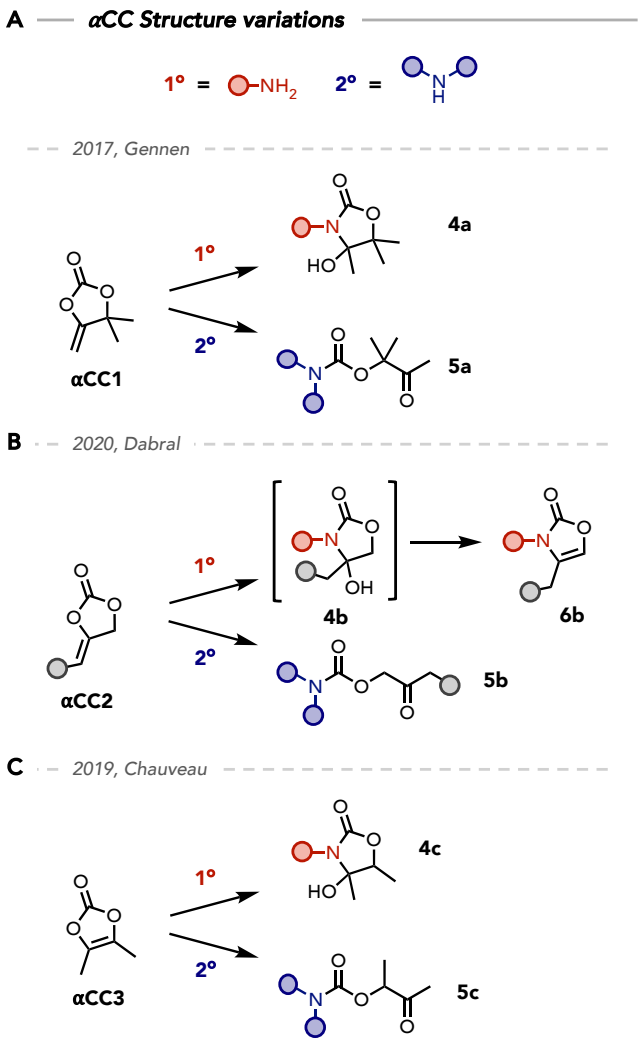

Scheme 16 – Reactions of **αCC** variants with primary and secondary amines. (A) Substituted exovinylene cyclic carbonate; (B) Unsubstituted exovinylene cyclic carbonate; (C) disubstituted endovinylene cyclic carbonate.

4.1.2. Effect of the amine

The reaction of **αCC1** and amines is slower with increased steric hindrance around the amine function[103]. Kinetic experiments established the order of reactivity for three representative amines as follows: heptylamine > benzylamine > cyclohexylamine. Despite variations in reaction rate, the reactions reached quantitative conversion after 24 h. The *oxo*-carbamate intermediate **3** is observed during the reaction for all amines and gets consumed as the reaction proceeds, therefore driving the equilibrium toward products. The ring-closure into hydroxy-oxazolidone **4** occurs quickly for the aliphatic amine but is considerably slower for sterically hindered cycloaliphatic amine, such as cyclohexylamine (24 % of remaining **3** after 24 h). Interestingly, for hindered benzylamine, the ring-closure is exceptionally rapid, with the

intermediate **1** barely detectable during the reaction and leading to full selectivity toward **4**. The high reactivity of benzylamine toward ring-closure suggests that other factors than steric hindrance might influence this step. The addition of DBU as catalyst (5 mol%) significantly accelerates both amine addition and ring-closure steps, rendering the reaction with cyclohexylamine selective toward **4** after 24 h.

4.2. Polymerizations

The high efficiency of this chemistry to quantitatively provide carbamates at r.T and within 24 h was translated to the step-growth polymerization of linear polymers. Bifunctional **αCC** monomers were synthesized following different strategies, mostly based on the synthesis of bis(propargyl alcohol)s obtained from diketones[102,110] (toward substituted bis**αCC M14**-**M16**, **Scheme 17A**) or from bisepoxides[92] (toward unsubstituted bis**αCC M17**-**M18**, **Scheme 17B**). Another approach relies on the Heck coupling of monofunctional **αCC** toward **M19**[102] (**Scheme 17C**).

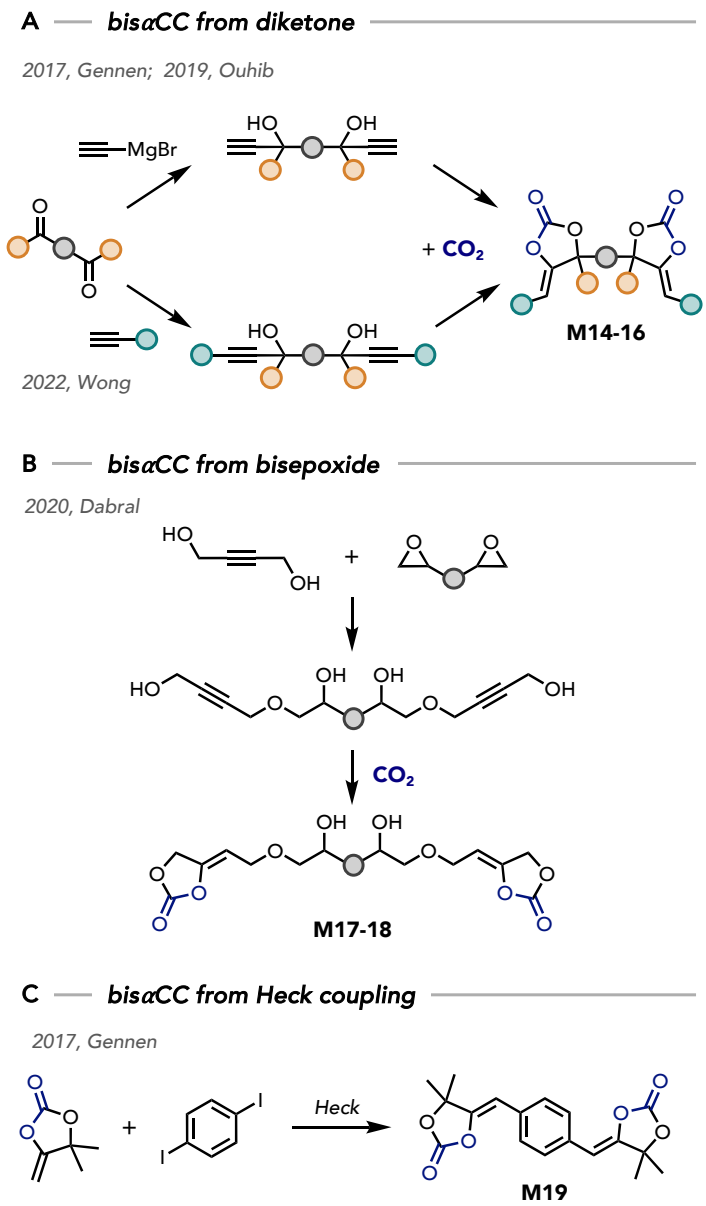

Scheme 17 – Synthesis of bis**αCC** from (A) diketones, (B) bisepoxides, and (C) using Heck coupling reaction.

4.2.1. Poly(*oxo*-urethane)s

Gennen demonstrated the polymerization of **M14** and **M19** with secondary diamines at r.T, using $CHCl_3$ or DMF as solvents (**Scheme 18A**)[102]. DMF was superior as demonstrated by a 2- to 3-fold increase in molecular weight of the polymers compared to $CHCl_3$. The monomer structure was varied for the polymerization in DMF, affording M_n of 13,500 g·mol^{-1} (M_w 40,000 g·mol^{-1}) for **M19** and 5,000 g·mol^{-1} (M_w 7,000 g·mol^{-1}) for **M14** after 24h of polymerization (**Scheme 18A**). This suggests that **M19** might have increased reactivity compared to **M14**.

However, it's important to note that the molar mass determined by SEC is relative and heavily influenced by the molecular structure. The addition of a catalytic amount of DBU increased the molecular weight to M_n 25,000 g·mol^{-1} (M_w 73,000 g·mol^{-1}) for **M19** and M_n 11,000 g·mol^{-1} (M_w 16,000 g·mol^{-1}) for **M14**.

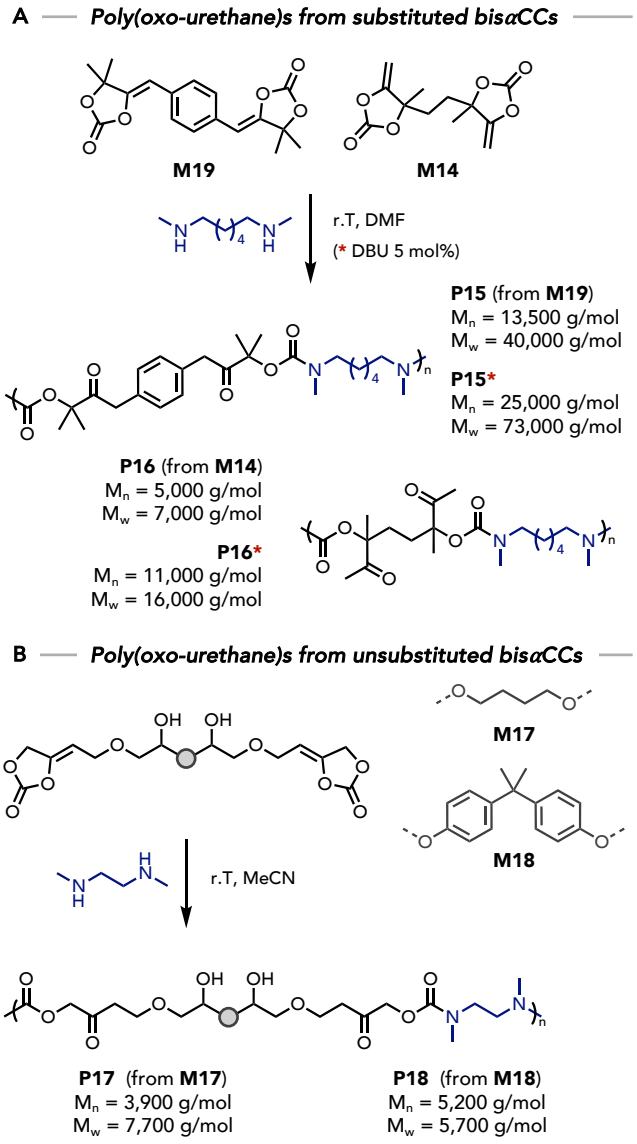

Scheme 18 – Poly(*oxo*-urethane) synthesis from (A) substituted bisαCCs and (B) unsubstituted bisαCCs.

Unsubstituted bisαCCs **M17** and **M18** were co-polymerized with a secondary diamine at r.T in acetonitrile, affording polymers with moderate molar mass up to M_n 5,200 g·mol^{-1} and M_w up to 7,700 g·mol^{-1}, with a full conversion in monomers after 24 h[92] (**Scheme 18B**). However, the solvent was not varied nor the addition of a catalyst to optimize the reaction conditions.

4.2.2. Poly(hydroxy-oxazolidone)s

Gennen synthesized poly(hydroxy-oxazolidone)s by reacting **M19** with primary diamines at r.T in DMF, providing polymers of high molecular weight after only 3 h (up to M_n = 22,000; M_w = 77,000 g·mol^{-1}) (**Scheme 19A**). These polymers became insoluble after 24 h of reaction, likely due to increased molecular weight. Polymerization using **M14** provided soluble polymers after 24h, characterized by a M_n of 21,500 g·mol^{-1} (M_w 31,000 g·mol^{-1}). In both cases, the reaction medium became very viscous and even gelled.

Habets expanded the scope of polymers with a spirocyclic monomer **M15**, along **M14**, to polymerize with a broad range of primary diamines at r.T in DMF for 24 h (**Scheme 19B**). Using **M14** as monomer, moderately high molecular weight poly(hydroxyoxazolidone)s were obtained using unhindered diamine monomers (M_n 20,400 - 24,900 g·mol^{-1}; M_w 36,100 - 44,800 g·mol^{-1}) with a full selectivity toward the hydroxy-oxazolidone **4** linkage. However, using more hindered benzylic MXDA resulted in lower molecular weight (M_n 4,000 g·mol^{-1}; M_w 7,600 g·mol^{-1}), with a complete selectivity toward the cyclic linkage **4**, in line with the model experiments (*vide infra*). Highly hindered and rigid cyclohexyldiamine was even less efficient, resulting in low molecular weight polymers (M_n 3,000 g·mol^{-1}; M_w 4,700 g·mol^{-1}) and in a partial selectivity toward the hydroxy-oxazolidone linkage (32% of *oxo*-urethane linkage **3** persisted after 24 h). EDR148 also produced low molecular weight polymers (M_n 4,200 g·mol^{-1}; M_w 8,400 g·mol^{-1}) despite its unhindered structure, certainly affected by the negative inductive effect of β-ethoxy bonds. The addition of 5 mol% of DBU was evaluated for the challenging amines. For EDR148, the molecular weight significantly increased to M_n of 15,500 g·mol^{-1} (M_w = 25,500 g·mol^{-1}), demonstrating the beneficial effect of a catalyst for challenging substrates. However, the DBU-catalyzed addition of more hindered cyclohexyl- and benzylic diamines yielded insoluble polymers, possibly due to molecular weight exceeding solubility thresholds. All the poly(hydroxy-oxazolidone)s derived from **M15** were insoluble in all organic solvents.

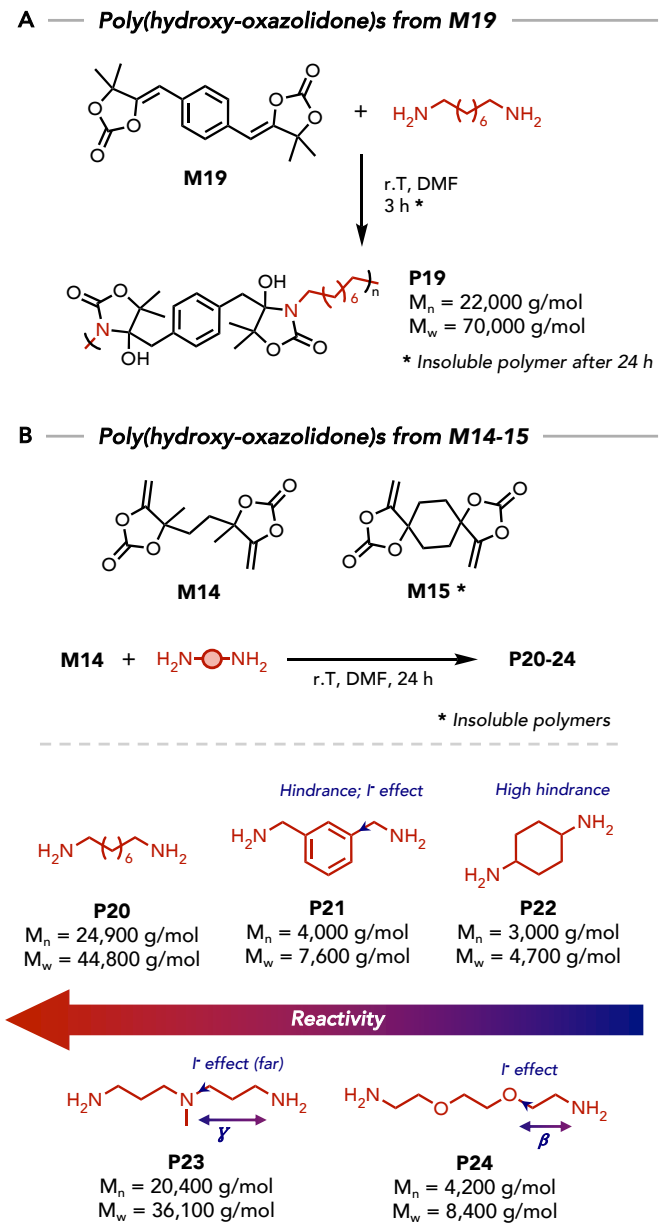

Scheme 19 – Poly(hydroxy-oxazolidone) synthesis from (A) **M19** and 1,8-octanediamine and (B) **M14-15** and several diamines.

This isocyanate-free chemistry has shown great promise for producing elusive poly(oxazolidone)s with moderate molecular weight at r.T, while this class of PU is generally synthesized in harsh conditions (> 150 °C, catalysts) from epoxides and isocyanates. A major limitation is the low solubility of the synthesized polymers, likely due to the combined effects of structural rigidity and the dense hydrogen bonding network formed by the pending hydroxyl functions of the polymer backbone. To address this issue, Wong very recently incorporated solubilizing groups on the double bond of the challenging monomer **M15** to enhance the solubility of the polymer in solvents, yielding monomers **M16a-d**[111] (**Scheme 20**). High

temperatures (80 °C) were mostly used in the work, but one example was achieved at r.T from **M16b** and 1,4-butanediamine in the presence of DBU (25 mol%). The polymer contained exclusively hydroxyoxazolidone **2** linkages but was characterized by a low molecular weight (M_n 3,400 g·mol^{-1}; M_w 6,800 g·mol^{-1}). The polymerization occurred in diluted conditions (0.125 M in reactive functions), in contrast to previous works from Gennen and Habets (0.335 M), which could significantly affect the reaction rate. The introduction of solubilizing groups resulted in improved solubility of the polymers in various solvents, particularly when the groups included the more flexible ether-containing chain in **M16d**.

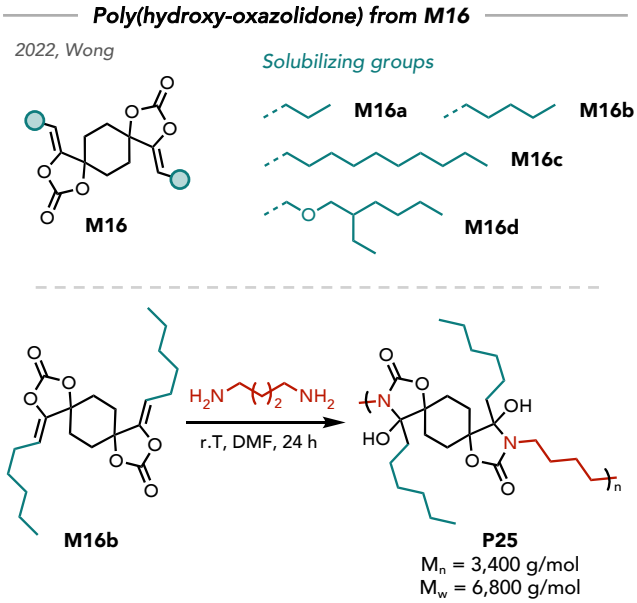

Scheme 20 – Poly(hydroxy-oxazolidone) **P25** synthesis from **M16**.

The tertiary alcohol in the hydroxyoxazolidone linkage **4** has shown to provide opportunities for further functionalization through a dehydration reaction to yield poly(alkylidene oxazolidone)s. This was first demonstrated by Habets with the dehydration of, for instance, **P20** and **P21**, by reflux in acetic acid (120 °C) for 2 h, furnishing **P20dehy** and **P21dehy** respectively[103] (**Scheme 21A**). Similarly, Wong performed this reaction on **P25**, but at r.T in the presence of trifluoroacetic acid (TFA, 25 mol%) and molecular sieves (3Å)[111]. While **P21dehy** exhibited only the expected α-alkylidene oxazolidone linkage, **P20dehy** contained 58 % of the α-alkylidene oxazolidone linkage and 42 % of the β-analog. It was rationalized that a Wagner-Meerwein rearrangement led to the formation of the more stable trisubstituted alkene in the β-linkage. The feasibility of this rearrangement seemed ruled by the hindrance of the amine group. In the case of **P25dehy**, no rearrangement occurred in the absence of a neighboring labile methyl group (**Scheme 21B**). The thermal stability of the dehydrated polymers generally

improved compared to poly(hydroxy-oxazolidone)s, enabling their characterization by DSC. Polymers **P20dehy** and **P21dehy** were characterized by T_gs values of 89 and 130 °C respectively, while the polymer **P25dehy** was semi-crystalline with a T_g of 85 °C and a T_m of 207 °C.

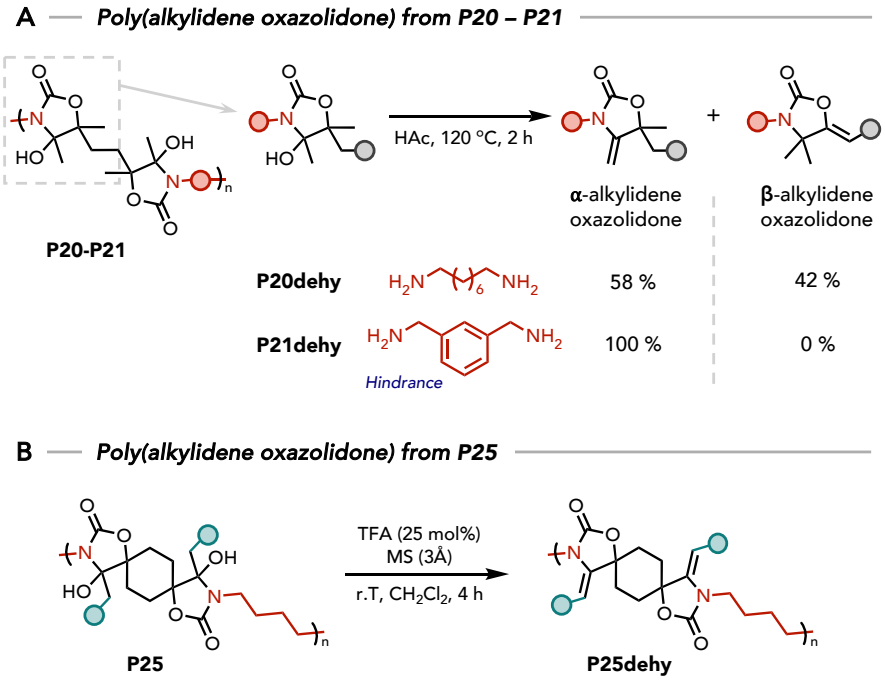

Scheme 21 – (A) Dehydration of poly(hydroxyoxazolidone)s **P20** and **P21** to yield a poly(alkylidene oxazolidone)s embedding one or two different linkages depending on the amine steric hindrance. (B) Dehydration of poly(hydroxy-oxazolidone) **P25**.

The α-alkylidene cyclic carbonate chemistry is an emerging toolbox for the synthesis of regioregular and well-defined NIPUs in mild conditions. By the selection of the amine nature (primary or secondary), both acyclic and cyclic polyurethanes can be produced. However, many aspects of this chemistry remain unexplored, such as the effect of the cyclic carbonate structure on the reaction rate, the identification of optimal catalysts, solvent effects, and the development of materials with practical applications that leverage the unique properties of this chemistry.

5. NIPUs by polycondensation methods

5.1. Transurethanisation

NIPUs can be synthesized using polycondensation methods, typically through the well-established transurethanisation reaction where biscarbamates **M20** react with diols. The monomeric diols replace a leaving alcohol condensate to form a new carbamate bond (**Scheme 22A**). To shift the equilibrium toward high conversion and therefore, high molecular weight, the condensate must be removed from the reaction medium. Consequently, this reaction requires high temperatures and reduced pressure in the presence of suitable catalysts. This approach is highly attractive as the resulting polymers possess the same molecular structure as isocyanate-based PUs. However, performing transurethanisation at r.T is illusory due to the need to remove the alcohol condensates.

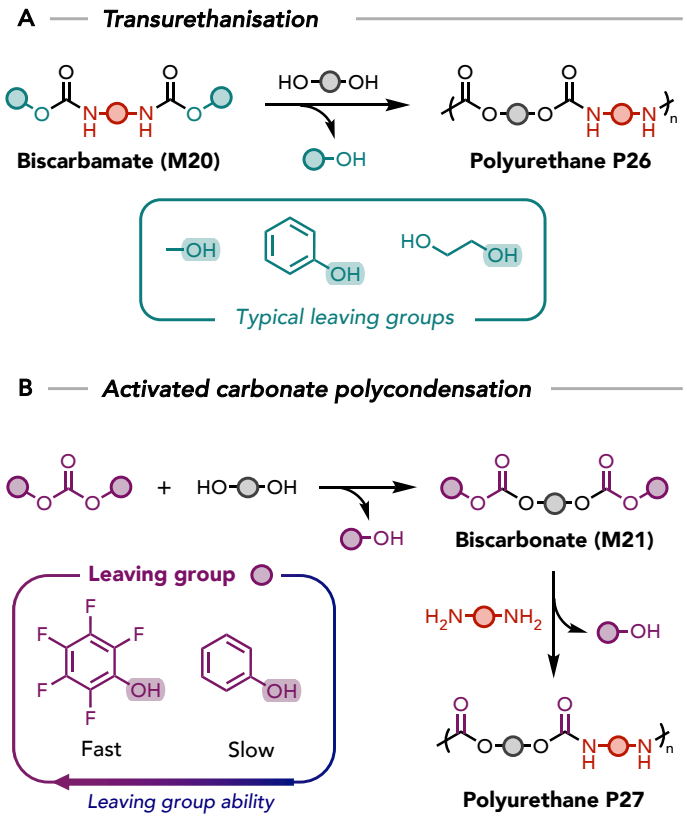

Scheme 22 – NIPUs by polycondensation through (A) transurethanisation, and (B) activated carbonates.

5.2. Polycondensation from activated carbonates and diamines

Polycondensation into polymers with identical chemical structures can be achieved by engineering carbonates into so-called '*activated carbonates*'[112–114]. The strategy relies on the synthesis of a biscarbonate **M21** terminated with excellent leaving groups. By reaction of this monomer with a diamine in mild conditions, the carbonate is selectively cleaved to release the desired leaving group, yielding carbamate linkages (**Scheme 22B**). Biscarbonates can be synthesized from chosen diols to tune the polymer properties, also altered by the choice of the diamine during polymerization. For instance, Sardon designed biscarbonates using both rigid (1,6-hexanediol) and flexible (PEG) linkers, which were used in different ratios to tailor the final polymer properties. The polymerization was conducted in water, with an equimolar ratio between the biscarbonate and the amine, along with triethylamine in equimolar ratio *vs* reactive functions. Polymers **P27** with M_n of around 16,000 g·mol^{-1} (M_w 32,000 g·mol^{-1}) were obtained after only 1 h of reaction at r.T without needing reduced pressure, though it must be kept in mind that polymers were obtained from oligomeric biscarbonates (PEG-derived) and diamines. The polymers exhibited crystallinity due to the PEG domains and a low T_g of around -55 °C. A significant drawback from this approach is the release of toxic and hazardous pentafluorophenol during polymerization. Additionally, the biscarbonate was synthesized from bis(pentafluorophenyl)carbonate, which originates from phosgene. Substituting this effective leaving group with more environmentally friendly phenol significantly slowed down the reaction. Although it was not discussed by the authors, the presence of triethylamine might benefit to the reaction by quenching the acidic released phenolic species, hence shifting the reaction equilibrium.

5.3. Polycondensation from CO_2-derived carbamates and dihalides

Wu recently described a polycondensation strategy combining diamines and dihalides in the presence of CO_2 to synthesize polyurethanes[115] (**Scheme 23**). This method relies on the formation of carbamates from amines and CO_2 in mild conditions and in the presence of a base (1 eq. *vs* reactive functions). The resulting carbamate adducts undergo step-growth polymerization with a dihalide (bromide here), producing a polyurethane and an acid-base condensate. Previous reports required higher temperatures, resulting in defects within the polymer backbone and stoichiometric unbalance[116]. The authors found that a cyclopropeneimine base enabled chemoselectivity at r.T and yielded soluble carbamate adducts, unlike other commercial superbases such as DBU or TBD. Their methodology involved adding the base in equimolar amount to the amine with CO_2, thereby forming the

carbamate adduct. After the addition of the dihalide in a second step, the polymers were obtained after 24 h at r.T under 1 atm of CO_2, and were characterized by a moderate to high molecular weight (4,000 to 420,000 $g \cdot mol^{-1}$) depending on the diamine. Aromatic, hindered, and deactivated through inductive effect amines were less efficient than aliphatic diamines. Interestingly, secondary diamines were effective monomers to provide NIPUs bearing *N*-substituted carbamate linkages **P29**. The T_g of the polymers was greatly influenced by the monomers structure, ranging from -20 to 140 °C. Although the authors mentioned to reach molecular weight up to 420,000 $g \cdot mol^{-1}$, this was achieved using one specific monomer and exhibiting unusual low dispersity (near 1) for polymers produced by a step-growth process (typical dispersity of 2). Although the base is used in equimolar ratio and is not commercially available, the authors claimed that it can be quantitatively recovered without chromatographic separation.

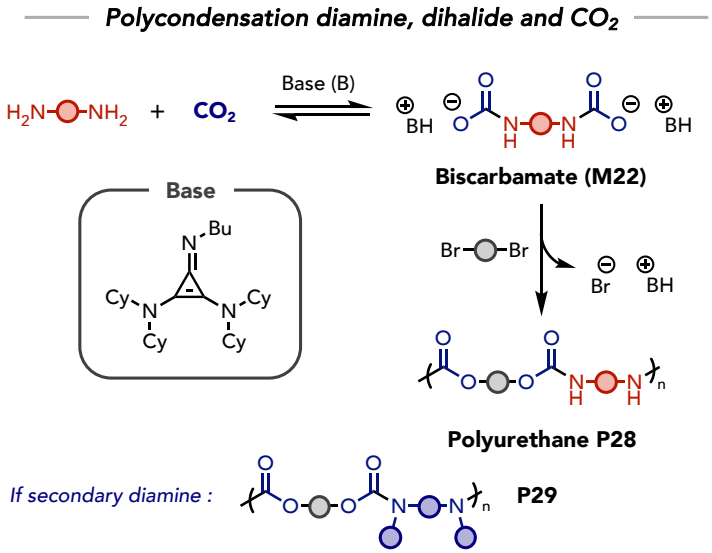

Scheme 23 – Polycondensation of diamines, dihalides and CO_2 into NIPUs **P28** and **P29** with an intermediate in-situ generated biscarbamates adduct **M22**.

6. NIPUs by ROP of cyclic carbamate

Ring-opening polymerization (ROP) offers several advantages over step-growth polymerization strategies commonly used for NIPUs synthesis: the ability to reach high molecular weight even at incomplete conversion, a control over the molecular weight, the possibility to reach low dispersities and a control over the polymer architecture (e.g. blocks, star-shaped polymers). However, due to the stability of the cyclic carbamates, their ROP is challenging, rendering this polymerization approach much less developed. Examples remain

scarce and the polymerizations are generally carried out at elevated temperatures (70 °C or higher)[117,118].

In 2019, two authors proposed the anionic ROP of five-membered cyclic carbamates at low temperature (0 °C to r.T). Zhang reported that ROP was only feasible on bicyclic oxazolidone fused to a six-membered ring **M23**, certainly due to the higher ring strain provided to the five-membered carbamate[119] (**Scheme 24**). The challenging ring-opening of the stable cyclic carbamate monomer **M23** was addressed by the introduction of a more electrophilic co-initiator bearing an electron-withdrawing acyl group on the carbamate. Activated by a strong base, e.g. BuLi, the nucleophilic nitrogen in the carbamate of **M23** can thereby attack the co-initiator. Following proton transfer, a new acyclic carbamate bond is created. The growing chain is therefore constituted of carbamate linkages with a cyclic carbamate chain-end, whose electrophilicity is activated by the acylurethane group, acting as new growing centers. Only low molar mass NIPUs were obtained (M_n = 7500 g·mol^{-1}) with a rather low dispersity (1.3) after polymerization in THF at 0 °C for 24 h. The effect of temperature remained unexplored by the authors. The resulting polyurethane was characterized by a high T_g of 150 °C.

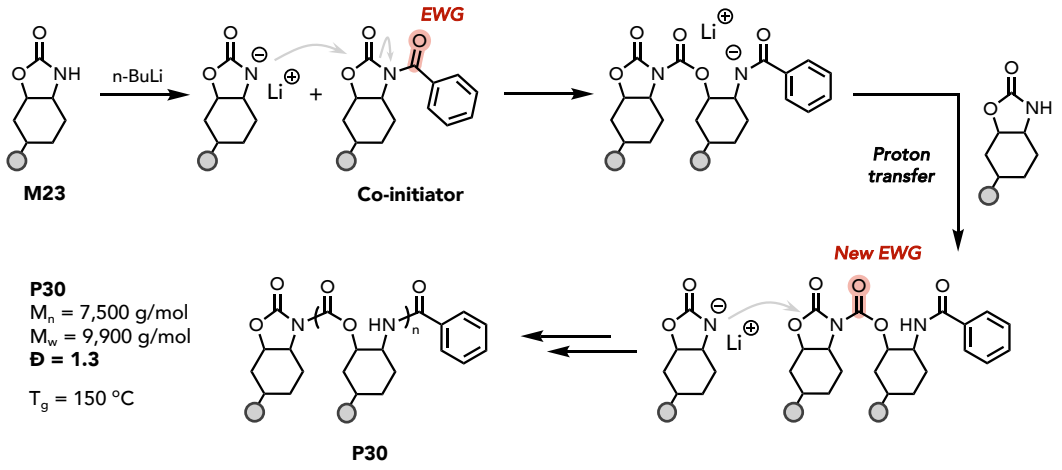

Scheme 24 – Synthesis of NIPU **P30** by ROP of cyclic carbamate monomer **M23**.

Haba proposed the polymerization of a similar monomer derived from sugar containing a fused 6-membered ring[120]. The monomer was polymerized in DMF at 0 °C in the presence of t-BuOK, conditions in which a M_n of 7,800 g·mol^{-1} was reached. Performing the reaction at r.T has led to a decrease in molecular weight (3,400 g·mol^{-1}) though this deviation was not rationalized.

7. Hybrid NIPUs

The difficulty to find efficient non-isocyanate ambient-curing systems prompted researchers to investigate hybrid NIPUs, where other well-established chemistries are involved and can promote efficient r.T polymerization.

7.1. UV-curable (meth)acrylate resins

PUs (meth)acrylate resins are widely used as they combine the desirable features of PUs and the advantages of acrylate-derived resins. Polyacrylates typically show superior optical properties, resistance to breakage, and high chemical resistance. Of high interest, the rapid free radical polymerization under UV allows for fast curing at r.T, rendering this technique environmentally friendly and energy efficient. They are therefore typically used in medical devices and dental health, coatings, adhesives, and 3D printing. A typical formulation contains monomers and/or oligomers, reactive diluents to reduce resin viscosity, a photoinitiator, and additives.

Given these advantages, research has focused on developing NIPU acrylate resins by the synthesis of acrylate precursors from existing urethane or oligo-urethanes.

Schimpf and Buchheit evaluated the aminolysis of glycerol carbonate methacrylate (GCMA) to provide hydroxyurethane linkages[121,122]. This synthon was easily produced from CO_2 fixation onto glycidyl methacrylate. The reaction of GCMA with amines left some **5CC** unreacted due to undesired aza-Michael addition of the amine onto the methacrylate function. By adding a small excess of GCMA, primarily hydroxyurethane methacrylates (**HUMA**, **M24**) derivatives were formed while minimizing the competitive side reaction (**Scheme 25A**). The structure of the precursor was easily tuned through a large choice of commercial polyamines. 4-acryloylmorpholine (ACMO) was added as reactive diluent in the formulation (ratio ACMO:precusor of 60:40). A wide diversity of polymers **P31** was obtained after UV curing for 2 x 10 min or 3D printing, with tunable thermal and mechanical properties (**Scheme 25B**). More flexible diamines provided polymers with T_g as low as 78 °C and the value was increased to 120 °C with more rigid diamines. As the **5CC** aminolysis provides hydroxyurethane **1**, the pendent hydroxyl groups were exploited for further functionalization, i.e. for introducing additional methacrylate moieties (**UMA**, **M25**). This allows for a more than 2-fold decrease in viscosity compared to **M24** by suppressing strong H-bonds. By the addition of more methacrylate units, a polymer with a T_g as high as 218 °C was produced.

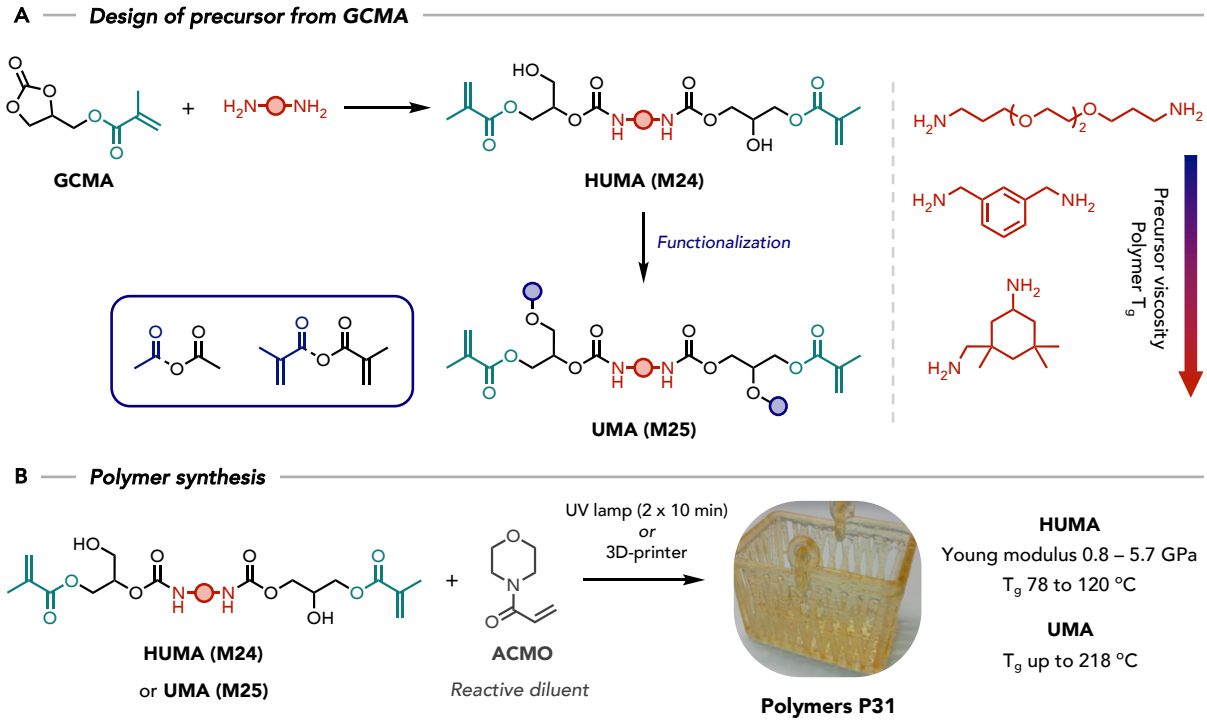

Scheme 25 – (A) Design of methacrylated precursors **M24-25**. (B) Polymerization of **M24-25** by UV curing in the presence of a reactive diluent into **P31**.

Meyer's team proposed the synthesis of **UMA** from widely available simple **5CC** (ethylene carbonate or propylene carbonate)[123–125]. By the reaction of **5CC** with a diamine, a bis(hydroxyurethane) **HU** was obtained. The two hydroxyl groups were then methacrylated into **UMA M26** (**Scheme 26A**). Interestingly, they also reported the synthesis of a mono-functional **UMA** (**mUMA**), which has shown very low viscosity and was therefore used in the formulation as reactive diluent (**Scheme 26B**). By using different ratios of **M26** and **mUMA**, and through the use of different diamine spacers, the polymer properties were tuned, with T_gs ranging from -11 to 100 °C. The high reactivity of these species made them ideal candidates for 3D printing. It was noticed that the structure of **5CC** and the diamine were important for the successful photocrosslinking reaction. For instance, when a simple aliphatic diamine such as 1,6-hexanediamine was used with ethylene carbonate as precursors, strong packing of the chains by H-bonding hindered diffusion and led to fast vitrification before the end of the reaction. This was solved by introducing branching using propylene carbonate as **5CC** or branched aliphatic diamines, or by the use of more flexible ether-containing diamines, providing full double bond conversion in 30 seconds. Carmenini recently proposed a similar strategy by using an itaconic acid-derived methacrylate for reaching high biobased content (up to 90 wt%) in the resin[126].

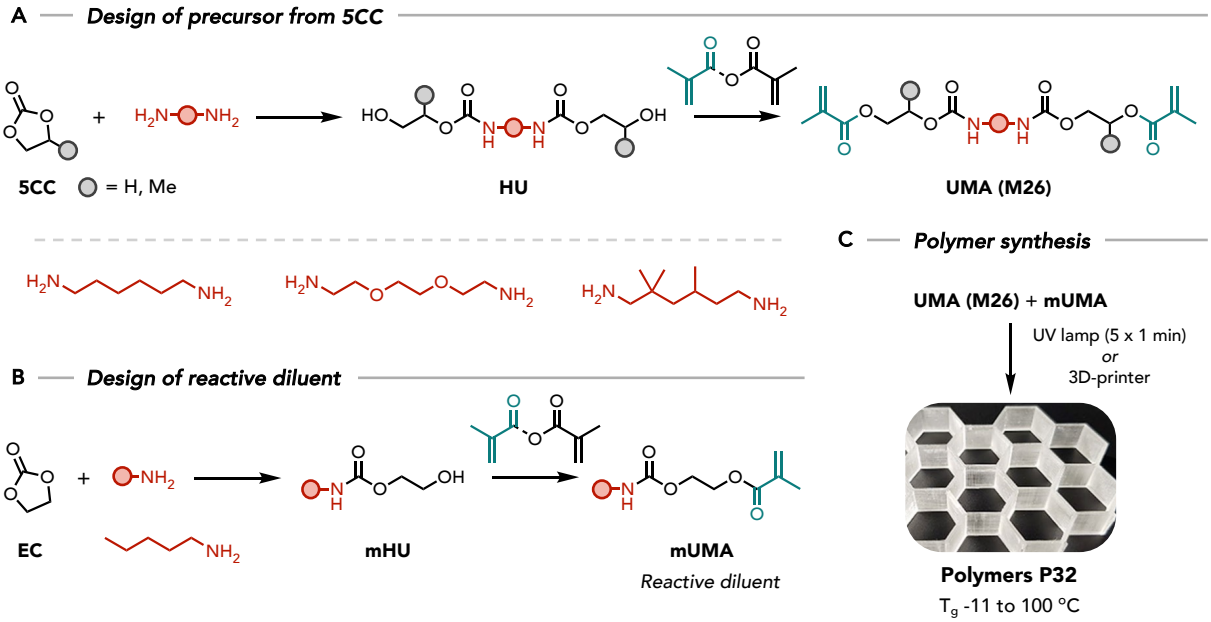

Scheme 26 – (A) Design of methacrylated precursors **M26**. (B) Design of a reactive diluent **mUMA**. (C) Polymerization of **M26** by UV curing in the presence of a reactive diluent (**mUMA**).

Ultimately, Zareanshahraki reported the synthesis of methacrylamide precursors by amidation of amine-terminated oligo-PHUs[127,128] to obtain methacrylamide-terminated PHU (**PHUMA**, **M27**) (**Scheme 27A**). Bi- and tri-functional monomers were added to **M27** and the resins were used for coating applications (**Scheme 27B**).

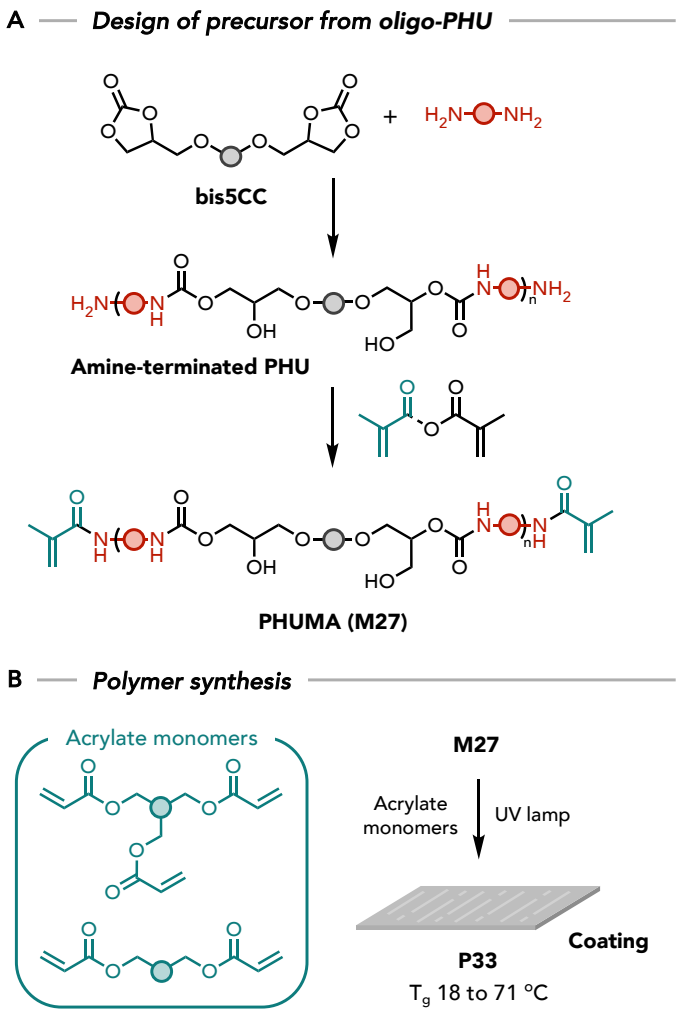

Scheme 27 – (A) Design of methacrylamide end-functionalized PHU precursors **M27**. (B) Polymerization of **M27** by UV curing in the presence of polyfunctional acrylate monomers.

7.2. Thiol-ene reaction

The thiol-ene reaction is part of the “click” reactions family, meaning the reaction is generally fast and efficient, is not sensitive to water nor oxygen, and works in mild conditions to give the desired product in high yield[129]. An advantage of this chemistry is the ability of photo-initiation of the reaction, giving a spatio-temporal control on the reactivity, notably to make polymeric materials. The material often presents high uniformity, and is well-defined, in contrast to materials made from acrylate-derived curing. The thiol-ene therefore represents a method of choice for making NIPU materials at r.T.

7.2.1. Linear polymers by thiol-ene

In 2014, Calle aimed at the synthesis of a AB thiol-alkene monomer **M28** embedding a carbamate function (**Scheme 28A**)[130]. This was achieved by reaction of cysteamine with allyl chloroformate. The reaction was scaled up to > 60 g of monomer in high yield (> 80 %). **M28** was polymerized in bulk under UV in the presence of a photoinitiator at r.T. After few minutes of reaction, the liquid monomer vitrified and turned into a solid, with 98 % of alkene conversion after 5 minutes. The polymer **P34** was characterized by a M_n of 14,300 g·mol^{-1} (M_w = 25,500 g·mol^{-1}), a T_g of -4 °C, and a T_m of 105 °C. This underlines the exceptional reaction rate of the thiol-ene reaction.

Recently, Xie leveraged the reversible capture of CO_2 by diamines in the presence of an organic base (TMG) to form carbamate adducts in a similar manner than the work of Wu (see **Scheme 23**, *vide infra*). These species reacted in one-pot with bromo-alkene derivatives to yield dienes monomers **M29** containing two urethane moieties in moderate yields (around 50 %) (**Scheme 28B**). **M29** was combined with dithiols to carry out UV-mediated thiol-ene reaction, furnishing poly(urethane-*co*-thioether)s **P35** of M_n up to 10,800 g·mol^{-1} (M_w 25,000 g·mol^{-1}) after 4-24 h of reaction in THF[131]. The properties of the polymers were varied through the choice of the diamine, the length of the bromoalkene, and the length of the aliphatic dithiol. Most of the polymers were semi-crystalline with a T_g varying between -30 and 0 °C, and a T_m between 100 and 130 °C.

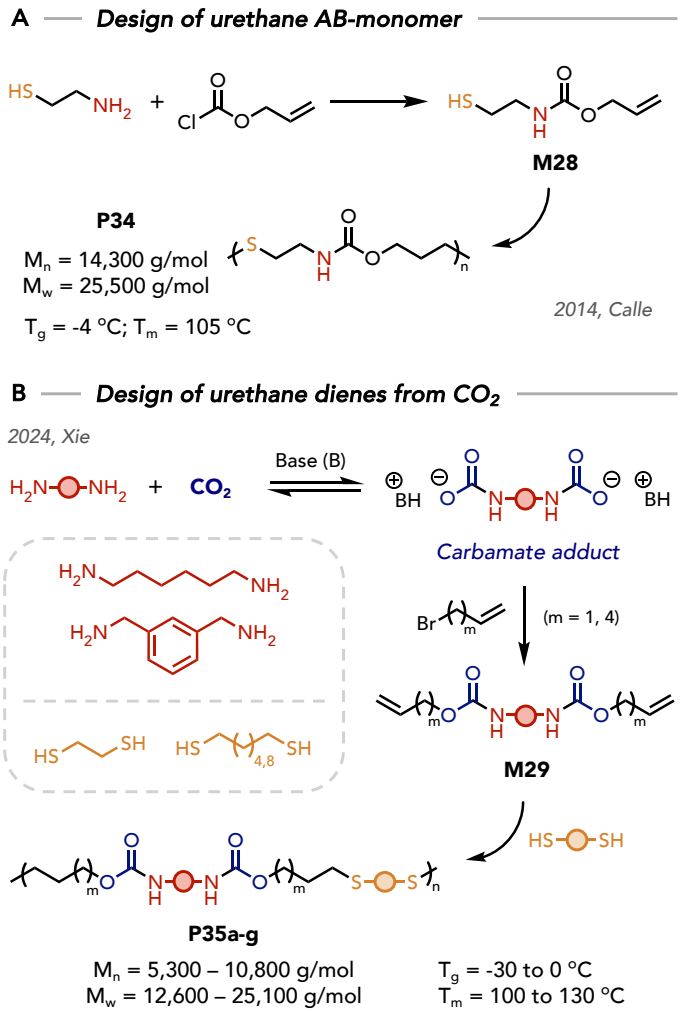

Scheme 28 – (A) Design of AB-monomer **M28** for NIPU thiol-ene polymerization into **P34**. (B) Design of dienes **M29** from the condensation of carbamate adducts with allyl halides. The thiol-ene polymerization with different dithiols provides polymers **P35**.

Other dienes were synthesized by Scheelje from limonene-based terpenes and carvone (**Scheme 29**)[132]. To introduce the urethane function within the monomers, the compounds were first epoxidized, then carbonated and finally, reacted with allylamine derivatives to target ene-terminated monomers **M30**. The dienes were used as monomers for the thiol-ene reaction at r.T in solvent (2-Me-THF) for 24 h in conjugation with different dithiols, providing a library of 9 polymers **P36** with molar masses up to M_n 31,200 g·mol^{-1} and M_w 56,200 g·mol^{-1}. The T_g for these materials was ranging from 0 to 30 °C.

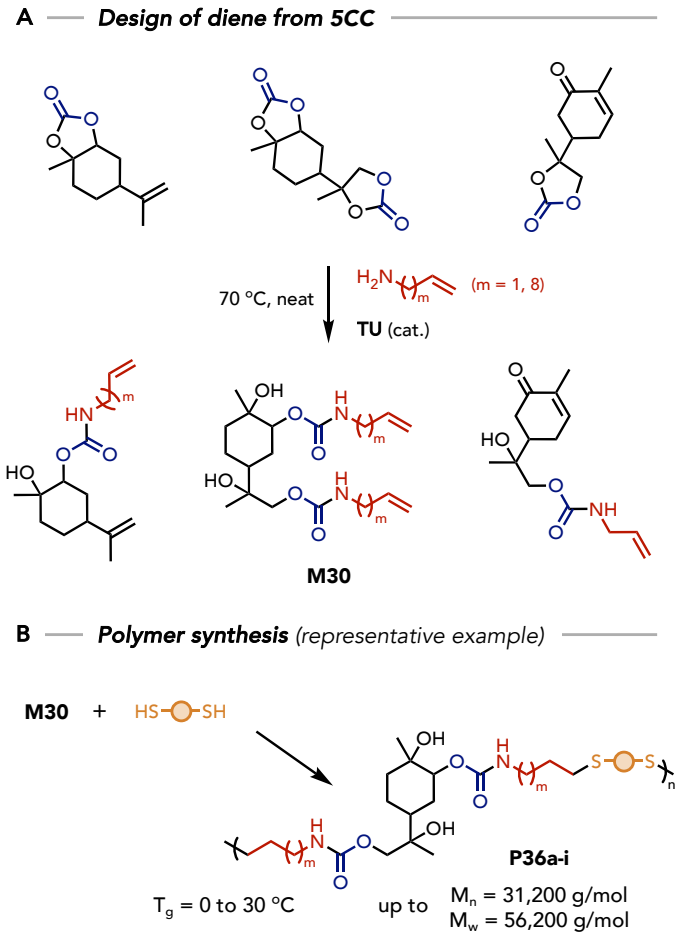

Scheme 29 – (A) Design of dienes **M30** by ring-opening aminolysis of **5CC**. (B) Polymerization with dithiols to yield **P36**.

7.2.2. Cross-linked polymers by thiol-ene

The UV-initiated thiol-ene has also been adopted in cross-linked NIPUs synthesis. Several strategies were here again proposed to produce ene-terminated precursors containing urethane bonds.

In two separate works, trimethylolpropane monoallyl ether cyclic carbonate (**6CC-allyl**) was used as a **6CC** precursor containing a reactive allyl group (**Scheme 30A**). Urethane bonds were introduced by reacting **6CC-allyl** with di-[133] or tri-[134] amines to provide di- or tri-functional linkers respectively. The ring-opening of these **6CC** by amines proceeds without catalyst at 60 °C to yield the ene monomers **M31** (**Scheme 30A**). In the first work by Hua, the trifunctional monomer was mixed with a dithiol and subjected to UV light to yield the network. The double bond conversion attained 90 % after few minutes, and was increased after longer illumination (95 % after 20 min). The polymer containing tertiary amines and the installed thioether bonds were further functionalized by quaternization of the amine and methylation of the thioether to

impart antibacterial activity to the material. In the second contribution by Warner, the bifunctional linker was cross-linked with mixtures of di-, tri-, and tetra-thiols to provide a set of polymers (**Scheme 30B**). FTIR indicated complete alkene consumption after 5 min of irradiation. All polymers were characterized by similar T_gs around 0 °C. However, the thiol functionality imparted the networks with very different mechanical properties, notably the Young's modulus which varied from 500 to 2,500 MPa. As a proof-of-concept, a spatially patterned material was 3D-printed through control of the polythiol composition in the resin. Additionally, the material displayed biocompatibility.

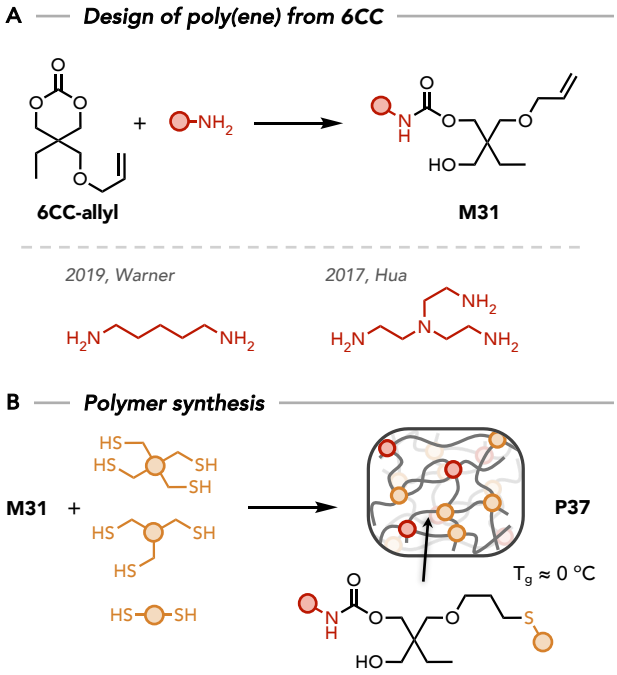

Scheme 30 – (A) Di- or tri-ene synthesis from **6CC-allyl** and di- or tri-amines respectively. (B) Polymer **P37** synthesis by thiol-ene of **M31** with di, tri-, and tetra-thiols.

Pierrard reported the synthesis of NIPUs networks by thiol-ene starting from bis**5CC** synthons following two distinct approaches. In the first one, oligomeric PPG-derived **5CC** was reacted with allylamine in the presence of DBU at 40 °C for 4 days[135] (**Scheme 31A**). The resin was formulated by adding a trithiol and a photoinitiator to the diene monomer **M32**. Networks **P38** were produced upon UV irradiation at r.T for 15 min (**Scheme 31B**). A gel time of 4 min was determined by rheology and the T_g was -23 or -5 °C depending on the length of PPG chain within the monomer. The fast reaction and the low viscosity of the formulation allowed for 3D-printing of the polymer.

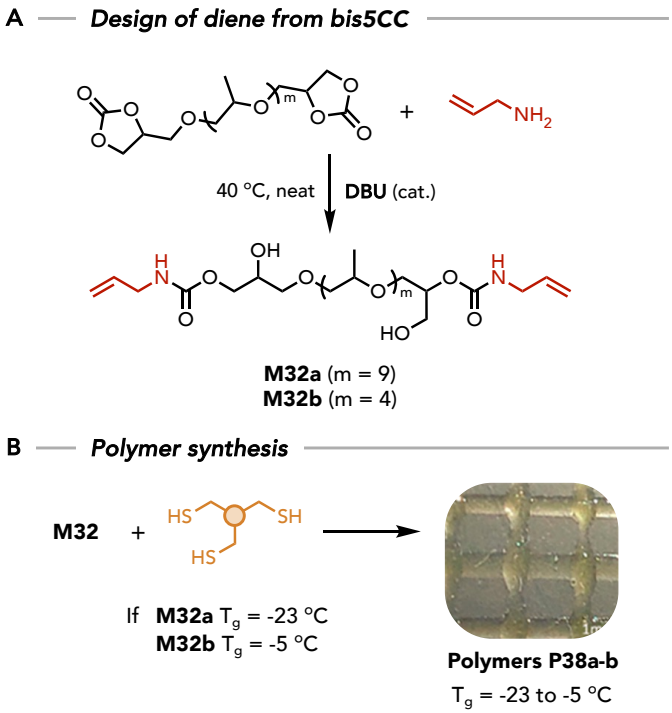

Scheme 31 – (A) Synthesis of dienes **M32** from aminolysis of PPG-derived bis**5CC** (of different lengths) by allylamine. (B) Polymers **P38** synthesis by thiol-ene with a trithiol.

In a second work, the same PPG-derived bis**5CC** was used to make a PHU polymer by reaction with a rigid diamine (MBCHA) at 70 °C for 4 days in bulk (**Scheme 32A**). The polymer was characterized by a moderate molar mass (M_n = 7200 g·mol^{-1}; M_w = 16,100 g·mol^{-1}). Allyl groups were introduced by the addition of a CO_2-derived allyl-containing **αCC** synthon, reactive to alcohols moieties in the presence of an organocatalyst[136]. The dissolved polymer in DMF was mixed with allyl-**αCC** (equimolar ratio *vs* hydroxyl groups) and DBU (10 mol%) at r.T for 24 h. The PHU was entirely functionalized with pendent carbonate functions terminated by a reactive alkene (**Scheme 32A**). This polyfunctional ene **M33** was then mixed with a photoinitiator and a poly(thiol) (di-, tri-, or tetra-functional), and irradiated under UV for 15 min to yield **P39** at r.T (**Scheme 32B**). Very low gel times of 6 to 8 seconds were determined by rheology whatever the thiol functionality. The network T_g was influenced by the thiol functionality, with values of 8, 25 and 42 °C with the di-, tri-, and tetra-thiol, respectively. The mechanical properties were also drastically impacted by the thiol functionality, with the Young's modulus ranging from 2.4 to 16.0 MPa. The elongation at break was also decreased with increased cross-linking density. By adjusting the viscosity with a high boiling point solvent (NMP), 3D printing was successfully achieved. The purified materials proved to be bio- and hemo-compatible, therefore being promising candidates for specialized medical devices.

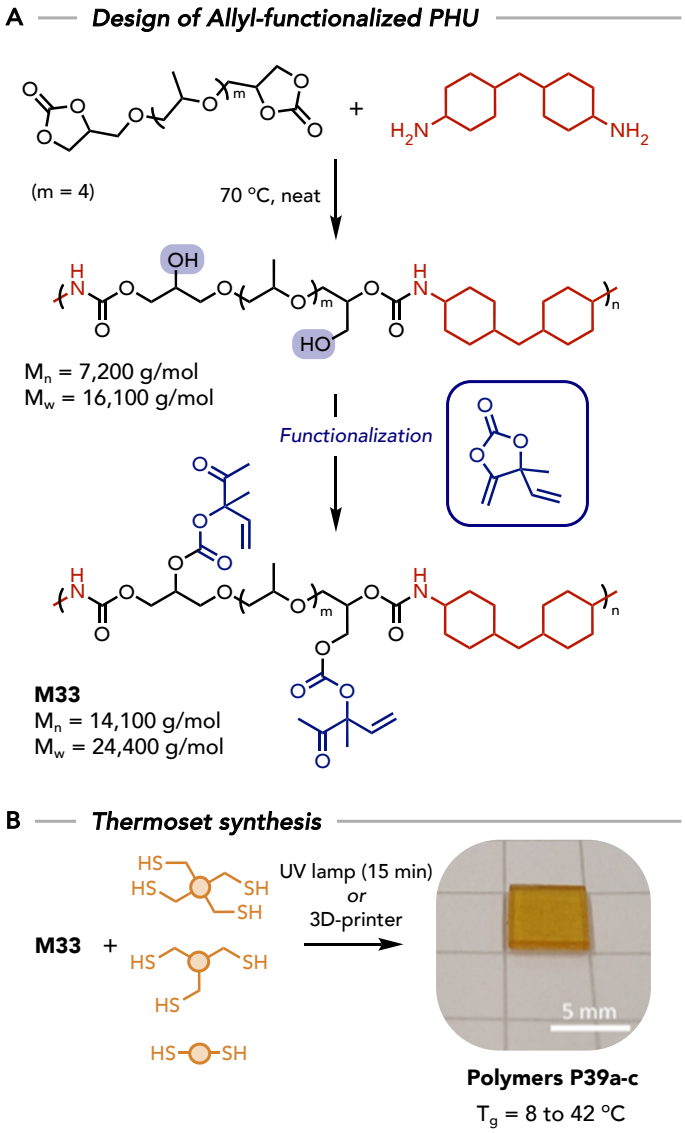

Scheme 32 – (A) Synthesis of a PHU polymer and functionalization using allyl-**αCC** into **M33**. (B) Resin photo-curing using **M33** and polyfunctional thiols into **P39**.

7.3. Epoxide – amine reaction

The reaction between epoxides and amines is a well-known process occurring at r.T, leading to the formation of amino-alcohols **7** (**Scheme 33**). Formulations of polyfunctional reactants have led to the development of epoxy resins, largely used in industrial and consumer contexts for their excellent properties: robust mechanical properties, excellent substrate adhesion, and chemical resistance[137]. They find applications in coatings and paints, adhesives, composite materials, or electronics. This chemistry is therefore of high interest for the development of hybrid NIPU thermoset materials, and has been especially developed in the field of PHUs as the polyamine can react with both cyclic carbonates and epoxy groups. The curing process is

therefore accelerated, and cross-link density can be increased due to the double reactivity of the amine as illustrated in **Scheme 33** (primary then secondary which is also reactive with epoxides). Two approaches were reported to produce hydrid NIPU materials. In the first one, amine-terminated pre-polymers containing urethane linkages are reacted with epoxides to build the network as a mimic of the polyamine hardener used in epoxy resin formulations. In the second, the curing is performed directly from all precursors in one pot by mixing the poly**5CC**, the polyamine, and the polyepoxide.

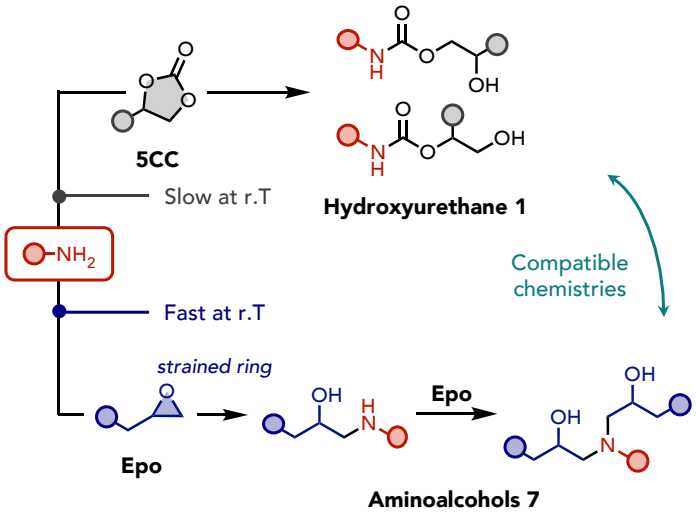

Scheme 33 – Slow aminolysis of **5CC** to yield hydroxyurethane **1**, and fast aminolysis of epoxide to yield amino-alcohols derivatives **7**. Both chemistries are compatible and can be carried out simultaneously.

7.3.1. Pre-polymer approach

Asemani reported the synthesis of amine-terminated PHU prepolymers by the reaction of an excess of diamine with a bis**5CC**. Both the structure of bis**5CC** and diamine were varied. The pre-polymers were then mixed with the polyepoxide, a catalyst (organobase) and other additives typically used in coatings (surface additive, defoamer, solvent for adjusting viscosity)[138] (**Scheme 34**). The coatings were cured for 7 days at r.T, but experienced tack-free between 4 and 12 h depending on the formulation. The properties were as performant as isocyanate-based PUs references found in the market, and the properties were overall largely varied upon selection of the prepolymer structure and epoxy curing agent.

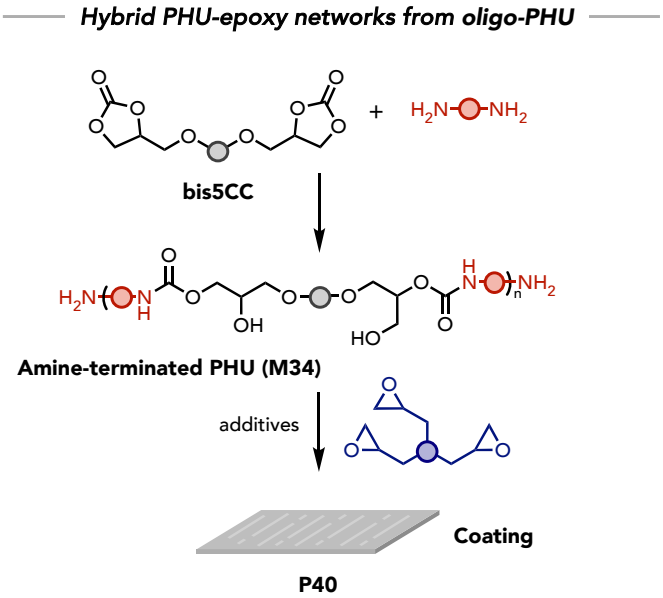

Scheme 34 – Synthesis of amine-terminated PHU (**M34**) and polymerization with polyepoxides into polymeric coatings **P40**.

In a second work, Genteno-Pedrazo synthesized amino-terminated PHUs prepolymers from carbonated soybean oil. The prepared polyamines were then reacted with bisepoxides in the presence of MEK as solvent to adjust the formulation viscosity[139]. The resin was cured at r.T and characterized after 28 days, time at which the hardness value of the coating reached a plateau. The coatings were however tack-free in less than 24 h. The authors evidenced that coating properties readily improve with this hybrid chemistry compared to pure PHUs formulations, with a considerable increased hardness.

7.3.2. One-step approach

Figovsky proposed the use of partially carbonated polyepoxides to have both cyclic carbonate and epoxy units on the same substrate[140]. The formulation was containing the partially carbonated poly**5CC**, commercial bisepoxides, and diamine hardeners. The curing of the formulation was achieved at r.T for 7 days. It must be noted that although the polymer contained urethane linkages, the authors used the carbonated **5CC** as modifier of epoxy resin formulation and the content in partially carbonated substrate was as low as 5 to 10%. However, they compared the properties to **5CC**-free formulation and demonstrated that the introduction of hydroxyurethane linkages were responsible for improved adhesion performance and higher strength of the polymer.

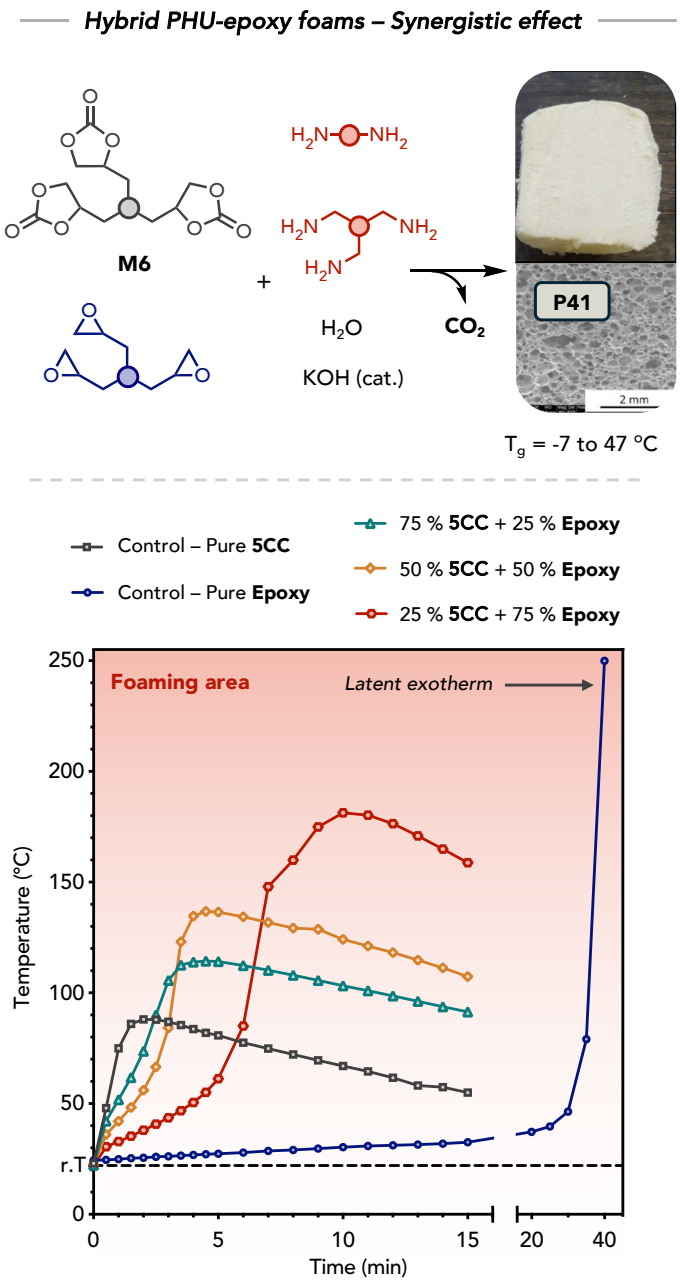

Figure 9 – Preparation of hybrid NIPU foams through the synergistic reaction of trifunctional **5CC** (**M6**) and a trifunctional epoxide with polyamines to provide exotherms. The hydrolysis of **5CC** by water releases CO_2 as blowing agent.

Bourguignon recently reported a methodology for producing self-blown hybrid PHU foams in a matter of minutes from formulations at r.T[12]. Previous works reported foaming in around 30 minutes at 100 °C from formulations composed of a trifunctional **5CC** (**M6**), a polyamine, water as a chemical foaming agent, KOH as catalyst, and a filler for foam homogeneity[58]. The addition of a trifunctional epoxide in the formulation promoted an exotherm needed to reach

the foaming temperature (starting at around 100 °C) when the formulations were prepared at r.T (**Figure 9**). Through control experiments, it was observed that the aminolysis and hydrolysis of **5CC** were exothermic processes, though at a too low extent for the foaming to occur. The epoxy-amine was however highly exothermic when the reaction medium reached about 50 °C. Cascade exotherms, initiated by the **5CC** aminolysis and hydrolysis, thus initiated the epoxy amine reaction, rapidly increasing the formulation temperature well beyond the foaming area. Using this strategy, the maximum foam expansion was reached in less than 1 minute after foaming initiation. The introduction of low amount of epoxide had only small effects on the final material properties. However, at higher content, both T_gs and thermal degradation temperature were increased. The compression modulus was drastically affected and readily increased with epoxide content, as expected from the more densely cross-linked structure. Modulation of the nature and functionality of both the epoxide and amine enabled to tune the mechanical properties of the foams. Foams of high bio-based content (90wt%) were also produced by selecting bio-based monomers. This concept might be applied to other materials to achieve fast curing. However, typical applications in the PU market such as adhesive and coatings couldn't benefit from this approach as they rely on application of thin films of formulation on substrates, allowing for high energy dissipation. In the context of NIPUs foams, other exothermic reactions that are compatible with the PHU chemistry might be great candidates for producing new hybrid PHU foams of diverse properties.

7.4. Epoxide – thiol reaction

The epoxy-thiol reaction, analog to the epoxy-amine reaction, is recognized as part of the "click reactions", typically high-yielding and fast in mild conditions leading to the formation of β-hydroxythioethers **8** (**Scheme 35A**). It is generally catalyzed by a base that deprotonates the thiol into a nucleophilic thiolate. This reaction has so far been applied to many applications, in the biological and pharmaceutical fields to the development of adhesives, coatings and composites[129].

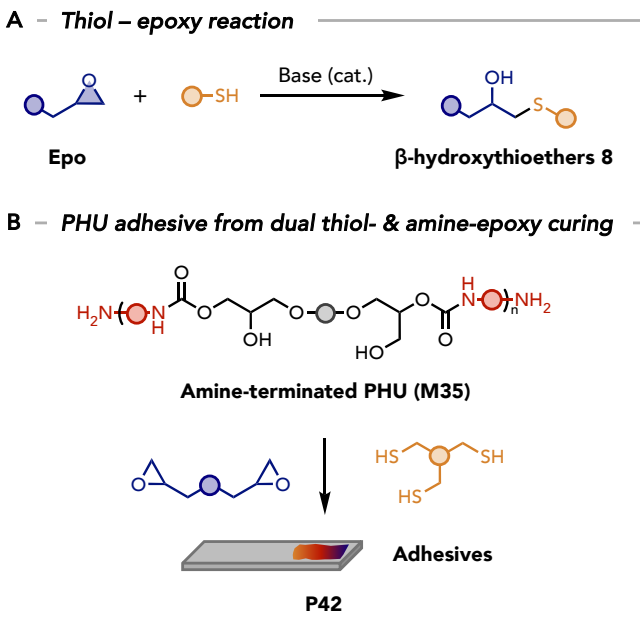

Scheme 35 – (A) Base-catalyzed reaction of thiol with epoxides (Epo) to yield β-hydroxythioethers **8**. (B) PHU adhesive **P42** from an amine-terminated PHU (**M35**) reacting with a bisepoxide and a trithiol.

This reaction was recently applied by Gomez-Lopez for the production of ambient-curable PHU adhesives[141]. Following a process similar to the epoxy-amine curing of PHU (**Scheme 34**), an amine-terminated PHU pre-polymer **M35** was first synthesized and was combined to a commercial bisepoxide and a trithiol (**Scheme 35B**). While the gel time exceeded 2 h in all cases and was not precisely determined by the authors, it was demonstrated that the addition of trithiol to the formation readily accelerated the increase in shear modulus. Interestingly, the curing occurred in the absence of an organobase catalyst, certainly because the amine monomers may act as base catalysts. IR analysis confirmed complete reaction in 24 h. The adhesive performances have shown to significantly improve from a pure amine-epoxy system to the dual amine-thiol-epoxy cure (leap-shear strength increasing from 7.6 to 12.8 MPa).

7.5. Chemistry of silanes and alkoxy silanes

7.5.1. Silane-amine reaction

Cornille reported the preparation of NIPU foams at r.T by leveraging the chemistry of silanes toward amines[142] (**Scheme 36A**). The formulations were based on a mixture of di- and tri-functional **5CC**, a diamine, and a polysiloxane chain containing reactive silane groups (**Scheme 36B**). The presence of a thiourea catalyst was also required for efficient cross-

linking. Upon PHU matrix formation, the amines reacted with the silane groups, aiding in the cross-linking of the material, and concomitantly releasing dihydrogen (H_2) that created pores within the network, thus forming PHU foams. The T_g of the foams ranged between 0 and 10 °C, and IR analyses showed consumption of the **5CC** and silane bonds after three days.

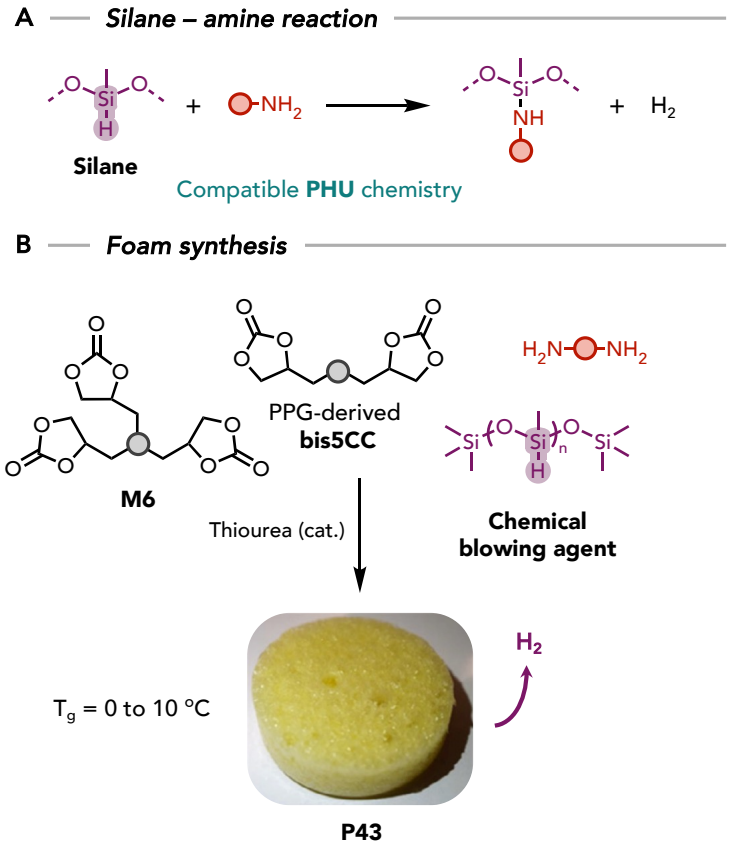

Scheme 36 – (A) Silane-amine chemistry releasing hydrogen gas. (B) Synthesis of foams **P43** using silanes as chemical blowing agent, releasing dihydrogen (H_2) gas in the polymer matrix.

7.5.2. Humidity-induced alkoxysilane cross-linking

Alkoxysilane are well-established cross-linkers, forming strong siloxane bonds after condensation of silanol, himself produced by hydrolysis of alkoxysilane. Chemical bonds can also be formed with the surface of various substrates, which makes these cross-linkers excellent candidates for coating and adhesive applications.

Gomez-Lopez reported the formation of **5CC**-terminated PHU pre-polymers by reaction of an excess of bis**5CC** with a diamine. The prepolymer was then functionalized with an amine bearing a triethoxysilane functional group (**Scheme 37**). Upon addition of a catalyst (acetic

acid), the material cured at r.T and provided adhesives **P44**, with a gel time of 5 h[143]. The process yielded better results at 100 °C, though the authors demonstrated that curing was possible at r.T.

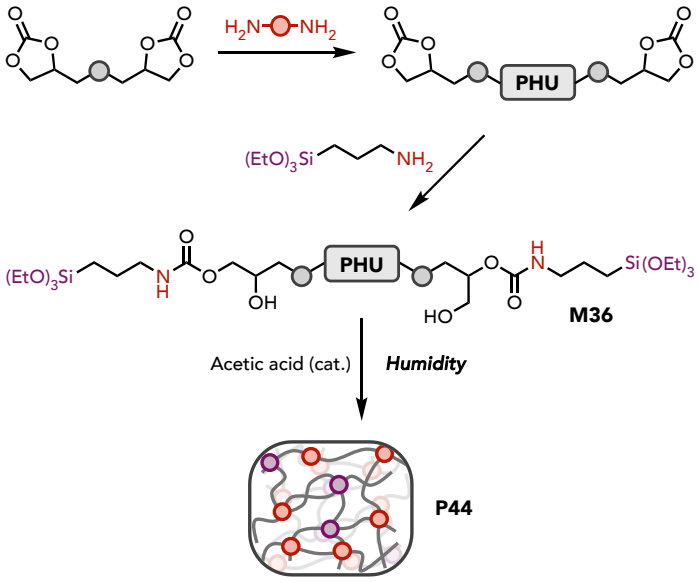

Scheme 37 – Synthesis of triethoxysilane-functionalized PHUs (**M36**) and their polymerization driven by humidity in the presence of acetic acid as catalyst.

Asemani recently reported a dual cure system based on the reaction of amine-terminated PHU prepolymers with both polyepoxides and epoxides bearing a triethoxysilane functional group[144]. This provided a dual curing system promoted by the epoxy-amine reaction and the moisture-driven polysiloxane formation. Curing was achieved at r.T for 7 days and the authors demonstrated that the dual cure process was faster than a simpler curing from polyepoxides only.

7.6. Michael addition

The Michael addition is a well-known robust reaction used in many contexts in organic synthesis (bioactive drugs, *β*-amino acids)[145] and polymer chemistry[146,147]. It consists in the reaction between a Michael acceptor, most often α,β-unsaturated carbonyl-containing groups (ester, ketone, amide, etc.) and a Michael donor such as amines. The reaction generally proceeds smoothly and quantitatively at r.T, rendering this reaction a good candidate to produce polymers in mild conditions.

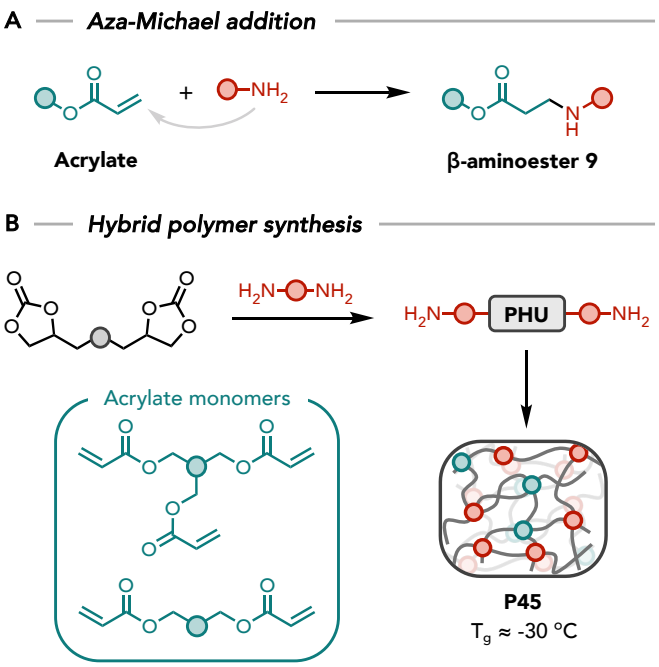

Scheme 38 – (A) The aza-Michael addition of amine onto acrylate moieties to form β-aminoesters **9**. (B) Synthesis of amine-terminated PHUs and their reaction with di- and tri-acrylate to provide hybrid polymers **P45**.

Cornille reported PHU formulations containing commercial polyacrylates, which can be attacked by amines through a Michael addition[148] (**Scheme 38A**). Amine-terminated pre-polymers were first synthesized by reaction of excess amine with a PPG-derived bis**5CC**. The telechelic polymers were then reacted with di- and tri-acrylates without catalyst nor solvent, providing full acrylate conversion after 48 h (**Scheme 38B**). The materials **P45** presented low T_g values of around -30 °C, certainly due to the very flexible nature of the PPG-derived precursors and of the created *β*-amino ester linkages. The cross-linking efficiency was validated by gel contents higher than 90 %.

The integration of hybrid chemistries in the development of NIPUs offers a compelling solution to the inherent room-temperature reactivity challenges encountered in promising technologies, particularly with the nowadays well-studied PHU chemistry from five-membered cyclic carbonate aminolysis. Efficient and well-established chemistries can be utilized, either on pre-synthesized urethane-containing synthons or along their formation to reach moderate to high molecular weight and efficient curing within desirable timeframes. Exploring synergistic reactions has demonstrated to be particularly valuable to expand the reactivity and applicability capabilities beyond simple combination of divergent chemical bonds. Moreover, incorporating additional functionalities can impart NIPUs with unique properties, such as chemical

resistance, improved adhesion, or the ability for rapid photo-curing in 3D-printed resins. There is still room for exploring and optimizing new processes to furnish hybrid NIPUs at r.T without relying on hazardous but yet efficient isocyanates for their production.

8. Conclusion

This review aimed at putting forward the developed technologies amenable to room temperature synthesis of NIPUs, of high interest in a climate where numerous regulations get implemented. These do not only serve to limit the wide usage of hazardous compounds but also to lower the energy footprint of many industrial processes. Developing NIPUs at room temperature is also economically favorable for finding large consumer applications and fitting into existing PU production facilities.

The most widely used approach is the reaction of five-membered cyclic carbonates and amines to furnish poly(hydroxyurethanes). This strategy has already been reported long time ago and is currently widely expanding with a multitude of applications, though the synthesis of scaffolds at r.T is very challenging compared to isocyanate-based PUs. The low reactivity of **5CC** has led to vast research to unlock boosted reactivity. Most common strategies are monomers design, catalysis, and solvent effect. There is however room for fundamental studies to understand and overcome remaining limitations, as well as to new promising applications for these polymers. Using larger rings (from six- to height-membered cyclic carbonates) readily increased the reactivity of the cyclic carbonates toward aminolysis, at the cost of being more prone to undesired side reactions. Moreover, these large rings are more challenging to prepare at large scale from readily available, cheap and non-toxic reagents.

α-alkylidene cyclic carbonates emerged as highly appealing building blocks for producing NIPUs at r.T, their strained structure allowing for fast, quantitative reactions without noticeable side reactions. This technology remains vastly unstudied and many avenues are still opened for researchers to better understand this chemistry and find applications to the so-produced polymers.

Polycondensation techniques at r.T are limited to a very limited amount of examples using and releasing toxic compounds. The atom efficiency of the process is also very poor. These reasons certainly explain why this approach is barely described in the literature.

Ring-opening polymerizations techniques are of high interest for their atom economy, possibility to reach very high molecular weights, and for the ability to control the polymer architecture. However, this method is scarcely described even at higher temperature due to the challenging ring-opening of stable cyclic carbamates, which so far only furnished low molecular weight polymers.

Finally, hybrid NIPUs have been more widely reported at r.T as they are generally founded on efficient and tolerable chemistries that are well-established to operate at r.T. It is interesting to note that many publications targeted specific applications for which the polymers properties were tuned through the choice of the optimal chemistry. Synergistic effects were also reported and must be sought as novel strategies toward isocyanate-based PU competitive materials such as fast and ambient-curable NIPUs foams, coatings and adhesives.

Importantly, most developed chemistries to achieve room temperature NIPU syntheses are not only profitable for finding isocyanate-based alternatives, but also afford new polymeric structures never studied in the past that are not accessible by conventional routes. This means that all the novel polymers developed in the last decades might be amenable to specific applications in which they would excel.

References

(1) Holden, G. Thermoplastic Elastomers. In *Applied Plastics Engineering Handbook*; Elsevier, 2024; pp 97–113. https://doi.org/10.1016/B978-0-323-88667-3.00020-5.

(2) Peyrton, J.; Avérous, L. Structure-Properties Relationships of Cellular Materials from Biobased Polyurethane Foams. *Materials Science and Engineering: R: Reports* **2021**, *145*, 100608. https://doi.org/10.1016/j.mser.2021.100608.

(3) Monie, F.; Vidil, T.; Grignard, B.; Cramail, H.; Detrembleur, C. Self-Foaming Polymers: Opportunities for the next Generation of Personal Protective Equipment. *Materials Science and Engineering: R: Reports* **2021**, *145*, 100628. https://doi.org/10.1016/j.mser.2021.100628.

(4) Sonnenschein, M. F. *Polyurethanes: Science, Technology, Markets, and Trends*, 1st ed.; Wiley, 2014. https://doi.org/10.1002/9781118901274.

(5) Engels, H.; Pirkl, H.; Albers, R.; Albach, R. W.; Krause, J.; Hoffmann, A.; Casselmann, H.; Dormish, J. Polyurethanes: Versatile Materials and Sustainable Problem Solvers for Today's Challenges. *Angew Chem Int Ed* **2013**, *52* (36), 9422–9441. https://doi.org/10.1002/anie.201302766.

(6) Eling, B.; Tomović, Ž.; Schädler, V. Current and Future Trends in Polyurethanes: An Industrial Perspective. *Macro Chemistry & Physics* **2020**, *221* (14), 2000114. https://doi.org/10.1002/macp.202000114.

(7) Das, A.; Mahanwar, P. A Brief Discussion on Advances in Polyurethane Applications. *Advanced Industrial and Engineering Polymer Research* **2020**, *3* (3), 93–101. https://doi.org/10.1016/j.aiepr.2020.07.002.

(8) Anastas, P.; Eghbali, N. Green Chemistry: Principles and Practice. *Chem. Soc. Rev.* **2010**, *39* (1), 301–312. https://doi.org/10.1039/B918763B.

(9) Vidal, F.; Van Der Marel, E. R.; Kerr, R. W. F.; McElroy, C.; Schroeder, N.; Mitchell, C.; Rosetto, G.; Chen, T. T. D.; Bailey, R. M.; Hepburn, C.; Redgwell, C.; Williams, C. K. Designing a Circular Carbon and Plastics Economy for a Sustainable Future. *Nature* **2024**, *626* (7997), 45–57. https://doi.org/10.1038/s41586-023-06939-z.

(10) Brahmachari, G. Design of Organic Transformations at Ambient Conditions: Our Sincere Efforts to the Cause of Green Chemistry Practice. *The Chemical Record* **2016**, *16* (1), 98–123. https://doi.org/10.1002/tcr.201500229.

(11) Karpf, M. Organic Synthesis at High Temperatures. Gas-Phase Flow Thermolysis [New Synthetic Methods (57)]. *Angew. Chem. Int. Ed. Engl.* **1986**, *25* (5), 414–430. https://doi.org/10.1002/anie.198604141.

(12) Bourguignon, M.; Grignard, B.; Detrembleur, C. Cascade Exotherms for Rapidly Producing Hybrid Nonisocyanate Polyurethane Foams from Room Temperature Formulations. *J. Am. Chem. Soc.* **2024**, *146* (1), 988–1000. https://doi.org/10.1021/jacs.3c11637.

(13) Bürgel, T.; Fedtke, M. Reactions of Cyclic Carbonates with Amines: Model Studies for Curing Process. *Polymer Bulletin* **1991**, *27* (2), 171–177. https://doi.org/10.1007/BF00296027.

(14) Bürgel, T.; Fedtke, M. Epoxy Resins with Cyclic Carbonate Structures: Model Studies for Amine Curing. *Polymer Bulletin* **1993**, *30* (1), 61–68. https://doi.org/10.1007/BF00296235.

(15) Garipov, R. M.; Sysoev, V. A.; Mikheev, V. V.; Zagidullin, A. I.; Deberdeev, R. Ya.; Irzhak, V. I.; Berlin, Al. Al. Reactivity of Cyclocarbonate Groups in Modified Epoxy–Amine Compositions. *Doklady Physical Chemistry* **2003**, *393* (1–3), 289–292. https://doi.org/10.1023/B:DOPC.0000003463.07883.c9.

(16) Levina, M. A.; Krasheninnikov, V. G.; Zabalov, M. V.; Tiger, R. P. Nonisocyanate Polyurethanes from Amines and Cyclic Carbonates: Kinetics and Mechanism of a Model Reaction. *Polym. Sci. Ser. B* **2014**, *56* (2), 139–147. https://doi.org/10.1134/S1560090414020092.

(17) Cornille, A.; Blain, M.; Auvergne, R.; Andrioletti, B.; Boutevin, B.; Caillol, S. A Study of Cyclic Carbonate Aminolysis at Room Temperature: Effect of Cyclic Carbonate Structures and Solvents on Polyhydroxyurethane Synthesis. *Polym. Chem.* **2017**, *8* (3), 592–604. https://doi.org/10.1039/C6PY01854H.

(18) Zabalov, M. V.; Tiger, R. P.; Berlin, A. A. Reaction of Cyclocarbonates with Amines as an Alternative Route to Polyurethanes: A Quantum-Chemical Study of Reaction Mechanism. *Dokl Chem* **2011**, *441* (2), 355–360. https://doi.org/10.1134/S0012500811120032.

(19) Zabalov, M. V.; Tiger, R. P.; Berlin, A. A. Mechanism of Urethane Formation from Cyclocarbonates and Amines: A Quantum Chemical Study. *Russ Chem Bull* **2012**, *61* (3), 518–527. https://doi.org/10.1007/s11172-012-0076-8.

(20) Blain, M.; Cornille, A.; Boutevin, B.; Auvergne, R.; Benazet, D.; Andrioletti, B.; Caillol, S. Hydrogen Bonds Prevent Obtaining High Molar Mass PHU s. *J of Applied Polymer Sci* **2017**, *134* (45), 44958. https://doi.org/10.1002/app.44958.

(21) Besse, V.; Camara, F.; Méchin, F.; Fleury, E.; Caillol, S.; Pascault, J.-P.; Boutevin, B. How to Explain Low Molar Masses in PolyHydroxyUrethanes (PHUs). *European Polymer Journal* **2015**, *71*, 1–11. https://doi.org/10.1016/j.eurpolymj.2015.07.020.

(22) Lamarzelle, O.; Durand, P.-L.; Wirotius, A.-L.; Chollet, G.; Grau, E.; Cramail, H. Activated Lipidic Cyclic Carbonates for Non-Isocyanate Polyurethane Synthesis. *Polym. Chem.* **2016**, *7* (7), 1439–1451. https://doi.org/10.1039/C5PY01964H.

(23) Lamarzelle, O.; Hibert, G.; Lecommandoux, S.; Grau, E.; Cramail, H. A Thioglycerol Route to Bio-Based Bis-Cyclic Carbonates: Poly(Hydroxyurethane) Preparation and Post-

Functionalization. *Polym. Chem.* **2017**, *8* (22), 3438–3447. https://doi.org/10.1039/C7PY00556C.

(24) Bourguignon, M.; Grignard, B.; Detrembleur, C. Introducing Polyhydroxyurethane Hydrogels and Coatings for Formaldehyde Capture. *ACS Appl. Mater. Interfaces* **2021**, *13* (45), 54396–54408. https://doi.org/10.1021/acsami.1c16917.

(25) Tomita, H.; Sanda, F.; Endo, T. Model Reaction for the Synthesis of Polyhydroxyurethanes from Cyclic Carbonates with Amines: Substituent Effect on the Reactivity and Selectivity of Ring-opening Direction in the Reaction of Five-membered Cyclic Carbonates with Amine. *J. Polym. Sci. A Polym. Chem.* **2001**, *39* (21), 3678–3685. https://doi.org/10.1002/pola.10009.

(26) He, Y.; Goel, V.; Keul, H.; Möller, M. Synthesis, Characterization, and Selectivity of Bifunctional Couplers. *Macro Chemistry & Physics* **2010**, *211* (22), 2366–2381. https://doi.org/10.1002/macp.201000340.

(27) Levina, M. A.; Zabalov, M. V.; Krasheninnikov, V. G.; Tiger, R. P. Comparative Reactivity of Cyclocarbonate Groups of Oligomeric Triglycerides Based on Soybean Oil and Model Compounds in the Reactions of Nonisocyanate Urethane Formation. *Polym. Sci. Ser. B* **2018**, *60* (5), 563–570. https://doi.org/10.1134/S1560090418050081.

(28) Ruiz, L.; Aghmiz, A.; Masdeu-Bultó, A. M.; Lligadas, G.; Ronda, J. C.; Galià, M.; Cádiz, V. Upgrading Castor Oil: From Heptanal to Non-Isocyanate Poly(Amide-Hydroxyurethane)s. *Polymer* **2017**, *124*, 226–234. https://doi.org/10.1016/j.polymer.2017.07.070.

(29) Cornille, A.; Auvergne, R.; Figovsky, O.; Boutevin, B.; Caillol, S. A Perspective Approach to Sustainable Routes for Non-Isocyanate Polyurethanes. *European Polymer Journal* **2017**, *87*, 535–552. https://doi.org/10.1016/j.eurpolymj.2016.11.027.

(30) Bähr, M.; Bitto, A.; Mülhaupt, R. Cyclic Limonene Dicarbonate as a New Monomer for Non-Isocyanate Oligo- and Polyurethanes (NIPU) Based upon Terpenes. *Green Chem.* **2012**, *14* (5), 1447. https://doi.org/10.1039/c2gc35099h.

(31) Schimpf, V.; Ritter, B. S.; Weis, P.; Parison, K.; Mülhaupt, R. High Purity Limonene Dicarbonate as Versatile Building Block for Sustainable Non-Isocyanate Polyhydroxyurethane Thermosets and Thermoplastics. *Macromolecules* **2017**, *50* (3), 944–955. https://doi.org/10.1021/acs.macromol.6b02460.

(32) Scholten, P. B. V.; Demarteau, J.; Gennen, S.; De Winter, J.; Grignard, B.; Debuigne, A.; Meier, M. A. R.; Detrembleur, C. Merging CO_2-Based Building Blocks with Cobalt-Mediated Radical Polymerization for the Synthesis of Functional Poly(Vinyl Alcohol)s. *Macromolecules* **2018**, *51* (9), 3379–3393. https://doi.org/10.1021/acs.macromol.8b00492.

(33) Maltby, K. A.; Hutchby, M.; Plucinski, P.; Davidson, M. G.; Hintermair, U. Selective Catalytic Synthesis of 1,2- and 8,9-Cyclic Limonene Carbonates as Versatile Building Blocks

for Novel Hydroxyurethanes. *Chemistry A European J* **2020**, *26* (33), 7405–7415. https://doi.org/10.1002/chem.201905561.

(34) Maquilón, C.; Brandolese, A.; Alter, C.; Hövelmann, C. H.; Della Monica, F.; Kleij, A. W. Renewable Beta-Elemene Based Cyclic Carbonates for the Preparation of Oligo(Hydroxyurethane)s. *ChemSusChem* **2022**, *15* (17), e202201123. https://doi.org/10.1002/cssc.202201123.

(35) Ochiai, B.; Matsuki, M.; Miyagawa, T.; Nagai, D.; Endo, T. Kinetic and Computational Studies on Aminolysis of Bicyclic Carbonates Bearing Alicyclic Structure Giving Alicyclic Hydroxyurethanes. *Tetrahedron* **2005**, *61* (7), 1835–1838. https://doi.org/10.1016/j.tet.2004.12.014.

(36) Maisonneuve, L.; Lamarzelle, O.; Rix, E.; Grau, E.; Cramail, H. Isocyanate-Free Routes to Polyurethanes and Poly(Hydroxy Urethane)s. *Chem. Rev.* **2015**, *115* (22), 12407–12439. https://doi.org/10.1021/acs.chemrev.5b00355.

(37) Webster, D. C.; Crain, A. L. Synthesis and Applications of Cyclic Carbonate Functional Polymers in Thermosetting Coatings. *Progress in Organic Coatings* **2000**, *40* (1–4), 275–282. https://doi.org/10.1016/S0300-9440(00)00114-4.

(38) Diakoumakos, C. D.; Kotzev, D. L. Non-Isocyanate-Based Polyurethanes Derived upon the Reaction of Amines with Cyclocarbonate Resins. *Macromolecular Symposia* **2004**, *216* (1), 37–46. https://doi.org/10.1002/masy.200451205.

(39) Nohra, B.; Candy, L.; Blanco, J.; Raoul, Y.; Mouloungui, Z. Aminolysis Reaction of Glycerol Carbonate in Organic and Hydroorganic Medium. *J Americ Oil Chem Soc* **2012**, *89* (6), 1125–1133. https://doi.org/10.1007/s11746-011-1995-5.

(40) Blain, M.; Jean-Gérard, L.; Auvergne, R.; Benazet, D.; Caillol, S.; Andrioletti, B. Rational Investigations in the Ring Opening of Cyclic Carbonates by Amines. *Green Chem.* **2014**, *16* (9), 4286–4291. https://doi.org/10.1039/C4GC01032A.

(41) Alves, M.; Méreau, R.; Grignard, B.; Detrembleur, C.; Jérôme, C.; Tassaing, T. DFT Investigation of the Reaction Mechanism for the Guanidine Catalysed Ring-Opening of Cyclic Carbonates by Aromatic and Alkyl-Amines. *RSC Adv.* **2017**, *7* (31), 18993–19001. https://doi.org/10.1039/C7RA00220C.

(42) Guzmán Agudelo, A. F.; Pérez-Sena, W. Y.; Kebir, N.; Salmi, T.; Ríos, L. A.; Leveneur, S. Influence of Steric Effects on the Kinetics of Cyclic-Carbonate Vegetable Oils Aminolysis. *Chemical Engineering Science* **2020**, *228*, 115954. https://doi.org/10.1016/j.ces.2020.115954.

(43) Quienne, B.; Poli, R.; Pinaud, J.; Caillol, S. Enhanced Aminolysis of Cyclic Carbonates by β-Hydroxylamines for the Production of Fully Biobased Polyhydroxyurethanes. *Green Chem.* **2021**, *23* (4), 1678–1690. https://doi.org/10.1039/D0GC04120C.

(44) Lambeth, R. H.; Henderson, T. J. Organocatalytic Synthesis of (Poly)Hydroxyurethanes from Cyclic Carbonates and Amines. *Polymer* **2013**, *54* (21), 5568–5573. https://doi.org/10.1016/j.polymer.2013.08.053.

(45) Ochiai, B.; Inoue, S.; Endo, T. Salt Effect on Polyaddition of Bifunctional Cyclic Carbonate and Diamine. *J. Polym. Sci. A Polym. Chem.* **2005**, *43* (24), 6282–6286. https://doi.org/10.1002/pola.21081.

(46) Maisonneuve, L.; More, A. S.; Foltran, S.; Alfos, C.; Robert, F.; Landais, Y.; Tassaing, T.; Grau, E.; Cramail, H. Novel Green Fatty Acid-Based Bis-Cyclic Carbonates for the Synthesis of Isocyanate-Free Poly(Hydroxyurethane Amide)s. *RSC Adv.* **2014**, *4* (49), 25795–25803. https://doi.org/10.1039/C4RA03675A.

(47) Blain, M.; Yau, H.; Jean-Gérard, L.; Auvergne, R.; Benazet, D.; Schreiner, P. R.; Caillol, S.; Andrioletti, B. Urea- and Thiourea-Catalyzed Aminolysis of Carbonates. *ChemSusChem* **2016**, *9* (16), 2269–2272. https://doi.org/10.1002/cssc.201600778.

(48) Levina, M. A.; Zabalov, M. V.; Krasheninnikov, V. G.; Tiger, R. P. Green Chemistry of Polyurethanes: The Catalytic n-Butylaminolysis of Ethylene Carbonate as a Model Chain-Growth Reaction in the Formation of Nonisocyanate Polyurethanes. *Polym. Sci. Ser. B* **2017**, *59* (5), 497–505. https://doi.org/10.1134/S1560090417050074.

(49) Sopeña, S.; Laserna, V.; Guo, W.; Martin, E.; Escudero-Adán, E. C.; Kleij, A. W. Regioselective Organocatalytic Formation of Carbamates from Substituted Cyclic Carbonates. *Adv Synth Catal* **2016**, *358* (13), 2172–2178. https://doi.org/10.1002/adsc.201600290.

(50) De La Cruz-Martínez, F.; Francés-Poveda, E.; North, M.; Castro-Osma, J. A.; Lara-Sánchez, A. Base-Catalyzed Highly Regioselective Synthesis of Bio-Based Hydroxyurethanes. *Eur J Org Chem* **2024**, e202400275. https://doi.org/10.1002/ejoc.202400275.

(51) Guo, W.; Gónzalez-Fabra, J.; Bandeira, N. A. G.; Bo, C.; Kleij, A. W. A Metal-Free Synthesis of N-Aryl Carbamates under Ambient Conditions. *Angew Chem Int Ed* **2015**, *54* (40), 11686–11690. https://doi.org/10.1002/anie.201504956.

(52) Lombardo, V. M.; Dhulst, E. A.; Leitsch, E. K.; Wilmot, N.; Heath, W. H.; Gies, A. P.; Miller, M. D.; Torkelson, J. M.; Scheidt, K. A. Cooperative Catalysis of Cyclic Carbonate Ring Opening: Application Towards Non-Isocyanate Polyurethane Materials. *Eur J Org Chem* **2015**, *2015* (13), 2791–2795. https://doi.org/10.1002/ejoc.201500313.

(53) Zabalov, M. V.; Levina, M. A.; Tiger, R. P. Molecular Organization of Reagents in the Kinetics and Catalysis of Liquid-Phase Reactions: XIII. Cyclic Transition States Involving Solvent Molecules in the Mechanism of Aminolysis of Cyclocarbonates in an Alcohol Medium. *Kinet Catal* **2020**, *61* (5), 721–729. https://doi.org/10.1134/S0023158420050134.

(54) Zabalov, M. V.; Levina, M. A.; Krasheninnikov, V. G.; Tiger, R. P. Reactivity of New Monomers of the Polyurethanes Green Chemistry, the Reaction Mechanism, and the Medium Effect. *Polym. Sci. Ser. B* **2023**, *65* (4), 467–474. https://doi.org/10.1134/S1560090423701063.

(55) Zabalov, M. V.; Tiger, R. P. The Supermolecule Method, as Applied to Studies of Liquid-Phase Reaction Mechanisms Taking Cyclocarbonate Aminolysis in Dioxane as an Example: Specific Features. *Russ Chem Bull* **2016**, *65* (3), 631–639. https://doi.org/10.1007/s11172-016-1347-6.

(56) Zabalov, M. V.; Tiger, R. P. Specificities of Application of the Supermolecule Method to the Calculation of Reaction Mechanisms in a Protonodonor Medium. Ethylene Carbonate Aminolysis in Methanol. *Theor Chem Acc* **2017**, *136* (9), 95. https://doi.org/10.1007/s00214-017-2124-9.

(57) Olsén, P.; Oschmann, M.; Johnston, E. V.; Åkermark, B. Synthesis of Highly Functional Carbamates through Ring-Opening of Cyclic Carbonates with Unprotected α-Amino Acids in Water. *Green Chem.* **2018**, *20* (2), 469–475. https://doi.org/10.1039/C7GC02862H.

(58) Bourguignon, M.; Grignard, B.; Detrembleur, C. Water-Induced Self-Blown Non-Isocyanate Polyurethane Foams. *Angew Chem Int Ed* **2022**, *61* (51), e202213422. https://doi.org/10.1002/anie.202213422.

(59) Monie, F.; Vidil, T.; Grau, E.; Grignard, B.; Detrembleur, C.; Cramail, H. A Sip of Water in Your Thermoset: The Role of H2O as an Accelerator of the Crosslinking Reaction of Polyhydroxyurethane Networks. April 17, 2024. https://doi.org/10.26434/chemrxiv-2024-7x7z6.

(60) Fortman, D. J.; Brutman, J. P.; Hillmyer, M. A.; Dichtel, W. R. Structural Effects on the Reprocessability and Stress Relaxation of Crosslinked Polyhydroxyurethanes. *J of Applied Polymer Sci* **2017**, *134* (45), 44984. https://doi.org/10.1002/app.44984.

(61) Chen, X.; Li, L.; Jin, K.; Torkelson, J. M. Reprocessable Polyhydroxyurethane Networks Exhibiting Full Property Recovery and Concurrent Associative and Dissociative Dynamic Chemistry via Transcarbamoylation and Reversible Cyclic Carbonate Aminolysis. *Polym. Chem.* **2017**, *8* (41), 6349–6355. https://doi.org/10.1039/C7PY01160A.

(62) Bakkali-Hassani, C.; Berne, D.; Bron, P.; Irusta, L.; Sardon, H.; Ladmiral, V.; Caillol, S. Polyhydroxyurethane Covalent Adaptable Networks: Looking for Suitable Catalysts. *Polym. Chem.* **2023**, *14* (31), 3610–3620. https://doi.org/10.1039/D3PY00579H.

(63) Levina, M. A.; Zabalov, M. V.; Krasheninnikov, V. G.; Tiger, R. P. Kinetics and Quantum Chemical Aspects of the Mechanism of the Guanidine (TBD) Catalyzed Aminolysis of Cyclocarbonate Containing Soybean Oil Triglycerides as the Model Process of Green Chemistry of Polyurethanes. *Reac Kinet Mech Cat* **2020**, *129* (1), 65–83. https://doi.org/10.1007/s11144-019-01683-w.

(64) Steblyanko, A.; Choi, W.; Sanda, F.; Endo, T. Addition of Five-Membered Cyclic Carbonate with Amine and Its Application to Polymer Synthesis. *J. Polym. Sci. A Polym. Chem.* **2000**, *38* (13), 2375–2380. https://doi.org/10.1002/1099-0518(20000701)38:13<2375::AID-POLA100>3.0.CO;2-U.

(65) Annunziata, L.; Diallo, A. K.; Fouquay, S.; Michaud, G.; Simon, F.; Brusson, J.-M.; Carpentier, J.-F.; Guillaume, S. M. α,ω-Di(Glycerol Carbonate) Telechelic Polyesters and Polyolefins as Precursors to Polyhydroxyurethanes: An Isocyanate-Free Approach. *Green Chem.* **2014**, *16* (4), 1947–1956. https://doi.org/10.1039/C3GC41821A.

(66) Chen, Q.; Gao, K.; Peng, C.; Xie, H.; Zhao, Z. K.; Bao, M. Preparation of Lignin/Glycerol-Based Bis(Cyclic Carbonate) for the Synthesis of Polyurethanes. *Green Chem.* **2015**, *17* (9), 4546–4551. https://doi.org/10.1039/C5GC01340B.

(67) Fleischer, M.; Blattmann, H.; Mülhaupt, R. Glycerol-, Pentaerythritol- and Trimethylolpropane-Based Polyurethanes and Their Cellulose Carbonate Composites Prepared via the Non-Isocyanate Route with Catalytic Carbon Dioxide Fixation. *Green Chem.* **2013**, *15* (4), 934. https://doi.org/10.1039/c3gc00078h.

(68) Wu, Z.; Cai, W.; Chen, R.; Qu, J. Synthesis and Properties of Ambient-Curable Non-Isocyanate Polyurethanes. *Progress in Organic Coatings* **2018**, *119*, 116–122. https://doi.org/10.1016/j.porgcoat.2018.02.006.

(69) Bourguignon, M.; Thomassin, J.-M.; Grignard, B.; Jerome, C.; Detrembleur, C. Fast and Facile One-Pot One-Step Preparation of Nonisocyanate Polyurethane Hydrogels in Water at Room Temperature. *ACS Sustainable Chem. Eng.* **2019**, acssuschemeng.9b02624. https://doi.org/10.1021/acssuschemeng.9b02624.

(70) Capar, Ö.; Tabatabai, M.; Klee, J. E.; Worm, M.; Hartmann, L.; Ritter, H. Fast Curing of Polyhydroxyurethanes *via* Ring Opening Polyaddition of Low Viscosity Cyclic Carbonates and Amines. *Polym. Chem.* **2020**, *11* (43), 6964–6970. https://doi.org/10.1039/D0PY01172J.

(71) Bourguignon, M.; Thomassin, J.; Grignard, B.; Vertruyen, B.; Detrembleur, C. Water-Borne Isocyanate-Free Polyurethane Hydrogels with Adaptable Functionality and Behavior. *Macromol. Rapid Commun.* **2021**, *42* (3), 2000482. https://doi.org/10.1002/marc.202000482.

(72) Tomita, H.; Sanda, F.; Endo, T. Reactivity Comparison of Five- and Six-Membered Cyclic Carbonates with Amines: Basic Evaluation for Synthesis of Poly(Hydroxyurethane). *J. Polym. Sci. A Polym. Chem.* **2001**, *39* (1), 162–168. https://doi.org/10.1002/1099-0518(20010101)39:1<162::AID-POLA180>3.0.CO;2-O.

(73) Maisonneuve, L.; Wirotius, A.-L.; Alfos, C.; Grau, E.; Cramail, H. Fatty Acid-Based (Bis) 6-Membered Cyclic Carbonates as Efficient Isocyanate Free Poly(Hydroxyurethane) Precursors. *Polym. Chem.* **2014**, *5* (21), 6142–6147. https://doi.org/10.1039/C4PY00922C.

(74) Tomita, H.; Sanda, F.; Endo, T. Polyaddition of Bis(Seven-membered Cyclic Carbonate) with Diamines: A Novel and Efficient Synthetic Method for Polyhydroxyurethanes. *J. Polym. Sci. A Polym. Chem.* **2001**, *39* (23), 4091–4100. https://doi.org/10.1002/pola.10058.

(75) Tomita, H.; Sanda, F.; Endo, T. Polyaddition Behavior of Bis(Five- and Six-Membered Cyclic Carbonate)s with Diamine. *J. Polym. Sci. A Polym. Chem.* **2001**, *39* (6), 860–867. https://doi.org/10.1002/1099-0518(20010315)39:6<860::AID-POLA1059>3.0.CO;2-2.

(76) Lambeth, R. H.; Mathew, S. M.; Baranoski, M. H.; Housman, K. J.; Tran, B.; Oyler, J. M. Nonisocyanate Polyurethanes from Six-membered Cyclic Carbonates: Catalysis and Side Reactions. *J of Applied Polymer Sci* **2017**, *134* (45), 44941. https://doi.org/10.1002/app.44941.

(77) Yuen, A.; Bossion, A.; Gómez-Bengoa, E.; Ruipérez, F.; Isik, M.; Hedrick, J. L.; Mecerreyes, D.; Yang, Y. Y.; Sardon, H. Room Temperature Synthesis of Non-Isocyanate Polyurethanes (NIPUs) Using Highly Reactive N-Substituted 8-Membered Cyclic Carbonates. *Polym. Chem.* **2016**, *7* (11), 2105–2111. https://doi.org/10.1039/C6PY00264A.

(78) Fanjul-Mosteirín, N.; Aguirresarobe, R.; Sadaba, N.; Larrañaga, A.; Marin, E.; Martin, J.; Ramos-Gomez, N.; Arno, M. C.; Sardon, H.; Dove, A. P. Crystallization-Induced Gelling as a Method to 4D Print Low-Water-Content Non-Isocyanate Polyurethane Hydrogels. *Chem. Mater.* **2021**, *33* (18), 7194–7202. https://doi.org/10.1021/acs.chemmater.1c00913.

(79) Besse, V.; Foyer, G.; Auvergne, R.; Caillol, S.; Boutevin, B. Access to Nonisocyanate Poly(Thio)Urethanes: A Comparative Study. *J. Polym. Sci. Part A: Polym. Chem.* **2013**, *51* (15), 3284–3296. https://doi.org/10.1002/pola.26722.

(80) Gregory, G. L.; Jenisch, L. M.; Charles, B.; Kociok-Köhn, G.; Buchard, A. Polymers from Sugars and CO_2: Synthesis and Polymerization of a d -Mannose-Based Cyclic Carbonate. *Macromolecules* **2016**, *49* (19), 7165–7169. https://doi.org/10.1021/acs.macromol.6b01492.

(81) Nederberg, F.; Lohmeijer, B. G. G.; Leibfarth, F.; Pratt, R. C.; Choi, J.; Dove, A. P.; Waymouth, R. M.; Hedrick, J. L. Organocatalytic Ring Opening Polymerization of Trimethylene Carbonate. *Biomacromolecules* **2007**, *8* (1), 153–160. https://doi.org/10.1021/bm060795n.

(82) Hedrick, J. L.; Piunova, V.; Park, N. H.; Erdmann, T.; Arrechea, P. L. Simple and Efficient Synthesis of Functionalized Cyclic Carbonate Monomers Using Carbon Dioxide. *ACS Macro Lett.* **2022**, *11* (3), 368–375. https://doi.org/10.1021/acsmacrolett.2c00060.

(83) Yuen, A. Y.; Bossion, A.; Veloso, A.; Mecerreyes, D.; Hedrick, J. L.; Dove, A. P.; Sardon, H. Efficient Polymerization and Post-Modification of *N* -Substituted Eight-Membered Cyclic Carbonates Containing Allyl Groups. *Polym. Chem.* **2018**, *9* (18), 2458–2467. https://doi.org/10.1039/C8PY00231B.

(84) Venkataraman, S.; Ng, V. W. L.; Coady, D. J.; Horn, H. W.; Jones, G. O.; Fung, T. S.; Sardon, H.; Waymouth, R. M.; Hedrick, J. L.; Yang, Y. Y. A Simple and Facile Approach to Aliphatic *N* -Substituted Functional Eight-Membered Cyclic Carbonates and Their

Organocatalytic Polymerization. *J. Am. Chem. Soc.* **2015**, *137* (43), 13851–13860. https://doi.org/10.1021/jacs.5b06355.

(85) Tempelaar, S.; Mespouille, L.; Coulembier, O.; Dubois, P.; Dove, A. P. Synthesis and Post-Polymerisation Modifications of Aliphatic Poly(Carbonate)s Prepared by Ring-Opening Polymerisation. *Chem. Soc. Rev.* **2013**, *42* (3), 1312–1336. https://doi.org/10.1039/C2CS35268K.

(86) Yu, W.; Maynard, E.; Chiaradia, V.; Arno, M. C.; Dove, A. P. Aliphatic Polycarbonates from Cyclic Carbonate Monomers and Their Application as Biomaterials. *Chem. Rev.* **2021**, *121* (18), 10865–10907. https://doi.org/10.1021/acs.chemrev.0c00883.

(87) McGuire, T. M.; López-Vidal, E. M.; Gregory, G. L.; Buchard, A. Synthesis of 5- to 8-Membered Cyclic Carbonates from Diols and CO2: A One-Step, Atmospheric Pressure and Ambient Temperature Procedure. *Journal of CO2 Utilization* **2018**, *27*, 283–288. https://doi.org/10.1016/j.jcou.2018.08.009.

(88) Vara, B. A.; Struble, T. J.; Wang, W.; Dobish, M. C.; Johnston, J. N. Enantioselective Small Molecule Synthesis by Carbon Dioxide Fixation Using a Dual Brønsted Acid/Base Organocatalyst. *J. Am. Chem. Soc.* **2015**, *137* (23), 7302–7305. https://doi.org/10.1021/jacs.5b04425.

(89) Whiteoak, C. J.; Kielland, N.; Laserna, V.; Escudero-Adán, E. C.; Martin, E.; Kleij, A. W. A Powerful Aluminum Catalyst for the Synthesis of Highly Functional Organic Carbonates. *J. Am. Chem. Soc.* **2013**, *135* (4), 1228–1231. https://doi.org/10.1021/ja311053h.

(90) Ngassam Tounzoua, C.; Grignard, B.; Detrembleur, C. Exovinylene Cyclic Carbonates: Multifaceted CO_2-Based Building Blocks for Modern Chemistry and Polymer Science. *Angew Chem Int Ed* **2022**, *61* (22), e202116066. https://doi.org/10.1002/anie.202116066.

(91) Johnson, C.; Dabral, S.; Rudolf, P.; Licht, U.; Hashmi, A. S. K.; Schaub, T. Liquid-liquid-phase Synthesis of *Exo* -Vinylene Carbonates from Primary Propargylic Alcohols: Catalyst Design and Recycling. *ChemCatChem* **2021**, *13* (1), 353–361. https://doi.org/10.1002/cctc.202001551.

(92) Dabral, S.; Licht, U.; Rudolf, P.; Bollmann, G.; Hashmi, A. S. K.; Schaub, T. Synthesis and Polymerisation of α-Alkylidene Cyclic Carbonates from Carbon Dioxide, Epoxides and the Primary Propargylic Alcohol 1,4-Butynediol. *Green Chem.* **2020**, *22* (5), 1553–1558. https://doi.org/10.1039/C9GC04320A.

(93) Ouyang, L.; Tang, X.; He, H.; Qi, C.; Xiong, W.; Ren, Y.; Jiang, H. Copper-Promoted Coupling of Carbon Dioxide and Propargylic Alcohols: Expansion of Substrate Scope and Trapping of Vinyl Copper Intermediate. *Adv Synth Catal* **2015**, *357* (11), 2556–2565. https://doi.org/10.1002/adsc.201500088.

(94) Fischler, H.-M.; Heine, H.-G.; Hartmann, W. Darstellung Einiger Dialkylsubstituierter Vinylencarbonate Und Ihre Photosensibilisierte Cycloaddition an Äthylen. *Tetrahedron Letters* **1972**, *13* (17), 1701–1704. https://doi.org/10.1016/S0040-4039(01)84725-0.

(95) Svahn, C. M.; Merenyi, F.; Karlson, L. Tranexamic Acid Derivatives with Enhanced Absorption. *J. Med. Chem.* **1986**, *29* (4), 448–453. https://doi.org/10.1021/jm00154a004.

(96) Onida, K.; Haddleton, A. J.; Norsic, S.; Boisson, C.; D'Agosto, F.; Duguet, N. Organocatalytic Synthesis of Substituted Vinylene Carbonates. *Adv Synth Catal* **2021**, *363* (22), 5129–5137. https://doi.org/10.1002/adsc.202100870.

(97) Qiao, C.; Engel, P. D.; Ziegenhagen, L. A.; Rominger, F.; Schäfer, A.; Deglmann, P.; Rudolf, P.; Comba, P.; Hashmi, A. S. K.; Schaub, T. An Organocatalytic Route to *Endo* -Vinylene Carbonates from Carbon Dioxide-Based *Exo* -Vinylene Carbonates. *Adv Synth Catal* **2024**, *366* (2), 291–298. https://doi.org/10.1002/adsc.202301374.

(98) Bruneau, C.; Dixneuf, P. H. Catalytic Incorporation of CO2 into Organic Substrates: Synthesis of Unsaturated Carbamates, Carbonates and Ureas. *Journal of Molecular Catalysis* **1992**, *74* (1), 97–107. https://doi.org/10.1016/0304-5102(92)80227-8.

(99) Titov, I. Yu.; Chernysheva, N. B.; Chudinov, Yu. B.; Bogolyubov, A. A.; Semenov, V. V. 4-Methylenedioxolan-2-Ones as Convenient Synthons for the Preparation of Natural Products of the Berbine and Calycotomine Series. *Russian Chemical Bulletin* **2006**, *55* (3), 569–575. https://doi.org/10.1007/s11172-006-0293-0.

(100) Shi, M.; Shen, Y.; Chen, Y.-J. Reactions of 5,5Dimethyl4-Methylene-1,3-Dioxolan-2-One with Amines in the Presence of Palladium Catalyst. *Heterocycles* **2002**, *57*. https://doi.org/10.3987/COM-01-9379.

(101) Gennen, S.; Grignard, B.; Jérôme, C.; Detrembleur, C. CO_2-Sourced Non-Isocyanate Poly(Urethane)s with pH-Sensitive Imine Linkages. *Adv. Synth. Catal.* **2019**, *361* (2), 355–365. https://doi.org/10.1002/adsc.201801230.

(102) Gennen, S.; Grignard, B.; Tassaing, T.; Jérôme, C.; Detrembleur, C. CO_2-Sourced α-Alkylidene Cyclic Carbonates: A Step Forward in the Quest for Functional Regioregular Poly(Urethane)s and Poly(Carbonate)s. *Angew. Chem. Int. Ed.* **2017**, *56* (35), 10394–10398. https://doi.org/10.1002/anie.201704467.

(103) Habets, T.; Siragusa, F.; Grignard, B.; Detrembleur, C. Advancing the Synthesis of Isocyanate-Free Poly(Oxazolidones)s: Scope and Limitations. *Macromolecules* **2020**, *53* (15), 6396–6408. https://doi.org/10.1021/acs.macromol.0c01231.

(104) Qiu, J.; Zhao, Y.; Zhao, Y.; Wang, H.; Li, Z.; Wang, J.; Jiao, T. Cu(I)/Ionic Liquids Promote the Conversion of Carbon Dioxide into Oxazolidinones at Room Temperature. *Molecules* **2019**, *24* (7), 1241. https://doi.org/10.3390/molecules24071241.

(105) Song, Q.-W.; Liu, P.; Han, L.-H.; Zhang, K.; He, L.-N. Upgrading CO2 by Incorporation into Urethanes through Silver-Catalyzed One-Pot Stepwise Amidation Reaction. *Chinese Journal of Chemistry* **2018**, *36* (2), 147–152. https://doi.org/10.1002/cjoc.201700572.

(106) Song, Q.-W.; Chen, W.-Q.; Ma, R.; Yu, A.; Li, Q.-Y.; Chang, Y.; He, L.-N. Bifunctional Silver(I) Complex-Catalyzed CO_2 Conversion at Ambient Conditions: Synthesis of α-Methylene Cyclic Carbonates and Derivatives. *ChemSusChem* **2015**, *8* (5), 821–827. https://doi.org/10.1002/cssc.201402921.

(107) Kikuchi, S.; Yoshida, S.; Sugawara, Y.; Yamada, W.; Cheng, H.-M.; Fukui, K.; Sekine, K.; Iwakura, I.; Ikeno, T.; Yamada, T. Silver-Catalyzed Carbon Dioxide Incorporation and Rearrangement on Propargylic Derivatives. *Bulletin of the Chemical Society of Japan* **2011**, *84* (7), 698–717. https://doi.org/10.1246/bcsj.20110078.

(108) Dabral, S.; Bayarmagnai, B.; Hermsen, M.; Schießl, J.; Mormul, V.; Hashmi, A. S. K.; Schaub, T. Silver-Catalyzed Carboxylative Cyclization of Primary Propargyl Alcohols with CO_2. *Org. Lett.* **2019**, *21* (5), 1422–1425. https://doi.org/10.1021/acs.orglett.9b00156.

(109) Chauveau, C.; Fouquay, S.; Michaud, G.; Simon, F.; Carpentier, J.-F.; Guillaume, S. M. α,ω-Di(Vinylene Carbonate) Telechelic Polyolefins: Synthesis by Metathesis Reactions and Studies as Potential Precursors toward Hydroxy-Oxazolidone-Based Polyolefin NIPUs. *European Polymer Journal* **2019**, *116*, 144–157. https://doi.org/10.1016/j.eurpolymj.2019.03.052.

(110) Ouhib, F.; Grignard, B.; Van Den Broeck, E.; Luxen, A.; Robeyns, K.; Van Speybroeck, V.; Jerome, C.; Detrembleur, C. A Switchable Domino Process for the Construction of Novel CO_2-Sourced Sulfur-Containing Building Blocks and Polymers. *Angew. Chem. Int. Ed.* **2019**, *58* (34), 11768–11773. https://doi.org/10.1002/anie.201905969.

(111) Wong, A. R.; Barrera, M.; Pal, A.; Lamb, J. R. Improved Characterization of Polyoxazolidinones by Incorporating Solubilizing Side Chains. *Macromolecules* **2022**, *55* (24), 11006–11012. https://doi.org/10.1021/acs.macromol.2c02104.

(112) Sardon, H.; Engler, A. C.; Chan, J. M. W.; Coady, D. J.; O'Brien, J. M.; Mecerreyes, D.; Yang, Y. Y.; Hedrick, J. L. Homogeneous Isocyanate- and Catalyst-Free Synthesis of Polyurethanes in Aqueous Media. *Green Chem.* **2013**, *15* (5), 1121. https://doi.org/10.1039/c3gc40319j.

(113) Bossion, A.; Jones, G. O.; Taton, D.; Mecerreyes, D.; Hedrick, J. L.; Ong, Z. Y.; Yang, Y. Y.; Sardon, H. Non-Isocyanate Polyurethane Soft Nanoparticles Obtained by Surfactant-Assisted Interfacial Polymerization. *Langmuir* **2017**, *33* (8), 1959–1968. https://doi.org/10.1021/acs.langmuir.6b04242.

(114) Hosokawa, S.; Nagao, A.; Hashimoto, Y.; Matsune, A.; Okazoe, T.; Suzuki, C.; Wada, H.; Kakiuchi, T.; Tsuda, A. Non-Isocyanate Polyurethane Synthesis by Polycondensation of

Alkylene and Arylene Bis(Fluoroalkyl) Bis(Carbonate)s with Diamines. *Bulletin of the Chemical Society of Japan* **2023**, *96* (7), 663–670. https://doi.org/10.1246/bcsj.20230066.

(115) Wu, D.; Martin, R. T.; Piña, J.; Kwon, J.; Crockett, M. P.; Thomas, A. A.; Gutierrez, O.; Park, N. H.; Hedrick, J. L.; Campos, L. M. Cyclopropenimine-Mediated CO_2 Activation for the Synthesis of Polyurethanes and Small-Molecule Carbonates and Carbamates. *Angew Chem Int Ed* **2024**, *63* (18), e202401281. https://doi.org/10.1002/anie.202401281.

(116) Chen, Z.; Hadjichristidis, N.; Feng, X.; Gnanou, Y. Poly(Urethane–Carbonate)s from Carbon Dioxide. *Macromolecules* **2017**, *50* (6), 2320–2328. https://doi.org/10.1021/acs.macromol.7b00142.

(117) Rokicki, G.; Parzuchowski, P. G.; Mazurek, M. Non-isocyanate Polyurethanes: Synthesis, Properties, and Applications. *Polymers for Advanced Techs* **2015**, *26* (7), 707–761. https://doi.org/10.1002/pat.3522.

(118) Grignard, B.; Gennen, S.; Jérôme, C.; Kleij, A. W.; Detrembleur, C. Advances in the Use of CO_2 as a Renewable Feedstock for the Synthesis of Polymers. *Chem. Soc. Rev.* **2019**, *48* (16), 4466–4514. https://doi.org/10.1039/C9CS00047J.

(119) Zhang, D.; Zhang, Y.; Fan, Y.; Rager, M.-N.; Guérineau, V.; Bouteiller, L.; Li, M.-H.; Thomas, C. M. Polymerization of Cyclic Carbamates: A Practical Route to Aliphatic Polyurethanes. *Macromolecules* **2019**, *52* (7), 2719–2724. https://doi.org/10.1021/acs.macromol.9b00436.

(120) Haba, O.; Akashika, Y. Anionic Ring-opening Polymerization of a Five-membered Cyclic Urethane Derived from d -glucosamine. *J. Polym. Sci. Part A: Polym. Chem.* **2019**, *57* (24), 2491–2497. https://doi.org/10.1002/pola.29511.

(121) Buchheit, H.; Bruchmann, B.; Stoll, K.; Mülhaupt, R. Functionalized Acrylic Polyhydroxy Urethanes as Molecular Tool Box for Photocurable Thermosets and 3D Printing. *Journal of Polymer Science* **2021**, *59* (10), 882–892. https://doi.org/10.1002/pol.20210115.

(122) Schimpf, V.; Asmacher, A.; Fuchs, A.; Bruchmann, B.; Mülhaupt, R. Polyfunctional Acrylic Non-Isocyanate Hydroxyurethanes as Photocurable Thermosets for 3D Printing. *Macromolecules* **2019**, *52* (9), 3288–3297. https://doi.org/10.1021/acs.macromol.9b00330.

(123) Singh, N.; Bakhshi, H.; Meyer, W. Developing Non-Isocyanate Urethane-Methacrylate Photo-Monomers for 3D Printing Application. *RSC Adv.* **2020**, *10* (72), 44103–44110. https://doi.org/10.1039/D0RA06388F.

(124) Bakhshi, H.; Kuang, G.; Wieland, F.; Meyer, W. Photo-Curing Kinetics of 3D-Printing Photo-Inks Based on Urethane-Acrylates. *Polymers* **2022**, *14* (15), 2974. https://doi.org/10.3390/polym14152974.

(125) Kuang, G.; Bakhshi, H.; Meyer, W. Urethane-Acrylate-Based Photo-Inks for Digital Light Processing of Flexible Materials. *J Polym Res* **2023**, *30* (4), 141. https://doi.org/10.1007/s10965-023-03519-7.

(126) Carmenini, R.; Spanu, C.; Locatelli, E.; Sambri, L.; Comes Franchini, M.; Maturi, M. Isocyanate-Free Urethanediol Itaconates as Biobased Liquid Monomers in Photopolymerization-Based 3D Printing. *Prog Addit Manuf* **2024**. https://doi.org/10.1007/s40964-024-00598-w.

(127) Zareanshahraki, F.; Mannari, V. Formulation and Optimization of Radiation-Curable Nonisocyanate Polyurethane Wood Coatings by Mixture Experimental Design. *J Coat Technol Res* **2021**, *18* (3), 695–715. https://doi.org/10.1007/s11998-020-00453-x.

(128) Zareanshahraki, F.; Asemani, H. R.; Skuza, J.; Mannari, V. Synthesis of Non-Isocyanate Polyurethanes and Their Application in Radiation-Curable Aerospace Coatings. *Progress in Organic Coatings* **2020**, *138*, 105394. https://doi.org/10.1016/j.porgcoat.2019.105394.

(129) Hoyle, C. E.; Bowman, C. N. Thiol–Ene Click Chemistry. *Angew Chem Int Ed* **2010**, *49* (9), 1540–1573. https://doi.org/10.1002/anie.200903924.

(130) Calle, M.; Lligadas, G.; Ronda, J. C.; Galià, M.; Cádiz, V. An Efficient Nonisocyanate Route to Polyurethanes via Thiol-ene Self-addition. *J. Polym. Sci. Part A: Polym. Chem.* **2014**, *52* (21), 3017–3025. https://doi.org/10.1002/pola.27347.

(131) Xie, S.; Li, Y.; Chai, Y.; Chen, Q.; North, M.; Xie, H. Introducing the Reversible Reaction of CO_2 with Diamines into Nonisocyanate Polyurethane Synthesis. *ACS Macro Lett.* **2024**, *13* (1), 14–20. https://doi.org/10.1021/acsmacrolett.3c00621.

(132) Scheelje, F. C. M.; Meier, M. A. R. Non-Isocyanate Polyurethanes Synthesized from Terpenes Using Thiourea Organocatalysis and Thiol-Ene-Chemistry. *Commun Chem* **2023**, *6* (1), 239. https://doi.org/10.1038/s42004-023-01041-x.

(133) Warner, J. J.; Wang, P.; Mellor, W. M.; Hwang, H. H.; Park, J. H.; Pyo, S.-H.; Chen, S. 3D Printable Non-Isocyanate Polyurethanes with Tunable Material Properties. *Polym. Chem.* **2019**, *10* (34), 4665–4674. https://doi.org/10.1039/C9PY00999J.

(134) Hua, G.; Odelius, K. Isocyanate-Free, UV-Crosslinked Poly(Hydroxyurethane) Networks: A Sustainable Approach toward Highly Functional Antibacterial Gels. *Macromolecular Bioscience* **2017**, *17* (11), 1700190. https://doi.org/10.1002/mabi.201700190.

(135) Pierrard, A.; Aqil, A.; Detrembleur, C.; Jérôme, C. Thermal and UV Curable Formulations of Poly(Propylene Glycol)–Poly(Hydroxyurethane) Elastomers toward Nozzle-Based 3D Photoprinting. *Biomacromolecules* **2023**, *24* (10), 4375–4384. https://doi.org/10.1021/acs.biomac.2c00860.

(136) Pierrard, A.; Melo, S. F.; Thijssen, Q.; Van Vlierberghe, S.; Lancellotti, P.; Oury, C.; Detrembleur, C.; Jérôme, C. Design of 3D-Photoprintable, Bio-, and Hemocompatible

Nonisocyanate Polyurethane Elastomers for Biomedical Implants. *Biomacromolecules* **2024**, *25* (3), 1810–1824. https://doi.org/10.1021/acs.biomac.3c01261.

(137) *Handbook of Thermoset Plastics*, Fourth edition.; Dodiuk, H., Ed.; PDL handbook series; William Andrew: Oxford Cambridge, MA, 2022.

(138) Asemani, H.; Zareanshahraki, F.; Mannari, V. Design of Hybrid Nonisocyanate Polyurethane Coatings for Advanced Ambient Temperature Curing Applications. *J of Applied Polymer Sci* **2019**, *136* (13), 47266. https://doi.org/10.1002/app.47266.

(139) Centeno-Pedrazo, A.; Freixa, Z.; Feola, R.; Lunzer, F.; Garcia-Suarez, E. J.; Ortiz, P. Bringing Non-Isocyanate Polyurethanes Closer to Industrial Implementation Using Carbonated Soybean Oil-Based Amino Hardeners. *Progress in Organic Coatings* **2023**, *185*, 107925. https://doi.org/10.1016/j.porgcoat.2023.107925.

(140) Figovsky, O.; Shapovalov, L.; Birukova, O.; Leykin, A. Modification of Epoxy Adhesives by Hydroxyurethane Components on the Basis of Renewable Raw Materials. *Polym. Sci. Ser. D* **2013**, *6* (4), 271–274. https://doi.org/10.1134/S1995421213040047.

(141) Gomez-Lopez, A.; Grignard, B.; Calvo, I.; Detrembleur, C.; Sardon, H. Accelerating the Curing of Hybrid Poly(Hydroxy Urethane)-Epoxy Adhesives by the Thiol-Epoxy Chemistry. *ACS Appl. Polym. Mater.* **2022**, *4* (12), 8786–8794. https://doi.org/10.1021/acsapm.2c01195.

(142) Cornille, A.; Guillet, C.; Benyahya, S.; Negrell, C.; Boutevin, B.; Caillol, S. Room Temperature Flexible Isocyanate-Free Polyurethane Foams. *European Polymer Journal* **2016**, *84*, 873–888. https://doi.org/10.1016/j.eurpolymj.2016.05.032.

(143) Gomez-Lopez, A.; Grignard, B.; Calvo, I.; Detrembleur, C.; Sardon, H. Monocomponent Non-Isocyanate Polyurethane Adhesives Based on a Sol–Gel Process. *ACS Appl. Polym. Mater.* **2020**, *2* (5), 1839–1847. https://doi.org/10.1021/acsapm.0c00062.

(144) Asemani, H. R.; Mannari, V. Dual-Curable Coatings Obtained from Multi-Functional Non-Isocyanate Polyurethane Oligomers. *J Coat Technol Res* **2022**, *19* (5), 1393–1407. https://doi.org/10.1007/s11998-022-00614-0.

(145) Yu. Rulev, A. Aza-Michael Reaction: A Decade Later – Is the Research Over? *Eur J Org Chem* **2023**, *26* (26), e202300451. https://doi.org/10.1002/ejoc.202300451.

(146) Desmet, G. B.; D'hooge, D. R.; Omurtag, P. S.; Espeel, P.; Marin, G. B.; Du Prez, F. E.; Reyniers, M.-F. Quantitative First-Principles Kinetic Modeling of the Aza-Michael Addition to Acrylates in Polar Aprotic Solvents. *J. Org. Chem.* **2016**, *81* (24), 12291–12302. https://doi.org/10.1021/acs.joc.6b02218.

(147) Taplan, C.; Guerre, M.; Du Prez, F. E. Covalent Adaptable Networks Using β-Amino Esters as Thermally Reversible Building Blocks. *J. Am. Chem. Soc.* **2021**, *143* (24), 9140–9150. https://doi.org/10.1021/jacs.1c03316.

(148) Cornille, A.; Ecochard, Y.; Blain, M.; Boutevin, B.; Caillol, S. Synthesis of Hybrid Polyhydroxyurethanes by Michael Addition. *European Polymer Journal* **2017**, *96*, 370–382. https://doi.org/10.1016/j.eurpolymj.2017.09.028.

Heteroatom-rich polymers are pivotal actors in the plastics industry, representing a significant market share due to their diverse applications across various sectors. The functional group within these polymers defines the polymer family to which they belong and imparts them with specific properties for tailored applications. In polyurethanes (PUs), the carbamate linkage provides strong hydrogen bonding, reflecting in the polymers' properties with high toughness, excellent adhesion, and versatility. Similarly, other hetero-atom rich polymer families, the most notable being the polycarbonates (PCs), polyesters, and polyamides (PAs), bring unique properties suited for different applications. Emerging classes of polymers containing sulfur atoms, notably the sulfur-derived above-mentioned polymer classes such as polythiourethanes (PTUs) or polythiocarbonates (PTCs), introduce unique advantages over their oxygenated counterparts. This includes enhanced chemical resistance, structural flexibility, or improved optical performance.

However, the current production of most polymers relies on fossil resources and hazardous reagents. It is therefore of prime importance to explore new synthetic possibilities from renewable or waste resources, such as CO_2. Additionally, exploring recycling options is crucial in the current societal climate pushing toward a more sustainable and circular economy, thereby reducing the dramatic environmental consequences of plastic waste.

Our research group recently developed an innovative and promising synthetic route toward regio-regular and high molecular weight heteroatom-rich polymers in mild conditions. It was demonstrated that various nucleophiles (amines, alcohols, thiols) readily react with CO_2-sourced sourced α-alkylidene bis(cyclic carbonate)s (bisαCC) by step-growth polymerization at room temperature to obtain many polymer classes, including PUs, PCs, PTCs, and poly(cyclic carbonate-co-thioether)s (PCCs) (**Scheme 1**).

Among them, poly(hydroxy-oxazolidone)s, a special family of NIPUs, is obtained from the reaction of primary diamines with bisαCC without catalyst. A thorough study of the synthesis of these polymers highlighted their lack of solubility, hampering in-depth characterization and development of applications. Similarly, linear PUs are obtained from secondary diamines in the same conditions. However, examples remain scarce due to the limited availability of commercial multifunctional monomers.

When bisαCC is reacted with dithiols in the presence of an organobase (DBU), PTCs are mainly formed and rearrange in a domino process into PCCs. By addition of an additive (fluorinated alcohol), DBU is partially deactivated, and the amount of cyclic carbonate is limited. However, selectivity highly depends on the substrate and a control remains limited.

Polyols are reactive toward bisαCC in the presence of an organobase (DBU), leading to amorphous or semi-crystalline PCs. These polymers have already been applied as promising electrolytes for solid-state batteries.

This chemistry has already drawn attention from big companies such as BASF, as attested by recent patents on the production of new bisαCC and their incorporation in formulations. Only a few academic research groups, including ours, have explored the synthetic aspects of this chemistry and the range of applications remains extremely limited, certainly due to the novelty of the αCC chemistry field.

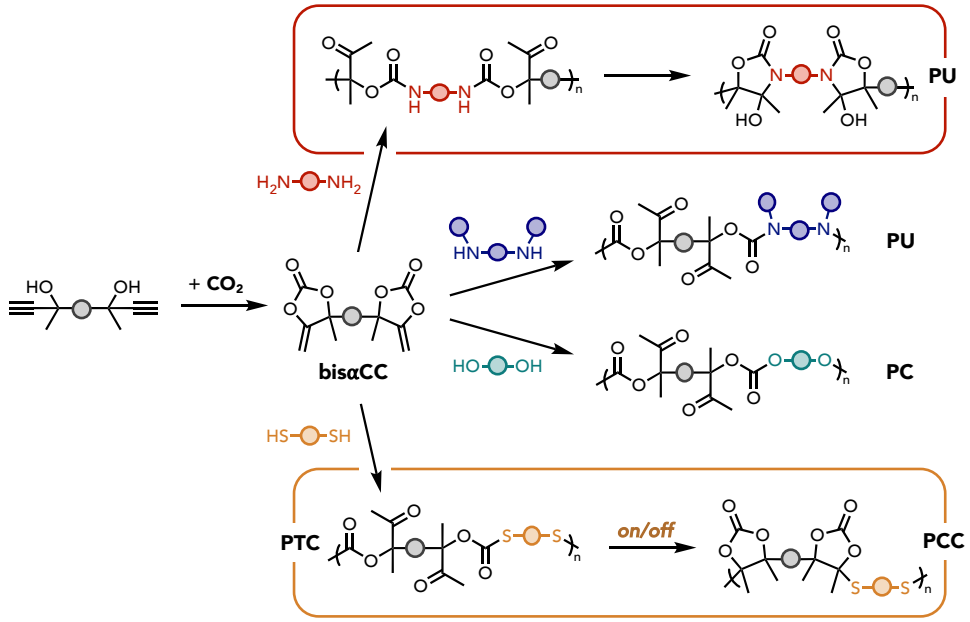

Scheme 1 – Library of polymers obtained by the reaction of bisαCC with various nucleophiles (Polyurethane, PU; Polycarbonate, PC; Polythiocarbonate, PTC; Poly(cyclic carbonate), PCC).

The aim of this thesis is to advance the chemistry of α-alkylidene cyclic carbonates with a focus on reactions involving amines and thiols to synthesize new hybrid polymers, especially poly(oxazolidone)s – a class of PUs. By optimizing reaction conditions and organocatalysts, we aim at guiding the chemoselective addition of both nucleophiles and to control the functionalities distribution within the polymer structure (i.e. oxazolidone for amines; thiocarbonate or cyclic carbonate for thiols). This would enable to construct polymers with on-demand functionality and properties from the same feedstock. This work also includes thorough characterization of the novel polymers and investigation of their properties. To promote circularity, we explored degradation and/or re-valorization pathways.

In Chapter I are summarized advances and strategies for NIPUs synthesis at room temperature – a significant challenge in polymer chemistry. It critically examines and identifies gaps in fundamental research and discusses the developed technologies to achieve high molecular weight NIPUs or well-defined thermosets structures. A promising technology, yet relatively unstudied, is the chemistry of α-alkylidene cyclic carbonates (αCCs) with amines to provide cyclic urethanes functionalities.

In Chapter II, the simultaneous polymerization of bisαCC with diamines and dithiols to create hybrid polymers is investigated. The study is initiated by model reactions to assess amine and thiol chemistries compatibility, and to identify the nature of the reaction products as well as their kinetics of formation. Optimized conditions are translated to the construction of novel hybrid poly(oxazolidone)s with improved solubility. The thermal properties of the polymers are assessed, and post-functionalization strategies of the hydroxy-oxazolidone linkage are explored, such as the thermal dehydration into exovinylene oxazolidone, and the subsequent cationic thiol-ene reaction.

In Chapter III, the room temperature cationic thiol-ene reaction between exovinylene oxazolidones and thiols is studied in depth on model compounds, revealing the fast and reversible nature of the resulting cyclic *N,S*-acetal oxazolidone linkage. Polymer networks are constructed from newly designed bifunctional exovinylene oxazolidone monomers and exhibit remarkable tunable mechanical properties. The covalent adaptable network (CAN) nature of the material is assessed by rheology experiments. Diverse end-of-life scenarios are then explored to recycle these thermoset materials.

In Chapter IV, the aminolysis of densely substituted cyclic carbonates derived from the thiol-αCC chemistry (cyclic carbonate-co-thioethers) is explored. Model reactions are first achieved to investigate the reactions kinetics and optimize the reaction conditions. In-depth DFT computational investigation supports experimental results and unravels the reaction mechanism. The manifold is applied to the deconstruction of high molecular weight PCCs displaying promising mechanical properties competing with polyolefins substitutes. The degradation products are valorized by the aforementioned *N,S*-acetal oxazolidone chemistry to furnish new recyclable polymer networks.

In Chapter V, the labile thiocarbonate bond from thiol-αCC chemistry is selectively produced by a new catalyst to address the previous lack of selectivity. A liquid bisαCC monomer is designed for the solvent-free formulation of PTCs thermosets and their recyclability is

evaluated as covalent adaptable networks. Finally, the applicability of PTCs as solid polymer electrolytes after combination with a lithium salt was explored.

Each chapter of the thesis is separated by an interlude to clarify how they are inter-connected. This thesis is based on peer-reviewed or under submission articles, and the results were selected for the frame of the thesis. A list of publications is available at the end of thesis, listing other published works during the timeframe of the thesis.

Chapter II

Facile construction of functional poly(monothiocarbonate) copolymers under mild operating conditions

*Thomas Habets, Fabiana Siragusa, Alejandro J. Müller, Quentin Grossman, Davide Ruffoni, Bruno Grignard, and Christophe Detrembleur**

Reference: *Polym. Chem. 2022, 13, 3076-3090*

Abstract

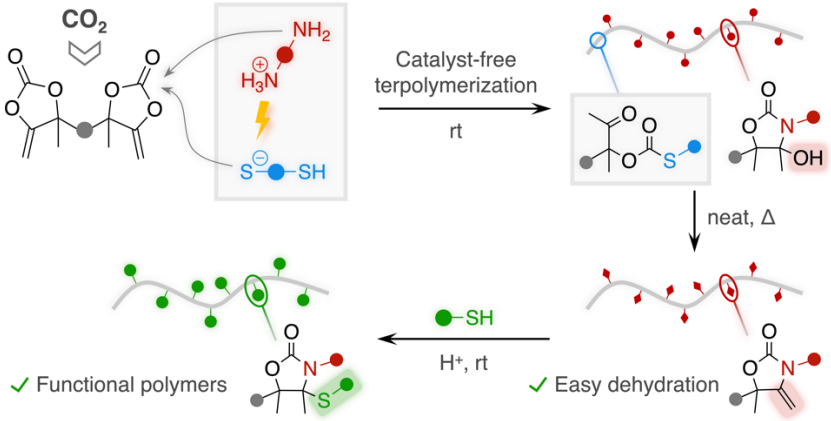

The installation of both oxazolidone and thiocarbonate linkages within a single polymer backbone remains elusive by simple procedures under mild conditions. In this work, we report the construction of copolymers containing these two linkages by the one-pot terpolymerization of diamines, dithiols and a CO2-sourced activated dicyclic carbonate of the α-alkylidene type. This process is facile and efficient with many commercially available diamine and dithiol comonomers, and occurs at room temperature under catalyst-free conditions. In contrast to polyoxazolidones that are insoluble in many organic solvents, the copolymers are highly soluble, facilitating their processing as adhesives. The polymers present an unusual thermal behavior with the presence of two glass transition temperatures. Importantly, they can undergo facile and quantitative dehydration by a simple thermal treatment at moderate temperature (110–160 °C) without using any catalyst or dehydrating agent, thereby furnishing novel polymers presenting both thiocarbonate and α-alkylidene oxazolidone linkages. The pendant double bonds are exploited for the facile thiol–ene functionalization with a scope of commercially available thiols under mild conditions. This work gives access to functional poly(monothiocarbonate)-based copolymers under mild operating conditions without requiring specific equipment.

Introduction

The valorization of sulfur for the synthesis of high-performance polymers is intensively investigated by different means, i.e. by exploiting elemental sulfur[1] obtained from petroleum refining or other sulfur-containing building blocks such as COS, CS_2 or thiol-based organic compounds (mercaptans, thioethers, thiolactones, etc.)[2,3]. Various polymeric scaffolds of different functionalities are now accessible, and present unique thermal and physical properties, generally distinct from the oxygen-based analogues (divergent thermal properties, improved refractive index, affinity to metals)[2–6]. However, the palette of available synthons and polymerization conditions to furnish these sulfur-containing polymers remains limited compared to the more conventional oxygen-based ones.

Among sulfur-based polymer families, poly(monothiocarbonate)s deserved important interest as the introduction of sulfur atom in the carbonate functionality imparts enthralling features such as excellent optical and electrical properties, biocompatibility, and appreciable binding to metal ions[7]. However, these polymers are scarcely studied and applicative examples remain rare, certainly due to the lack of facile and versatile synthetic pathways. Main routes to their production consist in the polycondensation of dithiols with bis(chloroformate)s[4,6,8] (Scheme 1A) and the ring-opening polymerization (ROP) of cyclic thiocarbonates by either cationic[9–11] or anionic pathways[12] (Scheme 1B). Although polymerizations are conducted in ambient conditions, they are both based on the use of extremely harmful reactants (phosgene/thiophosgene) and the condensation reaction requires an excess of base to neutralize the HCl condensate.

More recently, the chain-growth copolymerization of epoxides with carbonyl sulfide (COS) catalyzed by either metal catalysts[13–15] or organic Lewis pairs[16–18] emerged as a promising alternative (Scheme 1C). Defect-free poly(monothiocarbonate)s were obtained at room temperature with a nearly stoichiometric [COS]:[epoxide] ratio. Although nearly full selectivity was obtained in some conditions, the chain-growth is in competition with the formation of stable five-membered cyclic thiocarbonates through backbiting reactions[19]. This route was extended to the preparation of block copolymers using alcohol-terminated PEG prepolymers as initiating species[20]. Importantly, the terpolymerization of epoxides with both COS and CO_2 gave access to poly(thiocarbonate-*co*-carbonate)s using a dual metal-based catalytic system[21] (Scheme 1Cii). However, the polymerizations have to be conducted in a pressurized autoclave filled with COS using dry vessel/reagents as water molecules can act as initiating species. Moreover, the structural change of the polymer was mainly restricted to the choice of the epoxide.

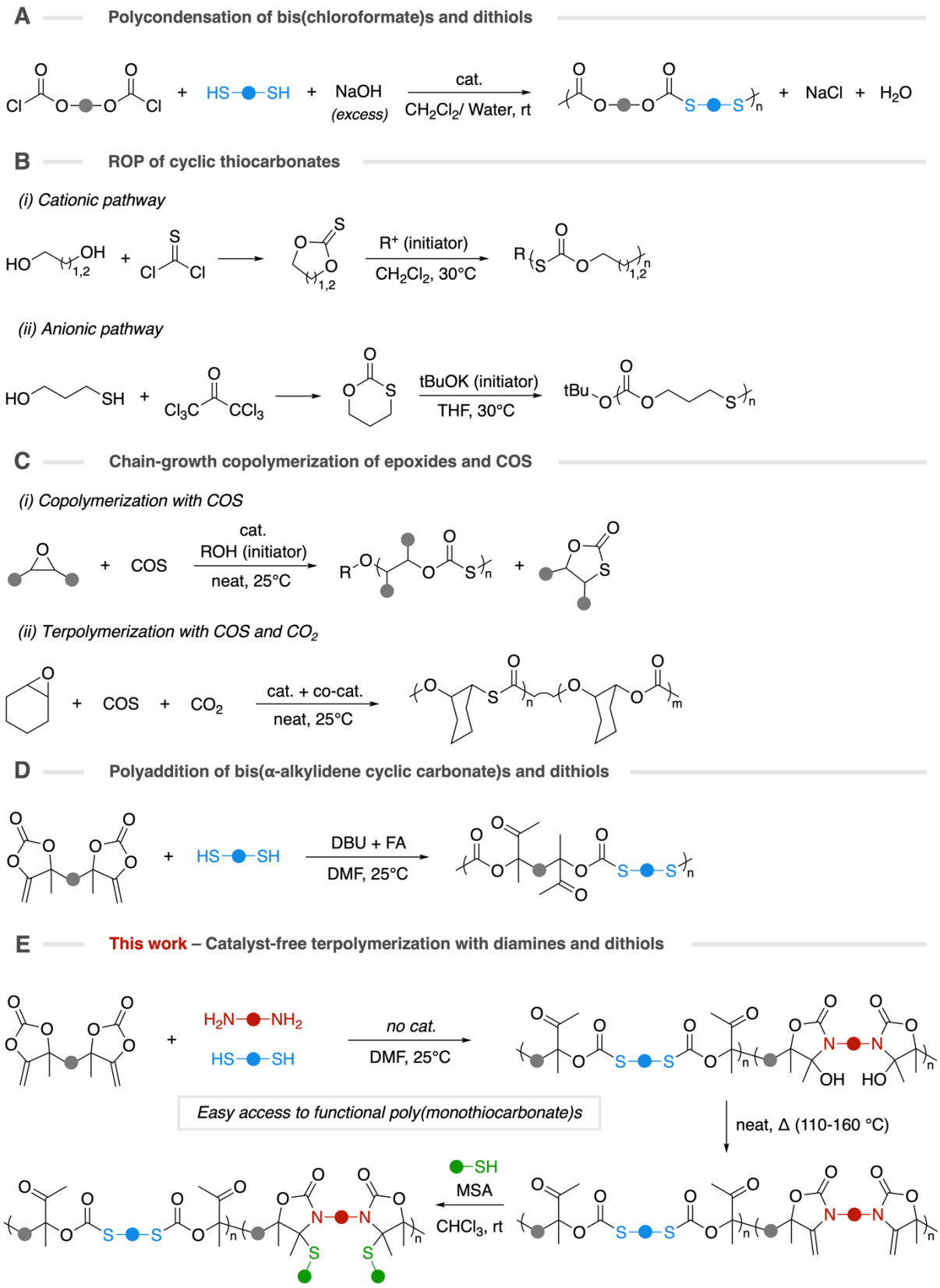

Scheme 1 – Synthetic routes toward poly(monothiocarbonate)s (A-D) and (E) terpolymerization of bisαCCs with diamines and dithiols toward functional poly(monothiocarbonate-co-oxazolidone)s.

Lately, some of us reported the organocatalyzed polyaddition of dithiols onto bis(α-alkylidene cyclic carbonate)s (bisαCCs) to furnish functional poly(monothiocarbonate)s[22] (Scheme 1D). In the presence of a binary catalytic system composed of DBU and a fluorinated alcohol, poly(monothiocarbonate)s bearing pendent ketones were obtained. Nevertheless, the polymers presented some cyclic carbonate defects (about 20 mol%) that originated from a rearrangement of the oxo-monothiocarbonate moieties. Despite the presence of these defects, the reaction proceeded under ambient conditions (room temperature, ambient atmosphere) at low catalyst loading (1 mol%). It also permitted to deliver a large diversity of poly(monothiocarbonate)s by changing the nature of the dithiol and bisαCC. When the same procedure was utilized in the presence of DBU without the fluorinated alcohol, defect-free poly(cyclic carbonate-*co*-thioether)s of much higher T_g were obtained[22,23]. Importantly, the content of monothiocarbonate in the polymer backbone was easily tuned by adapting the amount of fluorinated alcohol cocatalyst, a simple mean to design the polymer with the target T_g from an identical monomer composition.

Among the polymers accessible by the bisαCCs chemistry[22–29], poly(hydroxy-oxazolidone)s obtained by the polyaddition of di-primary amines to bisαCCs are particularly appealing due to their high chemical and thermal stability, and glass transition temperature[24,25]. They are also a source of poly(α-alkylidene-oxazolidone)s after dehydration, with pending exovinylene groups that can potentially serve for further chemical functionalization. These chemical groups are thus appealing for providing new functional poly(monothiocarbonate)-type polymers, provided that thiols and diamines can be copolymerized with bisαCCs while limiting the content of cyclic carbonate linkages.

This work describes how polymers containing both monothiocarbonate and hydroxyoxazolidone linkages can be easily constructed from readily available dithiols and diamines under ambient conditions (Scheme 1E). By studying and optimizing the reactions on model compounds, and then transposing them to polymerizations, these polymers can now be obtained without using any catalyst. We have also established conditions for quantitatively dehydrating the hydroxyoxazolidone linkages without affecting the sensitive thiocarbonate ones. The alkylidene oxazolidone groups of the dehydrated polymers were then exploited for further functionalization by the robust thiol-ene reaction. Preliminary investigations of the use of these polymers (dehydrated or not) as adhesives on aluminum substrate were then reported. Beside their complete structural characterizations by ^{1}H- and ^{13}C-NMR studies, their thermal properties were assessed by thermogravimetric analysis (TGA) and differential scanning calorimetry (DSC). This work described for the first time the construction of these types of polymers under very mild operating conditions.

Experimental section

General procedure for the synthesis of polymers without catalyst

BisαCC (508 mg, 2 mmol, 1 eq.) was added to a reaction tube together with the dithiol (1 mmol, 0.5 eq.) and DMF (1 mL). The diamine (1 mmol, 0.5 eq.) was then added and the tube was stirred at 25°C under N_2 atmosphere. After 24h, an aliquot of the crude product was taken out for SEC and ^{1}H-NMR characterizations. The polymer was purified by precipitation in diethyl ether followed by centrifugation at 10,000 rpm for 10min. The solid was then solubilized and dialyzed in THF for 24h. The polymer was precipitated in diethyl ether and the solid was recovered by filtration. The solid was washed several times with diethyl ether and was dried overnight under vacuum at 60°C.

General procedure for the synthesis of polymers with DBU

BisαCC (508 mg, 2 mmol, 1 eq.) was added to a reaction tube together with the dithiol (1 mmol, 0.5 eq.) and DMF (1 mL). The diamine (1 mmol, 0.5 eq.) and DBU (0.04 mmol, 0.02 eq.) were then added and the tube was stirred at 25°C under N_2 atmosphere. After 24h, an aliquot of the crude product was taken out for SEC and ^{1}H-NMR characterizations. Formic acid (0.2 mmol, 0.1 eq.) was added to quench the reaction (by protonation of DBU), and the mixture was stirred at 25°C for 15 minutes. The polymer was purified by precipitation in water followed by lyophilization. The solid was then solubilized in THF and the operation was repeated. The solid was then solubilized and dialyzed in THF. After 24h, the polymer was precipitated in diethyl ether and the solid was recovered by filtration. The solid was washed several times with diethyl ether and was dried overnight under vacuum at 60°C.

General procedure for the polymer dehydration

200 mg of polymer were poured in an aluminum dish and placed for 2h in a pre-heated oven at the polymer dehydration temperature (determined by TGA; dehydration temperatures of the different polymers are summarized in Table 3). The dehydration was performed under air.

General procedure for polymer functionalization

The dehydrated polymer was dissolved in 1.5 mL of $CHCl_3$ at a 0.5 M concentration of alkene functionality (0.75 mmol; 1 eq.). The thiol was then added (2.25 mmol; 3 eq.) followed by MSA (0.075 mmol; 0.1 eq.). The mixture was stirred at 25°C for 24h under air atmosphere. After

24h, the polymer was precipitated in diethyl ether, solubilized and dialyzed for 48h in $CHCl_3$. The polymer was precipitated in diethyl ether and the solid was recovered by filtration. The solid was washed several times with diethyl ether and was dried overnight under vacuum at rt.

Preparation of lap-shear samples

Aluminum (AlMg3 Dure type) substrates for lap shear testing were prepared by cutting the material into rectangular pieces of 6 cm long x 1.5 cm wide and 3 mm thick. A centered hole of 6 mm diameter was drilled into one of the two adherents at 8 mm of the length end. The surface treatment of adherents was achieved by washing and wiping with acetone. The substrate was then introduced into a basic aqueous bath (NaOH 40 g/L) for 1 minute, then introduced into an acidic aqueous bath (25 %w H_2SO_4, 2 w% $Na_2Cr_2O_7$, 73 w% water) for 1 minute. The substrate was washed with water and wiped between each step.
Galvanized steel (provided by ARCEO) substrates were prepared by cutting the material into rectangular pieces of 5 cm long x 1 cm wide and 0.18 mm thick. The surface treatment of adherents was achieved by washing and wiping with acetone and water.
PE-HD substrates (provided by Alfa Aesar) substrates were prepared by cutting the material into rectangular pieces of 5 cm long x 1 cm wide and 3.18 mm thick. The surface treatment of adherents was achieved by washing and wiping with acetone and water.
Polymer solutions in THF (0.5 g/mL) were prepared and 50 µL of the solution was placed on each adherent face. The adherents were overlapped at 1 x 1.5 cm in a lap shear configuration (Figure 8A). The substrates were let drying for 1h at rt, then 72h at 60°C, and cooled 1h at rt.

Results and discussion

We studied the terpolymerization of bisαCCs with dithiols and primary diamines. The ring-opening of the alkylidene cyclic carbonate group by the thiol was expected to provide the monothiocarbonate linkage, while the hydroxyoxazolidone one would be obtained by its ring-opening by the primary amine. As previously demonstrated, the polyaddition of primary diamines onto bisαCCs did not require a catalyst at room temperature, whereas a strong organobase (i.e. DBU) was necessary for the polymerization with dithiols. Although not applied to polymerizations, weaker bases (e.g. triethylamine, TEA) also catalyzed the ring-opening of alkylidene cyclic carbonates by a thiol to selectively deliver monothiocarbonates, however extremely slowly[22]. Capitalizing on these observations, we hypothesized that the primary diamine co-monomer (a weak base) might catalyze the addition of the dithiol to selectively provide the monothiocarbonate linkages when considering the terpolymerization. We thus first

carried out reactions on model monofunctional compounds to evaluate the feasibility of this approach under catalyst-free conditions, prior extension to polymerizations.

Model reactions

We first studied the reaction of 4,4-dimethyl-5-methylene-1,3-dioxolan-2-one (**αCC**) with a scope of different amines **A1-3** and thiols **T1-2** (Scheme 2). These monofunctional model molecules were selected to enable significant structural variations, thus facilitating some reactivity trends establishment.

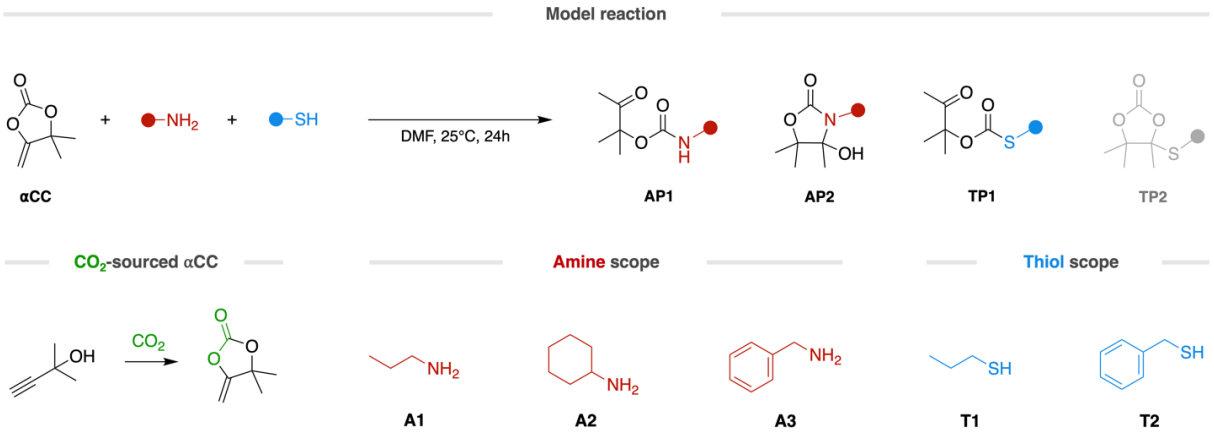

Scheme 2 – Substrate scope for the model reactions of αCC with amines and thiols.

Reaction conditions were chosen to mimic those that will be implemented in polymerizations, i.e. 2 M concentration of **αCC** in *N,N*-dimethylformamide (DMF) at 25°C. These conditions were selected as they were demonstrated to be well-suited for the polymerizations of diamines or dithiols with bisαCCs[22,25]. A [αCC]:[amine]:[thiol] ratio of 2:1:1 was selected, again to mimic the polymerization that will be carried out later, and all reactions were monitored for 24h by ^{1}H-NMR spectroscopy. Four products were expected to be produced: (1) the oxo-urethane **AP1** (by aminolysis of αCC), (2) the hydroxyoxazolidone **AP2** (by intramolecular cyclization of **AP1**), (3) the monothiocarbonate **TP1** (by ring-opening of αCC by the thiol) and (4) the tetrasubstituted cyclic carbonate **TP2** (by rearrangement of **TP1**) (Scheme 2). Results are collected in Table 1.

Remarkably, the thiols ring-opened αCCs with the selective formation of the monothiocarbonate **TP1**, demonstrating that all tested primary amines catalyzed this reaction,

and did not promote the rearrangement of **TP1** into **TP2**. The selective formation of monothiocarbonates is thus possible under these operating conditions.

In contrast, mixtures of oxo-urethane **AP1** and hydroxyoxazolidones **AP2** were collected in all cases and there was no selective formation of one of the two products. The **AP1**/**AP2** molar ratio depended on the structure of the amines, and not on the tested thiol. Reaction with benzylamine **A3** provided the best selectivity in hydroxyoxazolidone **AP2** (91%) with the two tested thiols (Table 1, entries 3 and 6).

Some rationalization of both thiolation and aminolysis of αCCs is discussed below.

Table 1 – Selected data after 24h for the catalyst-free model reaction between αCC and the different amines and thiols.[a]

Entry	Thiol	Amine	αCC conv. (%)	SH conv. (%)	NH_2 conv. (%)	Ratio AP1/AP2	Ratio TP1/TP2
1	T1	**A1**	88	74	100	55 / 45	100 / 0
2		**A2**	91	92	90	68 / 32	100 / 0
3		**A3**	76	59	93	9 / 91	100 / 0
4	T2	**A1**	93	86	100	40/ 60	100 / 0
5		**A2**	95	95	95	71 / 29	100 / 0
6		**A3**	86	73	98	9 / 91	100 / 0

[a] Conditions: [αCC]:[Amine]:[Thiol] = 2:1:1, 25°C, DMF.

Figure 1 shows the rate of consumption of the amine (**A1**-**A3**) and the thiol (**T1**) when reacted with **αCC** over a period of 24h at rt. The thiol conversion was strongly dependent on the nature of the amine. For the two tested thiols, the most sterically hindered amine (cyclohexylamine, **A2**) accelerated the consumption of the thiol that was almost complete after 1h of reaction (*vs* 68% and 48% for **A1** and **A3**, respectively). Two main factors influenced the rate of the thiol conversion: the amine basicity and its steric hindrance. As the amine plays the role of the basic catalyst for the thiolation, its activity is linked to its pKa value (higher is the pKa and higher will be its activity). Moreover, the addition rate of the amine to αCC defines the lifespan of the catalyst in the reaction medium - faster is consumed the amine and lower the concentration of the catalyst will be, and thus the thiolation rate. Consequently, the slower the amine is consumed, the longer the thiolation will be activated. Amines characterized by bulky structures and higher pKa are thus expected to be beneficial for the thiol conversion. This is clearly what is observed with cyclohexylamine **A2**, the amine with the highest pKa (pKa **A1** = 10.57, pKa **A2** = 10.64, pKa **A3** = 9.35)[30] and with the most steric hindrance. Figure 1 illustrates this synergistic effect, with the bulkier amine **A2** that added more slowly to αCC, in line with our

previous work dealing with the aminolysis of αCC. Note that when mixing both the amine **A2** and the thiol **T2** in pure form, colorless crystals were rapidly formed (Scheme 3). Their analysis by ^{1}H-NMR and IR spectroscopies revealed that they consisted in the corresponding ammonium thiolate (see ESI for details, Figures S7-8). The role of the amine was thus to generate the thiolate prone to ring open **αCC** and provide the monothiocarbonate (Scheme 3).

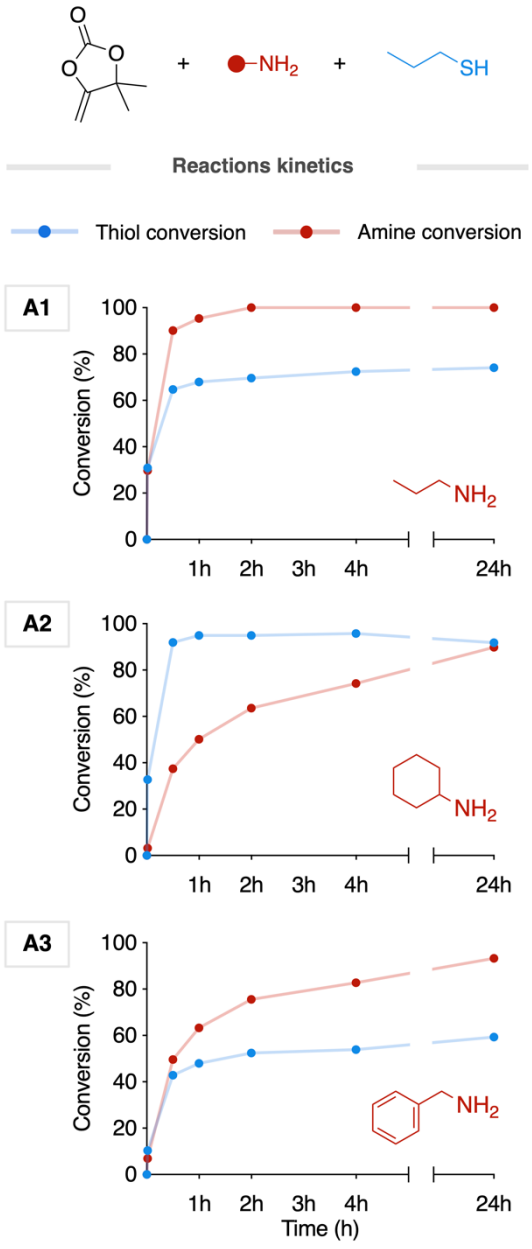

Figure 1 – Model reaction kinetic profiles for the three different amines **A1**-**3** with **αCC** and the thiol **T1**.

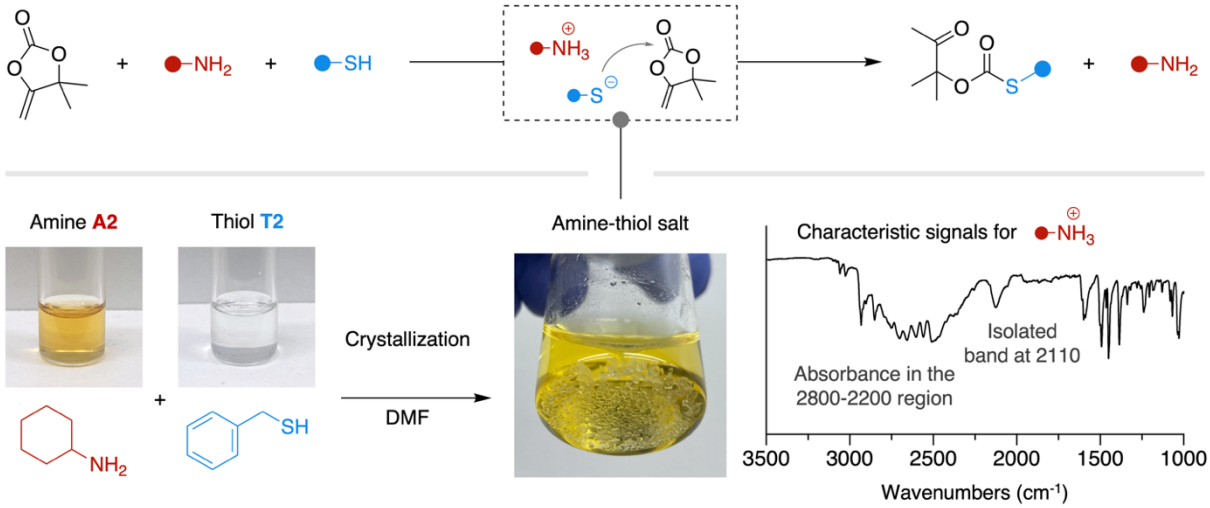

Scheme 3 – Catalytic role of the amine in generating the reactive thiolate species for the formation of the monothiocarbonate product **TP1**. When mixing the amine **A2** and the thiol **T2** in DMF, crystallization occurs. Analysis of the solid by ATR-IR spectroscopy evidences the ammonium salt nature of the product.

In line with our previous work, the aminolysis of αCCs and the intramolecular cyclization of the formed oxo-urethane into hydroxyoxazolidone were slowed down when increasing the steric hindrance of the amine[25]. This explains the lower selectivity towards the hydroxyoxazolidone when the cyclohexylamine was used (Table 1).

As the DBU-catalyzed addition of the thiol **T2** onto **αCC** was demonstrated to be very fast, quantitative and selective towards the tetrasubstituted ethylene carbonate **TP2** product in less than 2h at rt[22], we studied the same reaction in the presence of the amine **A3** ([**αCC**]/[**A3**]/[**T2**] = 2/1/1; 2 mol% DBU). Figure 2 shows that DBU strongly accelerated the conversion of the thiol. Surprisingly, the monothiocarbonate **TP1** was selectively obtained, with no trace of **TP2**. This observation is thus in sharp contrast to the reaction of **αCC** with **T2** without the amine **A3**.

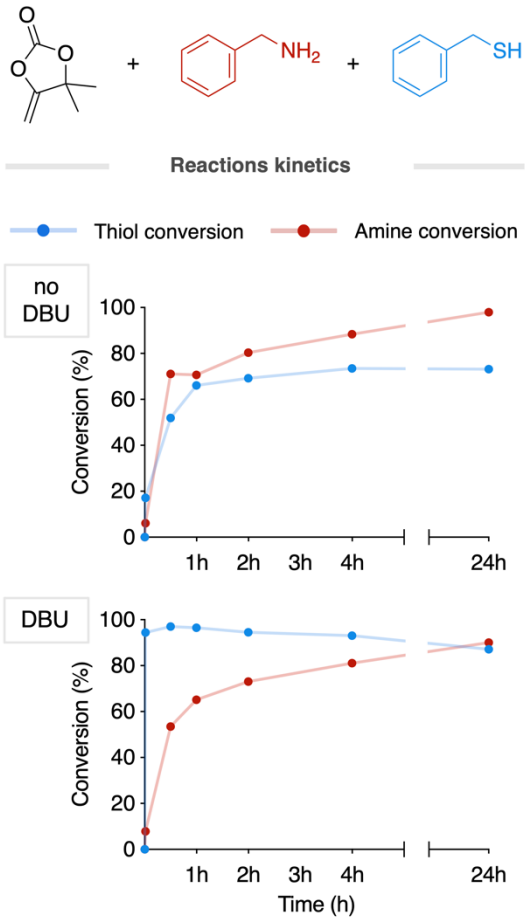

Figure 2 – Model reaction kinetic profiles for the amine **A3** and the thiol **T2** with **αCC** without and with DBU (2 mol%).

As only strong bases (e.g. DBU, MTBD, TBD) were able to catalyze the rearrangement of **TP1** into **TP2**, we hypothesized that one of the components of the reaction between αCC, the thiol and the primary amine partially deactivated DBU. Only the primary amine and the hydroxyoxazolidone **AP2** are external to the αCC-thiol chemistry. As **AP2** revealed to be a major product of the reaction, a hypothetical interaction between DBU and **AP2** was envisaged. In order to verify this hypothesis, the hydroxyoxazolidone **AP2** (synthesized from **A3**) and DBU were both mixed in different ratios in DMF-d_7 and the mixtures were analyzed by ^{1}H-NMR spectroscopy (Figure 3). When adding oxazolidone to DBU, a notable shift was observed for one DBU peak (from 2.309 to 2.335 ppm) until an equimolar 1:1 ratio. Adding more oxazolidone to reach a 0.5:1 ratio did not further shift the peak, suggesting a 1:1 association between the two molecules[31]. The oxazolidone peaks were more slightly shifted, although specific peaks were more notably impacted. In addition to the total disappearance of the sharp alcohol peak at 6.28 ppm to become a broad close-to-baseline signal, a higher peak shift (from 1.266 to 1.256 ppm) was observed for the methyl close to the alcohol function. These results evidence

an interaction between the basic site of the DBU and the alcohol moiety of the hydroxyoxazolidone. This interaction by hydrogen bonding was expected to decrease the basicity and thus the activity of DBU, which avoided the formation of **TP2**.

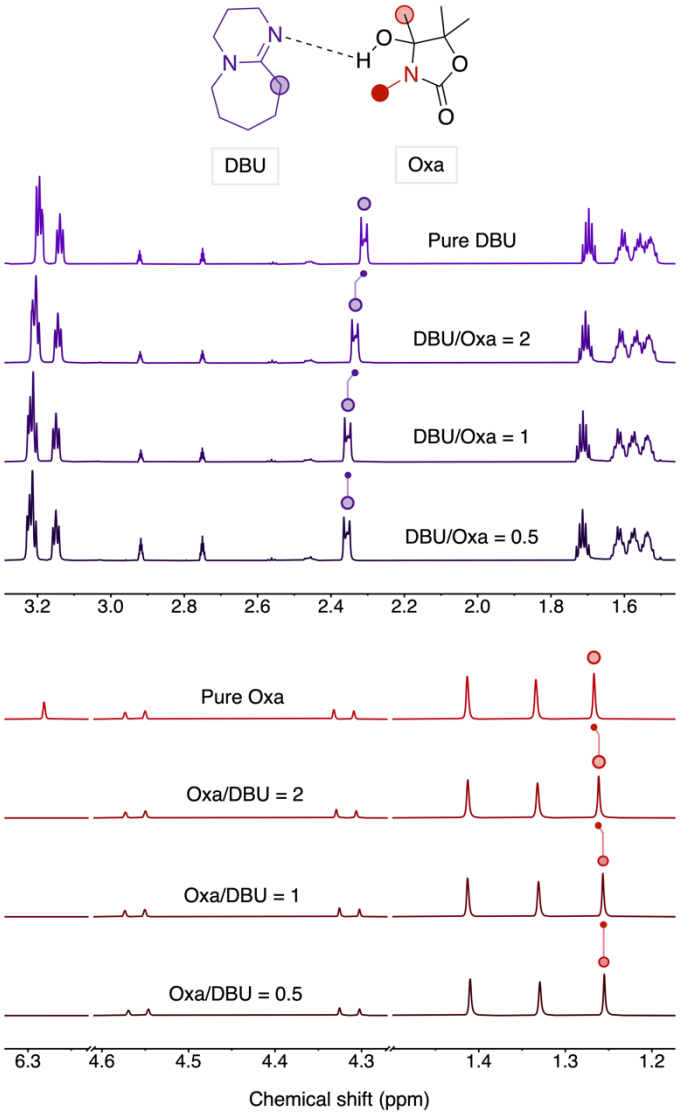

Figure 3 – ^{1}H-NMR spectra of different mixtures of the hydroxyoxazolidone **AP2** (from **A3**) with DBU in DMF-d_7. Highly shifting peaks were highlighted in the spectra and were attributed to the respective protons of both compounds.

Polymerizations

The polyadditions of bis(α-alkylidene cyclic carbonate) (**bisαCC**) to a series of diamines **AA1-3** and dithiols **TT1-2** having similar molecular structures to model compounds were then investigated (Scheme 4). Polymerizations were conducted at 25°C for 24h in DMF. The

[bisαCC]:[diamine]:[dithiol] ratio was kept constant at 2:1:1. Although the polymerizations were carried out under nitrogen atmosphere, similar results were obtained under air, illustrating that they were not sensitive to air moisture nor oxygen. The chemical structure of the polymers was fully characterized by ^{1}H- and ^{13}C-NMR spectroscopies, and all spectra and peak assignments are provided in supporting information. The types of linkage were analyzed and quantified, and results are provided in Table 2. Figure 4 illustrates representative ^{1}H-NMR spectra of the so-formed polymers with the main linkages assignments.

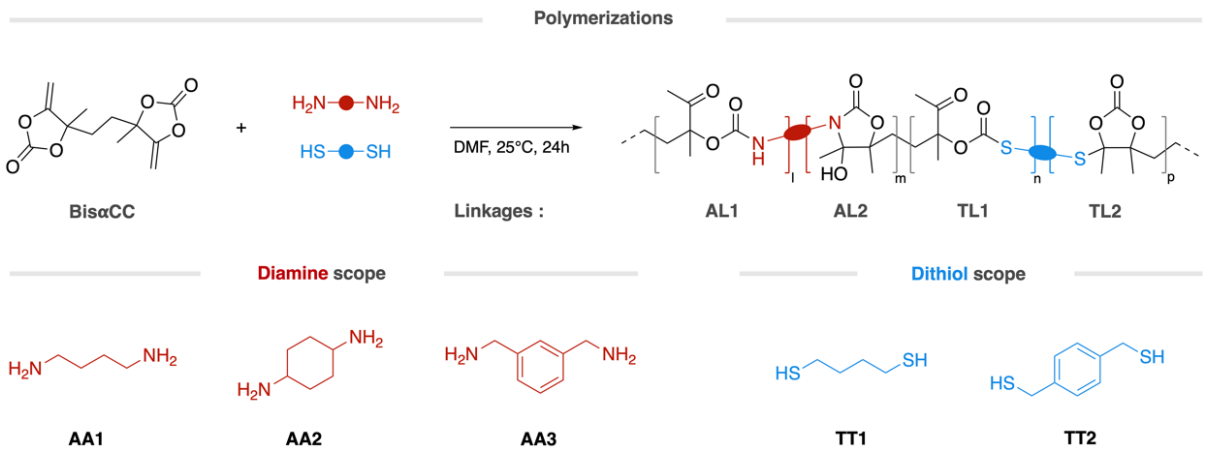

Scheme 4 – Substrate scope for the polymerization of bisαCC with diamines and dithiols, associated linkages and polymer microstructure.

Table 2 – Molecular characteristics and linkages selectivity for the polymers obtained after 24h of reaction. Polymerizations were carried out at 25 °C in DMF.

Entry	Polymer	Diamine	Dithiol	Cat.[a]	M_n (g/mol)[b]	M_w (g/mol)[b]	D[b]	Ratio AL1/AL2[c]	Ratio TL1/TL2[c]
1	P(A1T1)	AA1	TT1	--	3500	6100	1.76	16 / 84	100 / 0
2	P(A1T1)C			DBU	12900	24500	1.89	0 / 100	88 / 12
3	P(A1T2)		TT2	--	5400	11400	2.11	11 / 89	92 / 8
4	P(A2T1)	AA2	TT1	--	9900	16300	1.54	55 /45	100 / 0
5	P(A2T1)C			DBU	9700	16100	1.65	23 / 77	86 / 14
6	P(A2T2)		TT2	--	8900	14500	1.64	67 / 33	92 / 8
7	P(A3T1)	AA3	TT1	--	3400	5600	1.64	0 / 100	100 / 0
8	P(A3T1)C			DBU	10200	16800	1.65	0 / 100	92 / 8
9	P(A3T2)		TT2	--	4700	9100	1.93	0 / 100	92 / 8

[a] 2 mol% DBU *vs* bisαCC.

[b] determined on the crude product by SEC in DMF/LiBr by using a PS calibration.

[c] linkage ratios determined by ^{1}H-NMR in DMSO-d_6 of the pure products.

In the absence of DBU, the aliphatic **AA1** and benzylic **AA3** diamines delivered the lower molar mass scaffolds owing to the slow thiol **TT1** addition (Table 2, entries 1 and 7), in line with the model reactions. Higher molar mass polymers were obtained using the benzylic dithiol **TT2** with the same diamines (Table 2, entries 3 and 9). In agreement with the model reactions showing faster reactions when a cycloaliphatic amine was used, the cycloaliphatic diamine **AA2** delivered polymeric scaffolds of significantly higher molar mass (M_w of 16300 and 14500 g/mol with **TT1** and **TT2** respectively) (Table 2, entries 4 and 6).

The polymers were characterized by oxo-urethane/hydroxyoxazolidone (**AL1/AL2**) linkages ratios that follow the trends observed on the model compounds. A high hydroxyoxazolidone linkage content was obtained using the aliphatic diamine **AA1** (84 and 89% using dithiols **TT1** and **TT2**, respectively) (Table 2, entries 1 and 3). The cycloaliphatic diamine **AA2** provided polymers with lower hydroxyoxazolidone content (45 and 33% using dithiols **TT1** and **TT2**, respectively) (Table 2, entries 4 and 6). Remarkably, the benzylic diamine **AA3** delivered chains comprising exclusive hydroxyoxazolidone linkages **AL2** (Table 2, entries 7 and 9). Figure 4 shows the ^{1}H NMR spectra of pure polymers obtained by the catalyst-free terpolymerization using the three different diamines and the dithiol **TT1**. The typical resonances of the linear urethane NH (at 7.3 ppm) and its ketone methyl group (at 2.0 ppm) are clearly observed for polymers from diamines **AA1** and **AA2**. Polymers from **AA3** only display the characteristic hydroxyoxazolidone OH signal (at 6.0 ppm), confirming the quantitative cyclization of oxo-urethane **AL1**. For all three polymers, only the signals characteristic of the monothiocarbonate from **TT1** are observed (S-$\underline{CH_2}$-CH_2 at 2.8 ppm and the ketone CH_3 at 2.2 ppm). All polymerizations delivered chains with a total oxo-thiocarbonate linkage **TL1** selectivity using dithiol **TT1**. This selectivity remains high (92%), however slightly lower when using benzylic dithiol **TT2** (Table 2, entries 3, 6 and 9). All polymers were soluble in DMF, DMSO, THF, acetone, and some of them in $CHCl_3$ (Table S1).

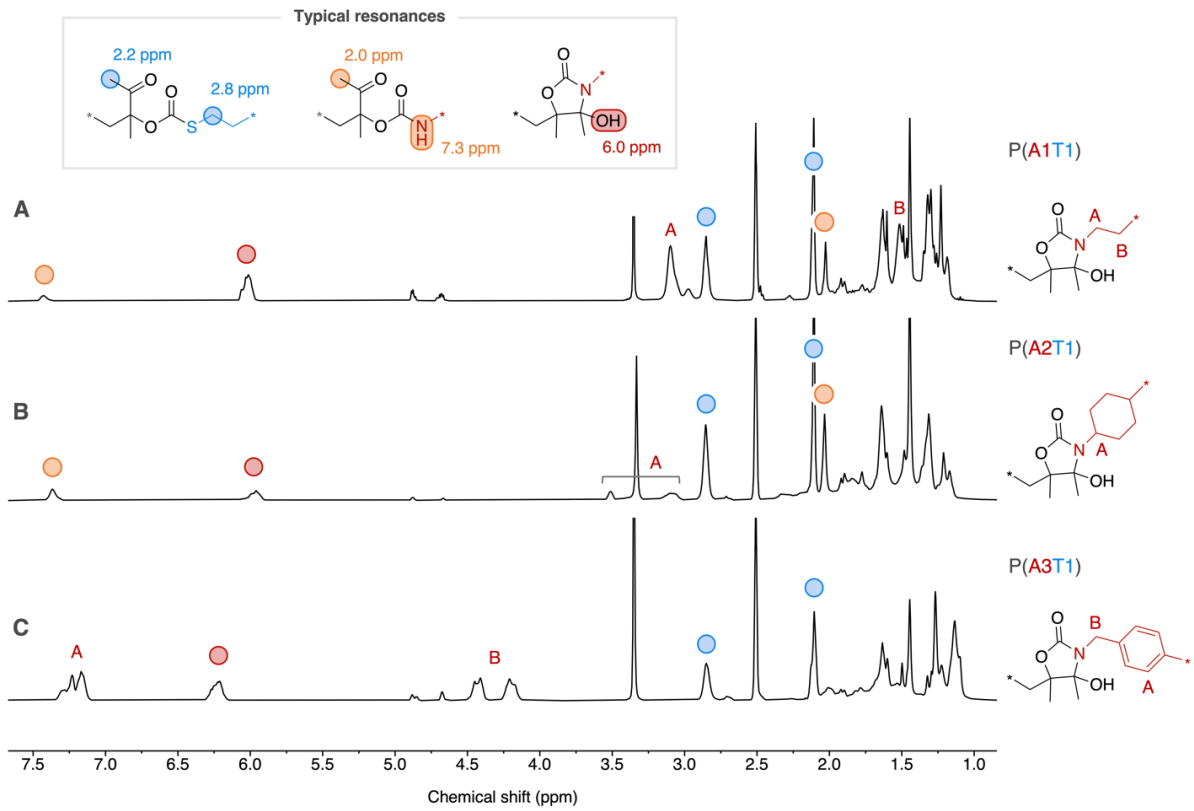

Figure 4 – Stacked ^{1}H NMR spectra in DMSO-d_6 of pure (A) P(A1T1), (B) P(A2T1), (C) P(A3T1) (full peaks assignments are provided in ESI).

When the polymerizations with **TT1** were carried out in the presence of DBU **(**2 mol% *vs* bisαCC), higher molar masses were obtained when using **AA1** or **AA3**, as DBU accelerated both the thiolation and aminolysis (Table 2, entries 2 and 8). The DBU-promoted polymerization with **AA2** did not further increase the molar mass as the catalyst-free reaction was already providing appreciable polymer lengths (Table 2, comparison entries 4 and 5). The addition of DBU accelerated the oxo-urethane cyclization rate and an exclusive hydroxyoxazolidone linkage **AL2** was embedded within the polymer chain from **AA1**. Polymer from **AA2** showed a notable increase of linkage cyclization from 45 to 77%. In contrast to model reactions, the presence of DBU slightly increased the content of tetrasubstituted ethylene carbonate **TL2** (12-14%).

By changing the content of DBU, we were able to finely tune the polymer microstructure, more particularly the type of linkages **TL1** and **TL2**. This is exemplified by increasing the content of DBU for the **bisαCC/AA1/TT1** terpolymerization. Figure 5 shows that the tetrasubstituted cyclic carbonate **TL2** linkage content presented a linear relationship with the DBU content, from about 10% with 2.5 mol% DBU to about 50% with 10 mol%. This plot is therefore a guide to construct the polymer with the desired linkage type and content.

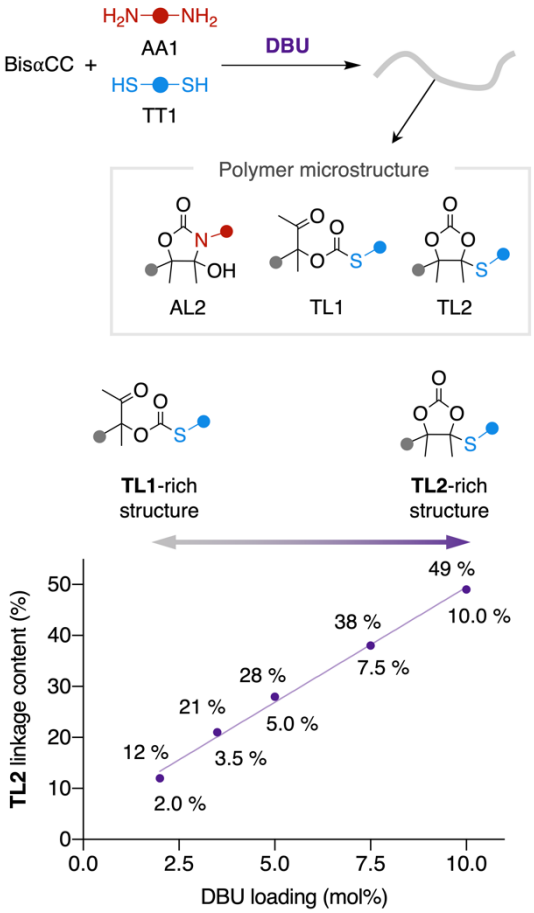

Figure 5 – Linear relationship between the DBU loading and the amount of **TL2** linkage within the polymer backbone (more details are provided in ESI, Figures S55-56 & Table S2).

Thermal properties of the polymers

In contrast to previously synthesized poly(hydroxyoxazolidone)s displaying insolubility in many solvents, the herein synthesized polymers have shown increased solubility and could thus be properly purified from residual solvent and reagents. Hence, their thermal properties could be accurately determined.

The thermal degradation temperature of the polymers was first determined through thermogravimetric analysis (TGA). All thermograms presented a similar and well-defined 3-steps degradation pattern (Figure 6A). The first mass loss is attributed to the hydroxyoxazolidone dehydration, affording a new polymer with exovinylene functionalities, followed by the degradation of the polymer backbone. As the first step of the mass loss sequence accounts for a polymer metamorphosis, the temperature at 10% of degradation ($T_{deg,10\%}$) was determined after this first step and has shown to be around 270°C for all scaffolds

(Table 3). However, the dehydration step was shifting in temperature depending on the polymer structure. In order to reach a higher accuracy for determining the dehydration temperature, TGA analyses were performed at a lower heating rate (2 K/min instead of 20 K/min). The dehydration temperature was then determined as the beginning of the mass loss peak observed in derivative thermogravimetry (DTG) plot (Figure 6B). The dehydration temperature seemed mainly governed by the steric hindrance of the diamine monomer. Polymers prepared from **AA1** were characterized by dehydration temperatures in the 110-120°C range while those obtained from bulkier **AA3** and **AA2** led to a dehydration temperature ranging from 130-145 and 145-160°C, respectively.

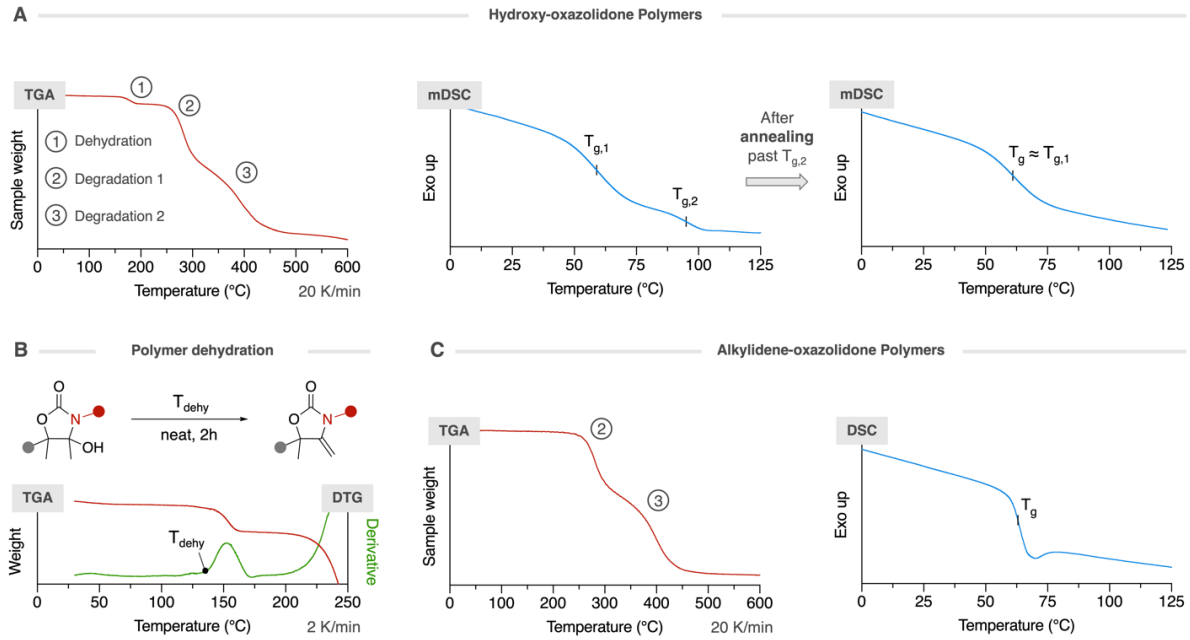

Figure 6 – (A) TGA and mDSC patterns for the hydroxyoxazolidone-containing polymers. The mDSC pattern is also displayed after polymer annealing. (B) Dehydration of the hydroxyoxazolidone-containing polymer. The TGA at slow heating rate (2 K/min) and its derivative (DTG) are both displayed for the hydroxyoxazolidone-containing polymer. The dehydration temperature T_{dehy} is determined as the start of the mass loss peak in DTG. (C) TGA and DSC patterns for the alkylidene oxazolidone-containing polymers.

Table 3 – Thermal properties of pure polymers and their dehydrated homologs.

	Hydroxyoxazolidone-containing polymers					Dehydrated polymers	
Entry	Polymer	T_{dehy} (°C)[a]	$T_{deg,10\%}$ (°C)[a]	$T_{g,1}$ (°C)[b]	$T_{g,2}$ (°C)[b]	$T_{deg,10\%}$ (°C)	T_g (°C)[b]
1	P(A1T1)	110	274	47	--[c]	272	51
2	P(A1T1)C	120	270	54	97	270	55
3	P(A1T2)	120	272	59	95	268	63
4	P(A2T1)	160	270	68	129	268	68
5	P(A2T1)C	145	270	69	114	270	74
6	P(A2T2)	160	267	84	125	268	88
7	P(A3T1)	130	277	65	96	276	68
8	P(A3T1)C	140	273	66	121	272	62
9	P(A3T2)	145	275	87	124	274	81

[a]The dehydration and degradation temperatures were determined by TGA. All TGA thermograms and DSC scans are provided in ESI. [b]Glass transition temperatures were determined by modulated DSC for the hydroxyoxazolidone-containing polymers (using the reversing heat flow curve) and by DSC for the dehydrated ones. [c] $T_{g,2}$ could not be determined due to overlapping with dehydration event.

Afterwards, the polymers were characterized by modulated DSC (mDSC) experiments to determine the polymers T_g's. Surprisingly, all polymers were characterized by two broad and weak T_g's (Figures S45-S54). Both seemed to be tightly correlated to the steric hindrance of the monomers. The first $T_{g,1}$ was the lowest for polymers prepared from the less hindered diamine, thus for polymers P(A1T1) and P(A1T1)C ($T_{g,1}$ = 47-54 °C, see Table 3, entries 1-2). Using more hindered diamines or dithiols had both the effect of increasing $T_{g,1}$ up to 87 °C (Table 3, entries 6 and 9). The second $T_{g,2}$ seemed to be more impacted by the polymer molar mass as that of P(A3T1) has shown to be drastically lower than T(A3T1)C despite their very similar chemical structure (96 and 121°C, respectively; Table 3, entries 7 and 8). $T_{g,2}$ could not be determined for P(A1T1) due to the overlap with the dehydration event and the second hypothetical transition located in the same temperature range (Figure S46).

The occurrence of two distinct T_g's is unusual for such polymers as this behavior is expected for blends or segregated block-copolymers. To shed light on this intriguing result, additional mDSC experiments were conducted (see ESI for more details). The investigation indicated that the second T_g is an irreversible event and annealing the polymer above this temperature provides a material characterized by a single T_g corresponding to $T_{g,1}$ of the starting material. The post-annealing chemical structure integrity was maintained as determined by ^{1}H-NMR. This polymer behavior shows similarities with the one of poly(acrylonitrile) (PAN), whose

thermal properties are still under debate and are characterized by two distinct T_g's too[32,33]. The annealing above the second T_g of PAN also provided a single-T_g material, without any modification of its chemical structure. Based on these works on PAN, we hypothesized the presence of a minor secondary glassy phase within the main glassy matrix, where both phases were characterized by a different T_g. However, a deeper study of this unusual thermal behavior must be conducted in order to fully understand the origin of this two secondary transitions pattern, which is out of scope of this work. The presence of these two T_g's is in sharp contrast with the thermal behavior of previously studied monothiocarbonate-rich polymers that were characterized by a single T_g[22]. By incorporating hydroxyoxazolidone units within the monothiocarbonate-rich polymer chains, a second T_g at higher value was thus observed, suggesting that the hydroxyoxazolidone linkages restricted the chain mobility by increasing the chain rigidity and by the presence of hydrogen bounding.

Polymer dehydration

Our previous work on poly(hydroxyoxazolidone)s has shown that they could be quantitatively dehydrated into poly(alkylidene oxazolidone)s by refluxing them in acetic acid for 2h[25]. However, adapting this procedure to the present copolymers, that contain both hydroxyoxazolidone and monothiocarbonate linkages, is inappropriate due to the sensitivity of the thiocarbonate linkage to these operating conditions. As we attributed the first mass loss observed in TGA to the polymer dehydration, we thus performed a simple thermal annealing at this dehydration temperature to provide the new exovinylene-bearing polymers (Figure 6B). This procedure was easy to implement on the neat material and did not require further purification steps, in contrast to the previous procedure dealing with acetic acid as dehydrating agent. Hence, all polymers were treated for 2h at their dehydration temperature under air atmosphere and a quantitative dehydration was obtained for all scaffolds. This was confirmed by ^{1}H-NMR analysis that showed a total disappearance of the characteristic tertiary alcohol proton resonance (δ = 6-6.25 ppm) and the appearance of olefinic signals (δ = 4.10-4.30 ppm) (Figure 7A-B). Comparison of integrals of the signal characteristic of these olefinic protons to those corresponding to the polymer chains at 4.6 ppm (assigned to the methylene benzylic protons N-$\underline{CH_2}$-C_6H_4-) or 7.25 ppm (assigned to the aromatic protons) also confirmed the complete dehydration of the polymer. It is worth noting that dehydration through this thermal treatment was selective toward α-alkylidene oxazolidone linkages while the previous chemical process furnished a mixture of α- and β-alkylidene oxazolidone linkages when unhindered diamines were used. These experiments further confirm that the first mass loss observed by

TGA for the hydroxyoxazolidone-containing polymers (Figure 6A & Table 3) corresponded to their dehydration.

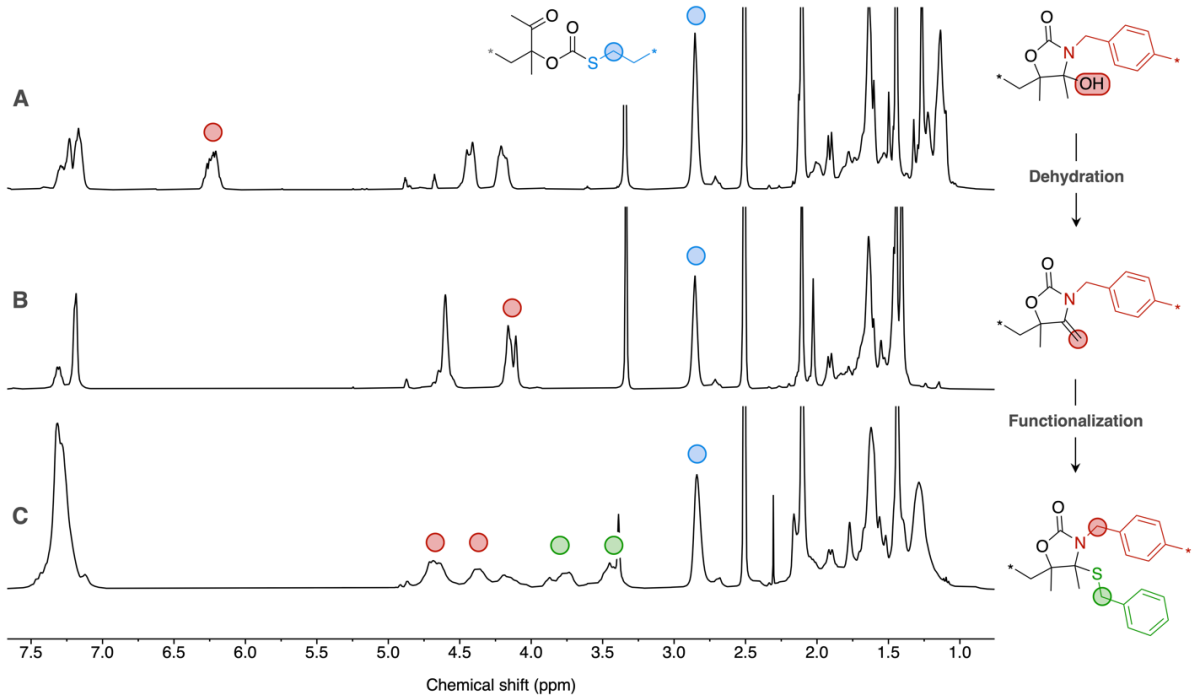

Figure 7 – Stacked ^{1}H-NMR spectra in DMSO-d_6 of (A) pure P(A3T1)C, (B) dehydrated polymer, (C) polymer functionalized with benzyl mercaptan (full peaks assignments are provided in ESI).

The thermal properties of these polymers were studied by TGA (Figures S84-92) and DSC (Figures S93-101) experiments, and data are summarized in Table 3. The degradation follows a 2-steps pattern along temperature corresponding to the two last steps observed in hydroxyoxazolidone-containing polymers and the temperature at 10% of degradation was determined at around 270°C for all scaffolds. These polymers were characterized by a single T_g whose value is yet similar to the first T_g of the hydroxyoxazolidone-containing polymers (Figure 6C).

Polymer functionalization

The presence of olefin groups in polymers is highly attractive as these groups are known to be easily functionalizable. Among the available palette of reactions, the thiol-ene reaction is a key reaction for polymer functionalization as its high rate, selectivity and versatility often categorize it as a click reaction. Different mechanistic routes are involved depending on the alkene and

reagents involved. The most studied pathways are the radical and the anionic routes, both leading to the anti-Markovnikov addition product. A less studied but yet interesting route is the cationic thiol-ene reaction leading to the Markovnikov product[34]. The latter reaction proceeds under mild conditions in the presence of an acid catalyst, which proton can be abstracted by an electron-rich alkene, followed by the nucleophilic addition of the thiol onto the carbocation intermediate. To our knowledge, there is no example of thiol-ene modified alkylidene oxazolidone yet. As these compounds are characterized by an electron-rich nitrogen group in α-position of the olefin, we envisioned that they might be adequate substrates for undergoing the cationic pathway, leading to the formation of elusive tetrasubstituted oxazolidones bearing a thioether bond (Scheme 5A).

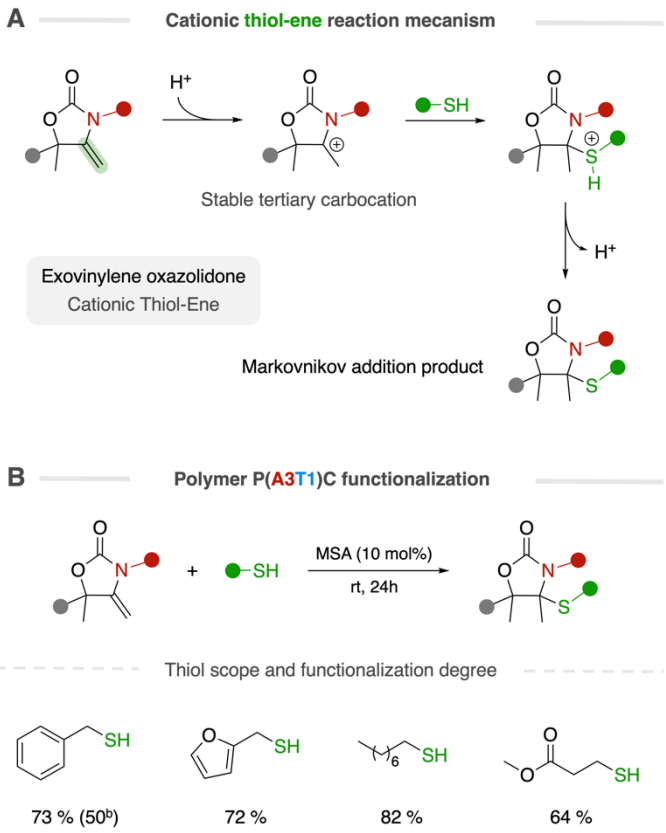

Scheme 5 – (A) Reaction mechanism for the cationic thiol-ene on α-alkylidene oxazolidone to provide tetrasubstituted oxazolidones. (B) Functionalization of P(A3T1C) using 4 different thiols[a] and the obtained functionalization degree.

[a] Conditions: [alkene] = 0.5 M in chloroform, MSA 10 mol%, rt, 24h.

[b] With MSA 5 mol%.

The polymer P(A3T1)C post-dehydration (Table 3, entry 8) was selected as a representative material for the functionalization experiments (Scheme 5B). The functionalization was first

carried out with benzyl mercaptan and methane sulfonic acid (MSA; 5 mol%) as the catalyst, providing a functionalization degree of 50% after 24h at rt. By increasing the catalyst loading to 10 mol%, this functionalization degree was raised to 73%. The Markovnikov product was confirmed by ^{1}H-NMR analysis with the consumption of the olefinic protons (at 4.14 ppm), the splitting of the amine benzylic protons (N-$\underline{CH_2}$-C_6H_4-; 4.67 and 4.37 ppm) and the appearance of the thioether functionality (S-$\underline{CH_2}$-C_6H_5; 3.77 and 3.45 ppm) (Figure 7B-C). These assignments were confirmed by HSQC and HMBC analyses (Figure S104-105). The functionalization was successfully extended to furanmethanethiol, n-octanethiol and methyl 3-mercaptopropionate with a functionalization degree of 72 %, 82% and 64 %, respectively. These experiments highlight the facile functionalization of α-alkylidene oxazolidone moieties under mild conditions, opening new opportunities to easily deliver a broad scope of functionalities to the polymer backbone.

Adhesion properties

As one of the important applications of polyurethanes are as adhesives[35], and because our polymers belong to a special variant of polyurethanes, we investigated their potential to glue aluminum substrates in this preliminary study. To this end, a solution of the polymers in THF was casted onto cleaned aluminum plates, and the assembly was dried at 60°C for 3 days to remove the solvent without dehydrating the hydroxyoxazolidone moieties. The adhesion performance of the samples was then evaluated by lap-shear experiments (Figure 8A) and the lap shear strength of all samples is summarized in Table 4.

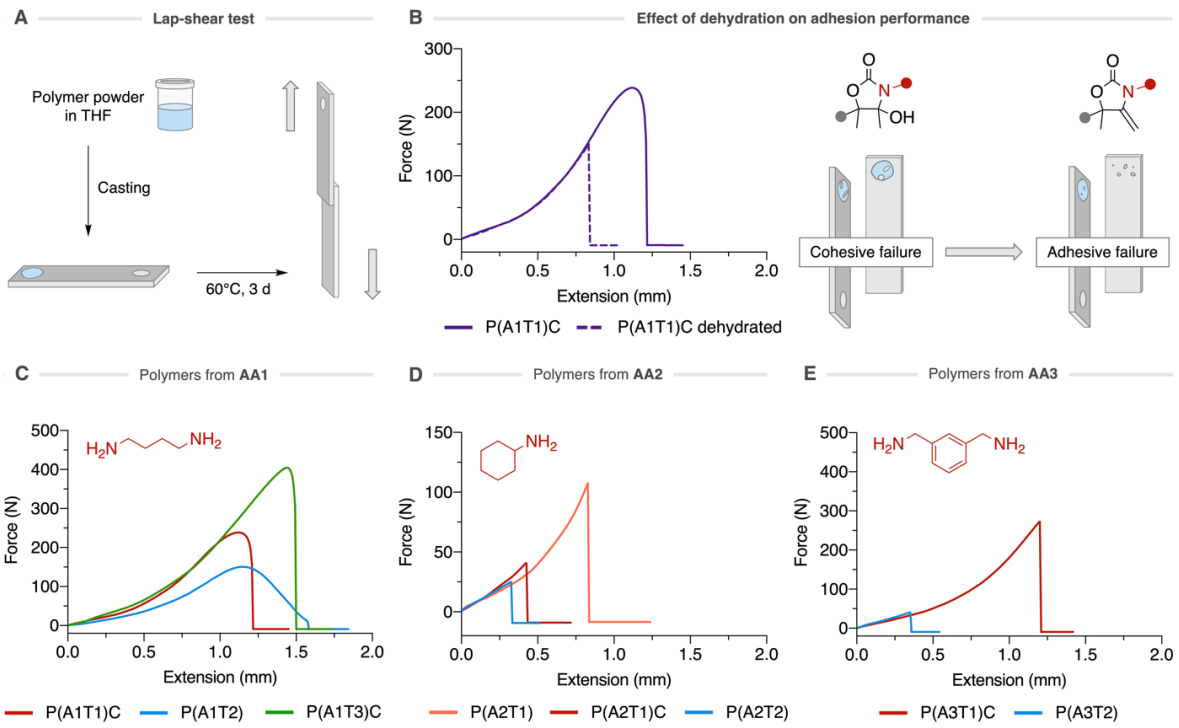

Figure 8 – (A) Schematic representation of the adhesive specimens preparation. (B) Force-extension plot for P(A1T1)C before and after dehydration. Schematic representation of the failure for both samples. (C-E) Force-extension plots for polymers made from diamines **AA1**, **AA2**, and **AA3** respectively.

Table 4 – Calculated lap-shear strengths for the polymer adhesives.

Entry	Polymer	Lap-shear strength (MPa)
1	P(A1T1)C	1.5 ± 0.1
2	P(A1T2)	1.1 ± 0.3
3	P(A2T1)	0.7 ± 0.1
4	P(A2T1)C	0.3 ± 0.1
5	P(A2T2)	0.2 ± 0.1
6	P(A3T1)C	1.8 ± 0.2
7	P(A3T2)	0.3 ± 0.1
8	P(A1T3)C	2.7 ± 0.2

As expected, polymers from the rigid **AA2** monomer yielded brittle materials that did not overpass a lap shear strength of 0.7 MPa (Table 4, entries 3-5). The best results were achieved with more flexible polymers, thus for P(A1T1)C and P(A3T1)C, with lap shear strengths of 1.5 and 1.8 MPa, respectively (Table 6, entries 1 and 6). All failures were cohesive, with both surfaces remaining covered by the adhesive, meaning that the adhesion strength of the

polymers to the substrate was underestimated. The influence of the dehydration of the polymer on the adhesive properties was also assessed. P(A1T1)C was deposited on the aluminum substrate, and once the two substrates were glued together, the polymer was dehydrated for 2h at 120°C. The lap shear strength measurement however showed that the performance of the adhesive was decreased (Figure 8B) with an adhesive failure at 1.1 MPa. This adhesive failure suggests that the loss of the hydroxyl functions was detrimental to the adhesion of the material to the substrate.

In order to further develop the potential of these adhesives, we prepared an additional polymer of reasonable molar mass (M_w = 22700 g/mol) by copolymerizing bisαCC with a mixture of flexible amine (**AA1**) and thiol (**TT3**) (Scheme 6). The macromolecular characteristics and the T_g of the polymer are summarized in Scheme 6. The lap shear strength of this polymer (applied to the aluminum substrate following an identical protocol as above) was significantly higher, i.e. 2.7 MPa (Table 4, entry 8) with an adhesive failure. When tested on galvanized steel and on high density polyethylene (HDPE), this polymer provided lower lap shear strength values of 0.7 (± 0.1) and 0.3 (± 0.1) MPa, respectively, with an adhesive failure in both cases. Although these two values are rather low, there is room to optimize them by modulating the structure and functionality of the polymers. However, this optimization is out of scope of this paper.

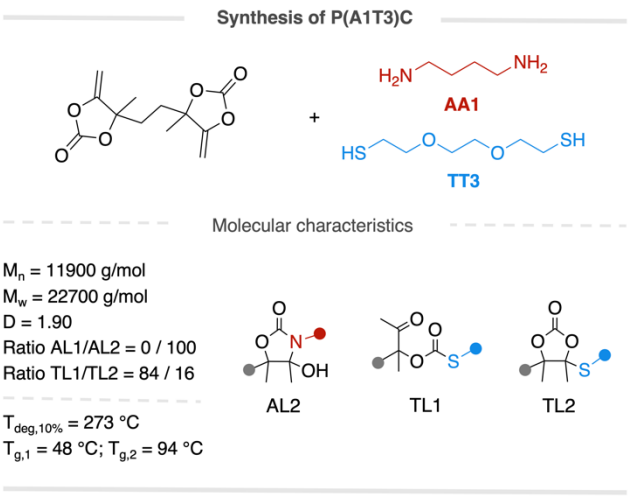

Scheme 6: Synthesis of P(A1T3)C and its molecular characteristics. Full characterization is provided in ESI.

Conclusion

This work reported the facile terpolymerization of CO_2-based activated bis(cyclic carbonate)s with dithiols and di-primary amines, to furnish polymers containing both monothiocarbonate (by thiolation of the cyclic carbonate) and hydroxyoxazolidone (by aminolysis of the cyclic carbonate) linkages. The main objective was to give access to functional poly(monothiocarbonate)-type copolymers under mild conditions. Importantly, the polymerizations proceeded under ambient conditions (room temperature, ambient atmosphere) without requiring any external catalyst. The diamine had a dual role: acting as the comonomer and as catalyst for the thiolation of the cyclic carbonate as demonstrated for model reactions. Bulky cycloaliphatic diamine provided faster polymerizations compared to less basic or unhindered diamines. The addition of a strong organobase (DBU) in low amount (2 mol%) enabled to furnish polymers of higher molar mass as the polymerizations were accelerated, however at the expense of a decrease in selectivity in monothiocarbonate linkage. Importantly, by tuning the DBU content from 0 to 10 mol%, the content of monothiocarbonate linkages were tuned in a linear fashion from 100% to 50%, and inversely from 0% to 50% in tetrasubstituted cyclic carbonate linkages.

The polymers presented unusual thermal properties with the presence of two T_g's, one between 50-85 °C and the second one, in the 95-130 °C range. All polymers presented a 3-steps degradation pattern that started by a loss of water and degradation temperatures were around 270 °C. The quantitative dehydration of all polymers was easily achieved by a thermal treatment of the neat polymer at its dehydration temperature for 2h, affording new α-alkylidene oxazolidone-functionalized copolymers that did not require any purification step. They were characterized by T_g values similar to the first transition of the hydroxyoxazolidone-containing polymers and a degradation temperature similar to these hydroxy-containing scaffolds. The olefins were exploited for functionalization by the cationic thiol-ene reaction with diversified thiols, yielding poly(monothiocarbonate)s bearing tetrasubstituted oxazolidones bearing thioether pendants with a functionalization degree up to 84% at room temperature.

All polymers prepared in this paper were soluble in many organic solvents. Some of them were evaluated as adhesives for aluminum substrates with promising adhesion performance. Lower values were noted on galvanized steel and HDPE for the preliminary tests. The range of possible structure and functionality variations of the polymers is large (structure of the amine, thiol, cyclic carbonate, post-polymerization modification by thiol-ene), such that the performance of the materials might be further optimized.

This work thus illustrates how functional poly(monothiocarbonate)s can be easily obtained under ambient conditions from a simple chemistry that does not require specific equipments.

References

(1) Lee, T.; Dirlam, P. T.; Njardarson, J. T.; Glass, R. S.; Pyun, J. Polymerizations with Elemental Sulfur: From Petroleum Refining to Polymeric Materials. *J. Am. Chem. Soc.* **2022**, *144* (1), 5–22. https://doi.org/10.1021/jacs.1c09329.

(2) Mutlu, H.; Ceper, E. B.; Li, X.; Yang, J.; Dong, W.; Ozmen, M. M.; Theato, P. Sulfur Chemistry in Polymer and Materials Science. *Macromol. Rapid Commun.* **2019**, *40* (1), 1800650. https://doi.org/10.1002/marc.201800650.

(3) Kausar, A.; Zulfiqar, S.; Sarwar, M. I. Recent Developments in Sulfur-Containing Polymers. *Polymer Reviews* **2014**, *54* (2), 185–267. https://doi.org/10.1080/15583724.2013.863209.

(4) Berti, C.; Marianucci, E.; Pilati, F. Sulfur Containing Polymers: 1. Copolymers of 1,3-Benzeneditiol with Phosgene and Bisphenol-A. *Polymer Bulletin* **1985**, *14* (1), 85–91. https://doi.org/10.1007/BF00254920.

(5) Yue, T.-J.; Wang, L.-Y.; Ren, W.-M. The Synthesis of Degradable Sulfur-Containing Polymers: Precise Control of Structure and Stereochemistry. *Polym. Chem.* **2021**, *12* (46), 6650–6666. https://doi.org/10.1039/D1PY01065D.

(6) Marianucci, E.; Berti, C.; Pilati, F.; Manaresi, P.; Guaita, M.; Chiantore, O. Refractive Index of Poly(Thiocarbonate)s and Poly(Dithiocarbonate)s. *Polymer* **1994**, *35* (7), 1564–1566. https://doi.org/10.1016/0032-3861(94)90361-1.

(7) Luo, M.; Zhang, X.-H.; Darensbourg, D. J. Poly(Monothiocarbonate)s from the Alternating and Regioselective Copolymerization of Carbonyl Sulfide with Epoxides. *Acc. Chem. Res.* **2016**, *49* (10), 2209–2219. https://doi.org/10.1021/acs.accounts.6b00345.

(8) Pilati, F.; Berti, C.; Marianucci, E. Sulfur-Containing Polymers: Thermal Behavior of Copolymers Containing Thiocarbonate Groups. *Polymer Degradation and Stability* **1987**, *18* (1), 63–72. https://doi.org/10.1016/0141-3910(87)90083-8.

(9) Kameshima, H.; Nemoto, N.; Sanda, F.; Endo, T. Cationic Ring-Opening Polymerization of Five-Membered Cyclic Thiocarbonate Bearing an Adamantane Moiety via Selective Ring-Opening Direction. *Macromolecules* **2002**, *35* (15), 5769–5773. https://doi.org/10.1021/ma012094i.

(10) Endo, T.; Nemoto, N.; Sanda, F. Living Ring-opening Polymerization of Cyclic Thiocarbonate. *Macromolecular Symposia* **2003**, *192* (1), 25–30. https://doi.org/10.1002/masy.200390035.

(11) Kricheldorf, H. R.; Damrau, D.-O. Polymers of Carbonic Acid, 26. Synthesis and Ionic Polymerization of 1,3-Dioxane-2-Thione. *Macromol. Chem. Phys.* **1998**, *199* (11), 2589–2596. https://doi.org/10.1002/(SICI)1521-3935(19981101)199:11<2589::AID-MACP2589>3.0.CO;2-P.

(12) Sanda, F.; Kamatani, J.; Endo, T. The First Anionic Ring-Opening Polymerization of Cyclic Monothiocarbonate via Selective Ring-Opening with C−S Bond Cleavage. *Macromolecules* **1999**, *32* (17), 5715–5717. https://doi.org/10.1021/ma9905472.

(13) Ren, W.-M.; Yue, T.-J.; Li, M.-R.; Wan, Z.-Q.; Lu, X.-B. Crystalline and Elastomeric Poly(Monothiocarbonate)s Prepared from Copolymerization of COS and Achiral Epoxide. *Macromolecules* **2017**, *50* (1), 63–68. https://doi.org/10.1021/acs.macromol.6b02089.

(14) Yue, T.; Bhat, G. A.; Zhang, W.; Ren, W.; Lu, X.; Darensbourg, D. J. Facile Synthesis of Well-Defined Branched Sulfur-Containing Copolymers: One-Pot Copolymerization of Carbonyl Sulfide and Epoxide. *Angew Chem Int Ed* **2020**, *59* (32), 13633–13637. https://doi.org/10.1002/anie.202005806.

(15) Luo, M.; Zhang, X.-H.; Du, B.-Y.; Wang, Q.; Fan, Z.-Q. Well-Defined High Refractive Index Poly(Monothiocarbonate) with Tunable Abbe's Numbers and Glass-Transition Temperatures via Terpolymerization. *Polym. Chem.* **2015**, *6* (27), 4978–4983. https://doi.org/10.1039/C5PY00773A.

(16) Yang, J.; Wang, H.; Hu, L.; Hong, X.; Zhang, X. A Double-Site Lewis Pair for Highly Active and Living Synthesis of Sulfur-Containing Polymers. *Polym. Chem.* **2019**, *10* (48), 6555–6560. https://doi.org/10.1039/C9PY01371G.

(17) Zhang, C.-J.; Wu, H.-L.; Li, Y.; Yang, J.-L.; Zhang, X.-H. Precise Synthesis of Sulfur-Containing Polymers via Cooperative Dual Organocatalysts with High Activity. *Nat Commun* **2018**, *9* (1), 2137. https://doi.org/10.1038/s41467-018-04554-5.

(18) Yang, J.; Wu, H.; Li, Y.; Zhang, X.; Darensbourg, D. J. Perfectly Alternating and Regioselective Copolymerization of Carbonyl Sulfide and Epoxides by Metal-Free Lewis Pairs. *Angew Chem Int Ed* **2017**, *56* (21), 5774–5779. https://doi.org/10.1002/anie.201701780.

(19) Li, Y.; Duan, H.-Y.; Luo, M.; Zhang, Y.-Y.; Zhang, X.-H.; Darensbourg, D. J. Mechanistic Study of Regio-Defects in the Copolymerization of Propylene Oxide/Carbonyl Sulfide Catalyzed by (Salen)CrX Complexes. *Macromolecules* **2017**, *50* (21), 8426–8437. https://doi.org/10.1021/acs.macromol.7b01867.

(20) Yang, J.-L.; Cao, X.-H.; Zhang, C.-J.; Wu, H.-L.; Zhang, X.-H. Highly Efficient One-Pot Synthesis of COS-Based Block Copolymers by Using Organic Lewis Pairs. *Molecules* **2018**, *23* (2), 298. https://doi.org/10.3390/molecules23020298.

(21) Yue, T.; Ren, B.; Zhang, W.; Lu, X.; Ren, W.; Darensbourg, D. J. Randomly Distributed Sulfur Atoms in the Main Chains of CO_2 -Based Polycarbonates: Enhanced Optical Properties. *Angew Chem Int Ed* **2021**, *60* (8), 4315–4321. https://doi.org/10.1002/anie.202012565.

(22) Ouhib, F.; Grignard, B.; Van Den Broeck, E.; Luxen, A.; Robeyns, K.; Van Speybroeck, V.; Jerome, C.; Detrembleur, C. A Switchable Domino Process for the Construction of Novel CO_2-Sourced Sulfur-Containing Building Blocks and Polymers. *Angew. Chem. Int. Ed.* **2019**, *58* (34), 11768–11773. https://doi.org/10.1002/anie.201905969.

(23) Ouhib, F.; Meabe, L.; Mahmoud, A.; Grignard, B.; Thomassin, J.-M.; Boschini, F.; Zhu, H.; Forsyth, M.; Mecerreyes, D.; Detrembleur, C. Influence of the Cyclic versus Linear Carbonate Segments in the Properties and Performance of CO_2 -Sourced Polymer Electrolytes for Lithium Batteries. *ACS Appl. Polym. Mater.* **2020**, *2* (2), 922–931. https://doi.org/10.1021/acsapm.9b01130.

(24) Gennen, S.; Grignard, B.; Tassaing, T.; Jérôme, C.; Detrembleur, C. CO_2-Sourced α-Alkylidene Cyclic Carbonates: A Step Forward in the Quest for Functional Regioregular Poly(Urethane)s and Poly(Carbonate)s. *Angew. Chem. Int. Ed.* **2017**, *56* (35), 10394–10398. https://doi.org/10.1002/anie.201704467.

(25) Habets, T.; Siragusa, F.; Grignard, B.; Detrembleur, C. Advancing the Synthesis of Isocyanate-Free Poly(Oxazolidones)s: Scope and Limitations. *Macromolecules* **2020**, *53* (15), 6396–6408. https://doi.org/10.1021/acs.macromol.0c01231.

(26) Siragusa, F.; Van Den Broeck, E.; Ocando, C.; Müller, A. J.; De Smet, G.; Maes, B. U. W.; De Winter, J.; Van Speybroeck, V.; Grignard, B.; Detrembleur, C. Access to Biorenewable and CO_2-Based Polycarbonates from Exovinylene Cyclic Carbonates. *ACS Sustainable Chem. Eng.* **2021**, *9* (4), 1714–1728. https://doi.org/10.1021/acssuschemeng.0c07683.

(27) Dabral, S.; Licht, U.; Rudolf, P.; Bollmann, G.; Hashmi, A. S. K.; Schaub, T. Synthesis and Polymerisation of α-Alkylidene Cyclic Carbonates from Carbon Dioxide, Epoxides and the Primary Propargylic Alcohol 1,4-Butynediol. *Green Chem.* **2020**, *22* (5), 1553–1558. https://doi.org/10.1039/C9GC04320A.

(28) Grignard, B.; Gennen, S.; Jérôme, C.; Kleij, A. W.; Detrembleur, C. Advances in the Use of CO_2 as a Renewable Feedstock for the Synthesis of Polymers. *Chem. Soc. Rev.* **2019**, *48* (16), 4466–4514. https://doi.org/10.1039/C9CS00047J.

(29) Ngassam Tounzoua, C.; Grignard, B.; Detrembleur, C. Exovinylene Cyclic Carbonates: Multifaceted CO_2-Based Building Blocks for Modern Chemistry and Polymer Science. *Angew Chem Int Ed* **2022**, *61* (22), e202116066. https://doi.org/10.1002/anie.202116066.

(30) Lange, N. A.; Dean, J. A. *Lange's Handbook of Chemistry*, 15th ed.; McGraw-Hill: New York St. Louis San Francisco [etc.], 1998.

(31) Lowe, A. J.; Pfeffer, F. M.; Thordarson, P. Determining Binding Constants from ^{1}H NMR Titration Data Using Global and Local Methods: A Case Study Using [*n*]Polynorbornane-Based Anion Hosts. *Supramolecular Chemistry* **2012**, *24* (8), 585–594. https://doi.org/10.1080/10610278.2012.688972.

(32) Bashir, Z. Polyacrylonitrile, an Unusual Linear Homopolymer with Two Glass Transitions. *Indian Journal of Fibre & Textile Research* **1999**, *24*, 1–9.

(33) Bashir, Z. THE HEXAGONAL MESOPHASE IN ATACTIC POLYACRYLONITRILE: A NEW INTERPRETATION OF THE PHASE TRANSITIONS IN THE POLYMER. *Journal of Macromolecular Science, Part B* **2001**, *40* (1), 41–67. https://doi.org/10.1081/MB-100000053.

(34) Sutherland, B. P.; Kabra, M.; Kloxin, C. J. Expanding the Thiol–X Toolbox: Photoinitiation and Materials Application of the Acid-Catalyzed Thiol–Ene (ACT) Reaction. *Polym. Chem.* **2021**, *12* (10), 1562–1570. https://doi.org/10.1039/D0PY01593H.

(35) *Szycher's Handbook of Polyurethanes*, 0 ed.; Szycher PhD, M., Ed.; CRC Press, 2012. https://doi.org/10.1201/b12343.

Supporting Information

1. Materials and Instrumentation

Materials

All chemicals were used as received. 1,4-Butanedithiol (97%), 1,4-Diaminobutane (99%), 1,8-Diazabicyclo[5.4.0]undec-7-ene (DBU, 99%), 1-Propanethiol (99%), 2-Furanmethanethiol (98%), 2,2′-(Ethylenedioxy)diethanethiol (95%), 3-Mercaptopropionic acid (99%), Benzylamine (99%), Benzyl mercaptan (99%), Cyclohexylamine (99%), m-Xylylenediamine (99%) were purchased from Sigma Aldrich. Propylamine (99%) was purchased from Fluka. Cyclohexane-1,4-diamine (99%), Methanesulphonic acid (98%) were purchased from Fluorochem. 1,4-Benzenedimethanethiol (98%) was purchased from TCI. Formic acid (85%) was purchased from Mobilab.

4,4-dimethyl-5-methylene-1,3-dioxolan-2-one (αCC)[1], 4,4′-(ethane-1,2-diyl)bis(4-methyl-5-methyl- ene-1,3-dioxolan-2-one) (bisαCC)[1] and 3-benzyl-4-hydroxy-4,5,5-trimethyloxazolidin-2-one[2] were synthesized according to procedures described elsewhere.

Dialysis membrane Spectra/Por 7 (MWCO 1 kD) was purchased from Repligen.

Instrumentation

Nuclear magnetic resonance (NMR) spectroscopy. ^{1}H- and ^{13}C-NMR analyses were performed on a Bruker 400 MHz spectrometer at 25 °C in the Fourier transform mode. 16 scans for ^{1}H spectra and 512 scans for ^{13}C spectra were recorded. ^{1}H- and ^{13}C-NMR analyses for the DBU-oxazolidone interaction experiments were performed on a Bruker Ultrashield Plus 700 MHz spectrometer at 25 °C in the Fourier transform mode. 16 scans for ^{1}H spectra and 32 scans for ^{13}C spectra were recorded.

Size exclusion chromatography (SEC). Number-average molecular weight (Mn) and dispersity (D) of the polymers were determined by size exclusion chromatography (SEC) in dimethylformamide (DMF) containing LiBr (0.025 M) at 55 °C (flow rate: 1 mL/min) with a Waters chromatograph equipped with three columns (PSS gram 1000Å (x2), 30 Å) and a precolumn, a dual absorbance detector (Waters 2487) and a refractive index detector (Waters 2414).

Thermogravimetric analysis (TGA). TGA analysis was performed on a TGA2 instrument from Mettler Toledo. *Determination of degradation temperature.* Around 5 to 10 mg of sample was heated at 10 °C/min from 30 to 50 °C and flushed for 10 min at 50 °C. The sample was then heated at 20 °C/min until 600 °C. All the experiment was conducted under nitrogen atmosphere (20 mL/min). *Determination of dehydration temperature.* Around 5 to 10 mg of sample was

heated at 2 °C/min from 30 to 250 °C. All the experiment was conducted under nitrogen atmosphere (20 mL/min).

Differential scanning calorimetry (DSC). DSC analysis was performed on a DSC 250 (TA Instruments). All the experiments were performed under ultrapure nitrogen flow. Samples of 4–6 mg were used and placed in hermetic aluminum pans. *Analysis of hydroxyoxazolidone copolymers.* The sample was heated from 25 to 90 °C at a rate of 10 °C/min and cooled to -40°C at a rate of 10 °C/min. The temperature modulated segment was set with an amplitude of 2 °C with a period of 60 seconds. The sample was then heated to 200 °C at a rate of 2 °C/min. The glass transition temperatures were determined using the reversing heat flow curve. *Analysis of dehydrated polymers.* The sample was heated from 25 to 140 °C at a rate of 10 °/min, cooled to -80 °C at a rate of 10 °C/min, and heated to 160 °C at a rate of 10 °C/min.

Fourier Transform Infrared Spectra (F-TIR). FTIR measurements were carried out on a Nicolet IS5 spectrometer (Thermo Fisher Scientific) equipped with a diamond attenuated transmission reflectance (ATR) device. 32 scans were recorded for each sample over the range 4000-500 cm^{-1} with a normal resolution of 4 cm^{-1}.

Lap-Shear Tests. Lap shear adhesion measurements were conducted on a MTS Criterion Model 43 system equipped with a 1 kN load cell with a displacement rate of 5 mm min^{-1}. A homemade setup was designed for avoiding failure in brittle samples on sample locking when aluminum substrates were used (Figure S123). The lap shear strength was calculated using the formula:

$$\tau = \frac{F}{A}$$

where τ is the lap shear strength (mPa), F is the applied force (N) and A the overlapped area (constant in this study as 150 mm^2). Each sample was measured three times.

2. Model reactions

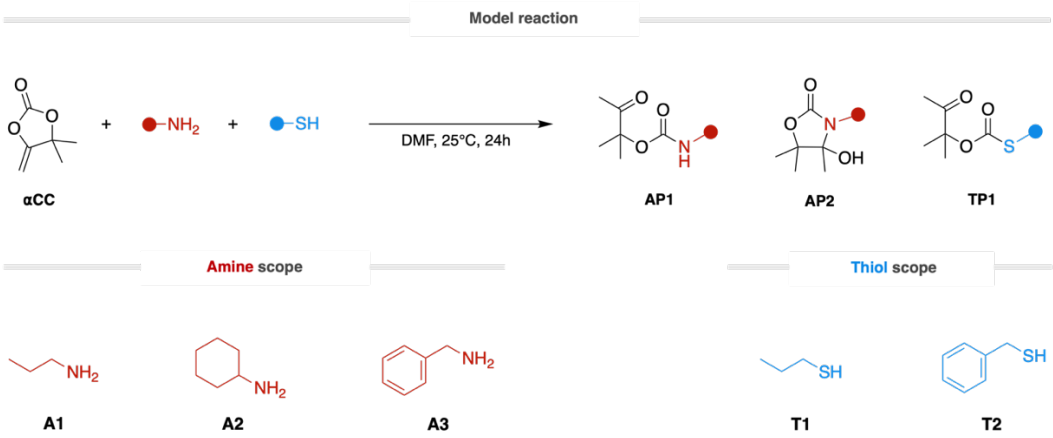

Scheme S1 – Substrate scope for the model reaction of αCC with amines and thiols.

Model reactions between αCC and a scope of different monofunctional amines **A1-3** and thiols **T1-2** have been carried out under different conditions. The kinetics were monitored by ^{1}H-NMR spectroscopy by sampling over time (1 min, 30 min, 1h, 2h, 4h, 24h).

General procedure

αCC (512 mg, 4 mmol, 2 eq.), the thiol (2 mmol, 1 eq.) and DMF (2 mL) were added to a reaction tube. Then, the amine (2 mmol, 1 eq.) was added and the reaction medium was stirred at 25°C under N_2 atmosphere. When used, DBU (0.08 mmol, 0.04 eq.) was added after all other components.

The NMR samples were prepared by mixing 100 µL of the reaction medium, a drop of formic acid to quench the reaction, and 700 µL of DMSO-d_6. The tube was then stored at -20°C prior analysis

The conversion in αCC, amine, thiol, and the oxo-urethane **AP1** cyclization (into **AP2**) were calculated following the respective equations:

$$\text{conv}(\alpha\text{CC})\ (\%) = 1 - \frac{I(\alpha\text{CC})}{I(\alpha\text{CC})+I(\text{AP1})+I(\text{AP2})+I(\text{TP1})}$$

$$\text{conv}(\text{amine})\ (\%) = \frac{(\ I(\text{AP1})+I(\text{AP2})\ ) \times 2}{I(\alpha\text{CC})+I(\text{AP1})+I(\text{AP2})+I(\text{TP1})}$$

$$\text{conv}(\text{thiol})\ (\%) = \frac{I(\text{TP1}) \times 2}{I(\alpha\text{CC})+I(\text{AP1})+I(\text{AP2})+I(\text{TP1})}$$

$$\text{cyclization}(\text{amine})\ (\%) = \frac{I(\text{AP2})}{I(\text{AP1})+I(\text{AP2})}$$

where *conv* is the conversion, *cyclization* the cyclization, *I* the normalized integration.

The peaks selected for the integration are attributed to their respective compounds and can be found below for each model reaction. Peaks relative to solvents appear at 2.5 ppm (DMSO-d_6), 2.73 and 2.89 ppm (DMF).

Model reaction with **A1** and **T1**

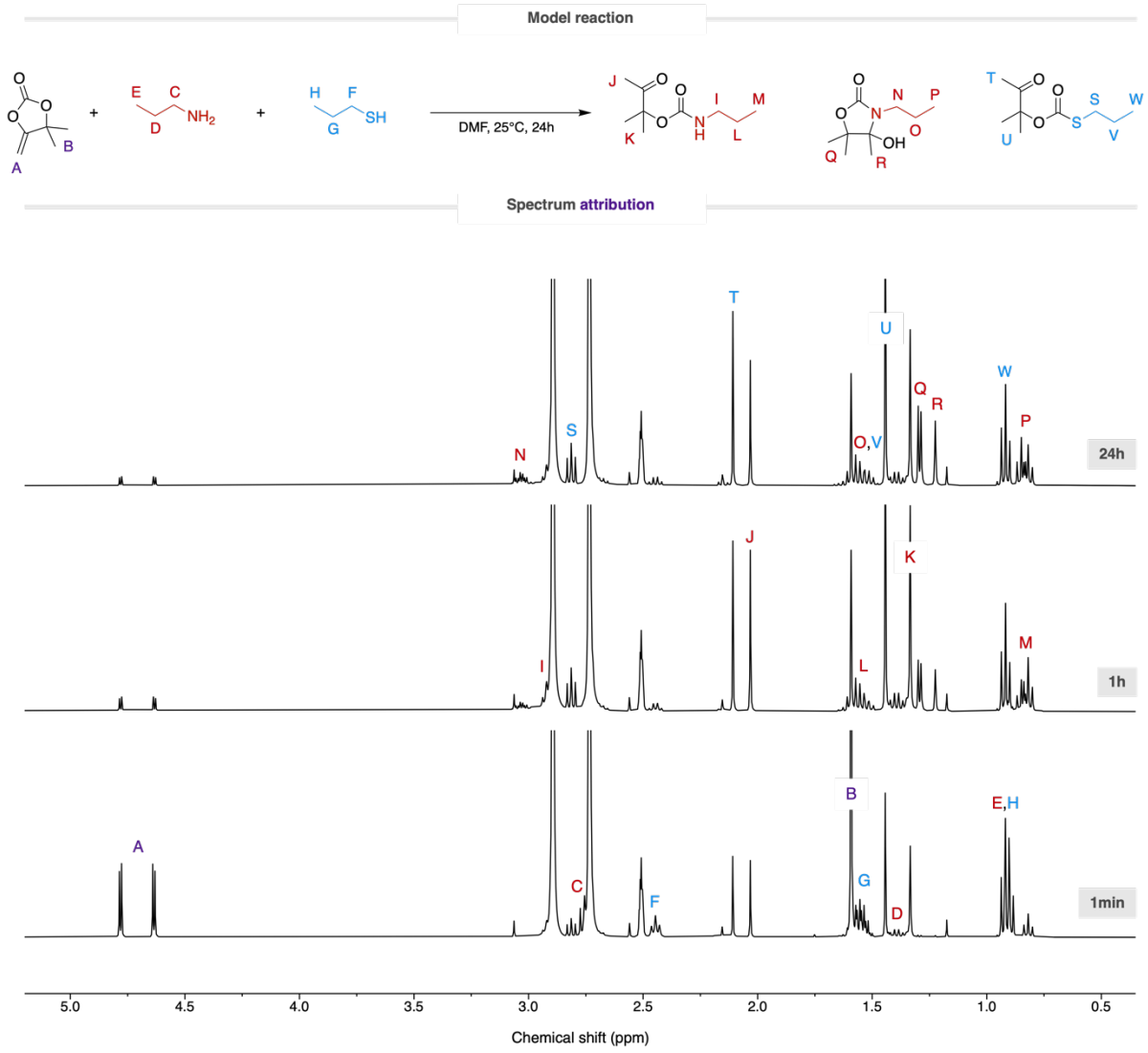

Figure S1 – Kinetic study of the model reaction between αCC, **A1**, and **T1** followed by ^{1}H-NMR spectroscopy (400 MHz, DMSO-d_6).

Compound	Peak	δ (ppm)
αCC	A	4.64
AP1	J	2.04
AP2	R	1.23
TP1	T	2.11

Model reaction with **A2** and **T1**

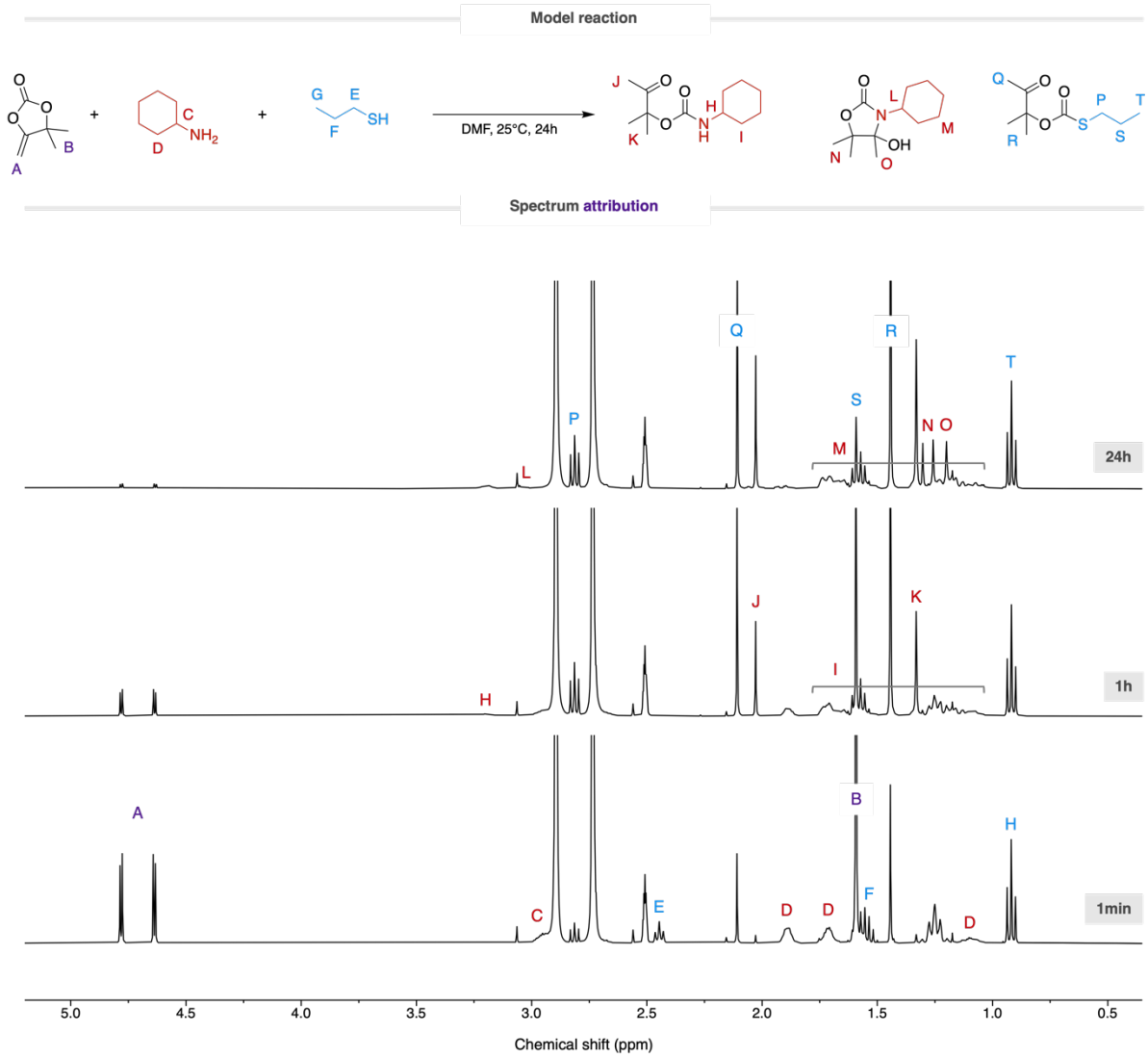

Figure S2 – Kinetic study of the model reaction between αCC, **A2**, and **T1** followed by ^{1}H-NMR spectroscopy (400 MHz, DMSO-d_6).

Compound	Peak	δ (ppm)
αCC	A	4.64
AP1	J	2.03
AP2	O	1.20
TP1	Q	2.11

Model reaction with **A3** and **T1**

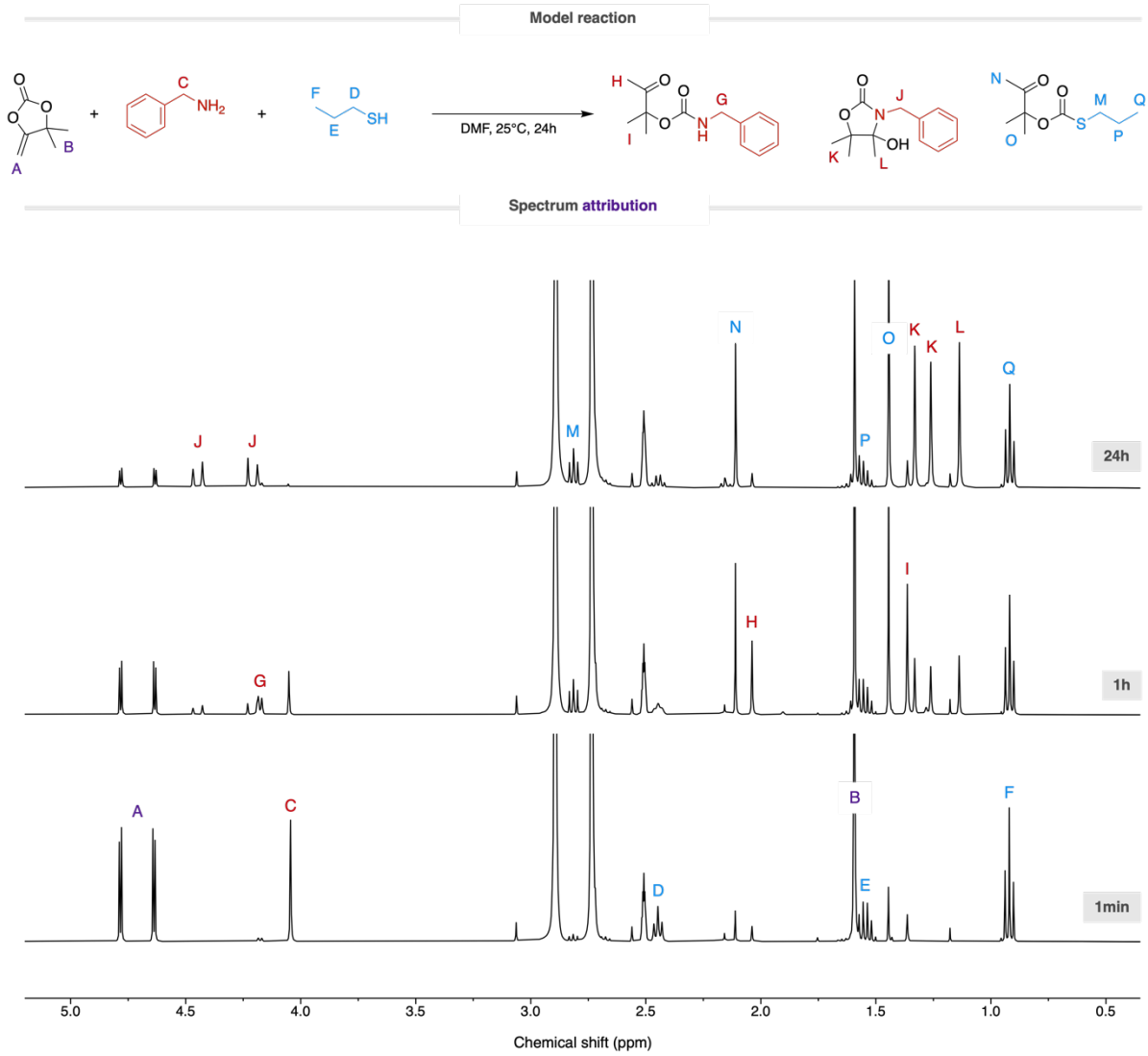

Figure S3 – Kinetic study of the model reaction between αCC, **A3**, and **T1** followed by ^{1}H-NMR spectroscopy (400 MHz, DMSO-d_6).

Compound	Peak	δ (ppm)
αCC	A	4.64
AP1	H	2.04
AP2	L	1.14
TP1	N	2.11

Model reaction with **A1** and **T2**

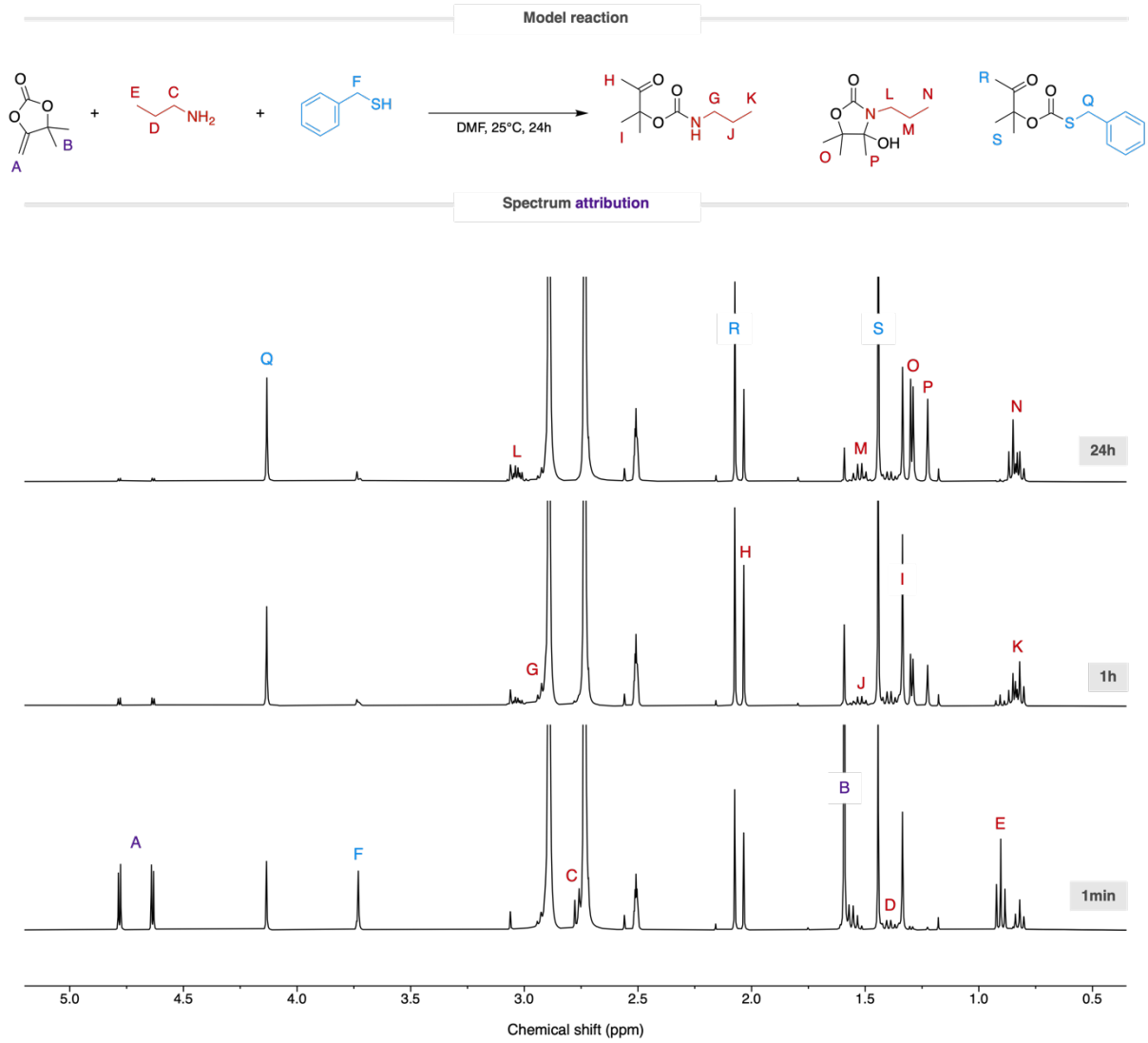

Figure S4 – Kinetic study of the model reaction between αCC, **A1**, and **T2** followed by ^{1}H-NMR spectroscopy (400 MHz, DMSO-d_6).

Compound	Peak	δ (ppm)
αCC	A	4.64
AP1	H	2.03
AP2	P	1.22
TP1	R	2.07

Model reaction with **A2** and **T2**

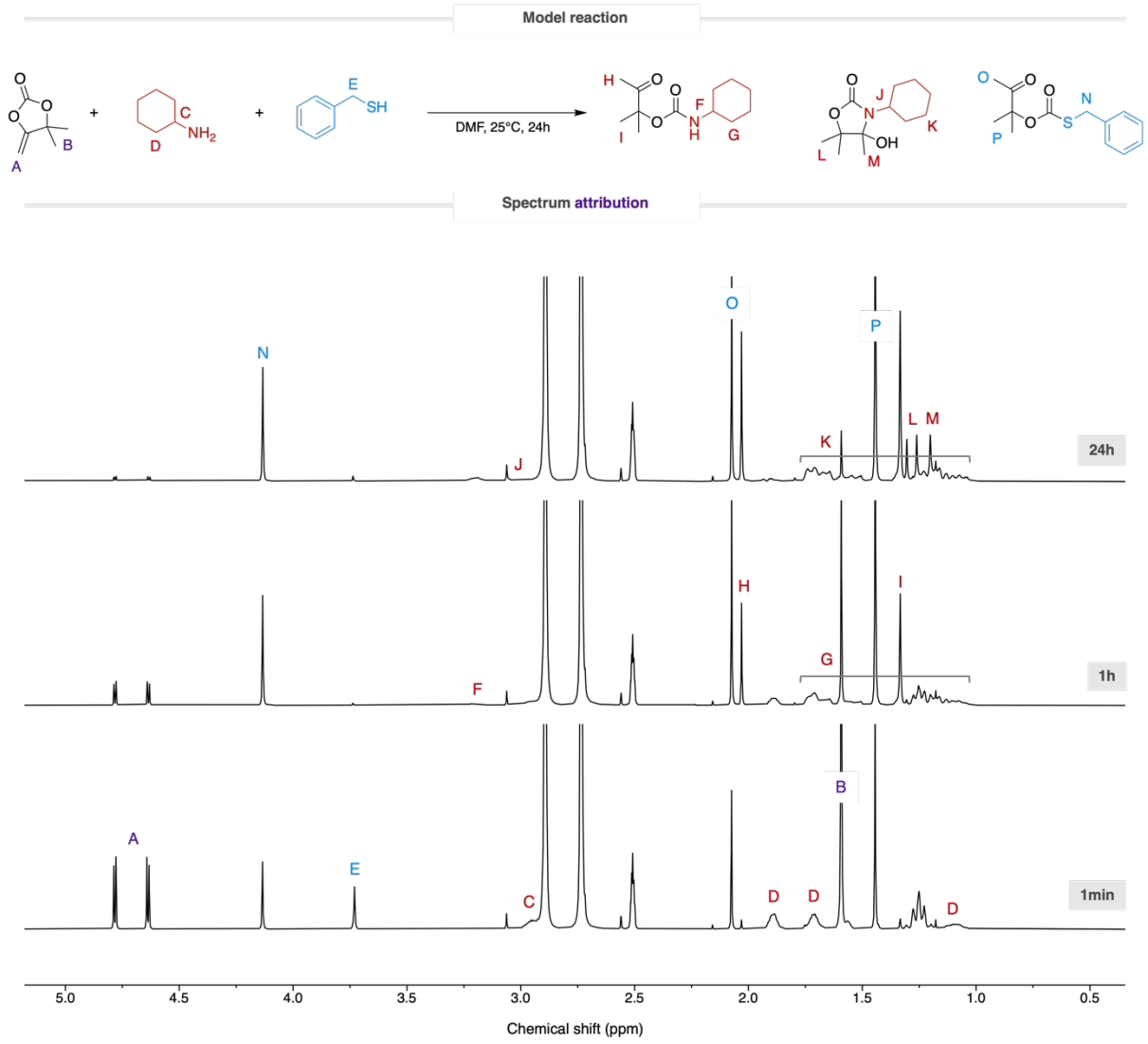

Figure S5 – Kinetic study of the model reaction between αCC, **A2**, and **T2** followed by ^{1}H-NMR spectroscopy (400 MHz, DMSO-d_6).

Compound	Peak	δ (ppm)
αCC	A	4.64
AP1	H	2.03
AP2	M	1.20
TP1	O	2.07

Model reaction with **A3** and **T2**

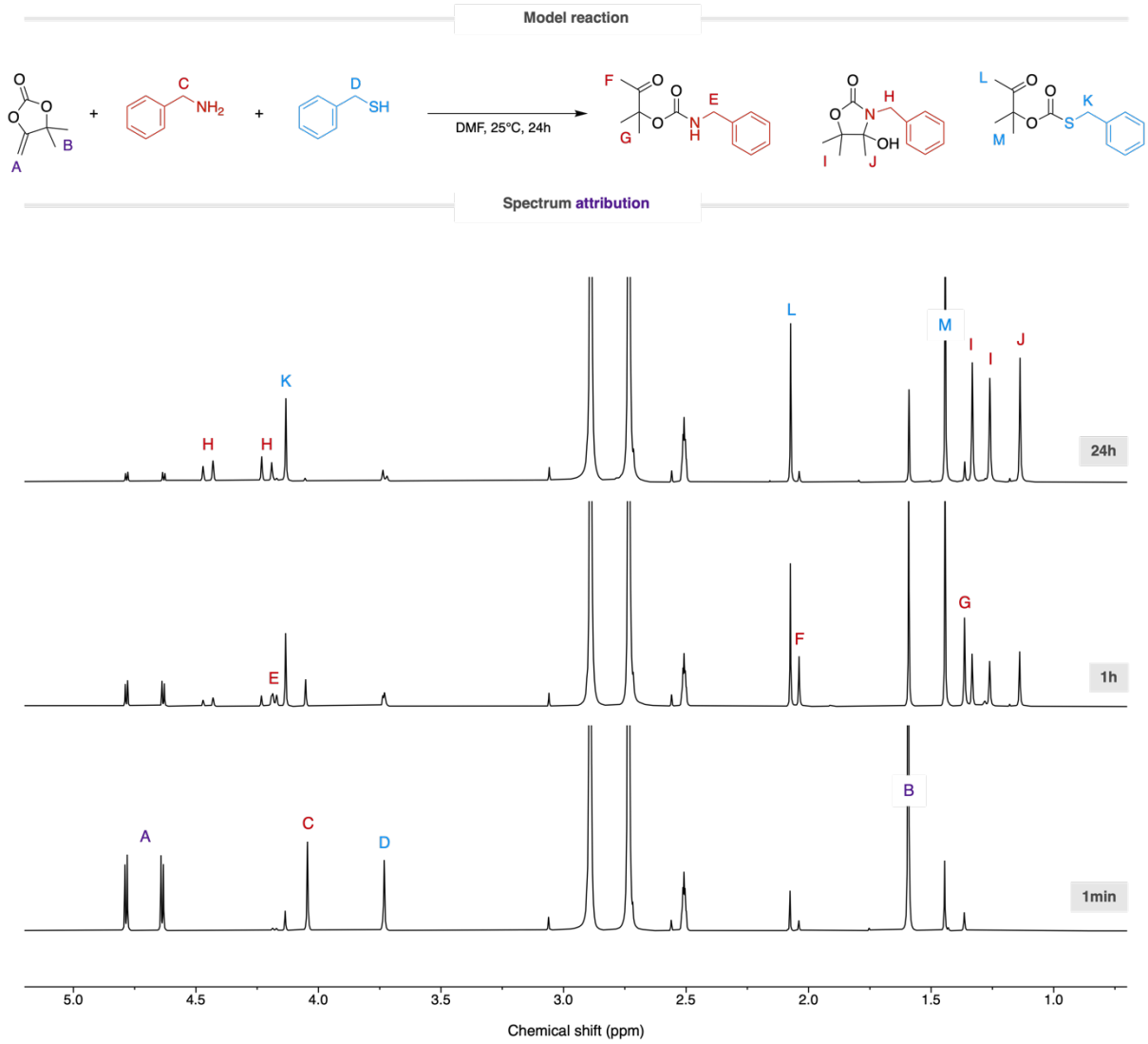

Figure S6 – Kinetic study of the model reaction between αCC, **A3**, and **T2** followed by ^{1}H-NMR spectroscopy (400 MHz, DMSO-d_6).

Compound	Peak	δ (ppm)
αCC	A	4.64
AP1	F	2.04
AP2	J	1.14
TP1	L	2.07

3. Evidence for reactive thiolate generation

Thiols are acidic compounds and primary amines are characterized by rather high basicity. Mixing the amine **A2** (yellow liquid) the thiol **T2** (colorless liquid) in DMF leads to a slow crystallization of a white solid. This solid salt can be isolated by filtration followed by washing with diethyl ether. The formation of this salt has already been reported in the literature[3].

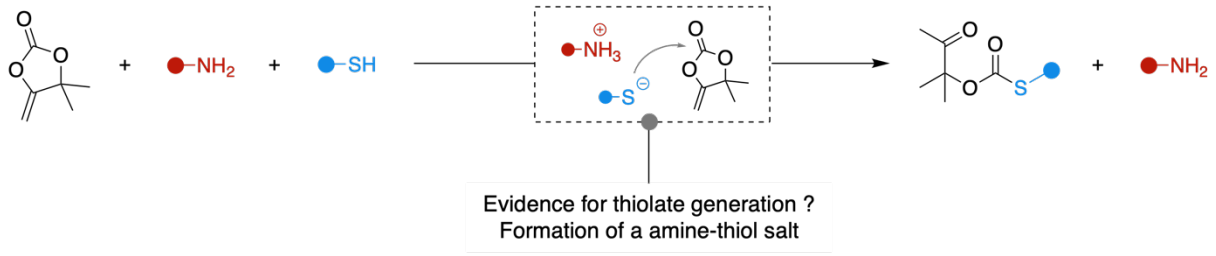

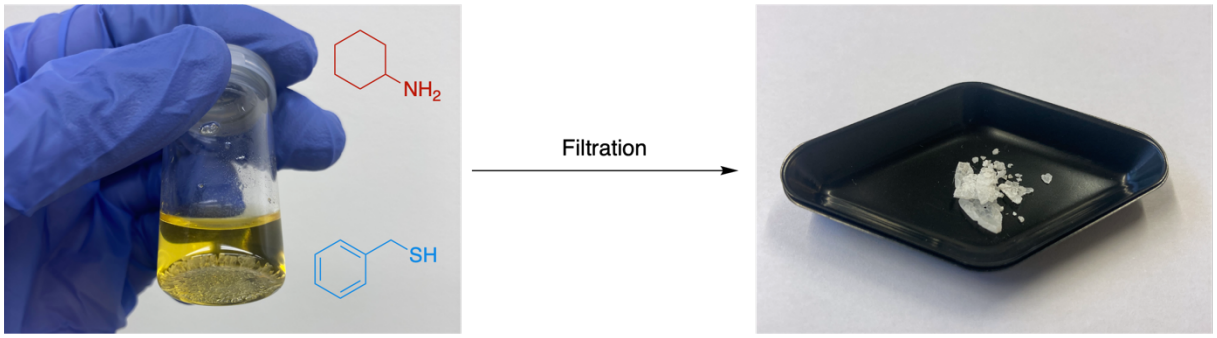

Scheme S2 – Catalytic role of the amine to generate thiolates species for the formation of the monothiocarbonate **TP1**. Mixing cyclohexylamine **A2** and benzyl mercaptan **T2** in DMF give rise to the formation of white crystals.

The formation of the salt is highlighted in both solid and dissolved forms. By ^{1}H-NMR spectroscopy in $CDCl_3$ as deuterated solvent (the salt has shown insolubility in DMSO-d_6), the formation of a salt is highlighted by a disappearance of the thiol hydrogen at 1.78 ppm (triplet) and the metamorphosis of the methylene at 3.76 ppm from a doublet to a singlet due to the absence of neighboring hydrogen (Figure S7). An ATR-IR spectrum has also been recorded and displays typical vibrations of primary amine salts[4,5], characterized by a wide absorbance in the region from 2800 to 2200 cm^{-1} and the presence of a lone band at 2110 cm^{-1} (Figure S8).

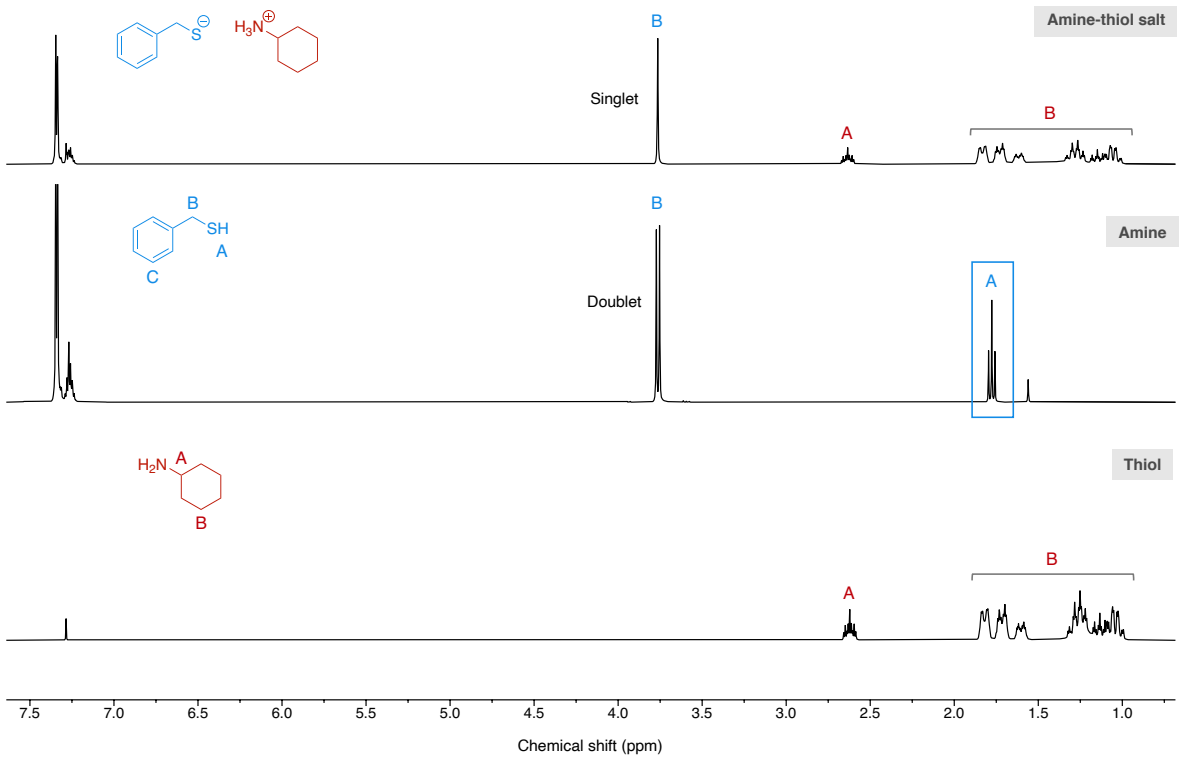

Figure S7 – ^{1}H-NMR spectra of the thiol, the amine, and the amine-thiol salt (400 MHz, DMSO-d_6).

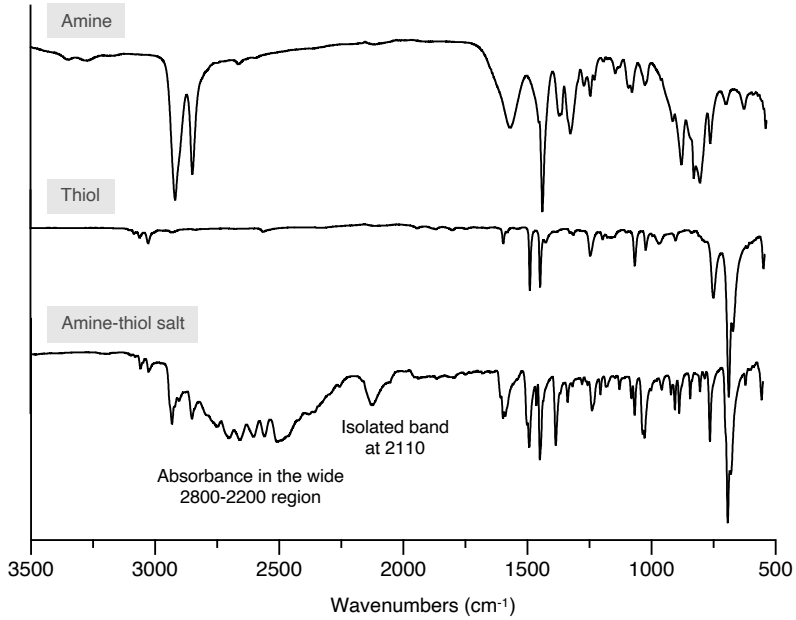

Figure S8 – ATR-IR spectra of the amine, the thiol, and the amine-thiol salt.

4. Solubility table of the synthesized polymers

The solubility was assessed by stirring 20 mg of the selected polymer in 500 µL of solvent at room temperature. The polymer was denoted as soluble if a transparent solution was obtained. If the polymer was not dissolved within 24 h, it was denoted as insoluble.

Table S1 – Solubility of the pure polymers in different organic solvents at rt.

	DMSO	DMF	THF	Acetone	$CHCl_3$
P(A1T1)	✓	✓	✓	✓	✓
P(A1T1)C	✓	✓	✓	✓	×
P(A1T2)	✓	✓	✓	✓	×
P(A2T1)	✓	✓	✓	✓	✓
P(A2T1)C	✓	✓	✓	✓	×
P(A2T2)	✓	✓	✓	✓	✓
P(A3T1)	✓	✓	✓	✓	×
P(A3T1)C	✓	✓	✓	✓	×
P(A3T2)	✓	✓	✓	✓	×

5. NMR characterization of the pure polymers

P(A1T1)

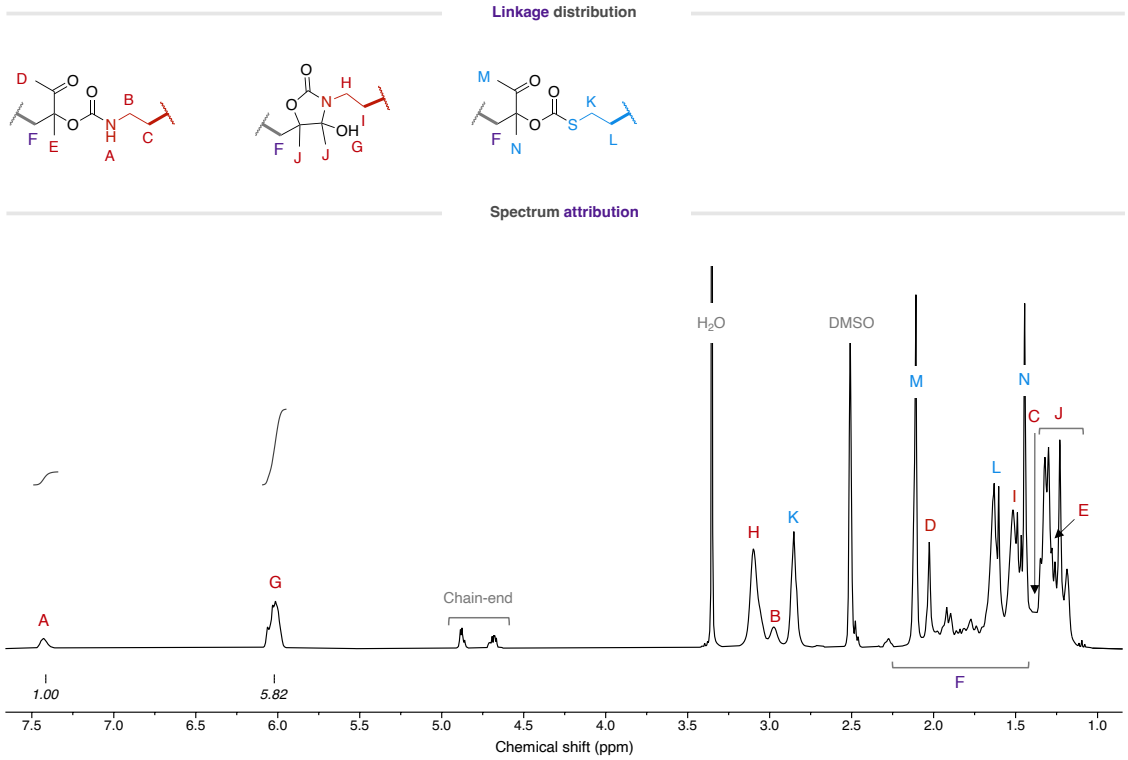

Figure S9 – ^{1}H-NMR spectrum of P(A1T1) (400 MHz, DMSO-d_6).

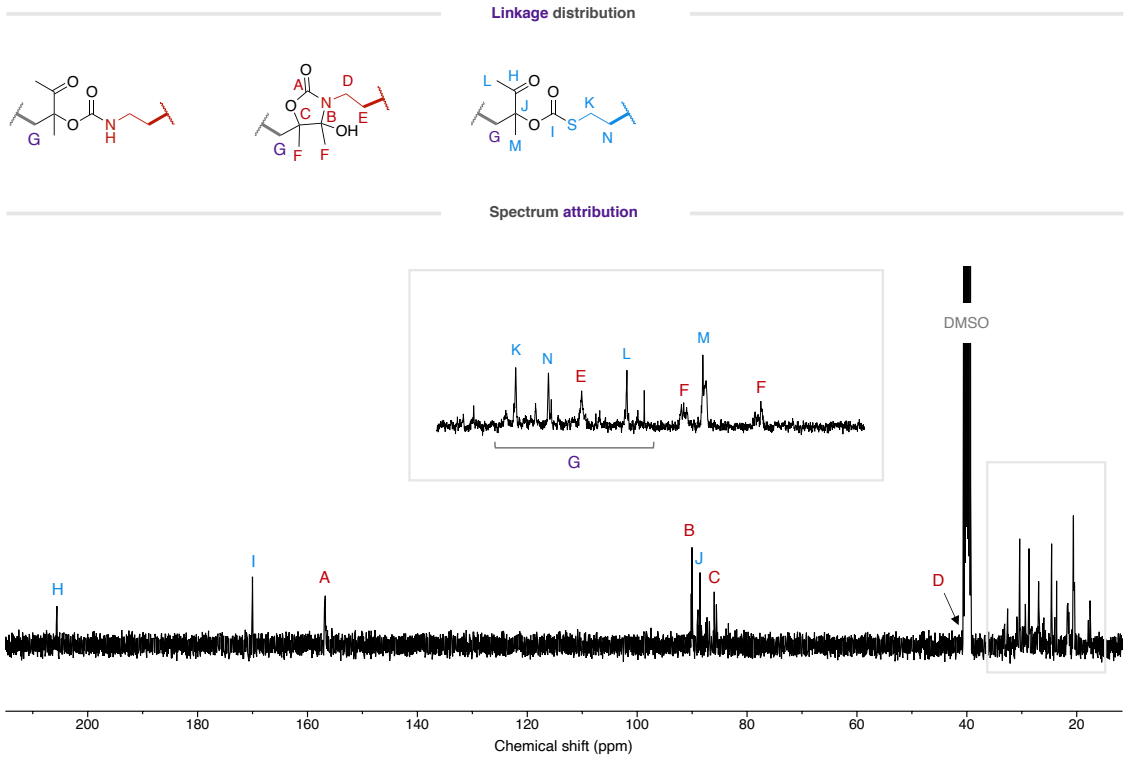

Figure S10 – ^{13}C-NMR spectrum of P(A1T1) (101 MHz, DMSO-d_6).

P(A1T1)C

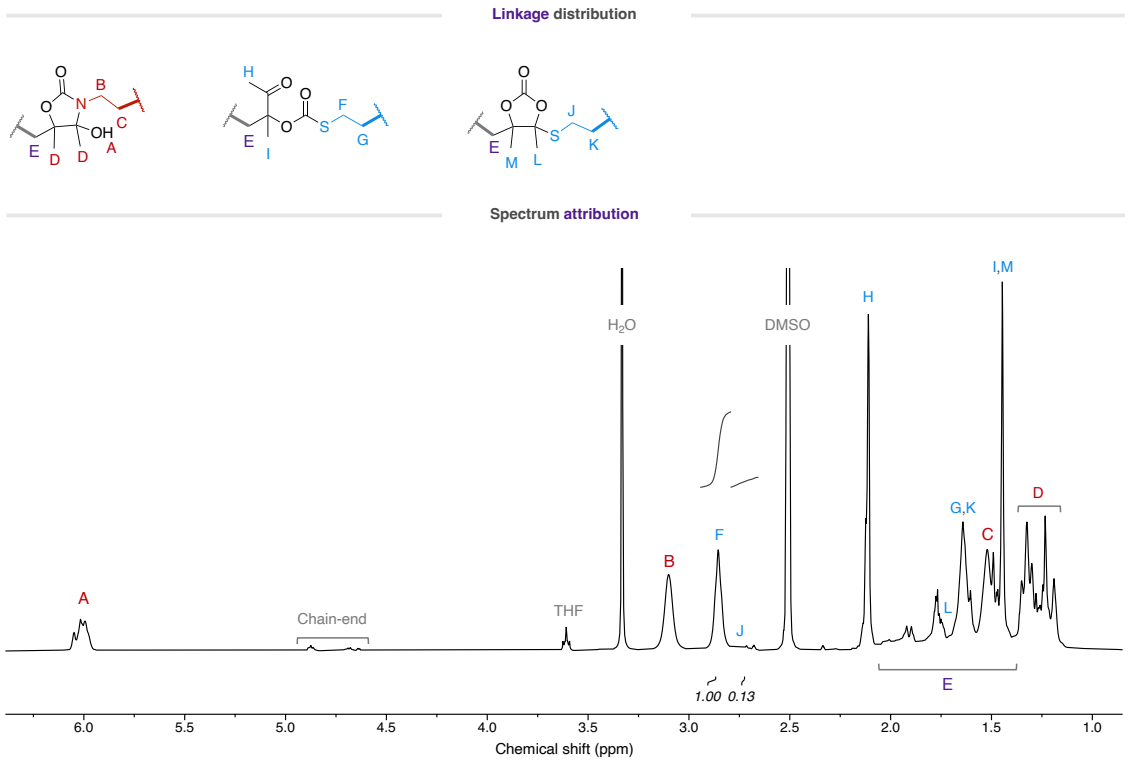

Figure S11 – ^{1}H-NMR spectrum of P(A1T1)C (400 MHz, DMSO-d_6).

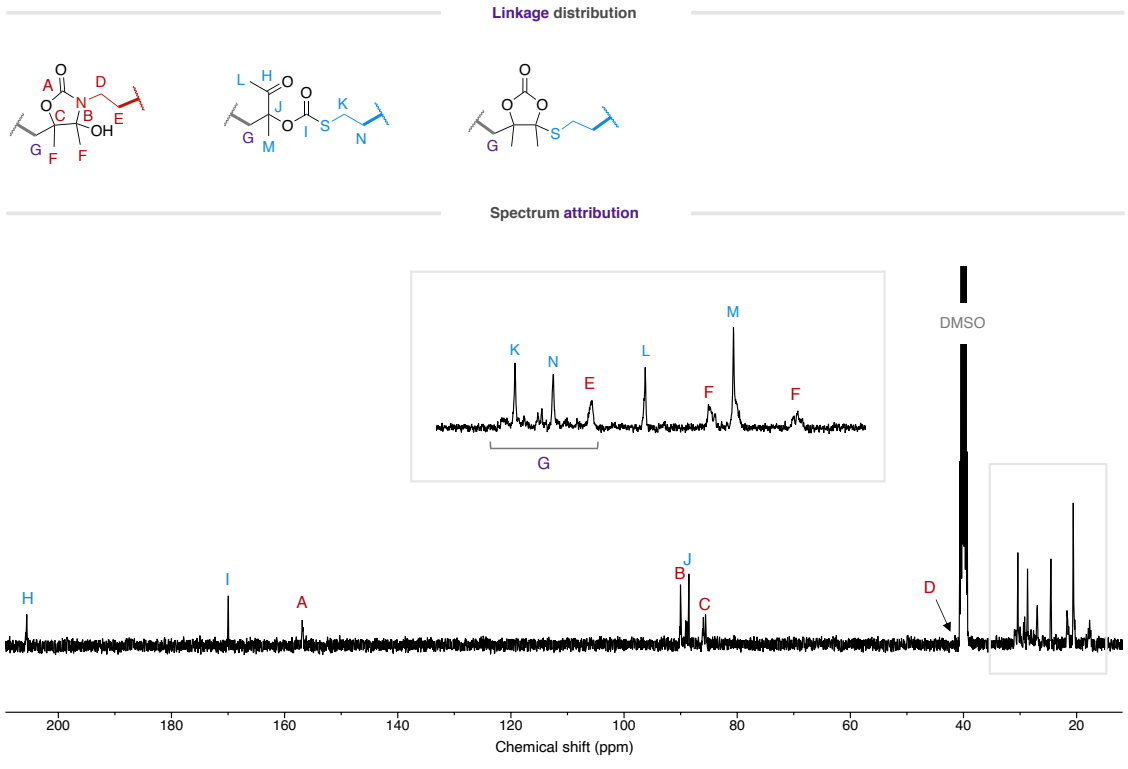

Figure S12 – ^{13}C-NMR spectrum of P(A1T1)C (101 MHz, DMSO-d_6).

P(A1T2)

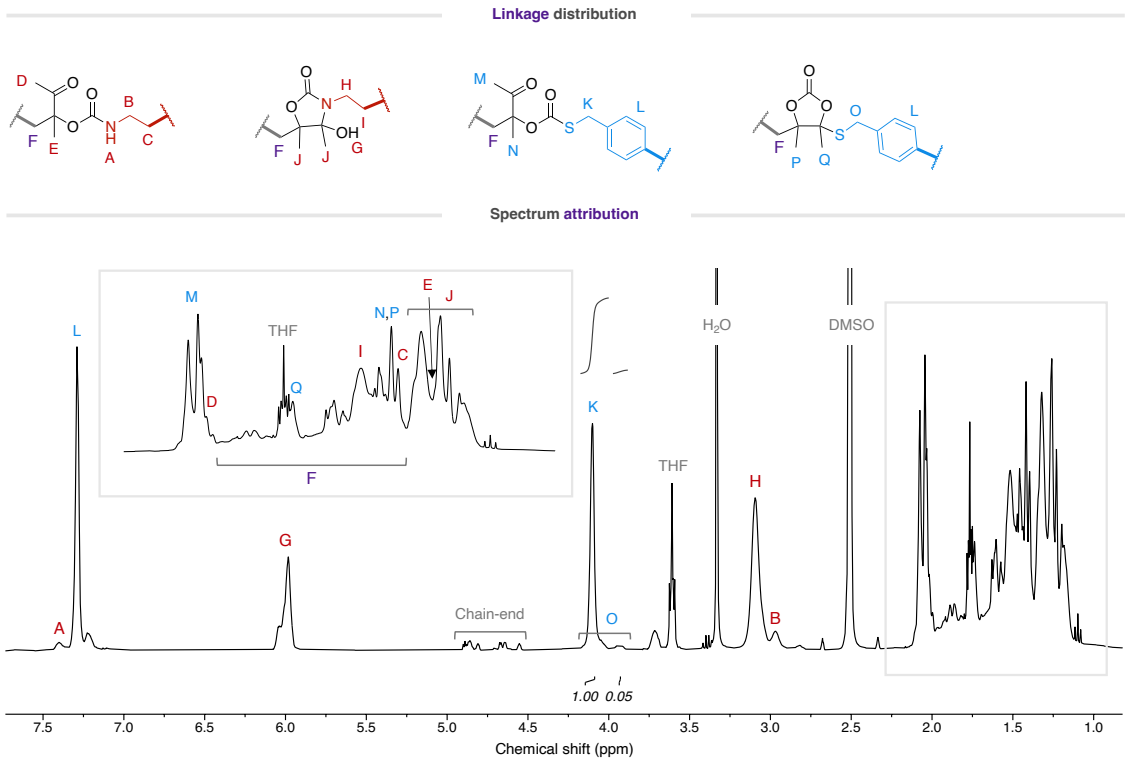

Figure S13 – ^{1}H-NMR spectrum of P(A1T2) (400 MHz, DMSO-d_6).

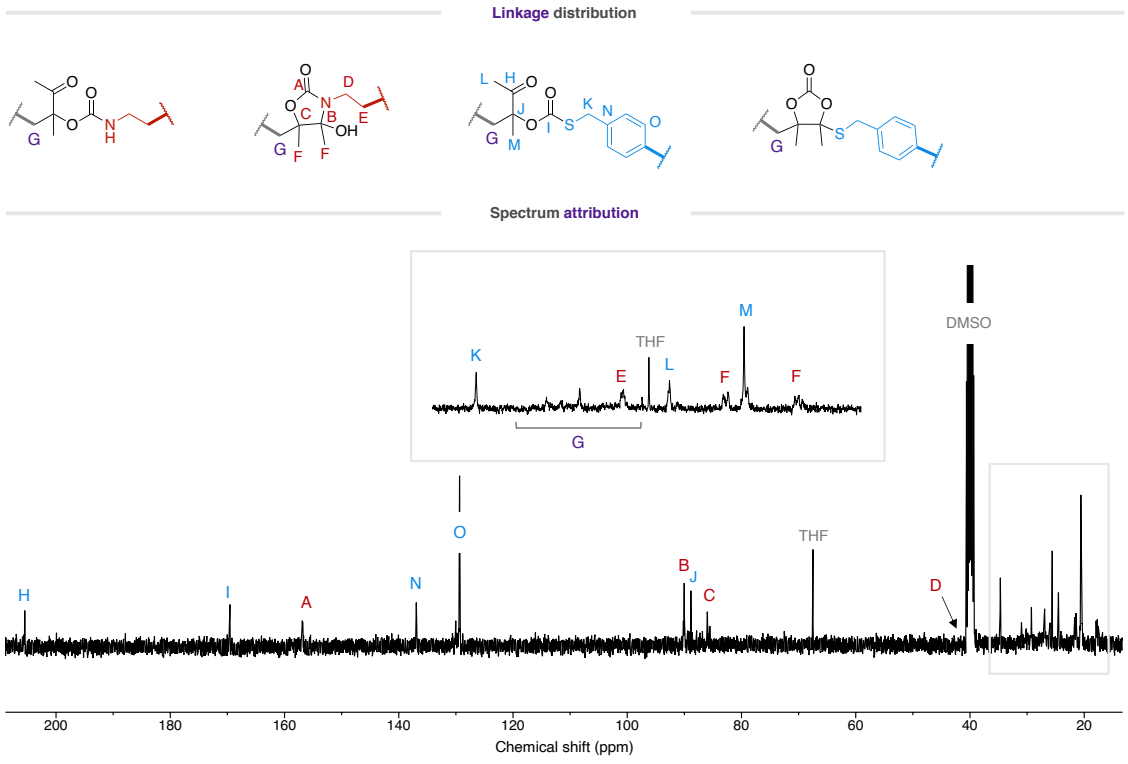

Figure S14 – ^{13}C-NMR spectrum of P(A1T2) (101 MHz, DMSO-d_6).

P(A2T1)

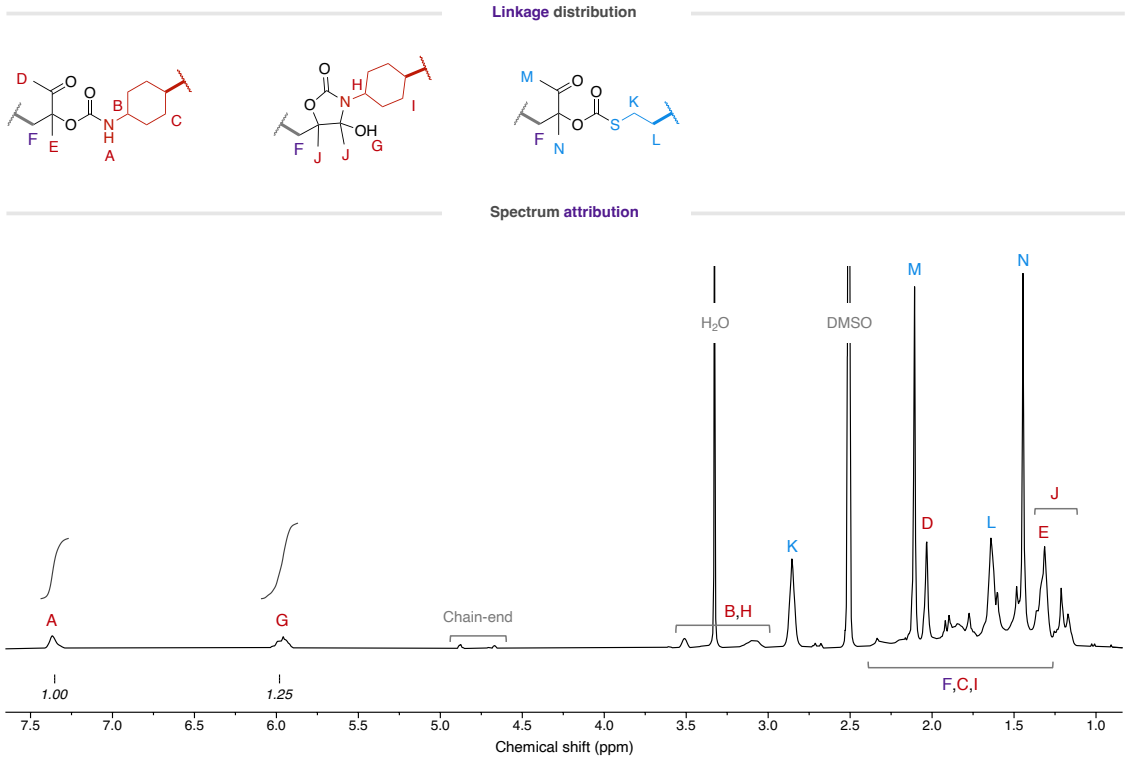

Figure S15 – ^{1}H-NMR spectrum of P(A2T1) (400 MHz, DMSO-d_6).

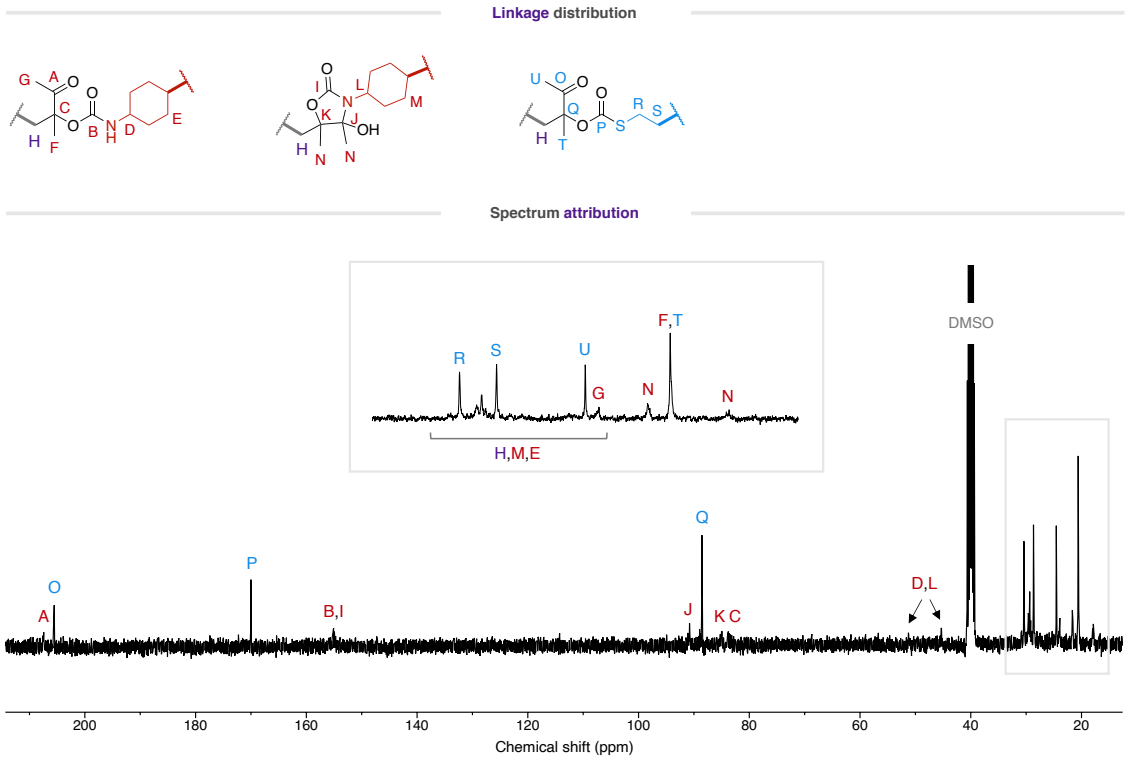

Figure S16 – ^{13}C-NMR spectrum of P(A2T1) (101 MHz, DMSO-d_6).

P(A2T1)C

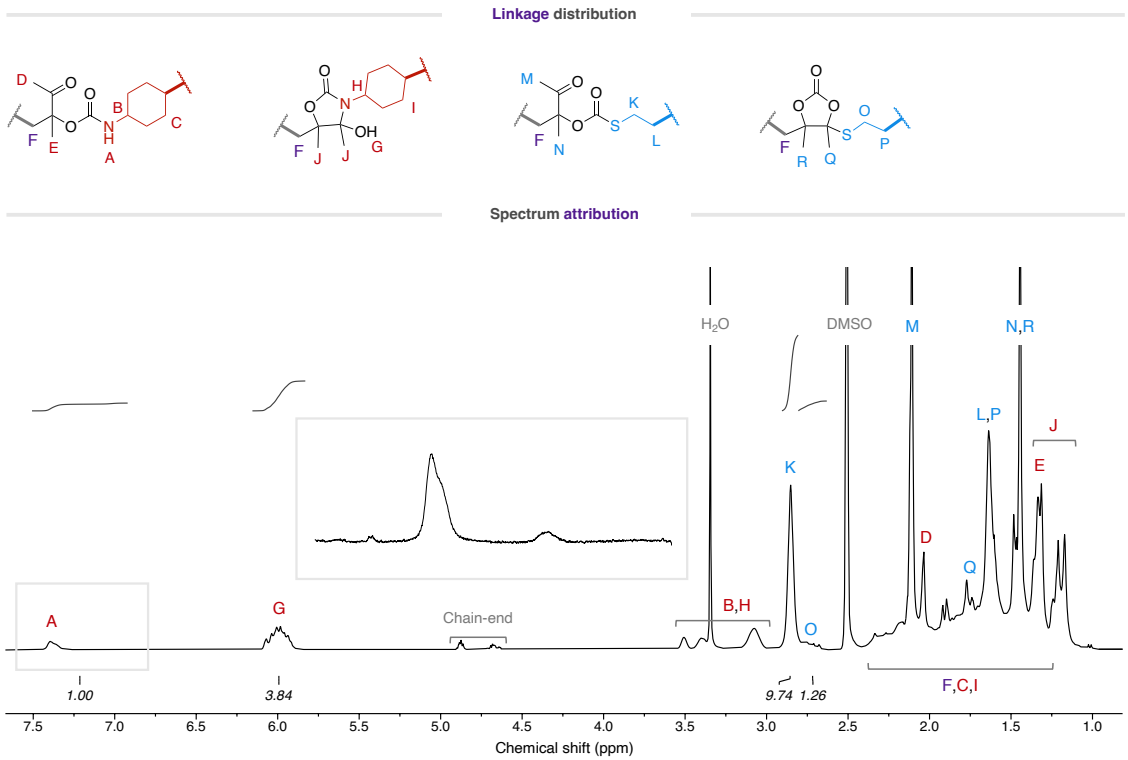

Figure S17 – ^{1}H-NMR spectrum of P(A2T1) (400 MHz, DMSO-d_6).

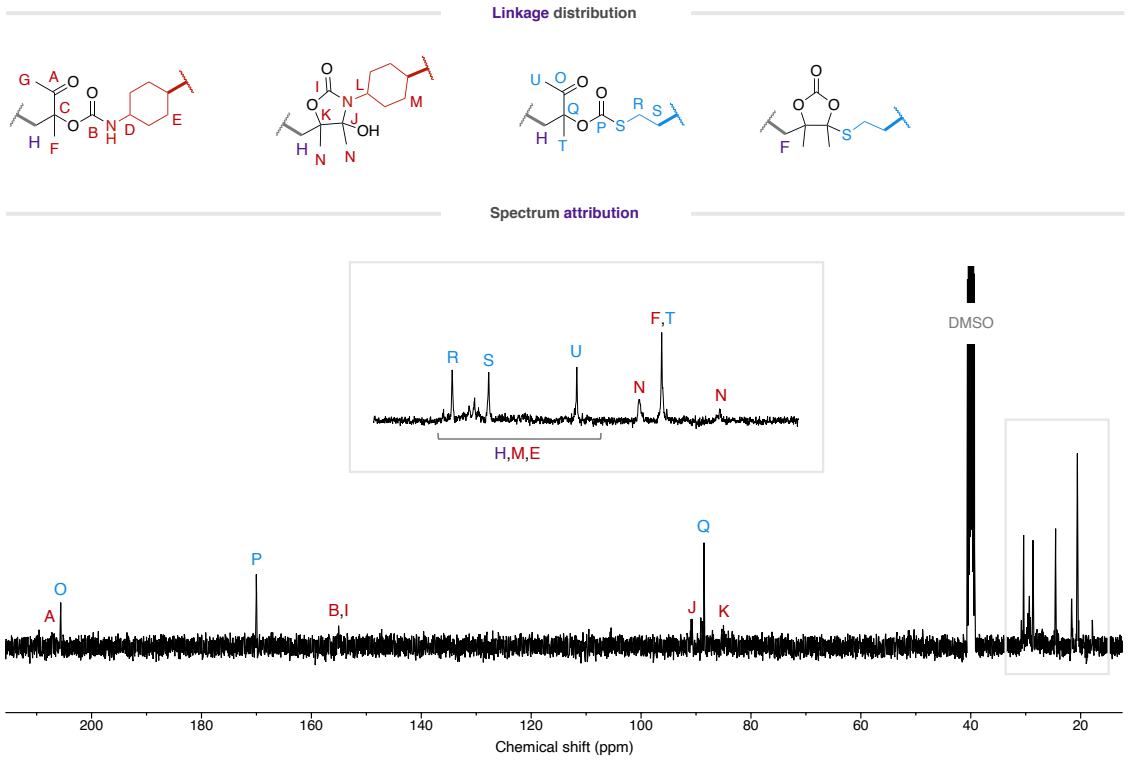

Figure S18 – ^{13}C-NMR spectrum of P(A2T1)C (101 MHz, DMSO-d_6).

P(A2T2)

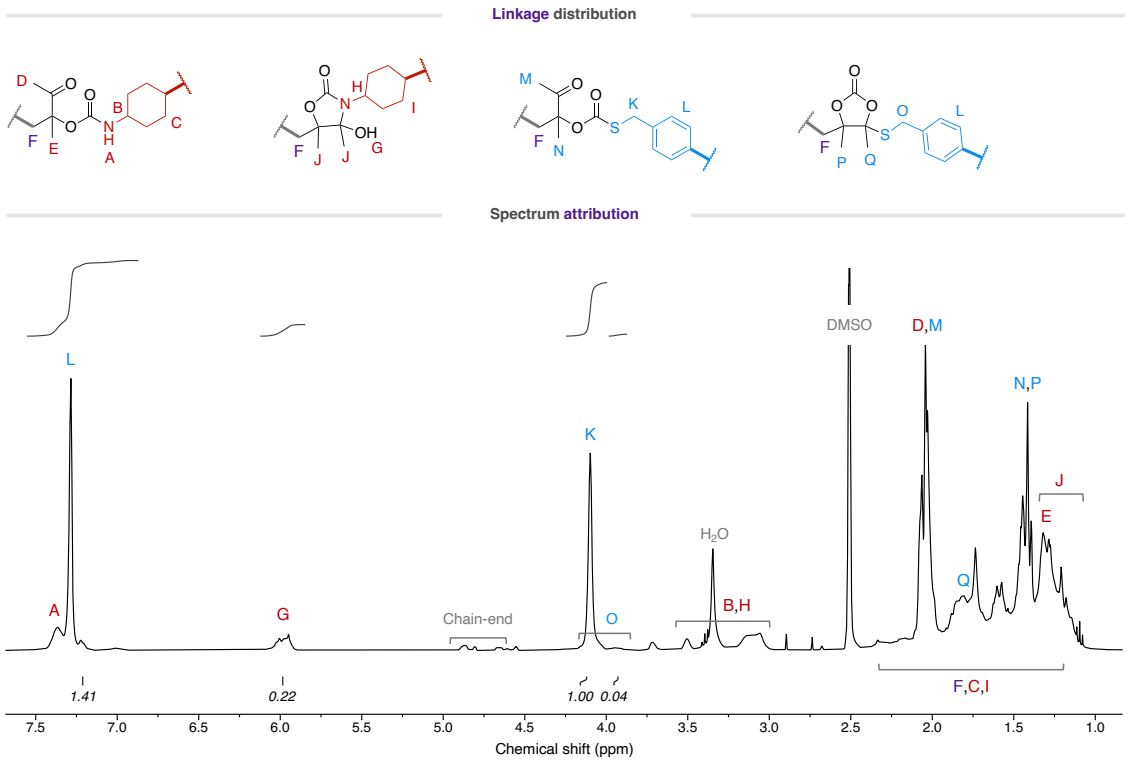

Figure S19 – ^{1}H-NMR spectrum of P(A2T2) (400 MHz, DMSO-d_6).

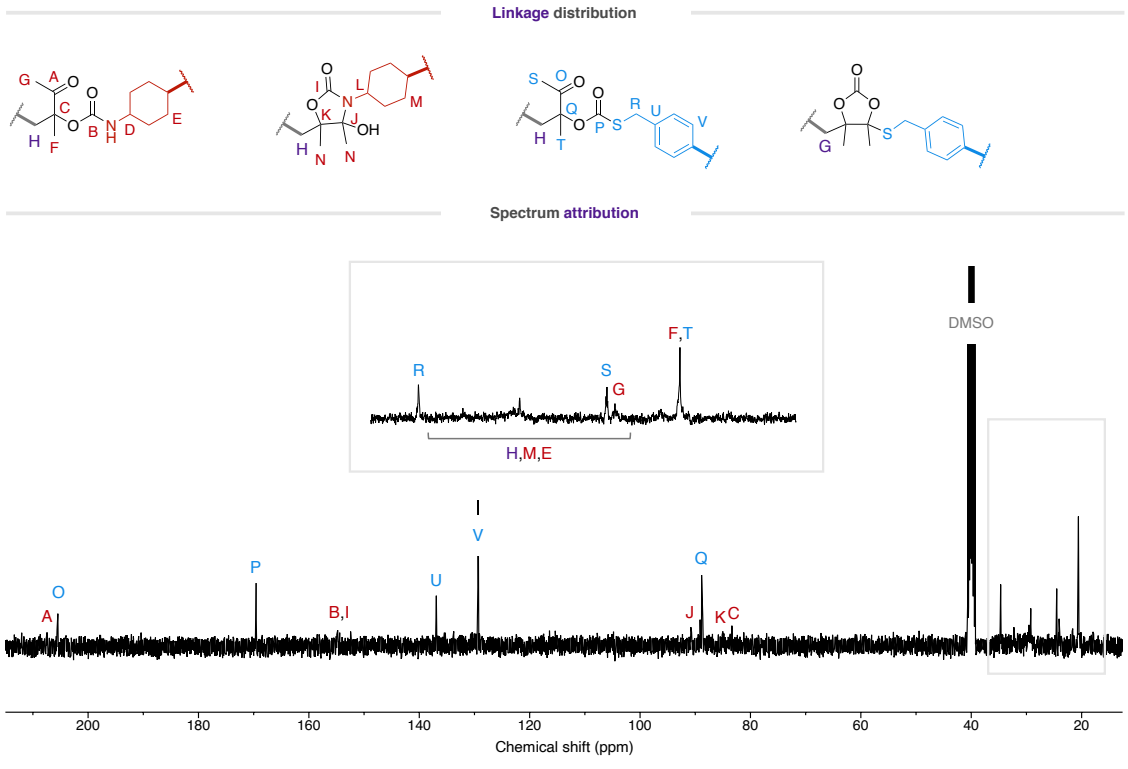

Figure S20 – ^{13}C-NMR spectrum of P(A2T2) (101 MHz, DMSO-d_6).

P(A3T1)

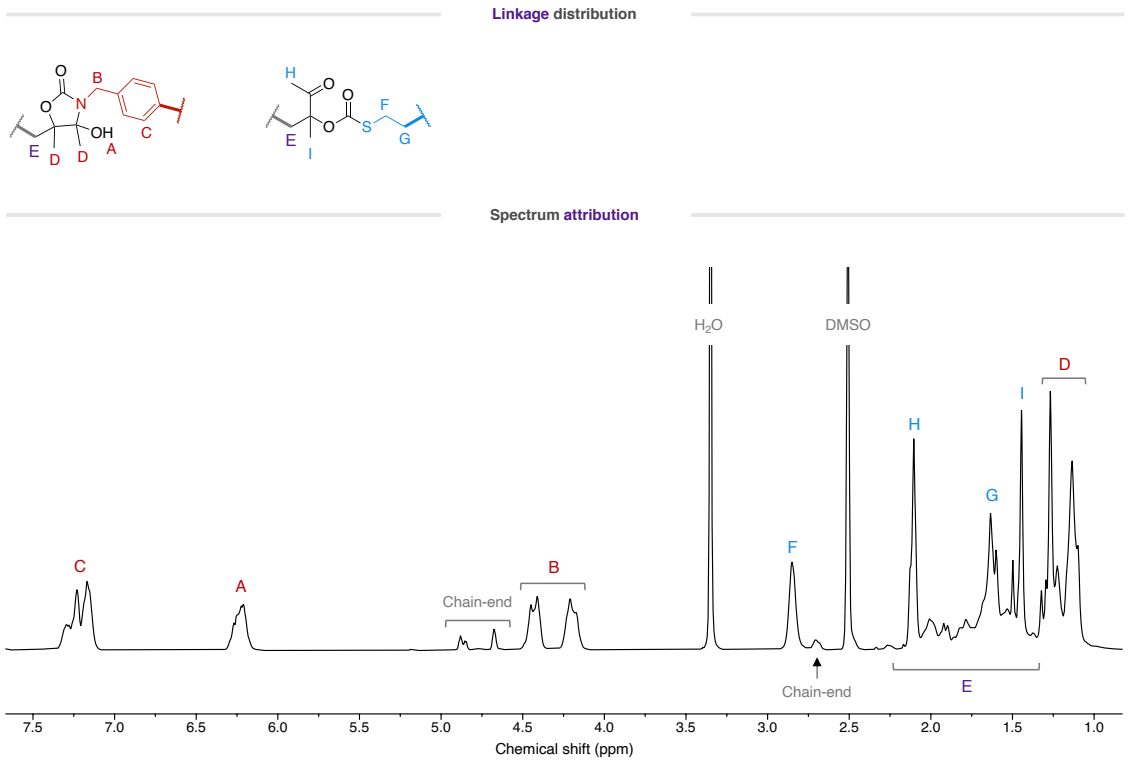

Figure S21 – ^{1}H-NMR spectrum of P(A3T1) (400 MHz, DMSO-d_6).

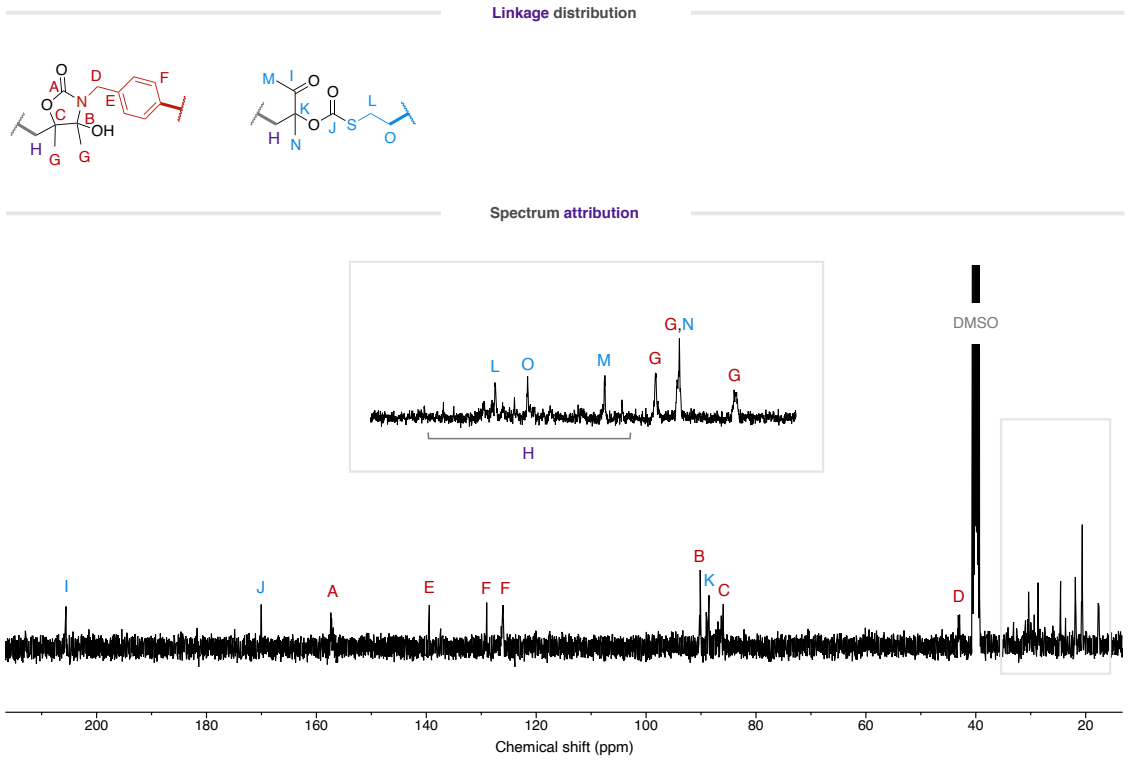

Figure S22 – ^{13}C-NMR spectrum of P(A3T1) (101 MHz, DMSO-d_6).

P(A3T1)C

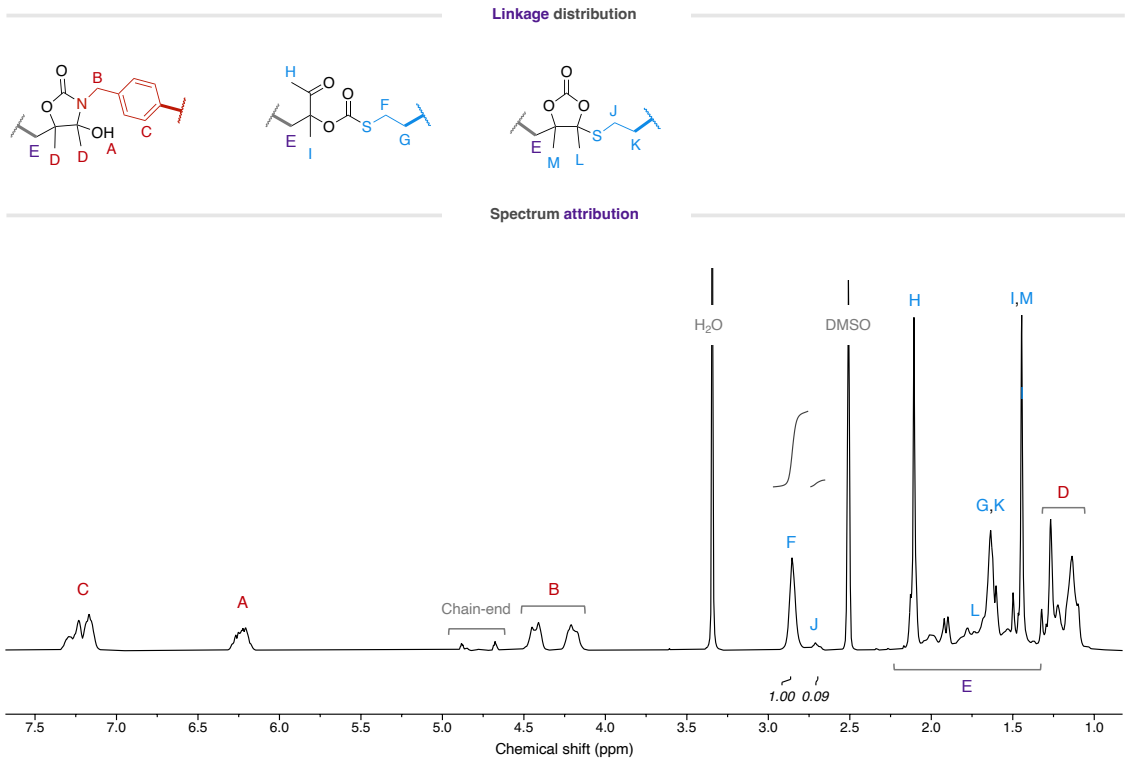

Figure S23 – ^{1}H-NMR spectrum of P(A3T1)C (400 MHz, DMSO-d_6).

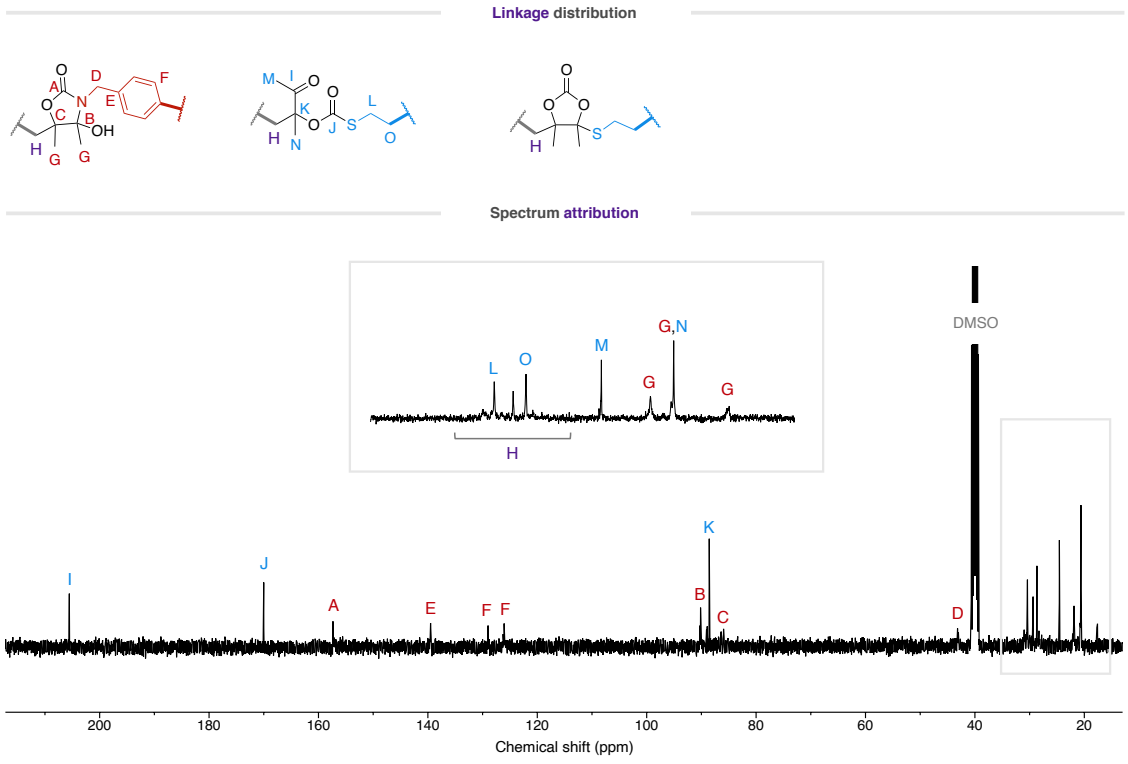

Figure S24 – ^{13}C-NMR spectrum of P(A3T1)C (101 MHz, DMSO-d_6).

P(A3T2)

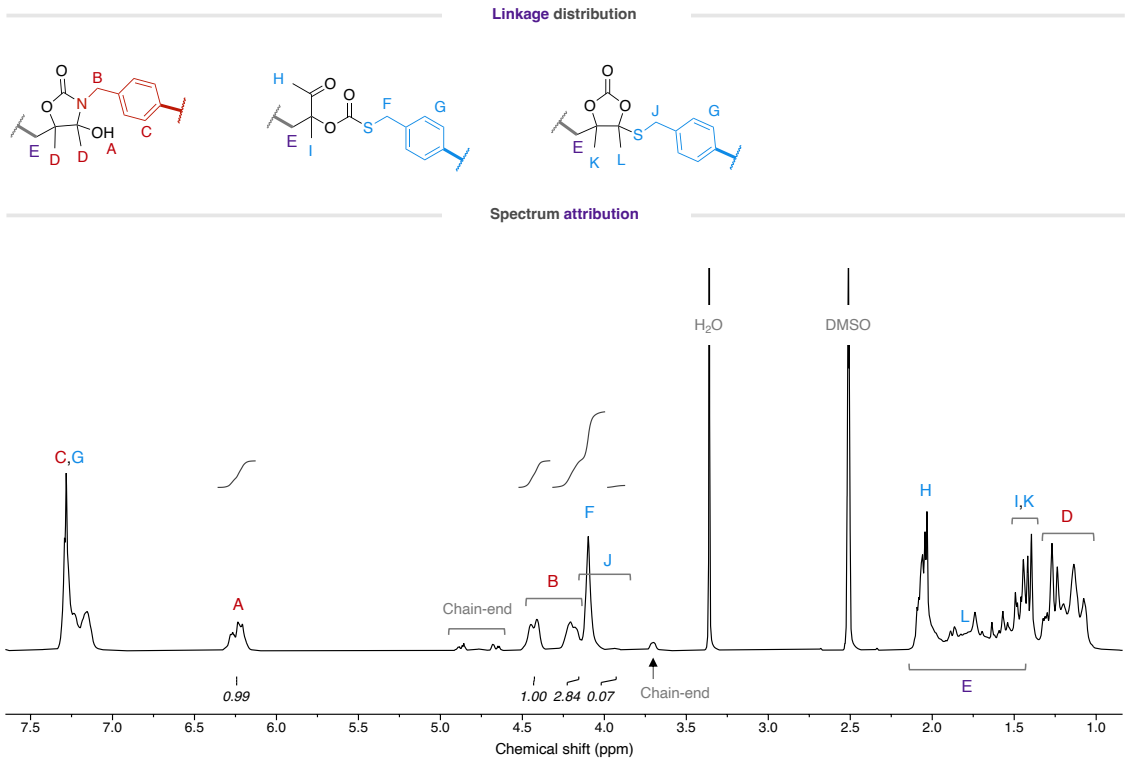

Figure S25 – ^{1}H-NMR spectrum of P(A3T2) (400 MHz, DMSO-d_6).

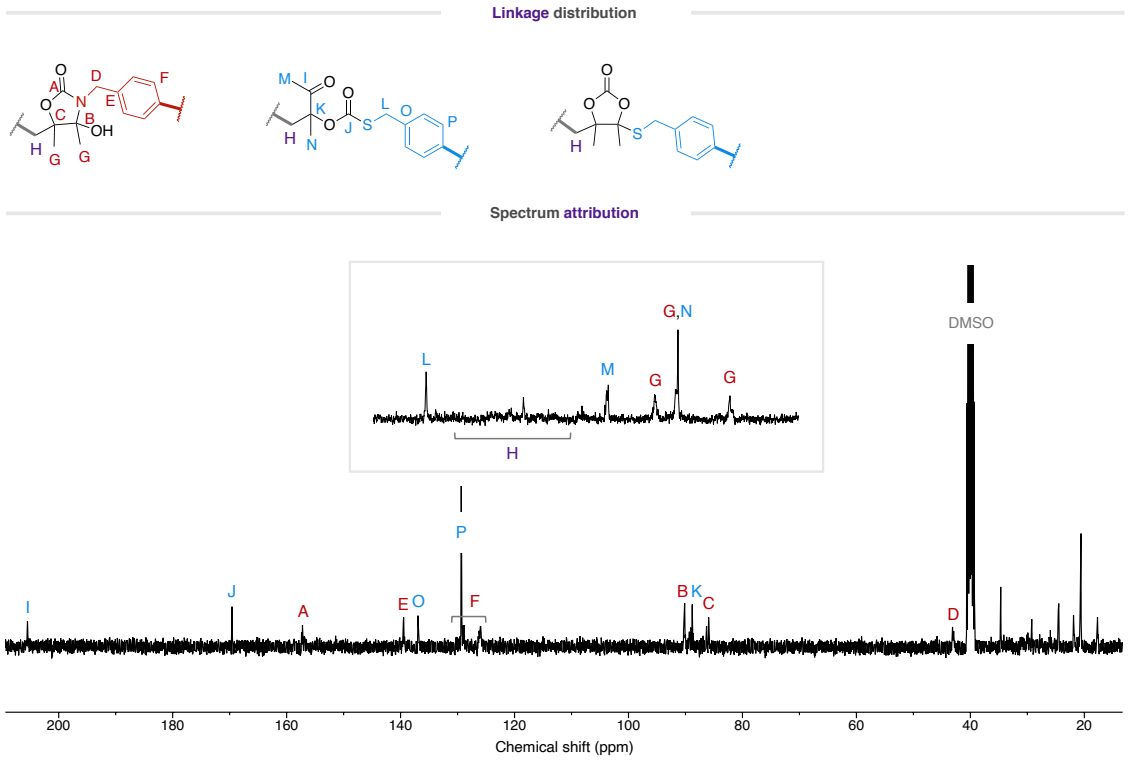

Figure S26 – ^{13}C-NMR spectrum of P(A3T2) (101 MHz, DMSO-d_6).

6. SEC chromatograms of crude reactions

Typical SEC chromatograms of crude reaction medium are shown below for polymers synthesized without catalyst and with 2 mol% of DBU.

P(A1T1)

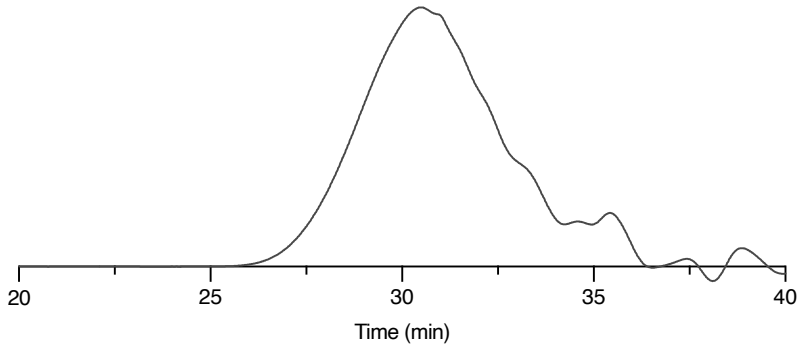

Figure S27 – SEC chromatogram (before purification) of P(A1T1).

P(A1T1)C

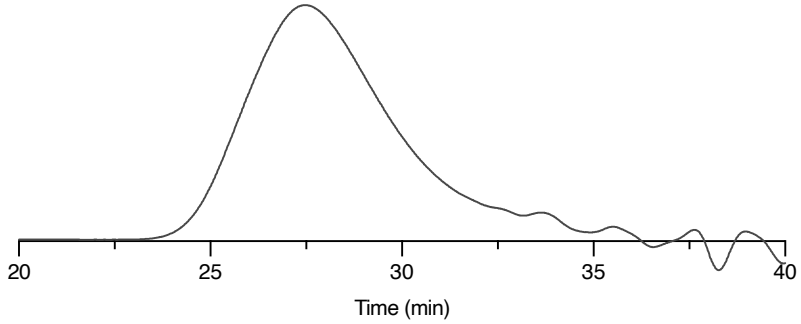

Figure S28 – SEC chromatogram (before purification) of P(A1T1)C.

P(A1T2)

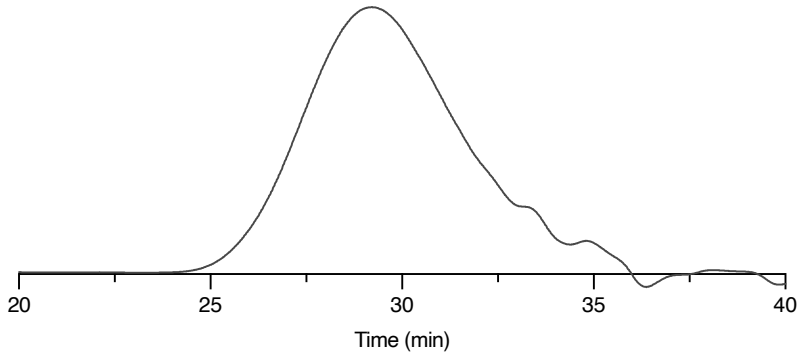

Figure S29 – SEC chromatogram (before purification) of P(A1T2).

P(A2T1)

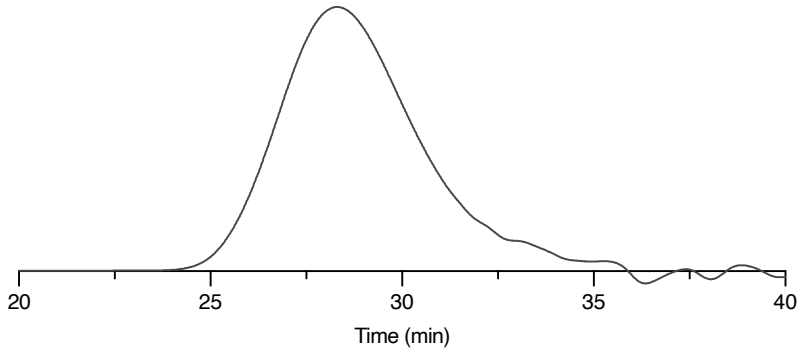

Figure S30 – SEC chromatogram (before purification) of P(A2T1).

P(A2T1)C

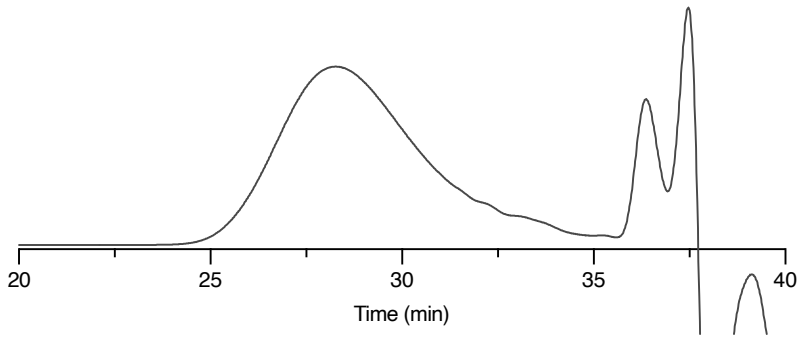

Figure S31 – SEC chromatogram (before purification) of P(A2T1)C.

P(A2T2)

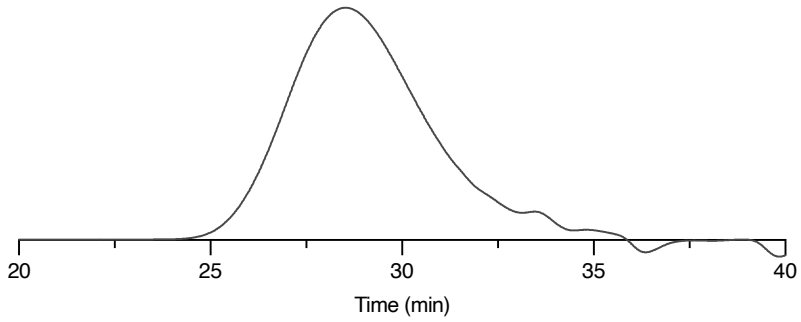

Figure S32 – SEC chromatogram (before purification) of P(A2T2).

P(A3T1)

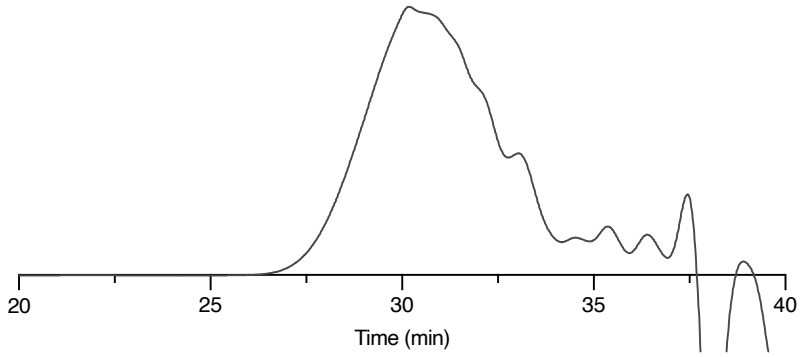

Figure S33 – SEC chromatogram (before purification) of P(A3T1).

P(A3T1)C

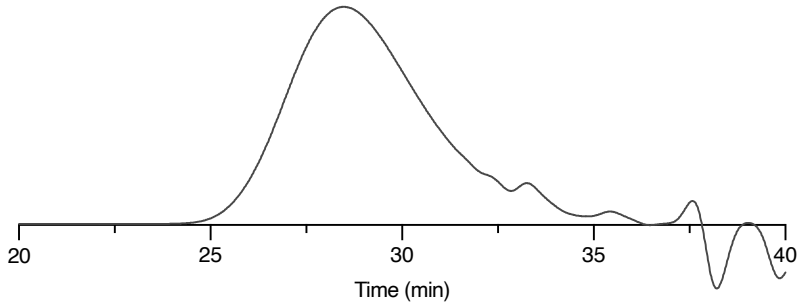

Figure S34 – SEC chromatogram (before purification) of P(A3T1)C.

P(A3T2)

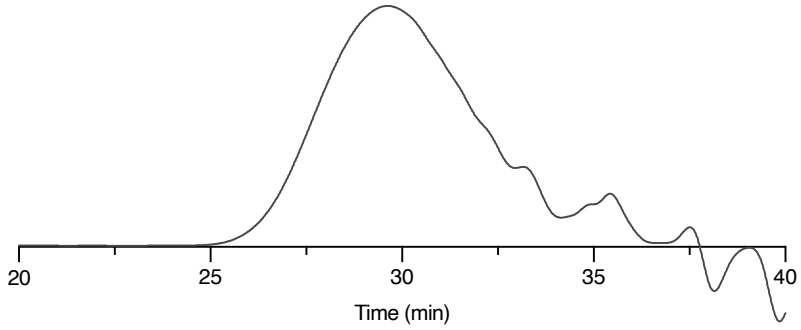

Figure S35 – SEC chromatogram (before purification) of P(A3T2).

7. TGA analyses of pure polymers

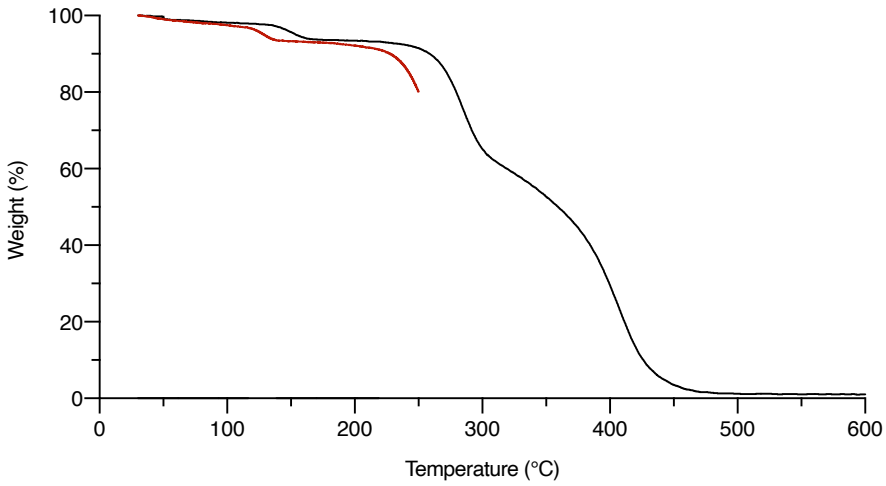

Figure S36 – TGA plot of P(A1T1) at a heating rate of 20 K/min (black) and 2 K/min (red).

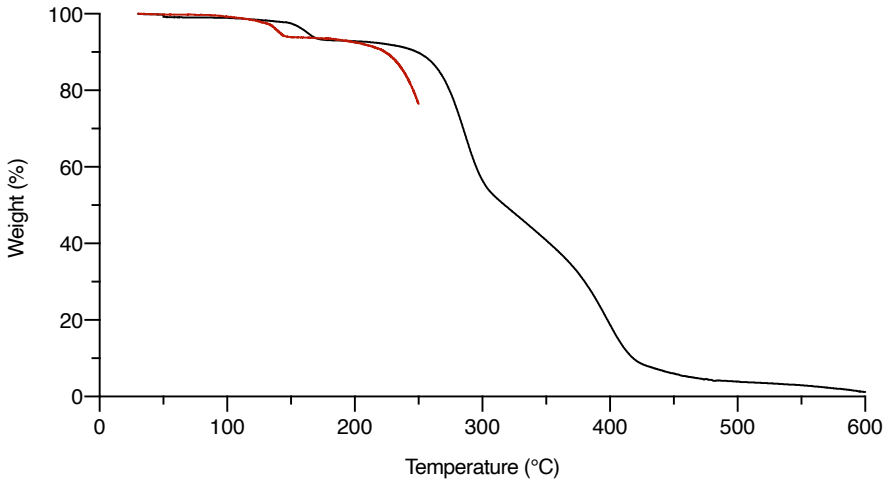

Figure S37 – TGA plot of P(A1T1)C at a heating rate of 20 K/min (black) and 2 K/min (red).

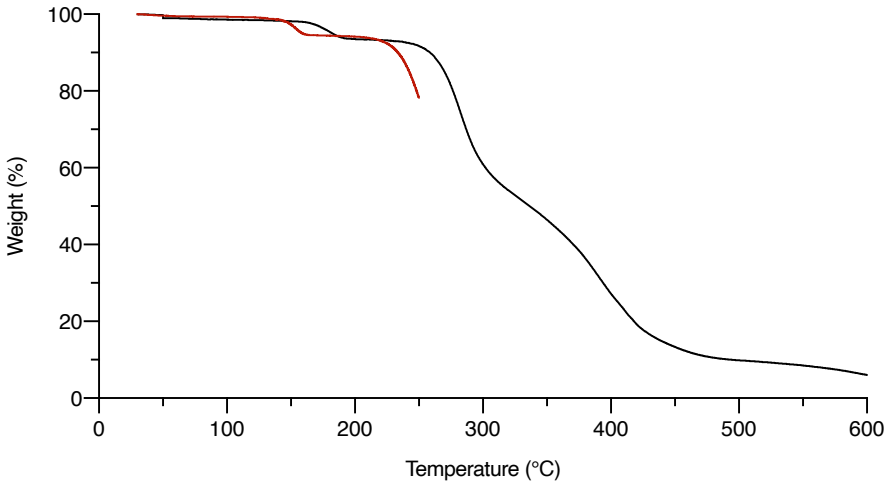

Figure S38 – TGA plot of P(A1T2) at a heating rate of 20 K/min (black) and 2 K/min (red).

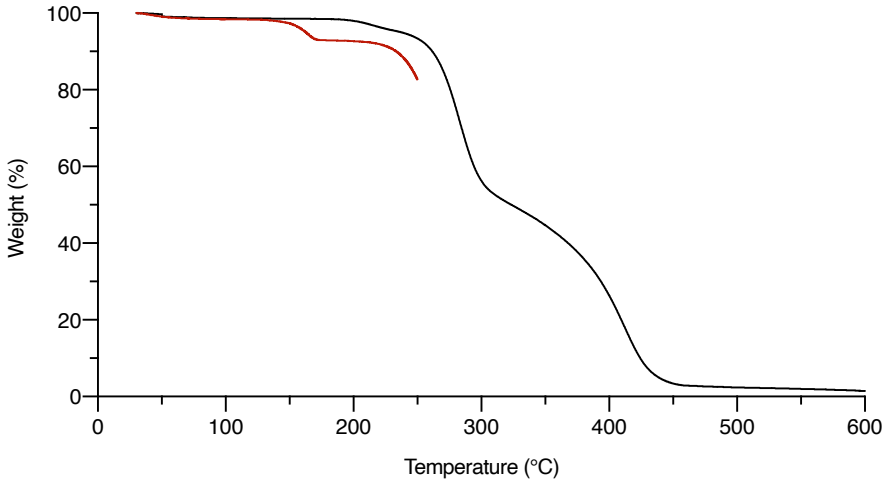

Figure S39 – TGA plot of P(A2T1) at a heating rate of 20 K/min (black) and 2 K/min (red).

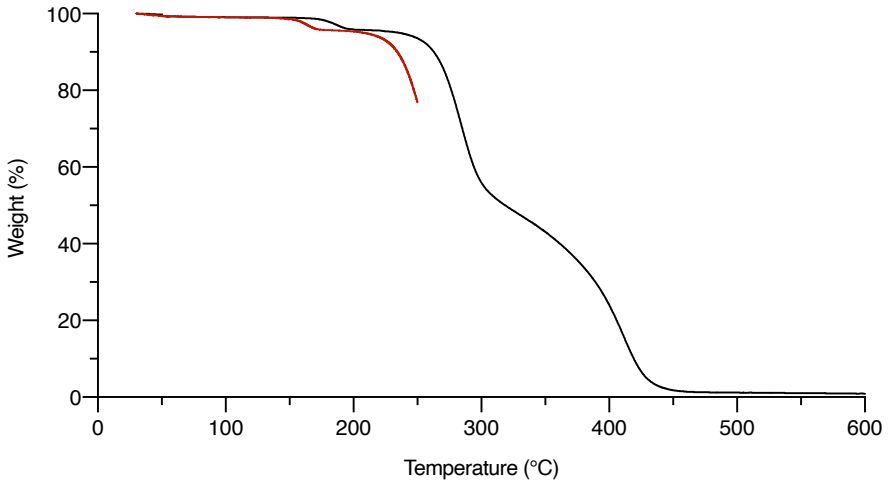

Figure S40 – TGA plot of P(A2T1)C at a heating rate of 20 K/min (black) and 2 K/min (red).

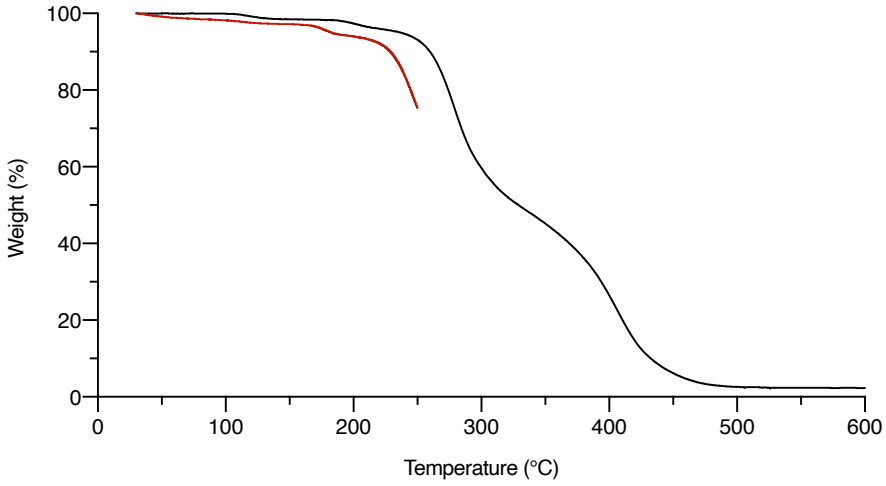

Figure S41 – TGA plot of P(A2T2) at a heating rate of 20 K/min (black) and 2 K/min (red).

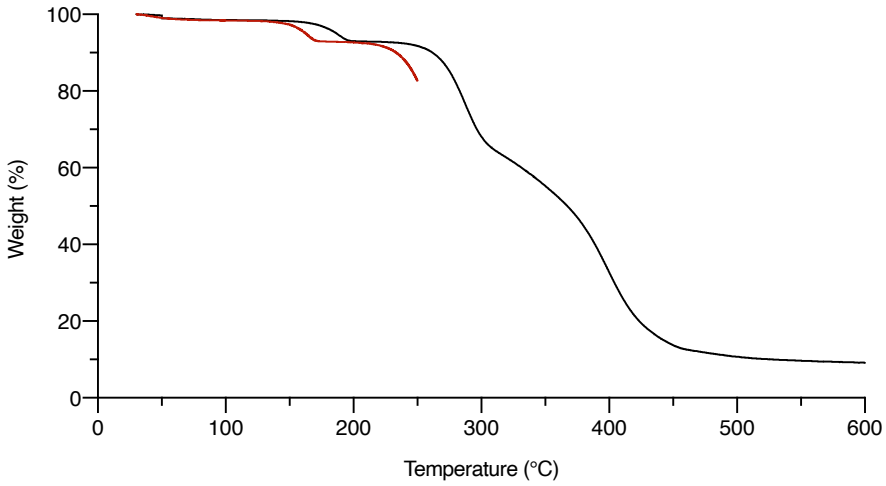

Figure S42 – TGA plot of P(A3T1) at a heating rate of 20 K/min (black) and 2 K/min (red).

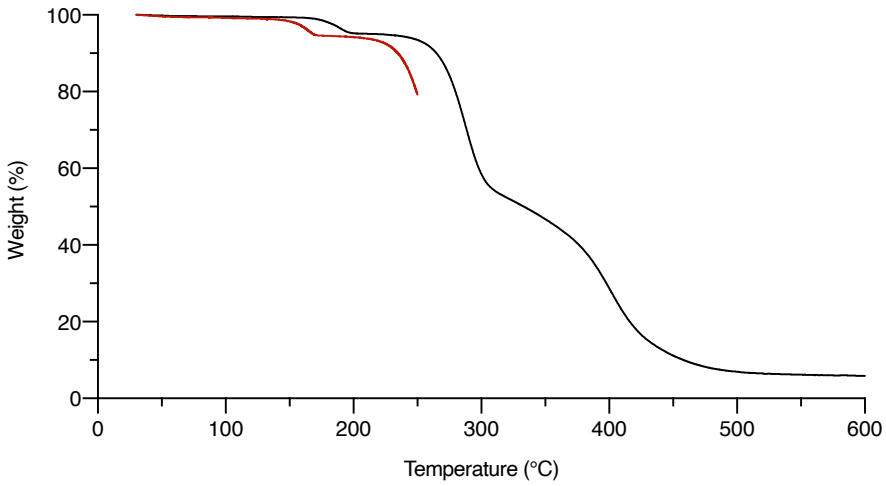

Figure S43 – TGA plot of P(A3T1)C at a heating rate of 20 K/min (black) and 2 K/min (red).

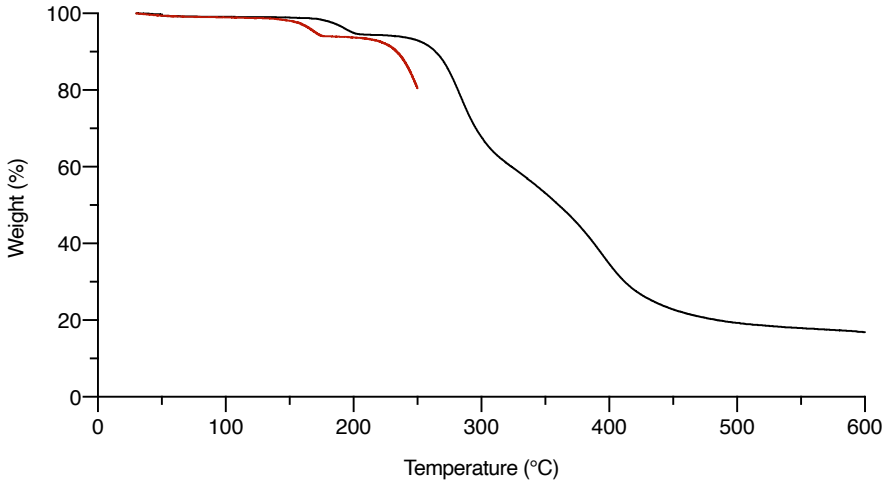

Figure S44 – TGA plot of P(A3T2) at a heating rate of 20 K/min (black) and 2 K/min (red).

8. DSC analyses of pure polymers

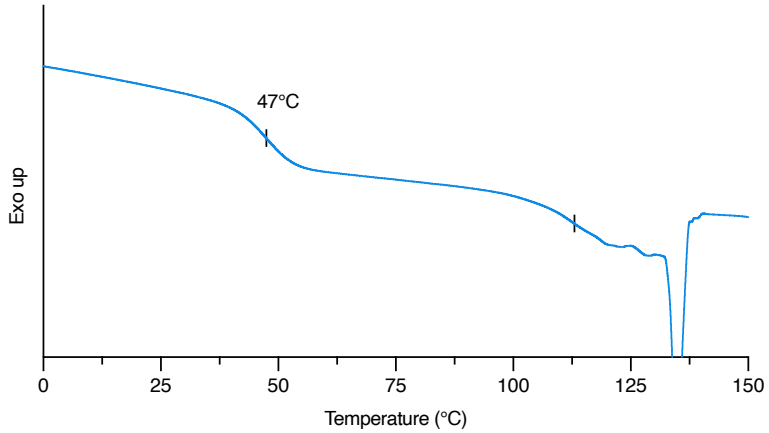

Figure S45 – Reversing heat flow by modulated DSC of P(A1T1).

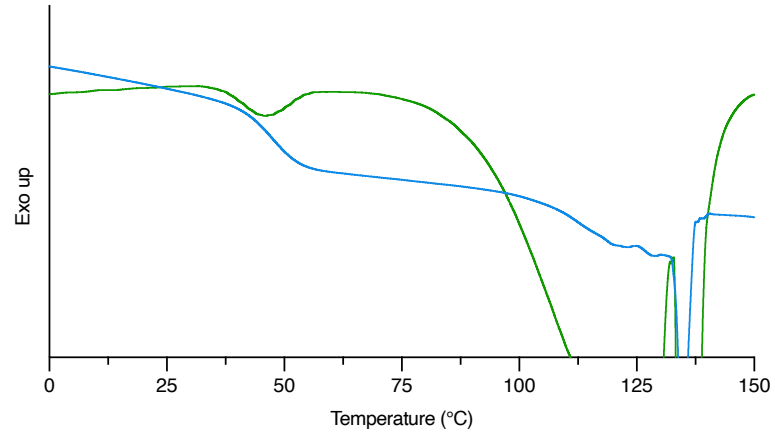

Figure S46 – Reversing heat flow (blue) and non-reversing heat flow (green) by modulated DSC of P(A1T1). The non-reversing curve displays a strong peak due to dehydration overlapping with the potential second T_g region.

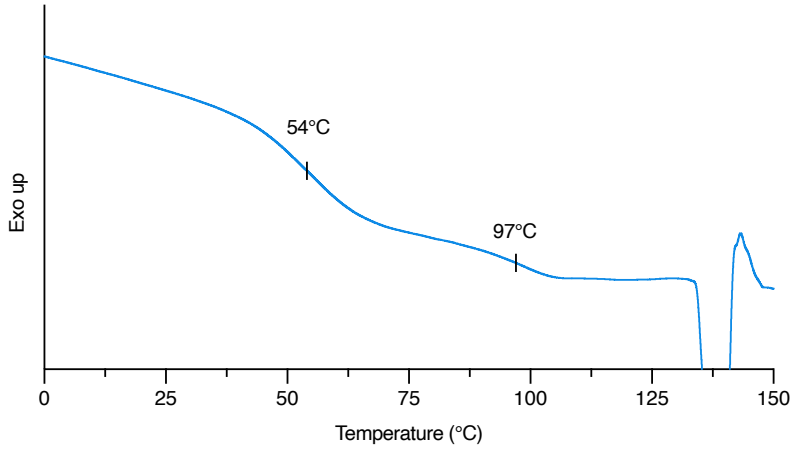

Figure S47 – Reversing heat flow by modulated DSC of P(A1T1)C.

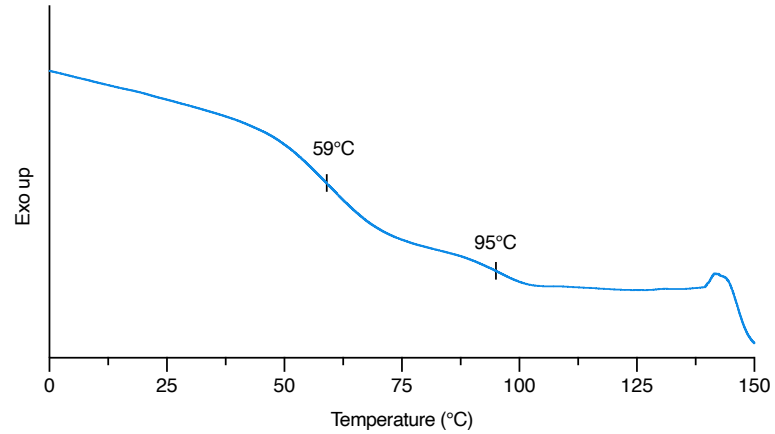

Figure S48 – Reversing heat flow by modulated DSC of P(A1T2).

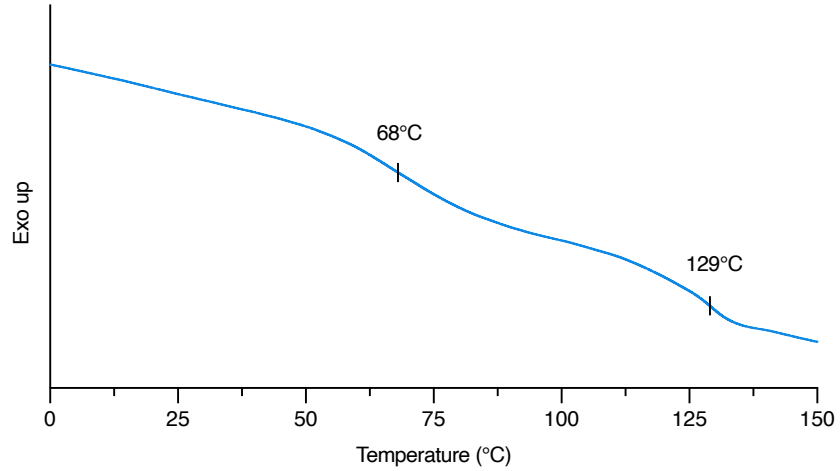

Figure S49 – Reversing heat flow by modulated DSC of P(A2T1).

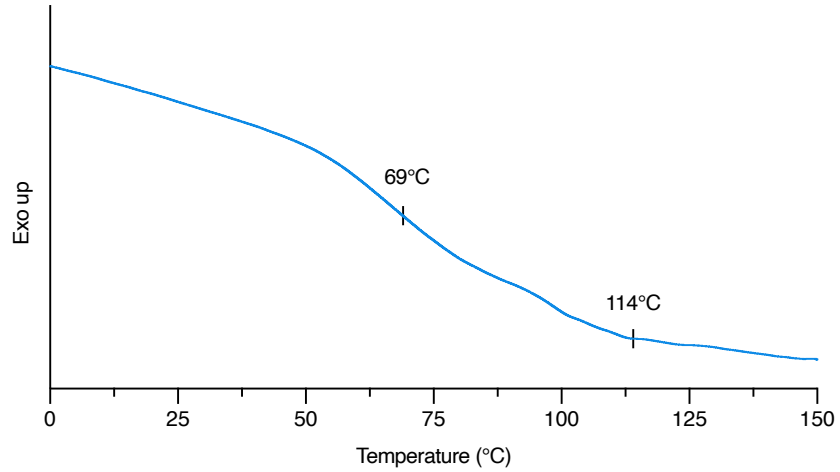

Figure S50 – Reversing heat flow by modulated DSC of P(A2T1)C.

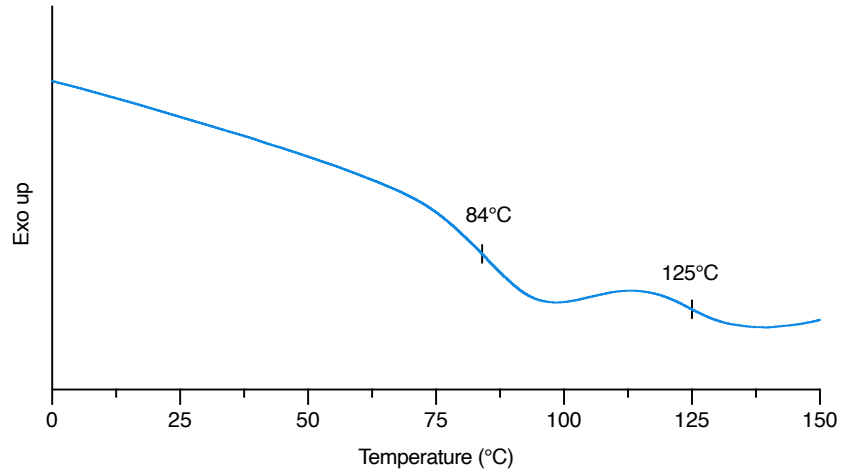

Figure S51 – Reversing heat flow by modulated DSC of P(A2T2).

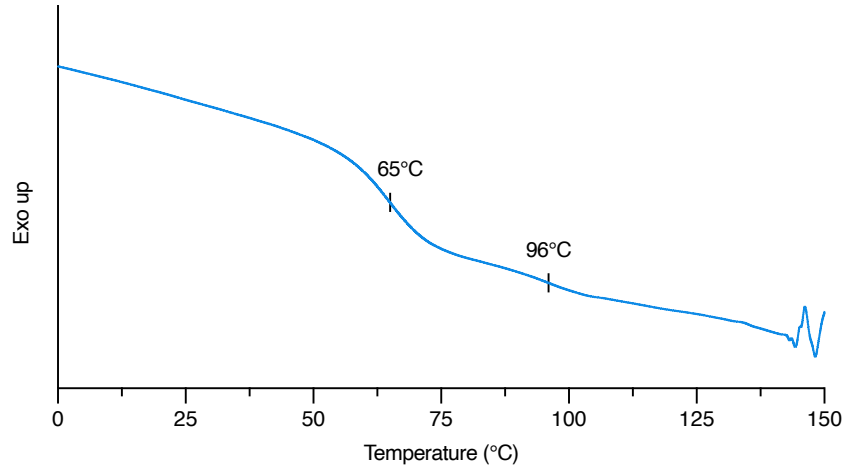

Figure S52 – Reversing heat flow by modulated DSC of P(A3T1).

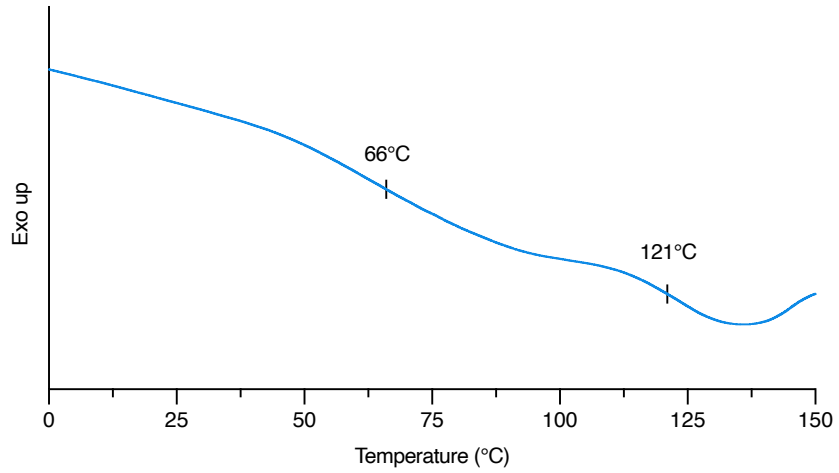

Figure S53 – Reversing heat flow by modulated DSC of P(A3T1)C.

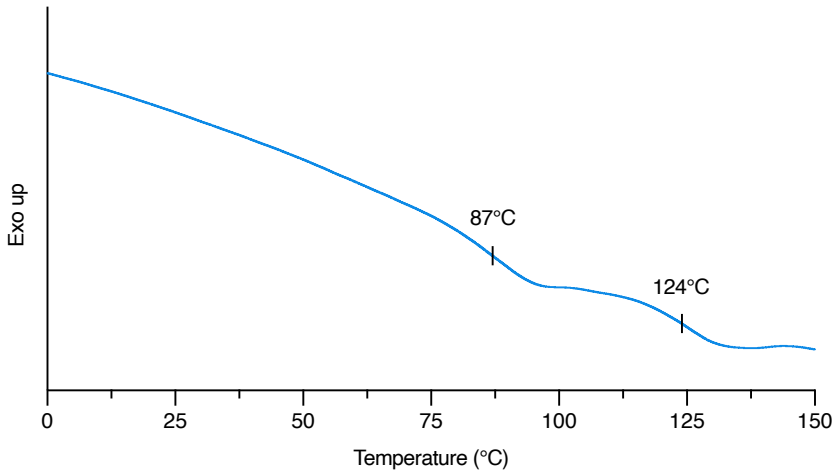

Figure S54 – Reversing heat flow by modulated DSC of P(A3T2).

9. Modulated DSC experiments

Conventional DSC experiments didn't lead to any exploitable results. However, the modulated DSC technique is characterized by a higher sensitivity which has lead to the observation to 2 weak and broad T_gs for all copolymers. In order to shed light on this unusual feature, several experiments were achieved on the polymer P(A1T2), chosen for an optimal temperature window between the second transition and the dehydration reaction at higher temperature which can be observed on the non-reversing heat flow curve. For most polymers, the dehydration peak start was close to the second transition. After selection of the polymer, the herein described experiments were conducted:

General procedure:

- Heating from 25 to 90 °C (10 °C/min)
- Cooling to -40 °C (10 °C/min)
- *Modulation of temperature (amplitude 2°C; period 60 s)*
- Heating to 200 °C (2 °C/min)

This procedure leads to the observation of two weak and broad T_g.

Annealing above the second T_g:

- Heating from 25 to 90 °C (10 °C/min)
- Cooling to -40 °C (10 °C/min)
- *Modulation of temperature (amplitude 2°C; period 60 s)*
- Heating to 110 °C (2 °C/min) [Annealing of polymer]
- Cooling to -40 °C (10 °C/min)
- Heating to 130 °C (2 °C/min)

With this procedure, the first part of the experiment stays the same except that the sample is heated up to 110 °C. The second T_g of the polymer, determined in the first curve, is observed at 95°C. On the next cycle (after annealing without isothermal), only the first T_g is observed.

As dehydrated polymers are characterized by a single T_g similar to the first T_g of the hydroxy-polymers, a new experiment was achieved with post-experience polymer chemical structure analysis.

Annealing above the second T_g with post-experiment characterization:

- Heating from 25 to 90 °C (10 °C/min)
- Cooling to -40 °C (10 °C/min)

- *Modulation of temperature (amplitude 2°C; period 60 s)*
- Heating to 110 °C (2 °C/min) [Annealing of polymer]

As this experiment stops just after polymer annealing, the sample was subsequently taken out of the pan and analyzed by ^{1}H-NMR analysis. No trace of dehydration was observed and the chemical structure of the polymer was intact. Then, these experiments indicate that the second transition may be an irreversible event which disappears after fast annealing.

Other experiments were conducted:

- Slow cooling (rate of 2 °C/min) after annealing
- Isothermal of 30 minutes at 85°C (between the two transitions) on cooling
- Fast cooling (rate of 150 °C/min) after annealing

However, these supplementary experiments didn't affect the curves.

10. Polymerizations with various DBU loadings

The polymerization of **bisαCC** was considered with **AA1** and **TT1** using different loadings of DBU. The linkage ratio **TL1** / **TL2** was determined by integration of characteristic peaks for each functionality (peak F for **TL1**; peak J for **TL2**). As the residual DMF peaks were overlapping with the 2 signals of interest, the lone peak of DMF at 7.95 ppm was simply integrated and used to subtract the theorical DMF integration from the F and J signals (Figure S56).

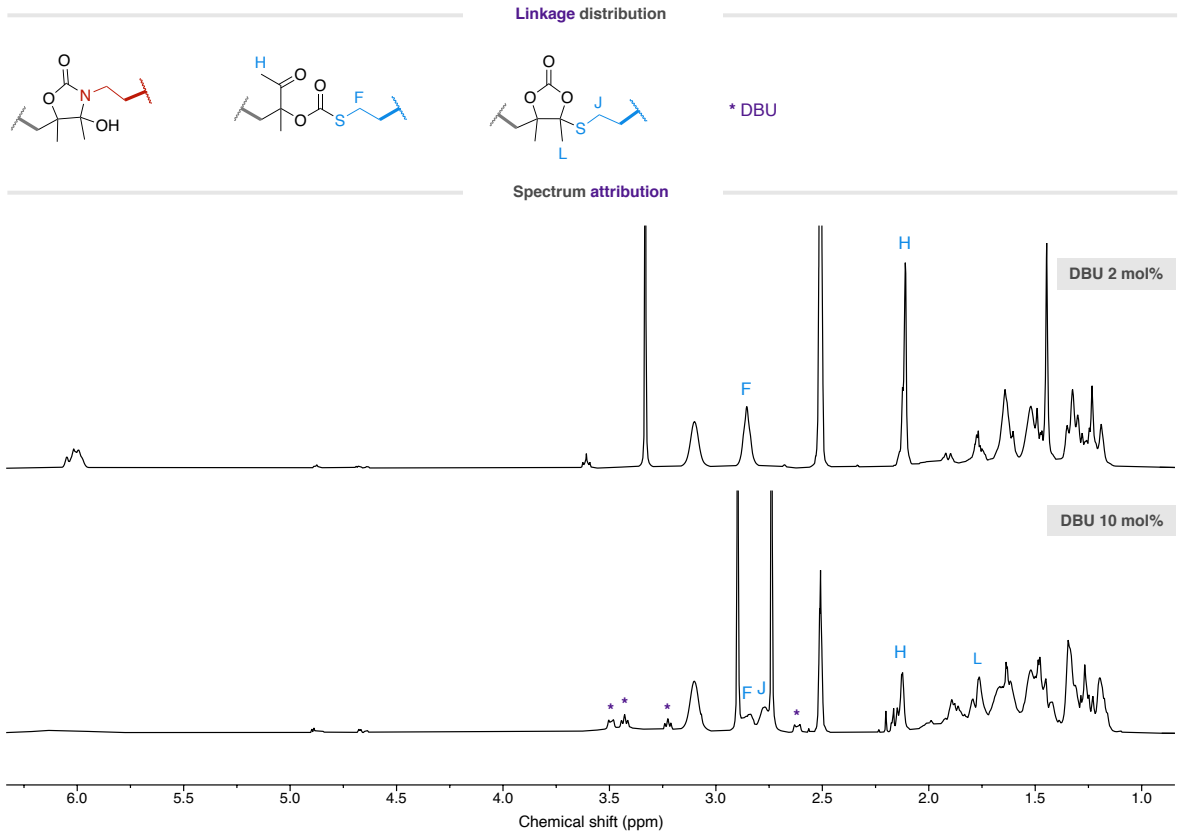

Figure S55 – ^{1}H-NMR spectrum of polymers made from **AA1** and **TT1** with 2 mol% and 10 mol% of DBU (400 MHz, DMSO-d_6). The polymer made from 2 mol% of DBU is pure (P(A1T1)C) and the polymer made from 10 mol% of DBU was analyzed after one precipitation in diethyl ether.

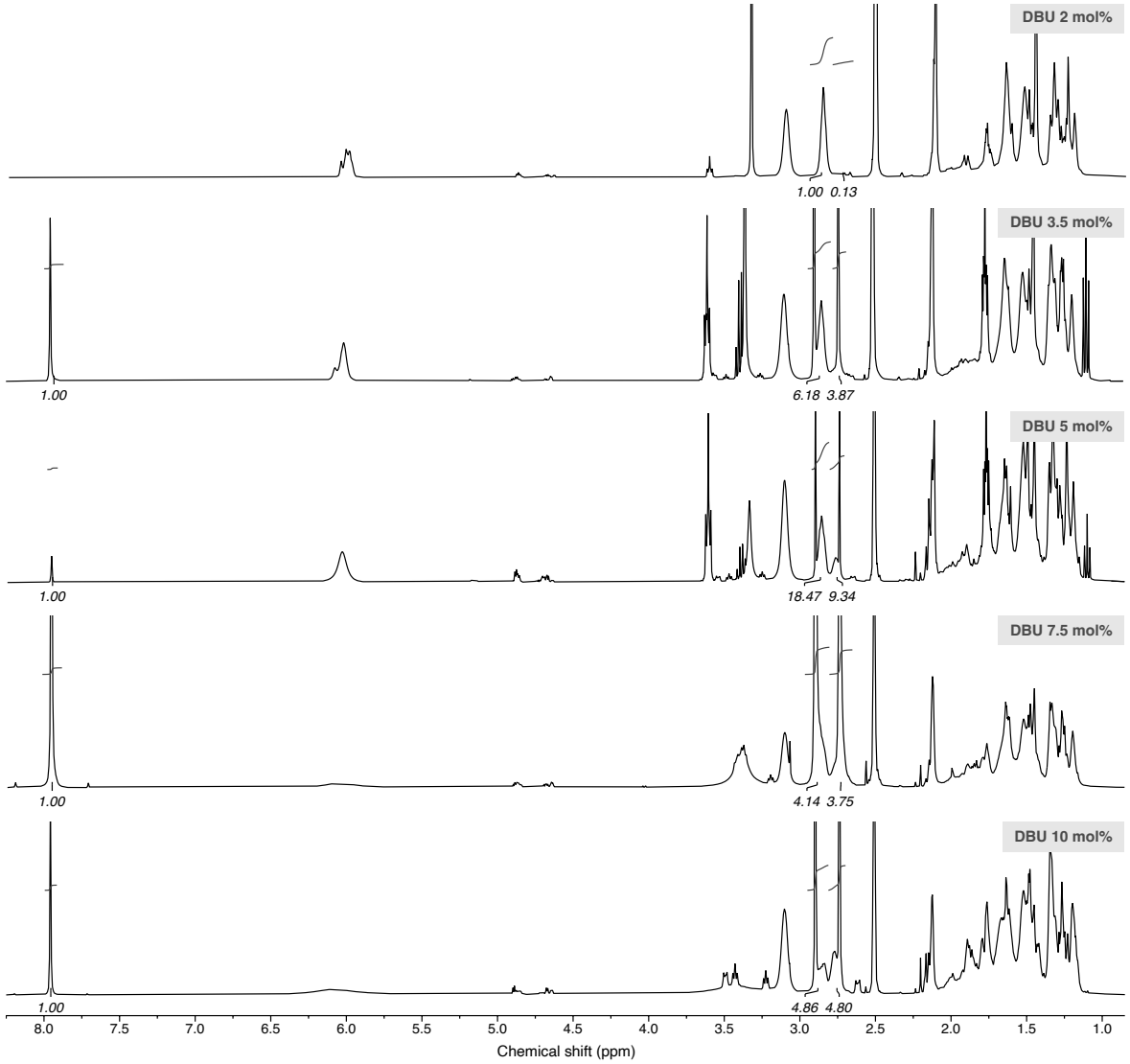

Figure S56 – ^{1}H-NMR spectrum of polymers made from **AA1** and **TT1** with 2 mol% to 10 mol% of DBU (400 MHz, DMSO-d_6). The polymer made from 2 mol% of DBU is pure (P(A1T1)C) and the other polymers were analyzed after one precipitation in diethyl ether.

Table S2 - Molecular characteristics and linkages selectivity for the polymerization of BisαCC with **AA1** and **TT1** after 24h of reaction with different DBU loadings. Polymerizations were carried out at 25 °C in DMF.

Entry	Diamine	Dithiol	DBU (mol%)	M_n (g/mol)[a]	M_w (g/mol)[a]	D[a]	Ratio AL1/AL2	Ratio TL1/TL2
1	AA1	TT1	--	3500	6100	1.76	16 / 84	100 / 0
2			2	12900	24500	1.89	0 / 100	88 / 12
3			3.5	11400	20600	1.80	0 / 100	79 / 21
4			5	9800	16800	1.72	0 / 100	72 / 28
5			7.5	8900	15000	1.70	0 / 100	62 / 38
6			10	11100	19600	1.78	0 / 100	51 / 49

[a]Determined in the crude product by SEC in DMF/LiBr by using a PS calibration

11. NMR characterization of dehydrated polymers

P(A1T1) dehydrated

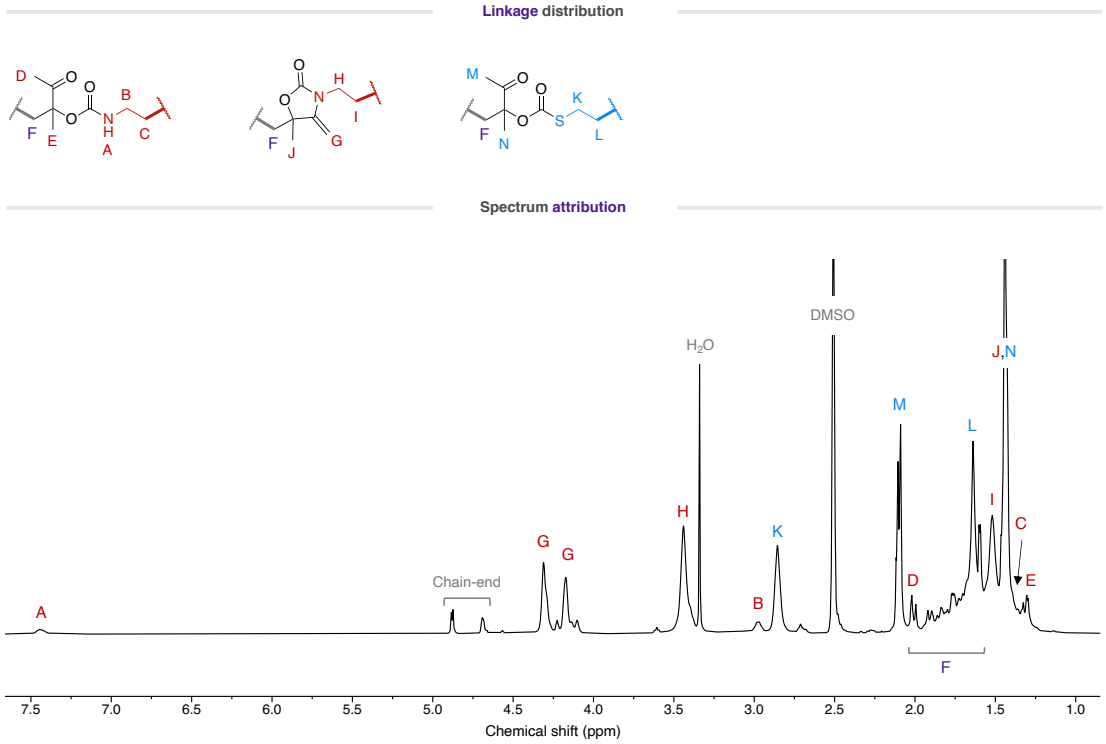

Figure S57 – ^{1}H-NMR spectrum of dehydrated P(A1T1) (400 MHz, DMSO-d_6).

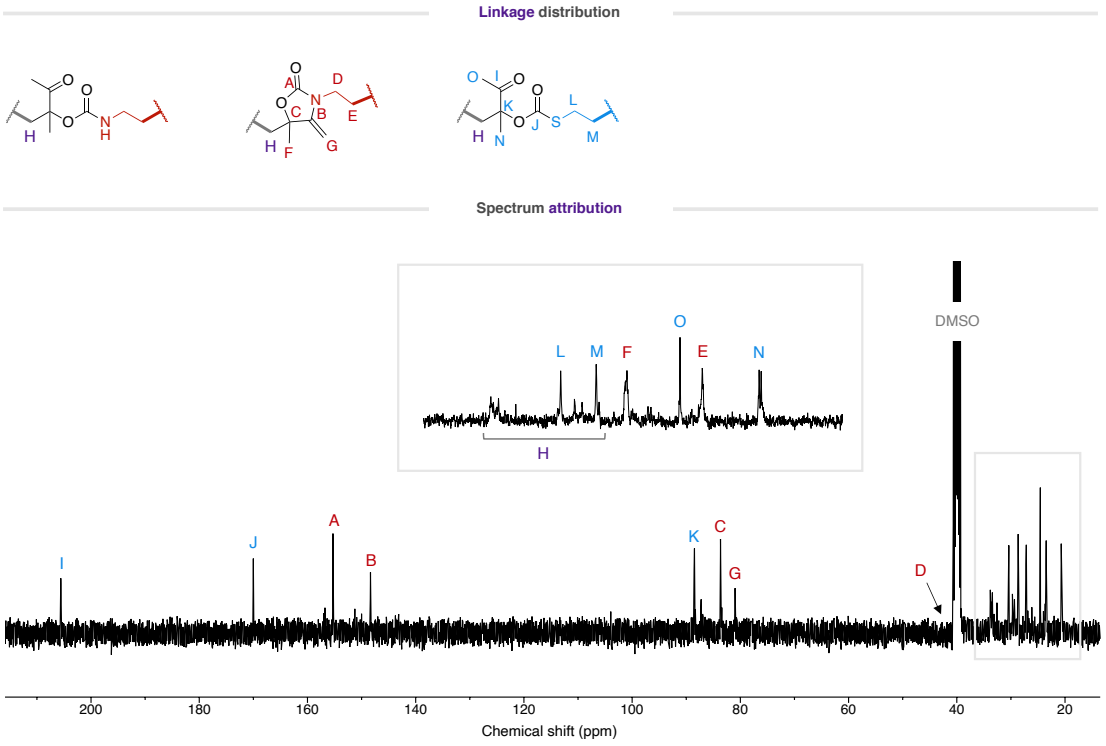

Figure S58 – ^{13}C-NMR spectrum of dehydrated P(A1T1) (101 MHz, DMSO-d_6).

P(A1T1)C dehydrated

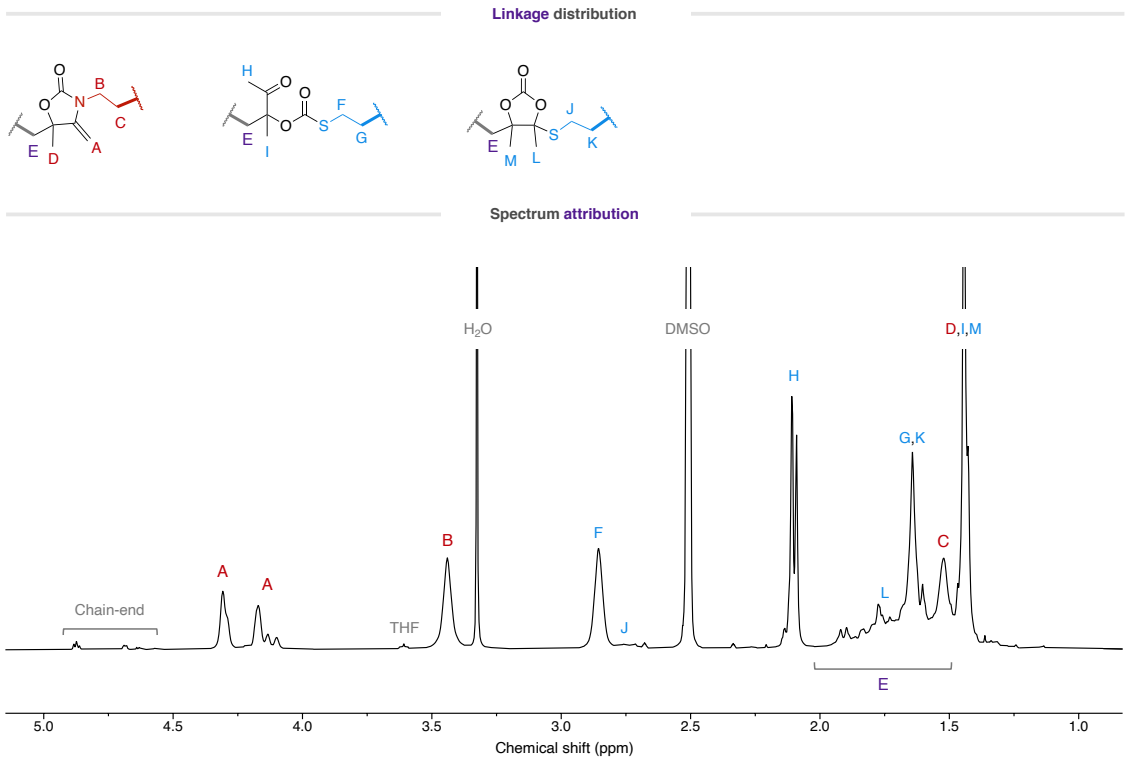

Figure S59 – ^{1}H-NMR spectrum of dehydrated P(A1T1)C (400 MHz, DMSO-d_6).

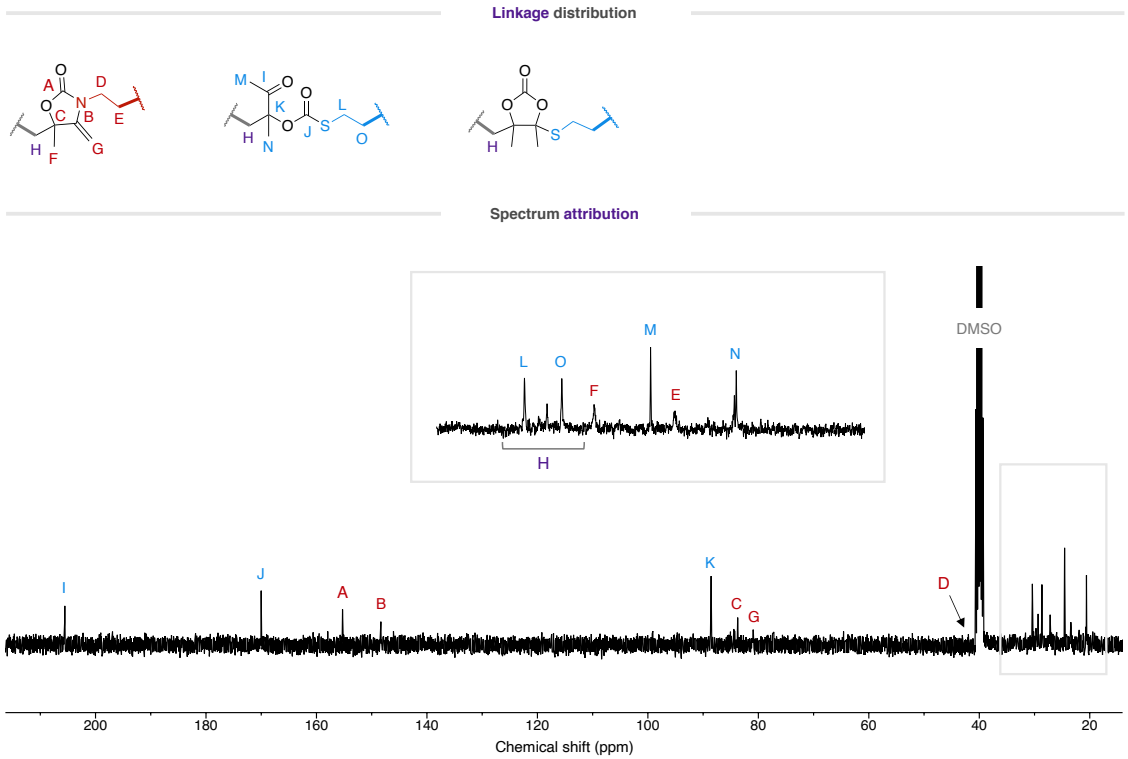

Figure S60 – ^{13}C-NMR spectrum of dehydrated P(A1T1)C (101 MHz, DMSO-d_6).

P(A1T2) dehydrated

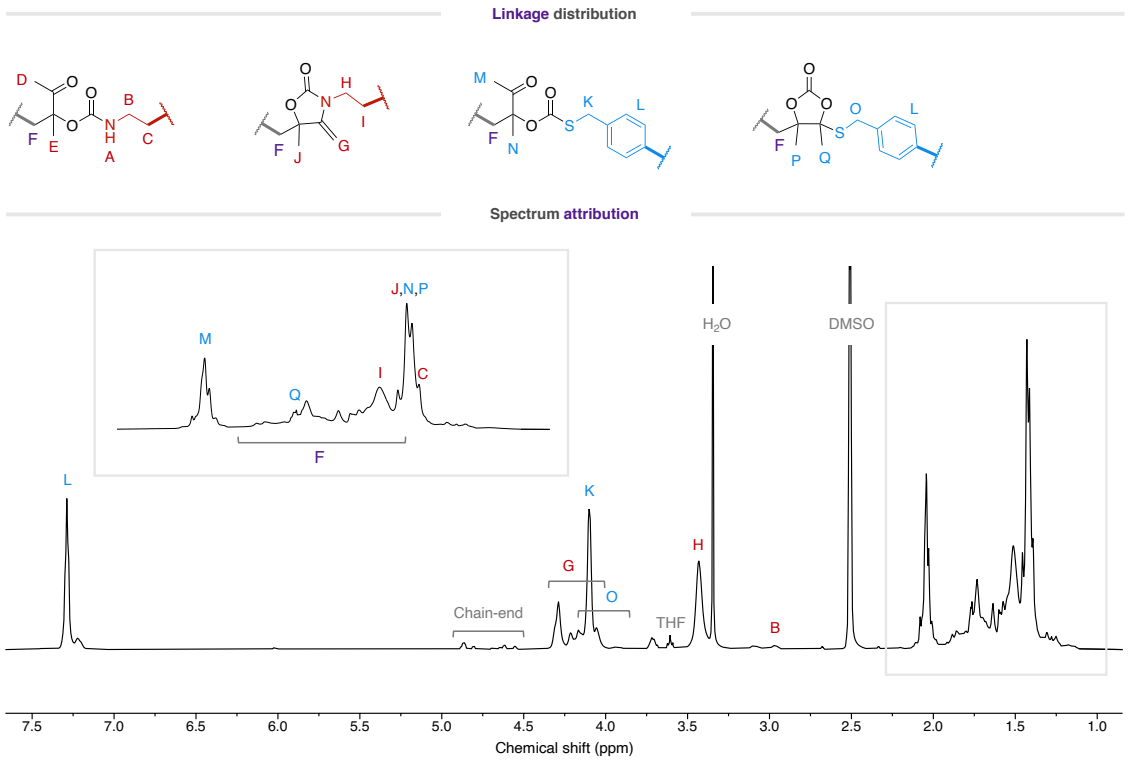

Figure S61 – ^{1}H-NMR spectrum of dehydrated P(A1T2) (400 MHz, DMSO-d_6).

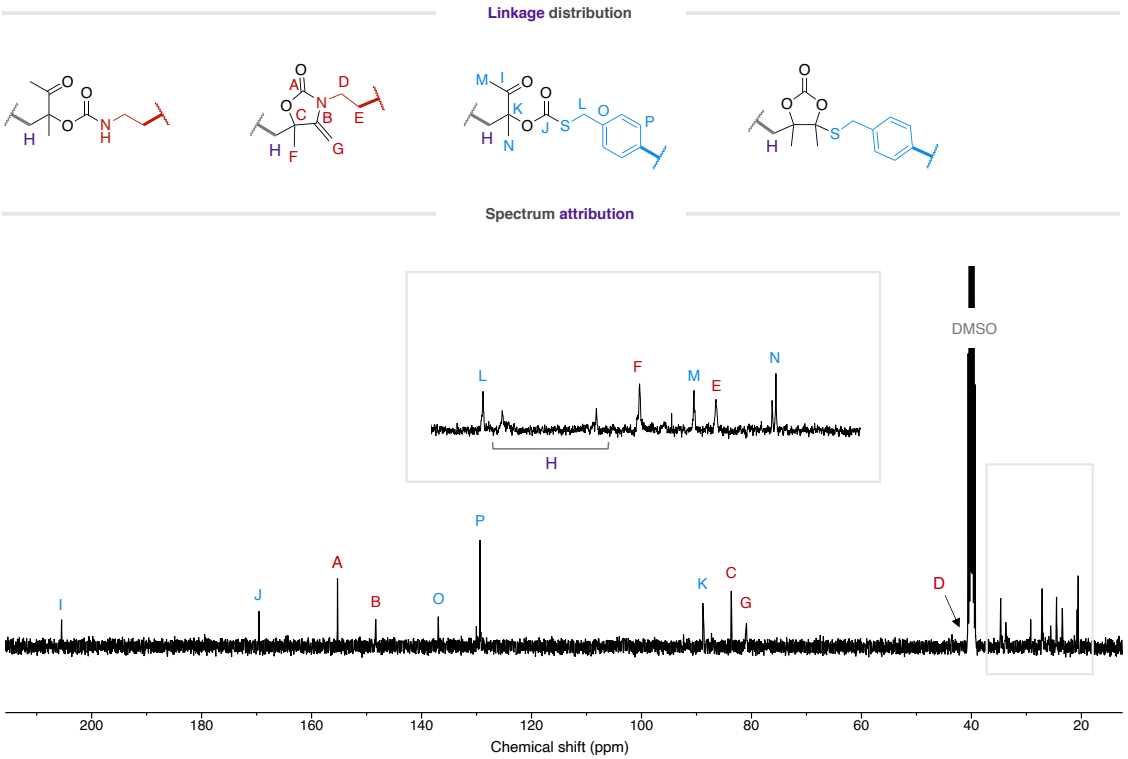

Figure S62 – ^{13}C-NMR spectrum dehydrated of P(A1T2) (101 MHz, DMSO-d_6).

P(A2T1) dehydrated

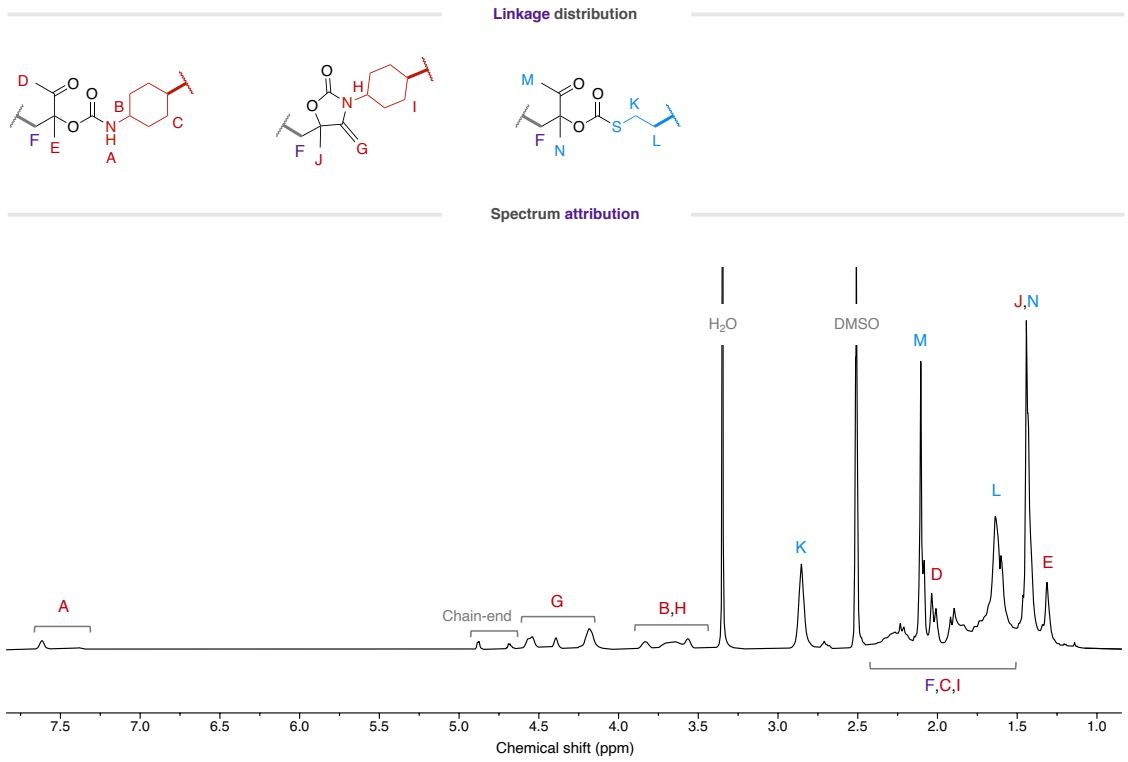

Figure S63 – ^{1}H-NMR spectrum of dehydrated P(A2T1) (400 MHz, DMSO-d_6).

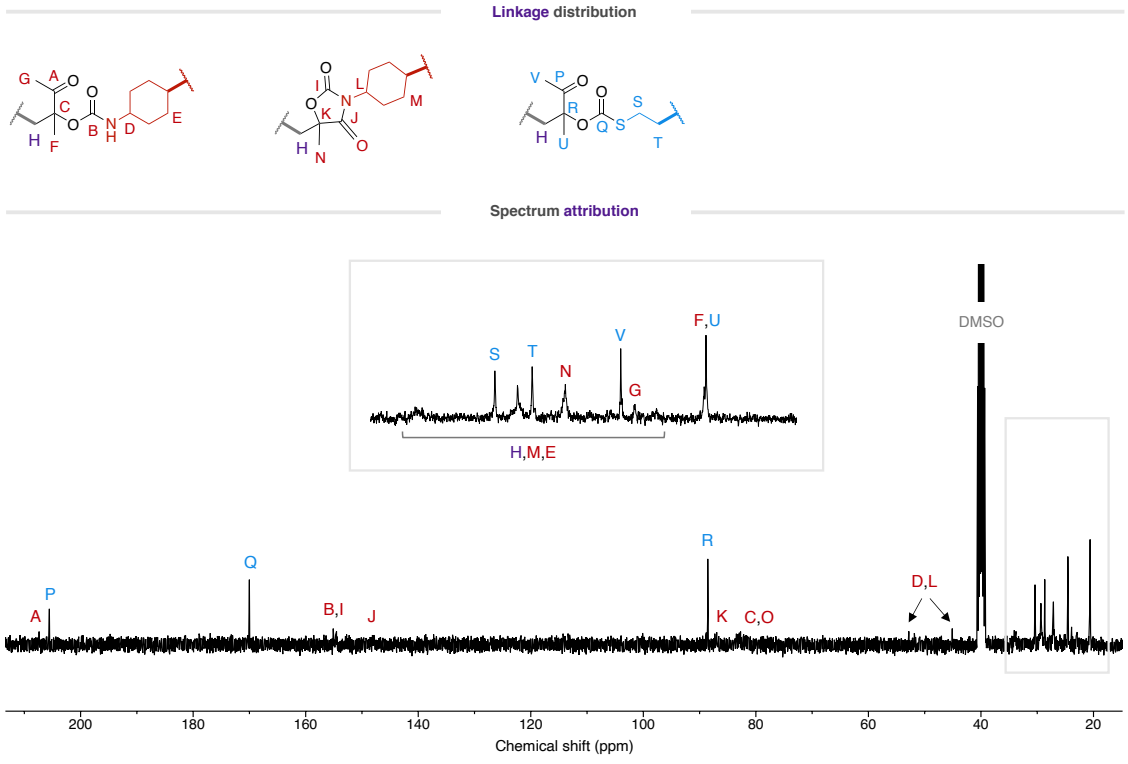

Figure S64 – ^{13}C-NMR spectrum of dehydrated P(A2T1) (101 MHz, DMSO-d_6).

P(A2T1)C dehydrated

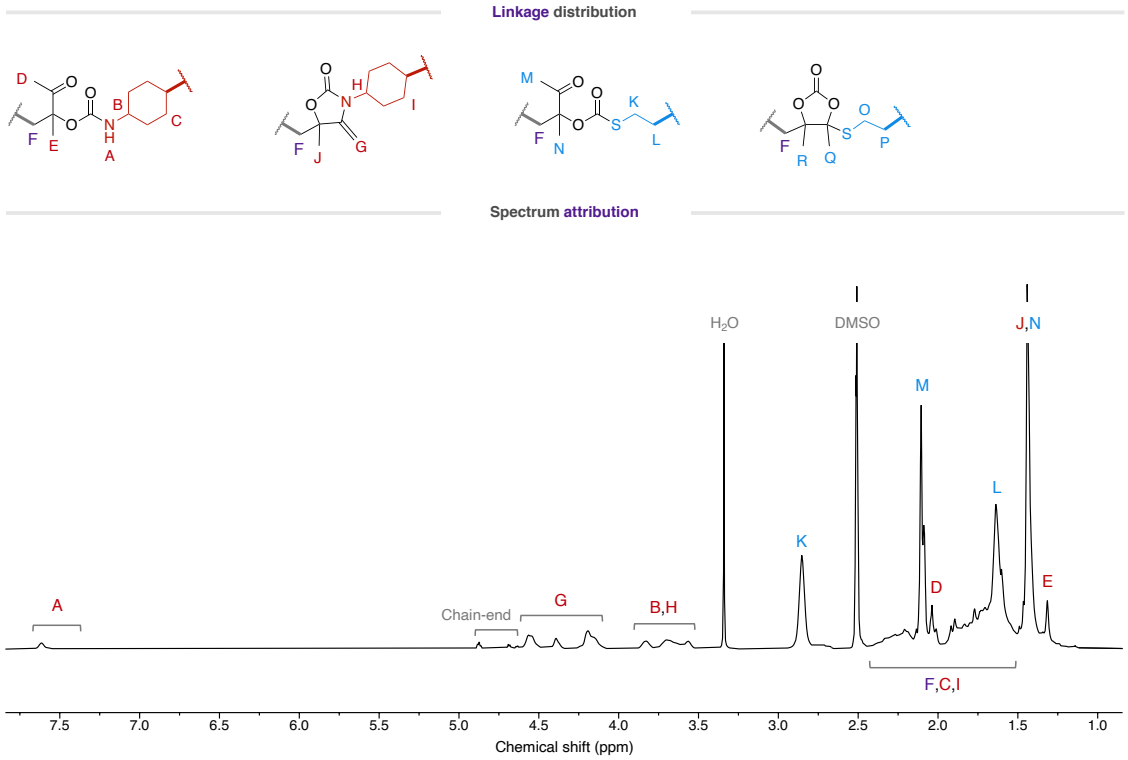

Figure S65 – ^{1}H-NMR spectrum of dehydrated P(A2T1)C (400 MHz, DMSO-d_6).

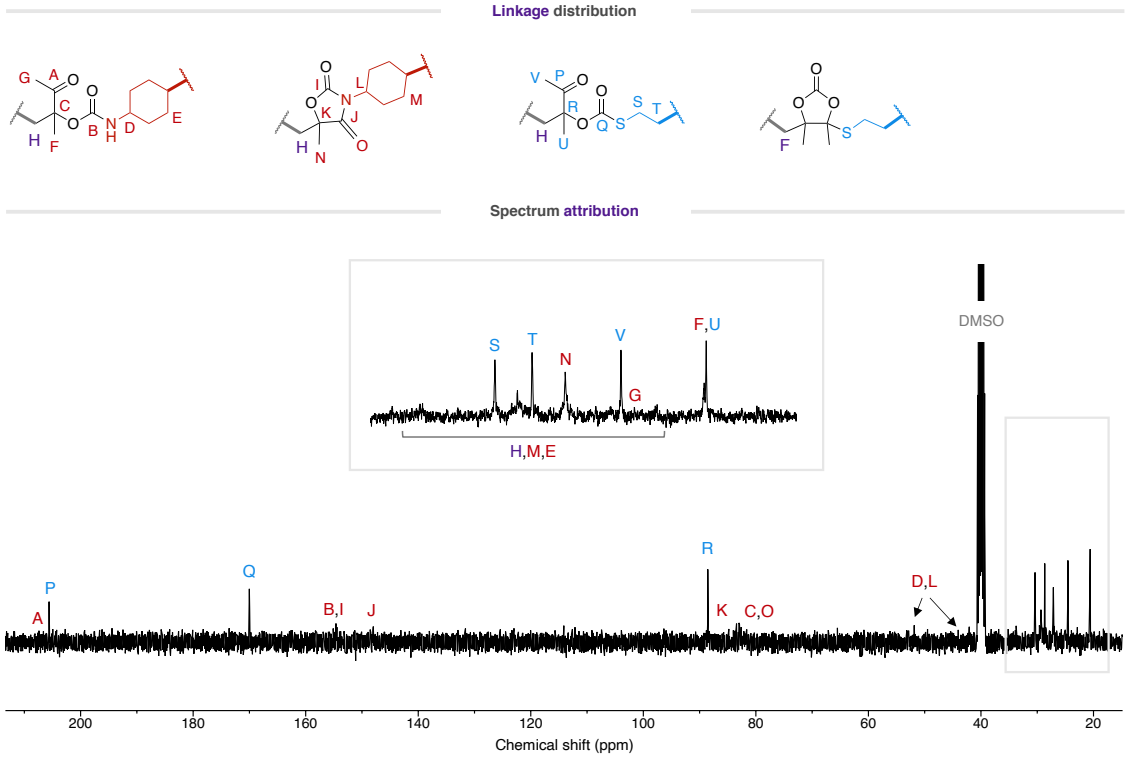

Figure S66 – ^{13}C-NMR spectrum of dehydrated P(A2T1)C (101 MHz, DMSO-d_6).

P(A2T2) dehydrated

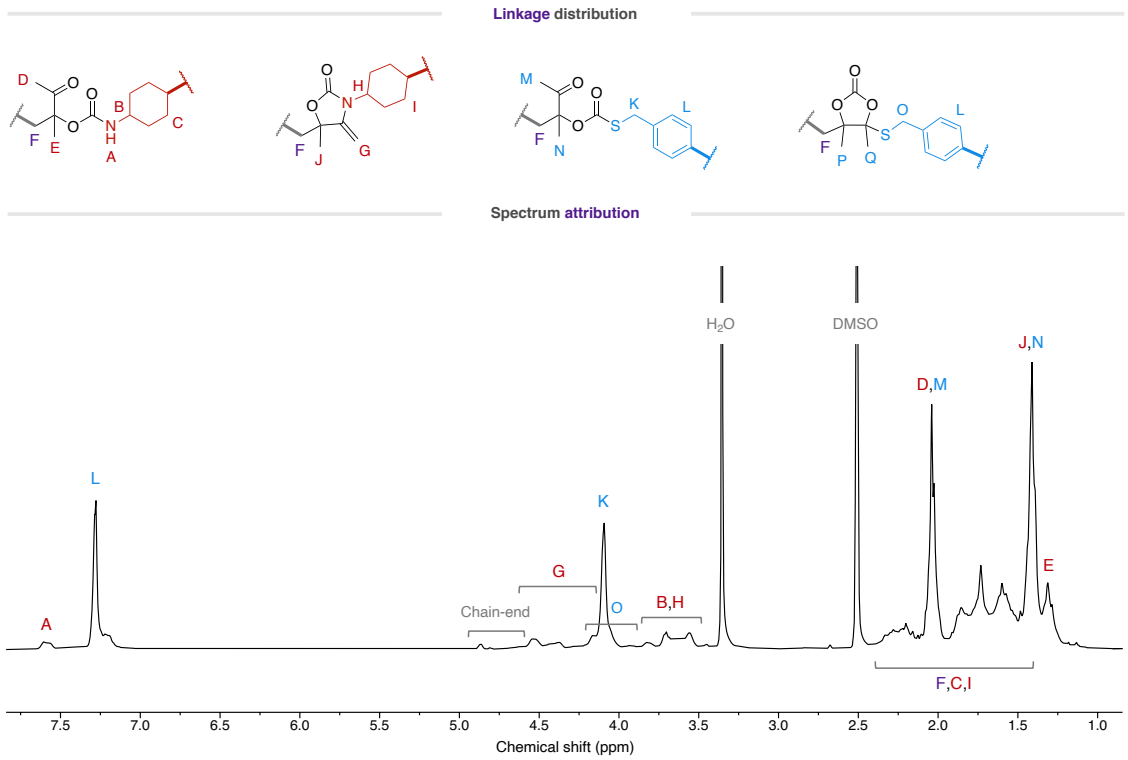

Figure S67 – ^{1}H-NMR spectrum of dehydrated P(A2T2) (400 MHz, DMSO-d_6).

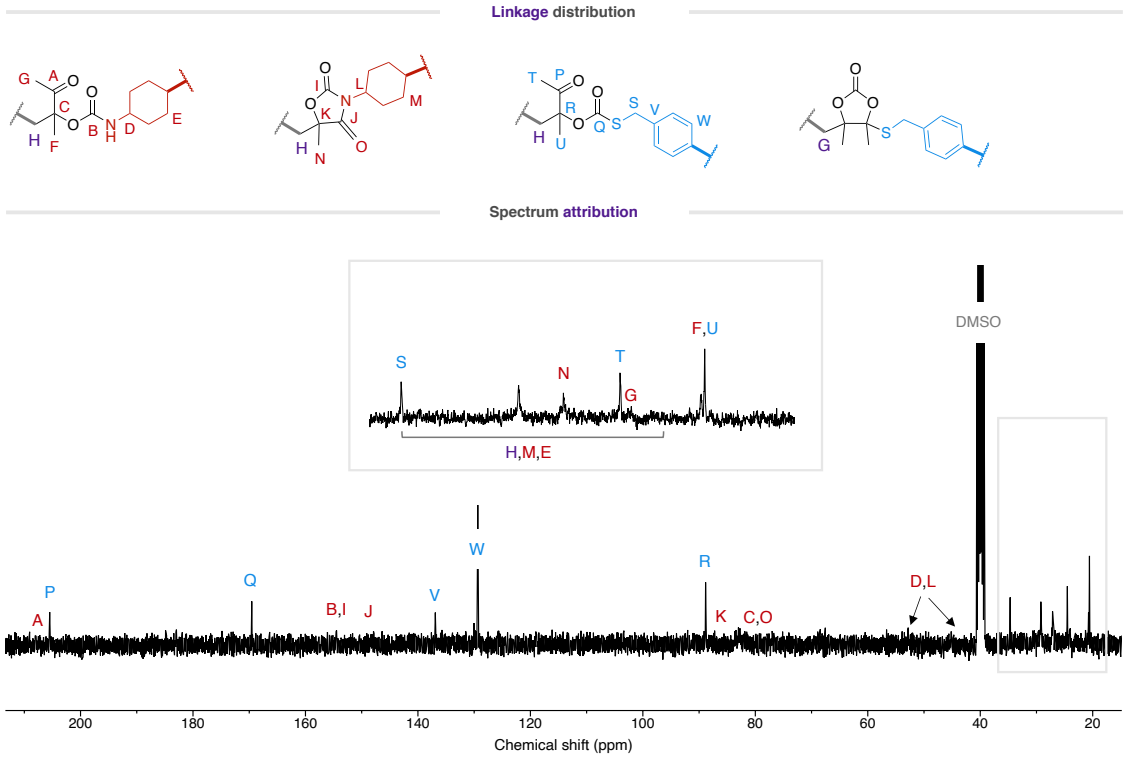

Figure S68 – ^{13}C-NMR spectrum dehydrated of P(A2T2) (101 MHz, DMSO-d_6).

P(A3T1) dehydrated

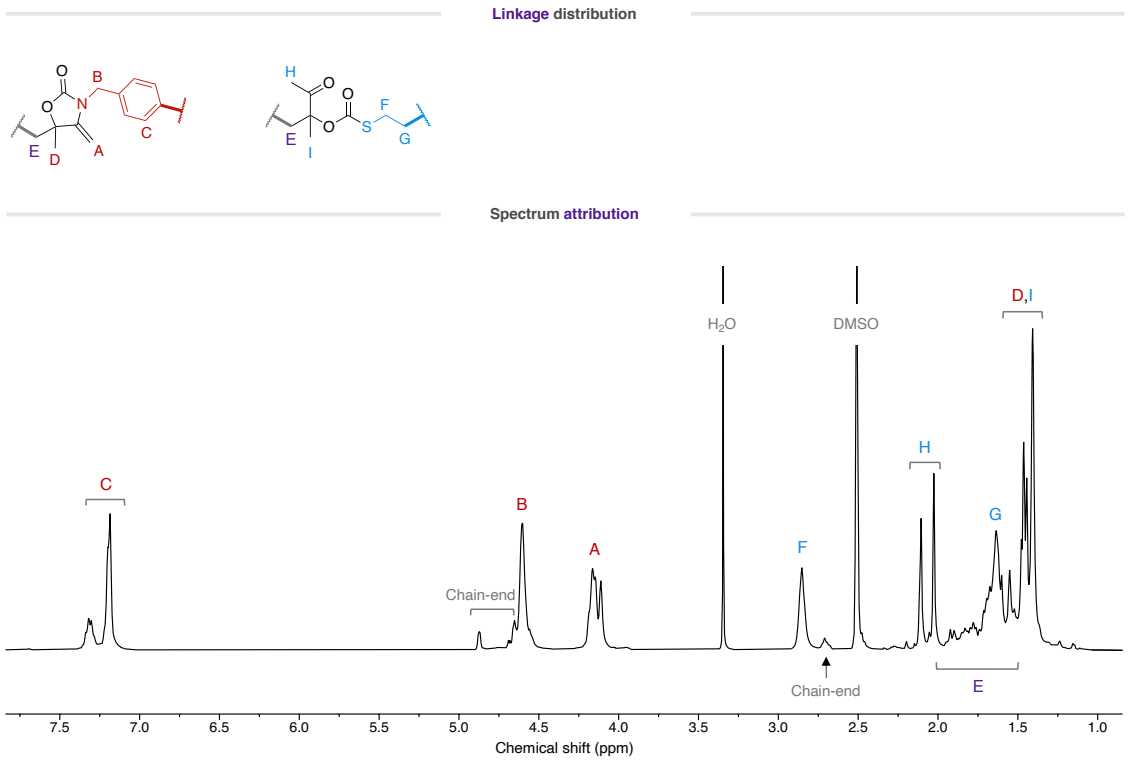

Figure S69 – ^{1}H-NMR spectrum dehydrated of P(A3T1) (400 MHz, DMSO-d_6).

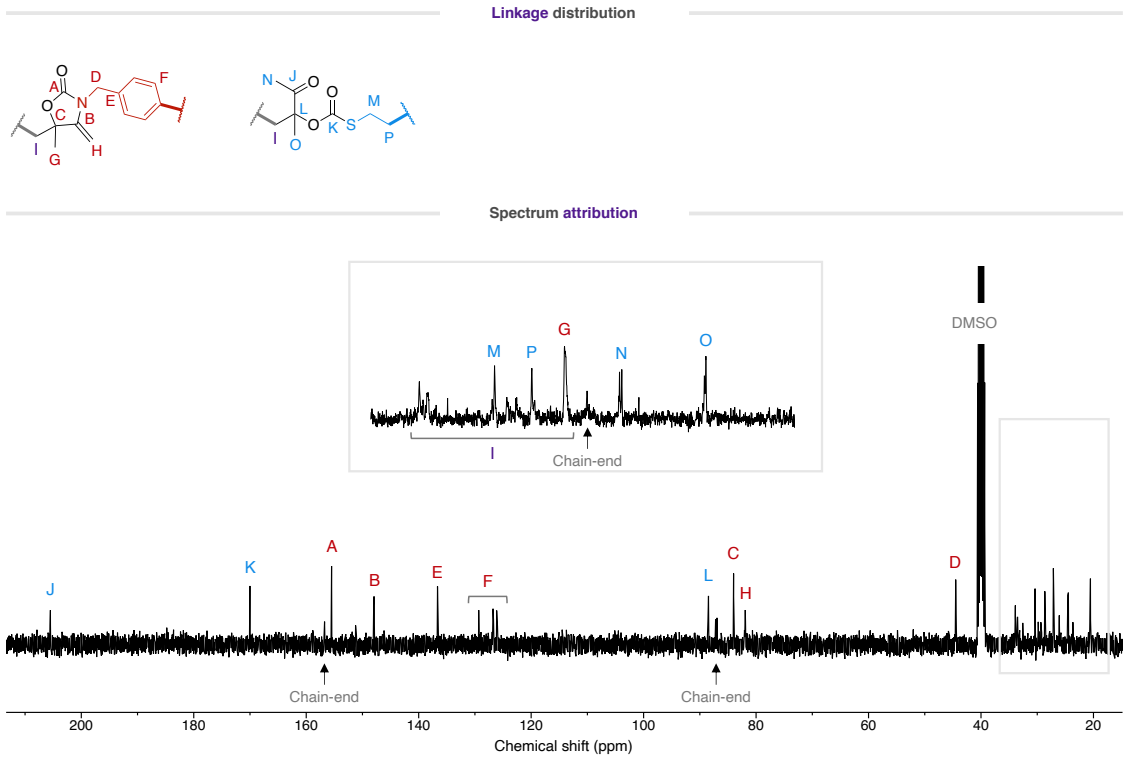

Figure S70 – ^{13}C-NMR spectrum of dehydrated P(A3T1) (101 MHz, DMSO-d_6).

P(A3T1)C dehydrated

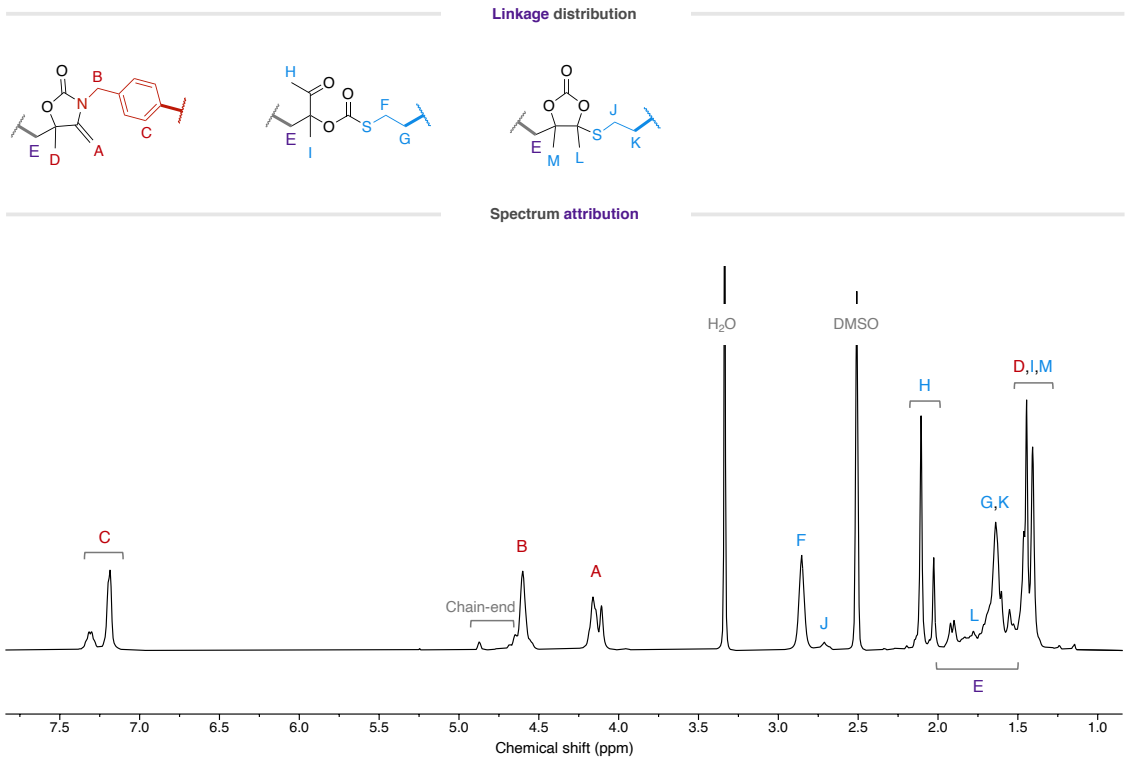

Figure S71 – ^{1}H-NMR spectrum of dehydrated P(A3T1)C (400 MHz, DMSO-d_6).

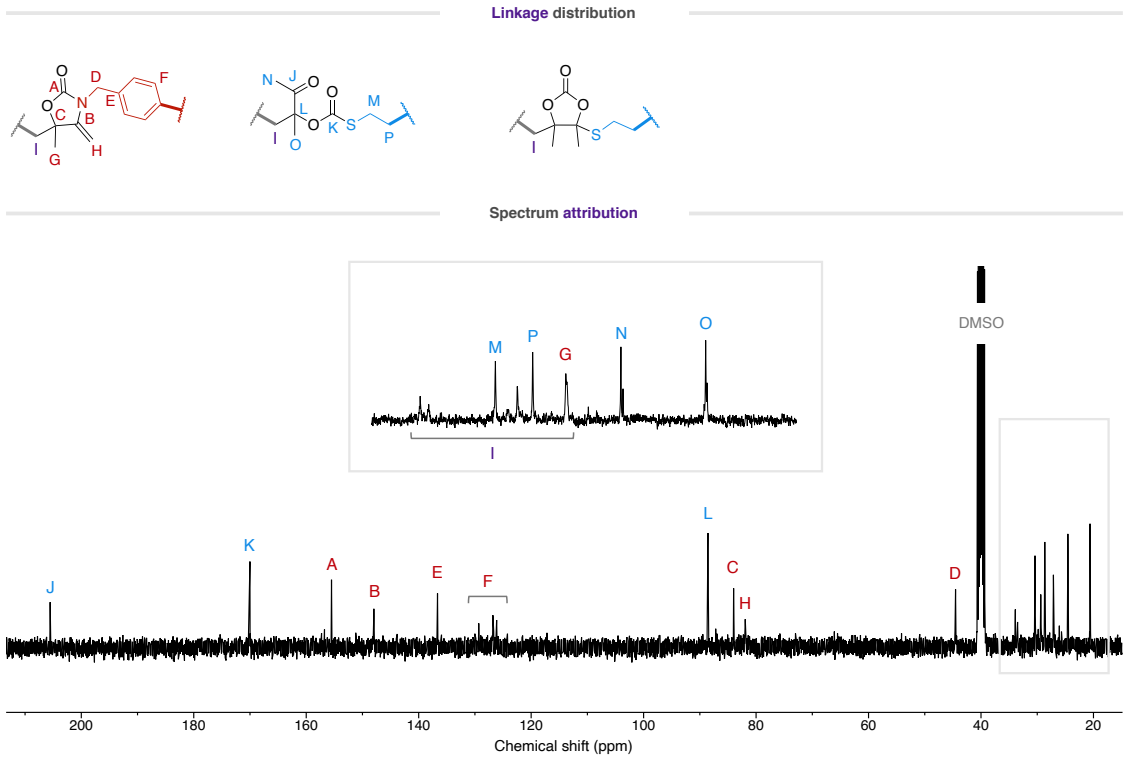

Figure S72 – ^{13}C-NMR spectrum of dehydrated P(A3T1)C (101 MHz, DMSO-d_6).

P(A3T2) dehydrated

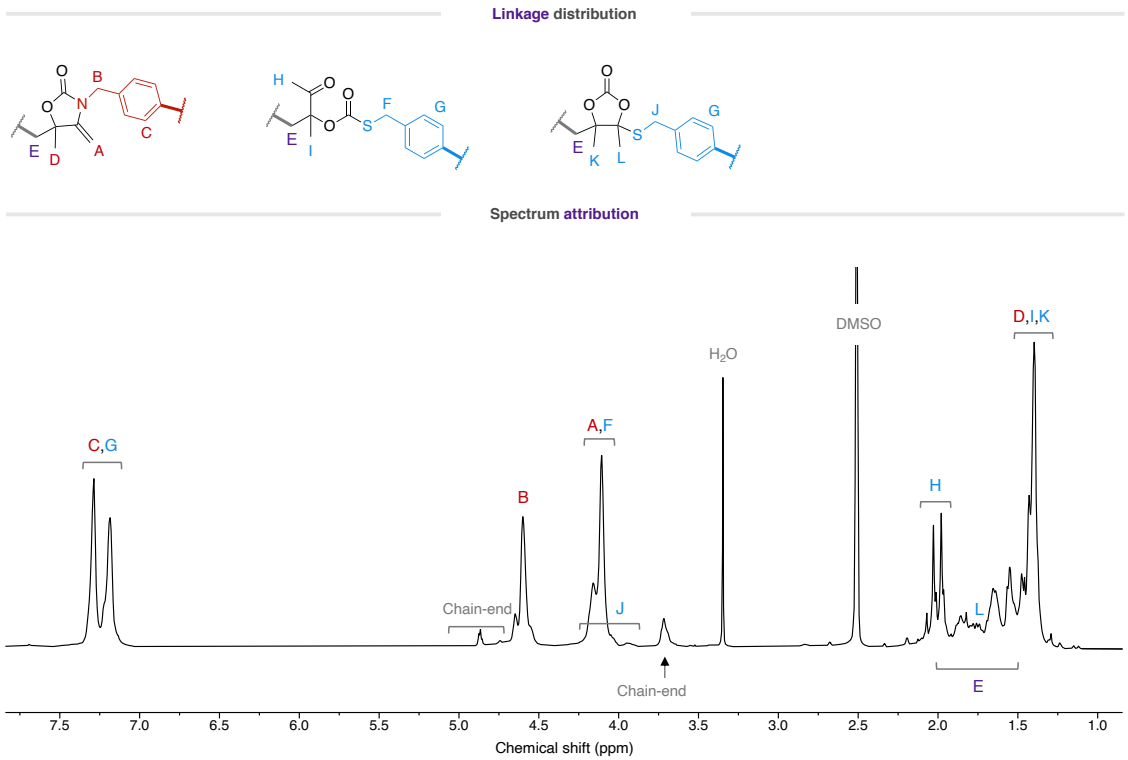

Figure S73 – ^{1}H-NMR spectrum of dehydrated P(A3T2) (400 MHz, DMSO-d_6).

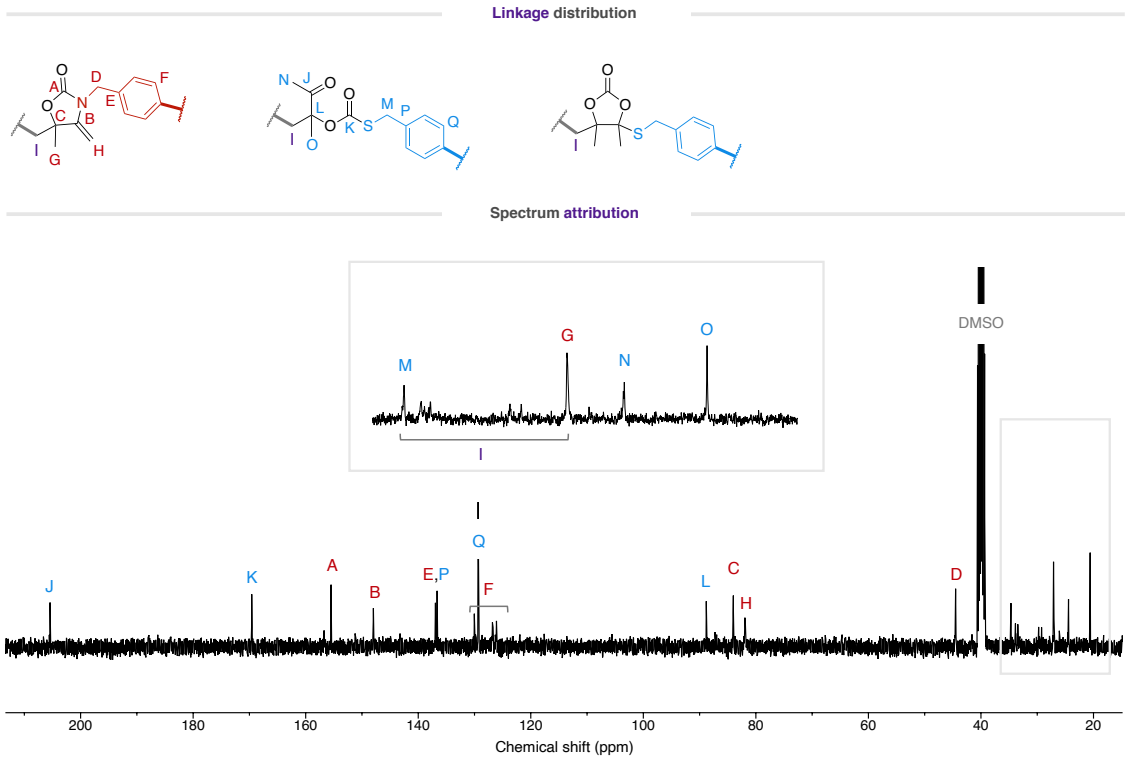

Figure S74 – ^{13}C-NMR spectrum of dehydrated P(A3T2) (101 MHz, DMSO-d_6).

12. SEC chromatograms of dehydrated polymers

Typical SEC chromatograms of pure hydroxyoxazolidone copolymers (dotted) and dehydrated α-alkylidene oxazolidone polymers (line) are shown below.

P(A1T1)

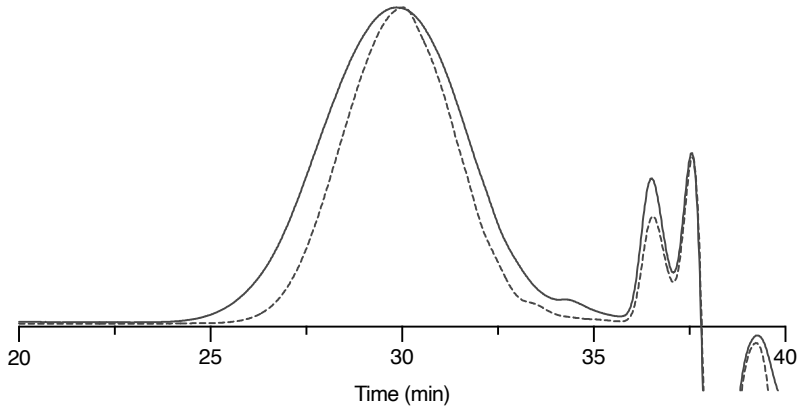

Figure S75. SEC chromatograms of P(A1T1) after purification (dotted) and after dehydration (line).

P(A1T1)C

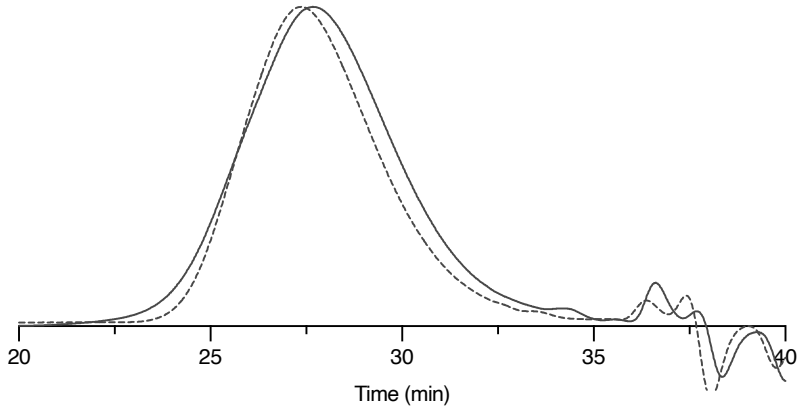

Figure S76. SEC chromatograms of P(A1T1)C after purification (dotted) and after dehydration (line).

P(A1T2)

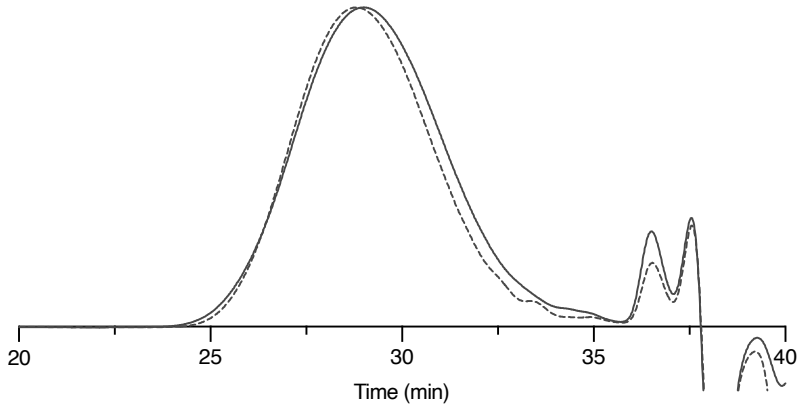

Figure S77. SEC chromatograms of P(A1T2) after purification (dotted) and after dehydration (line).

P(A2T1)

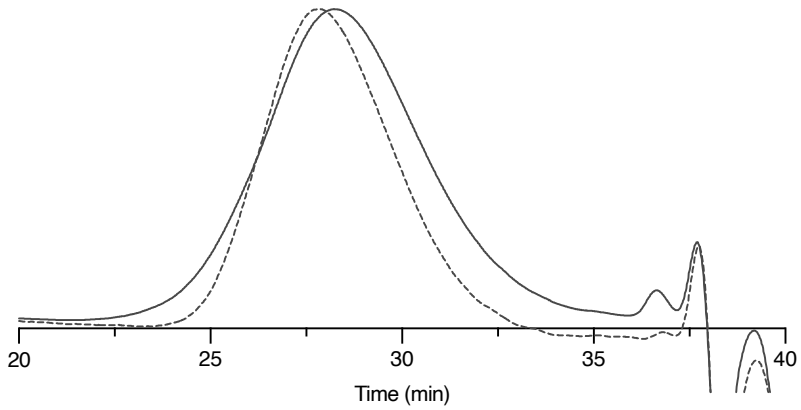

Figure S78. SEC chromatograms of P(A2T1) after purification (dotted) and after dehydration (line).

P(A2T1)C

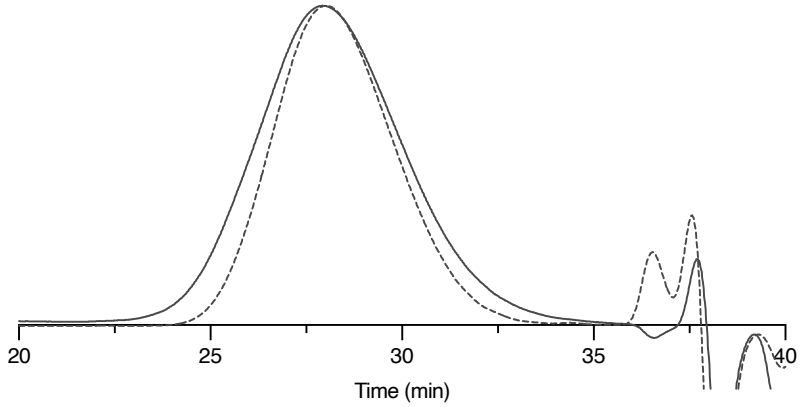

Figure S79. SEC chromatograms of P(A2T1)C after purification (dotted) and after dehydration (line).

P(A2T2)

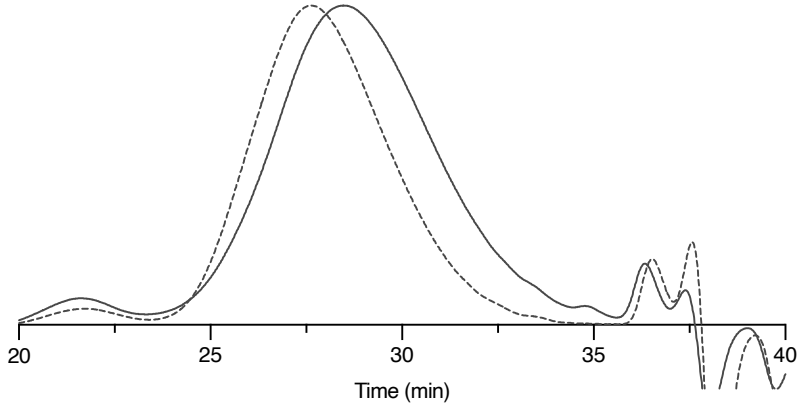

Figure S80. SEC chromatograms of P(A2T2) after purification (dotted) and after dehydration (line).

P(A3T1)

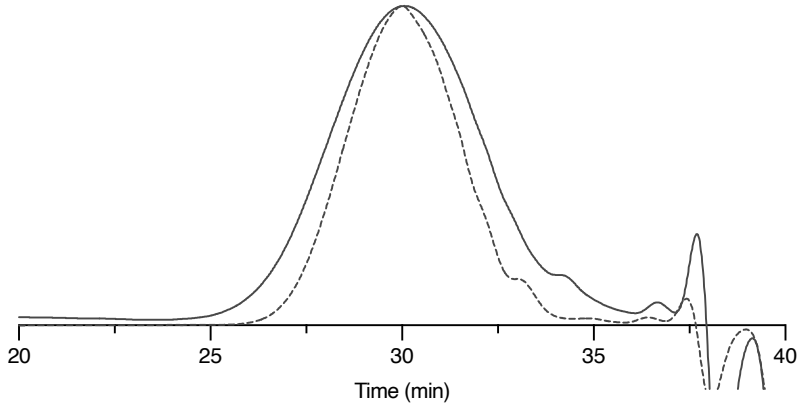

Figure S81. SEC chromatograms of P(A3T1) after purification (dotted) and after dehydration (line).

P(A3T1)C

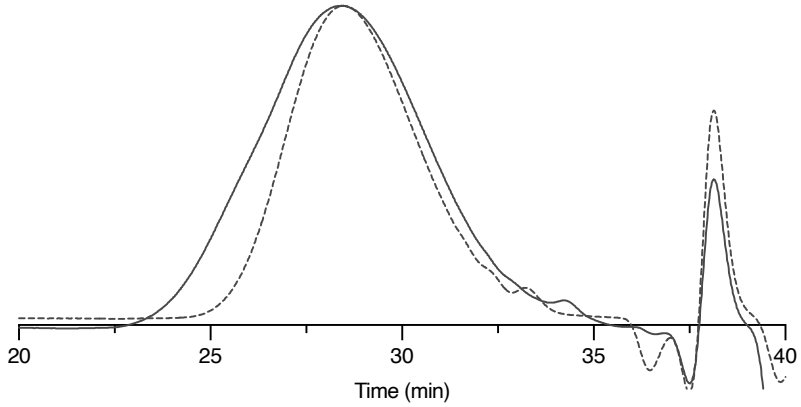

Figure S82. SEC chromatograms of P(A3T1)C after purification (dotted) and after dehydration (line).

P(A3T2)

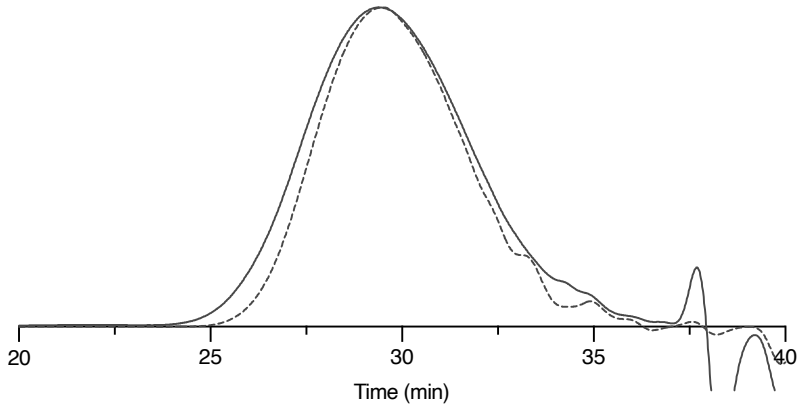

Figure S83. SEC chromatograms of P(A3T2) after purification (dotted) and after dehydration (line).

13. TGA analyses of dehydrated polymers

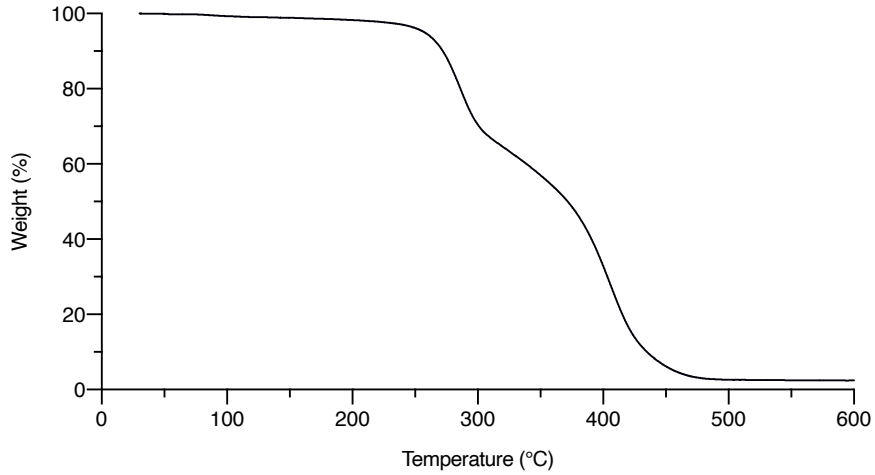

Figure S84 – TGA plot of dehydrated P(A1T1).

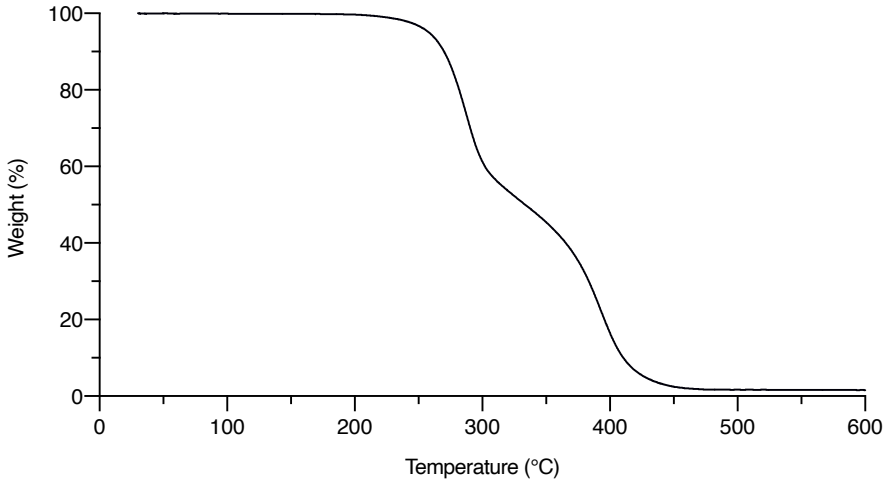

Figure S85 – TGA plot of dehydrated P(A1T1)C.

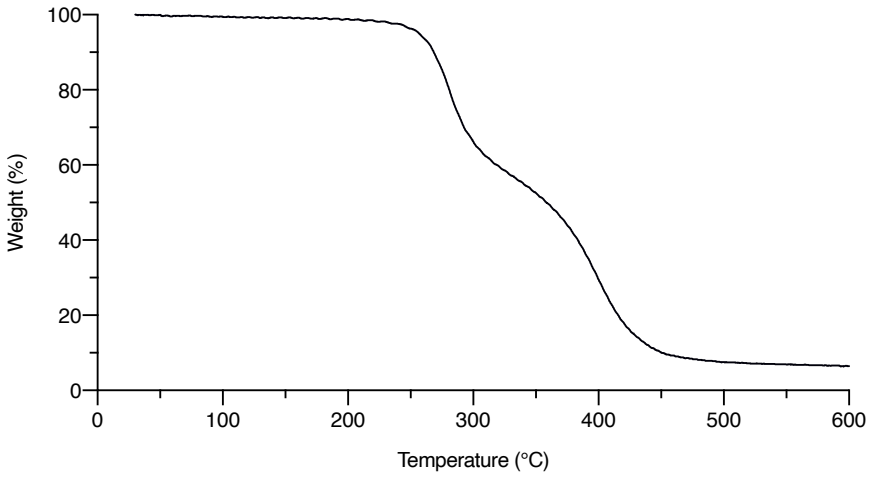

Figure S86 – TGA plot of dehydrated P(A1T2).

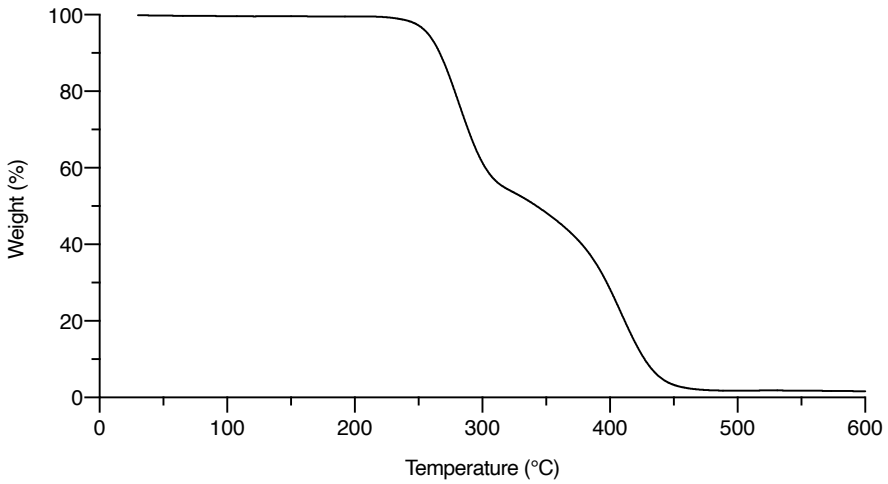

Figure S87 – TGA plot of dehydrated P(A2T1).

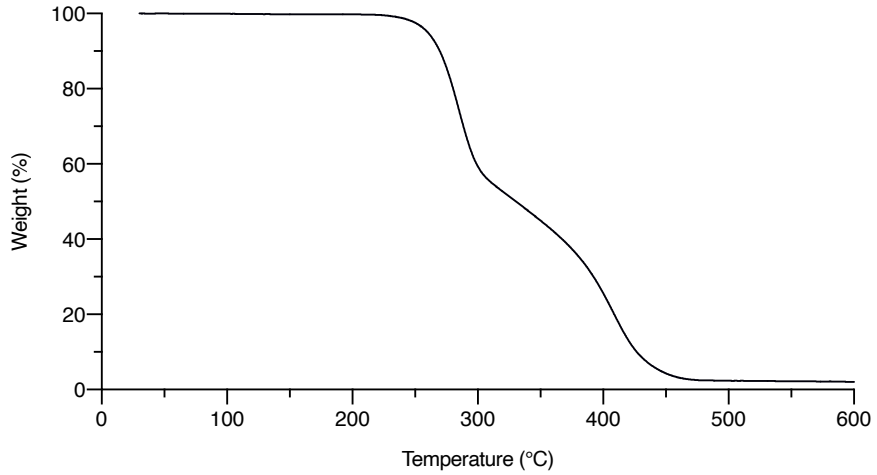

Figure S88 – TGA plot of dehydrated P(A2T1)C.

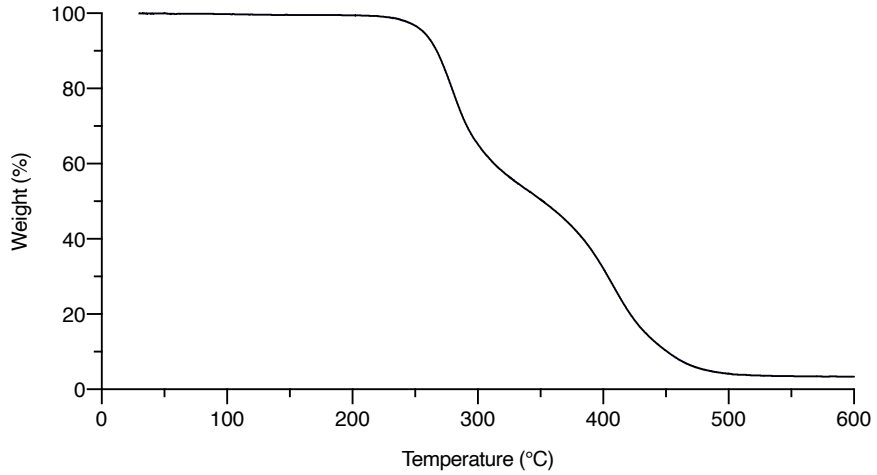

Figure S89 – TGA plot of dehydrated P(A2T2).

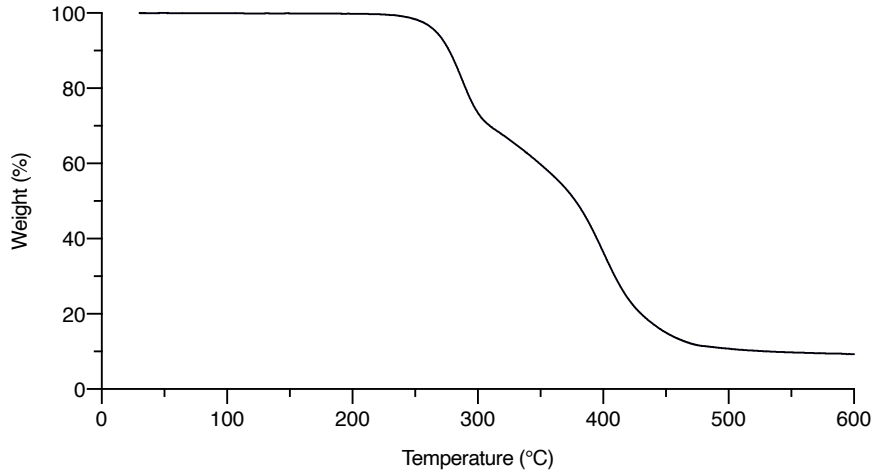

Figure S90 – TGA plot of dehydrated P(A3T1).

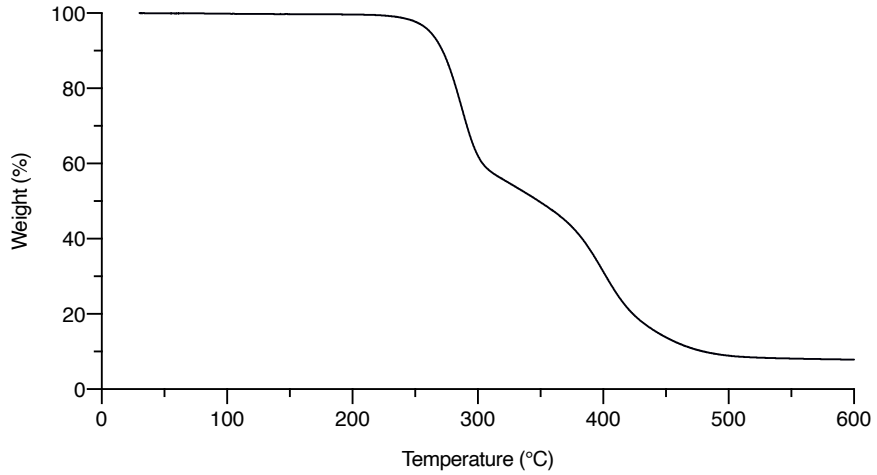

Figure S91 – TGA plot of dehydrated P(A3T1)C.

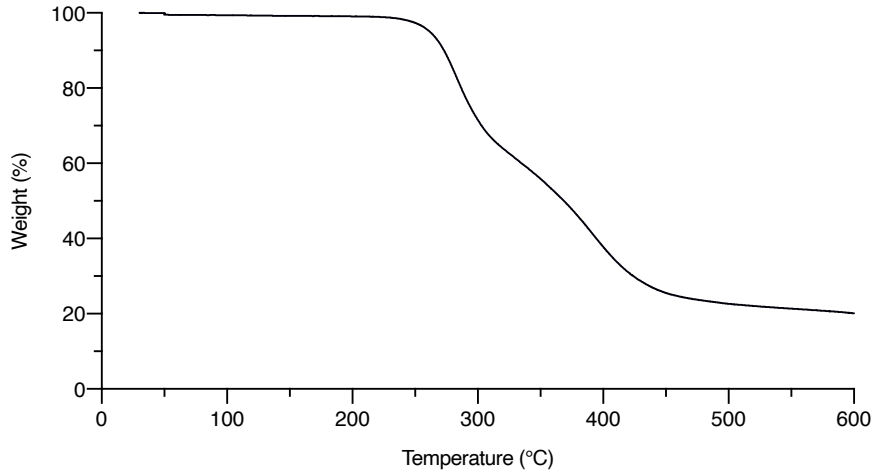

Figure S92 – TGA plot of dehydrated P(A3T2).

14. DSC analyses of dehydrated polymers

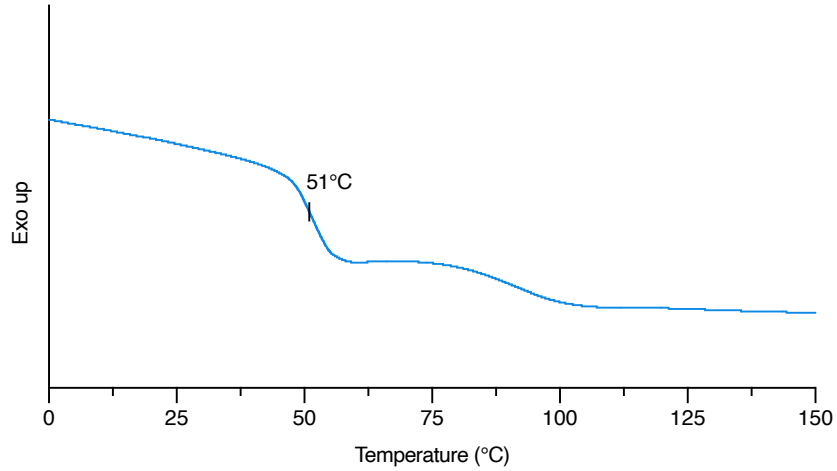

Figure S93 – DSC plot of dehydrated P(A1T1).

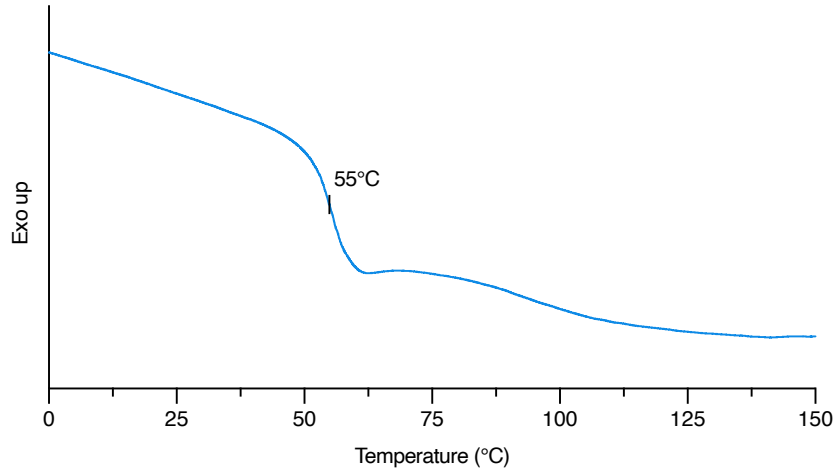

Figure S94 – DSC plot of dehydrated P(A1T1)C.

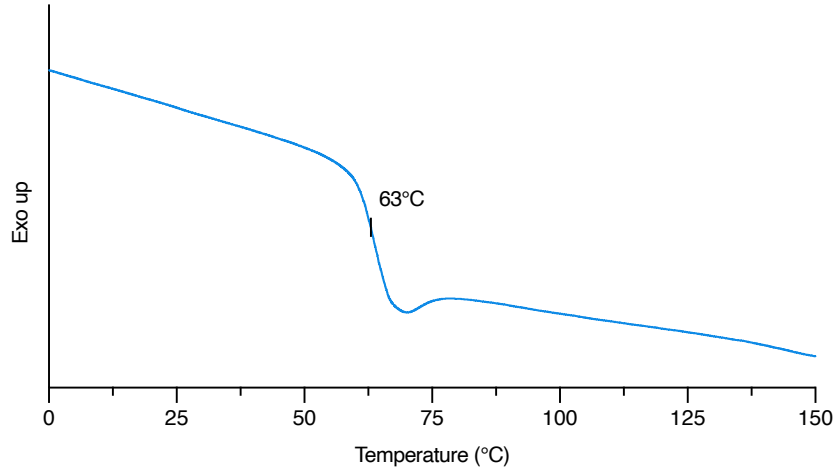

Figure S95 – DSC plot of dehydrated P(A1T2).

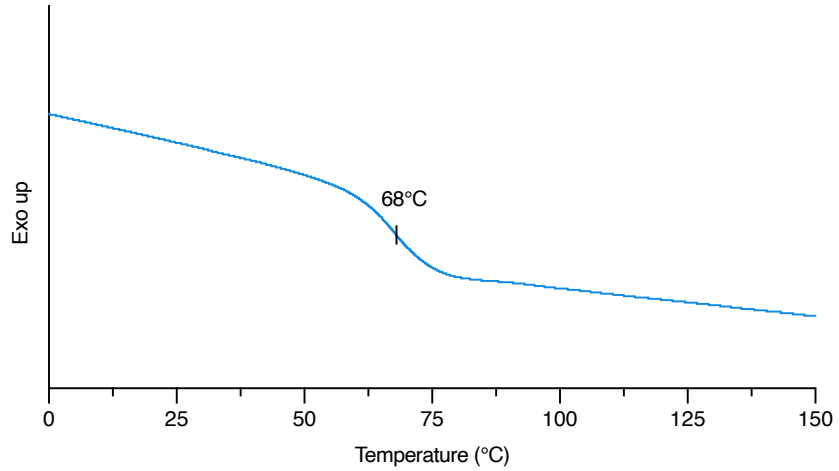

Figure S96 – DSC plot of dehydrated P(A2T1).

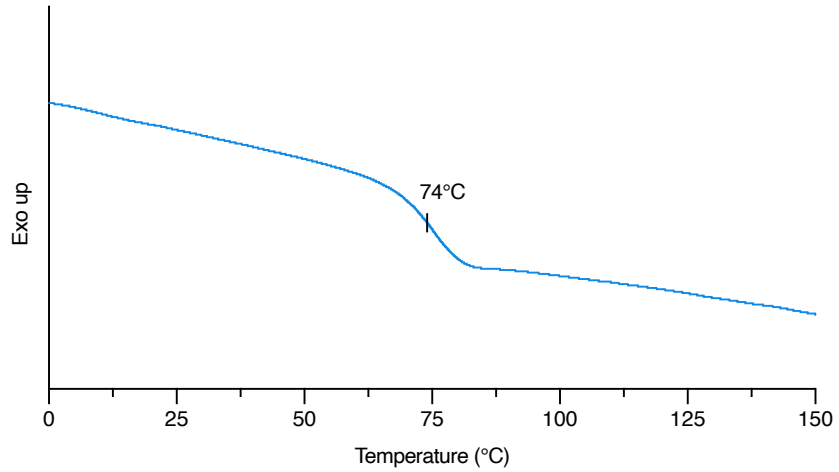

Figure S97 – DSC plot of dehydrated P(A2T1)C.

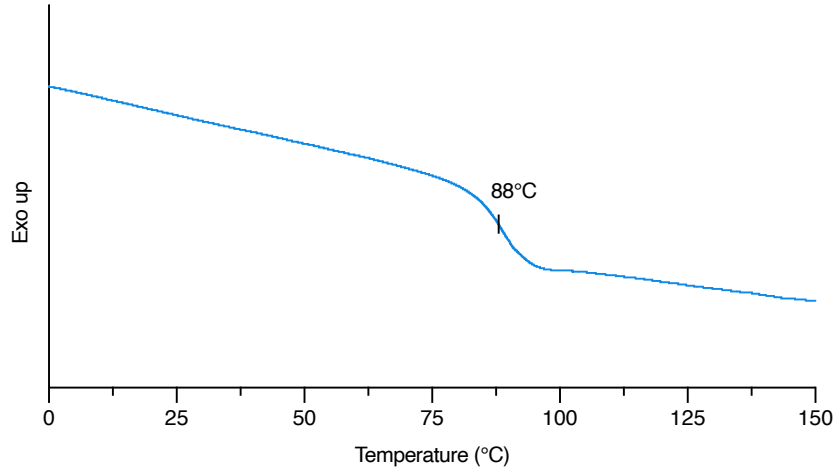

Figure S98 – DSC plot of dehydrated P(A2T2).

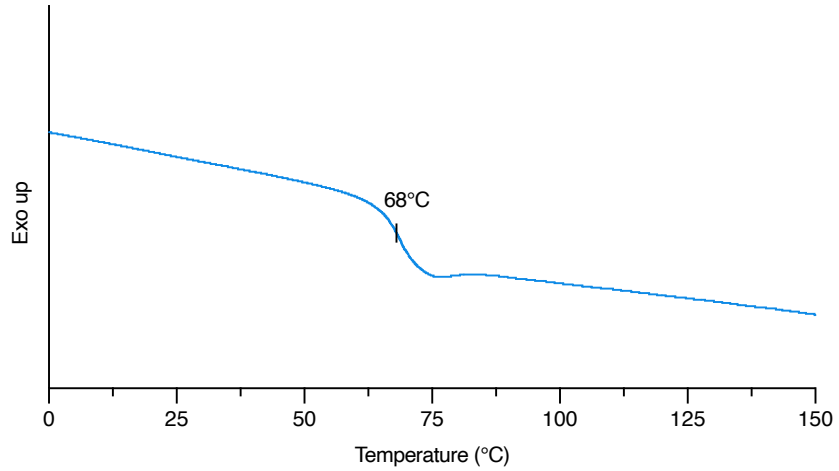

Figure S99 – DSC plot of dehydrated P(A3T1).

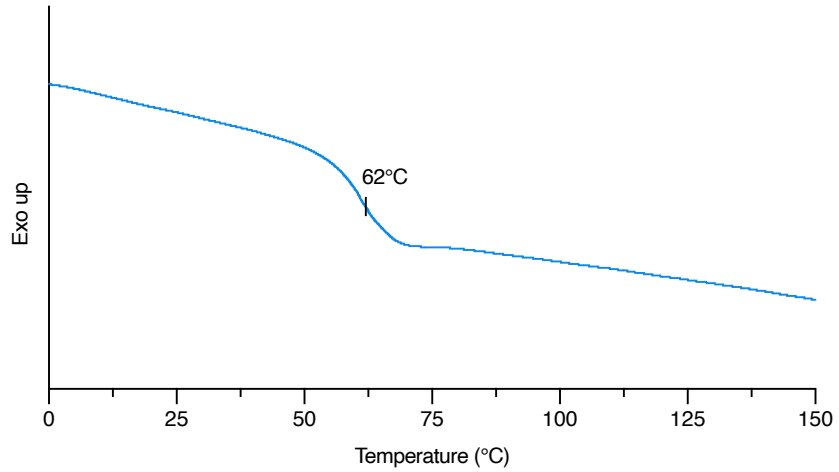

Figure S100 – DSC plot of dehydrated P(A3T1)C.

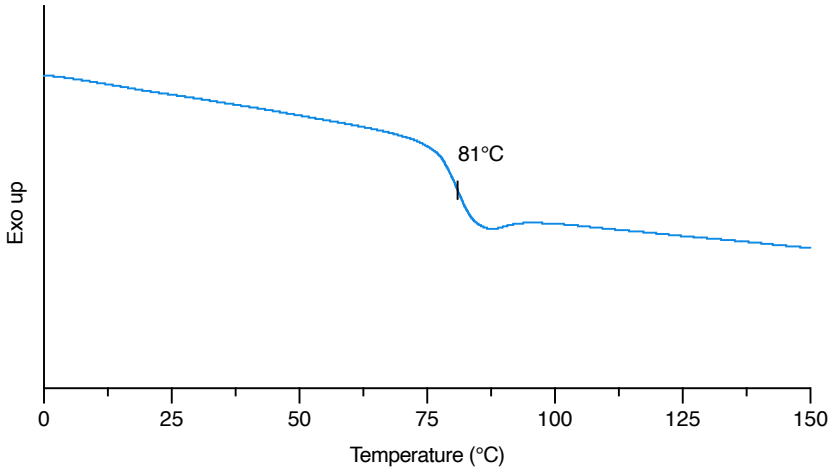

Figure S101 – DSC plot of dehydrated P(A3T2).

15. NMR characterization of functionalized polymers

P(A3T1)C dehydrated functionalized with benzyl mercaptan

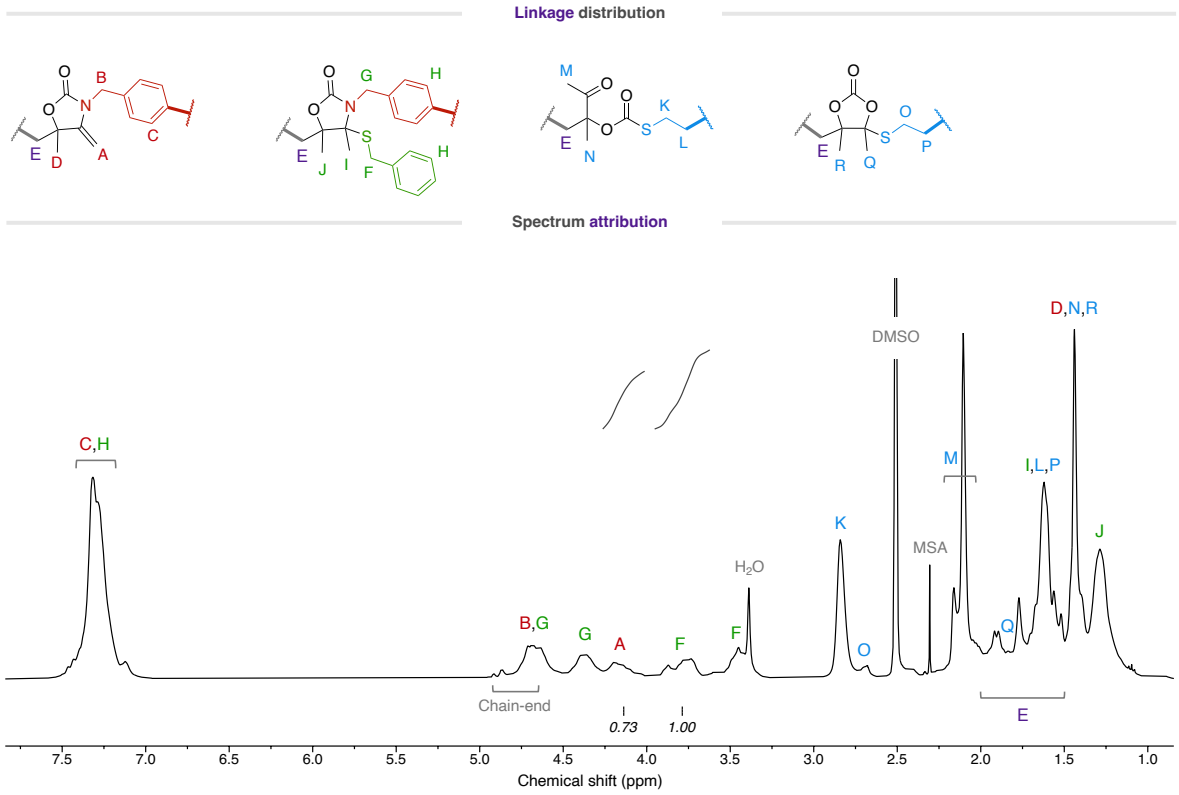

Figure S102 – ^{1}H-NMR spectrum of pure polymer functionalized with benzyl mercaptan (400 MHz, DMSO-d_6).

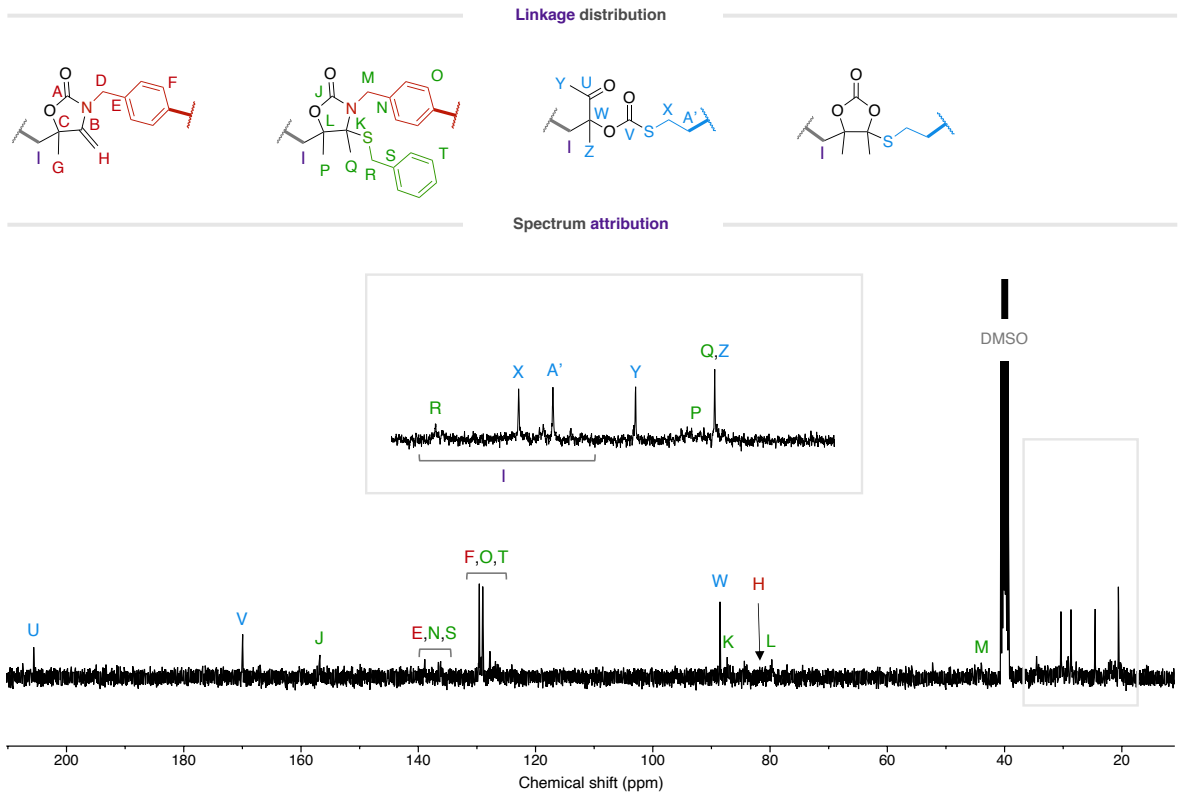

Figure S103 – ^{13}C-NMR spectrum of pure polymer functionalized with benzyl mercaptan (101 MHz, DMSO-d_6).

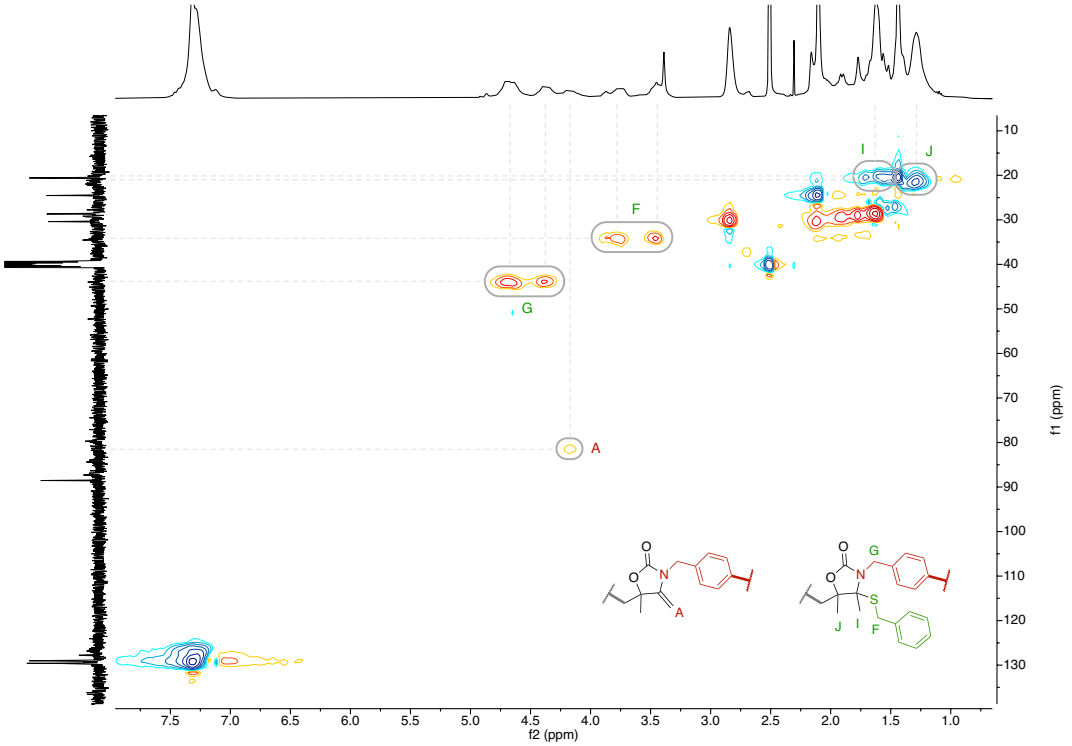

Figure S104 – ^{1}H-^{13}C HSQC NMR spectrum of pure polymer functionalized with benzyl mercaptan (400 MHz, DMSO-d_6).

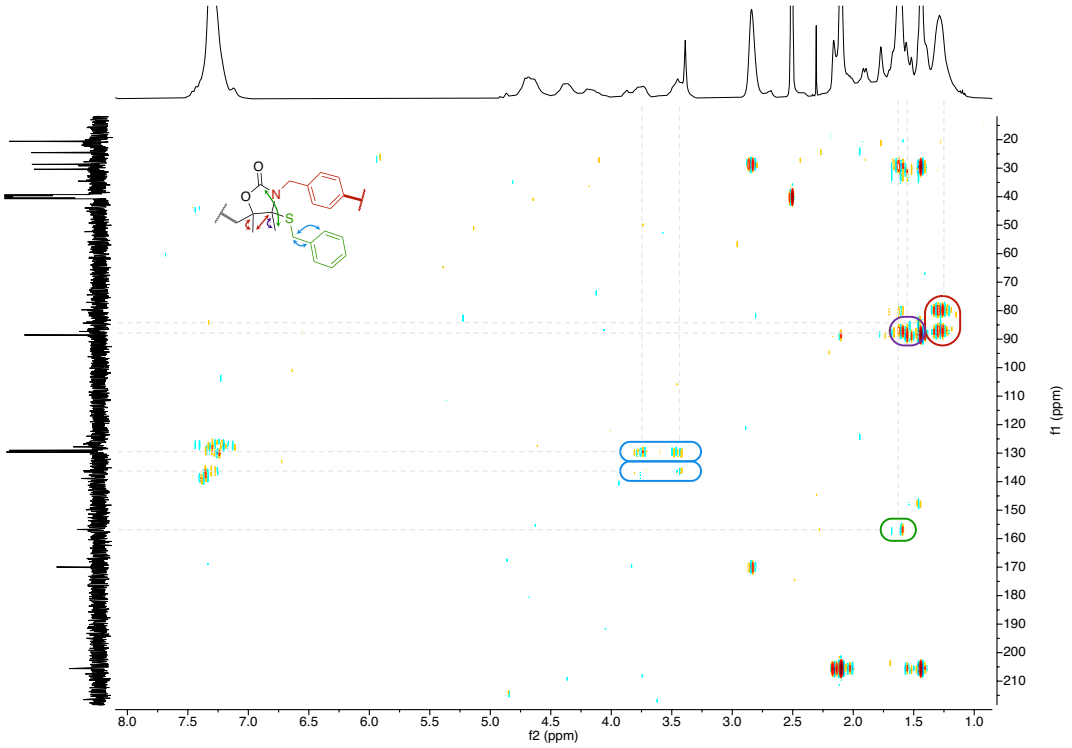

Figure S105 – ^{1}H-^{13}C HMBC NMR spectrum of pure polymer functionalized with benzyl mercaptan (400 MHz, DMSO-d_6).

P(A3T1)C dehydrated functionalized with furanmethanethiol

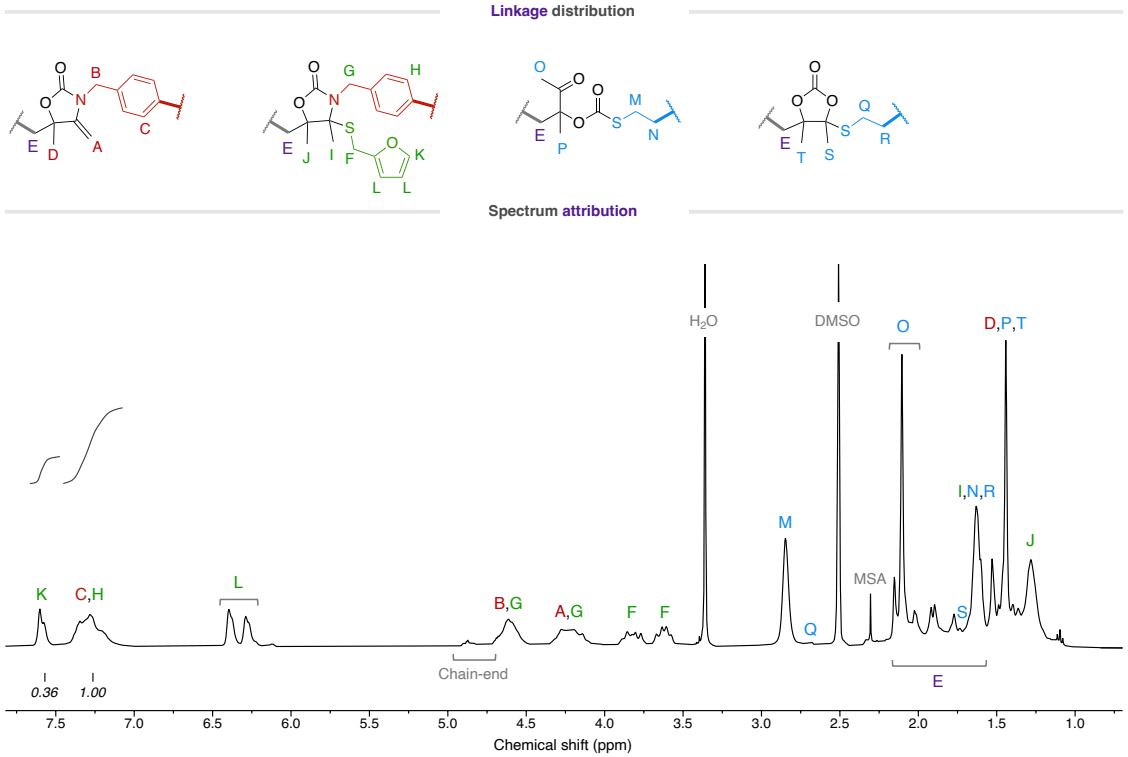

Figure S106 – ^{1}H-NMR spectrum of pure polymer functionalized with furanmethanethiol (400 MHz, DMSO-d_6).

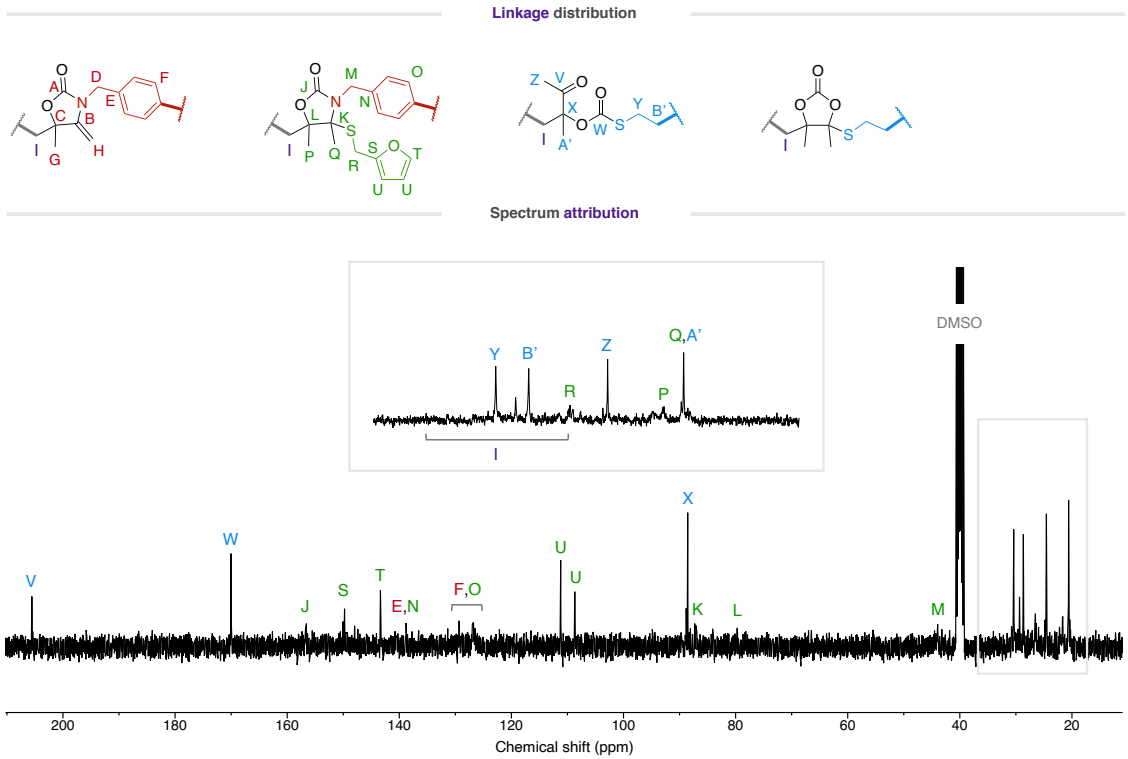

Figure S107 – ^{13}C-NMR spectrum of pure polymer functionalized with furanmethanethiol (101 MHz, DMSO-d_6).

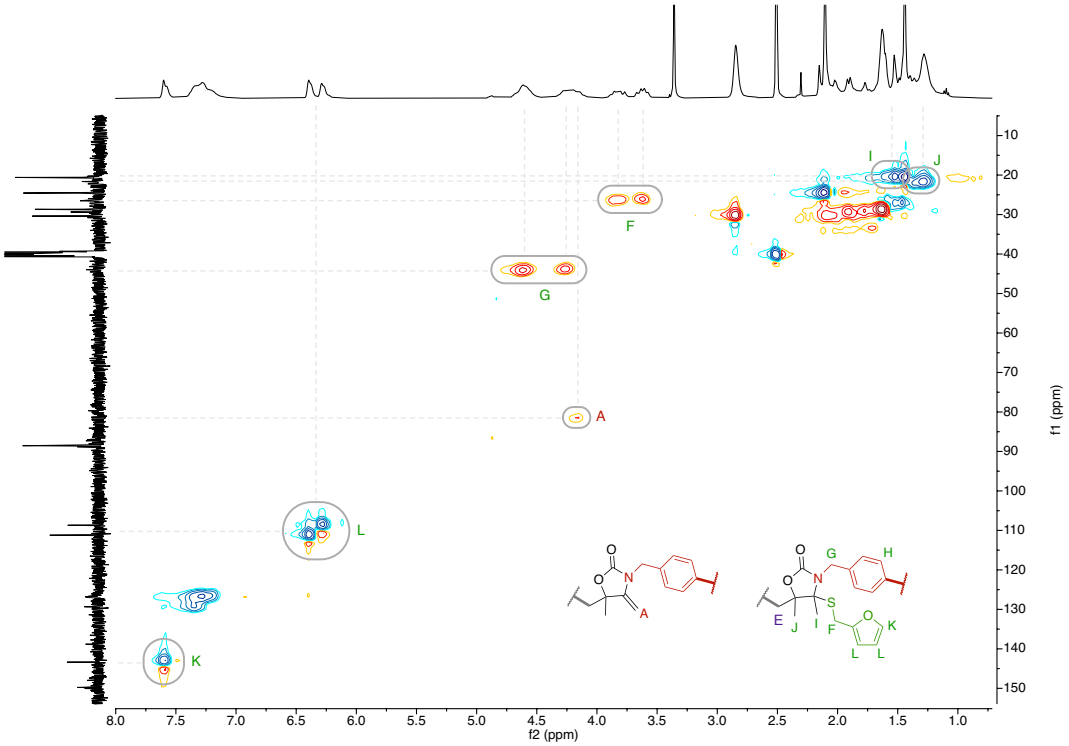

Figure S108 – ^{1}H-^{13}C HSQC NMR spectrum of pure polymer functionalized with furanmethanethiol (400 MHz, DMSO-d_6).

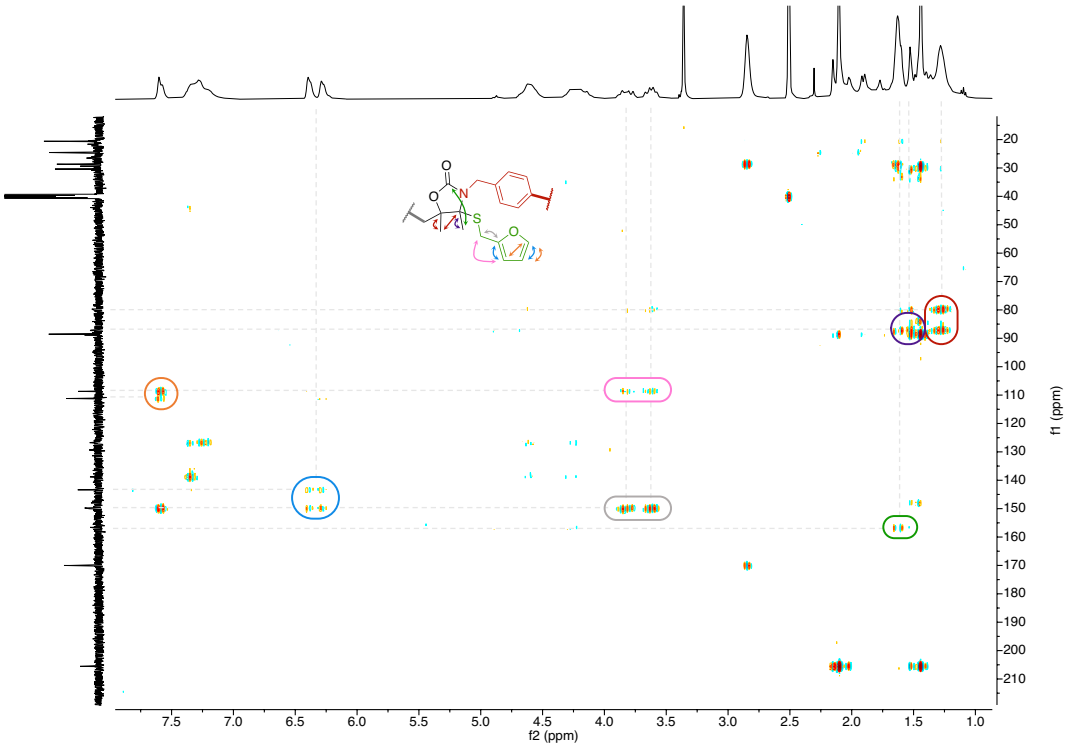

Figure S109 – ^{1}H-^{13}C HMBC NMR spectrum of pure polymer functionalized with furanmethanethiol (400 MHz, DMSO-d_6).

P(A3T1)C dehydrated functionalized with n-octanethiol

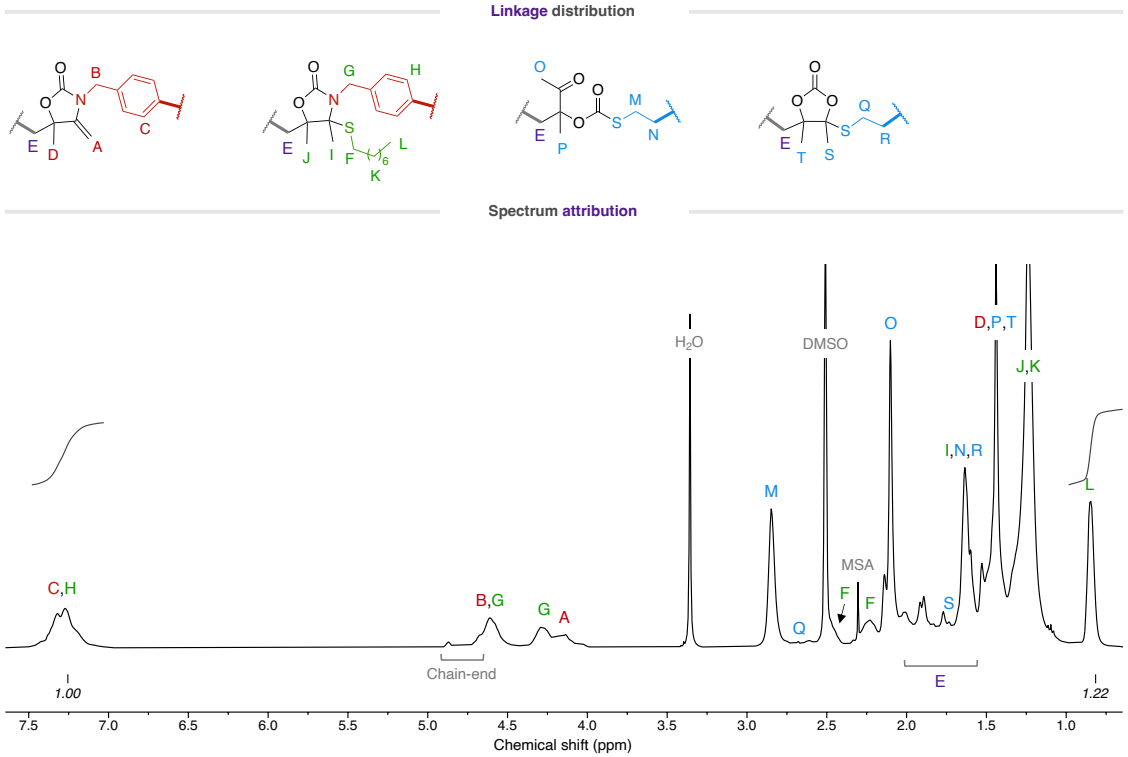

Figure S110 – ^{1}H-NMR spectrum of pure polymer functionalized with n-octanethiol (400 MHz, DMSO-d_6).

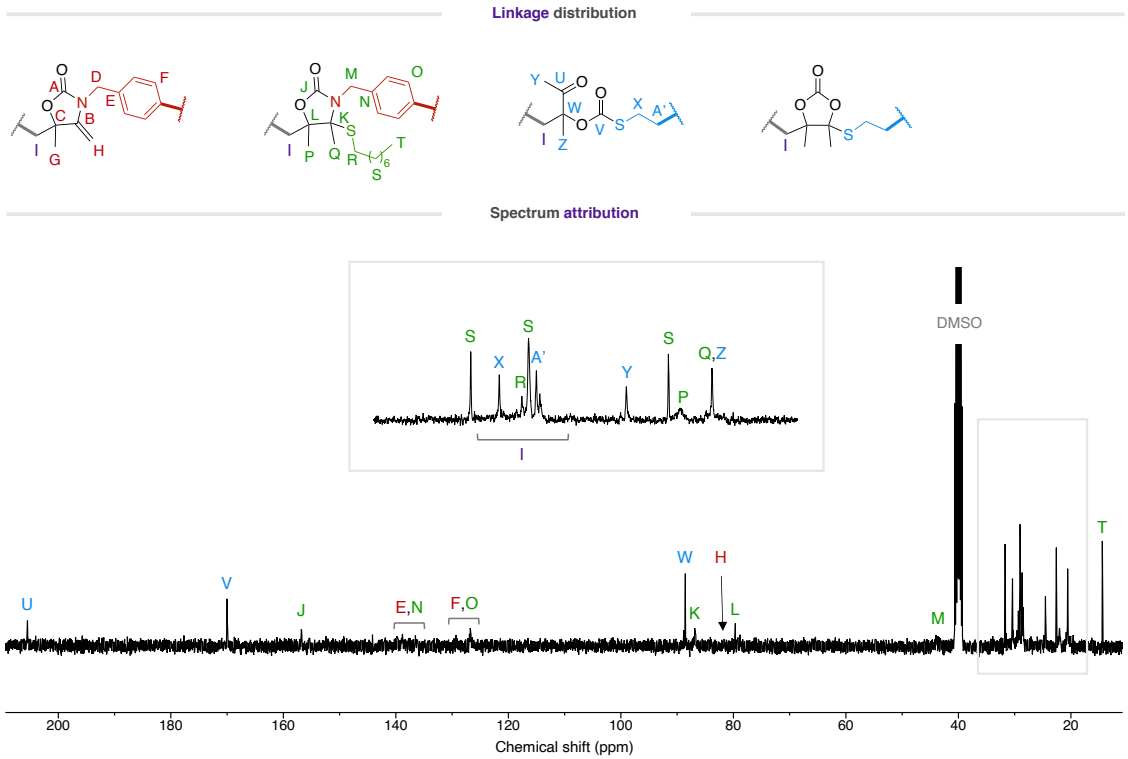

Figure S111 – ^{13}C-NMR spectrum of pure polymer functionalized with n-octanethiol (101 MHz, DMSO-d_6).

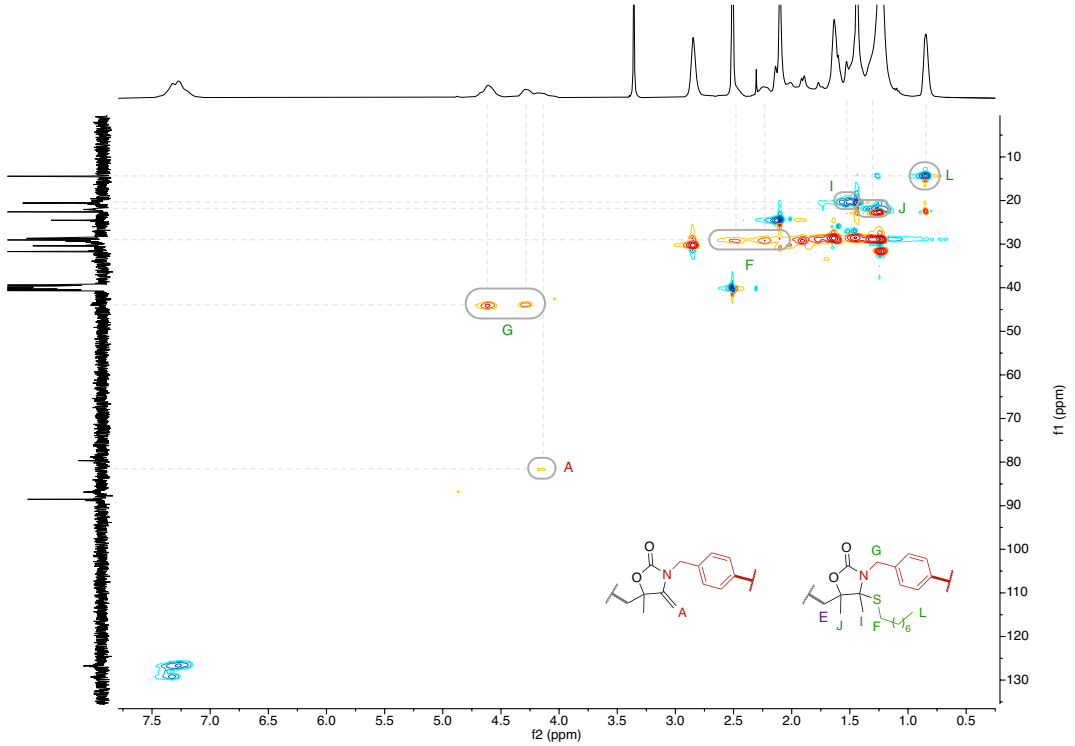

Figure S112 – ^{1}H-^{13}C HSQC NMR spectrum of pure polymer functionalized with n-octanethiol (400 MHz, DMSO-d_6).

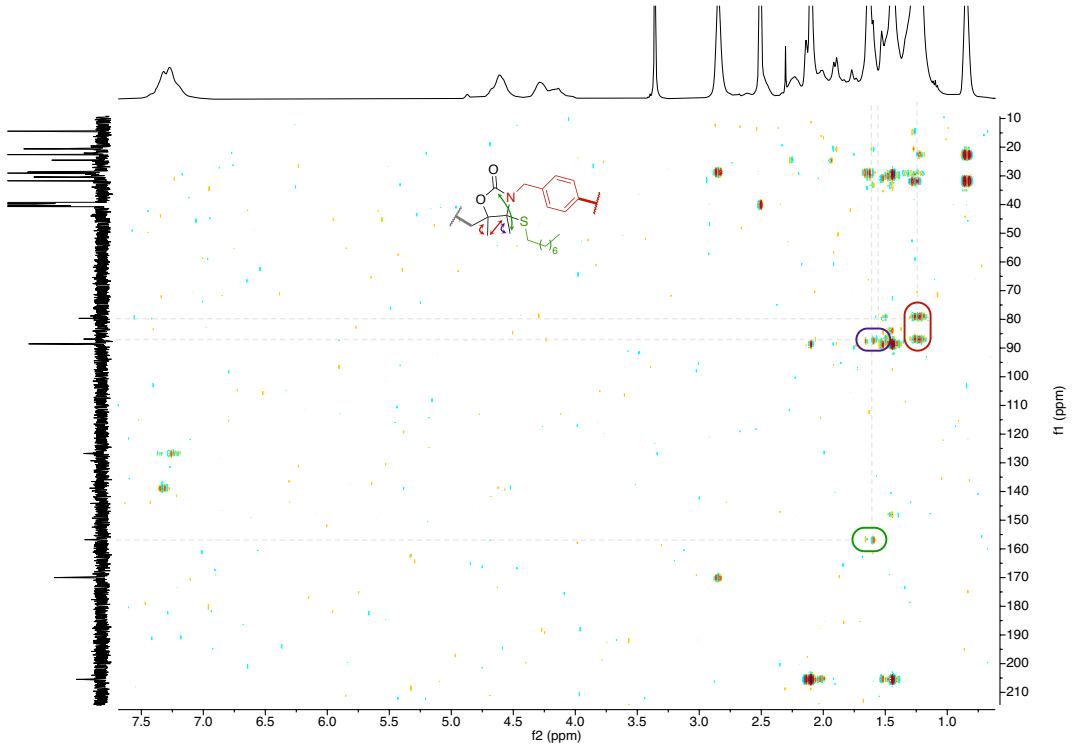

Figure S113 – ^{1}H-^{13}C HMBC NMR spectrum of pure polymer functionalized with n-octanethiol (400 MHz, DMSO-d_6).

P(A3T1)C dehydrated functionalized with methyl 3-mercaptopropionate

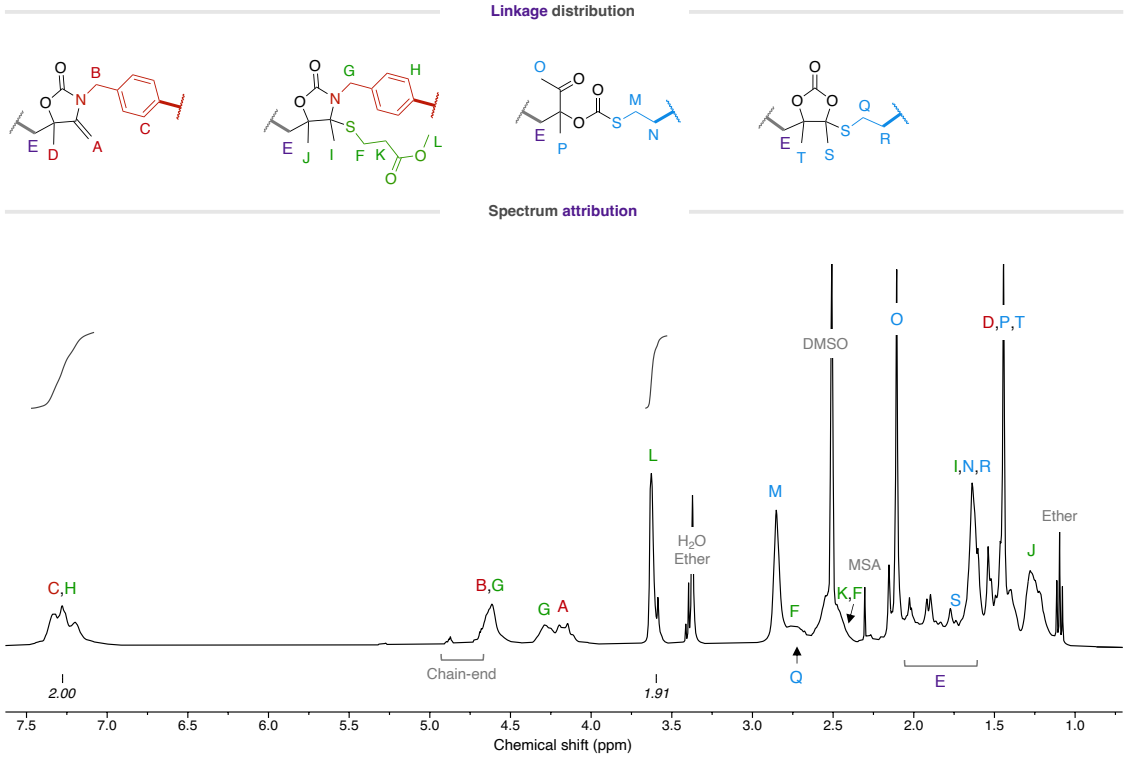

Figure S114 – ^{1}H-NMR spectrum of pure polymer functionalized with methyl 3-mercaptopropionate (400 MHz, DMSO-d_6).

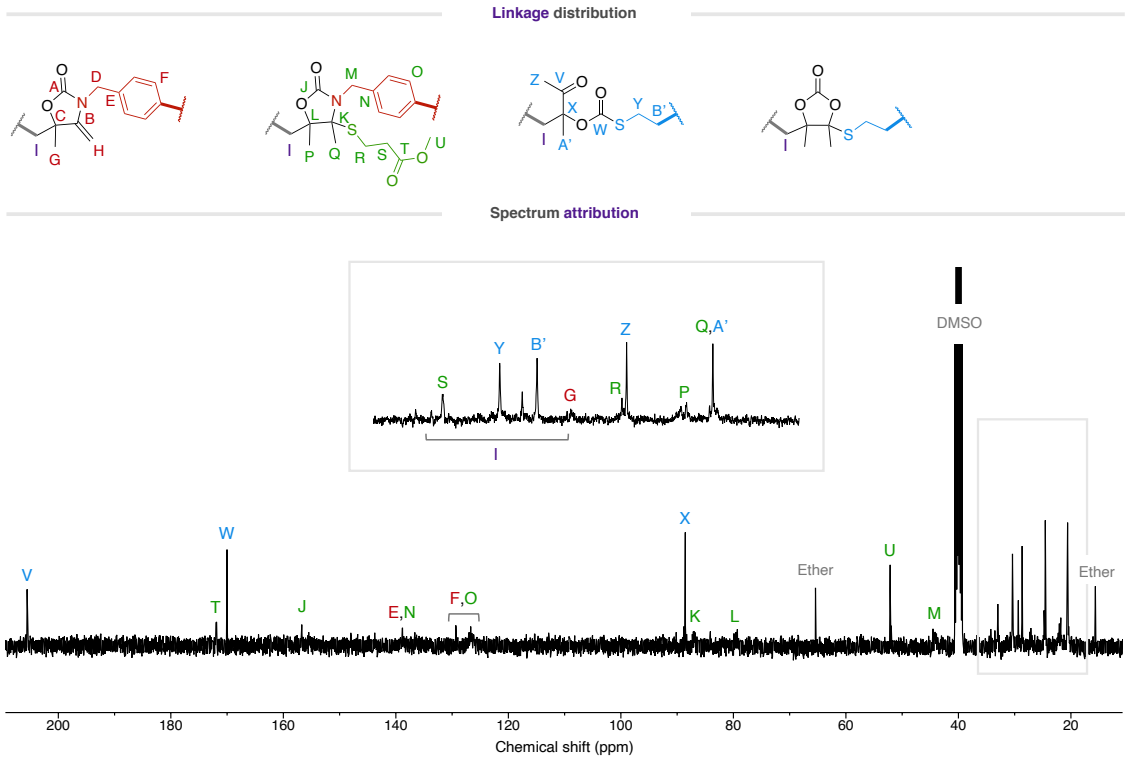

Figure S115 – ^{13}C-NMR spectrum of pure polymer functionalized with methyl 3-merceptopropionate (101 MHz, DMSO-d_6).

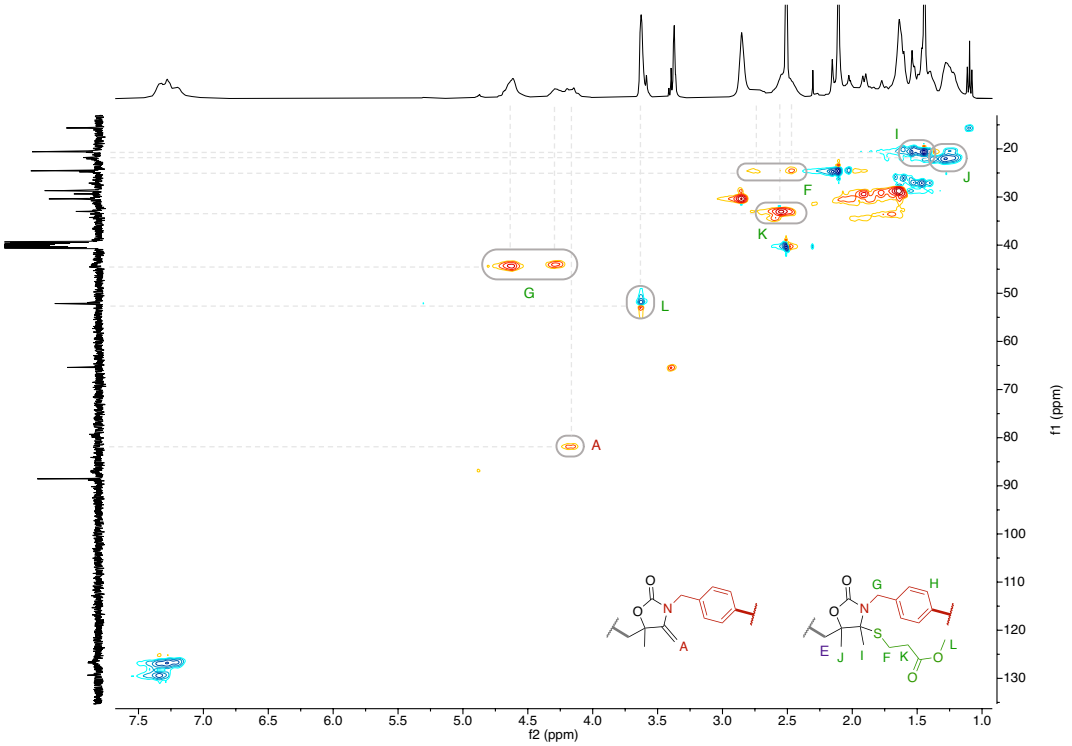

Figure S116 – ^{1}H-^{13}C HSQC NMR spectrum of pure polymer functionalized with methyl 3-mercaptopropionate (400 MHz, DMSO-d_6).

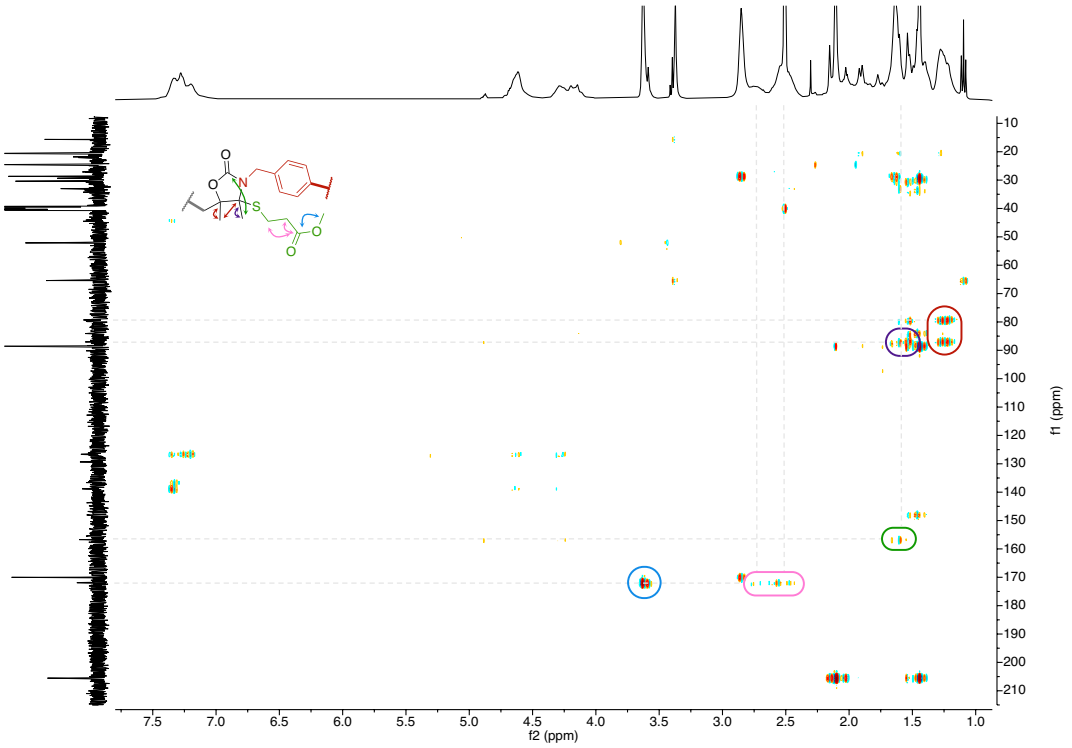

Figure S117 – ^{1}H-^{13}C HMBC NMR spectrum of pure polymer functionalized with methyl 3-mercaptopropionate (400 MHz, DMSO-d_6).

16. Characterization of polymer P(A1T3)C

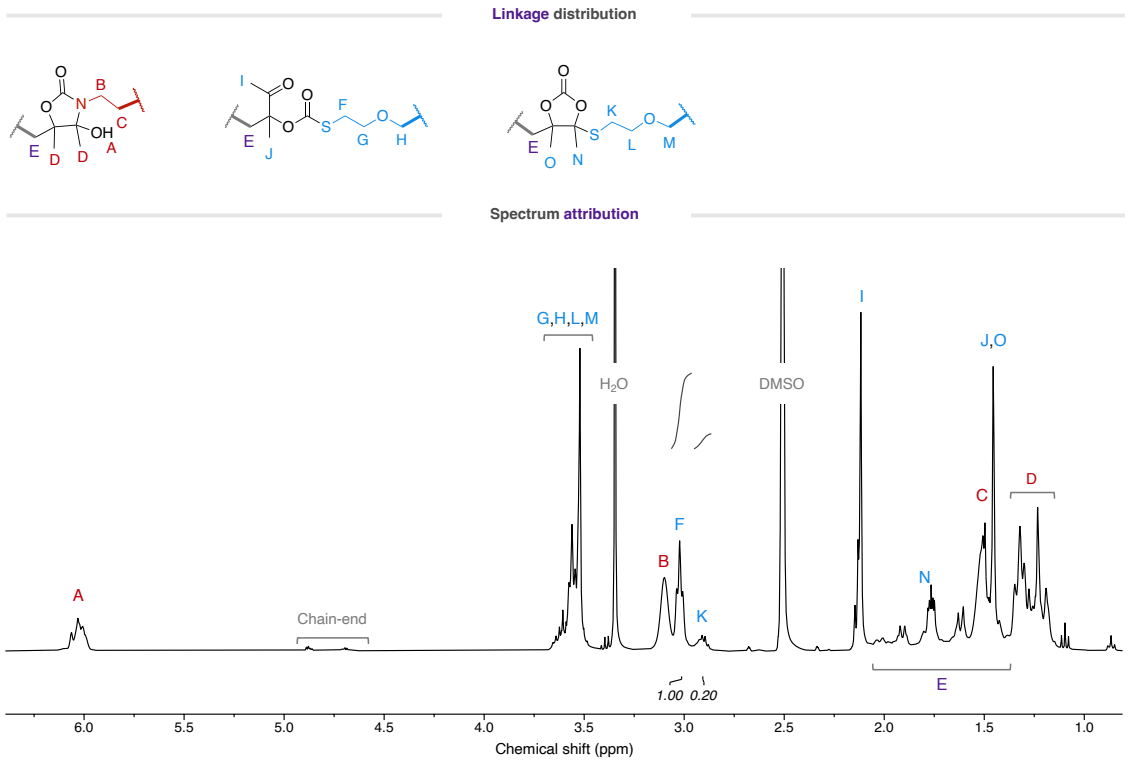

Figure S118 – ^{1}H-NMR spectrum of P(A1T3)C (400 MHz, DMSO-d_6).

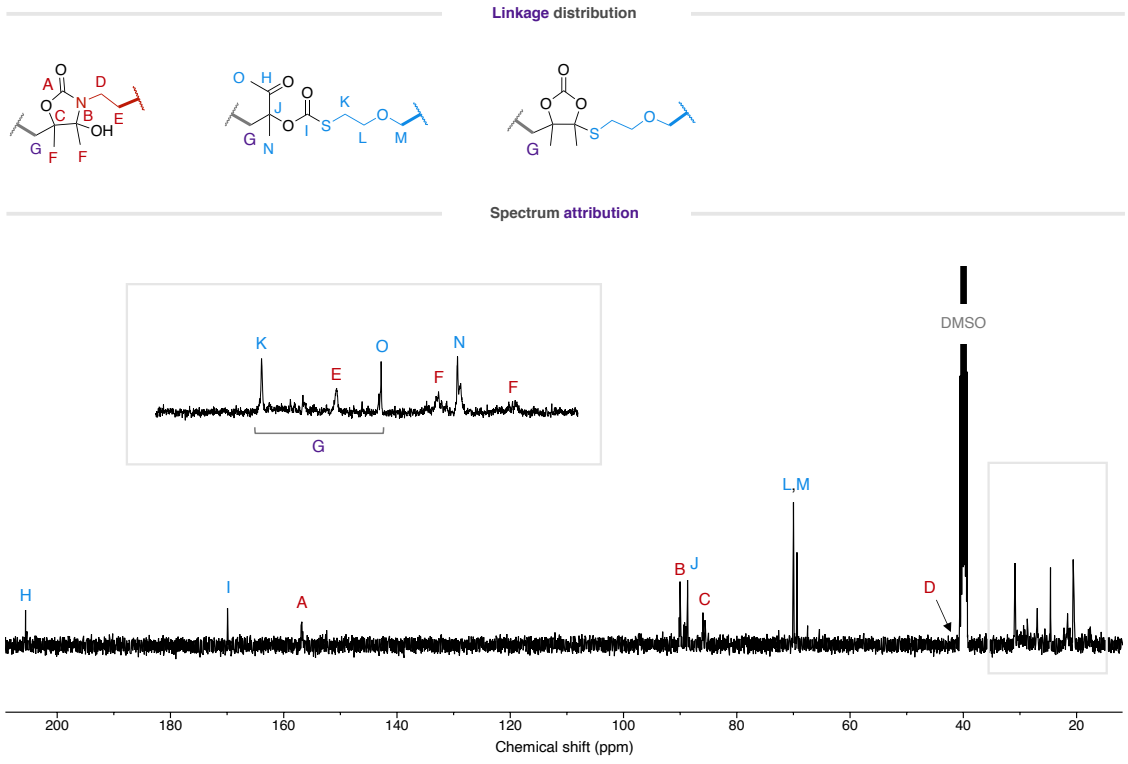

Figure S119 – ^{13}C-NMR spectrum of P(A1T3)C (101 MHz, DMSO-d_6).

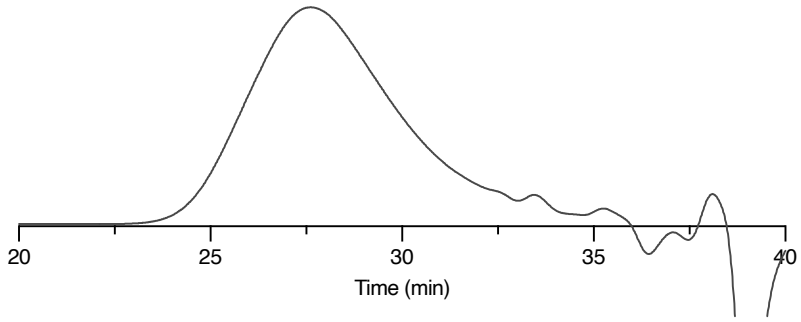

Figure S120 – SEC chromatogram (before purification) of P(A1T3)C.

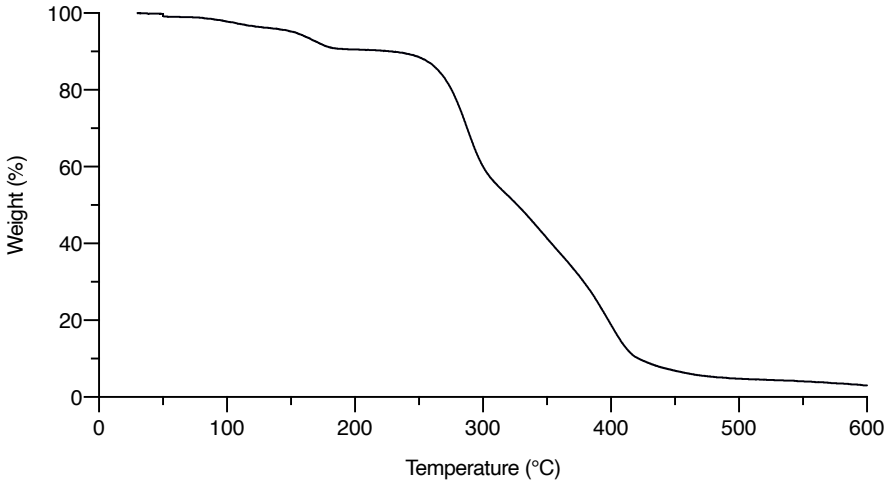

Figure S121 – TGA plot of P(A1T3)C.

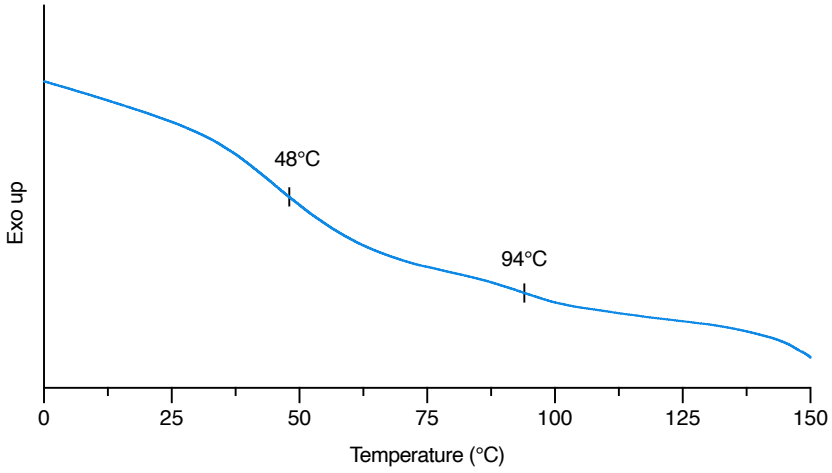

Figure S122 – Reversing heat flow by modulated DSC of P(A1T3)C.

17. Setup for the lap-shear tests experiments

As some specimens have shown high brittleness, some of the samples were breaking before the test when fixing them in the pneumatic clamps. To avoid this problem, a homemade setup made of a hook was developed, thus giving freedom to the sample when placing it in the clamps.

Figure S123 – Homemade setup for the lap-shear tests on prepared specimens.

18. References

(1) Gennen, S.; Grignard, B.; Tassaing, T.; Jérôme, C.; Detrembleur, C. CO_2-Sourced α-Alkylidene Cyclic Carbonates: A Step Forward in the Quest for Functional Regioregular Poly(Urethane)s and Poly(Carbonate)s. *Angew. Chem. Int. Ed.* 2017, *56* (35), 10394–10398. https://doi.org/10.1002/anie.201704467.

(2) Habets, T.; Siragusa, F.; Grignard, B.; Detrembleur, C. Advancing the Synthesis of Isocyanate-Free Poly(Oxazolidones)s: Scope and Limitations. *Macromolecules* 2020, *53* (15), 6396–6408. https://doi.org/10.1021/acs.macromol.0c01231.

(3) Oswald, A. A.; Noel, F.; Stephenson, A. J. Organic Sulfur Compounds. V. Alkylammonium Thiolate and Peroxide Salts; Possible Intermediates in Amine-Catalyzed Oxidation of Mercaptans by Hydroperoxides. *J. Org. Chem.* 1961, *26* (10), 3969–3974. https://doi.org/10.1021/jo01068a078.

(4) Thompson, W. E.; Warren, R. J.; Eisdorfer, I. B.; Zarembo, J. E. Identification of Primary, Secondary, and Tertiary Pharmaceutical Amines by the Infrared Spectra of Their Salts. *Journal of Pharmaceutical Sciences* 1965, *54* (12), 1819–1821. https://doi.org/10.1002/jps.2600541231.

(5) Chenon, B.; Sandorfy, C. HYDROGEN BONDING IN THE AMINE HYDROHALIDES: I. GENERAL ASPECTS. *Can. J. Chem.* 1958, *36* (8), 1181–1206. https://doi.org/10.1139/v58-173.

Chapter II highlighted the pivotal role of α-alkylidene cyclic carbonates as a versatile toolbox for engineering complex macromolecules under mild conditions. This enabled the simultaneous incorporation of various functionalities such as *oxo*-urethane, oxazolidone, *oxo*-thiocarbonate, and cyclic carbonate thioether within the polymer backbone. It emphasized the advantages of this hybrid chemistry in synthesizing soluble poly(oxazolidone)s, but also to furnish elusive copolymers that are challenging to obtain through conventional, harsher synthetic routes.

The work also uncovered key properties of hydroxy-oxazolidones, the most important being their thermal dehydration. Of high interest was the possibility to post-functionalize these polymers by the cationic thiol-ene reaction.

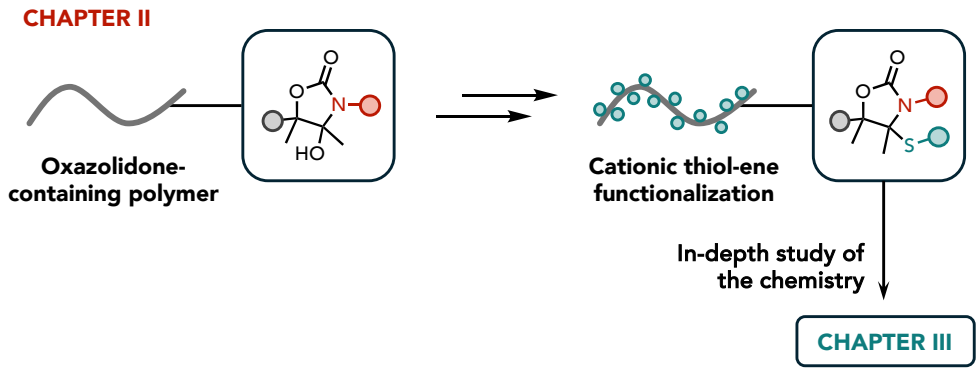

Capitalizing on the peculiar reactivity of exovinylene oxazolidones toward thiols by cationic thiol ene chemistry, Chapter III is dedicated to an in-depth study into this unexplored chemistry. This will be achieved through systematic model reactions and applications in macromolecular science to provide novel poly(oxazolidone)s.

Chapter III

Covalent Adaptable Networks through Dynamic *N,S*-Acetal Chemistry: Toward Recyclable CO_2-Based Thermosets

*Thomas Habets, Guillem Seychal, Marco Caliari, Jean-Marie Raquez, Haritz Sardon, Bruno Grignard, and Christophe Detrembleur**

Reference: *J. Am. Chem. Soc, 2023, 145, 46, 25450-25462*

Abstract

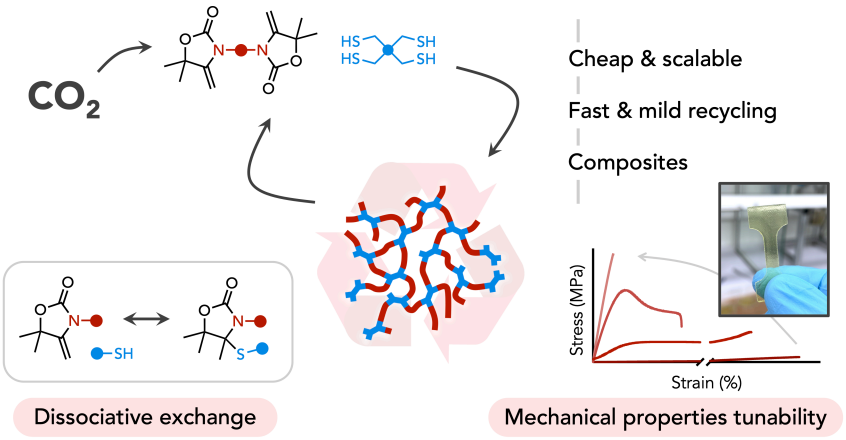

Finding new chemistry platforms for easily recyclable polymers has become a key challenge to face up environmental concerns and the growing plastics demand. Here, we report a dynamic chemistry between CO_2-sourced alkylidene oxazolidones and thiols, delivering circular non-isocyanate polyurethane networks embedding *N,S*-acetal bonds. The production of oxazolidone monomers from CO_2 is facile and scalable starting from cheap reagents. Their copolymerization with a polythiol occurs under mild conditions in the presence of a catalytic amount of acid to furnish polymer networks. The polymer structure is easily tuned by virtue of monomer design, translating in a wide panel of mechanical properties similar to commodity plastics, ranging from PDMS-like elastomers (with Young's modulus (E) of 2.9 MPa and elongation at break (ε_{break}) of 159%) to polystyrene-like rigid plastics (with E = 2400 MPa, ε_{break} = 3%). The highly dissociative nature of the *N,S*-acetal bonds is demonstrated and exploited to offer three different recycling scenarios to the thermosets: (1) the mechanical recycling by compression molding, extrusion or injection molding – with multiple recycling (at least 10 times) without any material properties deterioration, (2) the chemical recycling through depolymerization, followed by repolymerization, also applicable to composites, and (3) the upcycling of two different oxazolidone-based thermosets into a single one with distinct properties. This work highlights a new facile and scalable chemical platform for designing highly dynamic polymer networks containing elusive oxazolidone motifs. The versatility of this chemistry shows great potential for the preparation of materials (including composites) of tunable structure and properties, with multiple end-of-life scenarios.

Introduction

Plastics are ubiquitous in our daily life on account of their vast panel of applications within most economical sectors. The global plastic use accounted for 460 million tons in 2019 and, following worldwide trends, is expected to triple by 2060[1]. Regrettably, plastic waste became one of the greatest environmental threats causing irreversible damages to many ecosystems on the planet. Replacing them is not a feasible option as there are no viable alternatives so far which can match their outstanding features: low weight, affordability, versatility, and durability. A worldwide effort is devoted to re-think the plastics design through valorization of waste[2,3] or by utilizing biobased and/or CO_2-sourced molecules[4–6] to circumvent fully fossil-based chemistry. However, their recycling must be considered as importantly as their production to tackle environmental concerns[7–10]. Thus, appropriate solutions need to be developed in both the design and the recyclability of these materials.

In the recent years, covalent adaptable networks (CANs) have emerged as a new class of polymers whose properties lie between thermoplastics and thermosets[11–15]. Despite their cross-linked 'fixed' structure, recycling is enabled through exchange reactions between dynamic bonds under a certain trigger, most generally heat[16]. Many works already took advantage of bond dynamics to reprocess conventionally unrecyclable thermoset materials, notably via smart insertion of dynamic disulfide, boronic ester, acetal or Diels-Alder adducts bonds within the polymer matrix[17–21]. However, the reshaping process is most often limited by the high cross-link density and associated viscosity even at high temperature, restraining their processing to compression molding[22,23]. Most examples of CANs reprocessed using a larger arsenal of techniques are designed with lower cross-link densities[24] through long oligomeric or polymeric chains within their structure to reach lower viscosities at high temperature[20,25–28].

CANs can be categorized in two main categories depending on their bond exchange mechanism[29]. Associative CANs are characterized by a constant cross-link density during reprocessing as bonds associate before breaking, rendering their fast relaxation challenging. To address this issue, smart molecular engineering through additional functional groups and catalysts[16] was successfully implemented to extrude associative CANs imparted with enough short relaxation times[22]. In contrast, dissociative CANs contain bonds that follow a stepwise elimination and addition mechanism, resulting in a loss of cross-link density as a function of temperature.[30]

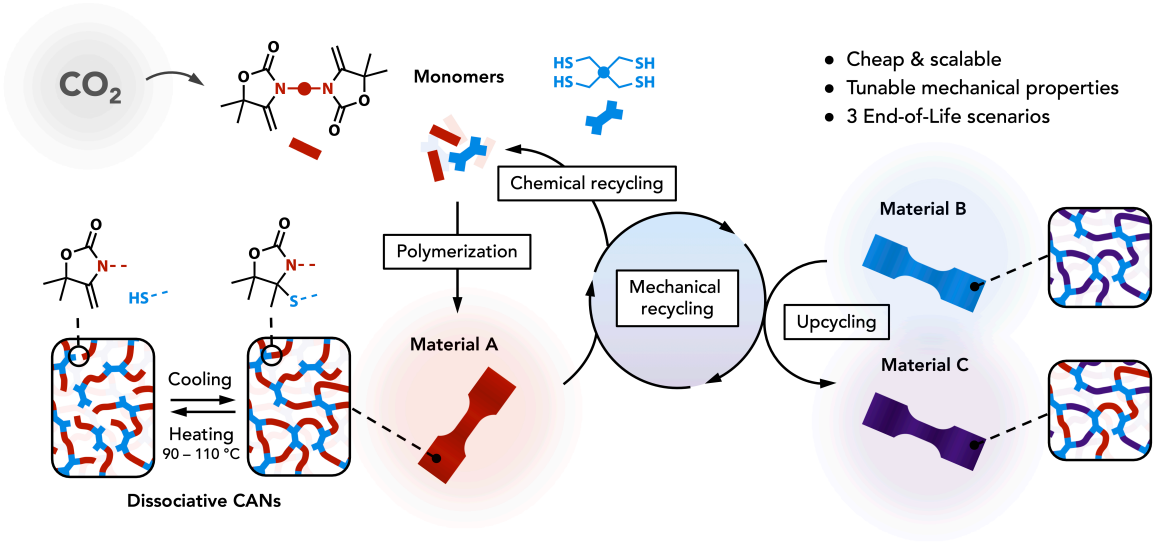

Scheme 1 – Illustration of the alkylidene oxazolidone – thiol chemistry, and overview of the three recycling scenarios of *N,S*-acetal oxazolidone-based dissociative CAN materials (mechanical, chemical and upcycling).

However, the addition of large amount of catalyst or the insertion of specific groups in the matrix are generally needed to shift enough the equilibrium toward the dissociated state to endow the material with enough low viscosity to be reprocessed like thermoplastics[24,31]. Another challenge associated with CANs is the access to milder reprocessing conditions. Most dynamic networks need long exposures to high temperatures and pressures to be reshaped, typically above 150 °C from some minutes to several hours[30,32–34]. Such harsh conditions might generate unwanted side reactions,[14,32,35–37] resulting in material properties alteration during multiple reshaping cycles. Fast reprocessing of CANs in mild conditions is therefore of key interest to facilitate recycling. Lastly, finding new chemistries of high potential in terms of recyclability, cost, scalability, and tunability toward materials with modular thermo-mechanical properties became a new pillar in the search for a more sustainable and affordable future for plastics.

In the last years, many works were devoted to design sustainable polymers containing degradable acetal linkages[38,39]. Recent contributions related to CANs have also shown that acetals and thioacetal derivatives undergo stress relaxation through bond exchange at elevated temperatures, rendering the acetal chemistry a promising platform for making greener materials[31,40–42].

In this work, we introduce a new highly dynamic chemistry based on *N,S*-acetals and its application in CANs. Unlike conventional synthetic approaches, *N,S*-acetals are synthesized by a facile cationic thiol-ene reaction between thiol and exovinylene oxazolidone obtained from

CO_2. Their utility is highlighted for the edition and reutilization of thermoset poly(oxazolidone)s, a type of emerging isocyanate-free polyurethanes with remarkable thermal and chemical stability[43–45]. Mechanistic and kinetic insights of the *N,S*-acetal formation and its dynamics were first illustrated on model compounds. Then, diverse CO_2-sourced exovinylene bisoxazolidone monomers were prepared and copolymerized with a polythiol at room temperature to provide thermosets featuring a wide diversity of mechanical properties ranging from PDMS-like elastomers to rigid polystyrene-like ones. The *N,S*-acetal bond in the thermosets was proven to be highly dynamic by means of rheology through stress relaxation and temperature sweep cycling experiments. This unique bond dynamics was then exploited for developing three different recycling scenarios: (i) the facile and rapid mechanical reprocessing by compression molding, extrusion or injection molding of densely cross-linked bulk material, (ii) the closed-loop chemical recycling through depolymerization into the offspring monomers, followed by their repolymerization, and (iii) an upcycling strategy by repurposing two different oxazolidone-based thermosets into a single one with new thermo-mechanical properties (Scheme 1). The utility of this new dynamic chemistry is exemplified by the facile manufacturing of a recyclable structural composite.

Overall, this work provides a new tool for the facile preparation of *N,S*-acetal compounds and recyclable polymer networks from CO_2. To date, there is no example of oxazolidone-based networks with intrinsic recyclability, and recent contributions on poly(oxazolidone)s were focused on linear polymer synthesis[46–50].

Results and discussion

Inspired by the “click” reaction of enamides with thiols in acidic conditions to provide *N,S*-acetals[51], we aimed to investigate whether the enecarbamate structure within alkylidene oxazolidones **2** exhibits similar reactivity (Figure 1a). Our group has previously confirmed the viability of this chemistry for post-functionalizing linear polymers containing alkylidene oxazolidone moieties[49]. However, a comprehensive understanding of the reaction at the molecular level remains unexplored. Intrigued by the potential of this reaction to deliver novel *N,S*-acetal oxazolidone scaffolds and the presumed dynamic nature of the *N,S*-acetal bond, we conducted initial studies at the model molecule level before implementing this chemistry to macromolecular engineering.

Model reactions

Alkylidene oxazolidones **2** can be obtained via the spontaneous and quantitative reaction between primary amines and CO_2-sourced α-alkylidene cyclic carbonates **αCC**. This reaction yields hydroxyoxazolidones **1**, which are subsequently dehydrated into the desired alkylidene oxazolidones **2** (Figure 1a). Previous works have introduced this last step[48,52], but existing approaches led to a mixture of **1** and **2**. To address this limitation, we developed a novel optimized protocol for the synthesis of **2** at high yields, ensuring both quantitative reaction and potential scalability.

In the frame of this study, we started from a cheap and abundantly available propargyl alcohol, 2-methylbut-3-yn-2-ol, that produced the corresponding α-alkylidene cyclic carbonate **αCC** by the room temperature reaction with CO_2 in the presence of a low catalyst loading (Ag_2CO_3/PPh_3; 1 mol%). After 14 h of reaction at 40 bar, 126 g of **αCC** was obtained in a single batch with a high isolated yield (76 %). The quantitative dehydration of **1** was then realized with methanesulfonic acid (MSA, 0.1 eq.) in refluxing continuously dried acetonitrile (Figure S1), and **2** was collected with a high isolated yield of 77-83% after purification. For the purpose of this work, two compounds were easily produced from two structurally different primary amines, i.e. propylamine (product **2a**) and benzylamine (product **2b**) (Figure 1b).

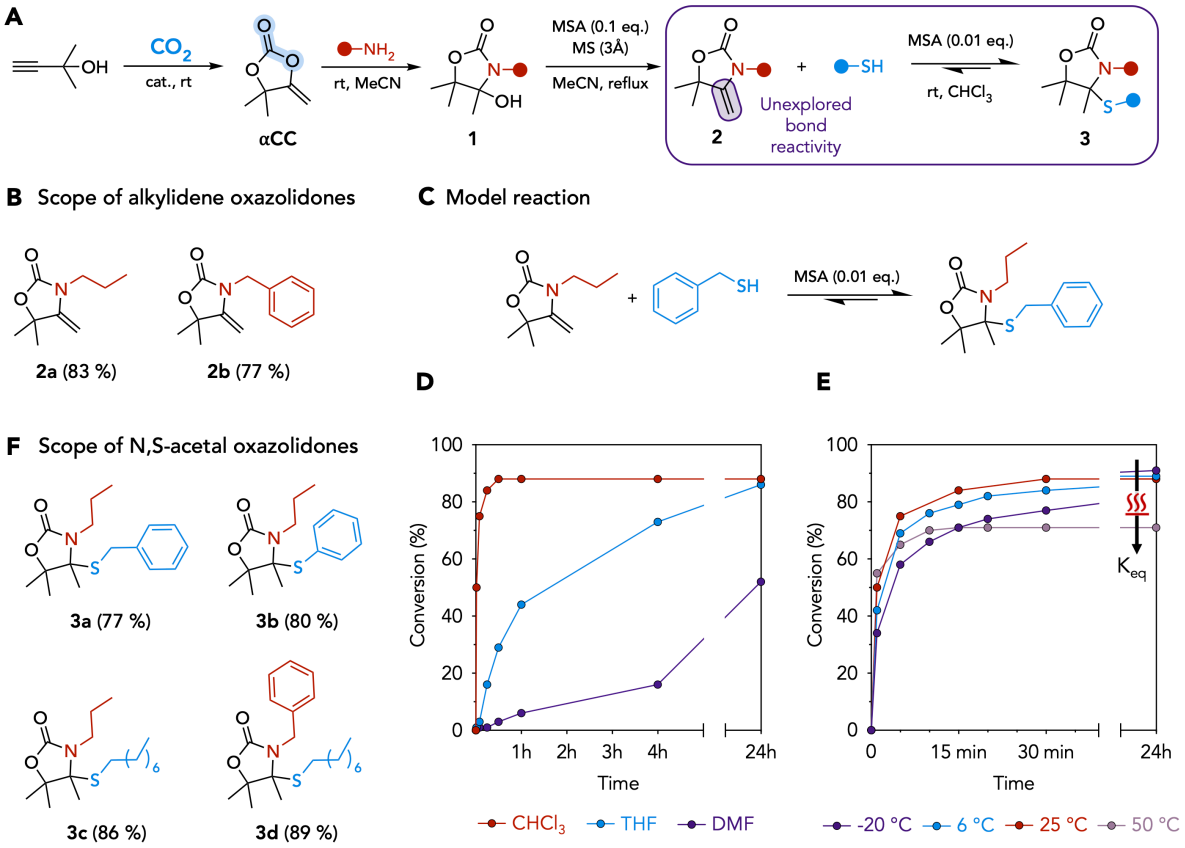

Figure 1. Overview of the synthetic pathway toward N,S-acetal oxazolidones and model reactions. (A) Carboxylation of 2-methylbut-3-yn-2-ol into reactive **αCC**, followed by its aminolysis into hydroxyoxazolidone **1**. Dehydration can be triggered to yield alkylidene oxazolidone **2**. N,S-acetal oxazolidones **3** are then obtained by the cationic addition of the thiol onto **2**. (B) Scope of synthesized alkylidene oxazolidones **2** (isolated yields in brackets). (C) Model reaction between **2a** and benzyl mercaptan to study the effect of (D) solvent and (E) temperature on the reaction kinetics. (F) Scope of synthesized alkylidene oxazolidones **2** (isolated yields in brackets).

With compounds **2** in our hands, we initiated our investigation by subjecting them to reaction with equimolar contents of thiols to yield *N,S*-acetal oxazolidones **3**. To assess how solvent and temperature influenced the reaction, we conducted reaction kinetics using the model oxazolidone **2a** and a commercial thiol, benzyl mercaptan, in the presence of MSA as acid catalyst (0.01 eq. compared to the oxazolidone), which has shown to efficiently catalyze the cationic thiol-ene reaction[51] (Figure 1d, Figures S2-S5).

Chloroform was the ideal solvent for the reaction, which ended after nearly 15 minutes with the formation of **3a** (Figure 1e). Importantly, the reaction never reached completion and a conversion of 88 % at equilibrium was obtained at 25 °C, in contrast to previously studied

enamides which quantitatively provided the product[51]. Solvents with a higher Lewis base character[53] significantly decreased the reaction rate. In THF, a similar conversion required over 4h of reaction and, in DMF, the reaction remained uncomplete after two days. Our findings indicate that solvents with a higher base nature tend to act as proton traps, affecting the alkylidene protonation efficiency, in accordance with the previous work of Kloxin et al[51]. Conversions were lower at higher temperature as the dissociated state was entropically favored (71 % at 50 °C) but were slightly increased at a lower temperature (89 % at 6 °C and 91 % at -20 °C) at the cost of longer reaction times (Figure 1f). This suggested that the conversion was dictated by the thermodynamic equilibrium between the associated and the dissociated state, the equilibrium constant being affected by temperature changes.

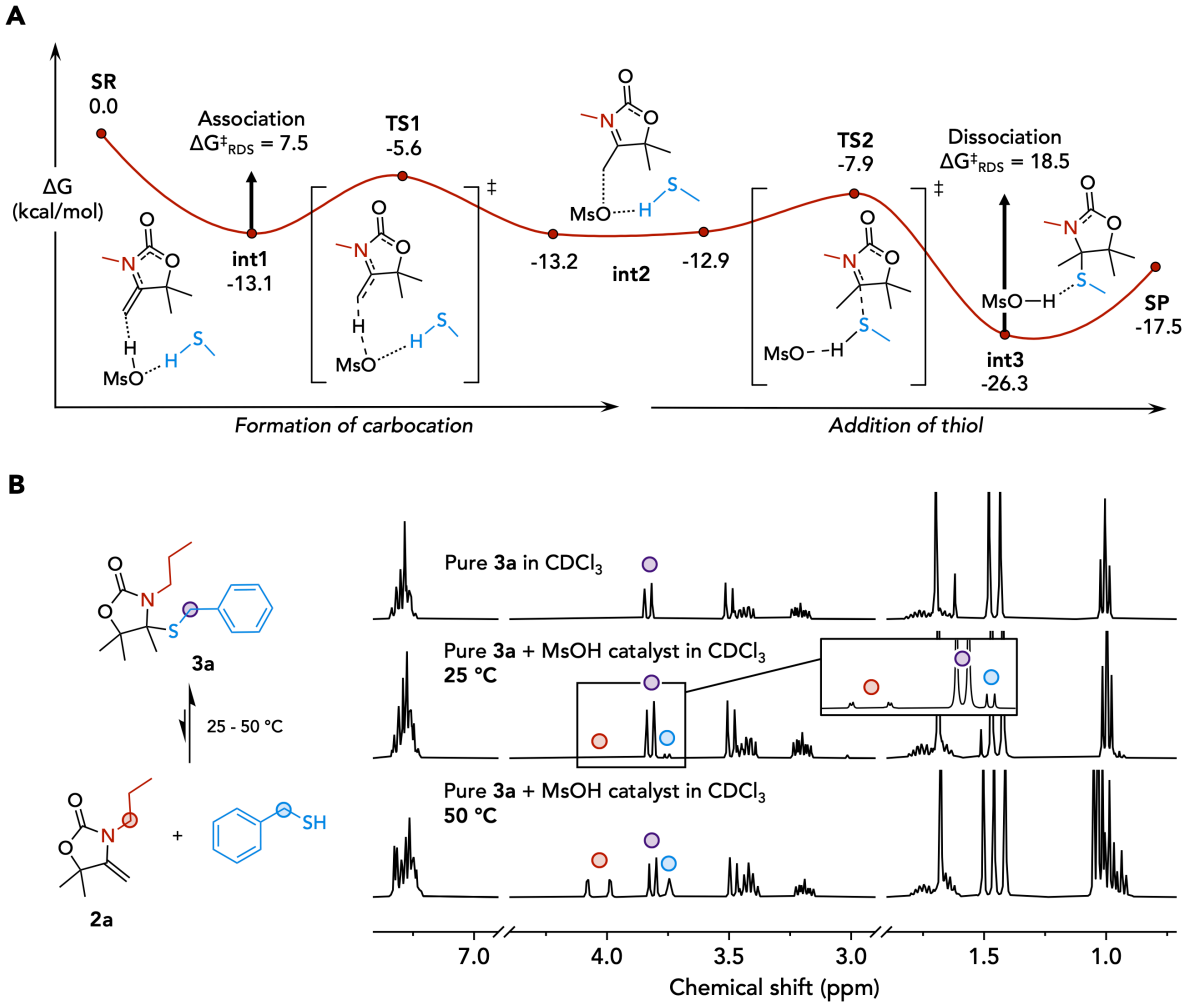

Figure 2. Energetics of the reaction pathway modelled by DFT and dissociative nature of the *N,S*-acetal oxazolidone moiety. (A) Gibbs-Free Energy profile with intermediates and transition states structures for the reaction of a model alkylidene oxazolidone with a model thiol. Vertical arrows indicate the energy barriers for both the association and the dissociation

reactions at their rate-determining step (RDS). (B) Dissociation experiment of 3a in the presence of MSA in deuterated chloroform ($CDCl_3$) analyzed by ^{1}H-NMR spectroscopy at different temperatures.

We probed the reactivity of **2a** with various thiols, i.e. octanethiol, benzyl mercaptan and thiophenol (Figure S6a). Octanethiol behaved similarly to benzyl mercaptan, with a slight increase of the reaction rate, certainly due to a decrease in steric hindrance around the thiol group. Thiophenol reacted rapidly, however its conversion remained low at equilibrium (73 %). Using the more hindered oxazolidone **2b** with octanethiol did not seem to significantly affect the reaction rate (Figure S6b).

The potential of this reaction can be leveraged by choosing ideal conditions (25 °C, excess of thiol) to synthesize novel *N,S*-acetal oxazolidone compounds **3a-d** (Figure 1c) with high isolated yields (up to 89 %). The full characterization of these molecules by NMR spectroscopy and HRMS can be found in Supporting Information (Figures S7-S14). This chemistry therefore opens an avenue to the facile construction of a vast library of compounds whose oxazolidone motifs are of high interest in many fields of chemistry (pharmacology, agriculture, synthetic intermediates, etc.).[54–57]

To have a better insight on the mechanism of this reaction, we performed density functional theory (DFT) calculations at the ωB97-XD/6-311++G(d,p) level of theory with a CPCM solvation model (ε=4.7113, chloroform) (Figure 2a). For simplicity's sake, the system was modelled with methyl groups as substituents for the N and S atoms, mimicking aliphatic chains used in the experimental model reactions. As it might have a drastic impact on calculations, MSA was used as catalyst in the system. Our results revealed that the reaction is performed in two separate steps. The starting reactants complex is very stable compared to separate reactants with a stabilization energy of 13.1 kcal·mol^{-1}. This is enabled by hydrogen bonding interactions between the different species and more especially due to the acidic proton of MSA in interaction with the negatively charged atom of the alkene (Figure S17). This interaction creates a high degree of delocalization in the oxazolidone ring thanks to the presence of the electron-rich nitrogen group in the vicinity of both the alkene and the carbonyl groups. The first step of the reaction, which is the rate-determining step (RDS) of the forward reaction, has a low activation barrier of 7.5 kcal·mol^{-1} explaining the experimentally observed high reaction rate. In this first step, the acidic proton of MSA is transferred to the terminal side of the alkene to form a stabilized carbocation, which is of very similar energy than the reactants complex **int1** (difference of 0.1 kcal·mol^{-1}). The high stabilization of this intermediate **int2** can be explained by the formation of a new stable pi bond between the nitrogen and the carbocation, resulting in a decrease of bond length from 1.373 to 1.292 Å (- 0.081 Å). The N-C(O) bond

readily increases its length of 0.073 Å as the nitrogen atom shares less electrons with the carbonyl group (Table S1). In a second time, the thiol adds onto the electrophilic carbon of the ring with a very low barrier of 5.0 kcal·mol^{-1}, thus breaking the pi bond created in the first step. In a concerted manner, the hydrogen of the thiol already in interaction with the catalyst is then completely transferred to form a stabilized complex of the product and the regenerated MSA **int3**, whose energy is -26.3 kcal·mol^{-1}. This enhanced product stability renders the reverse reaction less energetically favorable though the reverse barrier stays rather low with an activation energy of 18.5 kcal·mol^{-1}. These differences in energy support why the equilibrium was shifted towards the product under ambient reaction conditions, with only slight reversibility occurring at room temperature.

To further support that dissociation occurred under ambient conditions, to pure oxazolidone **3a** was added by MSA (0.01 eq.) in $CDCl_3$ and the mixture was analyzed by ^{1}H-NMR spectroscopy (Figure 2b). Besides *N,S*-acetal oxazolidone **3a**, we observed the formation of the alkylidene oxazolidone **2a** and the thiol in low amounts (≈ 3 mol%). Without MSA, only compound **3a** was observed. This result provided strong evidence that dissociation slightly occurred in the presence of MSA at room temperature. When increasing the temperature to 50 °C, a great effect on dissociation was observed with the formation of **2a** and the thiol in large amount (≈ 25 mol%).

The exchange kinetics was monitored at different temperatures using ^{1}H-NMR spectroscopy by reacting **3a** with a fivefold excess of octanethiol in the presence of MSA (0.01 eq. *vs* **3a**) (Figures 3a, S18). The reaction was monitored from 7 to 50 °C, showing slow exchange kinetics at 7 °C and strong acceleration of the reaction rate constant k at 50 °C, passing from 0.5×10^{-3} to 23×10^{-3} s^{-1}. The exchange reaction therefore showed a great temperature dependance. An Arrhenius plot was built from the different reaction rate constants k at different temperatures and an activation energy of 15.5 kcal.mol^{-1} was extracted for the bond exchange (Figure 3b-c), lying in the same range of *S,S*-acetal or vinylogous urethane bonds[42,58] (Table S2). This energy is also of same order as the dissociation energy determined by DFT (18.5 kcal.mol^{-1}). It must be noted that even in the presence of a high excess of thiol, the alkylidene oxazolidone **2a** could still be observed in traces amount by NMR during the reaction kinetics, further proving the dissociative mechanism (Figure S18). Overall, the alkylidene oxazolidone – thiol dynamic chemistry showed activity at room temperature with strong increase in bond dynamics when the temperature was increased, highlighting a high reversible character in mild conditions.

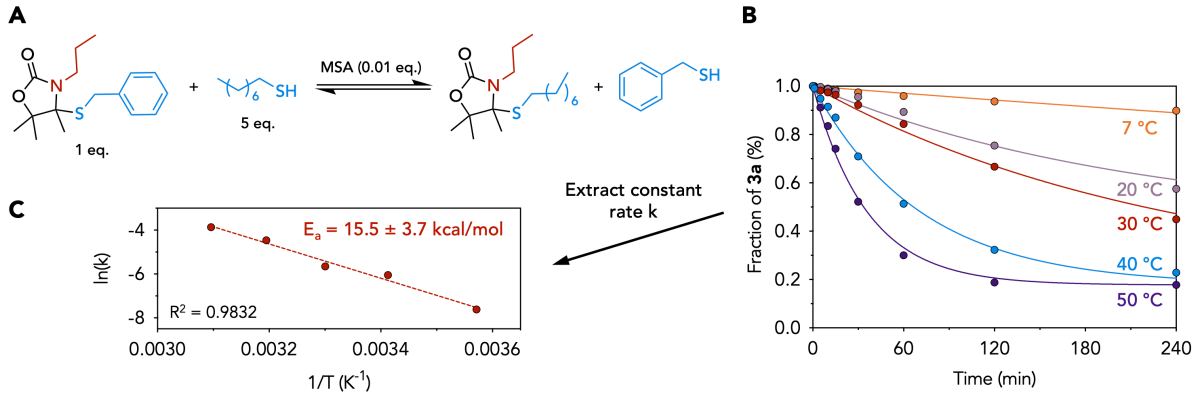

Figure 3. Exchange reaction kinetics at the model compound level. (A) Model reaction for the exchange kinetic study. (B) Kinetics of exchange at several temperatures (from 7 to 50 °C). (C) Arrhenius plot from the extracted reaction rate constants at the different temperatures of reaction.

Thermoset preparation and characterization

Taking advantage of the highly reversible character of this reaction, we explored its potential for the design of covalent adaptable networks based on *N,S*-acetal bonds. We exploited the versatile and facile α-alkylidene cyclic carbonate chemistry to design bifunctional alkylidene oxazolidone monomers of different structures (Figure 4a). Four compounds **2c-2f** were synthesized from different commercially available diamines: m-xylylenediamine (XDA), 2,2′-(Ethylenedioxy)bis(ethylamine) (DMDO), hexamethylenediamine (HMDA) and Priamine 1075 (PRI). This scope of diamines was chosen to access structurally diverse monomers, which are expected to impart networks with diamine-dependent properties. The synthesis of all four monomers was achieved by reacting CO_2-sourced **αCC** with a diamine in acetonitrile at r.T. Then, tandem dehydration was triggered without isolation of the bis(hydroxyoxazolidone) intermediate using the previously described dehydration setup. All substrates were easily purified by a chromatography-free process in high isolated yield (up to 84 %), rendering their synthesis facile, cheap, and up-scalable (see supporting information for details and a full characterization of these molecules, Figures S20-S27).

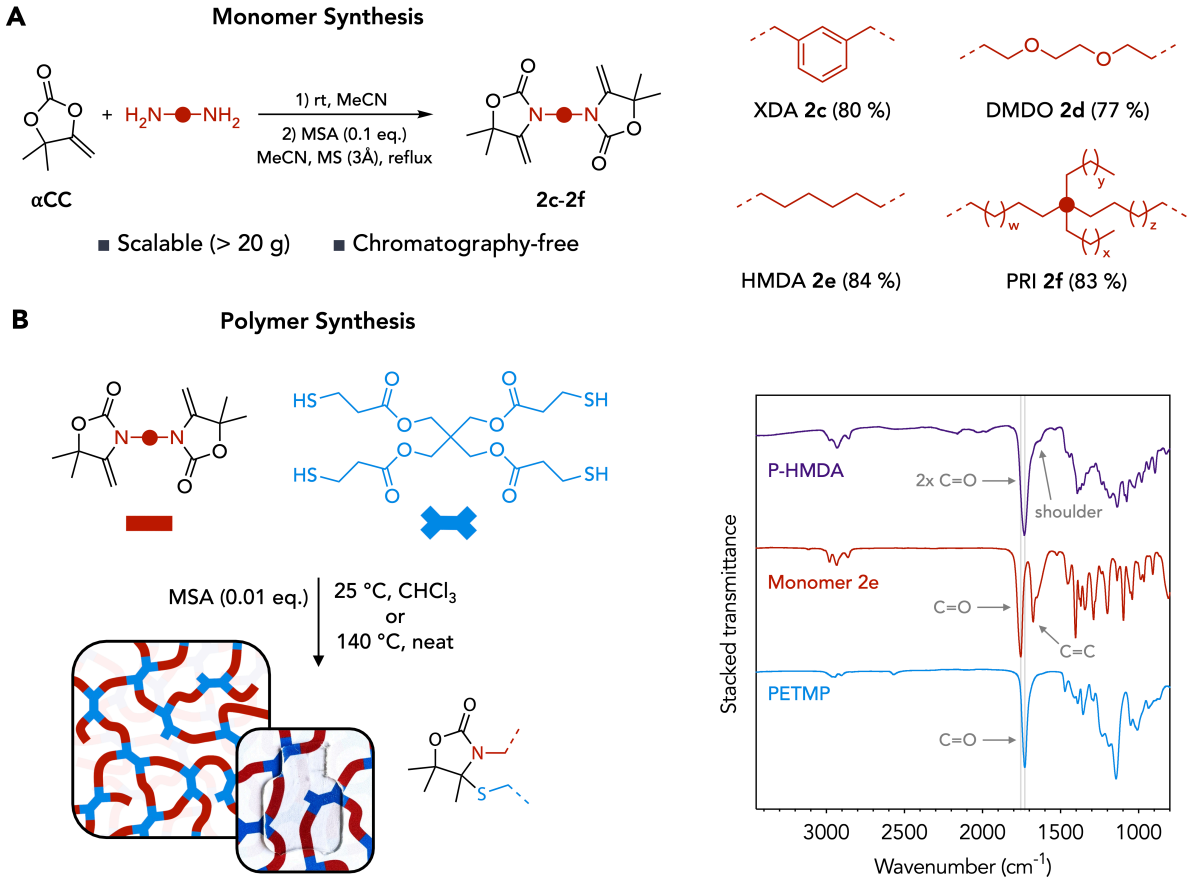

Figure 4. Monomer and polymer syntheses. (A) Tandem synthesis of bis(alkylidene oxazolidone)s 2c-2f from αCC and diamines (isolated yields in brackets). (B) Polymerization of a bis(alkylidene oxazolidone) with PETMP into a cross-linked material. A specimen of P-XDA is displayed to highlight its high transparency. ATR-IR spectra of P-HMDA and its respective monomers.

Different polymers were designed from the oxazolidone monomers **2c-f** and a 4-arm thiol, pentaerythritol tetrakis(3-mercaptopropionate) (PETMP) (Figure 4b). For all these syntheses, an equimolar ratio between the oxazolidone and the thiol functions was used, and the reactions were catalyzed by MSA (0.01 eq. *vs* oxazolidone monomer). The polymerization proceeded either in solution or in bulk (Figure S28). When achieved in solution, the mixture of the monomers in chloroform (2 M concentration of reactive functions) was stirred at r.T. until the formation of a gel (between 10 and 60 minutes depending on the monomer). The gel was then recovered and dried under vacuum at 70 °C followed by slow cooling to yield the pure material. Another option, which might be more easily adopted for large-scale production, was the bulk polymerization by stirring the components in the melt at 140 °C for 5 minutes followed by slow cooling to directly yield the pure material. In the two processes, the polymer networks were transparent with a special emphasis for P-XDA showing no coloration (Figure 4b).

Successful polymerization was confirmed via infrared (FT-IR) spectroscopy (Figure 4b). The networks were characterized by an intense elongation at 1732 cm^{-1} contributing for the stretching of the carbonyl groups of both the oxazolidone and ester groups. A very low intensity signal around 1620 cm^{-1} was indicative of some residual alkylidene function (Figures S29-30). This is in line with the previous model reaction study that revealed a non-quantitative conversion of the reactants. Nevertheless, high gel contents were obtained for all polymers in THF (from 87 to 99 %), attesting for the crosslinked nature of the materials (Table 1). A good swelling (between 140 and 314%) was observed for all polymers in THF (Table 1).

The thermal properties of the polymers were then studied by thermogravimetric analysis (TGA) and differential scanning calorimetry (DSC) (Table 1, Figures S31-38). All polymers displayed a temperature at 10 % of degradation ($T_{deg,10\%}$) around 300 °C except for P-PRI characterized by a higher value of 366 °C. The highest T_g was recorded for the aromatic P-XDA (T_g = 60 °C) with a more rigid backbone. On the other side, P-PRI picturing more chain mobility was characterized by the lowest T_g (8 °C). P-DMDO and P-HMDA had intermediate T_gs of 51 and 44 °C, respectively.

Table 1. Thermal properties, swelling ratios, gel contents and mechanical properties of the polymers.

Polymer	$T_{deg,10\%}$[a] (%)	T_g[b] (°C)	SR_{THF}[c] (%)	GC_{THF}[d] (%)	Young modulus[e] (MPa)	Yield Strength[e] (MPa)	Stress at break[e] (MPa)	Strain at break[e] (%)
P-XDA	296	60	196 ± 6	90.4 ± 0.6	--	--	--	--
P-DMDO	303	51	140 ± 4	99.0 ± 0.3	2438 ± 38	--[f]	46.5 ± 1.2	2.7 ± 0.1
P-HMDA	282	44	215 ± 5	94.8 ± 0.4	1778 ± 116	--[f]	12.6 ± 1.4	0.7 ± 0.1
P-PRI	366	8	287 ± 21	86.6 ± 1.3	2.9 ± 0.1	--[f]	2.2 ± 0.1	159 ± 4
P-(HMDA75)-(PRI25)	289	44	228 ± 1	93.8 ± 0.2	1851 ± 41	--[f]	34.0 ± 1.2	2.1 ± 0.1
P-(HMDA50)-(PRI50)	291	37	205 ± 6	91.2 ± 0.2	655 ± 72	8.6 ± 0.3	13.0 ± 0.3	81 ± 0.3
P-(XDA75)-(PRI25)	289	62	314 ± 6	86.1 ± 0.1	--	--	--	--
P-(XDA50)-(PRI50)	310	43	292 ± 12	93.7 ± 0.4	1238 ± 45	29.9 ± 1.0	20.8 ± 0.8	10 ± 1

[a]Temperature at 10% of degradation determined by TGA. [b]Glass transition temperature determined from the reversing curve of the first heating rate by modulated DSC. [c]Swelling ratio (SR) after immersion of the polymer for 24h in solvent (THF).[d]Gel content (GC) after immersion

of the polymer for 24h in solvent (THF). [e]Mechanical properties evaluated by tensile tests. [f]Materials experienced a brittle fracture.

To extend the scope of materials and modulate their thermo-mechanical properties, four additional polymers were synthesized by mixing pre-defined ratios of XDA or HMDA with PRI. The new polymers were labeled P-(A X)-(B Y) to denote their content in X wt% of monomer A and Y wt% of monomer B. Their temperature of degradation was quite similar, around 300 °C. We expected intermediate T_g for these polymers. Surprisingly, P(HMDA75)-(PRI25) was characterized by the same T_g as P-HMDA (44 °C), and P(XDA75)-(PRI25) was characterized by a similar T_g as P-XDA (62 °C and 60 °C, respectively). By increasing the PRI content to 50 wt% within the materials, their T_g dropped while remaining around 40 °C. Overall, the thermal properties of the networks were judiciously adjusted through the choice of the diamine chemical structure.

Next, the mechanical properties of the various polyoxazolidones thermosets were determined through tensile tests on specimens obtained by compression molding of the samples (Figure 5a). Unfortunately, P-XDA and P-(XDA75)-(PRI25) samples could not be tested due to their extreme brittleness. P-HMDA was a brittle material too, breaking at very low strain (0.7 %). Despite its similar T_g lying between P-XDA and P-HMDA, P-DMDO showed excellent mechanical properties with a Young modulus of 2400 MPa and a yield strength of 46 MPa, with a brittle fracture occurring at low strain (2.7 %). The extra toughness of this polymer compared to P-HMDA was attributed to the higher degree of mobility provided by the presence of the ether bonds within the polymer microstructure. On the other hand, P-PRI demonstrated elastomeric behavior, with a relatively low modulus of 2.9 MPa and an elongation at break of 159%. Interestingly, when PRI was added to the formulation of brittle P-XDA and P-HMDA, the resulting polymer's mechanical behavior was significantly altered. Specifically, P-(HMDA75)-(PRI25) exhibited a modulus of 1850 MPa and a brittle fracture, while increasing the PRI content in P(HMDA50)-(PRI50) decreased the modulus to 655 MPa and resulted in high plastic deformation with an elongation at break of 81%. P(XDA50)-(PRI50) exhibited a modulus of 1240 MPa and plastic deformation.

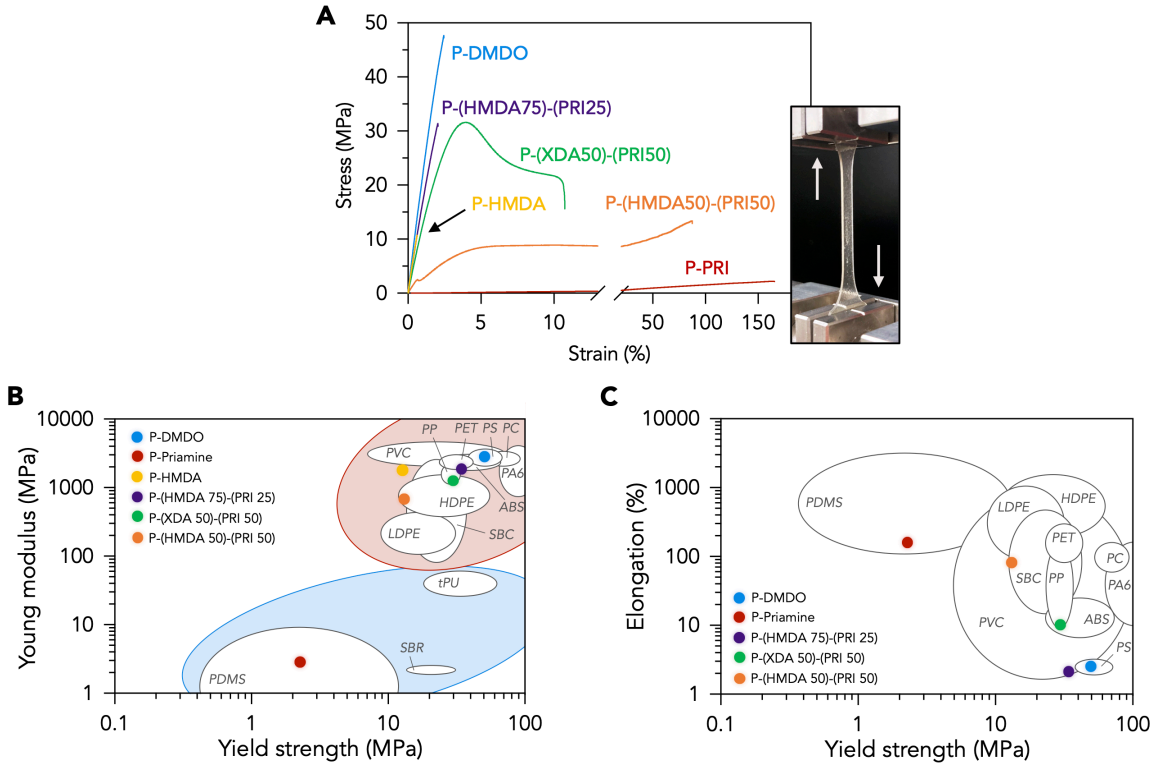

Figure 5. Mechanical properties of the polymers determined by tensile tests and comparison to commodity polymers. (A) Stress – strain curves of all polymers displaying a large range of properties. (B) Ashby plot showing Young modulus and yield strength compared to commodity polymers. (C) Similar Ashby plot showing elongation and yield strength. Commodity polymers mechanical properties were found in the literature[59].

To compare the properties of the synthesized polymers to commodity polymers, we plotted Ashby diagrams[60] based on three critical parameters: the Young's modulus, the yield strength, and the elongation at break (Figure 5b-c). These plots revealed a wide diversity in the mechanical properties of the synthesized polymers, with some of them exhibiting properties comparable to some commodity polymers. For example, P-DMDO had similar properties to polystyrene (PS), with a modulus, strength, and elongation within the literature values. Furthermore, P-PRI was located in the PDMS area of the diagram, while P(XDA50)-(PRI50) was situated in the polypropylene (PP) zone, albeit with low elongation. Despite P(HMDA75)-(PRI25) and P(HMDA50)-(PRI50) exhibiting intriguing properties, they did not meet those of the reported commodity polymers.

These results illustrate the huge potential of our new polymers to furnish materials of tunable mechanical properties by simply adapting the alkylidene oxazolidone monomer structure. Moreover, this study only represents a limited overview of the myriad of possibilities through

monomer design and formulation to develop a wide range of materials with on-demand modular properties to fit with the specification of diverse applications.

Dynamic behavior of the networks

The dynamic behavior of the networks was then characterized by rheology and exemplified for P-HMDA in Figure 6. First, the temperature-dependence on the storage (G') and loss modulus (G'') was assessed by a temperature sweep experiment (Figure 6a). Values below T_g could not be determined by rheology as the sample was hard, resulting in a poor surface contact between the rheometer plateau and the specimen[61]. They were obtained by dynamic mechanical thermal analysis (DMTA) from rt to 80 °C, showing a drop in storage modulus at the T_g of the polymer (Figure S39). Above T_g, the sample showed a higher value of G' than G'', indicating that the material was in a cross-linked rubber state. Importantly, G' showed a constant decreasing trend, attesting for the progressive loss of cross-linking density with increasing temperature. This result was in line with the dissociative nature of the bonds as observed in the model compounds study. The curves tend to cross above 80 °C where enough dissociation occurred to de-crosslink the material and enable flow. The crossover point between the two curves represents the gel-to-sol transition and was denoted $T_{gel\text{-}to\text{-}sol}$ for the different polymers (Table 2).

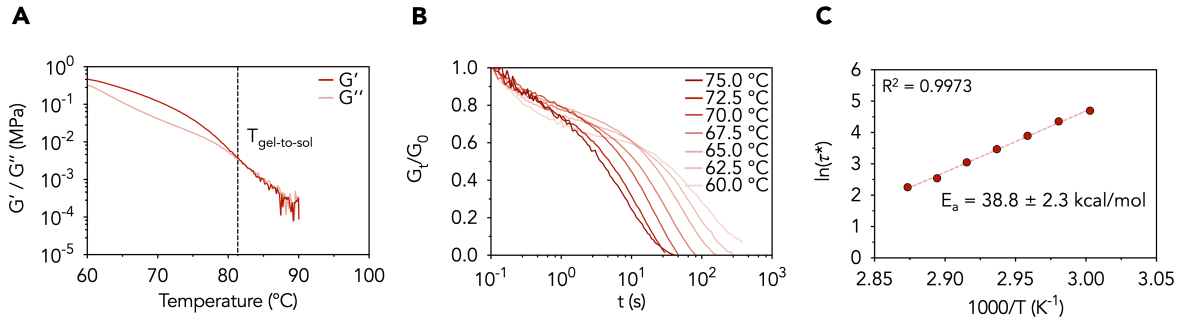

Figure 6. Rheological experiments conducted on P-HMDA. (A) Temperature sweep. (B) Stress relaxation at different temperatures whose extracted characteristic relaxation times could fit the (C) Arrhenius law to obtain an energy of activation.

Similar trends were observed for P-DMDO and P-PRI, each of them showing different $T_{gel\text{-}to\text{-}sol}$ transition temperatures (Figure S40-S42). P-DMDO presented a higher transition of 91 °C and P-PRI a lower one of 73 °C. As P-PRI was characterized by a low T_g, rheological data were recorded from room temperature. Interestingly, the value of G' was slowly decreasing from 30

to 55 °C, indicating a slight loss of cross-link density at low temperature. An abrupt drop was observed starting around 60 °C until the gel-to-sol transition at 72.6 °C.

Table 2. Gel-to-sol transition and flow activation energy for the polymers studied by rheology.

Polymer	$T_{gel\text{-}to\text{-}sol}$[a] (°C)	E_{flow}[b] (kcal·mol^{-1})
P-XDA	--[c]	--[c]
P-DMDO	91.3	26.4 ± 3.0
P-HMDA	81.4	38.8 ± 2.3
P-PRI	72.6	34.5 ± 2.8

[a] Gel-to-sol transition temperature as determined by temperature sweep rheology. [b] Flow activation energy (E_{flow}) as determined by stress relaxation measurements in rheology. [c] Could not be determined.

Stress-relaxation experiments were achieved before the flow transition threshold in the viscoelastic region of the networks. As observed in Figure 6b for P-HMDA, the material readily relaxed the applied stress through bond dynamics. The normalized stress relaxation curves have shown to follow a three-element Maxwell model, revealing the presence of three distinct relaxation modes during the material topology reorganization. However, most studies on CANs revealed that single-element Maxwell or stretched exponential models were generally accurately fitting the relaxation experiments data[12]. On the other side, multi-element Maxwell could be effectively used to describe materials with kinetically different exchange processes[62,63]. At each temperature were extracted three characteristic relaxation times (τ_1, τ_2 and τ_3). τ_1 and τ_2 showed to be independent from temperature changes and were both of relatively short timescale (0.1-0.7 s for τ_1 and 0.7-15 s for τ_2) (Figures S40-S42; Table S3). Thus, we hypothesized these relaxation modes to be attributed to chain rearrangement at stress exposition[64]. Although these two first relaxation modes with short timescales may not interfere in the network reprocessability, the use of a three-element Maxwell model is critical to correctly fit and extract reliable data. The last relaxation mode of characteristic relaxation time τ_3 was characterized by a strong temperature dependence and may be attributed to bond dynamics within the network. The different characteristic relaxation times τ_3 were plotted against temperature in a typical Arrhenius plot and an excellent linear correlation was observed, thus enabling the determination of a flow energy activation $E_{a,flow}$ of 38.8 kcal·mol^{-1} (Figure 6c). Stress relaxation experiments on P-DMDO and P-PRI showed that the polymer matrix and thereby, the monomer structure, had a strong influence on the viscoelastic behavior of the polymer (Table 2). P-DMDO was characterized by a lower $E_{a,flow}$ of 26.4 kcal·mol^{-1},

indicating a less pronounced sensitivity of the viscosity to temperature[14,65]. P-DMDO was indeed imparted with a shorter relaxation time τ_3 at 60 °C (88 s) but higher at 75 °C (15 s). This result was in line with the temperature sweep experiment displaying a higher $T_{gel\text{-}to\text{-}sol}$ transition for P-DMDO than P-HMDA despite their close T_g. On the other side, P-PRI was characterized by a lower but yet similar $E_{a,flow}$ as P-HMDA, of 34.5 kcal·mol^{-1}. The early gel-to-sol transition observed in P-PRI was rationalized by an increased chain mobility. However, matrix effects on CANs are yet still not fully understood and many parameters are thought to play a role such as polarity changes[64], solvation effects, cross-linking density and degree of chain flexibility[66]. Overall, monomer structure seems to have critical influence on the viscoelastic properties of *N,S*-acetal oxazolidone dynamic networks and a better rationalization of the experimental results might be needed to further understand all the structural effects. This study is however out of scope of this paper. The determined flow energy activation for the different studied polymers are in the same range of reported *S,S*-thioacetal dynamic networks reported by the group of Du Prez[42] (Table S2).

Overall, this rheological study suggests a high reprocessing ability for these materials which are able to relax extremely rapidly (relaxation times in the order of seconds) in their rubber state and can even flow as thermoplastics above their gel-to-sol transition temperature where the cross-linking integrity is lost.

Recycling of the networks

While most studies on CANs materials mainly display one or two recycling routes, this work exploited the highly reversible character of the alkylidene oxazolidone-thiol chemistry to provide three different end-of-life scenarios for the materials (Scheme 2). Multiplying the recycling possibilities for new emerging plastics is of great interest as the recycling approach might be selected depending on the market needs and the state of the material after use.

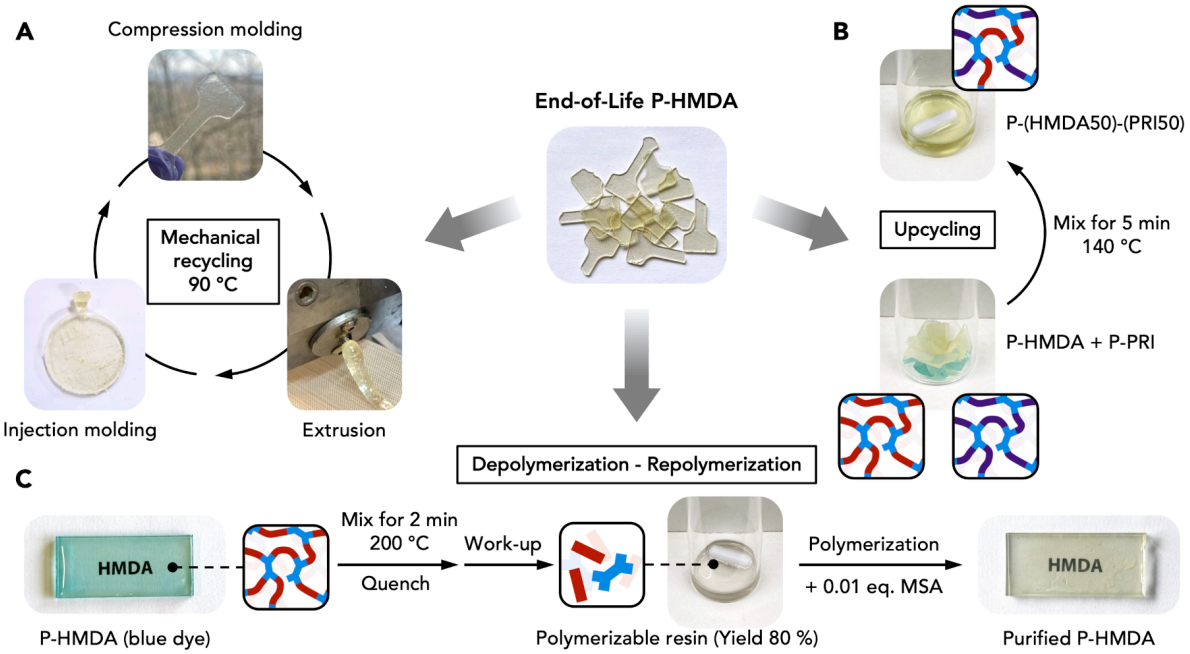

Scheme 2. End-of-life scenarios for P-HMDA. (A) Mechanical recycling using compression molding, extrusion, and injection molding. (B) Upcycling of P-HMDA and P-PRI toward P-(HMDA50)-(PRI50). (C) Chemical recycling through depolymerization and re-polymerization of contaminated P-HMDA.

Mechanical recycling

The most straightforward approach is the mechanical recycling (Scheme 2a). Although conventional networks cannot be reshaped, stress can be dissipated in CANs by virtue of bond dynamics and reshaping is therefore made possible. As highlighted by rheological investigations, the polymers reached very low complex viscosities η^* (in the range of 10 to 40 Pa·s at 90 °C) (Figure S43) and flowed at temperatures above the gel-to-sol transition. With this in mind, we first reprocessed P-HMDA by compression molding at 90 °C (in the flowing state) for 10 min under mild pressure (1 ton metric). Upon cooling, the material was recovered from the molds. We also successfully subjected P-HMDA to extrusion at high rate (150 rpm) or injection molding at 90 °C. Reshaping the network was thus possible through multiple industrially relevant techniques in mild conditions and in a short timeframe while most studied CANs require long exposition to high pressure and/or temperature[30,32–34]. In all cases, T_g as well as IR spectrum of the reprocessed polymer were identical to the starting material, suggesting no degradation (Figure S44).

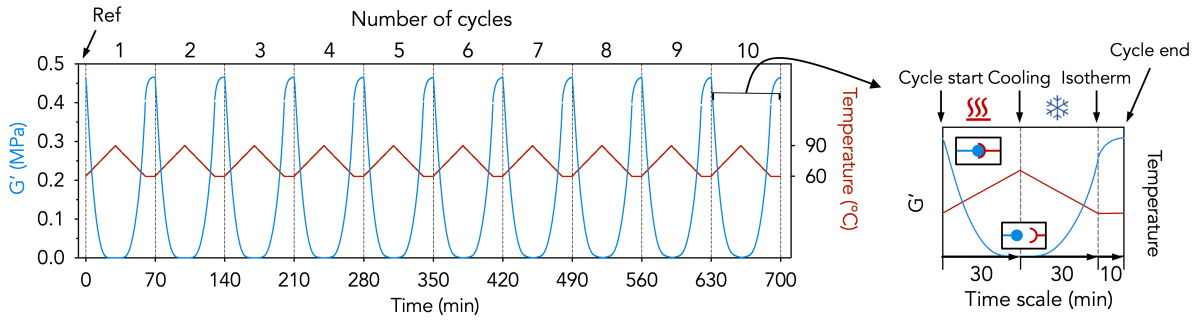

Figure 7. A temperature sweep cycling test was performed on P-HMDA at heating and cooling rates of 1 °C/min between 60 and 90 °C. The storage modulus G' was totally recovered (at 100%) at the end of each cycle.

We performed on-line storage modulus measurement as a function of time and temperature over up to 10 cycles (Figure 7). The sample, heated from 60 to 90 °C and cooled down to 60 °C at each cycle, displayed total recovery of the storage modulus. It must be noted that after cooling at 1 °C/min, around 85 % of the storage modulus was recovered. Additional 10 minutes at 60 °C allowed for a total recovery of G' before beginning a new cycle, highlighting that slow cooling was critical to recover the starting material properties. This experiment evidenced that the network underwent total disassembly to a flowing state at 90 °C by cycling above and below the gel-to-sol transition temperature with a total and reproducible recovery of the storage modulus, i.e. of the cross-link density within the material, without any hysteresis. This suggested that these materials might undergo a significant number of fast reprocessing cycles at mild temperatures, well below the degradation of the polymer, thus avoiding material degradation that might happen in CANs exposed to high pressure and temperatures for a prolonged period of time[14]. Tensile tests of reprocessed samples after fracture were performed and showed a good recovery of the Young's modulus which was very similar to the original material after two fracture-reprocessing cycles (Figure S45). However, both stress and strain at break were not fully recovered, as already observed for many healed materials containing dynamic linkages[35,67–70].

Upcycling

Recently, it was demonstrated that upcycling of CANs was possible through bond exchange between two distinct materials into a divergent one[71,72]. Dichtel et al. notably demonstrated that two soft and hard polyurethane networks could be mixed enough efficiently to provide a new material by extrusion at 200 °C. An akin strategy can be used in our case by mixing two different *N,S*-acetal oxazolidone dissociative CANs. Upon thermal treatment above the gel-to-sol

transition, bond rupture enabled the material to flow, delivering back alkylidene oxazolidone and thiol functionalities and, upon cooling, random re-association of the bonds was expected to provide a hybrid network consisting of mixed structures (Scheme 2b). This was illustrated by efficiently mixing identical contents of two different materials, P-HMDA and P-PRI, at 140 °C for 5 min under solvent-free conditions using a magnetic stirrer, and then to slowly cool down the mixture. DSC and IR analyses evidenced identical T_g and IR spectra than the previously synthesized P(HMDA50)-(PRI50), suggesting that the mixture of the two separate networks were converted into the mixed one (Figure S46). This approach enabled to easily upcycle the end-of-life networks into new ones exhibiting distinct properties.

Chemical recycling

The chemical recycling is the third considered end-of-life option (Scheme 2c). This approach, especially the one that considers the depolymerization into the constitutive monomers, is highly desirable as it generally allows to recover the monomers from impurities such as dyes and other additives[8,73].

Acidic hydrolysis of acetal linkages is a common and attractive way to promote degradation and recycling of polymers in mild conditions[31,41,74]. Thus, the presence of the *N,S*-acetal linkages could render poly(oxazolidone)s scaffolds sensitive to acidic aqueous environments. However, *N,S*-acetals derivatives might be more resistant than oxygen-containing *S,O*- and *O,O*-acetals[51]. Low swelling ratios were observed in water after 24h for all synthesized polymers, the highest value being 2% for P-DMDO. Lowering the pH using acidic aqueous solutions of H_2SO_4 at different concentrations (0.1, 1.0 and 5.0 M) did not lead to any degradation with gel contents as high as 99% and IR spectra showed no difference compared to the pristine polymer (Figure S47), attesting for the resistance of the polymers to acidic aqueous environment.

However, the versatility of the *N,S*-acetal oxazolidone chemistry and its high dissociative character at high temperatures allowed us to find another approach toward a recovery of the constitutive monomers. We synthesized P-HMDA containing a blue dye (methylene blue) as a model additive. In order to shift the equilibrium toward the monomers and thus to favor depolymerization, we heated the network at 200 °C for 2 minutes only. We then quenched the medium with a catalytic amount of triethylamine (3 eq. per equivalent of MSA) to avoid the MSA-catalyzed reverse reaction, quantitatively yielding a mixture of constitutive monomers and quenched catalyst (Figure S48). The mixture was purified by filtration through activated charcoal to remove the dye followed by a simple liquid extraction with water to remove triethylamine and MSA. After evaporation of the solvent, a colorless viscous resin was

obtained. ^{1}H-NMR analysis of the resin revealed the presence of the two starting monomers in equimolar amount that were recovered at 80 % yield (Figure S48). By adding MSA to this mixture and following the synthetic procedure, P-HMDA was recovered with identical DSC and IR results as the starting product (Figure S49).

Composite preparation and recycling

Thermosets are largely used in composites to furnish high performance light structural materials used for instance in wind turbine blades, aeronautics, automotive, etc.[75] However, the recycling of composites is an important issue due to the difficulty to separate the filler from the crosslinked polymer matrix. For the proof of concept to illustrate the potential of our technology in composite preparation and in their facile recycling, we prepared a composite composed of flax as the filler and P-DMDO as the network matrix. For that purpose, P-DMDO was hot pressed on flax under 3 bars of pressure at 100 °C for 15 minutes (Figure 8). This straightforward process was aided by the very low viscosity of the polymer above its gel-to-sol transition temperature, rendering the filler impregnation a facile task. As expected, the composite tensile strength was strongly increased compared to the lone polymer (170 *vs* 50 MPa) as well as the Young modulus (5700 *vs* 2400 MPa) (Figure 8). The strain at break passed from 2.7 % to 3.5 %.

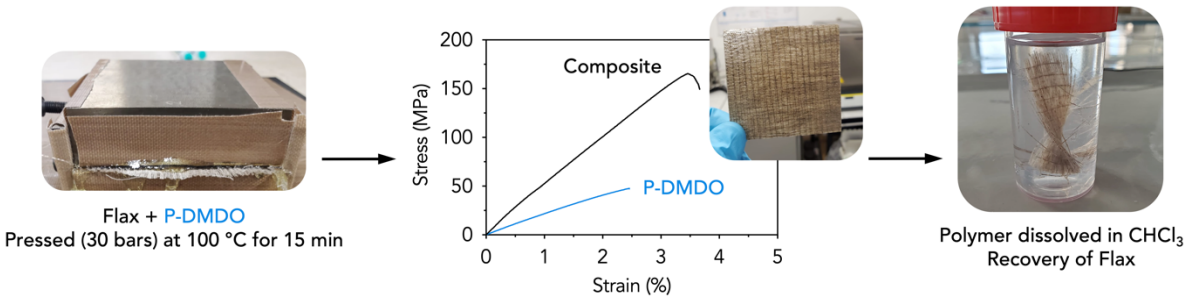

Figure 8. Composite preparation from flax and P-DMDO. Grinded P-DMDO was pressed with Flax to provide a composite material with excellent mechanical properties. Polymer-free flax could be recovered by dissociation of the polymer matrix in $CHCl_3$ (catalyzed by MSA within the polymer matrix).

To separate the fibers from the crosslinked matrix, we exploited the dynamics of the *N,S*-acetal type oxazolidone linkages. Based on our model reaction reported in Figure 2b, the *N,S*-acetal linkages slowly dissociated in chloroform. By immersing the composite (containing MSA catalyst in the polymer matrix) in a large volume of chloroform to displace the equilibrium

towards the dissociated state, P-DMDO was completely dissolved after one day at room temperature. While dissolution in organic solvent is generally unwanted for polymer networks and composites that should be solvent resistant, *N,S*-acetal based polyoxazolidone networks were only soluble in a large amount of this specific solvent. This allowed the recovery of the filler when needed (Figure S50). Under identical conditions, no dissolution was noted in THF nor DMF, consistently with the model reactions that demonstrated extremely slow kinetics of reaction in these solvents. An absence of dissolution was also noted in other solvents, therefore proving dissolution of these polymers is selective (Table S4).

Conclusion

In this work, the alkylidene oxazolidone – thiol chemistry that reversibly delivered *N,S*-acetal type oxazolidone scaffolds was studied at the model reaction level, attesting for fast kinetics in mild conditions with a great dynamic character. The synthesis of bifunctional alkylidene oxazolidone monomers was reported to be easy, affordable, and scalable starting from a readily available propargyl alcohol coupled with CO_2 and a primary diamine. Different polymer networks were synthesized from structurally divergent monomers and a commercially available tetrathiol in the presence of a catalytic amount of methane sulfonic acid (MSA). Networks with a wide range of mechanical properties were prepared, ranging from PDMS-like elastomers to rigid polystyrene-like ones. The highly dynamic character of the covalent adaptable networks was highlighted by rheological study reflecting observations made at the model level. High dissociation rates can be accessible in relatively mild conditions, thus enabling fast reprocessing with thermoplastic-like techniques such as extrusion and injection molding without promoting any side reactions and material alteration. Through this high dissociative exchange capability, two divergent materials were also mixed and upcycled by fast dissociation and random re-association events to furnish a new scaffold with distinct properties. At high temperatures, total dissociation was obtained in minutes timeframe, yielding back the initial monomers that could be repolymerized into the same network. Lastly, this chemistry showed potential to be easily applied to composite materials with recycling possibilities. Further work will be devoted to diversify thermal and mechanical properties of the networks with the objective to broaden the application field of this very promising family of easily recyclable polymer networks. Overall, this study shows great potential for constructing a wide range of circular materials that might find applications across the numerous domains covered by polyurethanes, and well beyond as the dynamic linkages might be introduced in other thermosets for improved recyclability.

References

(1) OECD. *Global Plastics Outlook: Policy Scenarios to 2060*; OECD, 2022. https://doi.org/10.1787/aa1edf33-en.

(2) Grignard, B.; Gennen, S.; Jérôme, C.; Kleij, A. W.; Detrembleur, C. Advances in the Use of CO_2 as a Renewable Feedstock for the Synthesis of Polymers. *Chem. Soc. Rev.* **2019**, *48* (16), 4466–4514. https://doi.org/10.1039/C9CS00047J.

(3) Xu, Y.; Lin, L.; Xiao, M.; Wang, S.; Smith, A. T.; Sun, L.; Meng, Y. Synthesis and Properties of CO2-Based Plastics: Environmentally-Friendly, Energy-Saving and Biomedical

Polymeric Materials. *Progress in Polymer Science* **2018**, *80*, 163–182. https://doi.org/10.1016/j.progpolymsci.2018.01.006.

(4) Cywar, R. M.; Rorrer, N. A.; Hoyt, C. B.; Beckham, G. T.; Chen, E. Y.-X. Bio-Based Polymers with Performance-Advantaged Properties. *Nat Rev Mater* **2021**, *7* (2), 83–103. https://doi.org/10.1038/s41578-021-00363-3.

(5) Hayes, G.; Laurel, M.; MacKinnon, D.; Zhao, T.; Houck, H. A.; Becer, C. R. Polymers without Petrochemicals: Sustainable Routes to Conventional Monomers. *Chem. Rev.* **2023**, *123* (5), 2609–2734. https://doi.org/10.1021/acs.chemrev.2c00354.

(6) Zhao, X.-L.; Tian, P.-X.; Li, Y.-D.; Zeng, J.-B. Biobased Covalent Adaptable Networks: Towards Better Sustainability of Thermosets. *Green Chem.* **2022**, *24* (11), 4363–4387. https://doi.org/10.1039/D2GC01325H.

(7) Jehanno, C.; Alty, J. W.; Roosen, M.; De Meester, S.; Dove, A. P.; Chen, E. Y.-X.; Leibfarth, F. A.; Sardon, H. Critical Advances and Future Opportunities in Upcycling Commodity Polymers. *Nature* **2022**, *603* (7903), 803–814. https://doi.org/10.1038/s41586-021-04350-0.

(8) Coates, G. W.; Getzler, Y. D. Y. L. Chemical Recycling to Monomer for an Ideal, Circular Polymer Economy. *Nat Rev Mater* **2020**, *5* (7), 501–516. https://doi.org/10.1038/s41578-020-0190-4.

(9) Kosloski-Oh, S. C.; Wood, Z. A.; Manjarrez, Y.; De Los Rios, J. P.; Fieser, M. E. Catalytic Methods for Chemical Recycling or Upcycling of Commercial Polymers. *Mater. Horiz.* **2021**, *8* (4), 1084–1129. https://doi.org/10.1039/D0MH01286F.

(10) Korley, L. T. J.; Epps, T. H.; Helms, B. A.; Ryan, A. J. Toward Polymer Upcycling—Adding Value and Tackling Circularity. *Science* **2021**, *373* (6550), 66–69. https://doi.org/10.1126/science.abg4503.

(11) Zheng, N.; Xu, Y.; Zhao, Q.; Xie, T. Dynamic Covalent Polymer Networks: A Molecular Platform for Designing Functions beyond Chemical Recycling and Self-Healing. *Chem. Rev.* **2021**, *121* (3), 1716–1745. https://doi.org/10.1021/acs.chemrev.0c00938.

(12) Zhang, V.; Kang, B.; Accardo, J. V.; Kalow, J. A. Structure–Reactivity–Property Relationships in Covalent Adaptable Networks. *J. Am. Chem. Soc.* **2022**, *144* (49), 22358–22377. https://doi.org/10.1021/jacs.2c08104.

(13) Kloxin, C. J.; Bowman, C. N. Covalent Adaptable Networks: Smart, Reconfigurable and Responsive Network Systems. *Chem. Soc. Rev.* **2013**, *42* (17), 7161–7173. https://doi.org/10.1039/C3CS60046G.

(14) Scheutz, G. M.; Lessard, J. J.; Sims, M. B.; Sumerlin, B. S. Adaptable Crosslinks in Polymeric Materials: Resolving the Intersection of Thermoplastics and Thermosets. *J. Am. Chem. Soc.* **2019**, *141* (41), 16181–16196. https://doi.org/10.1021/jacs.9b07922.

(15) Podgórski, M.; Fairbanks, B. D.; Kirkpatrick, B. E.; McBride, M.; Martinez, A.; Dobson, A.; Bongiardina, N. J.; Bowman, C. N. Toward Stimuli-Responsive Dynamic Thermosets through Continuous Development and Improvements in Covalent Adaptable Networks (CANs). *Adv. Mater.* **2020**, *32* (20), 1906876. https://doi.org/10.1002/adma.201906876.

(16) Montarnal, D.; Capelot, M.; Tournilhac, F.; Leibler, L. Silica-Like Malleable Materials from Permanent Organic Networks. *Science* **2011**, *334* (6058), 965–968. https://doi.org/10.1126/science.1212648.

(17) Clarke, R. W.; Sandmeier, T.; Franklin, K. A.; Reich, D.; Zhang, X.; Vengallur, N.; Patra, T. K.; Tannenbaum, R. J.; Adhikari, S.; Kumar, S. K.; Rovis, T.; Chen, E. Y.-X. Dynamic Crosslinking Compatibilizes Immiscible Mixed Plastics. *Nature* **2023**, *616* (7958), 731–739. https://doi.org/10.1038/s41586-023-05858-3.

(18) Bowman, C. N.; Kloxin, C. J. Covalent Adaptable Networks: Reversible Bond Structures Incorporated in Polymer Networks. *Angew. Chem. Int. Ed.* **2012**, *51* (18), 4272–4274. https://doi.org/10.1002/anie.201200708.

(19) Fortman, D. J.; Brutman, J. P.; De Hoe, G. X.; Snyder, R. L.; Dichtel, W. R.; Hillmyer, M. A. Approaches to Sustainable and Continually Recyclable Cross-Linked Polymers. *ACS Sustainable Chem. Eng.* **2018**, *6* (9), 11145–11159. https://doi.org/10.1021/acssuschemeng.8b02355.

(20) Röttger, M.; Domenech, T.; Van Der Weegen, R.; Breuillac, A.; Nicolaÿ, R.; Leibler, L. High-Performance Vitrimers from Commodity Thermoplastics through Dioxaborolane Metathesis. *Science* **2017**, *356* (6333), 62–65. https://doi.org/10.1126/science.aah5281.

(21) Adzima, B. J.; Aguirre, H. A.; Kloxin, C. J.; Scott, T. F.; Bowman, C. N. Rheological and Chemical Analysis of Reverse Gelation in a Covalently Cross-Linked Diels−Alder Polymer Network. *Macromolecules* **2008**, *41* (23), 9112–9117. https://doi.org/10.1021/ma801863d.

(22) Taplan, C.; Guerre, M.; Winne, J. M.; Du Prez, F. E. Fast Processing of Highly Crosslinked, Low-Viscosity Vitrimers. *Mater. Horiz.* **2020**, *7* (1), 104–110. https://doi.org/10.1039/C9MH01062A.

(23) Bapat, A. P.; Sumerlin, B. S.; Sutti, A. Bulk Network Polymers with Dynamic B–O Bonds: Healable and Reprocessable Materials. *Mater. Horiz.* **2020**, *7* (3), 694–714. https://doi.org/10.1039/C9MH01223K.

(24) Delahaye, M.; Tanini, F.; Holloway, J. O.; Winne, J. M.; Du Prez, F. E. Double Neighbouring Group Participation for Ultrafast Exchange in Phthalate Monoester Networks. *Polym. Chem.* **2020**, *11* (32), 5207–5215. https://doi.org/10.1039/D0PY00681E.

(25) Yang, K.; Grant, J. C.; Lamey, P.; Joshi-Imre, A.; Lund, B. R.; Smaldone, R. A.; Voit, W. Diels–Alder Reversible Thermoset 3D Printing: Isotropic Thermoset Polymers via Fused

Filament Fabrication. *Adv. Funct. Mater.* **2017**, *27* (24), 1700318. https://doi.org/10.1002/adfm.201700318.

(26) Cao, Y.; Rong, M. Z.; Zhang, M. Q. Covalent Adaptable Networks Impart Smart Processability to Multifunctional Highly Filled Polymer Composites. *Composites Part A: Applied Science and Manufacturing* **2021**, *151*, 106647. https://doi.org/10.1016/j.compositesa.2021.106647.

(27) Chen, S.; Wang, F.; Peng, Y.; Chen, T.; Wu, Q.; Sun, P. A Single Molecular Diels-Alder Crosslinker for Achieving Recyclable Cross-Linked Polymers. *Macromol. Rapid Commun.* **2015**, *36* (18), 1687–1692. https://doi.org/10.1002/marc.201500257.

(28) Feng, H.; Ma, S.; Xu, X.; Li, Q.; Wang, B.; Lu, N.; Li, P.; Wang, S.; Yu, Z.; Zhu, J. Facile Synthesis of Hemiacetal Ester-Based Dynamic Covalent Polymer Networks Combining Fast Reprocessability and High Performance. *Green Chem.* **2021**, *23* (22), 9061–9070. https://doi.org/10.1039/D1GC02773E.

(29) Winne, J. M.; Leibler, L.; Du Prez, F. E. Dynamic Covalent Chemistry in Polymer Networks: A Mechanistic Perspective. *Polym. Chem.* **2019**, *10* (45), 6091–6108. https://doi.org/10.1039/C9PY01260E.

(30) Elling, B. R.; Dichtel, W. R. Reprocessable Cross-Linked Polymer Networks: Are Associative Exchange Mechanisms Desirable? *ACS Cent. Sci.* **2020**, *6* (9), 1488–1496. https://doi.org/10.1021/acscentsci.0c00567.

(31) Li, Q.; Ma, S.; Li, P.; Wang, B.; Yu, Z.; Feng, H.; Liu, Y.; Zhu, J. Fast Reprocessing of Acetal Covalent Adaptable Networks with High Performance Enabled by Neighboring Group Participation. *Macromolecules* **2021**, *54* (18), 8423–8434. https://doi.org/10.1021/acs.macromol.1c01046.

(32) Fortman, D. J.; Brutman, J. P.; Cramer, C. J.; Hillmyer, M. A.; Dichtel, W. R. Mechanically Activated, Catalyst-Free Polyhydroxyurethane Vitrimers. *J. Am. Chem. Soc.* **2015**, *137* (44), 14019–14022. https://doi.org/10.1021/jacs.5b08084.

(33) Snyder, R. L.; Fortman, D. J.; De Hoe, G. X.; Hillmyer, M. A.; Dichtel, W. R. Reprocessable Acid-Degradable Polycarbonate Vitrimers. *Macromolecules* **2018**, *51* (2), 389–397. https://doi.org/10.1021/acs.macromol.7b02299.

(34) Obadia, M. M.; Mudraboyina, B. P.; Serghei, A.; Montarnal, D.; Drockenmuller, E. Reprocessing and Recycling of Highly Cross-Linked Ion-Conducting Networks through Transalkylation Exchanges of C–N Bonds. *J. Am. Chem. Soc.* **2015**, *137* (18), 6078–6083. https://doi.org/10.1021/jacs.5b02653.

(35) Delahaye, M.; Winne, J. M.; Du Prez, F. E. Internal Catalysis in Covalent Adaptable Networks: Phthalate Monoester Transesterification As a Versatile Dynamic Cross-Linking

Chemistry. *J. Am. Chem. Soc.* **2019**, *141* (38), 15277–15287. https://doi.org/10.1021/jacs.9b07269.

(36) Denissen, W.; Winne, J. M.; Du Prez, F. E. Vitrimers: Permanent Organic Networks with Glass-like Fluidity. *Chem. Sci.* **2016**, *7* (1), 30–38. https://doi.org/10.1039/C5SC02223A.

(37) Wang, S.; Ma, S.; Li, Q.; Yuan, W.; Wang, B.; Zhu, J. Robust, Fire-Safe, Monomer-Recovery, Highly Malleable Thermosets from Renewable Bioresources. *Macromolecules* **2018**, *51* (20), 8001–8012. https://doi.org/10.1021/acs.macromol.8b01601.

(38) Abel, B. A.; Snyder, R. L.; Coates, G. W. Chemically Recyclable Thermoplastics from Reversible-Deactivation Polymerization of Cyclic Acetals. *Science* **2021**, *373* (6556), 783–789. https://doi.org/10.1126/science.abh0626.

(39) Shen, T.; Chen, K.; Chen, Y.; Ling, J. Ring-Opening Polymerization of Cyclic Acetals: Strategy for Both Recyclable and Degradable Materials. *Macromol. Rapid Commun.* **2023**, *44* (13), 2300099. https://doi.org/10.1002/marc.202300099.

(40) Kariyawasam, L. S.; Rolsma, J.; Yang, Y. Chemically Recyclable Dithioacetal Polymers via Reversible Entropy-Driven Ring-Opening Polymerization**. *Angew Chem Int Ed* **2023**, *62* (26), e202303039. https://doi.org/10.1002/anie.202303039.

(41) Li, Q.; Ma, S.; Lu, N.; Qiu, J.; Ye, J.; Liu, Y.; Wang, S.; Han, Y.; Wang, B.; Xu, X.; Feng, H.; Zhu, J. Concurrent Thiol–Ene Competitive Reactions Provide Reprocessable, Degradable and Creep-Resistant Dynamic–Permanent Hybrid Covalent Networks. *Green Chem.* **2020**, *22* (22), 7769–7777. https://doi.org/10.1039/D0GC02823A.

(42) Van Herck, N.; Maes, D.; Unal, K.; Guerre, M.; Winne, J. M.; Du Prez, F. E. Covalent Adaptable Networks with Tunable Exchange Rates Based on Reversible Thiol–Yne Cross-Linking. *Angew. Chem. Int. Ed.* **2020**, *59* (9), 3609–3617. https://doi.org/10.1002/anie.201912902.

(43) Sendijarevic, V.; Sendijarevic, A.; Lekovic, H.; Lekovic, H.; Frisch, K. C. Polyoxazolidones for High Temperature Applications. *Journal of Elastomers & Plastics* **1996**, *28* (1), 63–83. https://doi.org/10.1177/009524439602800104.

(44) Sendijarevic, V.; Sendijarevic, A.; Frisch, K. C.; Reulen, P. Novel Isocyanate-Based Matrix Resins for High Temperature Composite Applications. *Polym. Compos.* **1996**, *17* (2), 180–186. https://doi.org/10.1002/pc.10603.

(45) Pankratov, V. A.; Frenkel', T. M.; Fainleib, A. M. 2-Oxazolidinones. *Russ. Chem. Rev.* **1983**, *52* (6), 576–593. https://doi.org/10.1070/RC1983v052n06ABEH002864.

(46) Gennen, S.; Grignard, B.; Tassaing, T.; Jérôme, C.; Detrembleur, C. CO_2-Sourced α-Alkylidene Cyclic Carbonates: A Step Forward in the Quest for Functional Regioregular Poly(Urethane)s and Poly(Carbonate)s. *Angew. Chem. Int. Ed.* **2017**, *56* (35), 10394–10398. https://doi.org/10.1002/anie.201704467.

(47) Ngassam Tounzoua, C.; Grignard, B.; Detrembleur, C. Exovinylene Cyclic Carbonates: Multifaceted CO_2-Based Building Blocks for Modern Chemistry and Polymer Science. *Angew Chem Int Ed* **2022**, *61* (22), e202116066. https://doi.org/10.1002/anie.202116066.

(48) Habets, T.; Siragusa, F.; Grignard, B.; Detrembleur, C. Advancing the Synthesis of Isocyanate-Free Poly(Oxazolidones)s: Scope and Limitations. *Macromolecules* **2020**, *53* (15), 6396–6408. https://doi.org/10.1021/acs.macromol.0c01231.

(49) Habets, T.; Siragusa, F.; Müller, A. J.; Grossman, Q.; Ruffoni, D.; Grignard, B.; Detrembleur, C. Facile Construction of Functional Poly(Monothiocarbonate) Copolymers under Mild Operating Conditions. *Polym. Chem.* **2022**, *13* (21), 3076–3090. https://doi.org/10.1039/D2PY00307D.

(50) Wong, A. R.; Barrera, M.; Pal, A.; Lamb, J. R. Improved Characterization of Polyoxazolidinones by Incorporating Solubilizing Side Chains. *Macromolecules* **2022**, *55* (24), 11006–11012. https://doi.org/10.1021/acs.macromol.2c02104.

(51) Sutherland, B. P.; Kabra, M.; Kloxin, C. J. Expanding the Thiol–X Toolbox: Photoinitiation and Materials Application of the Acid-Catalyzed Thiol–Ene (ACT) Reaction. *Polym. Chem.* **2021**, *12* (10), 1562–1570. https://doi.org/10.1039/D0PY01593H.

(52) Francis, T.; Thorne, M. P. Carbamates and 2-Oxazolidinones from Tertiary Alcohols and Isocyanates. *Can. J. Chem.* **1976**, *54* (1), 24–30. https://doi.org/10.1139/v76-006.

(53) Laurence, C.; Gal, J.-F. *Lewis Basicity and Affinity Scales: Data and Measurement*; John Wiley: Chichester, West Sussex, U.K, 2010.

(54) Pandit, N.; Singla, R. K.; Shrivastava, B. Current Updates on Oxazolidinone and Its Significance. *International Journal of Medicinal Chemistry* **2012**, *2012*, 1–24. https://doi.org/10.1155/2012/159285.

(55) Pulla, S.; Felton, C. M.; Ramidi, P.; Gartia, Y.; Ali, N.; Nasini, U. B.; Ghosh, A. Advancements in Oxazolidinone Synthesis Utilizing Carbon Dioxide as a C1 Source. *Journal of CO2 Utilization* **2013**, *2*, 49–57. https://doi.org/10.1016/j.jcou.2013.07.005.

(56) Sun, F.; Van Der Eycken, E. V.; Feng, H. Recent Advances in the Synthesis and Ring-Opening Transformations of 2-Oxazolidinones. *Adv. Synth. Catal.* **2021**, *363* (23), 5168–5195. https://doi.org/10.1002/adsc.202100746.

(57) Barbachyn, M. R.; Ford, C. W. Oxazolidinone Structure–Activity Relationships Leading to Linezolid. *Angew. Chem. Int. Ed.* **2003**, *42* (18), 2010–2023. https://doi.org/10.1002/anie.200200528.

(58) Denissen, W.; Rivero, G.; Nicolaÿ, R.; Leibler, L.; Winne, J. M.; Du Prez, F. E. Vinylogous Urethane Vitrimers. *Adv. Funct. Mater.* **2015**, *25* (16), 2451–2457. https://doi.org/10.1002/adfm.201404553.

(59) Lin, S.-K. Handbook of Polymers. By George Wypych, ChemTec Publishing, 2012; 680 Pages. Price $395.00, ISBN 978-1-895198-47-8. *Polymers* **2013**, *5* (1), 225–233. https://doi.org/10.3390/polym5010225.

(60) Ashby, M. F. *Materials Selection in Mechanical Design*, 2nd ed.; Butterworth-Heinemann: Oxford, OX ; Boston, MA, 1999.

(61) Lagron, A. B.; El-Zaatari, B. M.; Hamachi, L. S. Characterization Techniques to Assess Recyclability in Dynamic Polymer Networks. *Front. Mater.* **2022**, *9*, 915296. https://doi.org/10.3389/fmats.2022.915296.

(62) Van Lijsebetten, F.; De Bruycker, K.; Van Ruymbeke, E.; Winne, J. M.; Du Prez, F. E. Characterising Different Molecular Landscapes in Dynamic Covalent Networks. *Chem. Sci.* **2022**, *13* (43), 12865–12875. https://doi.org/10.1039/D2SC05528G.

(63) Maes, S.; Van Lijsebetten, F.; Winne, J. M.; Du Prez, F. E. *N* -Sulfonyl Urethanes to Design Polyurethane Networks with Temperature-Controlled Dynamicity. *Macromolecules* **2023**, *56* (5), 1934–1944. https://doi.org/10.1021/acs.macromol.2c02456.

(64) Schoustra, S. K.; Groeneveld, T.; Smulders, M. M. J. The Effect of Polarity on the Molecular Exchange Dynamics in Imine-Based Covalent Adaptable Networks. *Polym. Chem.* **2021**, *12* (11), 1635–1642. https://doi.org/10.1039/D0PY01555E.

(65) El-Zaatari, B. M.; Ishibashi, J. S. A.; Kalow, J. A. Cross-Linker Control of Vitrimer Flow. *Polym. Chem.* **2020**, *11* (33), 5339–5345. https://doi.org/10.1039/D0PY00233J.

(66) Spiesschaert, Y.; Taplan, C.; Stricker, L.; Guerre, M.; Winne, J. M.; Du Prez, F. E. Influence of the Polymer Matrix on the Viscoelastic Behaviour of Vitrimers. *Polym. Chem.* **2020**, *11* (33), 5377–5385. https://doi.org/10.1039/D0PY00114G.

(67) Joe, J.; Shin, J.; Choi, Y.; Hwang, J. H.; Kim, S. H.; Han, J.; Park, B.; Lee, W.; Park, S.; Kim, Y. S.; Kim, D. A 4D Printable Shape Memory Vitrimer with Repairability and Recyclability through Network Architecture Tailoring from Commercial Poly(*ε* -caprolactone). *Advanced Science* **2021**, *8* (24), 2103682. https://doi.org/10.1002/advs.202103682.

(68) Fortman, D. J.; Snyder, R. L.; Sheppard, D. T.; Dichtel, W. R. Rapidly Reprocessable Cross-Linked Polyhydroxyurethanes Based on Disulfide Exchange. *ACS Macro Lett.* **2018**, *7* (10), 1226–1231. https://doi.org/10.1021/acsmacrolett.8b00667.

(69) Yuan, D.; Delpierre, S.; Ke, K.; Raquez, J.-M.; Dubois, P.; Manas-Zloczower, I. Biomimetic Water-Responsive Self-Healing Epoxy with Tunable Properties. *ACS Appl. Mater. Interfaces* **2019**, *11* (19), 17853–17862. https://doi.org/10.1021/acsami.9b04249.

(70) Diggle, B.; Jiang, Z.; Li, R. W.; Connal, L. A. Self-Healing Polymer Network with High Strength, Tunable Properties, and Biocompatibility. *Chem. Mater.* **2021**, *33* (10), 3712–3720. https://doi.org/10.1021/acs.chemmater.1c00707.

(71) Swartz, J. L.; Sheppard, D. T.; Haugstad, G.; Dichtel, W. R. Blending Polyurethane Thermosets Using Dynamic Urethane Exchange. *Macromolecules* **2021**, *54* (23), 11126–11133. https://doi.org/10.1021/acs.macromol.1c01910.

(72) Chen, Z.; Sun, Y.-C.; Wang, J.; Qi, H. J.; Wang, T.; Naguib, H. E. Flexible, Reconfigurable, and Self-Healing TPU/Vitrimer Polymer Blend with Copolymerization Triggered by Bond Exchange Reaction. *ACS Appl. Mater. Interfaces* **2020**, *12* (7), 8740–8750. https://doi.org/10.1021/acsami.9b21411.

(73) Christensen, P. R.; Scheuermann, A. M.; Loeffler, K. E.; Helms, B. A. Closed-Loop Recycling of Plastics Enabled by Dynamic Covalent Diketoenamine Bonds. *Nat. Chem.* **2019**, *11* (5), 442–448. https://doi.org/10.1038/s41557-019-0249-2.

(74) Li, Q.; Ma, S.; Wang, S.; Yuan, W.; Xu, X.; Wang, B.; Huang, K.; Zhu, J. Facile Catalyst-Free Synthesis, Exchanging, and Hydrolysis of an Acetal Motif for Dynamic Covalent Networks. *J. Mater. Chem. A* **2019**, *7* (30), 18039–18049. https://doi.org/10.1039/C9TA04073K.

(75) Schenk, V.; Labastie, K.; Destarac, M.; Olivier, P.; Guerre, M. Vitrimer Composites: Current Status and Future Challenges. *Mater. Adv.* **2022**, *3* (22), 8012–8029. https://doi.org/10.1039/D2MA00654E.

Supporting Information

1. Materials and Instrumentation

Materials

Benzylamine (99%) was purchased from Sigma Aldrich.
Benzyl mercaptan (99%) was purchased from Sigma Aldrich.
2,2′-(Ethylenedioxy)diethanethiol (**DMDO**, 95%) was purchased from Sigma Aldrich.
Hexamethylenediamine (**HMDA**, 98%) was purchased from Sigma Aldrich.
Methanesulfonic acid (**MSA**, 99%) was purchased from Sigma Aldrich.
2-Methylbut-3-yn-2-ol (98%) was purchased from Sigma Aldrich.
Molecular sieves (3A, 2-5mm beads) were purchased from Thermo Scientific.
1-Octanethiol (98.5%) was purchased from Sigma Aldrich.
Pentaerythritol tetrakis(3-mercaptopropionate) (**PETMP**, 95%) was purchased from Sigma Aldrich.
Priamine 1075 (**PRI**) was kindly supplied by Croda.
Propylamine (99%) was purchased from Sigma Aldrich.
Silver carbonate (**Ag_2CO_3**, 99%) was purchased from Sigma Aldrich.
Triethylamine (99%) was purchased from Acros Organics.
Triphenylphosphine (99%) was purchased from Sigma Aldrich.
m-Xylylenediamine (**XDA**, 99%) was purchased from Sigma Aldrich.

All reagents were used as received without purification.

Instrumentation

Nuclear magnetic resonance (NMR) spectroscopy. ^{1}H- and ^{13}C-NMR analyses were performed on a Bruker 400 MHz spectrometer at 25 °C in the Fourier transform mode. 16 scans for ^{1}H spectra and 512 scans for ^{13}C spectra were recorded.
High resolution mass spectrometry (HRMS). ESI-MS data were acquired on a Waters Synapt G2-Si mass spectrometer (Waters, UK) equipped with an Electrospray ionization source used in the positive ion mode. Samples were prepared as followed, 1mg/mL solution in Acetonitrile solution were diluted 500 times to reach a final concentration of 2.10-6 g/mL. For the mass spectrometer parameters, the Electrospray ionization (ESI) conditions were capillary voltage 3.1 kV; cone voltage 30 V; source temperature 120 °C; desolvation temperature 150 °C. Dry nitrogen, the desolvation gas, is used as the ESI gas with a flow rate of 500 $L.h^{-1}$. Mass

accuracy measurement (HRMS) were performed by using lock spay unit, available on the source ion block, by infusing NaI solution as reference in order to perform internal calibration.

Fourier Transform Infrared Spectra (FT-IR). FTIR measurements were carried out on a Nicolet IS5 spectrometer (Thermo Fisher Scientific) equipped with a diamond attenuated transmission reflectance (ATR) device. 32 scans were recorded for each sample over the range 4000-500 cm^{-1} with a normal resolution of 4 cm^{-1}.

Thermogravimetric analysis (TGA). TGA analysis was performed on a TGA2 instrument from Mettler Toledo. Around 5 of sample was heated at 10 °C/min from 30 to 50 °C and flushed for 10 min at 50 °C. The sample was then heated at 20 °C/min until 600 °C. All the experiment was conducted under nitrogen atmosphere (20 mL/min).

Differential scanning calorimetry (DSC). DSC analysis was performed on a DSC 250 (TA Instruments). All the experiments were performed under ultrapure nitrogen flow. Samples of 4–6 mg were used and placed in hermetic aluminum pans. The sample was cooled to -40 °C and the temperature modulated segment was set with an amplitude of 1 °C with a period of 60 seconds. The sample was then heated to 120 °C at a rate of 2 °C/min. The glass transition temperatures were determined using the reversing heat flow curve.

Rheology. Rheology experiments were conducted on an ARES G2 rheometer from TA Instruments in shear geometry with a plate diameter of 8 mm. The samples were prepared by compression molding and were cut in their rubber state using a die cutter. Temperature sweeps were performed at a rate of 2 °C/min at a frequency of 1 Hz and at a constant strain of 1%. Stress relaxation experiments were performed with a constant shear strain of 1% within the linear viscoelastic region of the polymers.

Dynamic mechanical analysis (DMA). DMA experiment was performed on a DMA Q800 from TA Instruments. Temperature ramp experiment was performed in tension mode with 0.01 N of constant force and a frequency of 1 Hz. The sample was equilibrated at 30 °C and heated with a heating rate of 2 °C/min until 80 °C.

Swelling Ratio (SR) and Gel Content (GC). The swelling ratio (SR) was determined by immersion of a piece of material (between 100 and 200 mg) of mass m_i in THF (or neutralized THF with some drops of triethylamine). After 24h, the swollen sample was weighted as the mass of the gel m_{gel}. The SR was calculated using the following equation.

$$SR\ (\%) = \frac{m_{gel} - m_i}{m_i} \times 100$$

The gel content (GC) was determined by weighting the mass m_f after drying of the swollen sample using the following equation.

$$GC\ (\%) = \frac{m_f}{m_i} \times 100$$

Tensile tests. Tensile tests were conducted at room temperature using a ZwickRoell Z2.5 at a speed of 2 $mm.min^{-1}$ or 10 $mm.min^{-1}$ (in the case of the elastomeric P-PRI). Measurements were repeated 5 times on dogbone-shaped samples (ASTM-D1708) with a thickness of around 1 mm. The samples were prepared by compression molding and were cut in their rubber state using a die cutter. For reprocessing studies represented in Figure S45, the dogbone specimens of P-DMDO were reprocessed after fracture by compression molding at 100 °C (10 min, 1 ton metric) and were cut in their rubber state using a die cutter.

Compression molding. Polymer samples were cut into little pieces and pressed in a steel mold between Teflon sheets in a Carver press. All the samples were pressed at a temperature just above their flowing transition (between 80 and 100 °C) for 10 min under 1 ton metric of pressure. The mold was then removed from the press and slowly cooled down to r.T.

Extrusion. The polymer P-HMDA was cut in little pieces and introduced in a pre-heated DSM micro compounder at 90 °C. The polymer was mixed for few minutes at 90 °C and extruded at a screw speed of 150 rpm.

Injection molding. The polymer P-HMDA was cut in little pieces and introduced in the injection chamber of the DSM Xplore Mini for 10 min at 50 °C. It was then injected at 90 °C with a pressure of around 700 bars in the mold.

2. Synthetic Procedures toward model alkylidene oxazolidones

A. Synthesis of 4,4-dimethyl-5-methylene-1,3-dioxolan-2-one (αCC)

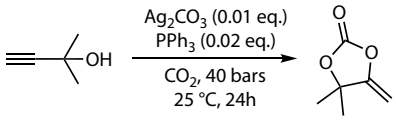

αCC was synthesized by modification of Q. Song's procedure[1]. 2-Methyl-3-butyn-2-ol (125 mL, 1.3 mol, 1 eq.), Ag_2CO_3 (3.585 g, 13 mmol, 0.01 eq.), Triphenylphosphine (6.82 g, 26 mmol, 0.02 eq.) and 20 mL of Chloroform were added in a 250 mL high pressure autoclave. The reactor was charged with 40 bars of CO_2 at 25°C. After 14h, the reactor was depressurized. The crude mixture was distilled under vacuum. The resulting transparent liquid was solubilized in 600 mL of diethyl ether and extracted with water (3 x 600 mL). The organic phase was dried over $MgSO_4$, filtered, and dried under vacuum. The pure product crystallized into a white solid (126.3 g, isolated yield 76 %); mp = 31 °C; **^{1}H NMR** (400 MHz, DMSO-d_6) δ 4.79 (d, J = 3.8 Hz, 1H), 4.65 (d, J = 3.8 Hz, 1H), 1.60 (s, 6H); **^{13}C NMR** (100 MHz, DMSO-d_6) δ 158.7, 151.3, 85.9, 85.6, 27.4.

B. Synthesis of 4-hydroxy-4,5,5-trimethyl-3-propyloxazolidin-2-one (1a)

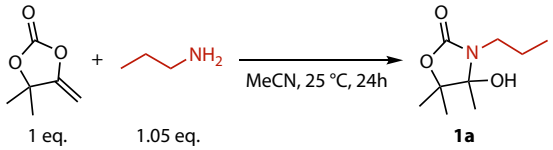

αCC (1.536 g, 12 mmol, 1 eq.), Propylamine (0.744 g, 12.6 mmol, 1.05 eq.), and acetonitrile (3 mL) were added to a round-bottom flask immerged in an ice bath. The mixture was stirred for 1h and 23h more at 25 °C. Solvent and excess amines were removed under vacuum to yield the product **1a** as white crystals (2.1 g, isolated yield 95 %); mp = 69 °C; **^{1}H NMR** (400 MHz, DMSO-d_6) δ 5.90 (s, 1H), 3.02 (m, 2H), 1.52 (sextuplet, J = 7.4 Hz, 2H), 1.29 (s, 3H), 1.28 (s, 3H), 1.22 (s, 3H), 0.85 (t, J = 7.4 Hz, 3H); **^{13}C NMR** (100 MHz, DMSO-d_6) δ 157.0, 89.7, 84.5, 41.6, 25.1, 22.8, 21.0, 20.9, 11.8.

C. Synthesis of 3-benzyl-4-hydroxy-4,5,5-trimethyloxazolidin-2-one (1b)

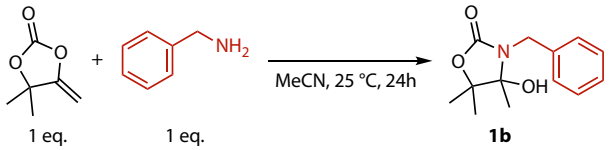

αCC (1.536 g, 12 mmol, 1 eq.), Benzylamine (1.284 g, 12 mmol, 1 eq.), and acetonitrile (3 mL) were added to a reaction tube and the mixture was stirred for 24h. The precipitate was then dissolved in more Acetonitrile (around 25 mL) and put at -20 °C overnight for recrystallization. The crystals were filtered, washed with cold diethyl ether, and dried under vacuum. The pure product **1b** was isolated as white crystals (2.48 g, isolated yield 88 %); mp = 145 °C; **^{1}H NMR** (400 MHz, DMSO-d_6) δ 7.31 (m, 5H), 6.15 (s, 1H), 4.43 (d, J = 16.2 Hz, 1H), 4.20 (d, J = 16.2 Hz, 1H), 1.32 (s, 3H), 1.26 (s, 3H), 1.12 (s, 3H); **^{13}C NMR** (100 MHz, DMSO-d_6) δ 157.5, 139.4, 128.8, 127.3, 89.8, 84.9, 43.1, 25.2, 21.2, 21.0.

D. Dehydration setup for the facile synthesis of alkylidene oxazolidone

A dehydration setup was designed to allow for quantitative dehydration of hydroxyoxazolidones **1** into **2** without the need of chromatography purification. The compound **1** was dissolved in acetonitrile and an acid catalyst (here, MSA) was added to catalyze dehydration. In order to push the reaction to full conversion, the acetonitrile forming an azeotrope with water was refluxed through an addition funnel containing molecular sieves (Figure S1). Water-free solvent is recovered during the reaction and the equilibrium can be shifted thanks to the molecular sieves acting as water scavenger. After reaction, the molecular sieves can be recovered and simply dried as there was no contact with any chemicals apart water and the solvent (here, acetonitrile).

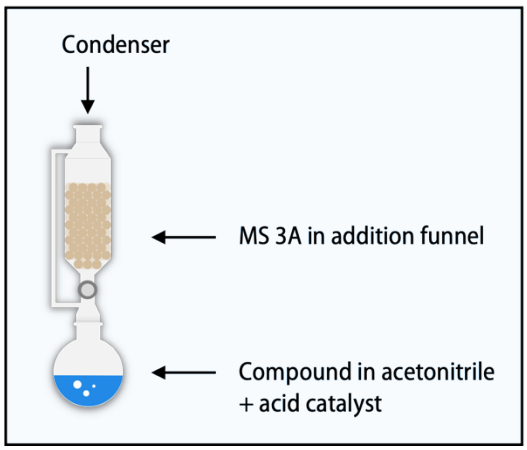

Figure S1 – Schematic representation of the dehydration setup.

E. General procedure for the synthesis of alkylidene oxazolidones (2a-b)

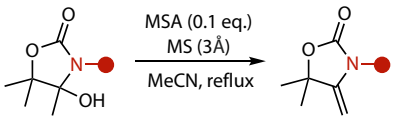

The hydroxyoxazolidone **1** (10 mmol, 1 eq.), MSA (1 mmol, 0.1 eq.) and acetonitrile (around 30 mL) were added to a round-bottom flask. A dehydration setup was installed on the flask and the mixture was refluxed for 24h. The crude was quenched with triethylamine (0.2 eq.) and cooled to room temperature. Ethyl acetate (50 mL) was added and extracted with water (3 x 50 mL). The organic phase was dried over $MgSO_4$, filtered, and dried under vacuum to yield pure **2**.

Synthesis of 5,5-dimethyl-4-methylene-3-propyloxazolidin-2-one (2a)

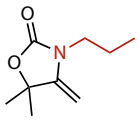

The pure product was isolated as a yellowish liquid (1.40 g, isolated yield 83 %); **^{1}H NMR** (400 MHz, DMSO-d_6) δ 4.21 (d, J = 2.6 Hz, 1H), 4.17 (d, J = 2.6 Hz, 1H), 3.36 (t, J = 7.1 Hz, 2H), 1.54 (sextuplet, J = 7.1 Hz, 2H), 0.85 (t, J = 7.5 Hz, 3 H); **^{13}C NMR** (100 MHz, DMSO-d_6) δ 155.3, 150.7, 82.1, 80.1, 42.5, 28.0, 19.7, 11.3.

Synthesis of 3-benzyl-5,5-dimethyl-4-methyleneoxazolidin-2-one (2b)

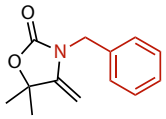

The pure product was isolated as a grayish oil (1.67 g, isolated yield 77 %); **^{1}H NMR** (400 MHz, DMSO-d_6) δ 7.31 (m, 5H), 4.62 (s, 2H), 4.16 (d, J = 2.7 Hz, 1H), 4.12 (d, J = 2.7 Hz, 1H), 1.48 (s, 6H); **^{13}C NMR** (100 MHz, DMSO-d_6) δ 155.5, 150.2, 136.3, 129.1, 127.9, 127.3, 82.6, 81.3, 44.5, 28.0.

3. Kinetic studies

A. Kinetics of reaction

Model reactions between alkylidene oxazolidones **2a-b** and thiols (benzyl mercaptan, octanethiol and thiophenol) were carried out under various conditions. The two components were mixed in equimolar ratio in a solvent with MSA and aliquots of the reaction mixture were sampled over time. The reactions were monitored by ^{1}H-NMR spectroscopy to determine the conversion in **2** at different time points. Representative NMR spectra for the different model reactions are shown in Figures S2-5 together with the resonances used for quantification.
Solvents used for the model reactions were dried over molecular sieves before use.

General procedure

2 (4 mmol, 1 eq.) and benzyl mercaptan (4 mmol, 1 eq.) were added to a reaction tube and the mixture was dissolved in 1 mL of solvent. The reaction was started by addition of MSA (0.01 eq.) and the mixture was stirred under nitrogen atmosphere.
To prepare the NMR sample, an aliquot was taken out of the reaction medium (100 µL) and was quenched with triethylamine. DMSO-d_6 (700 µL) was added and the tube was stored at -20 °C prior NMR analysis.

Model reaction of **2a** and benzyl mercaptan

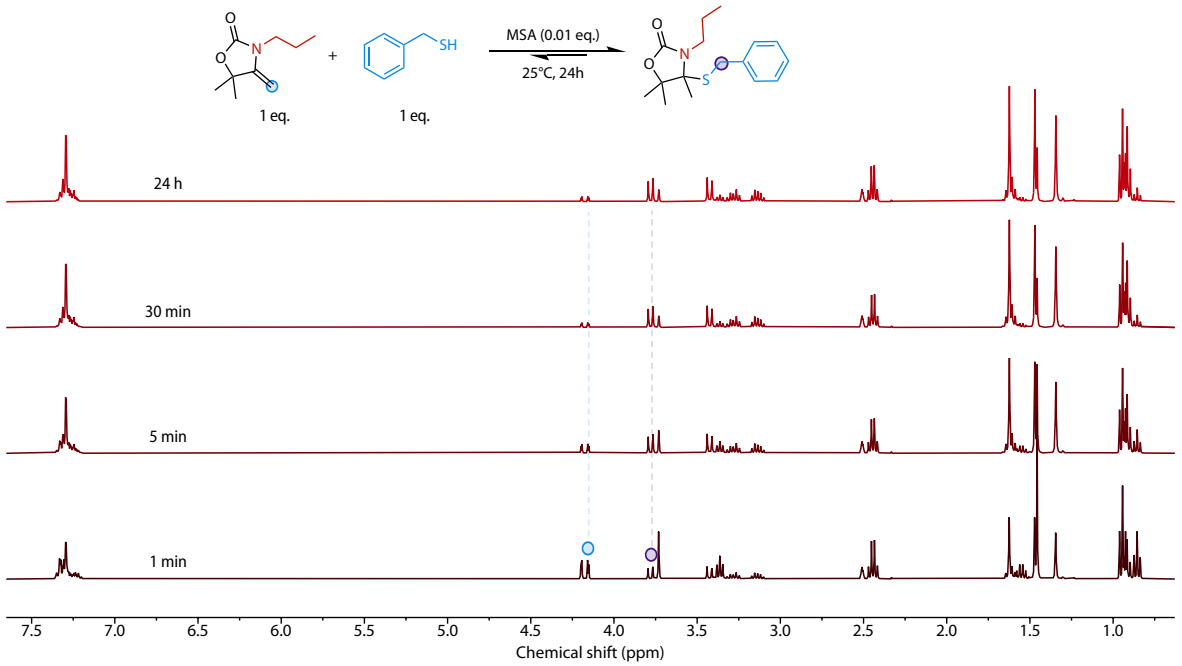

Figure S2 – Stacked ^{1}H-NMR spectra (400 MHz, DMSO-d_6) for the reaction of **2a** with benzyl mercaptan at 25°C along time.

For the reaction between **2a** and benzyl mercaptan, the resonance at 4.15 ppm (1H) was selected to follow **2a** and the resonance at 3.78 ppm (1H) to follow the product **3a**.
The following equation was used to determine the conversion:

$$Conv.(\%) = \left(\frac{I(3.78)}{I(4.15) + I(3.78)}\right) \times 100$$

Where *I* is the integral value of the selected peak.

Model reaction of **2a** and thiophenol

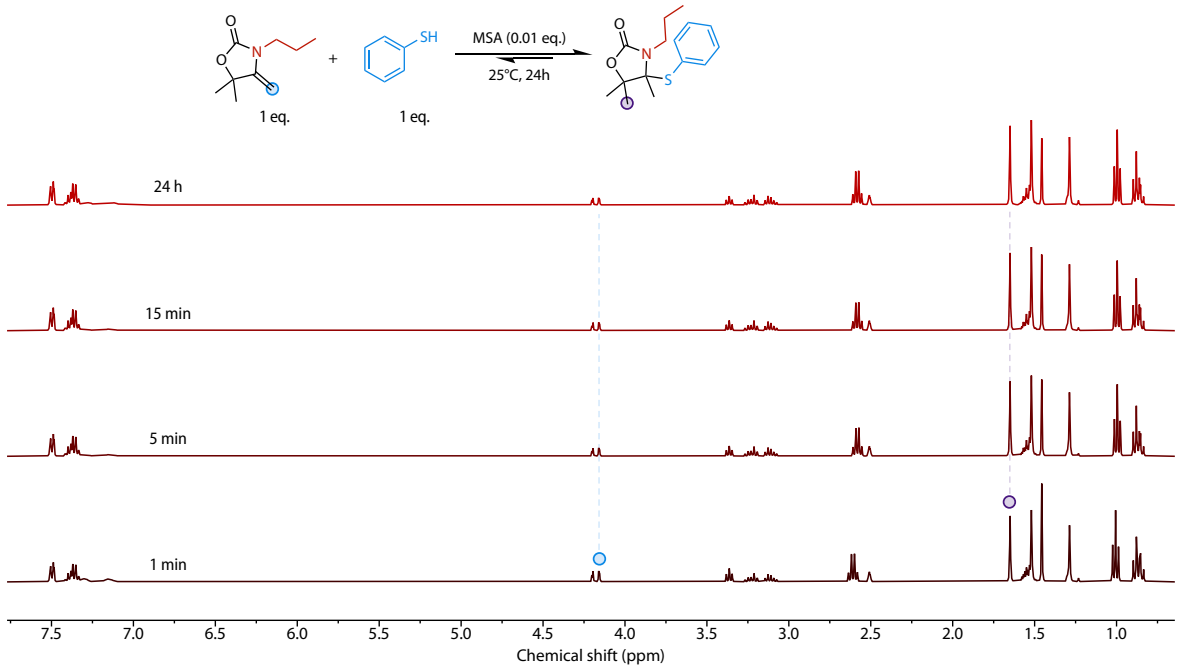

Figure S3 – Stacked ^{1}H-NMR spectra (400 MHz, DMSO-d_6) for the reaction of **2a** with thiophenol at 25°C along time.

For the reaction between **2a** and thiophenol, the resonance at 4.15 ppm (1H) was selected to follow **2a** and the resonance at 1.65 ppm (3H) to follow the product **3b**.
The following equation was used to determine the conversion:

$$Conv.(\%) = \left(\frac{\frac{I(1.65)}{3}}{I(4.15) + \frac{I(1.65)}{3}}\right) \times 100$$

Where *I* is the integral value of the selected peak.

Model reaction of **2a** and octanethiol

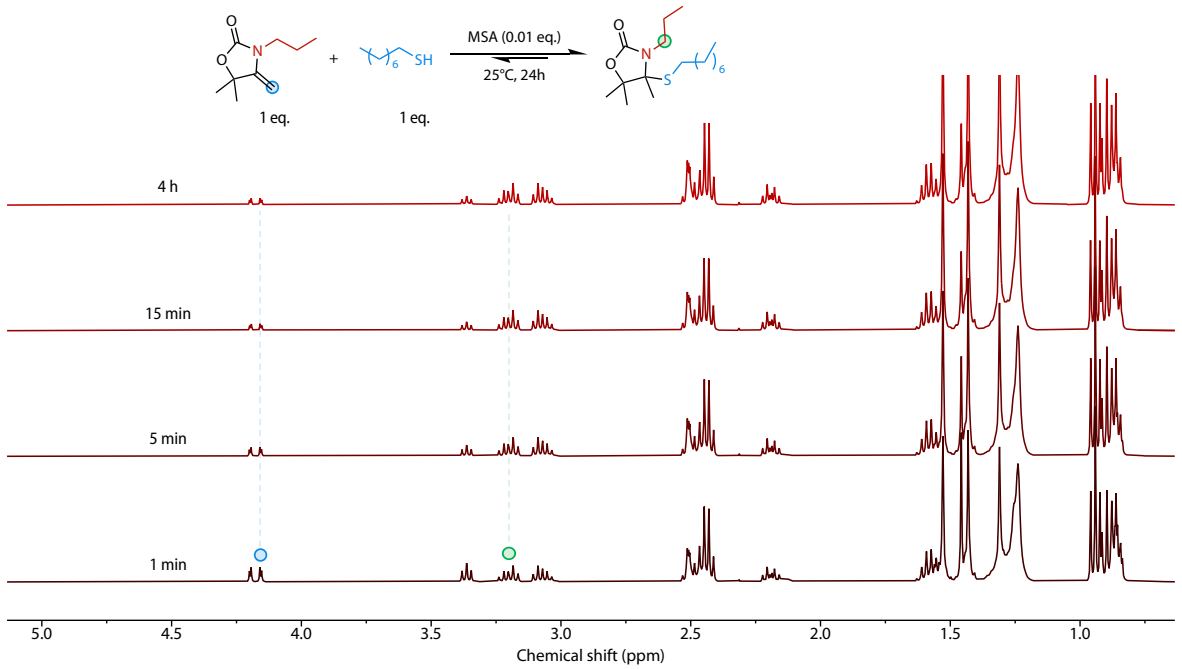

Figure S4 – Stacked ^{1}H-NMR spectra (400 MHz, DMSO-d_6) for the reaction of **2a** with octanethiol at 25°C along time.

For the reaction between **2a** and octanethiol, the resonance at 4.15 ppm (1H) was selected to follow **2a** and the resonance at 3.18 ppm (1H) to follow the product **3c**.
The following equation was used to determine the conversion:

$$Conv.(\%) = \left(\frac{I(3.18)}{I(4.15) + I(3.18)}\right) \times 100$$

Where *I* is the integral value of the selected peak.

Model reaction of **2b** and octanethiol

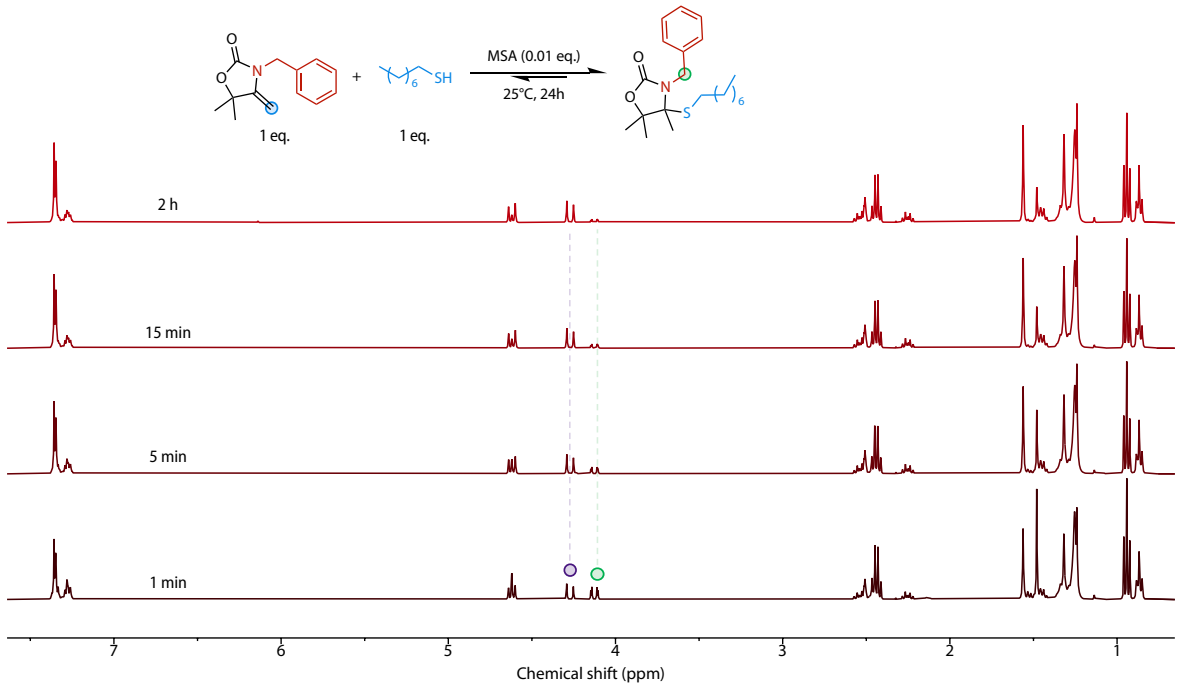

Figure S5 – Stacked ^{1}H-NMR spectra (400 MHz, DMSO-d_6) for the reaction of **2b** with octanethiol at 25°C along time.

For the reaction between **2a** and octanethiol, the resonance at 4.10 ppm (1H) was selected to follow **2b** and the resonance at 4.27 ppm (1H) to follow the product **3d**.
The following equation was used to determine the conversion:

$$Conv.(\%) = \left(\frac{I(4.27)}{I(4.10) + I(4.27)}\right) \times 100$$

Where *I* is the integral value of the selected peak.

Kinetic studies results

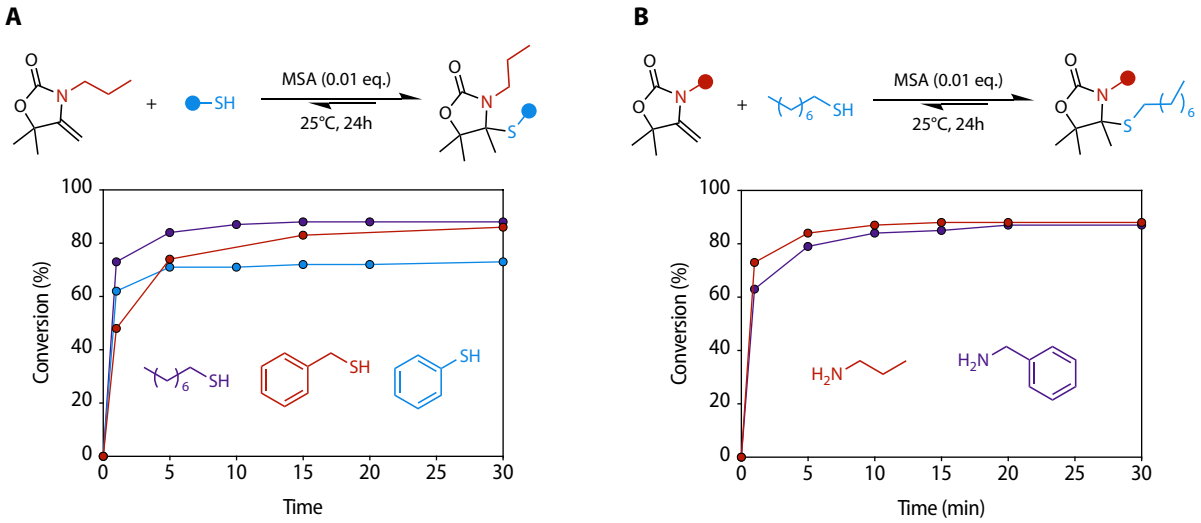

Figure S6 – Model reaction kinetic profiles for the reaction in $CHCl_3$ between (A) **2a** and different thiols and (B) **2a** or **2b** with octanethiol.

4. Synthetic Procedures: *N,S*-acetal oxazolidone compounds

General procedure for the synthesis of N,S-oxazolidones (3a-d)

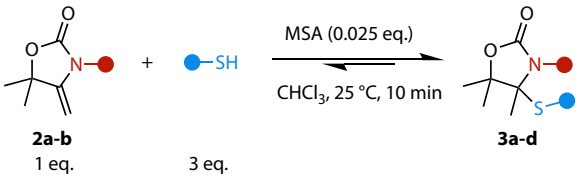

The oxazolidone **2** (3 mmol, 1 eq.), the thiol (9 mmol, 3 eq.) and 0.75 mL of $CHCl_3$ were added to a vial. MSA (7.2 mg, 0.075 mmol, 0.025 eq.) was added to the solution and the mixture was stirred for 10 minutes at 25 °C under air. The reaction was quenched by the addition of triethylamine (23 mg, 0.225 mmol, 0.075 eq.) and the crude medium was diluted with $CHCl_3$ (75 mL). The organic phase was then extracted 3 times with 75 mL NaOH aq. solution (1M) to remove the excess thiol and one time with 75 mL water. The organic phase was dried over $MgSO_4$ and dried under vacuum. The residue was purified by silica gel chromatography with diethylether / hexane (25/75).

4-(benzylthio)-4,5,5-trimethyl-3-propyloxazolidin-2-one (3a)

White solid (677 mg, isolated yield 77 %); mp = 43 °C; **^{1}H NMR** (400 MHz, DMSO-d_6) δ 7.35-7.22 (m, 5H), 3.78 (d, J = 11 Hz, 1H), 3.42 (d, J = 11 Hz, 1H), 3.32-3.22 (m, 1H), 3.18-3.08 (m, 1H), 1.62 (s, 3H), 1.61 (sextuplet, J = 7.4 Hz, 2H), 1.48 (s, 3H), 1.34 (s, 3H), 0.91 (t, J = 7.4 Hz, 3H); **^{13}C NMR** (100 MHz, DMSO-d_6) δ 156.8, 136.9, 129.4, 129.0, 127.7, 85.6, 79.1, 42.5, 34.1, 25.3, 23.6, 22.6, 20.8, 11.8. **HRMS (ESI)**: Calculated for $C_{16}H_{23}NO_2S$ [M+Na]$^+$: 316.1347. Found: 316.1347.

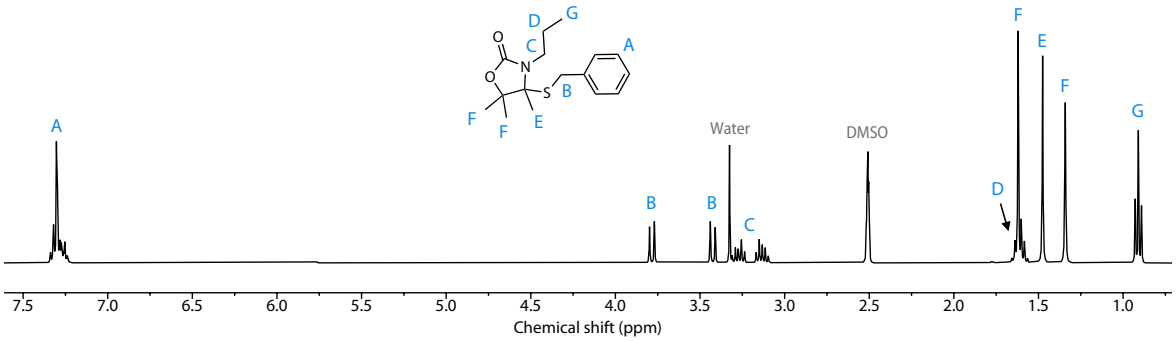

Figure S7 – ^{1}H-NMR spectrum (400 MHz, DMSO-d_6) of **3a**.

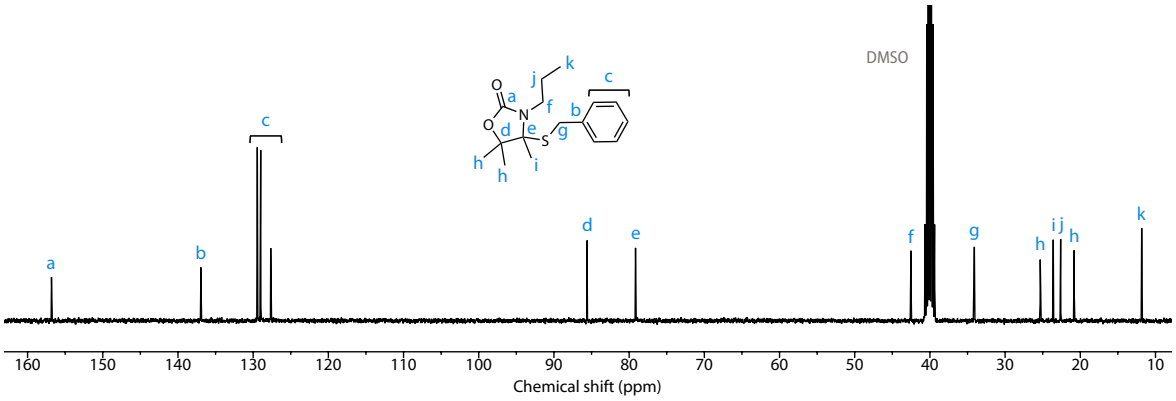

Figure S8 – ^{13}C-NMR spectrum (100 MHz, DMSO-d_6) of **3a**.

4,5,5-trimethyl-4-(phenylthio)-3-propyloxazolidin-2-one (3b)

White solid (670 mg, isolated yield 80 %); mp = 60 °C; **^{1}H NMR** (400 MHz, DMSO-d_6) δ 7.52-7.47 (m, 2H), 7.43-7.32 (m, 3H), 3.27-3.18 (m, 1H), 3.16-3.07 (m, 1H), 1.65 (s, 3H), 1.54 (sextuplet, J = 7.6 Hz, 2H), 1.52 (s, 3H), 1.29 (s, 3H), 0.88 (t, J = 7.4 Hz, 3H); **^{13}C NMR** (100 MHz, DMSO-d_6) δ 156.2, 137.0, 131.0, 129.8, 129.5, 86.1, 82.6, 43.1, 25.6, 23.3, 22.9, 21.1, 11.8. **HRMS (ESI)**: Calculated for $C_{15}H_{21}NO_2S$ [M+K]$^+$: 318.0930. Found: 318.0927.

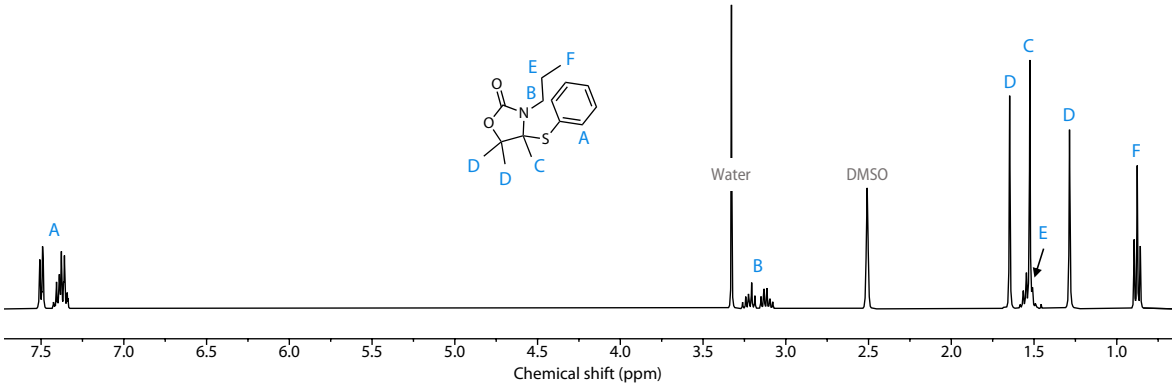

Figure S9 – ^{1}H-NMR spectrum (400 MHz, DMSO-d_6) of **3b**.

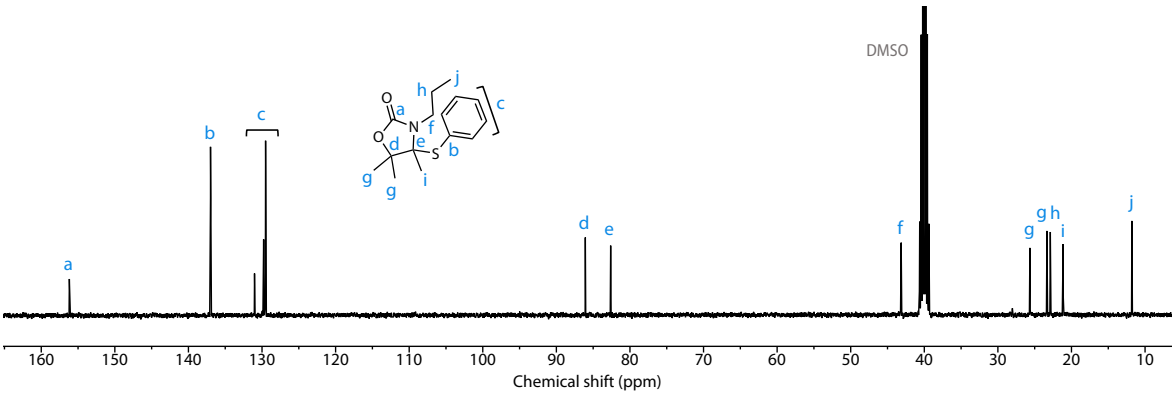

Figure S10 – ^{13}C-NMR spectrum (100 MHz, DMSO-d_6) of **3b**.

4,5,5-trimethyl-4-(octylthio)-3-propyloxazolidin-2-one (3c)

Colorless oil (813 mg, isolated yield 86 %); **^{1}H NMR** (400 MHz, DMSO-d_6) δ 3.24-3.13 (m, 1H), 3.11-3.00 (m, 1H), 2.54-2.45 (m, 1H), 2.23-2.14 (m, 1H), 1.58 (sextet, J = 7.4 Hz, 2H), 1.52 (s, 3H), 1.48-1.38 (m, 2H), 1.43 (s, 3H), 1.35-1.18 (m, 10H), 1.30 (s, 3H), 0.88 (t, J = 7.4 Hz, 3H), 0.85 (t, J = 7.1 Hz, 3H); **^{13}C NMR** (100 MHz, DMSO-d_6) δ 156.8, 85.5, 78.3, 42.5, 31.7, 29.2, 29.0, 28.9, 28.8, 28.6, 25.6, 23.5, 22.6, 22.5, 21.2, 14.4, 11.8. **HRMS (ESI)**: Calculated for $C_{17}H_{33}NO_2S$ $[M+Na]^+$: 338.2130. Found: 338.2125.

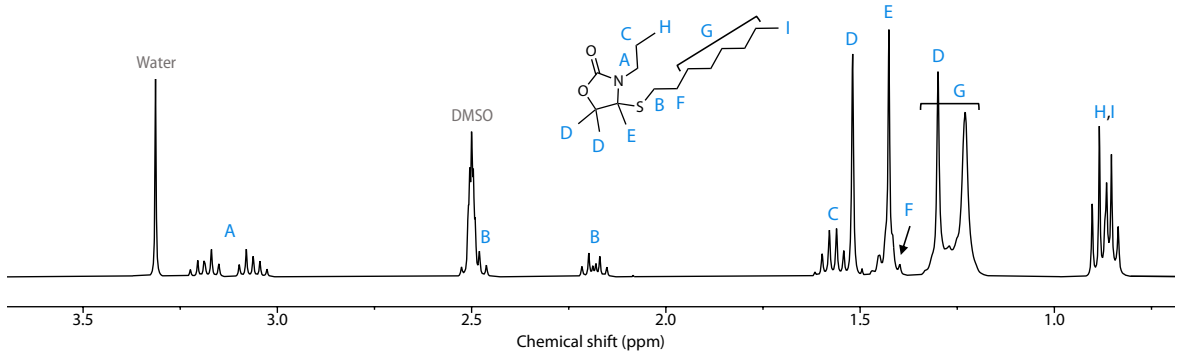

Figure S11 – ^{1}H-NMR spectrum (400 MHz, DMSO-d_6) of **3c**.

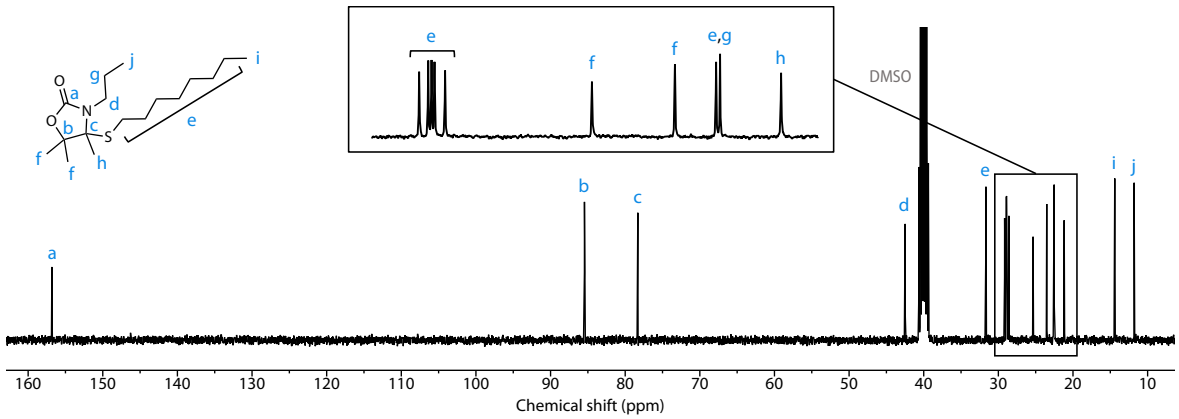

Figure S12 – ^{13}C-NMR spectrum (100 MHz, DMSO-d_6) of **3c**.

3-benzyl-4,5,5-trimethyl-4-(octylthio)oxazolidin-2-one (3d)

Colorless oil (969 mg, isolated yield 89 %); **^{1}H NMR** (400 MHz, DMSO-d_6) δ 7.39-7.32 (m, 4H), 7.32-7.24 (m, 1H), 4.60 (d, J = 15.9 Hz, 1H), 4.28 (d, J = 15.9 Hz, 1H), 2.58-2.49 (m, 1H), 2.29-2.20 (m, 1H), 1.56 (s, 3H), 1.51-1.39 (m, 2H), 1.37-1.2 (m, 10H), 1.32 (s, 3H), 1.24 (s, 3H), 0.91-0.82 (m, 3H); **^{13}C NMR** (100 MHz, DMSO-d_6) δ 157.2, 138.6, 129.0, 127.8, 127.7, 85.9, 78.5, 44.2, 31.7, 29.2, 29.0, 28.95, 28.90, 28.6, 25.5, 23.5, 22.5, 21.3, 14.4. **HRMS (ESI)**: Calculated for $C_{21}H_{33}NO_2S$ $[M+K]^+$: 402.1869. Found: 402.1867.

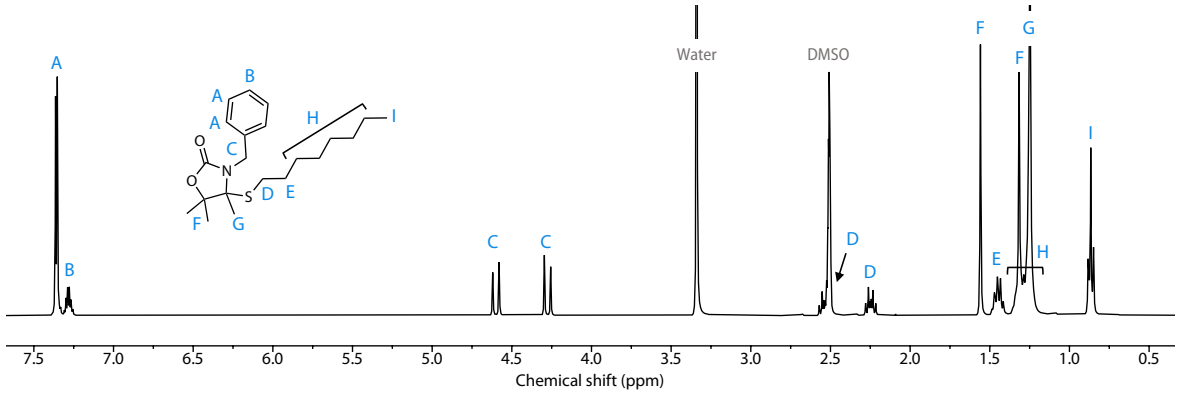

Figure S13 – ^{1}H-NMR spectrum (400 MHz, DMSO-d_6) of **3d**.

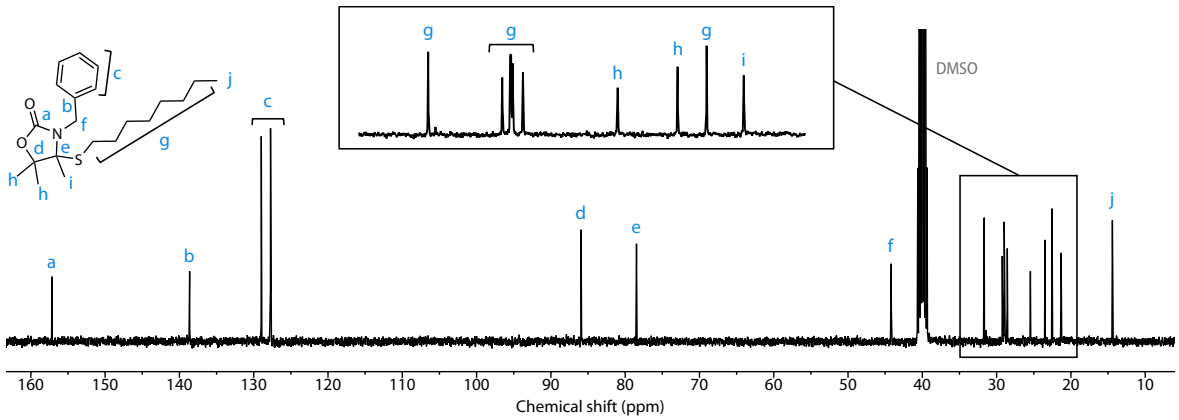

Figure S14 – ^{13}C-NMR spectrum (100 MHz, DMSO-d_6) of **3d**.

5. Computational details

Preliminary calculations of equilibrium structures were performed using a semi-empirical model (PM7)[2] to determine the most stable conformations. These semi-empirical calculations were performed using the MOPAC software[3]. The lowest energy structures obtained at the semi-empirical level were further investigated using the Density Functional Theory (DFT) method implemented in the Gaussian 16 package[4]. DFT calculations of geometries, energies and vibrational frequencies reported in this paper were carried out with the ωB97X-D functional[5] using the 6-311++G(d,p) basis set with the CPCM solvation model (chloroform). All frequencies of each structure have also been calculated to verify the presence of a single imaginary frequency for transition states and the absence of imaginary frequency for ground states. The intrinsic reaction coordinate (IRC) method has been used to verify that the obtained transition states were effectively connected to the desired minima. A wide range of possible configurations and interactions have been modelled and the more stable of them are reported in this work. To consider entropic effects, the energies mentioned in this study correspond to the Gibbs free energy.

The studied reaction pathway was discussed in the main manuscript. Intermediates on both sides of each transition states were annotated on the pathway displayed in Figure S15. Details on bond lengths along the reaction path (Figure S16, Table S1) and 3D structures of intermediates and transition states are provided here (Figure S17).

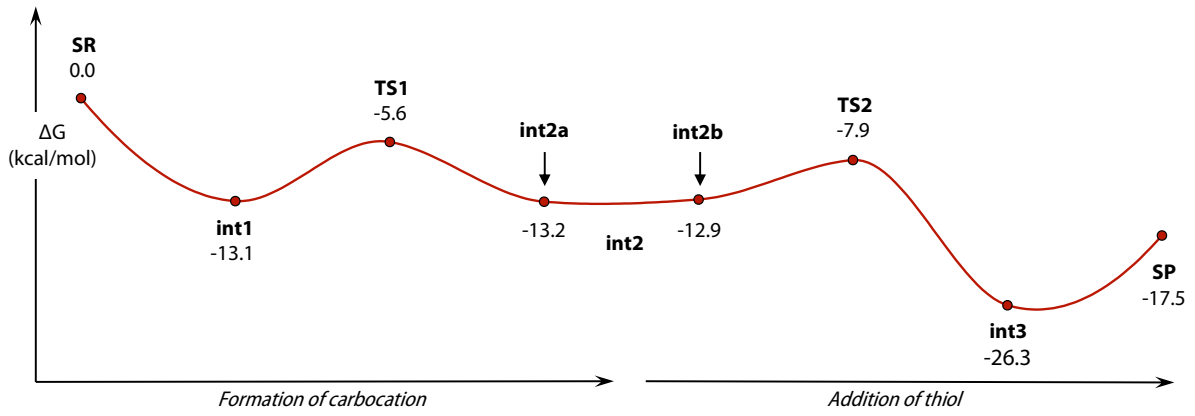

Figure S15 – Gibbs-Free Energy profile for the model reaction as studied by DFT.

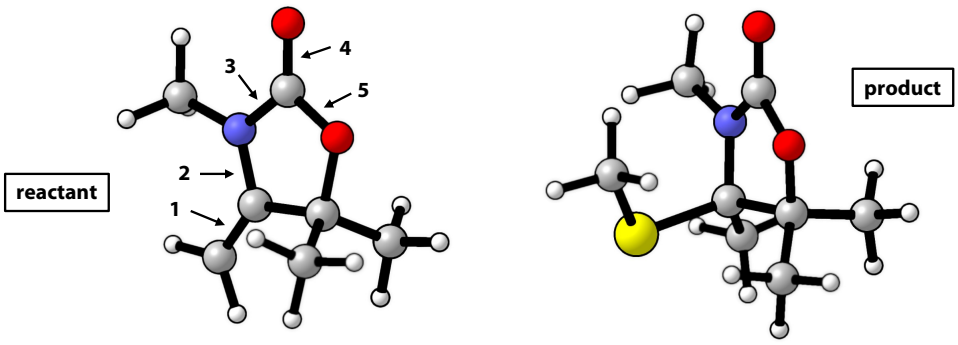

Figure S16 – 3D structures of the reactant and the product. A number was attributed to bonds whose length was followed along reaction coordinates.

Table S1 – Bond lengths for intermediates and transition states along the reaction path (expressed in Å).

	SR	**int1**	**TS1**	**int2a**	**int2b**	**TS2**	**int3**	**SP**
C-C (1)	1.332	1.340	1.388	1.461	1.461	1.484	1.524	1.525
C-N (2)	1.382	1.373	1.329	1.292	1.293	1.323	1.440	1.446
N-C (3)	1.382	1.379	1.413	1.452	1.450	1.423	1.366	1.363
C-O (4)	1.197	1.203	1.194	1.186	1.185	1.191	1.207	1.209
C-O (5)	1.346	1.339	1.328	1.318	1.320	1.327	1.348	1.348

From separate reactants, the partners can assemble into a stable complex whose stabilization energy is -13.1 kcal/mol. This is allowed by hydrogen bonds between the negatively charged carbon atom of the alkene and the acidic proton of MSA and between the acidic proton of the thiol and a free oxygen atom of MSA. The first interaction is already responsible for a slight bond (1) length increase of the alkene. Upon transfer of the acidic proton of MSA to the alkene through TS1, the so-formed carbocation in **int2** is stabilized by the nitrogen atom which can share electrons to build a stable pi bond. All bond lengths in the ring are strongly impacted by this step as indicated in Table S. The previous C=C alkene bond becomes a sigma C-C bond (1) with increased bond length (+0.121 Å). On the other side, the C-N bond (2) decreases with the creation of the stable pi bond. The nitrogen atom thus shares less electrons with the electron-poor carbon of the carbonyl group, resulting in a N-C(O) bond (3) length increase (+0.073 Å). Additional hydrogen bonds stabilize **int2**, rendering this intermediate as energetically stable as the reactants complex. The second step begins with **int2** where hydrogen bonds with the proton of the thiol and the proton of the oxazolidone methyl group are located on the same oxygen donor group of the MSA, whose negative charge is stabilized by

these interactions. The addition of the thiol on the electrophilic carbon takes place as the proton from the thiol is transferred to the MSA. The C=N (2) pi bond is suppressed, and the bond length readily increases (+0.147 Å). The nitrogen is then able to share back more electrons with the carbonyl atom resulting in a bond (3) length decrease (-0.084 Å). The product complex **int3** is stabilized of 8.8 kcal/mol on the account of hydrogen bonding between the acidic proton of regenerated MSA and the sulfur atom of the N,S-oxazolidone.

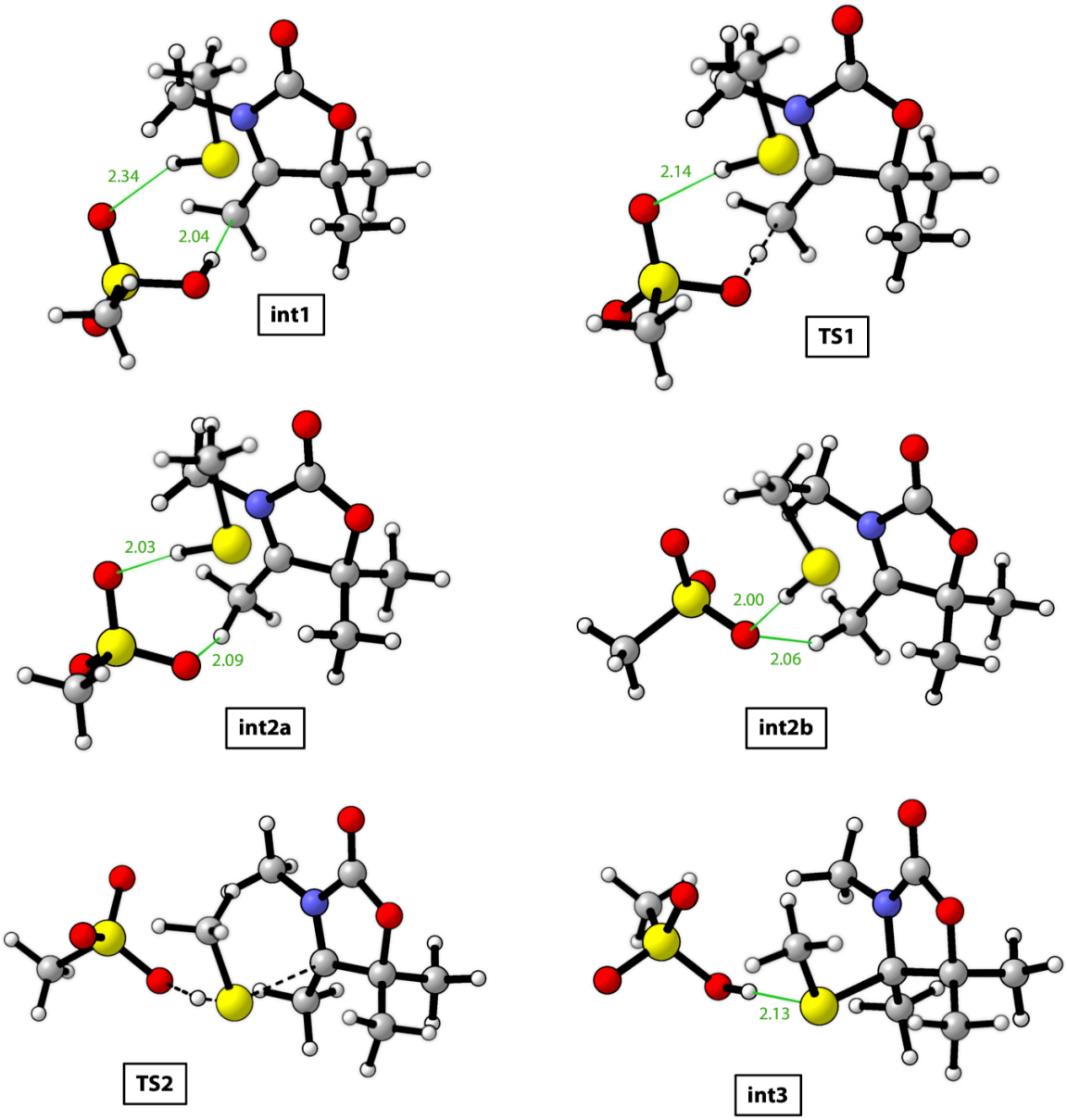

Figure S17 – 3D structures of optimized intermediates and transition states along the reaction path.

6. Model exchange reactions

The kinetics of the exchange reaction at the model molecule level was performed. **3a** was reacted with a fivefold excess of octanethiol, thus producing **3c** and benzyl mercaptan. The kinetics was performed by dissolving **3a** at a concentration of 0.25 M in $CDCl_3$. Octanethiol (5 eq.) and MSA (0.01 eq.) were added to the reaction mixture to initiate the exchange. Aliquots were taken at different times and were quenched with triethylamine prior ^{1}H-NMR analysis. Characteristic signals of **3a** and **3c** were followed to monitor the reaction (Figure S). For **3a**, the characteristic signal of the benzyl -$\underline{CH_2}$- at 3.80 ppm (in purple) was followed. For **3c**, an overlapping signal characteristic for the N-$\underline{CH_2}$- signal of both the reactants and products was followed (in green).

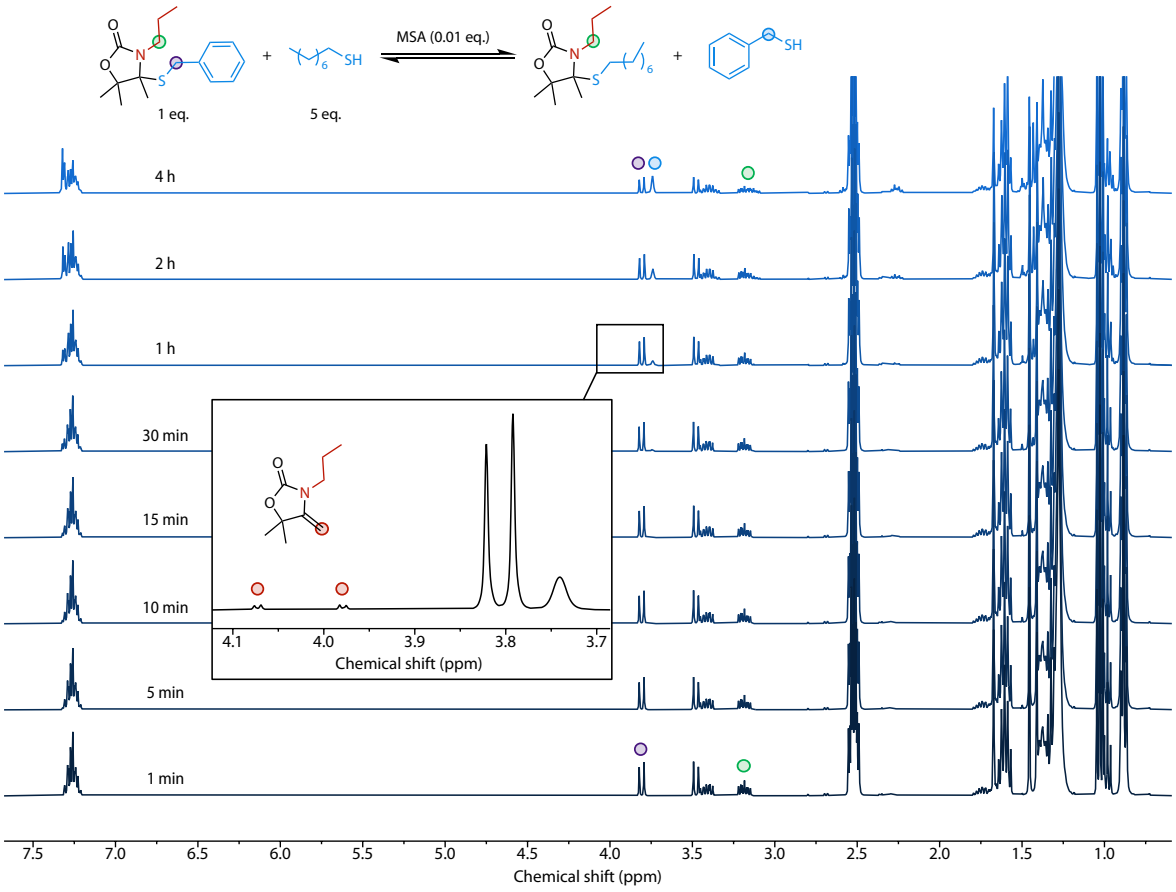

Figure S18 – Stacked ^{1}H-NMR spectra (400 MHz, $CDCl_3$) of the kinetics of the exchange reaction between **3a** and a fivefold excess of octanethiol at 25 °C.

In order to get an activation of energy for the exchange reaction, the same reaction was performed at five different temperatures (7 to 50 °C). A fit derived from the equation of the

isotope exchange kinetics could be used to extract rate constants k for all the reactions(Figure S19)[6].

$$[reactant] = 1 - (x_\infty - \exp\left(\frac{-kt}{x_\infty}\right))$$

Where x_∞ is the equilibrium concentration of the product (0.8225).

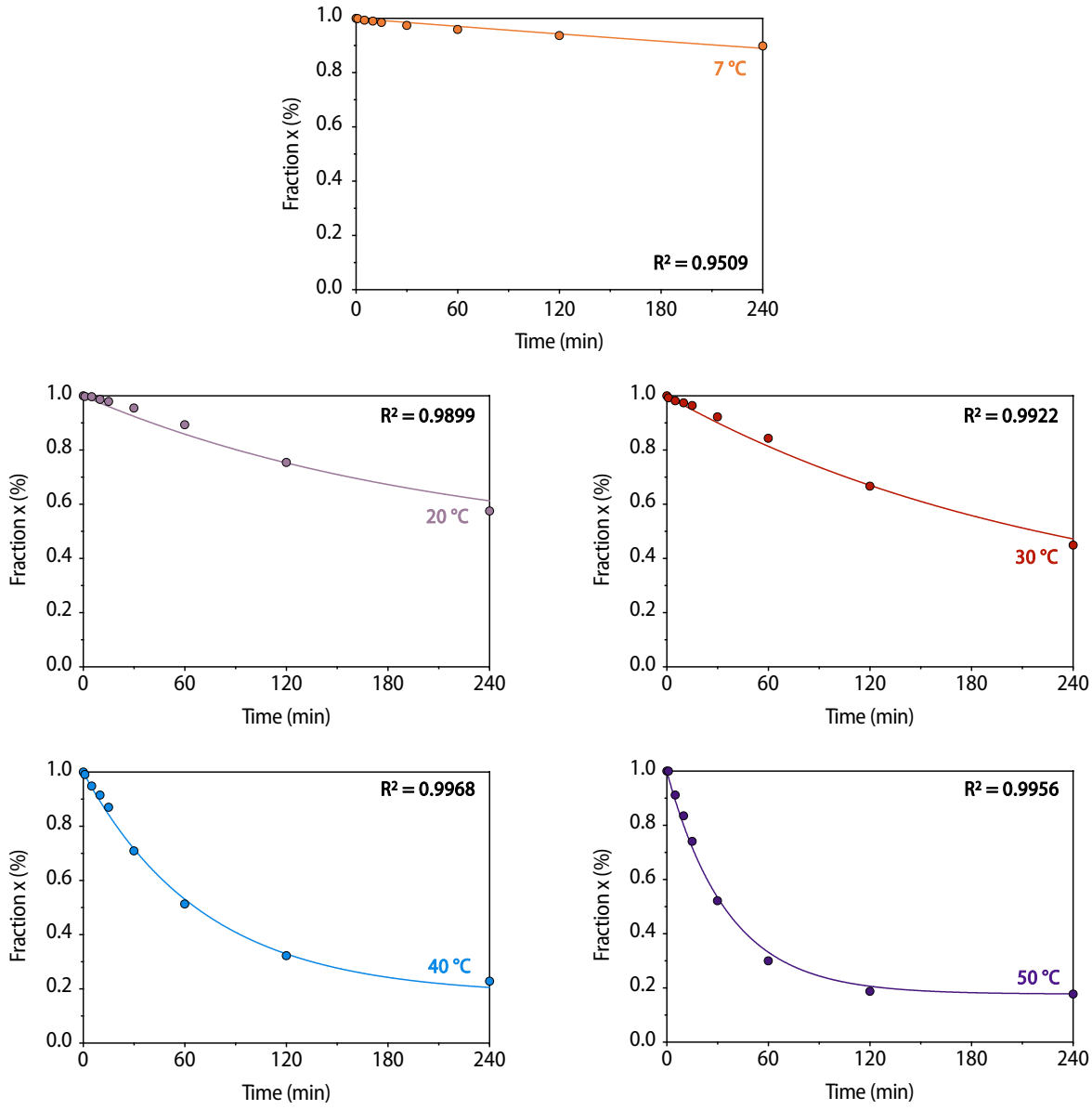

Figure S19 – Exchange reaction kinetic profiles for the reaction between **3a** and a fivefold excess of octanethiol at different temperatures. The kinetic data points (dots) were fitted to an equation to extract constant rates k (lines).

From the different rate constants at the different temperatures, an Arrhenius plot was built. From a linear regression fit, the activation of energy for the exchange reaction could be determined.

$$\ln(k) = \ln(A) - \frac{E_a}{RT}$$

Table S2 – Exchange activation energy of various dynamic bonds determined on both model compounds and polymer network matrices. Referred papers[7–14] are provided.

		Exchange activation energy (kcal/mol)		Ref.
Dynamic bond	Catalyst	Model compound	Polymer	
N,S-oxazolidone	MSA	15.5	26.4 – 38.8	
S,S-acetals	TBD	15.8 – 18.4	29.7 – 47.3	7
Vinylogous urethane	Catalyst-free	14.1	14.3	8
Vinylogous urea	Catalyst-free	12.5	10.5 – 14.3	9
Diketoenamine	Catalyst-free	6.9 – 14.8	11.7 – 14.3	10
Dioxaborolane	Catalyst-free	3.8	18.3	11
Phtalate monoster	Internal catalysis	22.9	28.7	12
Triazolinedione	$ZrAc_4$	26.0 – 27.8	25.8	13,14

7. Synthetic Procedures: alkylidene oxazolidones monomers

General procedure for the tandem synthesis of bis(alkylidene oxazolidone)s (2c-f)

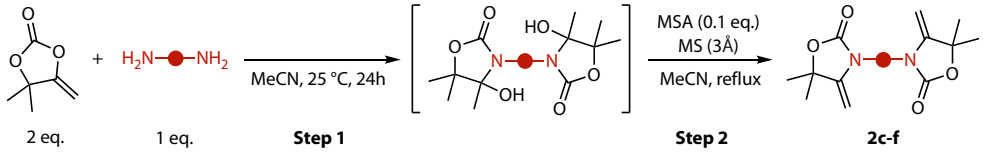

αCC (20.48 g, 0.16 mol, 2 eq.), the diamine (0.08 mol, 1 eq.) and acetonitrile (40 mL) were added to a round-bottom flask. The mixture was stirred in an ice bath for the first minutes of reaction and then at 25 °C. After 24h, MSA (0.1 eq.) and acetonitrile (80 mL) were added. The dehydration setup was installed on the flask and the mixture was refluxed for 24h. The crude was quenched with triethylamine (0.3 eq.) and cooled to room temperature. The mixture was diluted in dichloromethane (600 mL) and extracted with water (3 x 600 mL). The organic phase was dried over $MgSO_4$ and filtered. Solvent was partially removed under vacuum until around 100 mL is left. The solution was passed on a thin silica pad and 250 mL of dichloromethane is then passed on the pad. Solvent was then entirely removed under vacuum. When the monomer was solid, it was recrystallized in a suitable solvent system, filtered on Büchner, and washed with hexane to yield the pure product.
Deviations from this procedure are given for each product.

3,3'-(1,3-phenylenebis(methylene))bis(5,5-dimethyl-4-methyleneoxazolidin-2-one) (2c)

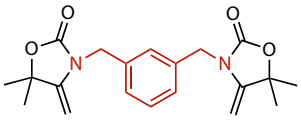

Recrystallized in Ethyl acetate 25 / Hexane 75 to yield white crystals (22.9 g, isolated yield 80%); mp = 107 °C; **^{1}H NMR** (400 MHz, DMSO-d_6) δ 7.34 (t, J = 7.5 Hz, 1H), 7.21 (d, J = 7.5 Hz, 2H), 7.08 (s, 1H), 4.60 (s, 4H), 4.13 (d, J = 2.7 Hz, 2H), 4.06 (d, J = 2.7 Hz, 2H), 1.46 (s, 6H); **^{13}C NMR** (100 MHz, DMSO-d_6) δ 155.4, 150.1, 136.8, 129.3, 126.7, 124.8, 82.6, 81.2, 44.36, 27.94. **HRMS (ESI)**: Calculated for $C_{20}H_{25}N_2O_4$ $[M+H]^+$: 357.1814. Found: 357.1820.

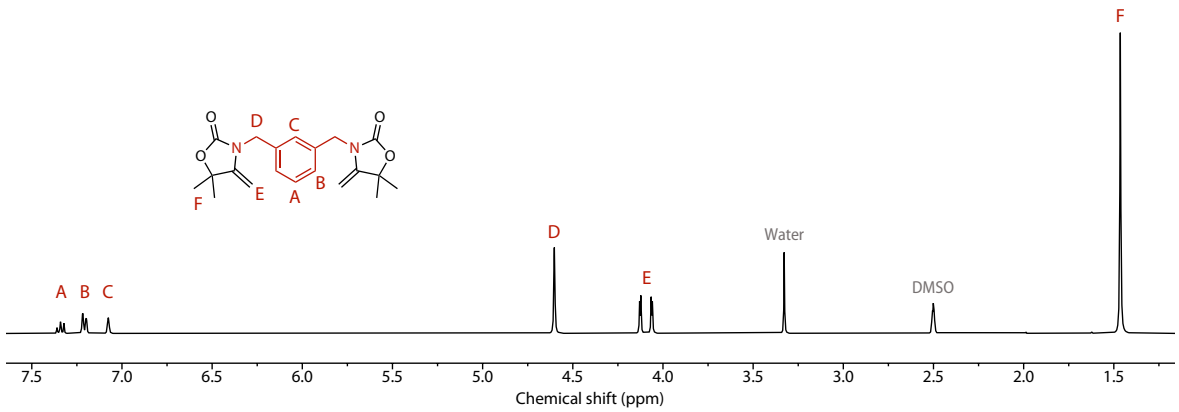

Figure S20 – ^{1}H-NMR spectrum (400 MHz, DMSO-d_6) of **2c**.

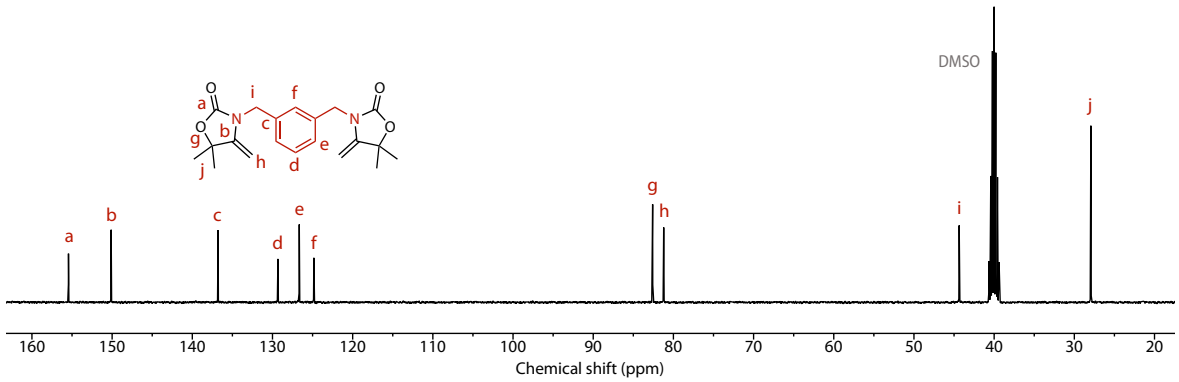

Figure S21 – ^{13}C-NMR spectrum (100 MHz, DMSO-d_6) of **2c**.

3,3'-((ethane-1,2-diylbis(oxy))bis(ethane-2,1-diyl))bis(5,5-dimethyl-4-methyleneoxazolidin-2-one) (2d)

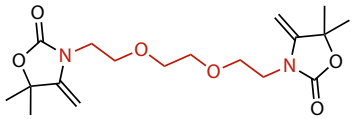

For the first step, DBU (0.05 eq.) was added to the reaction mixture. For the second step, 0.15 eq. of MSA was used rather than 0.1 eq. Recrystallized in Chloroform 10 / Hexane 90 to yield white crystals (22.8 g, isolated yield 77%); mp = 101 °C; **^{1}H NMR** (400 MHz, DMSO-d_6) δ 4.26 (d, J = 2.7 Hz, 2H), 4.18 (d, J = 2.7 Hz, 2H), 3.55 (s, 8H), 3.49 (s, 4H), 1.45 (s, 6H); **^{13}C NMR** (100 MHz, DMSO-d_6) δ 155.2, 150.5, 82.2, 80.5, 70.1, 66.2, 40.9, 27.94. **HRMS (ESI)**: Calculated for $C_{18}H_{29}N_2O_6$ $[M+H]^+$: 369.2026. Found: 369.2023.

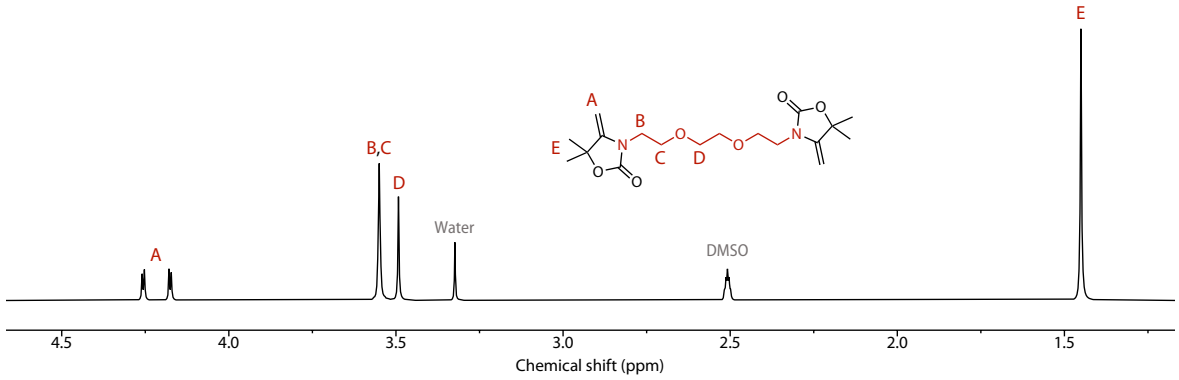

Figure S22 – ^{1}H-NMR spectrum (400 MHz, DMSO-d_6) of **2d**.

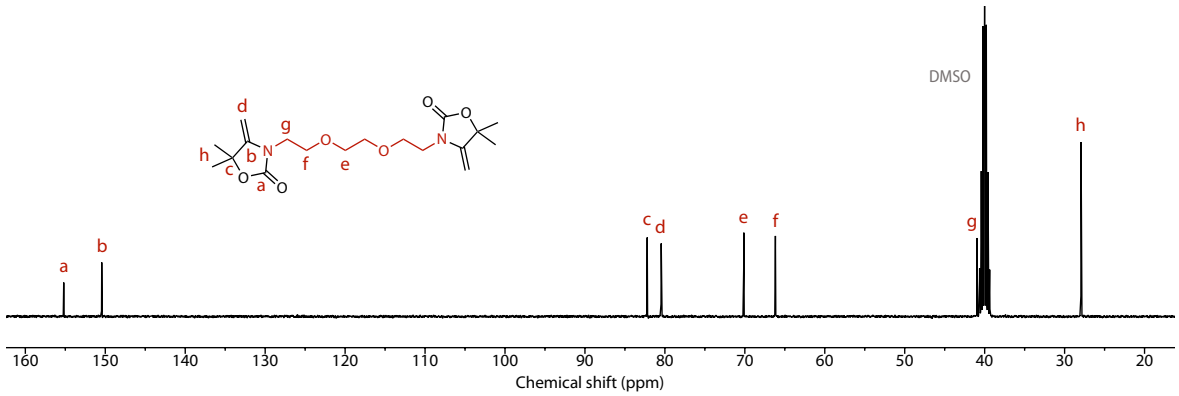

Figure S23 – ^{13}C-NMR spectrum (100 MHz, DMSO-d_6) of **2d**.

3,3'-(hexane-1,6-diyl)bis(5,5-dimethyl-4-methyleneoxazolidin-2-one) (2e)

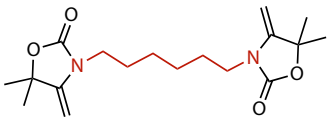

For the first step, DBU (0.05 eq.) was added to the reaction mixture. For the second step, 0.15 eq. of MSA was used rather than 0.1 eq. Recrystallized in Diethyl ether 40 / Hexane 60 to yield white crystals (22.65 g, isolated yield 84%); mp = 66 °C; **^{1}H NMR** (400 MHz, DMSO-d_6) δ 4.19 (d, J = 2.7 Hz, 2H), 4.16 (d, J = 2.7 Hz, 2H), 3.37 (t, J = 7.1 Hz, 4H), 1.55-1.46 (m, 4H), 1.44 (s, 12H), 1.33-1.21 (m, 4H); **^{13}C NMR** (100 MHz, DMSO-d_6) δ 155.2, 150.6, 82.1, 80.1, 40.9, 28.0, 26.2, 26.0. **HRMS (ESI)**: Calculated for $C_{18}H_{29}N_2O_4$ $[M+H]^+$: 337.2127. Found: 337.2122.

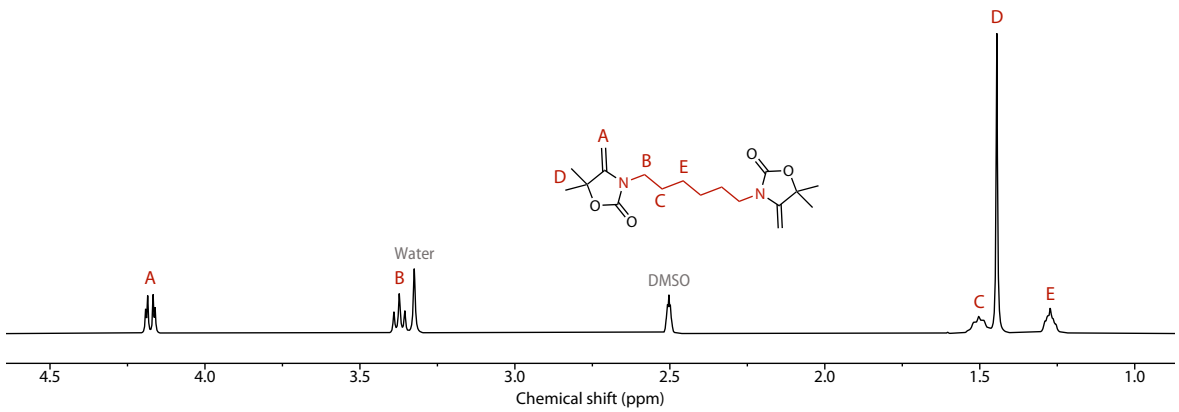

Figure S24 – ^{1}H-NMR spectrum (400 MHz, DMSO-d_6) of **2e**.

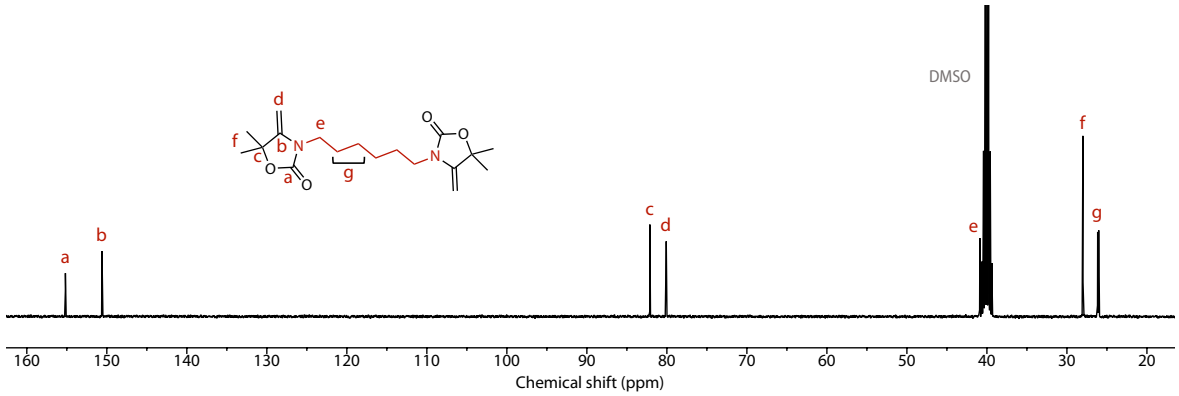

Figure S25 – ^{13}C-NMR spectrum (100 MHz, DMSO-d_6) of **2e**.

Bis(alkylidene oxazolidone) from Priamine 1075 PRI (2f)

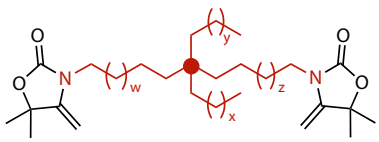

Instead of acetonitrile, toluene was used for both steps. For the first step, DBU (0.05 eq.) was added to the reaction mixture. For the second step, 0.15 eq. of MSA was used rather than 0.1 eq. Isolated as pale-yellow viscous liquid (51.23 g, isolated yield 83%); **^{1}H NMR** (400 MHz, $CDCl_3$) δ 4.07 (d, J = 2.9 Hz, 2H), 3.98 (d, J = 2.9 Hz, 2H), 3.43 (t, J = 7.4 Hz, 4H) 1.66-1.54 (m, 4H), 1.49 (s, 12H), 1.45-0.99 (m, 49H), 0.97-0.71 (m, 9H); **^{13}C NMR** (100 MHz, $CDCl_3$) δ 155.6, 151.1, 81.9, 79.0, 41.5, 31.9, 29.7, 29.6, 29.5, 29.4, 29.3, 28.0, 26.7, 26.3, 22.7, 14.1.

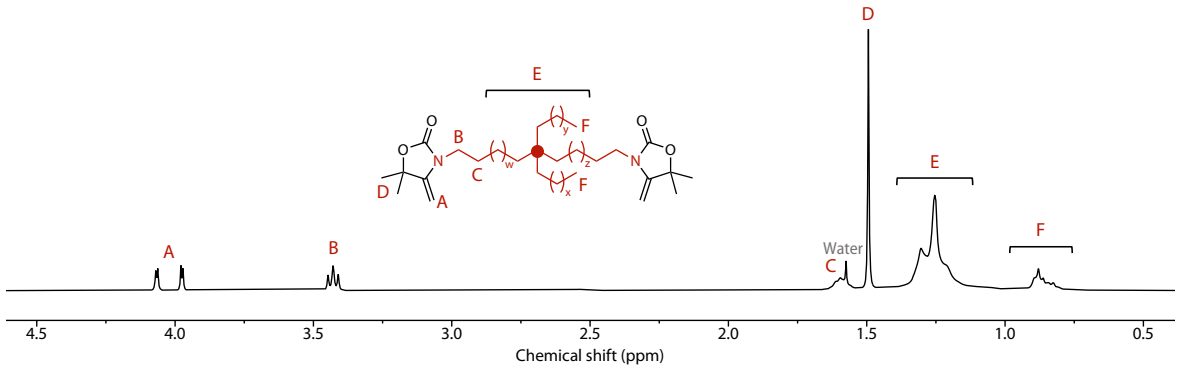

Figure S26 – ^{1}H-NMR spectrum (400 MHz, $CDCl_3$) of **2f**.

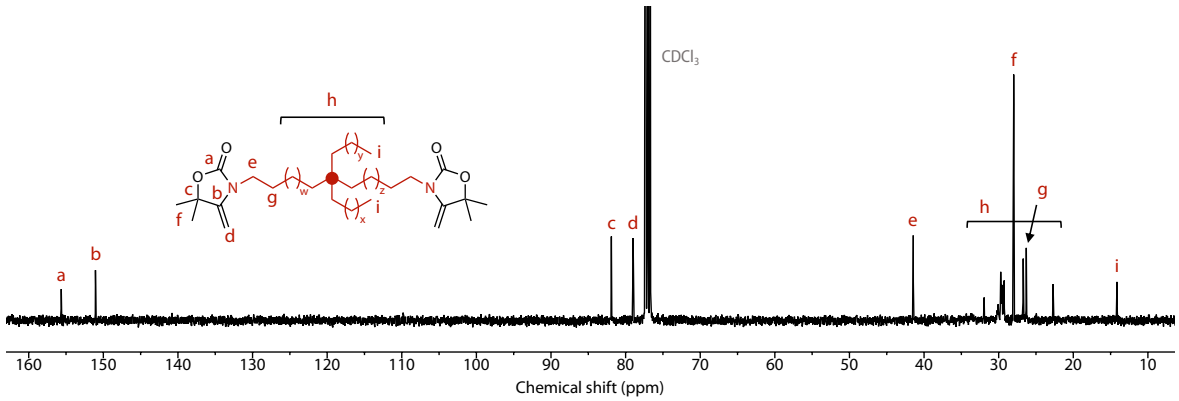

Figure S27 – ^{13}C-NMR spectrum (100 MHz, $CDCl_3$) of **2f**.

8. Polymer synthesis

In a baker containing 20 mL of $CHCl_3$ were added the monomer **2c-f** or a mix of monomers (20 mmol, 1 eq.) and PETMP (10 mmol, 0.5 eq.). Once the solution was homogeneous, MSA (0.01 eq.) was added and the mixture was stirred at room temperature. After 10 to 60 minutes, a gel was formed. The gel was easily recovered and dried under vacuum at 70 °C overnight. The pure polymer was then slowly cooled down to room temperature.

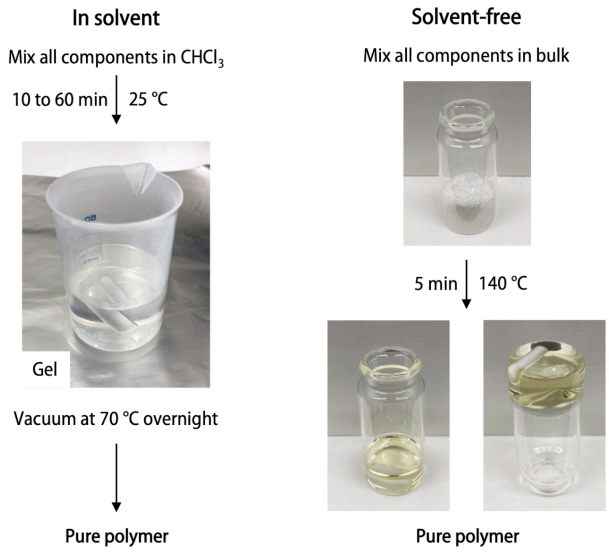

Figure S28 – Possible polymerization methods (for **P-HMDA** here): in solvent (left) and in bulk (right).

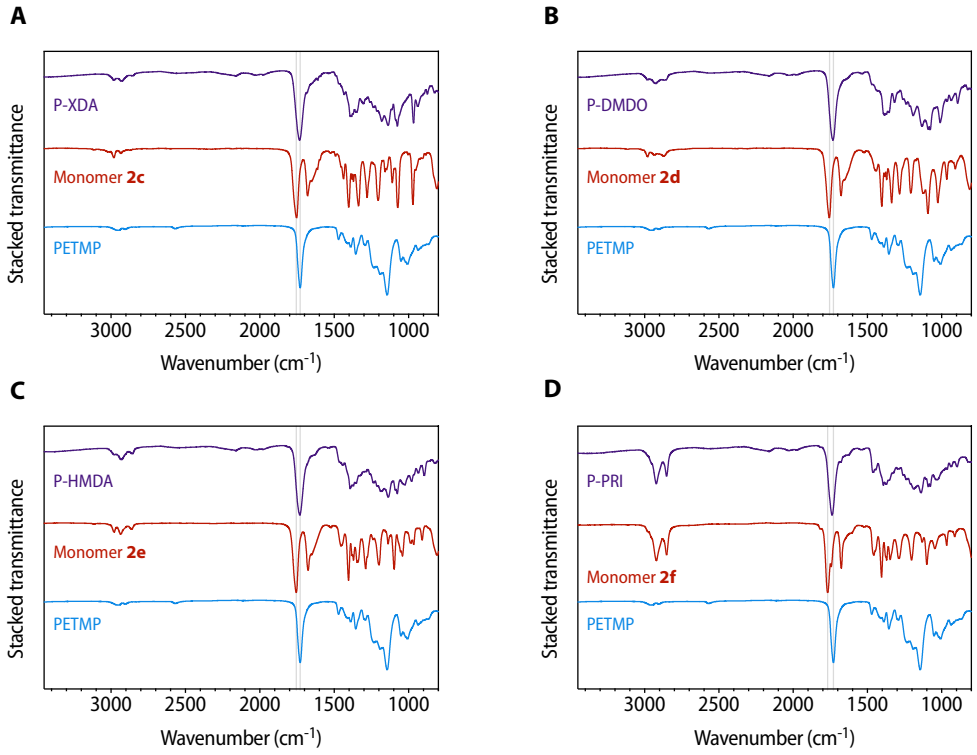

Figure S29 – ATR-IR spectra of (A) P-XDA, (B) P-DMDO, (C) P-HMDA, and (D) P-PRI and their respective monomers.

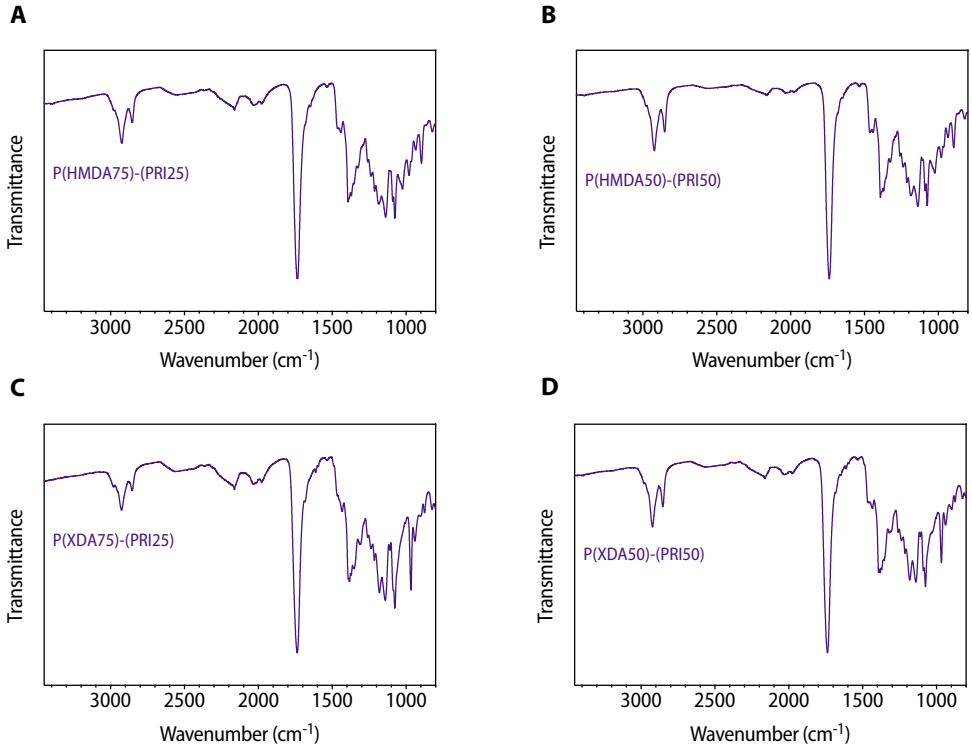

Figure S30 – ATR-IR spectra of (A) P(HMDA75)-(PRI25), (B) P(HMDA50)-(PRI50), (C) P(XDA75)-(PRI25), and (D) P(XDA50)-(PRI50).

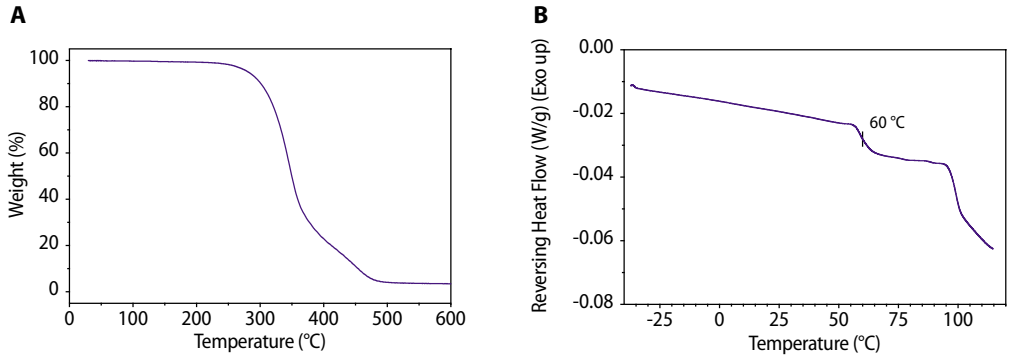

Figure S31 – (A) TGA and (B) mDSC curves for **P-XDA**.

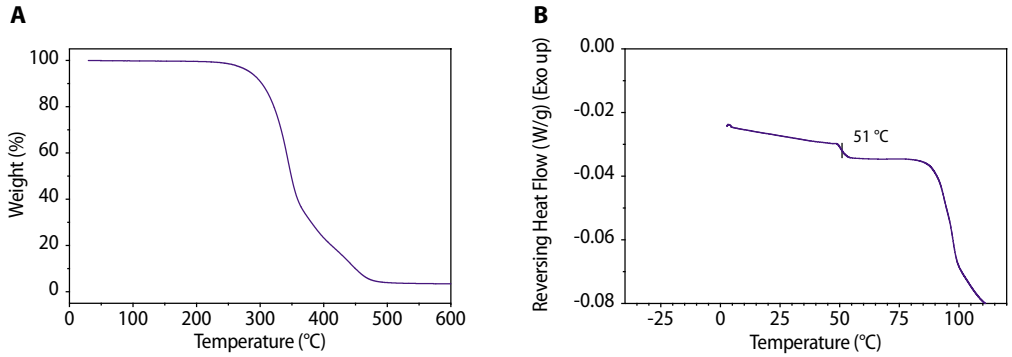

Figure S32 – (A) TGA and (B) mDSC curves for **P-DMDO**.

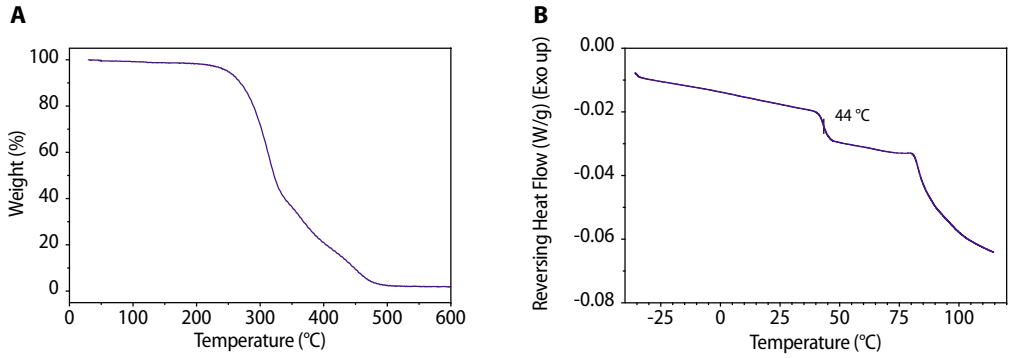

Figure S33 – (A) TGA and (B) mDSC curves for **P-HMDA**.

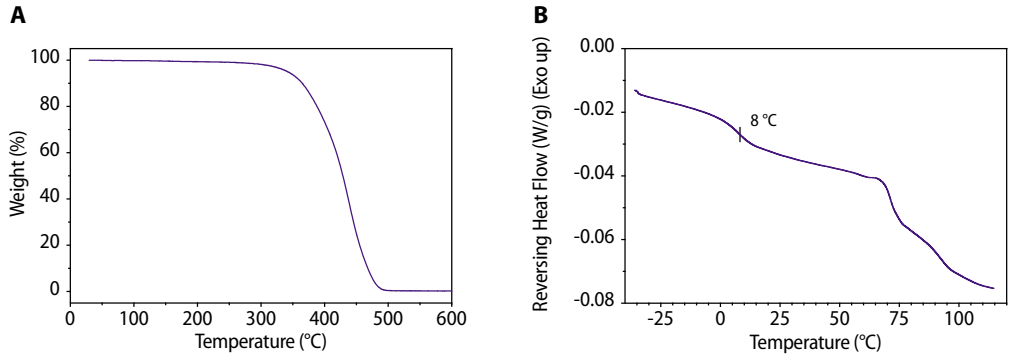

Figure S34 – (A) TGA and (B) mDSC curves for **P-PRI**.

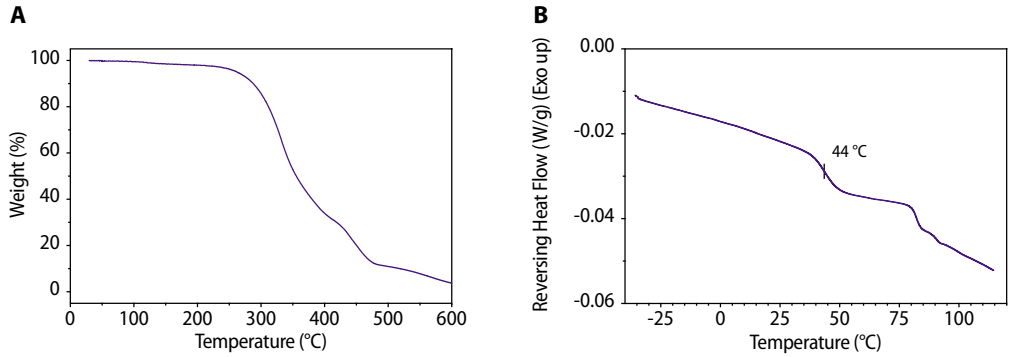

Figure S35 – (A) TGA and (B) mDSC curves for **P(HMDA75)-(PRI25)**.

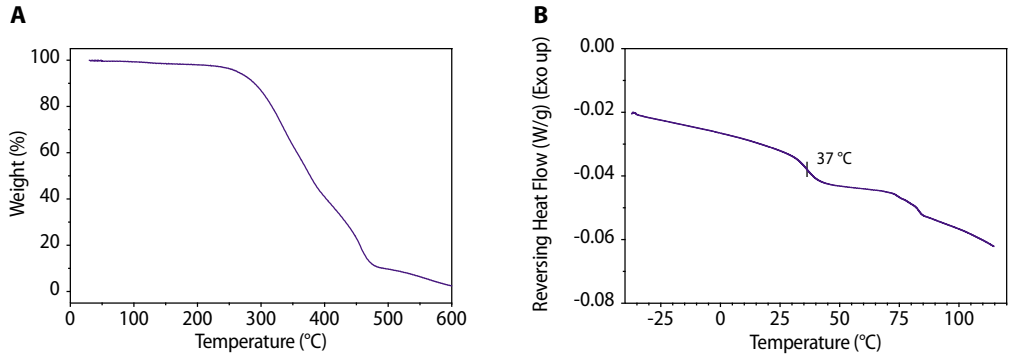

Figure S36 – (A) TGA and (B) mDSC curves for **P(HMDA50)-(PRI50)**.

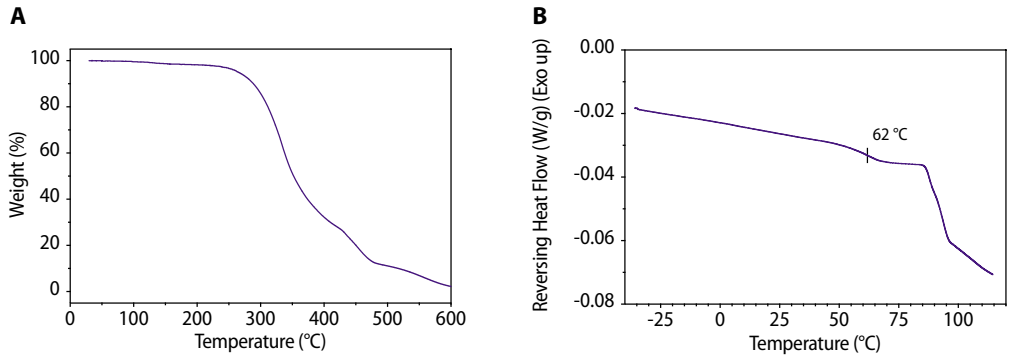

Figure S37 – (A) TGA and (B) mDSC curves for **P(XDA75)-(PRI25)**.

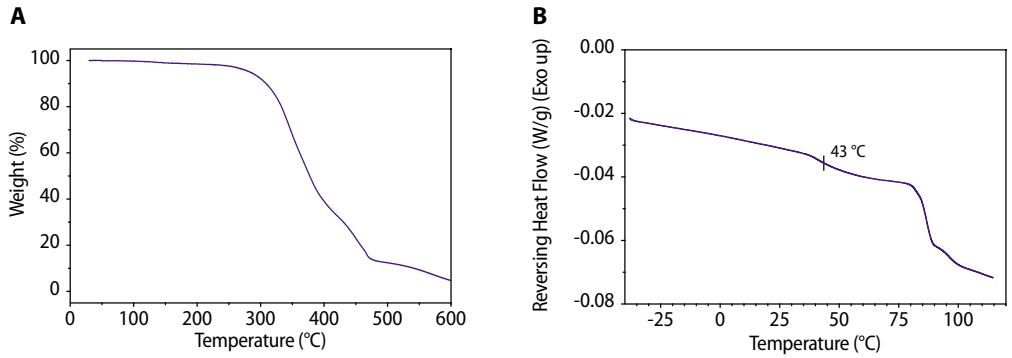

Figure S38 – (A) TGA and (B) mDSC curves for **P(XDA50)-(PRI50)**.

9. Dynamic Mechanical Analysis

As discussed in the manuscript, DMTA was performed to observe the thermal behavior of a typical network, P-DMDO, in temperatures inaccessible with our rheology setup. A temperature ramp was therefore performed from room temperature to 80 °C. This maximum temperature limit was selected to avoid polymer flow which might damage the instrument. As the temperature increased, a drop in storage modulus was observed due to the glass transition of the polymer, which showed to be very similar (2 °C of difference) to the one determined by DSC analysis.

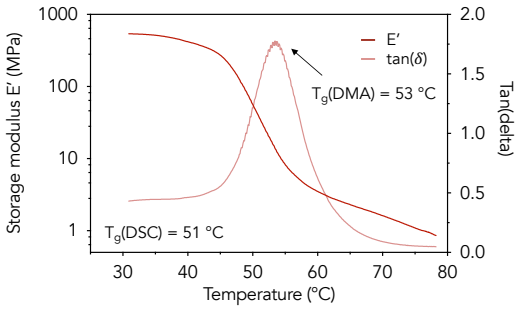

Figure S39 – Temperature ramp analysis by DMTA of P-DMDO, displaying a T_g very similar to the T_g determined by DSC.

10. Rheological data

Stress relaxation experiments were achieved at different temperatures for a given material. One- or two-element Maxwell and stretched exponential models didn't gave satisfactory results with low fitting accuracy. The data was then fitted to a three-element Maxwell model with which high values of R^2 could be obtained (typically $R^2 > 0.99$)

$$G(t) = G_0 + G_1 e^{-t/\tau_1} + G_2 e^{-t/\tau_2} + G_3 e^{-t/\tau_3}$$

Only the slowest relaxation time τ_3 showed a temperature-dependence behavior. An energy of activation could be determined from the slope of the linear fit in an Arrhenius plot following the equation:

$$\ln(\tau_3) = \ln(\tau_0) + \frac{E_a}{RT}$$

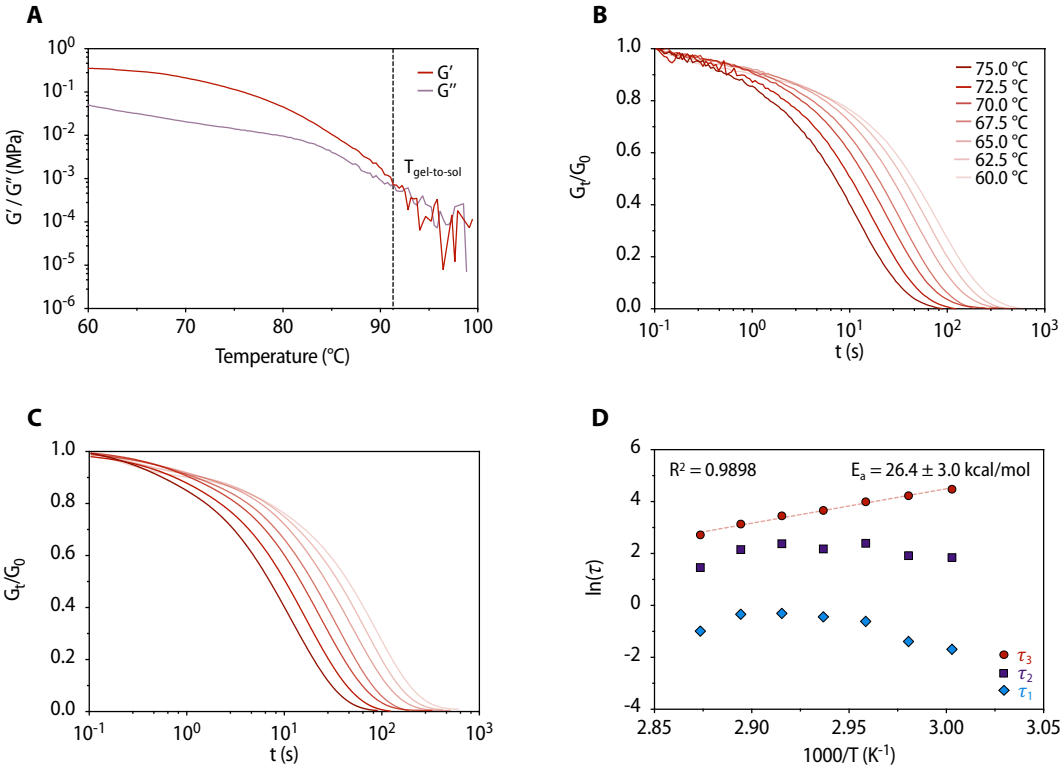

Figure S40 – For P-DMDO, different rheological experiments were conducted: (A) Temperature sweep, (B) Stress relaxation at different temperatures and (C) their respective curve fits. (D) The three relaxation times were plotted for each temperature, the third one used with the Arrhenius law to extract an energy of activation.

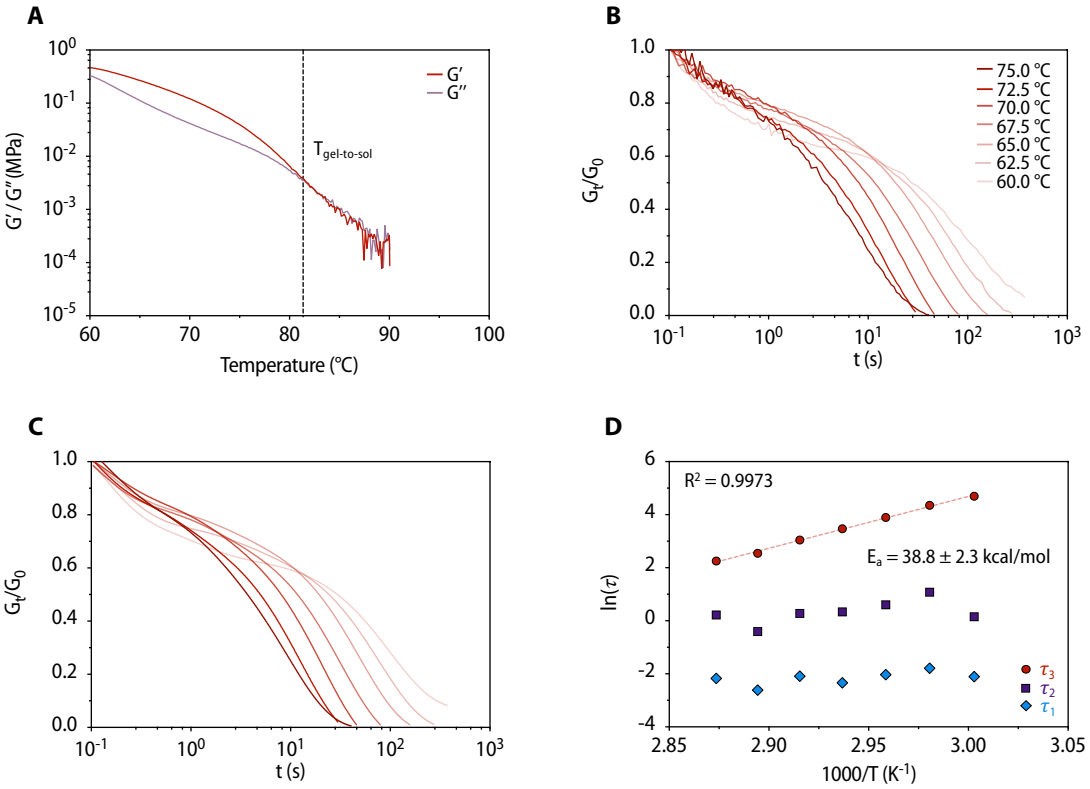

Figure S41 – For P-HMDA, different rheological experiments were conducted: (A) Temperature sweep, (B) Stress relaxation at different temperatures and (C) their respective curve fits. (D) The three relaxation times were plotted for each temperature, the third one used with the Arrhenius law to extract an energy of activation.

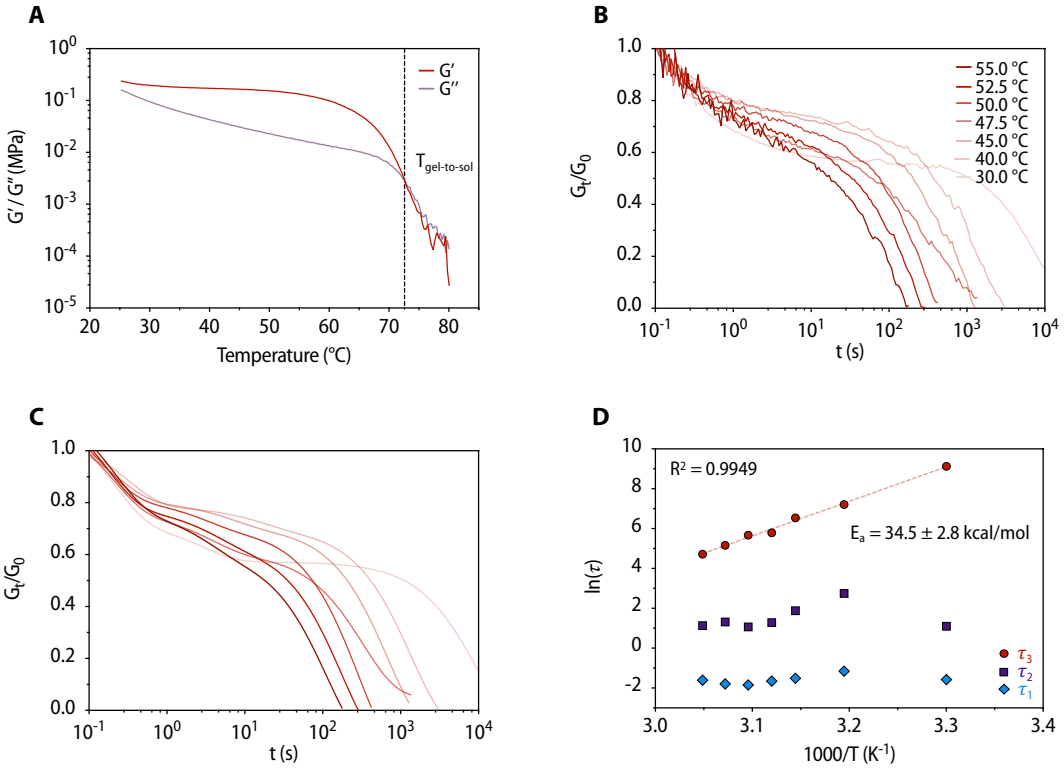

Figure S42 – For P-PRI, different rheological experiments were conducted: (A) Temperature sweep, (B) Stress relaxation at different temperatures and (C) their respective curve fits. (D) The three relaxation times were plotted for each temperature, the third one used with the Arrhenius law to extract an energy of activation.

Table S3 – From a fitting of the relaxation curve to the model, three relaxation times were determined at each temperature. The good fitting was highlighted by an excellent R^2 in all cases.

T (°C) DMDO	τ_1 (s)	τ_2 (s)	τ_3 (s)	R^2
60	0,1844	6,318	88,25	0.9999
62.5	0,2505	6,852	68,67	0.9999
65	0,5423	11	54,36	0.9999
67.5	0,6472	8,827	38,88	0.9999
70	0,7394	10,77	31,55	0.9999
72.5	0,7145	8,626	23,01	0.9995
75	0,3739	4,324	15,13	0.9998
T (°C) HMDA	τ_1 (s)	τ_2 (s)	τ_3 (s)	R^2
60	0,122	1,171	109,6	0.9995
62.5	0,1668	2,944	77,95	0.9996

65	0,1311	1,833	49,39	0.9998
67.5	0,09689	1,405	32,09	0.9996
70	0,124	1,318	21,05	0.9997
72.5	0,07337	0,6698	12,72	0.9994
75	0,1137	1,25	9,526	0.9986
T (°C) PRI	τ_1 (s)	τ_2 (s)	τ_3 (s)	R^2
30	0,2069	3,003	9239	0.9983
40	0,3147	15,58	1357	0.9980
45	0,222	6,537	688,6	0.9978
47,5	0,1927	3,598	328,8	0.9974
50	0,1578	2,92	290,7	0.9973
52,5	0,166	3,723	175,5	0.9963
55	0,2002	3,12	112,6	0.9886

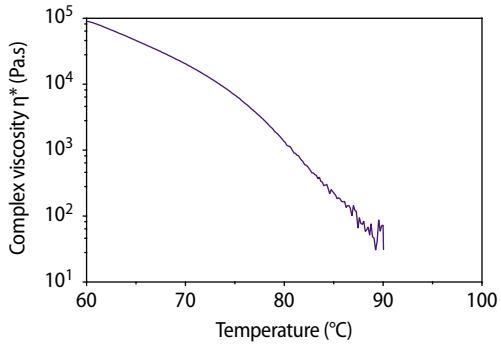

Figure S43 – Evolution of the complex viscosity of P-HMDA during a temperature sweep.

11. Polymer recycling

A. Mechanical recycling

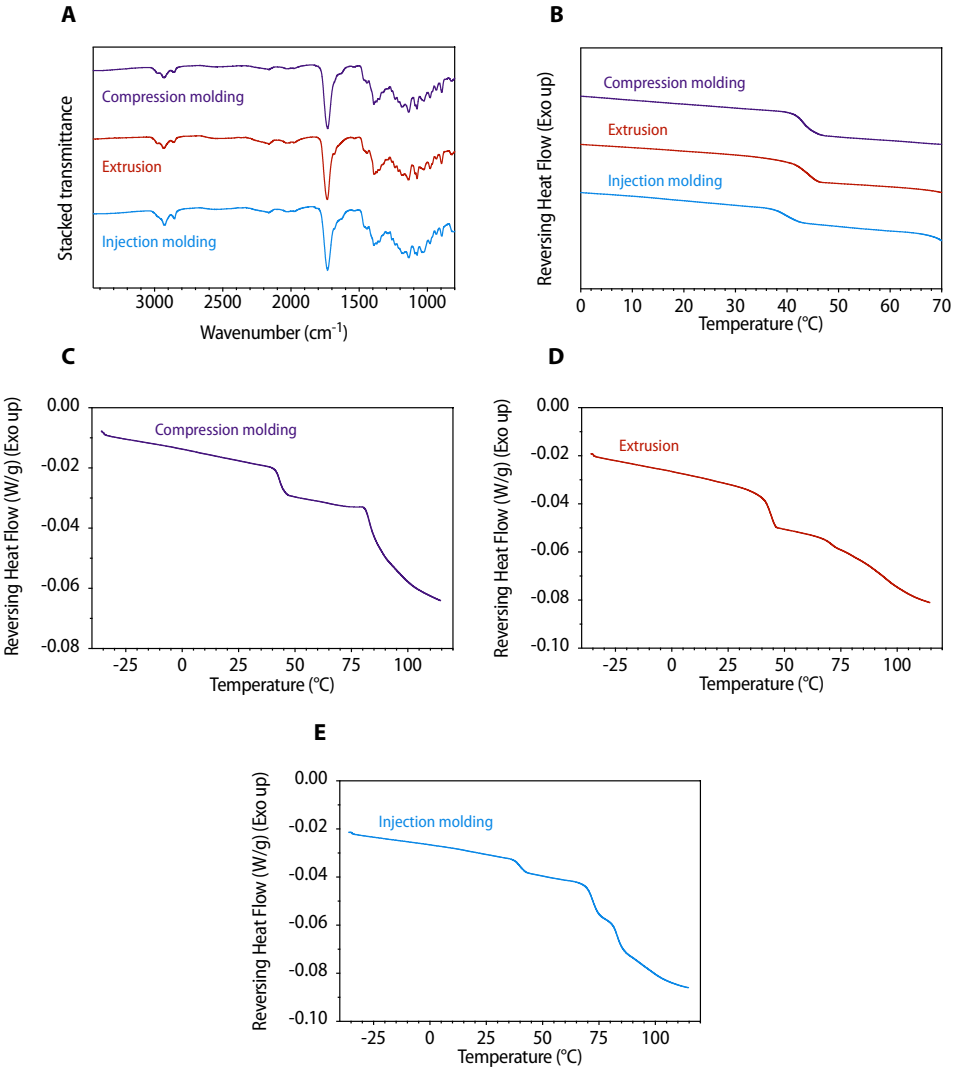

Figure S44 – (A) IR and (B) mDSC analyses of P-HMDA after mechanical recycling using various techniques. Complete DSC curves are provided in (C), (D) and (E). The endothermic phenomenon observed at around 75-80 °C in (C), (D) and (E) is attributed to dissociation within the polymer network.

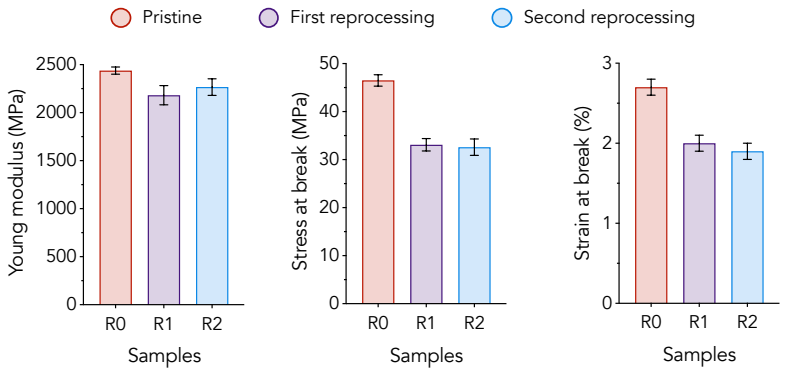

Figure S45 – Evolution of mechanical properties as determined by tensile tests after fracture and reprocessing of samples. R0 is the original material, R1 the material after one fracture and reprocessing, and R2 the material after two fractures and reprocessing.

B. Upcycling

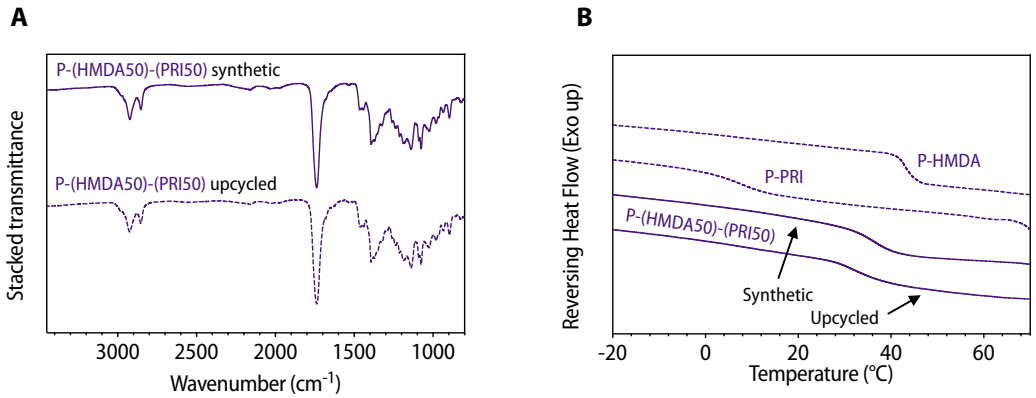

Figure S46 – (A) IR of synthetic and upcycled P-(HMDA50)-(PRI50). (B) mDSC analyses of P-HMDA, P-PRI, synthetic and upcycled P-(HMDA50)-(PRI50).

C. Chemical recycling

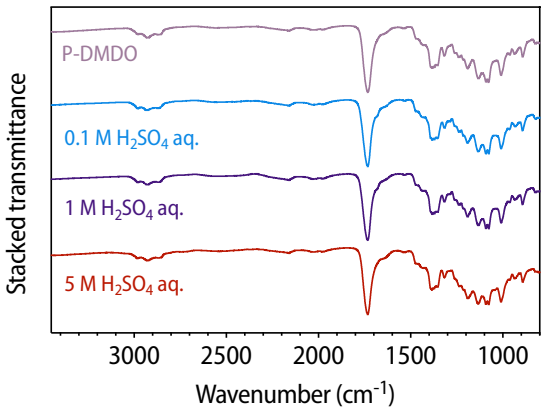

Figure S47 – After immersion of the polymer in H_2SO_4 aqueous solutions of different concentrations, the polymer was washed with water and dried under vacuum. The IR spectra show no difference after immersion in acidic water than the synthesized polymer.

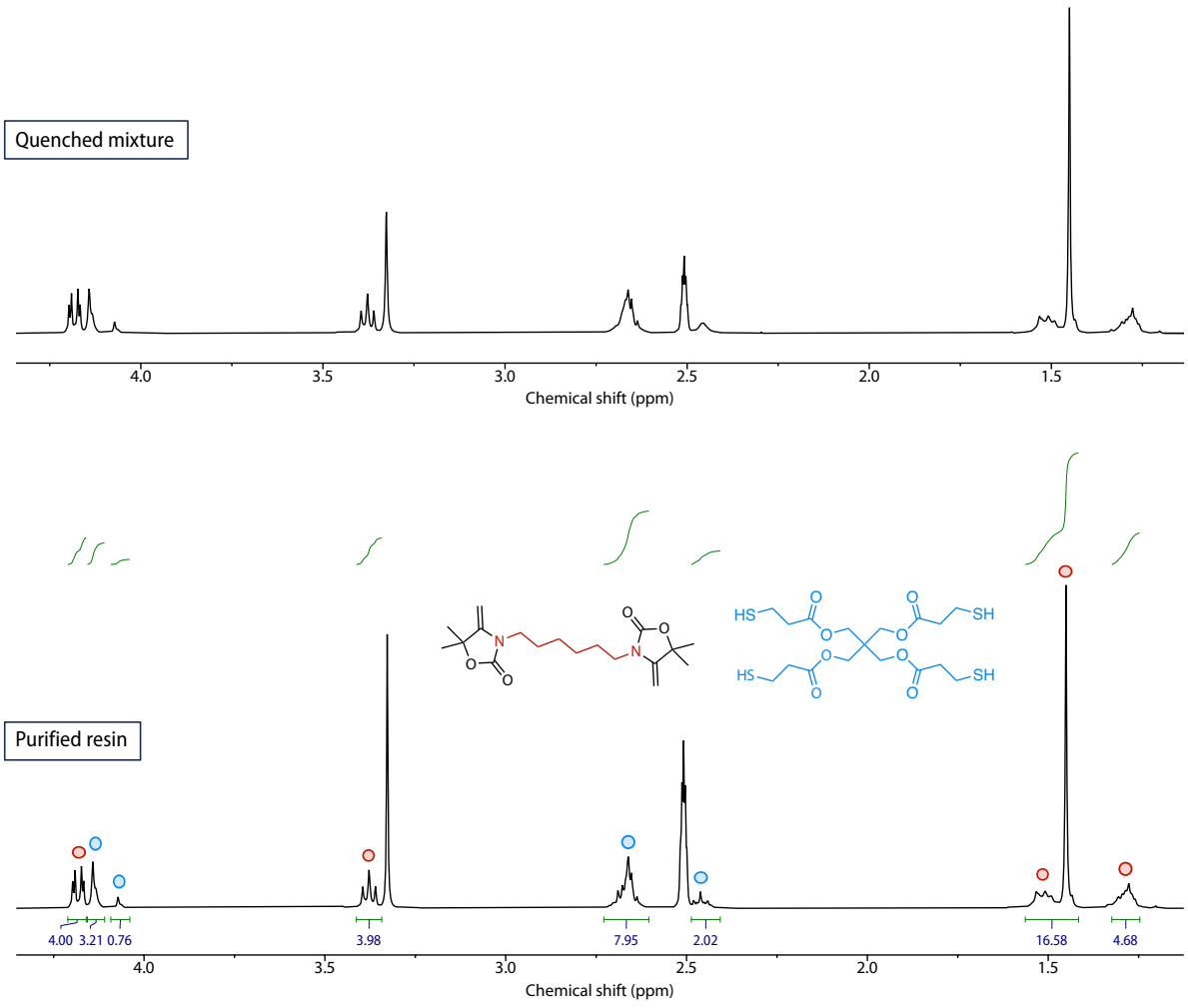

Figure S48 – ^{1}H-NMR spectrum (400 MHz, DMSO-d_6) of the **P-HMDA** resin after depolymerization and quench (top) and work-up (bottom). Integration of the signals shows the presence of the two compounds with functions in equimolar amounts.

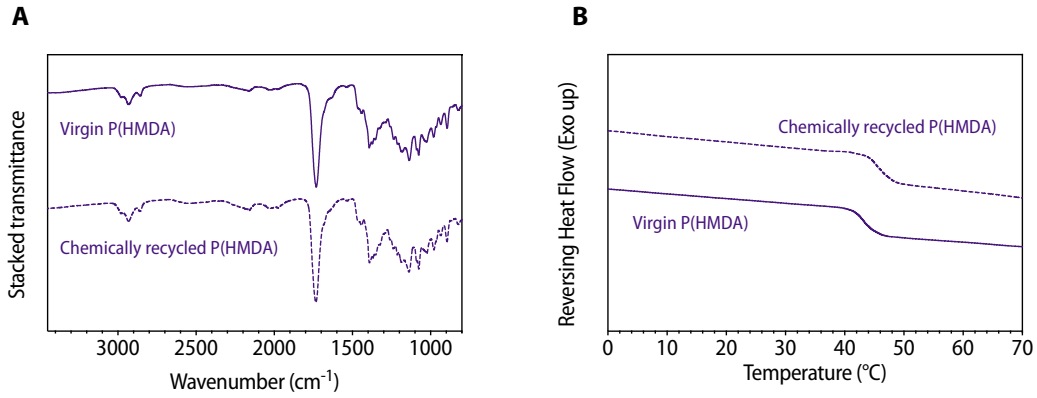

Figure S49 – (A) ATR-IR spectra and (B) mDSC curves of virgin P(HMDA) and the chemically recycled polymer.

12. Composite

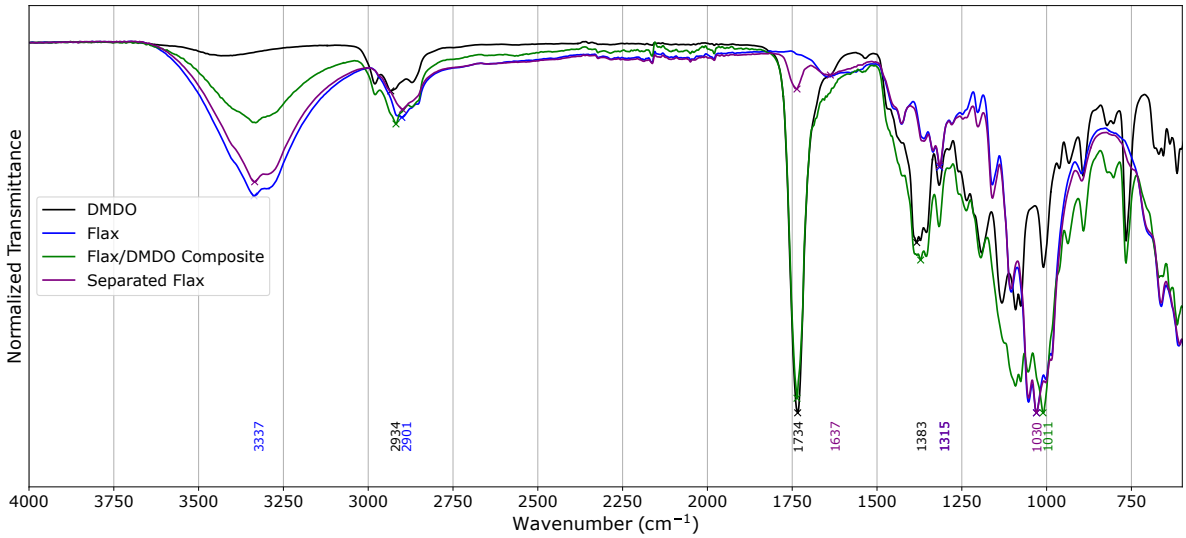

Figure S50 – Stacked ATR-IR spectra of P-DMDO polymer (black) and flax (blue). The Flax-DMDO composite (green) shows contribution of both constitutive components. The separated flax (purple) after dissolution of the polymer in $CHCl_3$ is very similar to the raw flax, with only very low contribution from P-DMDO as highlighted by the band at 1734 cm^{-1}.

13. Solvent resistance

The solvent resistance was assessed for a typical network (P-DMDO). To this aim, swelling ratios (SR) and gel contents (GC) were determined in solvents of very different nature: water as a polar and protic solvent, acetonitrile as a polar and aprotic solvent, THF as a solvent of medium polarity, and hexane as a solvent of low polarity. Chloroform allows for fast reaction kinetics and dissolution of the network (at rt, around 100 mg of P-DMDO in 30 mL of chloroform).

Table S4 – Swelling ratios and gel contents of P-DMDO in various solvents.

Solvent	H_2O	MeCN	THF	$CHCl_3$	Hexane
SR (%)	2.2 ± 0.1	90 ± 5	140 ± 4	soluble	1.1 ± 0.4
GC (%)	98.4 ± 0.4	89.3 ± 1.6	99.0 ± 0.3	soluble	99.8 ± 0.1

14. References

(1) Song, Q.-W.; Chen, W.-Q.; Ma, R.; Yu, A.; Li, Q.-Y.; Chang, Y.; He, L.-N. Bifunctional Silver(I) Complex-Catalyzed CO_2 Conversion at Ambient Conditions: Synthesis of α-Methylene Cyclic Carbonates and Derivatives. *ChemSusChem* **2015**, *8* (5), 821–827. https://doi.org/10.1002/cssc.201402921.

(2) Stewart, J. J. P. Optimization of Parameters for Semiempirical Methods VI: More Modifications to the NDDO Approximations and Re-Optimization of Parameters. *J Mol Model* **2013**, *19* (1), 1–32. https://doi.org/10.1007/s00894-012-1667-x.

(3) James J. P. Stewart. MOPAC2016. http://openmopac.net.

(4) Frisch, M. J.; Trucks, G. W.; Schlegel, H. B.; Scuseria, G. E.; Robb, M. A.; Cheeseman, J. R.; Scalmani, G.; Barone, V.; Petersson, G. A.; Nakatsuji, H.; Li, X.; Caricato, M.; Marenich, A. V.; Bloino, J.; Janesko, B. G.; Gomperts, R.; Mennucci, B.; Hratchian, H. P.; Ortiz, J. V.; Izmaylov, A. F.; Sonnenberg, J. L.; Williams-Young, D.; Ding, F.; Lipparini, F.; Egidi, F.; Goings, J.; Peng, B.; Petrone, A.; Henderson, T.; Ranasinghe, D.; Zakrzewski, V. G.; Gao, J.; Rega, N.; Zheng, G.; Liang, W.; Hada, M.; Ehara, M.; Toyota, K.; Fukuda, R.; Hasegawa, J.; Ishida, M.; Nakajima, T.; Honda, Y.; Kitao, O.; Nakai, H.; Vreven, T.; Throssell, K.; Montgomery, J. A., Jr.; Peralta, J. E.; Ogliaro, F.; Bearpark, M. J.; Heyd, J. J.; Brothers, E. N.; Kudin, K. N.; Staroverov, V. N.; Keith, T. A.; Kobayashi, R.; Normand, J.; Raghavachari, K.; Rendell, A. P.; Burant, J. C.; Iyengar, S. S.; Tomasi, J.; Cossi, M.; Millam, J. M.; Klene, M.; Adamo, C.; Cammi, R.; Ochterski, J. W.; Martin, R. L.; Morokuma, K.; Farkas, O.; Foresman, J. B.; Fox, D. J. Gaussian 16, Revision C.01, 2016.

(5) Chai, J.-D.; Head-Gordon, M. Long-Range Corrected Hybrid Density Functionals with Damped Atom–Atom Dispersion Corrections. *Phys. Chem. Chem. Phys.* **2008**, *10* (44), 6615. https://doi.org/10.1039/b810189b.

(6) Logan, S. R. The Kinetics of Isotopic Exchange Reactions. *J. Chem. Educ.* **1990**, *67* (5), 371. https://doi.org/10.1021/ed067p371.

(7) Van Herck, N.; Maes, D.; Unal, K.; Guerre, M.; Winne, J. M.; Du Prez, F. E. Covalent Adaptable Networks with Tunable Exchange Rates Based on Reversible Thiol–Yne Cross-Linking. *Angew. Chem. Int. Ed.* **2020**, *59* (9), 3609–3617. https://doi.org/10.1002/anie.201912902.

(8) Denissen, W.; Rivero, G.; Nicolaÿ, R.; Leibler, L.; Winne, J. M.; Du Prez, F. E. Vinylogous Urethane Vitrimers. *Adv. Funct. Mater.* **2015**, *25* (16), 2451–2457. https://doi.org/10.1002/adfm.201404553.

(9) Haida, P.; Signorato, G.; Abetz, V. Blended Vinylogous Urethane/Urea Vitrimers Derived from Aromatic Alcohols. *Polym. Chem.* **2022**, *13* (7), 946–958. https://doi.org/10.1039/D1PY01237A.

(10) Christensen, P. R.; Scheuermann, A. M.; Loeffler, K. E.; Helms, B. A. Closed-Loop Recycling of Plastics Enabled by Dynamic Covalent Diketoenamine Bonds. *Nat. Chem.* **2019**, *11* (5), 442–448. https://doi.org/10.1038/s41557-019-0249-2.

(11) Röttger, M.; Domenech, T.; Van Der Weegen, R.; Breuillac, A.; Nicolaÿ, R.; Leibler, L. High-Performance Vitrimers from Commodity Thermoplastics through Dioxaborolane Metathesis. *Science* **2017**, *356* (6333), 62–65. https://doi.org/10.1126/science.aah5281.

(12) Delahaye, M.; Winne, J. M.; Du Prez, F. E. Internal Catalysis in Covalent Adaptable Networks: Phthalate Monoester Transesterification As a Versatile Dynamic Cross-Linking Chemistry. *J. Am. Chem. Soc.* **2019**, *141* (38), 15277–15287. https://doi.org/10.1021/jacs.9b07269.

(13) Houck, H. A.; De Bruycker, K.; Billiet, S.; Dhanis, B.; Goossens, H.; Catak, S.; Van Speybroeck, V.; Winne, J. M.; Du Prez, F. E. Design of a Thermally Controlled Sequence of Triazolinedione-Based Click and Transclick Reactions. *Chem. Sci.* **2017**, *8* (4), 3098–3108. https://doi.org/10.1039/C7SC00119C.

(14) Van Herck, N.; Du Prez, F. E. Fast Healing of Polyurethane Thermosets Using Reversible Triazolinedione Chemistry and Shape-Memory. *Macromolecules* **2018**, *51* (9), 3405–3414. https://doi.org/10.1021/acs.macromol.8b00368.

In Chapter III, the *N,S*-acetal oxazolidone chemistry – previously discovered in chapter II – was studied and showed great promises as a versatile platform for synthesizing easily recyclable poly(oxazolidone)s with highly tunable mechanical properties.

We were intrigued whether other types of cyclic acetal molecules exhibited peculiar reactivity. The DBU-catalyzed reaction between α-alkylidene cyclic carbonates and thiols furnishes cyclic carbonate-co-thioethers possessing a cyclic *S,O*-acetal functionality. The reactivity of these synthons was therefore probed and revealed reactivity in the presence of different nucleophiles (thiols, amines) in different conditions.

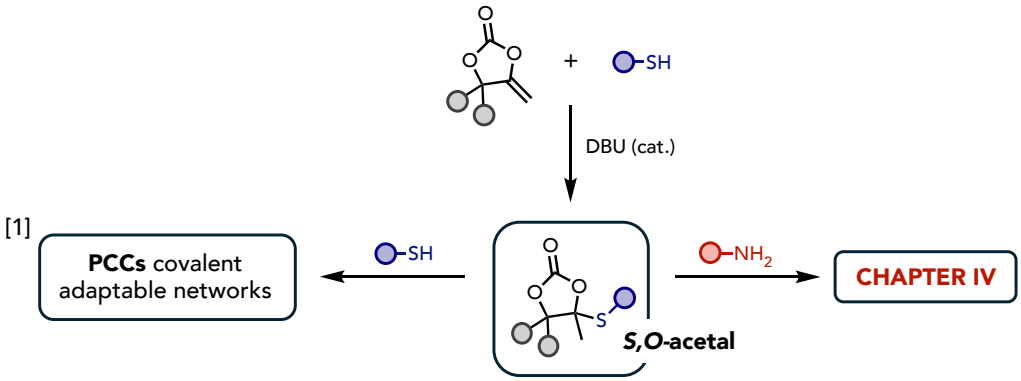

The aminolysis of cyclic carbonate-co-thioethers was studied and applied to the degradation of polymers in Chapter IV. The resulting degradation products were further valorized using the methodology outlined in chapter III. Although not included in this thesis, the thiolysis of cyclic carbonate thioether was explored in a collaborative project as a novel associative dynamic chemistry and evaluated to synthesize recyclable thermosets[1].

(1) Maes, S. ‡; Habets, T. ‡; Fischer, S. M.; Grignard, B.; Detrembleur, C.; Du Prez, F. E. Unprecedented Associative Exchange in CO_2-Sourced Cyclic *S,O*-Acetal-Based Covalent Adaptable Networks. Polym. Chem. 2024, 15 (22), 2296–2307.

Chapter IV

Fast, regioselective aminolysis of tetrasubstituted cyclic carbonates and application to recyclable thermoplastics and thermosets

*Thomas Habets, Raphaël Méreau, Fabiana Siragusa, Bruno Grignard, and Christophe Detrembleur**

Abstract

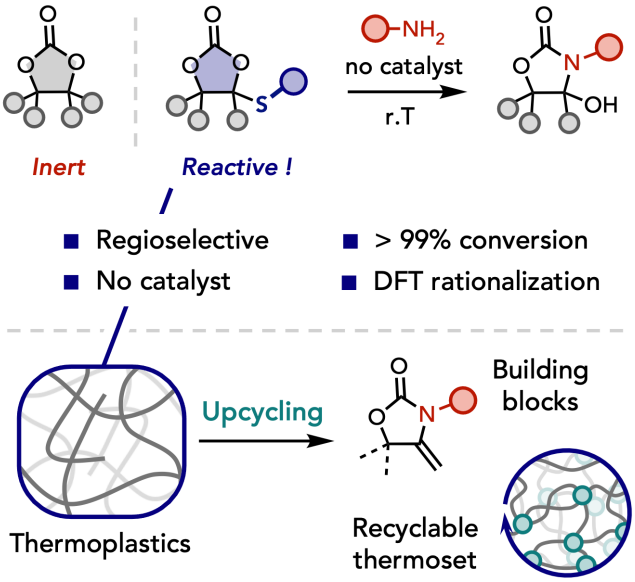

Herein is overcome the long-standing challenge of the ring-opening aminolysis of CO_2-derived tetrasubstituted cyclic carbonates at room temperature (r.T) under catalyst-free conditions. Molecular design of the cyclic carbonate by substitution of an alkyl group by a thioether unlocks quantitative conversion at r.T and ensures total regioselectivity toward highly substituted oxazolidone scaffolds. An in-depth rationalization of the high reactivity of these cyclic carbonate structures and of the aminolysis reaction mechanism is provided by a computational study supporting experimental observations. The high efficiency of the reaction is then translated to the deconstruction of polyolefins-resembling thermoplastics containing tetrasubstituted cyclic carbonate linkages to deliver building blocks that are re-used for designing recyclable thermosets bearing dynamic *N,S*-acetal linkages.

Introduction

Over the last decade, carbon dioxide (CO_2) has found value as a low cost and renewable resource to produce (commodity) chemicals or for designing complex macromolecular architectures[1–4]. Besides its direct copolymerization with epoxides into polycarbonates[2,5–7], CO_2 undergoes catalytic transformations into five-membered cyclic carbonates by coupling with epoxides[8–10] or vicinal alcohols[11–13]. Interestingly, these easily accessible 5-membered scaffolds offer many opportunities of post-modification for fine chemicals[14–16] (e.g. the preparation of carbamates by aminolysis) or serve as monomers in polymers synthesis (e.g. the production of isocyanate-free polyurethanes by copolymerization with polyamines)[17,18]. As most of the cyclic carbonates featured in organic transformations or polymer synthesis predominantly exhibit mono- or di-substitution, their aminolysis delivers two hydroxy-carbamate isomers due to the non-regioselective ring-opening of the cyclic carbonate. Some regioselectivity control is achieved by incorporating electron-withdrawing groups on the cyclic carbonates[19,20]. A full regiocontrol is only observed when introducing fluorine[21] or chlorine[22] atoms, or a neighboring cyclic carbonate with specific stereochemistry[23]. Besides this regioselectivity issue, the cyclic carbonates suffer from a poor reactivity at room temperature (r.T). Their aminolysis is thus accelerated by using catalysts[24,25] or amines of exacerbated reactivity.[26] Another option is to utilize 5-membered cyclic carbonates bearing exovinylene groups that are obtained by coupling CO_2 to propargylic alcohols. This class of highly reactive scaffolds are rapidly ring-opened by various nucleophiles in a regioselective manner, delivering regioregular products at r.T[27–31].

Densely substituted 5-membered cyclic carbonates of high complexity are now made available by various transformation modes of CO_2[32–39]. However, their aminolysis remains a challenge, rarely addressed in the literature. In 2016, Kleij reported the regioselective aminolysis of gem di- and tri-substituted cyclic carbonates at r.T in the presence of a high loading of TBD as organocatalyst (20 mol%)[40] (Scheme 1A). The steric congestion on one side of the cyclic carbonate was proposed to drive the selective bond scission[14,41]. The strategy was also extended to tetra-substituted cyclic carbonates with limited success, the reaction being extremely slow with the formation of side products. In 2018, some of us attempted the aminolysis of tetra-substituted cyclic carbonate-containing polymers using TBD as catalyst at 80 °C, affording only a low degree of conversion (23 %)[42].

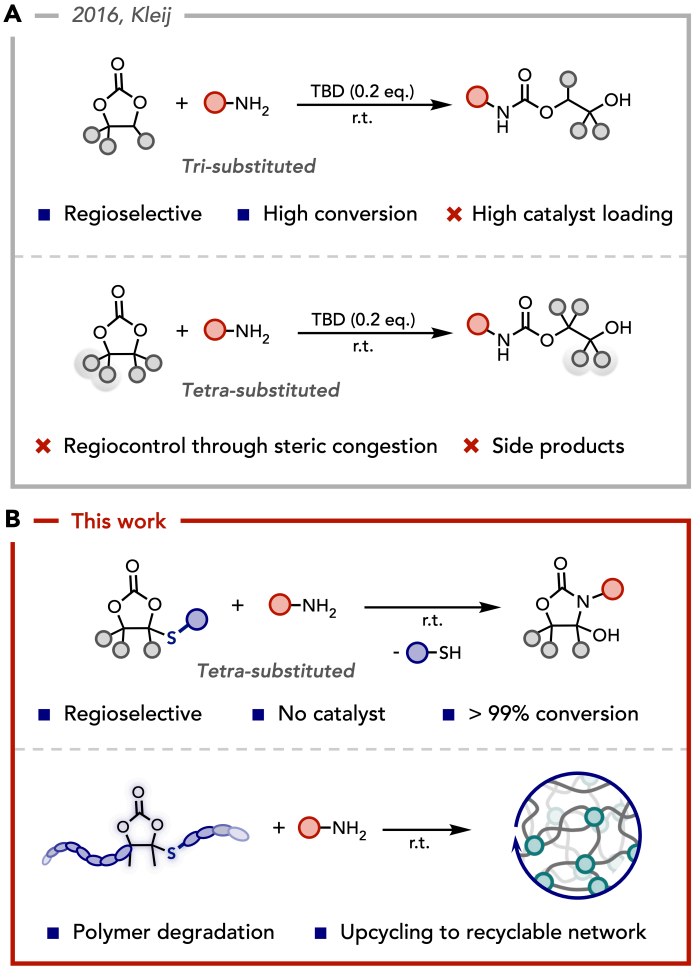

Scheme 1. (A) Prior work on the aminolysis of densely substituted cyclic carbonates[40]. (B) This work: a sulfur substitution strategy for the full, regioselective aminolysis of tetra-substituted cyclic carbonates. The concept was extended to polymer degradation and upcycling into recyclable thermosets.

Herein, we resolve the longstanding challenge of the ring-opening of tetrasubstituted 5-membered cyclic carbonates. Through molecular engineering, we show that replacing an alkyl group of densely substituted ethylene carbonates by a thioether moiety imparts the cyclic compound with unprecedent reactivity, yet enabling their fast and regioselective aminolysis at r.T under catalyst-free conditions (Scheme 1B). This reaction yields a thiol and an oxazolidone, i.e. a five-membered cyclic carbamate template commonly found in bioactive molecules[43–47] and high-performance polyurethanes[48,49]. Then, we showcase the utility of this new chemistry to polymer upcycling. Two thermoplastics embedding tetrasubstituted thioether-containing cyclic carbonate linkages, designed to approach mechanical properties of commodity polyolefins, are depolymerized. In line with the circularity objectives of our modern society, the resulting decomposition products are revalorized into covalent adaptable networks.

Results and discussion

We began our investigations by monitoring the aminolysis of a model conventional tetrasubstituted ethylene carbonate **4CC** with an excess of propylamine (3 eq.) at r.T in DMSO without any catalyst (Figure 1A). No reaction was observed after 24 h. Repeating the reaction at 120 °C left the reactants intact, underlying the inert nature of tetra-alkylated 5-membered cyclic carbonates in these conditions (Figures S9-10). Tetrasubstituted sulfur containing cyclic carbonates **4CCS** (Figure 1A) were then prepared to assess the influence of the substitution of an ethyl group by a thioether on the cyclic carbonate aminolysis. Two **4CCS** compounds were synthesized by the DBU-catalyzed addition of a CO_2-sourced α-alkylidene cyclic carbonate (4,4-dimethyl-5-methylene-1,3-dioxolan-2-one) with benzyl mercaptan (**4CCS-a**) or butanethiol (**4CCS-b**)[29]. Impressively, both compounds reacted quantitatively with propylamine at r.T in DMSO under catalyst-free conditions, in stark contrast to **4CC**. Kinetic insights of the **4CCS** aminolysis were collected by monitoring the reaction under various operating conditions (i.e. type of solvent, content and nature of the amine) by ^{1}H NMR spectroscopy (see SI Section 4 for details). When **4CCS-a** or **4CCS-b** were simply mixed with 3 eq. of propylamine at r.T, reactions were fast, ending in only 2 h (Figure 1A), showing negligible influence of the thioether substituent on the ring-opening. Remarkably, the reactions were selective with the exclusive formation of a hydroxyoxazolidone **1** and a thiol **2**. The reaction performed well in other solvents such as acetonitrile or THF and were complete in 2 h, however with a slightly lower rate than in DMSO (Figure S13).

The propylamine equivalence was found to affect the kinetics as illustrated for the aminolysis of **4CCS-a** (Figure S16). Decreasing the amine content below 3 eq. readily slowed down the reaction. The reaction using 2 eq. of amine was complete within 24 h, while with 1 eq. it became slow with a moderate **4CCS-a** conversion of 70% after 24 h. This was attributed to the quenching of the amine by the released acidic thiol, forming the amine-thiol salt adduct[50]. With 5 eq. of amine, the reaction was strongly accelerated and complete in only 30 min.

The scope of amines was then extended to bulky benzylamine or cyclohexylamine. As expected, the bulky groups on the amine somehow decreased the reaction rate. The reaction with benzylamine at r.T was complete within 24 h, while the reaction with cyclohexylamine reached a conversion of 96% after 24 h (Figure S17).

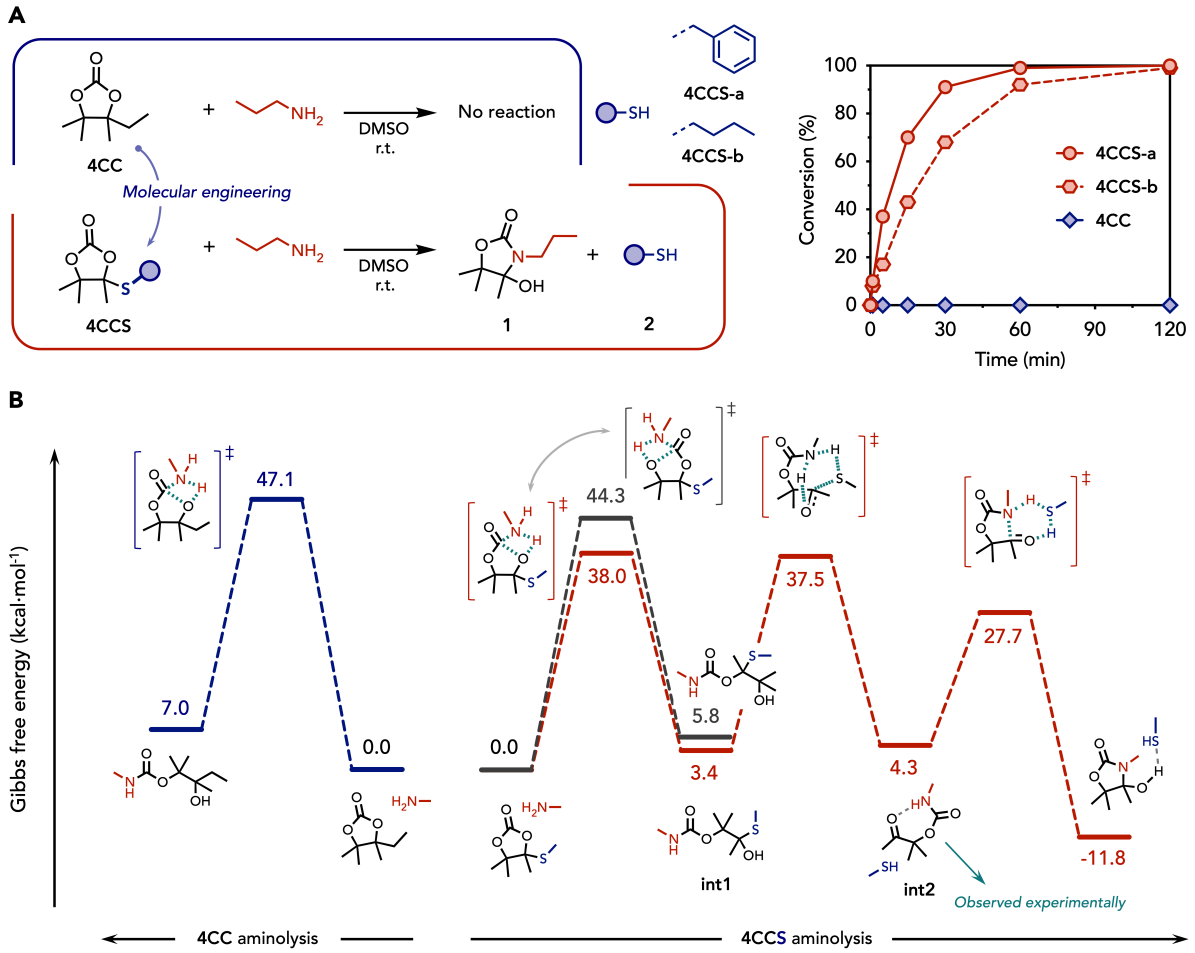

Figure 1. (A) Kinetic study on the aminolysis of **4CC** *vs* **4CCS**. (B) Energetics of the reaction pathways for **4CC** and **4CCS** determined by DFT.

DFT calculations were performed to unveil the increased reactivity of **4CCS** compared to **4CC**. Optimization and comparison of the two cyclic carbonate structures revealed a notable distinction in C-O bond lengths (Figure S22). While both bonds exhibited identical lengths in **4CC** (1.337 Å), the bond length in **4CCS** close to the sulfur atom side exceeded that on the opposite side (1.347 *vs* 1.334 Å). QTAIM and IGM analyses supported this observation, indicating asymmetric bond strength (see SI Section 5.1). Our experimental findings were further complemented by a detailed elucidation of the reaction mechanisms (see SI Sections 5.2-5.3 for details).

The ring-opening of **4CC** by the amine follows a well-established one-step mechanism involving the formation of a carbamate motif and the release of a tertiary alcohol[15,25], although it is thermodynamically disfavored by 7 kcal·mol^{-1} *vs* the reactants (Figure 1B, see Figure S24 for details). A striking difference was observed for **4CCS**, which ring-opening (C-O bond scission near S atom) was characterized by a lower energy barrier of 38.0 kcal·mol^{-1} compared

to 47.1 kcal·mol^{-1} for **4CC** (Figure 1B). Interestingly, the ring-opening on the opposite side of the ring in **4CCS** exhibited a high energy barrier of 44.3 kcal·mol^{-1} and a product destabilization by 5.8 kcal·mol^{-1}, rendering this pathway thermodynamically and kinetically less favorable (Figure S25). This finding strongly supports the regioselective control exerted by the sulfur atom. Unexpectedly, the ring face of attack proved critical, with the amine preferentially approaching near the sulfur atom despite apparent steric hindrance (Figure S27). This is likely attributed to stabilizing interactions between the sulfur's lone pair and the H-N bond of the amine (Figures S28-29).

Aminolysis of **4CCS** proceeds through the addition of the amine onto the electrophilic carbonyl group. Two closely competing pathways can then occur depending on the nature of the concomitant proton transfer. The amine proton is (i) directly transferred to the neighboring oxygen atom, providing a hemithioacetal **int1**. The *oxo*-urethane **int2** is subsequently formed by the release of the thiol (Figure 1B). Alternatively, the amine proton is (ii) transferred to the leaving thiolate with concomitant ketone formation, therefore bypassing the second step of the mechanism to directly afford the *oxo*-urethane **int2** (Figure S30, **TS1'**). The final common step involves ring-closure of **int2** into the hydroxyoxazolidone **1** through intramolecular nucleophilic attack of the -NH- group onto the electrophilic ketone. Interestingly, this step is aided by the thiol acting as a proton relay (Figure S26). The low energy barrier for this step corroborates the experimental observations that the *oxo*-urethane **int2** was experimentally barely detectable by NMR during the reaction kinetics (Figures S11, S15).

Modelling the reaction with a second amine showed that all reaction steps barriers were lowered by several kcal·mol^{-1}, suggesting that multiple amine molecules might participate to the mechanism through proton relay effects (see SI Section 5.4). This supports the experiments showing that the rate of **4CCS** aminolysis was significantly increased when raising the amine content.

Overall, both experimental and computational studies demonstrated the profound impact of the sulfur atom on unlocking both reactivity and regioselectivity in densely substituted cyclic carbonates, without requiring any catalyst.

We then exploited these findings for the preparation of high-performance thermoplastics with controlled degradability, aligning with current sustainability objectives in material science.

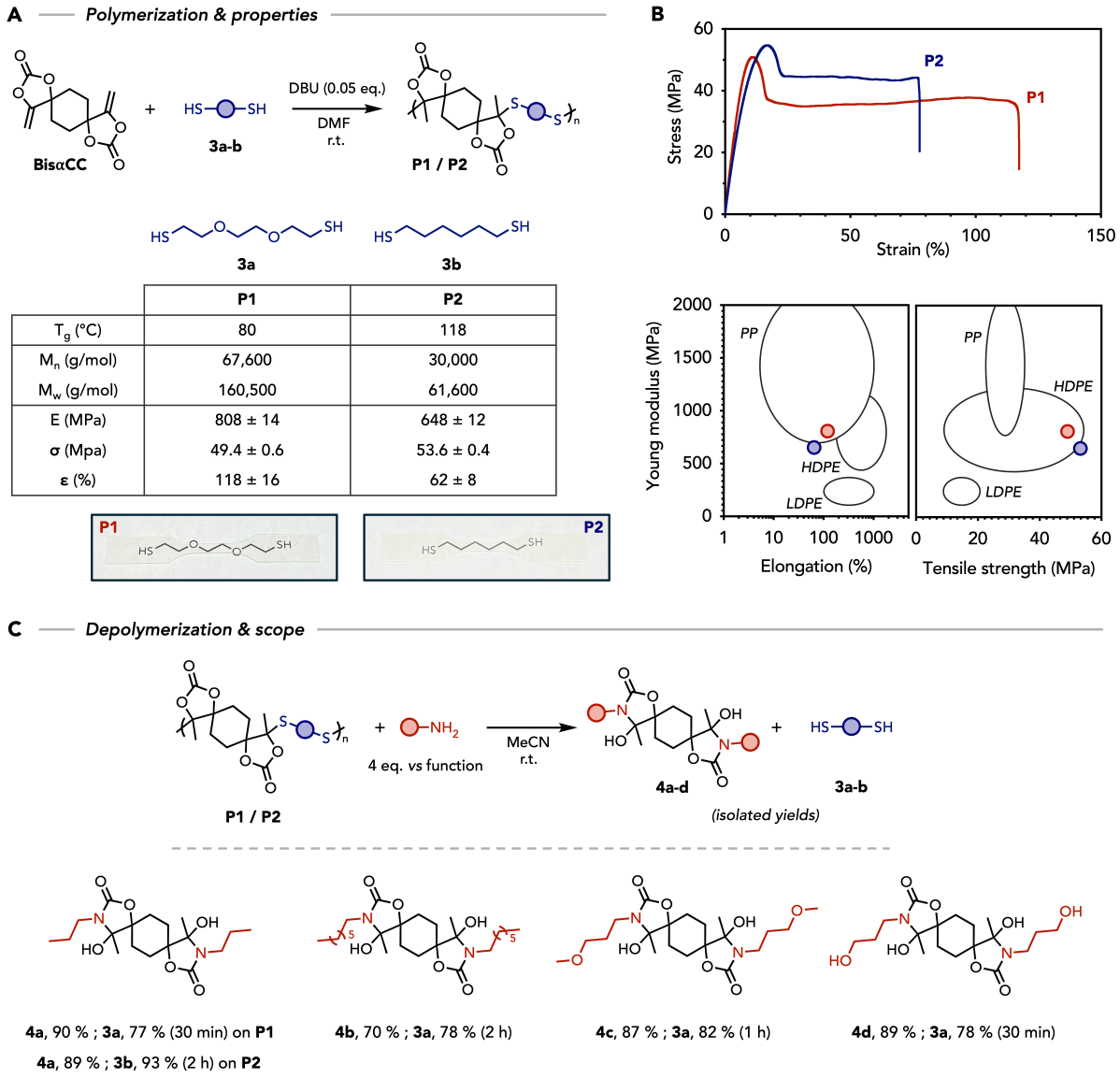

	P1	P2
T_g (°C)	80	118
M_n (g/mol)	67,600	30,000
M_w (g/mol)	160,500	61,600
E (MPa)	808 ± 14	648 ± 12
σ (Mpa)	49.4 ± 0.6	53.6 ± 0.4
ε (%)	118 ± 16	62 ± 8

Figure 2. (A) Synthesis of polymers **P1-2** and (B) their mechanical properties as compared to polyethylene (PE) and polypropylene (PP) using Ashby plots[51]. (C) Depolymerization using a scope of amines to provide **4a-d** and **3a-b**. Isolated yields and reactions time are provided.

Two highly substituted poly(cyclic carbonate-*co*-thioether)s were first synthesized by the r.T, DBU catalyzed step-growth polymerization of a CO_2-sourced spirocyclic bis(exovinylene cyclic carbonate) (**bisαCC**) with dithiols, i.e 2,2′-(Ethylenedioxy)diethanethiol (**3a**) and 1,6-Hexanedithiol (**3b**) (Figure 2a)[27,29,52]. The synthesis protocol was optimized to reach high molecular weight polymers, with the objective to enhance the materials mechanical properties – strongly dependent on macromolecular chain entanglement. At r.T, the high. Concentration of the medium during step-growth polymerization can lead to increased viscosity, preventing

efficient stirring and potentially causing vitrification. This phenomenon prevents the polymers end groups to react at a reasonable rate. To address this issue, we opted for a homemade mechanical stirring setup (Figure S35). After 24 h, the synthesis from **3a** and **3b** delivered polymer **P1 (**M_w = 160,500 g·mol^{-1}) and polymer **P2** (M_w = 61,600 g·mol^{-1}), respectively. When **P1** was synthesized using a traditional magnetic stirring, the high viscosity quickly inhibited efficient stirring and ultimately led to vitrified, resulting in a lower M_w of 84,400 g·mol^{-1}. Polymers **P1** and **P2** were characterized by ^{1}H and ^{13}C NMR, TGA, DSC and SEC (see SI Section 6). Once compression molded as dog bones (120 °C, 6 MT, 15 min for **P1**; 155 °C, 8 MT, 20 min for **P2**), both polymers were amorphous and highly transparent (Figure 2A). Despite their relatively similar chemical structure, they exhibited distinct T_gs, i.e. 80 °C for the more flexible ether-containing **P1** and 118 °C for **P2**. Both polymers were endowed with attractive mechanical properties, somehow lying between those of some grades of commodity HDPE and PP by displaying the low elongation of PP but a typical Young's modulus of HDPE materials (Figure 2B). Their tensile strength was however superior, reaching 53.6 MPa for **P2**. This underlines the potential of **P1** and **P2** to become easily recyclable substitutes to some polyolefins, which are particularly challenging to decompose/revalorize. Indeed, our facile cyclic carbonate aminolysis process was applied with success to the deconstruction of these thermoplastics **P1** and **P2**. For that purpose, **P1** and **P2** underwent total depolymerization at r.T in 30 min to 2 h with an excess of amines (Figure 2C) being either aliphatic (propyl- and heptyl-amine) or functional (3-methoxypropylamine and propanolamine). Bis(hydroxyoxazolidone) **4a-d** and the former dithiols **3a** or **3b** were collected as degradation products and easily isolated in high yields (up to 90% for the oxazolidone **4a-d** and up to 93% for the dithiols). The full characterization of the crude reaction media and the purified products is available in SI (Sections 7-8). It must be noted that the dithiols **3a** and **3b** were successfully recovered by conducting the reaction under inert atmosphere to prevent their oxidation into disulfide.

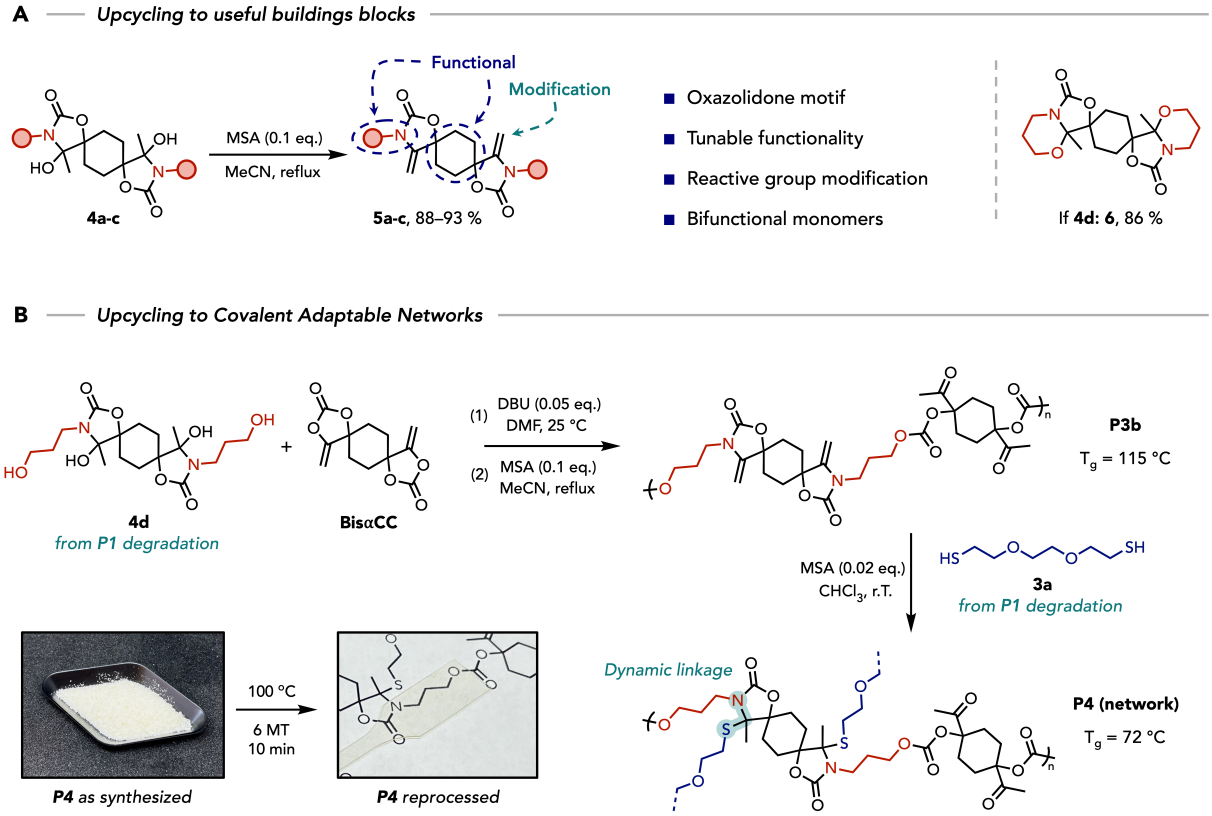

Figure 3 – (A) Dehydration of **4** into useful alkylidene scaffolds **5** and **6** (in the case of **4d**). (B) Upcycling of both **4d** and **3a** into a recyclable thermoset **P4**. **P4** can be reprocessed by compression molding.

On the path to circularity, the revalorization of products **4a-d** and dithiols **3a** and **3b** into new molecules and/or polymeric materials was explored. Previously, we and others established that hydroxy-oxazolidones were easily and quantitatively dehydrated into the corresponding exovinylene oxazolidones[30,49,50]. Following an optimized protocol,[53] products **4a-c** were thus transformed into bis(alkylidene oxazolidone)s **5a-5c** with high isolated yields of 86 to 93% (Figure 3A, Figures S63-68). These compounds **5** are versatile building blocks as they can be finely tuned through the bisαCC structure and the selected amine. They also offer subsequent modification possibilities through the double bond (Figure 3A). The dual functionality of the herein isolated molecules also renders them ideal candidates as monomers. Notably, they can be exploited for the preparation of poly(*N,S*-oxazolidone)s covalent adaptable networks (CANs) by cationic thiol-ene with polythiols.[53] It is important to note that the dehydration of **4d** quantitatively yielded a six-membered cyclic adduct **6** similar to reported five-membered derivatives[54] (Figure 3A, complete characterization in Figures S70-71), likely due to a cascade ring-closure *via* alcohol-ene reaction into a cyclic *N,O*-acetal.

In an effort to repurpose the two post-degradation feedstocks (i.e. the oxazolidone and the thiol), we synthesized a polymer containing alkylidene oxazolidone linkages subsequently cross-linkable by the recovered thiol to obtain a CAN following the strategy described in Figure 3B. The bis(hydroxyoxazolidone) **4d**, containing primary alcohol functions, was reacted with virgin bisαCC to produce poly(hydroxyoxazolidone-*co*-carbonate) **P3a** (M_w = 22,000 g.mol^{-1}; D = 1.7) at r.T in the presence of DBU as catalyst. The polymer was quantitatively dehydrated into the alkylidene analog **P3b** in a cascade one-pot process by refluxing in acetonitrile with methane sulfonic acid as catalyst (MSA; 0.1 eq.) (see SI Section 10 for details). The CAN **P4** featuring dynamic *N,S*-oxazolidone functions was then easily fabricated by the r.T crosslinking of **P3b** with dithiol **3a** via the MSA (2 mol% *vs* oxazolidone functions) catalyzed cationic thiol-ene (see SI Section 11 for the detailed experimental procedure). Following synthesis, the thermoset was reprocessed by compression molding at 100 °C for 10 min (6 MT of pressure) into a uniform transparent film, qualitatively demonstrating its reprocessability (Figure 3B).

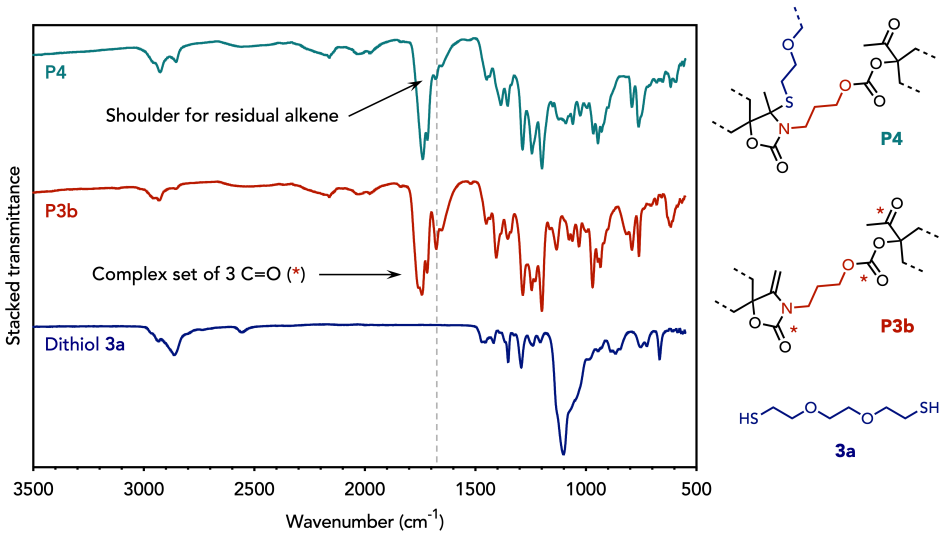

Figure 4 – Stacked ATR-IR spectra of **P4** and its constituting precursors **P3b** and **3a**.

Successful thermoset formation was confirmed by ATR-IR analysis (Figure 4), demonstrating a consumption of most alkene functions – this result is in line with our previous work on *N,S*-acetal CANs. The successful network formation was also confirmed by a high gel content of 98.5 % in THF, and a low swelling ratio (2.5 %). The thermoset exhibited the typical temperature response of highly dissociative dynamic networks with a loss of cross-link density above T_g (72 °C) and a flow transition at 129 °C ($T_{gel\text{-}to\text{-}sol}$) as determined by a temperature sweep experiment (Figure 5A and Figure S77)[55–57]. Stress relaxation experiments were performed to quantitatively assess the timescale over which **P4** can relax an applied stress through dynamic bonds reorganization. An initial experiment at 90 °C demonstrated that the

data does not conform to widely used models such as the single element Maxwell model. However, we found that two more sophisticated models accurately describe the relaxation behavior: the three-element Maxwell model and the double stretched exponential model – the first was used to describe the *N,S*-acetal CANs in Chapter III while the latter was recently employed by Torkelson & coworkers[58] (Figure 5B). The raw data was fitted to both models and relaxation times were extracted at each temperature. The short network reprocessing time (10 min at 100 °C) was consistent with the very short relaxation times (from around 2 min at 90 °C to few seconds at 125 °C; Figure 5C), aligning with our previous work on *N,S*-oxazolidone CANs[53]. Arrhenius plots were built from the extracted characteristic relaxation times and flow energies of activation (E_{flow}) were determined for each of the two models. The values were very similar (31.3 and 31.6 kcal·mol^{-1}) and fell within the range of previously determined values for *N,S*-acetal polymer networks (26.4 to 38.8 kcal·mol^{-1}). The detailed methodology for the characterization of **P4** and the determination of E_{flow} is found in SI Section 11.

The mechanical properties were typical of highly cross-linked networks with a brittle fracture, and **P4** was characterized by Youngs' modulus and strength that were similar to **P1**/**P2** (Figure 5D).

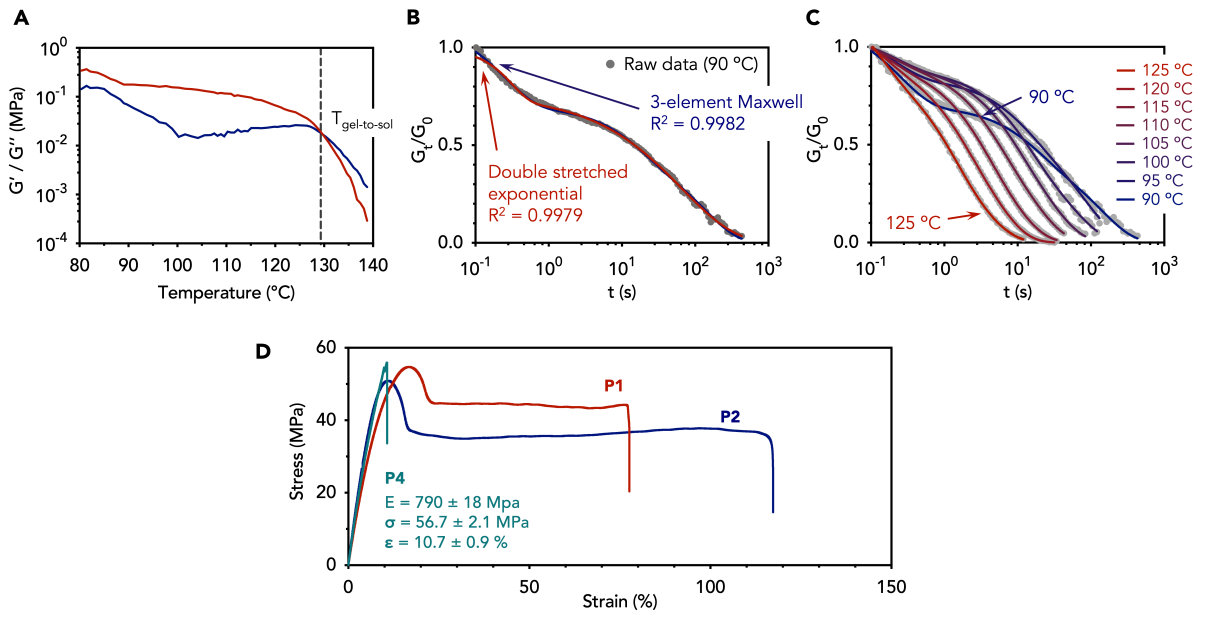

Figure 5 – (A) Temperature sweep of **P4** by rheology revealing a flow transition. (B) Raw stress relaxation data at 90 °C and fit curves using a three-element Maxwell model and a double stretched exponential model. (C) The stress relaxation data at all temperatures fitted to the three-element Maxwell model. (D) Mechanical properties of **P4** in comparison to **P1** and **P2**.

Conclusion

In summary, we developed a facile, regioselective ring-opening aminolysis of CO_2-sourced tetrasubstituted cyclic carbonates at room temperature under catalyst-free conditions. Substitution of the ring with a sulfur atom not only enhanced the reactivity of the tetrasubstituted ethylene carbonate, but also ensured full regioselectivity in the ring-opening, yielding highly substituted oxazolidones. A thorough modelling study confirmed the significant impact of the sulfur atom on the chemical structure of the tetrasubstituted cyclic carbonate and unveiled the ring-opening mechanisms along with their energetics. This concept was applied to the degradation of polyolefins-resembling thermoplastics embedding tetrasubstituted cyclic carbonate linkages, delivering oxazolidone scaffolds and thiols that were then reused in an open recycling loop for the facile construction of reprocessable covalent adaptable thermosets with dynamic *N,S*-acetal linkages. Besides opening many perspectives for the preparation of new organic synthons of the oxazolidone-type, this novel aminolysis process establishes as a new strategy to open highly substituted scaffolds and reinforces the importance of molecular design in achieving efficient and selective chemical transformations, of particular interest in organic and polymer chemistry.

References

(1) Liu, Q.; Wu, L.; Jackstell, R.; Beller, M. Using Carbon Dioxide as a Building Block in Organic Synthesis. *Nat Commun* **2015**, *6* (1), 5933. https://doi.org/10.1038/ncomms6933.

(2) Grignard, B.; Gennen, S.; Jérôme, C.; Kleij, A. W.; Detrembleur, C. Advances in the Use of CO_2 as a Renewable Feedstock for the Synthesis of Polymers. *Chem. Soc. Rev.* **2019**, *48* (16), 4466–4514. https://doi.org/10.1039/C9CS00047J.

(3) Dabral, S.; Schaub, T. The Use of Carbon Dioxide (CO_2) as a Building Block in Organic Synthesis from an Industrial Perspective. *Adv Synth Catal* **2019**, *361* (2), 223–246. https://doi.org/10.1002/adsc.201801215.

(4) Vidal, F.; Van Der Marel, E. R.; Kerr, R. W. F.; McElroy, C.; Schroeder, N.; Mitchell, C.; Rosetto, G.; Chen, T. T. D.; Bailey, R. M.; Hepburn, C.; Redgwell, C.; Williams, C. K. Designing a Circular Carbon and Plastics Economy for a Sustainable Future. *Nature* **2024**, *626* (7997), 45–57. https://doi.org/10.1038/s41586-023-06939-z.

(5) Siragusa, F.; Detrembleur, C.; Grignard, B. The Advent of Recyclable CO_2 -Based Polycarbonates. *Polym. Chem.* **2023**, *14* (11), 1164–1183. https://doi.org/10.1039/D2PY01258H.

(6) Rosetto, G.; Vidal, F.; McGuire, T. M.; Kerr, R. W. F.; Williams, C. K. High Molar Mass Polycarbonates as Closed-Loop Recyclable Thermoplastics. *J. Am. Chem. Soc.* **2024**, *146* (12), 8381–8393. https://doi.org/10.1021/jacs.3c14170.

(7) Bhat, G. A.; Darensbourg, D. J. Progress in the Catalytic Reactions of CO_2 and Epoxides to Selectively Provide Cyclic or Polymeric Carbonates. *Green Chem.* **2022**, *24* (13), 5007–5034. https://doi.org/10.1039/D2GC01422J.

(8) Cokoja, M.; Wilhelm, M. E.; Anthofer, M. H.; Herrmann, W. A.; Kühn, F. E. Synthesis of Cyclic Carbonates from Epoxides and Carbon Dioxide by Using Organocatalysts. *ChemSusChem* **2015**, *8* (15), 2436–2454. https://doi.org/10.1002/cssc.201500161.

(9) Guo, L.; Lamb, K. J.; North, M. Recent Developments in Organocatalysed Transformations of Epoxides and Carbon Dioxide into Cyclic Carbonates. *Green Chem.* **2021**, *23* (1), 77–118. https://doi.org/10.1039/D0GC03465G.

(10) Martín, C.; Fiorani, G.; Kleij, A. W. Recent Advances in the Catalytic Preparation of Cyclic Organic Carbonates. *ACS Catal.* **2015**, *5* (2), 1353–1370. https://doi.org/10.1021/cs5018997.

(11) Tamura, M.; Honda, M.; Nakagawa, Y.; Tomishige, K. Direct Conversion of CO_2 with Diols, Aminoalcohols and Diamines to Cyclic Carbonates, Cyclic Carbamates and Cyclic Ureas Using Heterogeneous Catalysts. *J of Chemical Tech & Biotech* **2014**, *89* (1), 19–33. https://doi.org/10.1002/jctb.4209.

(12) Honda, M.; Tamura, M.; Nakao, K.; Suzuki, K.; Nakagawa, Y.; Tomishige, K. Direct Cyclic Carbonate Synthesis from CO_2 and Diol over Carboxylation/Hydration Cascade Catalyst of CeO_2 with 2-Cyanopyridine. *ACS Catal.* **2014**, *4* (6), 1893–1896. https://doi.org/10.1021/cs500301d.

(13) Kindermann, N.; Jose, T.; Kleij, A. W. Synthesis of Carbonates from Alcohols and CO2. *Top Curr Chem (Z)* **2017**, *375* (1), 15. https://doi.org/10.1007/s41061-016-0101-8.

(14) Guo, W.; Gómez, J. E.; Cristòfol, À.; Xie, J.; Kleij, A. W. Catalytic Transformations of Functionalized Cyclic Organic Carbonates. *Angew Chem Int Ed* **2018**, *57* (42), 13735–13747. https://doi.org/10.1002/anie.201805009.

(15) Guo, W.; Gónzalez-Fabra, J.; Bandeira, N. A. G.; Bo, C.; Kleij, A. W. A Metal-Free Synthesis of N-Aryl Carbamates under Ambient Conditions. *Angew Chem Int Ed* **2015**, *54* (40), 11686–11690. https://doi.org/10.1002/anie.201504956.

(16) Ni, J.; Lanzi, M.; Kleij, A. W. Unusual DBU-Catalyzed Decarboxylative Formation of Allylic Thioethers from Vinyl Cyclic Carbonates and Thiols. *Org. Chem. Front.* **2022**, *9* (24), 6780–6785. https://doi.org/10.1039/D2QO01511K.

(17) Lanzi, M.; Kleij, A. W. Recent Advances in the Synthesis and Polymerization of New CO_2 -Based Cyclic †. *Chin. J. Chem.* **2024**, *42* (4), 430–443. https://doi.org/10.1002/cjoc.202300502.

(18) Maisonneuve, L.; Lamarzelle, O.; Rix, E.; Grau, E.; Cramail, H. Isocyanate-Free Routes to Polyurethanes and Poly(Hydroxy Urethane)s. *Chem. Rev.* **2015**, *115* (22), 12407–12439. https://doi.org/10.1021/acs.chemrev.5b00355.

(19) Lamarzelle, O.; Hibert, G.; Lecommandoux, S.; Grau, E.; Cramail, H. A Thioglycerol Route to Bio-Based Bis-Cyclic Carbonates: Poly(Hydroxyurethane) Preparation and Post-Functionalization. *Polym. Chem.* **2017**, *8* (22), 3438–3447. https://doi.org/10.1039/C7PY00556C.

(20) Cornille, A.; Blain, M.; Auvergne, R.; Andrioletti, B.; Boutevin, B.; Caillol, S. A Study of Cyclic Carbonate Aminolysis at Room Temperature: Effect of Cyclic Carbonate Structures and Solvents on Polyhydroxyurethane Synthesis. *Polym. Chem.* **2017**, *8* (3), 592–604. https://doi.org/10.1039/C6PY01854H.

(21) Tomita, H.; Sanda, F.; Endo, T. Model Reaction for the Synthesis of Polyhydroxyurethanes from Cyclic Carbonates with Amines: Substituent Effect on the Reactivity and Selectivity of Ring-opening Direction in the Reaction of Five-membered Cyclic Carbonates with Amine. *J. Polym. Sci. A Polym. Chem.* **2001**, *39* (21), 3678–3685. https://doi.org/10.1002/pola.10009.

(22) Ochiai, B.; Koda, K.; Endo, T. Branched Cationic Polyurethane Prepared by Polyaddition of Chloromethylated Five-membered Cyclic Carbonate and Diethylenetriamine in

Molten Salts. *J. Polym. Sci. A Polym. Chem.* **2012**, *50* (1), 47–51. https://doi.org/10.1002/pola.24969.

(23) Salvado, V.; Dolatkhani, M.; Grau, É.; Vidil, T.; Cramail, H. Sequence-Controlled Polyhydroxyurethanes with Tunable Regioregularity Obtained from Sugar-Based Vicinal Bis-Cyclic Carbonates. *Macromolecules* **2022**, *55* (16), 7249–7264. https://doi.org/10.1021/acs.macromol.2c01112.

(24) Blain, M.; Jean-Gérard, L.; Auvergne, R.; Benazet, D.; Caillol, S.; Andrioletti, B. Rational Investigations in the Ring Opening of Cyclic Carbonates by Amines. *Green Chem.* **2014**, *16* (9), 4286–4291. https://doi.org/10.1039/C4GC01032A.

(25) Alves, M.; Méreau, R.; Grignard, B.; Detrembleur, C.; Jérôme, C.; Tassaing, T. DFT Investigation of the Reaction Mechanism for the Guanidine Catalysed Ring-Opening of Cyclic Carbonates by Aromatic and Alkyl-Amines. *RSC Adv.* **2017**, *7* (31), 18993–19001. https://doi.org/10.1039/C7RA00220C.

(26) Quienne, B.; Poli, R.; Pinaud, J.; Caillol, S. Enhanced Aminolysis of Cyclic Carbonates by β-Hydroxylamines for the Production of Fully Biobased Polyhydroxyurethanes. *Green Chem.* **2021**, *23* (4), 1678–1690. https://doi.org/10.1039/D0GC04120C.

(27) Ngassam Tounzoua, C.; Grignard, B.; Detrembleur, C. Exovinylene Cyclic Carbonates: Multifaceted CO_2-Based Building Blocks for Modern Chemistry and Polymer Science. *Angew Chem Int Ed* **2022**, *61* (22), e202116066. https://doi.org/10.1002/anie.202116066.

(28) Gennen, S.; Grignard, B.; Tassaing, T.; Jérôme, C.; Detrembleur, C. CO_2-Sourced α-Alkylidene Cyclic Carbonates: A Step Forward in the Quest for Functional Regioregular Poly(Urethane)s and Poly(Carbonate)s. *Angew. Chem. Int. Ed.* **2017**, *56* (35), 10394–10398. https://doi.org/10.1002/anie.201704467.

(29) Ouhib, F.; Grignard, B.; Van Den Broeck, E.; Luxen, A.; Robeyns, K.; Van Speybroeck, V.; Jerome, C.; Detrembleur, C. A Switchable Domino Process for the Construction of Novel CO_2-Sourced Sulfur-Containing Building Blocks and Polymers. *Angew. Chem. Int. Ed.* **2019**, *58* (34), 11768–11773. https://doi.org/10.1002/anie.201905969.

(30) Wong, A. R.; Barrera, M.; Pal, A.; Lamb, J. R. Improved Characterization of Polyoxazolidinones by Incorporating Solubilizing Side Chains. *Macromolecules* **2022**, *55* (24), 11006–11012. https://doi.org/10.1021/acs.macromol.2c02104.

(31) Dabral, S.; Licht, U.; Rudolf, P.; Bollmann, G.; Hashmi, A. S. K.; Schaub, T. Synthesis and Polymerisation of α-Alkylidene Cyclic Carbonates from Carbon Dioxide, Epoxides and the Primary Propargylic Alcohol 1,4-Butynediol. *Green Chem.* **2020**, *22* (5), 1553–1558. https://doi.org/10.1039/C9GC04320A.

(32) Li, X.; Villar-Yanez, A.; Ngassam Tounzoua, C.; Benet-Buchholz, J.; Grignard, B.; Bo, C.; Detrembleur, C.; Kleij, A. W. Cascade Transformation of Carbon Dioxide and Alkyne-1, *n* -

Diols into Densely Substituted Cyclic Carbonates. *ACS Catal.* **2022**, *12* (5), 2854–2860. https://doi.org/10.1021/acscatal.1c05773.

(33) Laserna, V.; Martin, E.; Escudero-Adán, E. C.; Kleij, A. W. Substrate-Triggered Stereoselective Preparation of Highly Substituted Organic Carbonates. *ACS Catal.* **2017**, *7* (8), 5478–5482. https://doi.org/10.1021/acscatal.7b01748.

(34) Sopeña, S.; Cozzolino, M.; Maquilón, C.; Escudero-Adán, E. C.; Martínez Belmonte, M.; Kleij, A. W. Organocatalyzed Domino [3+2] Cycloaddition/Payne-Type Rearrangement Using Carbon Dioxide and Epoxy Alcohols. *Angew Chem Int Ed* **2018**, *57* (35), 11203–11207. https://doi.org/10.1002/anie.201803967.

(35) Longwitz, L.; Steinbauer, J.; Spannenberg, A.; Werner, T. Calcium-Based Catalytic System for the Synthesis of Bio-Derived Cyclic Carbonates under Mild Conditions. *ACS Catal.* **2018**, *8* (1), 665–672. https://doi.org/10.1021/acscatal.7b03367.

(36) Martínez, J.; Fernández-Baeza, J.; Sánchez-Barba, L. F.; Castro-Osma, J. A.; Lara-Sánchez, A.; Otero, A. An Efficient and Versatile Lanthanum Heteroscorpionate Catalyst for Carbon Dioxide Fixation into Cyclic Carbonates. *ChemSusChem* **2017**, *10* (14), 2886–2890. https://doi.org/10.1002/cssc.201700898.

(37) Fiorani, G.; Stuck, M.; Martín, C.; Belmonte, M. M.; Martin, E.; Escudero-Adán, E. C.; Kleij, A. W. Catalytic Coupling of Carbon Dioxide with Terpene Scaffolds: Access to Challenging Bio-Based Organic Carbonates. *ChemSusChem* **2016**, *9* (11), 1304–1311. https://doi.org/10.1002/cssc.201600238.

(38) Rintjema, J.; Epping, R.; Fiorani, G.; Martín, E.; Escudero-Adán, E. C.; Kleij, A. W. Substrate-Controlled Product Divergence: Conversion of CO_2 into Heterocyclic Products. *Angew Chem Int Ed* **2016**, *55* (12), 3972–3976. https://doi.org/10.1002/anie.201511521.

(39) Maeda, C.; Shimonishi, J.; Miyazaki, R.; Hasegawa, J.; Ema, T. Highly Active and Robust Metalloporphyrin Catalysts for the Synthesis of Cyclic Carbonates from a Broad Range of Epoxides and Carbon Dioxide. *Chemistry A European J* **2016**, *22* (19), 6556–6563. https://doi.org/10.1002/chem.201600164.

(40) Sopeña, S.; Laserna, V.; Guo, W.; Martin, E.; Escudero-Adán, E. C.; Kleij, A. W. Regioselective Organocatalytic Formation of Carbamates from Substituted Cyclic Carbonates. *Adv Synth Catal* **2016**, *358* (13), 2172–2178. https://doi.org/10.1002/adsc.201600290.

(41) De La Cruz-Martínez, F.; Francés-Poveda, E.; North, M.; Castro-Osma, J. A.; Lara-Sánchez, A. Base-Catalyzed Highly Regioselective Synthesis of Bio-Based Hydroxyurethanes. *Eur J Org Chem* **2024**, e202400275. https://doi.org/10.1002/ejoc.202400275.

(42) Scholten, P. B. V.; Demarteau, J.; Gennen, S.; De Winter, J.; Grignard, B.; Debuigne, A.; Meier, M. A. R.; Detrembleur, C. Merging CO_2-Based Building Blocks with Cobalt-Mediated

Radical Polymerization for the Synthesis of Functional Poly(Vinyl Alcohol)s. *Macromolecules* **2018**, *51* (9), 3379–3393. https://doi.org/10.1021/acs.macromol.8b00492.

(43) Chiu, S.-K.; Keifer, L.; Timberlake, J. W. Synthesis of Imidazolidinediones and Oxazolidinediones from Cyclization of Propargylureas and Propargyl Carbamates. *J. Med. Chem.* **1979**, *22* (6), 746–748. https://doi.org/10.1021/jm00192a026.

(44) Jo, Y. W.; Im, W. B.; Rhee, J. K.; Shim, M. J.; Kim, W. B.; Choi, E. C. Synthesis and Antibacterial Activity of Oxazolidinones Containing Pyridine Substituted with Heteroaromatic Ring. *Bioorganic & Medicinal Chemistry* **2004**, *12* (22), 5909–5915. https://doi.org/10.1016/j.bmc.2004.08.025.

(45) Fernandes, G. F. S.; Scarim, C. B.; Kim, S.-H.; Wu, J.; Castagnolo, D. Oxazolidinones as Versatile Scaffolds in Medicinal Chemistry. *RSC Med. Chem.* **2023**, *14* (5), 823–847. https://doi.org/10.1039/D2MD00415A.

(46) Armentano, B.; Curcio, R.; Brindisi, M.; Mancuso, R.; Rago, V.; Ziccarelli, I.; Frattaruolo, L.; Fiorillo, M.; Dolce, V.; Gabriele, B.; Cappello, A. R. 5-(Carbamoylmethylene)-Oxazolidin-2-Ones as a Promising Class of Heterocycles Inducing Apoptosis Triggered by Increased ROS Levels and Mitochondrial Dysfunction in Breast and Cervical Cancer. *Biomedicines* **2020**, *8* (2), 35. https://doi.org/10.3390/biomedicines8020035.

(47) Pathania, S.; Petrova-Szczasiuk, K.; Pentikäinen, O.; Singh, P. K. Oxazolidinones: Are They Only Good for the Discovery of Antibiotics? A Worm's Eye View. *Journal of Molecular Structure* **2023**, *1286*, 135630. https://doi.org/10.1016/j.molstruc.2023.135630.

(48) Altmann, H. J.; Clauss, M.; König, S.; Frick-Delaittre, E.; Koopmans, C.; Wolf, A.; Guertler, C.; Naumann, S.; Buchmeiser, M. R. Synthesis of Linear Poly(Oxazolidin-2-One)s by Cooperative Catalysis Based on *N* -Heterocyclic Carbenes and Simple Lewis Acids. *Macromolecules* **2019**, *52* (2), 487–494. https://doi.org/10.1021/acs.macromol.8b02403.

(49) Habets, T.; Siragusa, F.; Grignard, B.; Detrembleur, C. Advancing the Synthesis of Isocyanate-Free Poly(Oxazolidones)s: Scope and Limitations. *Macromolecules* **2020**, *53* (15), 6396–6408. https://doi.org/10.1021/acs.macromol.0c01231.

(50) Habets, T.; Siragusa, F.; Müller, A. J.; Grossman, Q.; Ruffoni, D.; Grignard, B.; Detrembleur, C. Facile Construction of Functional Poly(Monothiocarbonate) Copolymers under Mild Operating Conditions. *Polym. Chem.* **2022**, *13* (21), 3076–3090. https://doi.org/10.1039/D2PY00307D.

(51) Lin, S.-K. Handbook of Polymers. By George Wypych, ChemTec Publishing, 2012; 680 Pages. Price $395.00, ISBN 978-1-895198-47-8. *Polymers* **2013**, *5* (1), 225–233. https://doi.org/10.3390/polym5010225.

(52) Ouhib, F.; Meabe, L.; Mahmoud, A.; Grignard, B.; Thomassin, J.-M.; Boschini, F.; Zhu, H.; Forsyth, M.; Mecerreyes, D.; Detrembleur, C. Influence of the Cyclic versus Linear

Carbonate Segments in the Properties and Performance of CO_2 -Sourced Polymer Electrolytes for Lithium Batteries. *ACS Appl. Polym. Mater.* **2020**, *2* (2), 922–931. https://doi.org/10.1021/acsapm.9b01130.

(53) Habets, T.; Seychal, G.; Caliari, M.; Raquez, J.-M.; Sardon, H.; Grignard, B.; Detrembleur, C. Covalent Adaptable Networks through Dynamic *N* , *S* -Acetal Chemistry: Toward Recyclable CO_2 -Based Thermosets. *J. Am. Chem. Soc.* **2023**, *145* (46), 25450–25462. https://doi.org/10.1021/jacs.3c10080.

(54) Song, Q.-W.; Yu, B.; Li, X.-D.; Ma, R.; Diao, Z.-F.; Li, R.-G.; Li, W.; He, L.-N. Efficient Chemical Fixation of CO2 Promoted by a Bifunctional Ag2WO4/Ph3P System. *Green Chem.* **2014**, *16* (3), 1633. https://doi.org/10.1039/c3gc42406e.

(55) Elling, B. R.; Dichtel, W. R. Reprocessable Cross-Linked Polymer Networks: Are Associative Exchange Mechanisms Desirable? *ACS Cent. Sci.* **2020**, *6* (9), 1488–1496. https://doi.org/10.1021/acscentsci.0c00567.

(56) Scheutz, G. M.; Lessard, J. J.; Sims, M. B.; Sumerlin, B. S. Adaptable Crosslinks in Polymeric Materials: Resolving the Intersection of Thermoplastics and Thermosets. *J. Am. Chem. Soc.* **2019**, *141* (41), 16181–16196. https://doi.org/10.1021/jacs.9b07922.

(57) Denissen, W.; Winne, J. M.; Du Prez, F. E. Vitrimers: Permanent Organic Networks with Glass-like Fluidity. *Chem. Sci.* **2016**, *7* (1), 30–38. https://doi.org/10.1039/C5SC02223A.

(58) Fenimore, L. M.; Suazo, M. J.; Torkelson, J. M. Covalent Adaptable Networks Made by Reactive Processing of Highly Entangled Polymer: Synthesis-Structure-Thermomechanical Property-Reprocessing Relationship in Covalent Adaptable Networks. *Macromolecules* **2024**, *57* (6), 2756–2772. https://doi.org/10.1021/acs.macromol.3c02515.

Supporting Information

1. Materials and Instrumentation

Materials

Acetic acid (99 %) was purchased from Thermo Scientific.
3-Amino-1-propanol (99) was purchased from Sigma Aldrich.
Benzylamine (99 %) was purchased from Sigma Aldrich.
Benzyl mercaptan (99 %) was purchased from Sigma Aldrich.
1-Butanethiol (99 %) was purchased from Sigma Aldrich.
Cyclohexylamine (99 %) was purchased from Sigma Aldrich.
1,8-Diazabicyclo(5.4.0)undec-7-ene (**DBU**, 99 %) was purchased from Sigma Aldrich.
Dibenzyl disulfide (98 %) was purchased from Thermo Scientific.
Dibutyl disulfide (98.5 %) was purchased from TCI.
2,2′-(Ethylenedioxy)diethanethiol (95 %) was purchased from Sigma Aldrich.
Ethyl magnesium bromide solution (1.0 M in THF) was purchased from Sigma Aldrich.
Formic acid (95 %) was purchased from Sigma Aldrich.
Heptylamine (99 %) was purchased from Sigma Aldrich.
1,6-Hexanedithiol (97 %) was purchased from Thermo Scientific.
3-Hydroxy-3-methyl-2-butanone (95 %) was purchased from TCI.
Methanesulfonic acid (**MSA**, 99 %) was purchased from Sigma Aldrich.
3-Methyoxypropylamine (99 %) was purchased from TCI.
Molecular sieves (3 Å, 2-5mm beads) were purchased from Thermo Scientific.
Propylamine (99 %) was purchased from Sigma Aldrich.
Pyridine (99 %) was purchased from Sigma Aldrich.
Triethylamine (99 %) was purchased from Acros Organics.
Triphosgene (98 %) was purchased from TCI.

Unless stated, all reagents were used as received without purification.
DMSO was dried over activated molecular sieves (3 Å for 72 h at r.T).

Instrumentation

Nuclear magnetic resonance (NMR) spectroscopy. ^{1}H- and ^{13}C-NMR analyses were performed on a Bruker 400 MHz spectrometer at 25 °C in the Fourier transform mode. 16 scans for ^{1}H spectra and 512 scans for ^{13}C spectra were recorded.

High resolution mass spectrometry (HRMS). ESI-MS data were acquired on a Waters QToF Premier mass spectrometer (Waters, UK) equipped with an Electrospray ionization source used in the positive ion mode. Samples were prepared as followed, 1mg/mL solution in Methanol solution were diluted 500 times to reach a final concentration of 2.10^{-6} g/mL. For the mass spectrometer parameters, the Electrospray ionization (ESI) conditions were capillary voltage 3.1 kV; cone voltage 30 V; source temperature 80 °C; desolvation temperature 120 °C. Dry nitrogen, the desolvation gas, is used as the ESI gas with a flow rate of 500 $L.h^{-1}$. Mass accuracy measurement (HRMS) were performed by infusing NaI solution as reference in order to perform internal calibration.

Fourier Transform Infrared Spectra (FT-IR). FTIR measurements were carried out on a Nicolet IS5 spectrometer (Thermo Fisher Scientific) equipped with a diamond attenuated transmission reflectance (ATR) device. 32 scans were recorded for each sample over the range 4000-500 cm^{-1} with a normal resolution of 4 cm^{-1}.

Thermogravimetric analysis (TGA). TGA analysis was performed on a TGA2 instrument from Mettler Toledo. Around 5 of sample was heated at 10 °C/min from 30 to 50 °C and flushed for 10 min at 50 °C. The sample was then heated at 20 °C/min until 600 °C. All the experiment was conducted under nitrogen atmosphere (20 mL/min).

Differential scanning calorimetry (DSC). DSC analysis was performed on a DSC 250 (TA Instruments). All the experiments were performed under ultrapure nitrogen flow. ***Linear polymers.*** Samples of 4–6 mg were used and placed in hermetic aluminum pans. The sample was heated to 150 °C at rate of 10 °C/min followed by an isothermal segment of 5 min. The sample was then cooled to -40 °C at a rate of 10 °C/min followed by an isothermal segment of 2 min. The sample was finally heated to 200 °C at a rate of 10 °C/min. The glass transition temperature was determined using the last heating ramp. ***Covalent adaptable network.*** Samples of 4–6 mg were used and placed in hermetic aluminum pans. The sample was cooled to -40 °C and the temperature modulated segment was set with an amplitude of 1 °C with a period of 60 seconds. The sample was then heated to 160 °C at a rate of 2 °C/min. The glass transition temperatures were determined using the reversing heat flow curve. ***Compounds.*** Samples of 0.5-1.5 mg were used and placed in hermetic aluminum pans. The sample was loaded at a temperature of 25 °C in the instrument. The sample was heated to 200-300 °C

(depending on the compound melting point) at a rate of 10 °C/min. This curve was used for the determination of the melting point of the compound.

Rheology. Rheology experiments were conducted on an ARES G2 rheometer from TA Instruments in shear geometry with a plate diameter of 8 mm. The samples were prepared by compression molding and were cut in their rubber state using a die cutter. Temperature sweeps were performed at a rate of 3 °C/min at a frequency of 1 rad/s and at a constant strain of 1%. Stress relaxation experiments were performed with a constant shear strain of 3% within the linear viscoelastic region of the polymers.

Dynamic mechanical analysis (DMA). DMA experiment was performed on a DMA Q800 from TA Instruments. Temperature ramp experiment was performed in tension mode with 0.01 N of constant force and a frequency of 1 Hz. The sample was equilibrated at 30 °C and heated with a heating rate of 3 °C/min until 120 °C.

Swelling Ratio (SR) and Gel Content (GC). The swelling ratio (SR) was determined by immersion of a piece of material (between 100 and 200 mg) of mass m_i in THF. After 24h, the swollen sample was weighted as the mass of the gel m_{gel}. The SR was calculated using the following equation.

$$SR\ (\%) = \frac{m_{gel} - m_i}{m_i} \times 100$$

The gel content (GC) was determined by weighting the mass m_f after drying of the swollen sample using the following equation.

$$GC\ (\%) = \frac{m_f}{m_i} \times 100$$

Tensile tests. Tensile tests were conducted at room temperature using an Instron 34TM-10 equipped with a cell force of 500 N at a speed of 1 $mm.min^{-1}$. Measurements were repeated 5 times on dogbone-shaped films (ASTM-D638-V) with a thickness of 0.2-0.3 mm. The samples were prepared by compression molding and were cut at r.T for the linear polymers and in their rubber state for the cross-linked polymer using a die cutter.

Compression molding. Polymer samples were cut into little pieces and pressed between Teflon sheets in a carver press. **P1** was pressed at 120 °C for 15 min under 6 MT of pressure. **P2** was pressed at 155 °C for 20 min under 8 MT of pressure. **P4** was pressed at 100 °C for 10 min under 6 MT of pressure. The sample was then cut for tensile test or allowed to slowly cool down to r.T.

2. Synthetic Procedures

The compounds **4CC** and **4CCS-a**/**-b** were synthesized according to the following procedures. ^{1}H and ^{13}C NMR spectra of the compounds and their precursors can be found in Figures S1-8.

2,3-dimethylpentane-2,3-diol

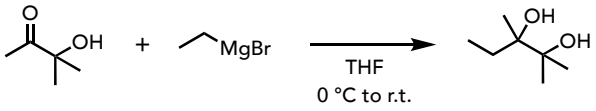

2,3-dimethylpentane-2,3-diol was synthesized by modification of A. Kleij's procedure[1]. 100 mL of ethyl magnesium bromide solution (1 M in THF, 0.1 mol, 2.5 eq.) were added to a two-necked round-bottom flask under N_2 atmosphere. The solution was cooled to 0 °C and a solution of 3-Hydroxy-3-methyl-2-butanone (4.08 g, 0.04 mol, 1 eq.) in 20 mL anhydrous THF was added dropwise. After stirring overnight, the reaction was quenched by the addition of 50 mL of saturated ammonium chloride (NH_4Cl) solution. The white precipitate was removed by filtration and 60 mL of diethyl ether were added to the filtrate. The aqueous phase was extracted with diethyl ether (3x 60 mL). The organic phases were combined and dried with $MgSO_4$ followed by filtration and removal of the solvent under vacuum. The residue was purified by silica gel chromatography with diethyl ether as eluent. The pure product was obtained as a transparent oil (2.12 g, isolated yield 40 %); **^{1}H NMR** (400 MHz, DMSO-d_6) δ 3.91 (s, 1H), 3.66 (s, 1H), 1.56-1.45 (m, 1H), 1.40-1.29 (m, 1H), 1.06 (s, 6H), 0.97 (s, 3H), 0.85 (t, J = 7.6 Hz, 3H); **^{13}C NMR** (100 MHz, DMSO-d_6) δ 75.6, 74.6, 28.2, 25.5, 25.4, 20.4, 8.7.

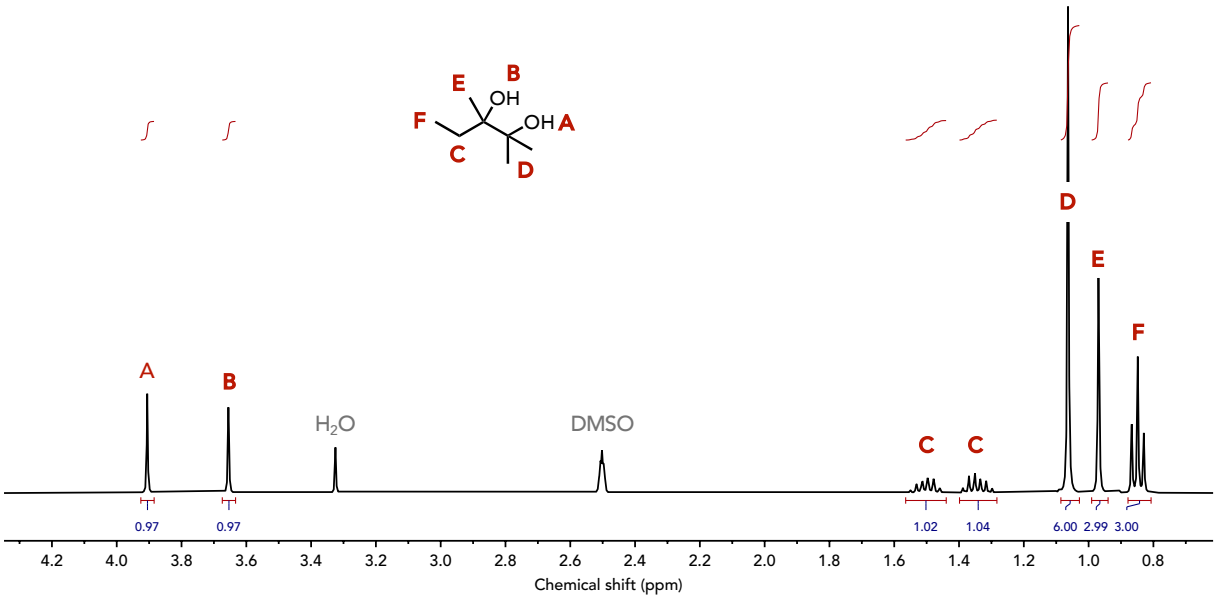

Figure S1 – ^{1}H-NMR spectrum (400 MHz, DMSO-d_6) of 2,3-dimethylpentane-2,3-diol.

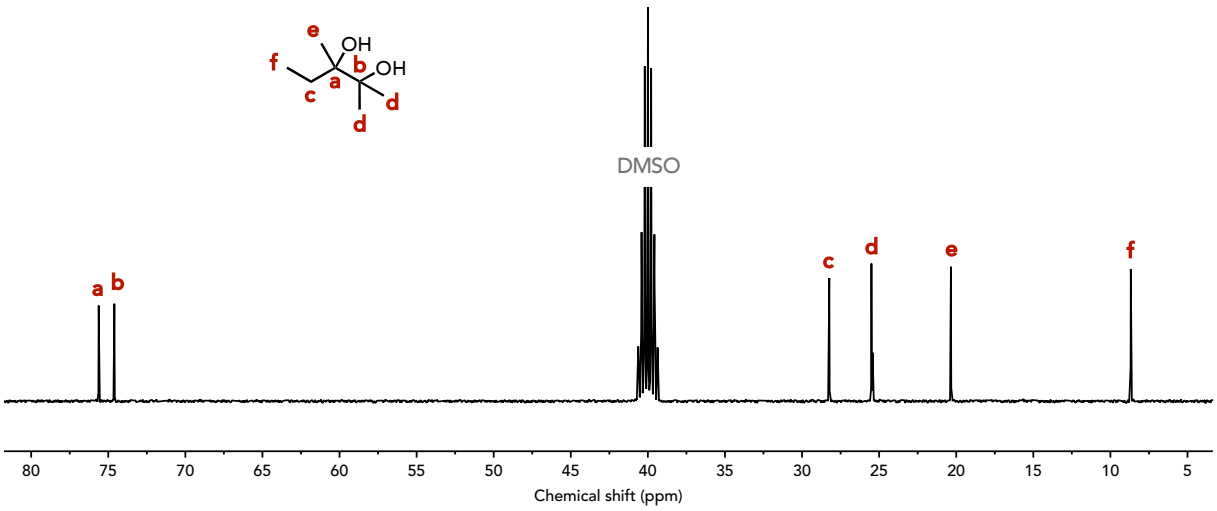

Figure S2 – ^{13}C-NMR spectrum (100 MHz, DMSO-d_6) of 2,3-dimethylpentane-2,3-diol.

4-ethyl-4,5,5-trimethyl-1,3-dioxolan-2-one (4CC)

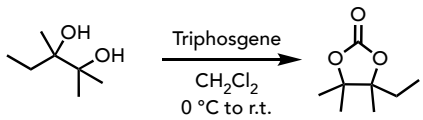

4-ethyl-4,5,5-trimethyl-1,3-dioxolan-2-one was synthesized by modification of A. Kleij's procedure[1]. 2,3-dimethylpentane-2,3-diol (1.98 g, 15 mmol, 1 eq.), pyridine (4.75 g, 60 mmol,

4 eq.) and dichloromethane (DCM) (90 mL) were added to a round-bottom flask. The mixture was cooled to 0 °C and a solution of triphosgene (2.23 g, 7.5 mmol, 0.5 eq.) in 7.5 mL DCM was added dropwise. The mixture was stirred overnight at room temperature under N_2 atmosphere. The reaction was quenched by the addition of 60 mL of saturated ammonium chloride (NH_4Cl) solution and 30 mL of water was then added. The aqueous phase was extracted with DCM (3x 100 mL). The organic phases were combined and dried with $MgSO_4$ followed by filtration and removal of the solvent under vacuum. The residue was purified by silica gel chromatography with dichloromethane as eluent. The pure product was obtained as a white solid (1.26 g, isolated yield 53 %); mp = 59 °C; **^{1}H NMR** (400 MHz, DMSO-d_6) δ 1.83-1.71 (m, 1H), 1.69-1.58 (m, 1H), 1.36 (s, 6H), 1.30 (s, 3H), 0.93 (t, J = 7.4 Hz, 3H); **^{13}C NMR** (100 MHz, DMSO-d_6) δ 153.7, 88.6, 87.0, 27.3, 22.9, 22.1, 18.5, 8.5.

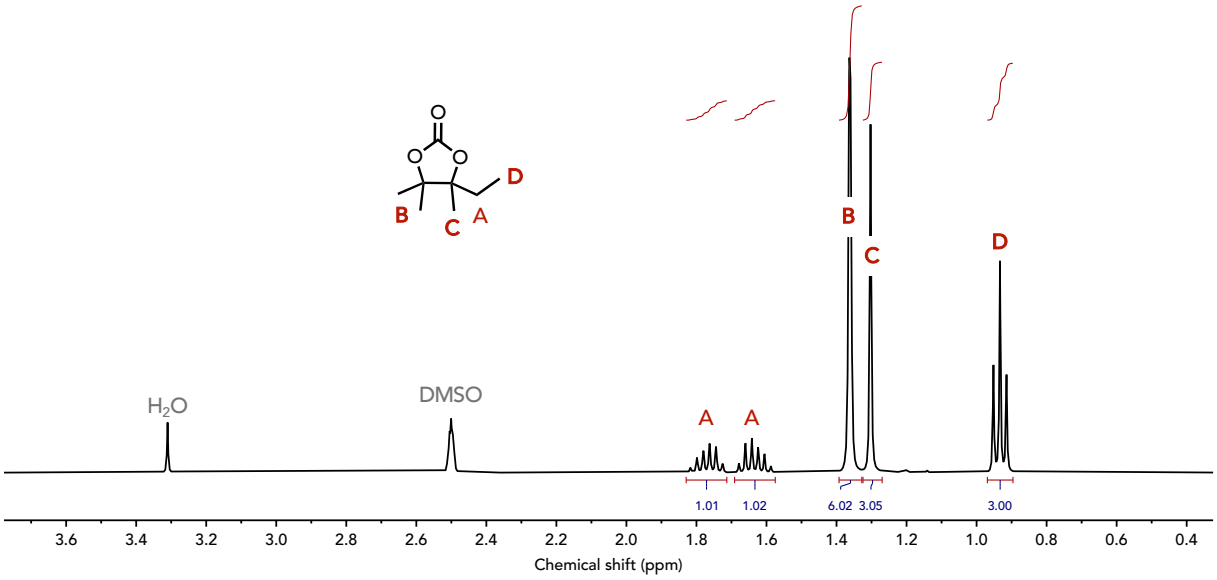

Figure S3 – ^{1}H-NMR spectrum (400 MHz, DMSO-d_6) of **4CC**.

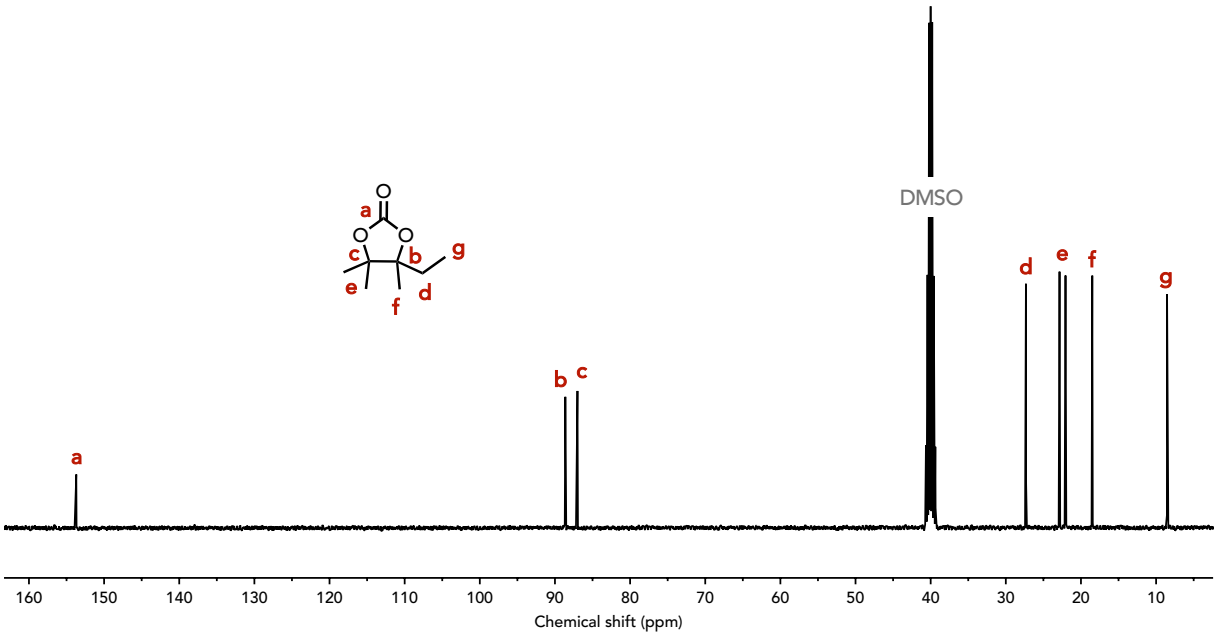

Figure S4 – ^{13}C-NMR spectrum (100 MHz, DMSO-d_6) of **4CC**.

4-(benzylthio)-4,5,5-trimethyl-1,3-dioxolan-2-one (4CCS-a)

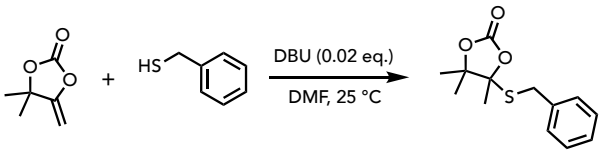

4CCS-a was synthesized by slightly modifying a previously reported procedure[2]. αCC (1.024 g, 8 mmol, 1 eq.), benzyl mercaptan (992 mg, 8 mmol, 1 eq.) and DMF (2 mL) were added in a reaction tube under N_2 atmosphere. DBU (24.3 mg, 0.16 mmol, 0.02 eq.) was added and the reaction medium was stirred at 25 °C for 24h. The mixture was then diluted with 100 mL of ethyl acetate and extracted 3 times with brine (3x100 mL). The organic phase was recovered, dried over $MgSO_4$ and filtered. The solvent was evaporated under vacuum at room temperature. The solid was then recrystallized in ethanol, filtered on a Büchner apparatus, and washed with cold ethanol. The pure product was isolated as a white solid (1.41 g, isolated yield 70 %). **^{1}H NMR** (400 MHz, DMSO-d_6) δ 7.36 (m, 5H), 4.08 (d, J = 12 Hz, 1H), 3.96 (d, J = 12 Hz, 1H), 1.80 (s, 3H), 1.51 (s, 3H), 1.46 (s, 3H). **^{13}C NMR** (100 MHz, DMSO-d_6) δ 152.8, 137.2, 129.6, 129.1, 127.8, 96.9, 88.1, 33.0, 23.5, 21.8, 21.7.

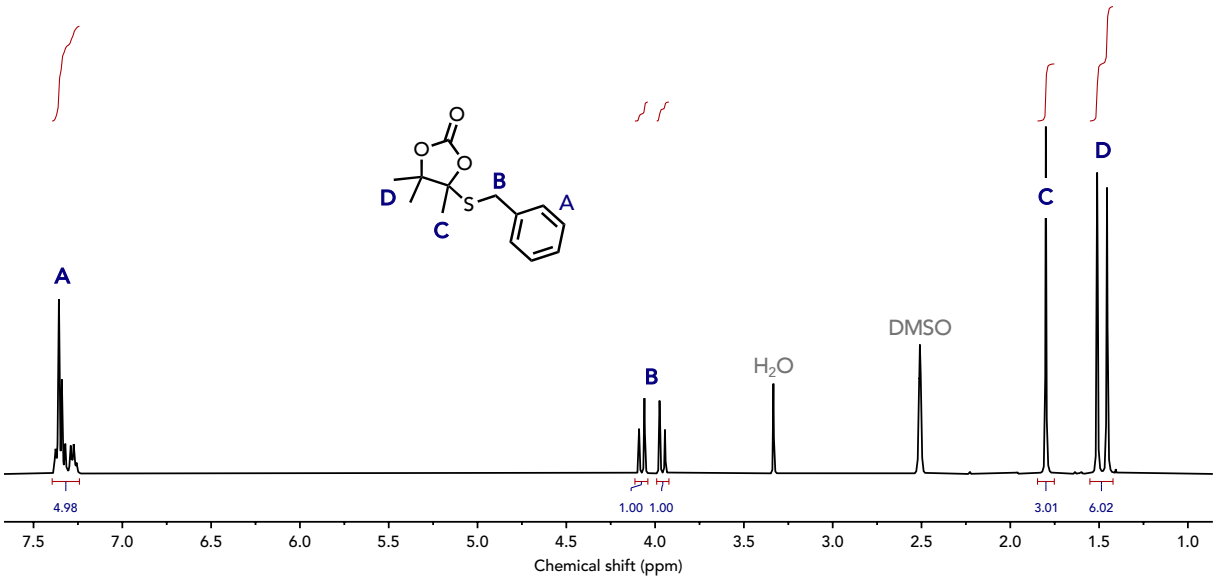

Figure S5 – ^{1}H-NMR spectrum (400 MHz, DMSO-d_6) of **4CCS-a**.

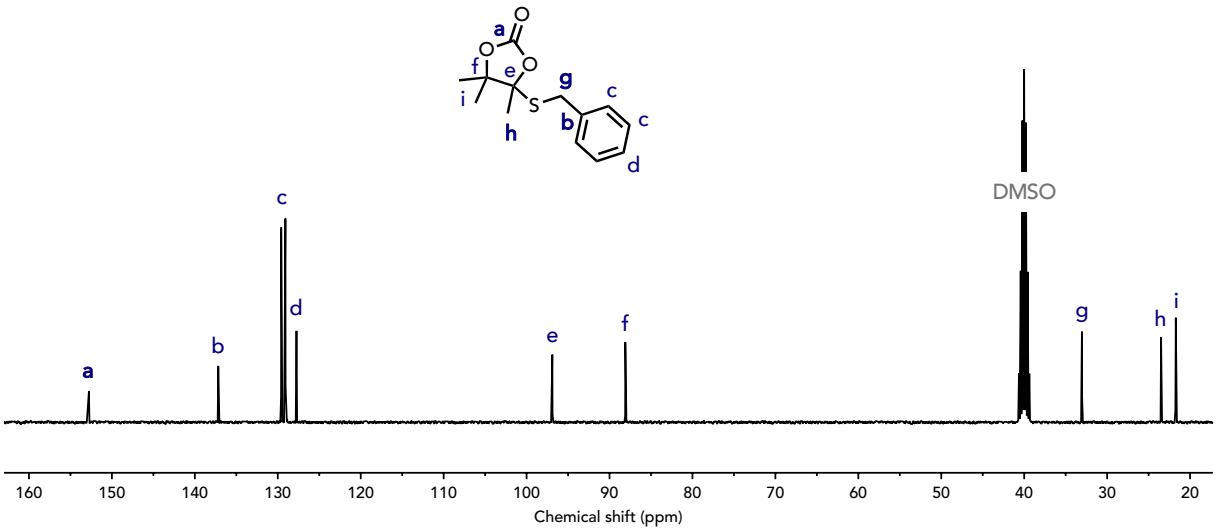

Figure S6 – ^{13}C-NMR spectrum (100 MHz, DMSO-d_6) of **4CCS-a**.

4-(butylthio)-4,5,5-trimethyl-1,3-dioxolan-2-one (4CCS-b)

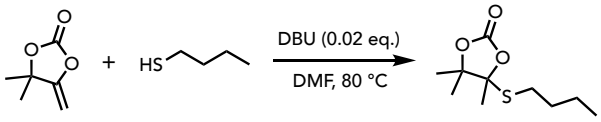

αCC (1.024 g, 8 mmol, 1 eq.), 1-butanethiol (722 mg, 8 mmol, 1 eq.) and DMF (2 mL) were added in a reaction tube under N_2 atmosphere. DBU (24.3 mg, 0.16 mmol, 0.02 eq.) was added and the reaction medium was stirred at 80 °C for 24h. The mixture was then diluted with 100 mL of ethyl acetate and extracted 3 times with brine (3x100 mL). The organic phase was recovered, dried over $MgSO_4$ and filtered. The solvent was evaporated under vacuum at room temperature. The product was diluted with diethyl ether (2 mL) and purified by silica gel chromatography using hexane/diethyl ether 75/25 as eluent. The pure product was isolated as transparent oil (874 mg, isolated yield 50 %). **^{1}H NMR** (400 MHz, DMSO-d_6) δ 2.73 (m, 2H), 1.73 (s, 3H), 1.54 (m, 2H), 1.50 (s, 3H), 1.43 (s, 3H), 1.37 (sext, J = 7.4 Hz, 2H), 0.88 (t, J = 7.4 Hz, 3H). **^{13}C NMR** (100 MHz, DMSO-d_6) δ 152.8, 96.8, 88.0, 31.6, 28.3, 23.5, 21.9, 21.8, 21.5, 13.9.

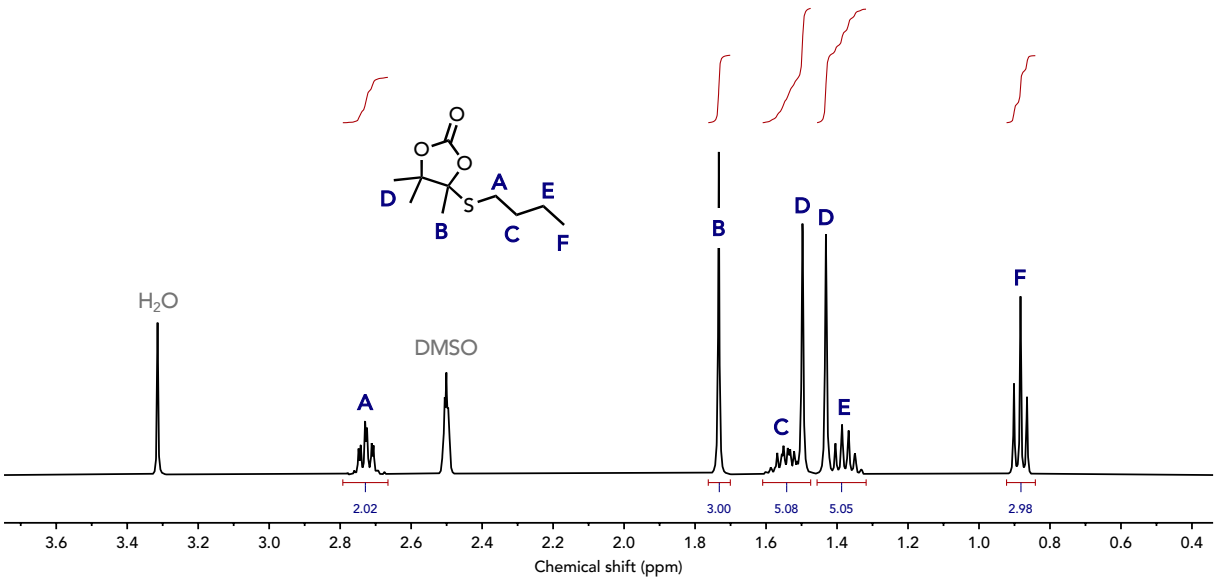

Figure S7 – ^{1}H-NMR spectrum (400 MHz, DMSO-d_6) of **4CCS-b**.

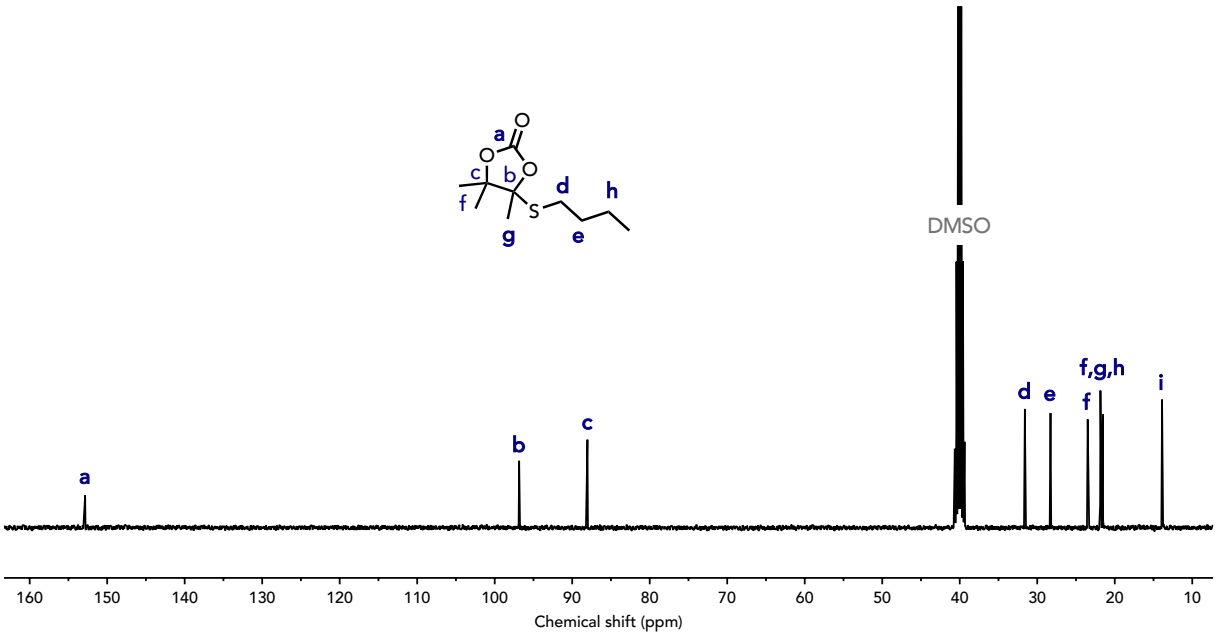

Figure S8 – ^{13}C-NMR spectrum (100 MHz, DMSO-d_6) of **4CCS-b**.

3. Kinetic experiments with 4CC

The aminolysis of **4CC** was monitored by ^{1}H-NMR spectroscopy to determine the conversion in **4CC** over time. However, no reaction was observed between **4CC** and propylamine at 25 °C after 24 h (Figure S9). The reaction condition was therefore intensified to trigger the reaction. **4CC** was reacted with heptylamine (instead of propylamine for its higher boiling point) at 120 °C for 24 h. Again, no reaction was observed (Figure S10). It must be noted that the peaks of the amines were shifted in the crude reaction samples due to the quenching by formic acid.

General procedure

4CC (316 mg, 2 mmol, 1 eq.) was added to a reaction tube with 1 mL of solvent (dry DMSO). The amine was added (6 mmol, 3 eq.) and the mixture was stirred under air at the desired temperature (25 or 120 °C). The NMR samples were prepared by sampling around 80 µL of the reaction medium at the desired time, diluting with DMSO-d_6, and quenching with formic acid. The tube was analyzed right away or stored at -20 °C prior NMR analysis.

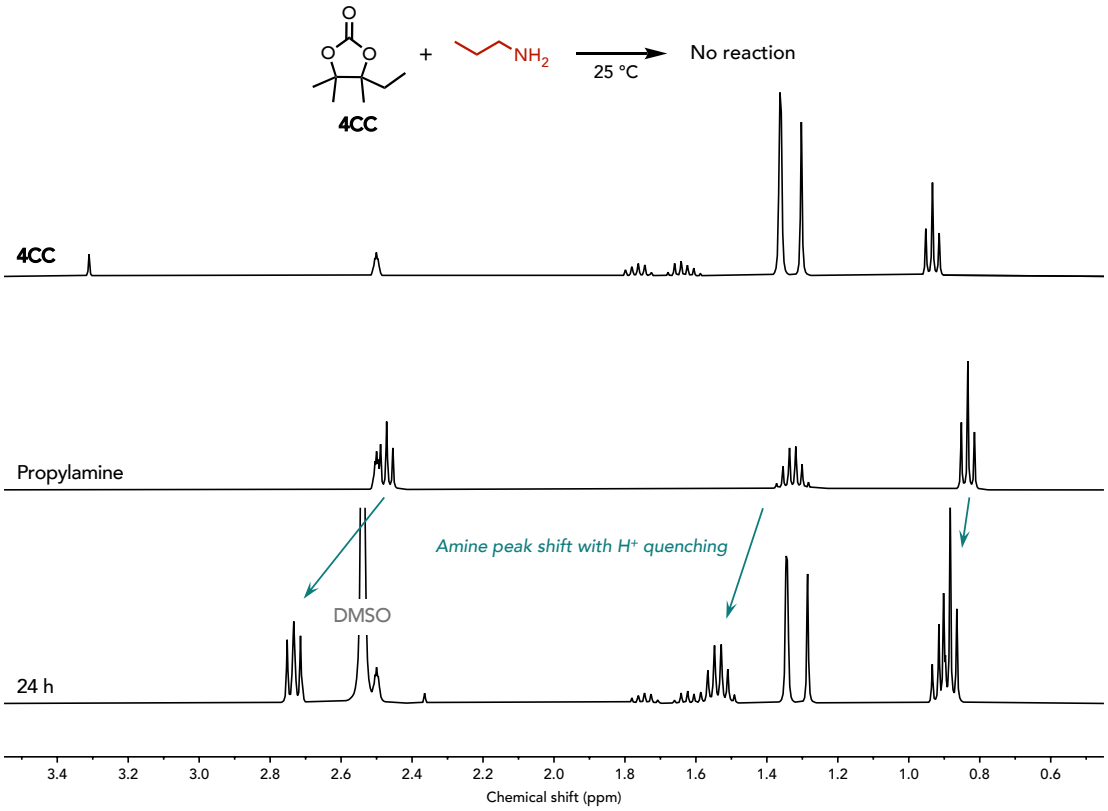

Figure S9 – Stacked ^{1}H-NMR spectra (400 MHz, DMSO-d_6) of **4CC**, propylamine, and of the quenched crude reaction between **4CC** and propylamine at 25 °C after 24h.

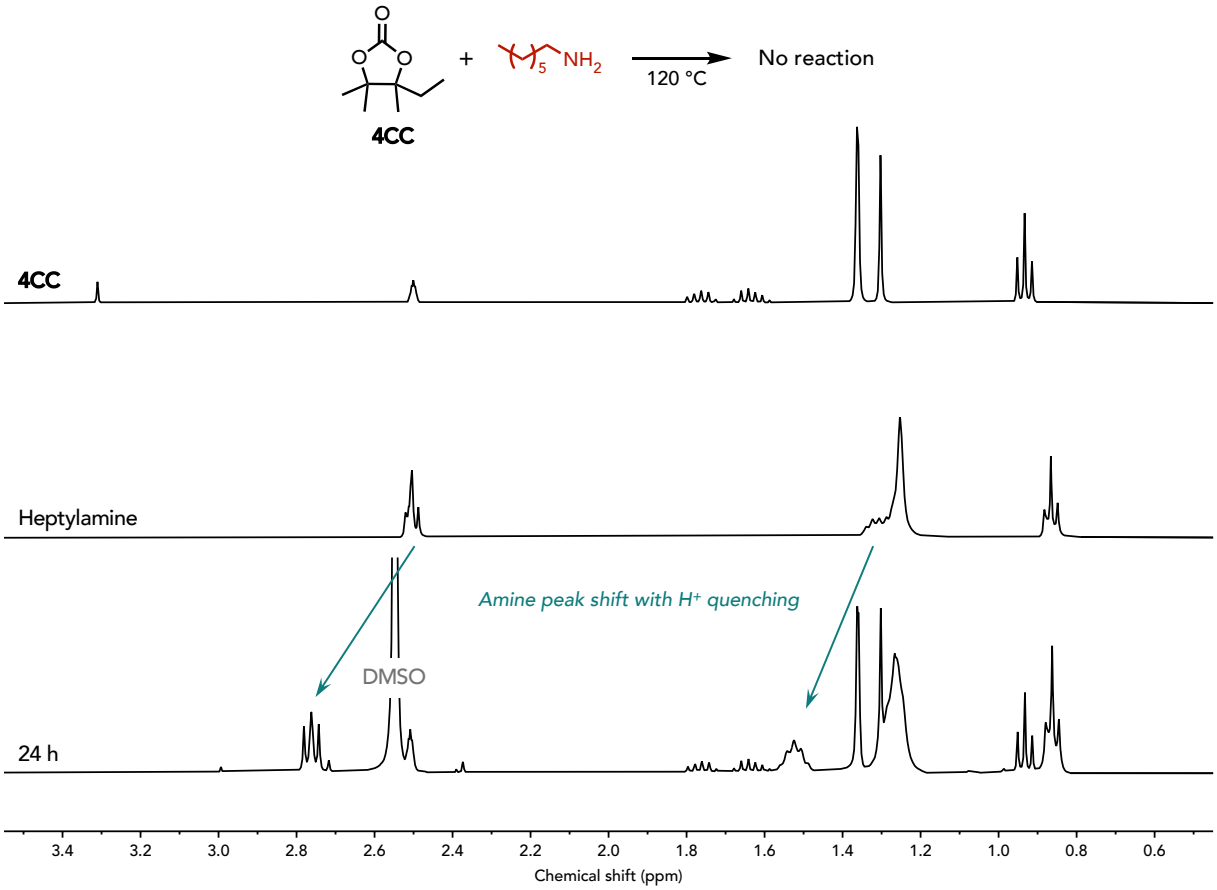

Figure S10 – Stacked ^{1}H-NMR spectra (400 MHz, DMSO-d_6) of **4CC**, heptylamine, and of the quenched crude reaction between **4CC** and heptylamine at 120 °C after 24h.

4. Kinetic experiments with 4CCS

General procedure

4CCS (2 mmol, 1 eq.) was added to a reaction tube with 1 mL of solvent (dry DMSO). The amine was added (6 mmol, 3 eq.) and the mixture was stirred under air at 25 °C. The NMR samples were prepared by sampling around 80 µL of the reaction medium at the desired time, diluting with DMSO-d_6, and quenching with formic acid. The tube was analyzed right away or stored at -20 °C prior NMR analysis.

The conversion in **4CCS** at the desired time was determined by integration of selected resonances in ^{1}H-NMR spectra for quantification.

It is noted that thiol oxidation into disulfide occurs during the reaction. This is highlighted with spectra of the pure thiols and their disulfide derivatives (Figures S20-21). However, overlapping of the different signals in the crude reaction mixture prevents the quantification of the amount of disulfide produced during the reaction.

Quantification of the conversion by ^{1}H-NMR spectroscopy

For the reaction between **4CCS-a** and propylamine (Figure S11), the resonance at 1.79 ppm (3H) was selected to follow **4CCS-a** and the resonance at 1.22 ppm (3H) was selected to follow the product **1a**. We also considered the reaction intermediate *oxo*-urethane by selecting the resonance at 2.03 ppm (3H). The following equation was used to determine the conversion:

$$Conv.(\%) = \left(\frac{I(1.22) + I(2.03)}{I(1.79) + I(1.22) + I(2.03)}\right) \times 100$$

Where *I* is the integral value of the selected resonance.

For the reaction between **4CCS-b** and propylamine (Figure S12), the resonance at 1.73 ppm (3H) was selected to follow **4CCS-a** and the resonance at 1.22 ppm (3H) was selected to follow the product **1a**. We also considered the reaction intermediate *oxo*-urethane by selecting the resonance at 2.03 ppm (3H). The following equation was used to determine the conversion:

$$Conv.(\%) = \left(\frac{I(1.22) + I(2.03)}{I(1.73) + I(1.22) + I(2.03)}\right) \times 100$$

Where *I* is the integral value of the selected resonance.

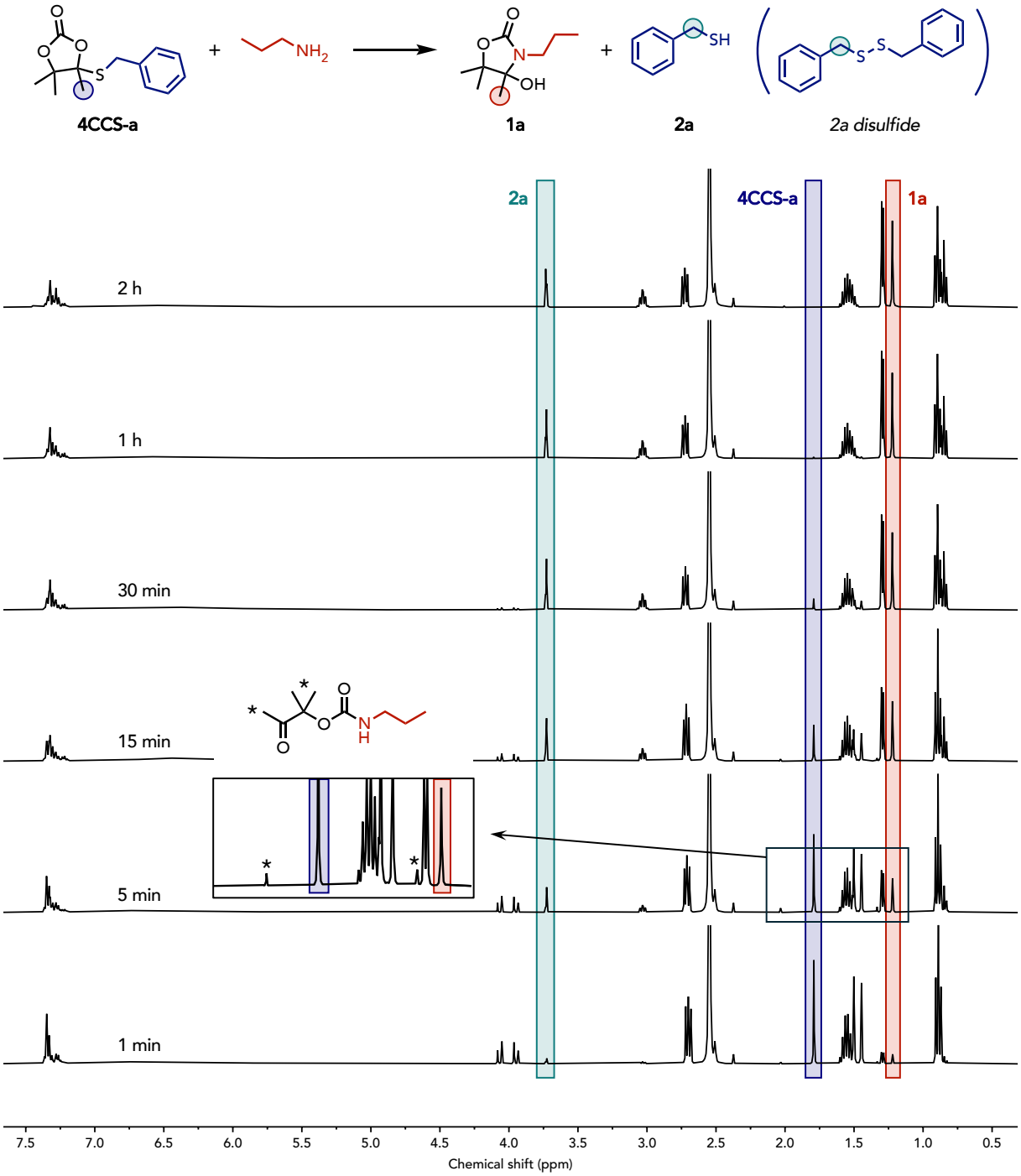

Figure S11 – Stacked ^{1}H-NMR spectra (400 MHz, DMSO-d_6) for the reaction between **4CCS-a** and propylamine in DMSO at 25 °C along time.

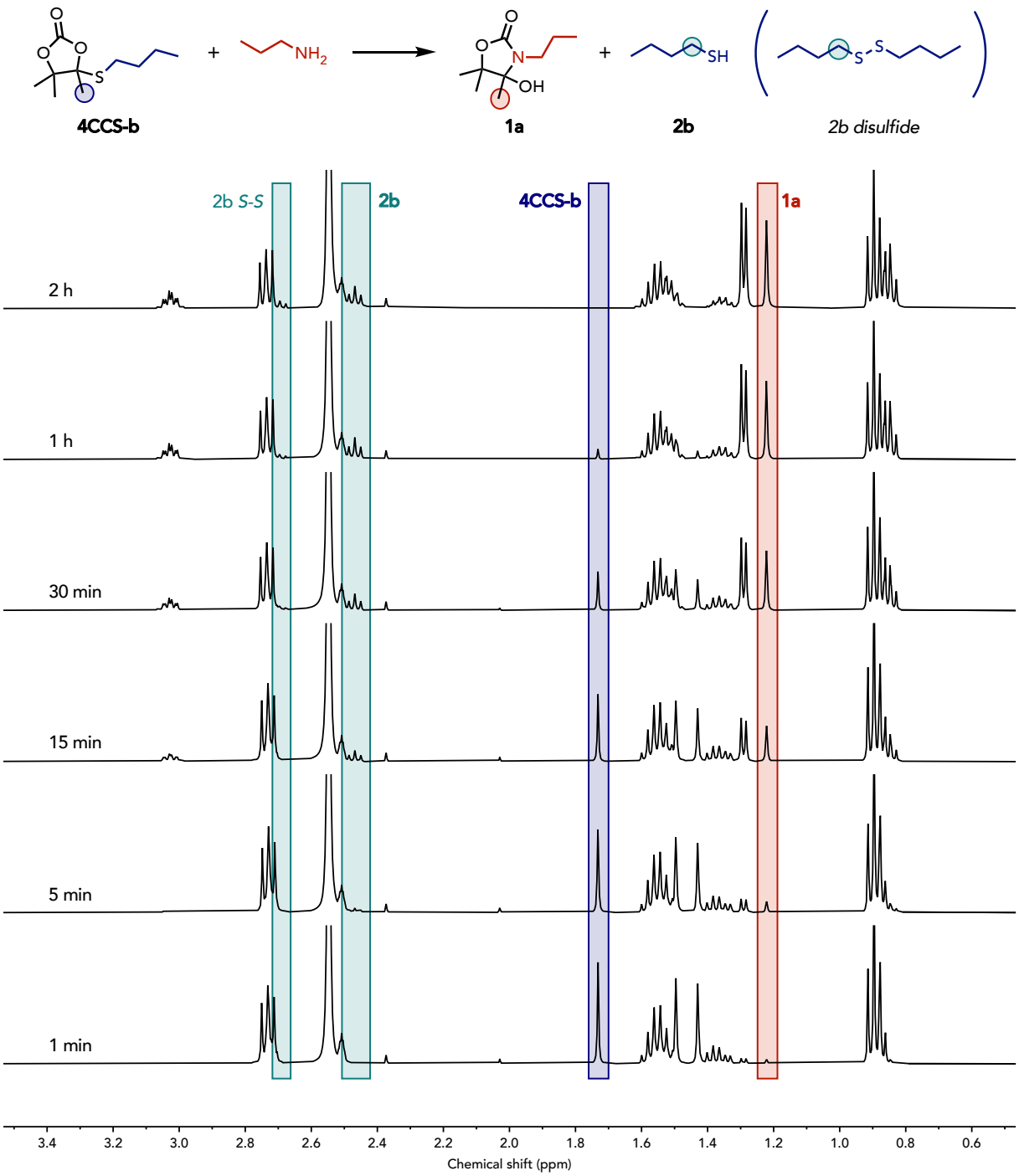

Figure S12 – Stacked ^{1}H-NMR spectra (400 MHz, DMSO-d_6) for the reaction between **4CCS-b** and propylamine in DMSO at 25 °C along time.

Reactions in other solvents

The kinetic experiments were performed according to the general procedure but in different solvents (MeCN and THF).

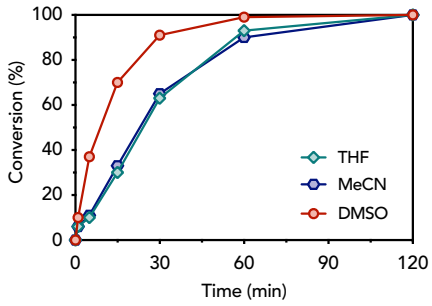

Figure S13 – Kinetic profiles for the reaction between **4CCS-a** and propylamine at 25 °C in different solvents.

Quantification of the conversion by ^{1}H-NMR spectroscopy

For the reaction between **4CCS-a** and propylamine in MeCN (Figure S14), the resonance at 1.79 ppm (3H) was selected to follow **4CCS-a** and the resonance at 1.22 ppm (3H) was selected to follow the product **1a**. We also considered the reaction intermediate *oxo*-urethane by selecting the resonance at 1.33 ppm (6H). The following equation was used to determine the conversion:

$$Conv.(\%) = \left(\frac{I(1.22) + \frac{I(1.33)}{2}}{I(1.79) + I(1.22) + \frac{I(1.33)}{2}} \right) \times 100$$

Where *I* is the integral value of the selected resonance.

For the reaction between **4CCS-a** and propylamine in THF (Figure S15), the resonance at 4.06 ppm (1H) was selected to follow **4CCS-a** and the resonance at 1.22 ppm (3H) was selected to follow the product **1a**. We also considered the reaction intermediate *oxo*-urethane by selecting the resonance at 2.03 ppm (3H). The following equation was used to determine the conversion:

$$Conv.(\%) = \left(\frac{\frac{I(1.22)}{3} + \frac{I(2.03)}{6}}{I(4.06) + \frac{I(1.22)}{3} + \frac{I(2.03)}{6}} \right) \times 100$$

Where *I* is the integral value of the selected resonance.

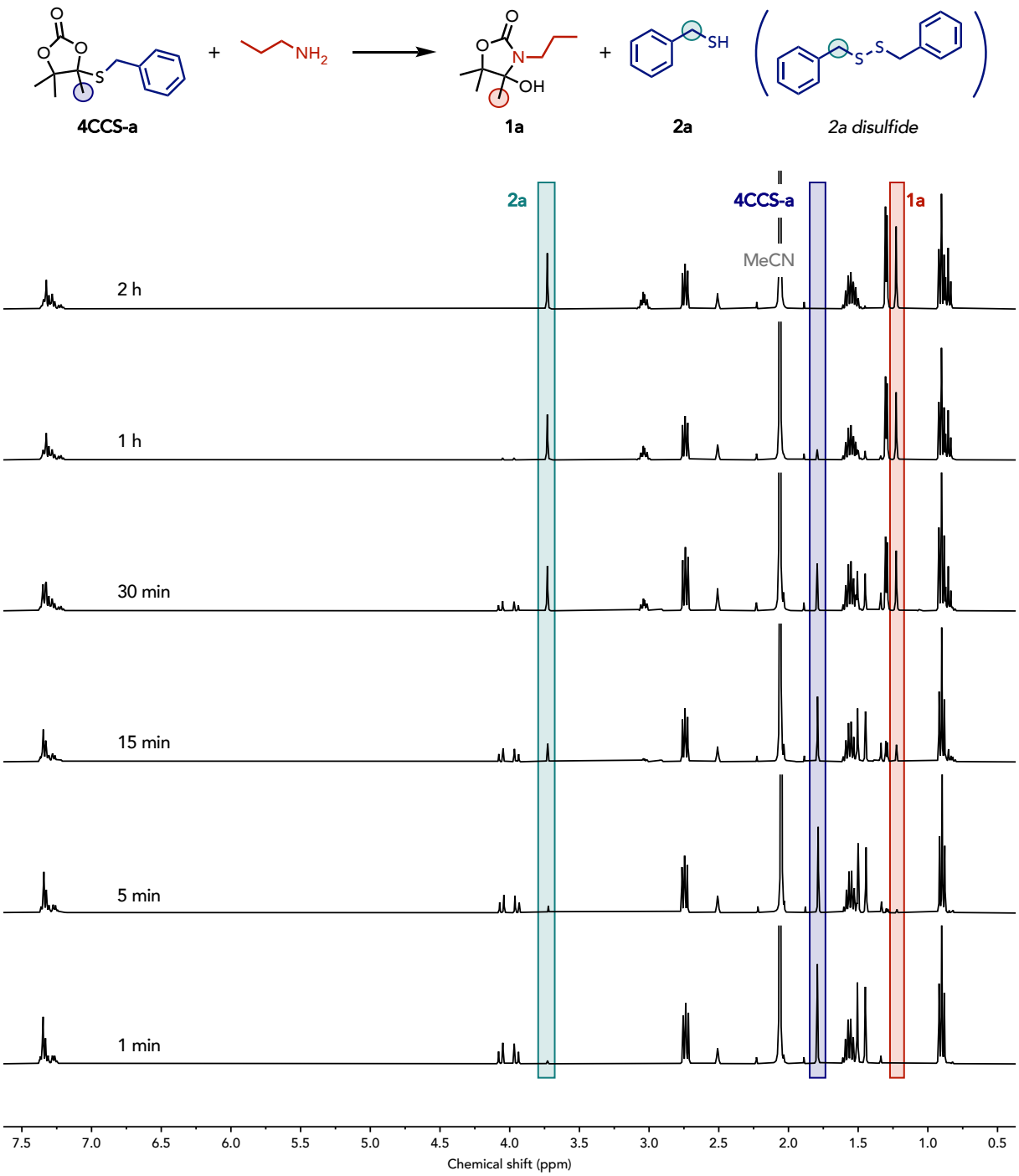

Figure S14 – Stacked ^{1}H-NMR spectra (400 MHz, DMSO-d_6) for the reaction between **4CCS-a** and propylamine in MeCN at 25 °C along time.

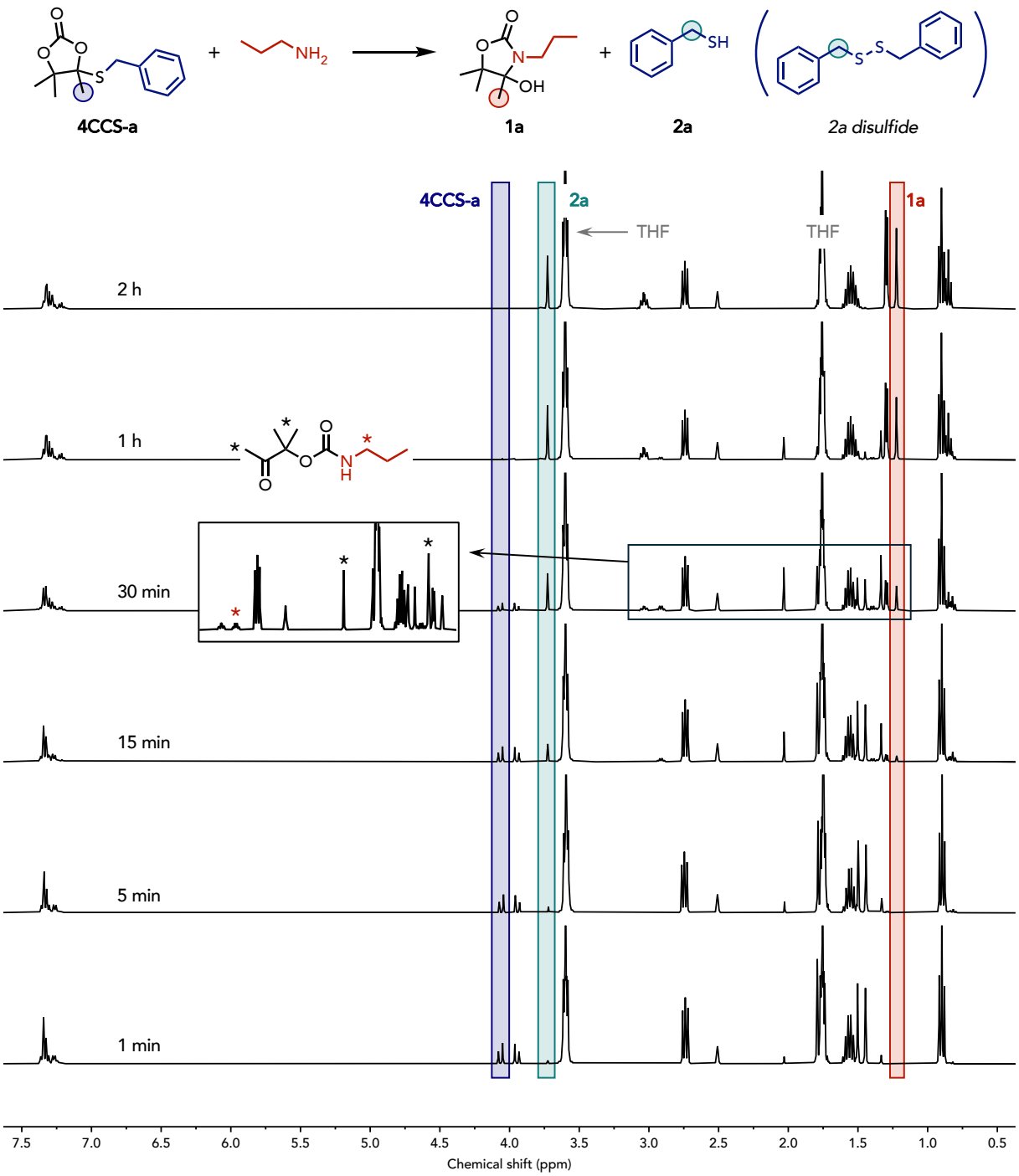

Figure S15 – Stacked ^{1}H-NMR spectra (400 MHz, DMSO-d_6) for the reaction between **4CCS-a** and propylamine in THF at 25 °C along time.

Reactions with different amounts of amine

The kinetic experiments were performed according to the general procedure but using different ratios of amine (propylamine) over **4CCS-a** (Figure S16A). The quantification by ^{1}H-NMR was achieved using the same resonances as above-mentioned (Figure S11).

The slow kinetics of reaction observed at 1 equivalence of amine could be ascribed to the formation of an amine-thiol salt (Figure S16B). The amine can indeed act as a Bronsted base and be quenched by the acidic thiol released during the course of the reaction.

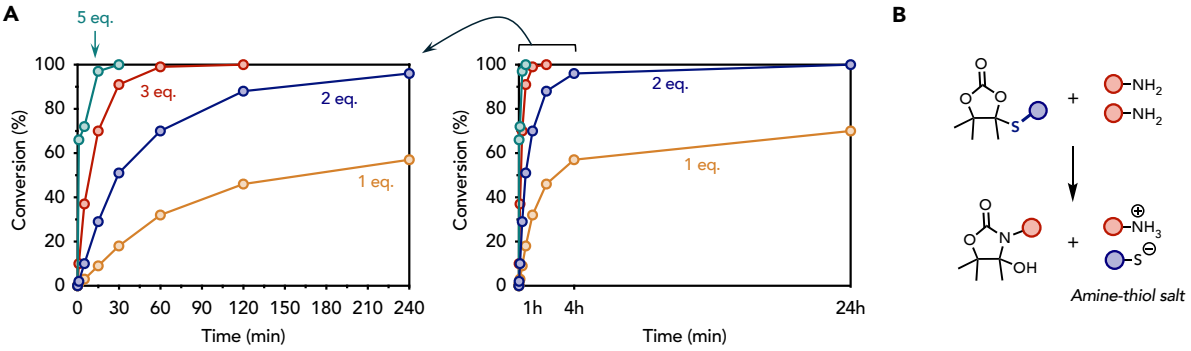

Figure S16 – (A) Kinetic profiles for the reaction between **4CCS-a** and different equivalents of propylamine (*vs* **4CCS-a**) at 25 °C in DMSO. (B) Aminolysis reaction of **4CCS** releasing an acidic thiol which is neutralized by a basic amine.

Reactions with different amines

The kinetic experiments were performed according to the general procedure but using different amines (benzylamine and cyclohexylamine compared to propylamine).

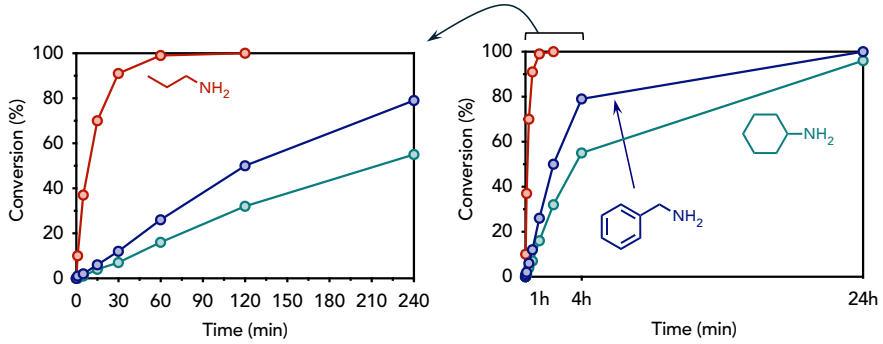

Figure S17 – Kinetic profiles for the reaction between **4CCS-a** and different amines (propylamine, benzylamine, cyclohexylamine) at 25 °C in DMSO.

Quantification of the conversion by ^{1}H-NMR spectroscopy

For the reaction between **4CCS-a** and benzylamine (Figure S18), the resonance at 1.80 ppm (3H) was selected to follow **4CCS-a** and the resonance at 1.14 ppm (3H) was selected to follow the product **1b**. The following equation was used to determine the conversion:

$$Conv.(\%) = \left(\frac{I(1.14)}{I(1.80) + I(1.14)}\right) \times 100$$

Where *I* is the integral value of the selected resonance.

For the reaction between **4CCS-a** and cyclohexylamine (Figure S19), the resonance at 4.06 ppm (1H) was selected to follow **4CCS-a**. The oxazolidone product **1b** was however difficult to follow over time due to overlapping signals or broadness of resonance leading to low intensity (Figure S19, resonance at 3.05 ppm). The reaction was therefore monitored as a function of thiol production using the characteristic signal at 3.73 ppm (2H). The following equation was used to determine the conversion:

$$Conv.(\%) = \left(\frac{\frac{I(3.73)}{2}}{I(4.06) + \frac{I(3.73)}{2}}\right) \times 100$$

Where *I* is the integral value of the selected resonance.

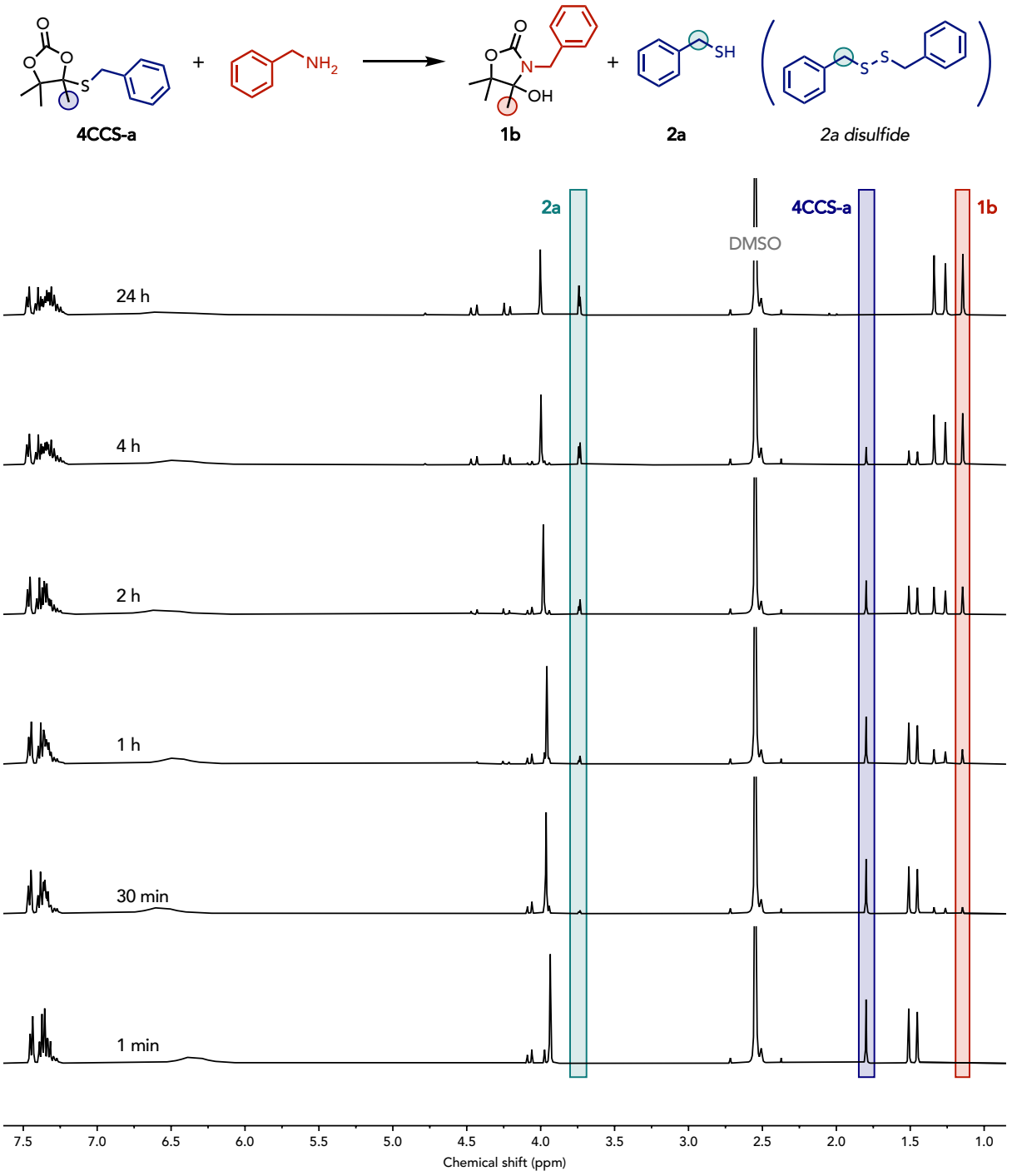

Figure S18 – Stacked ^{1}H-NMR spectra (400 MHz, DMSO-d_6) for the reaction between **4CCS-a** and benzylamine in DMSO at 25 °C along time.

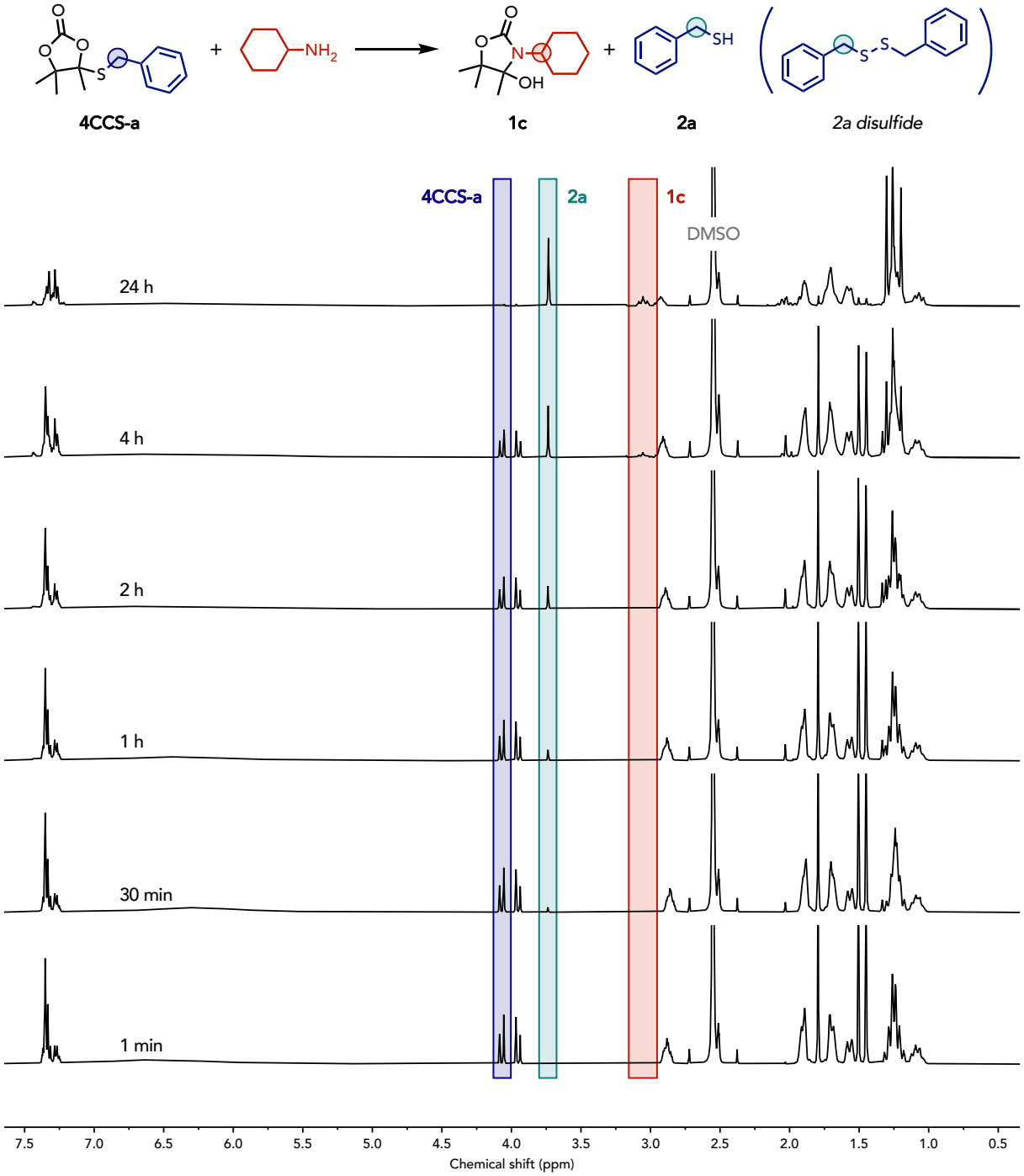

Figure S19 – Stacked ^{1}H-NMR spectra (400 MHz, DMSO-d_6) for the reaction between **4CCS-a** and cyclohexylamine in DMSO at 25 °C along time.

Thiol oxidation during the reaction

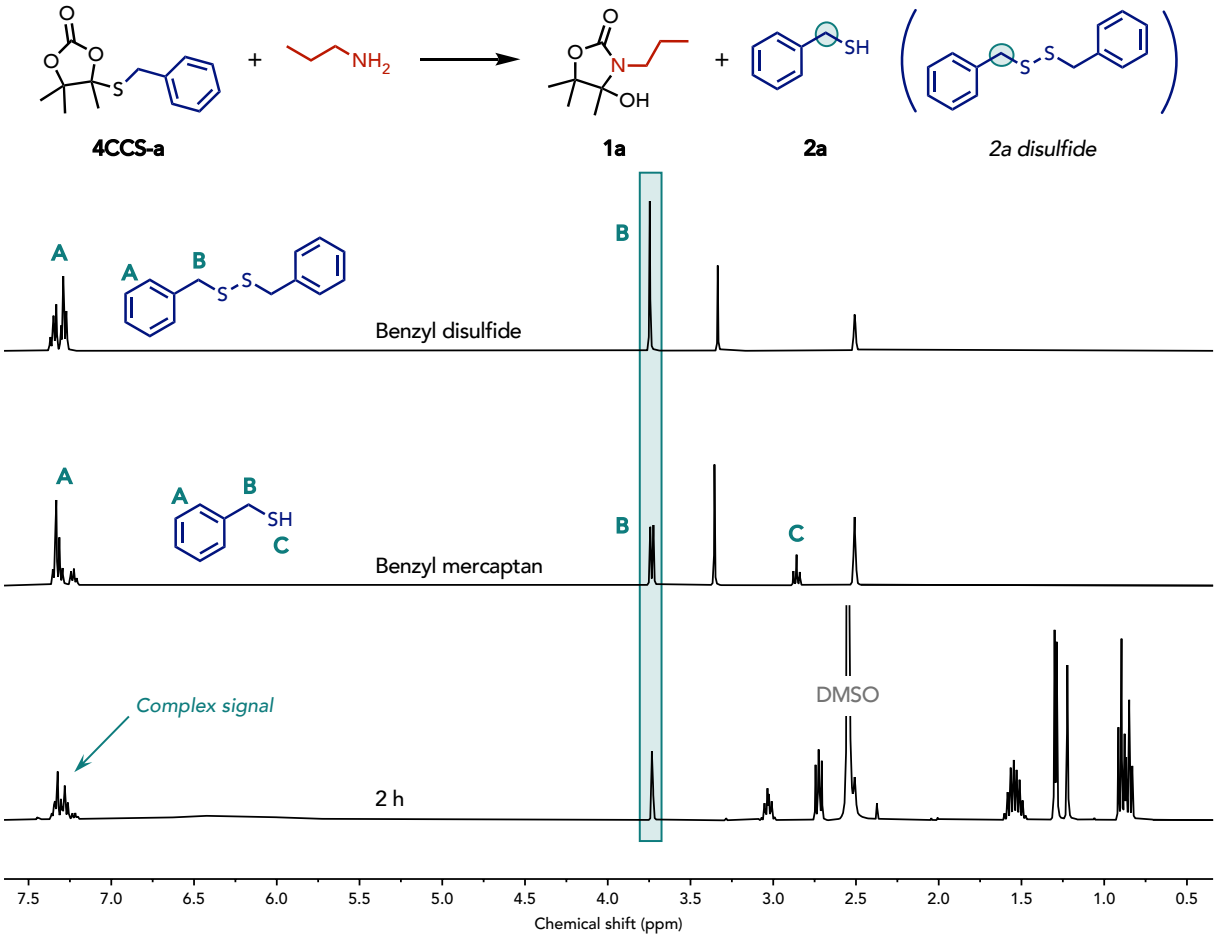

Figure S20 – Stacked ^{1}H-NMR spectra (400 MHz, DMSO-d_6) for the oxidation product of **2a**, pure **2a**, and the crude reaction mixture of **4CCS-a** with propylamine after 2 h.

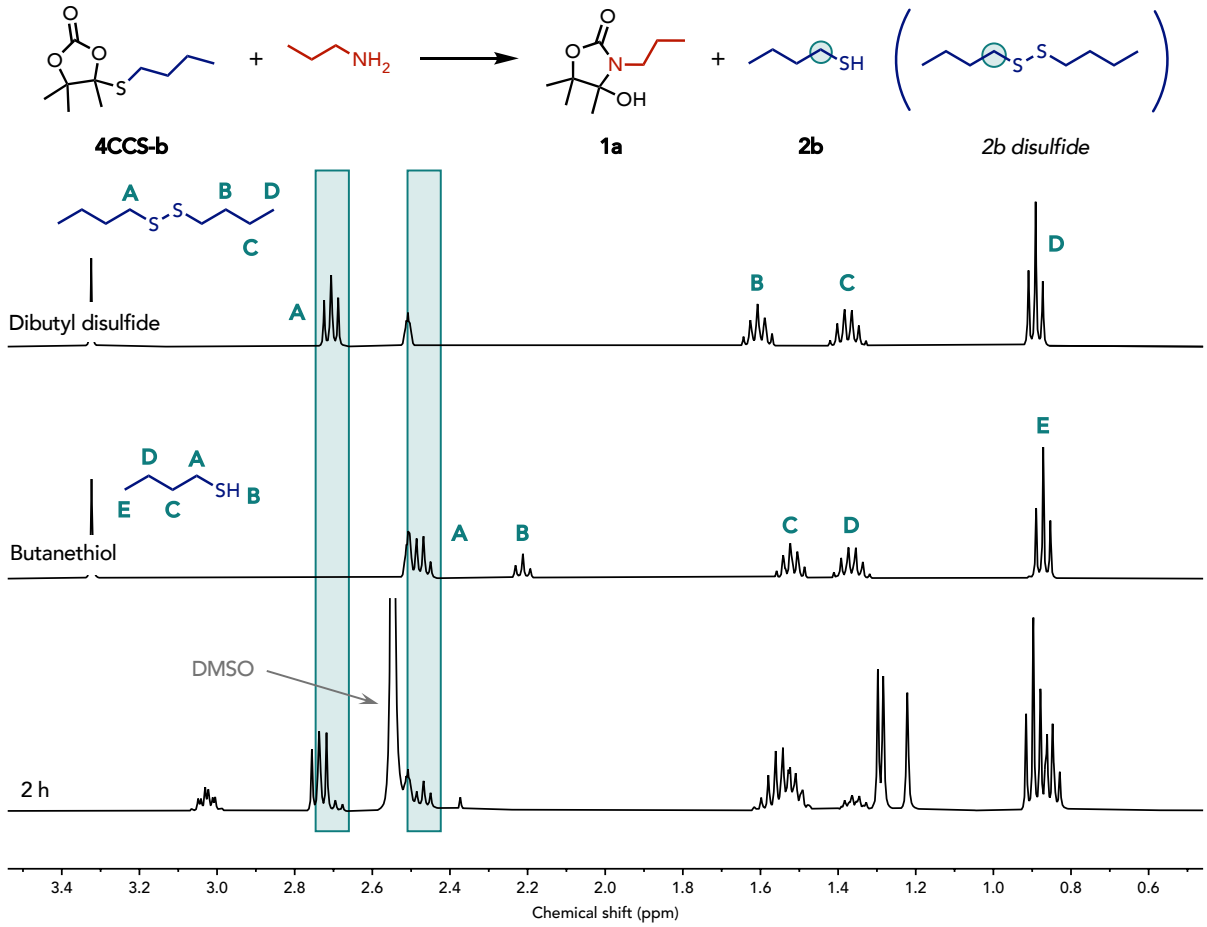

Figure S21 – Stacked ^{1}H-NMR spectra (400 MHz, DMSO-d_6) for the oxidation product of **2b**, pure **2b**, and the crude reaction mixture of **4CCS-b** with propylamine after 2 h.

5. Computational study

Computational details

Preliminary calculations of equilibrium structures were performed using a semi-empirical model (AM1-D3H4)[3,4] to determine the most stable conformations. These semi-empirical calculations were performed using the AMPAC software[5]. The CHAIN algorithm[6] was used for locating intermediates and transition states along the reaction path. The lowest energy structures obtained at the AM1-D3H4 level were further investigated using the Density Functional Theory method (DFT) implemented in the Gaussian 16 package[7]. DFT calculations of geometries, energies, and vibrational frequencies reported in this paper were carried out with the M06-2X functional[8] using the 6-311++G(d,p) basis set. Solvent effects (DMSO) were accounted for with PCM model[9] for all geometry optimizations, vibrational frequency and energies calculations.

All frequencies of each structure have also been calculated to verify the presence of a single imaginary frequency for transition states and the absence of imaginary frequency for ground states. The intrinsic reaction coordinate (IRC) method has been used to verify that the obtained transition states were effectively connected to the desired minima. To consider entropic effects, the energies mentioned in this study correspond to the Gibbs free energy (G).

The Intrinsic Bond Strength Index (IBSI)[10] was calculated using the IGMPlot program[11]. QTAIM analysis[12] were performed using the TopChem2 program[13].

Summary

To shed light on the experimental results comparing the reactivity of **4CC** and **4CCS**, a thorough mechanistic study was carried out by DFT calculations. To simplify the system and avoid undesirable effects of side chain groups, we performed all calculations using methylamine as the amine and methanethiol as substituent for the model **4CCS**. **4CC** was modelled as synthesized. We first compared the computed structural differences between the two cyclic carbonates to rationalize the divergent reactivity. We then proceeded to an understanding of the ring-opening mechanism that yields the expected products.

5.1 Structure-reactivity relationship

The cyclic carbonates **4CC** and **4CCS** were first optimized and different descriptors were used to rationalize the structure-reactivity relationship. This was achieved through (i) bond lengths, (ii) perturbation theory, (iii) AIM (Atoms in Molecules), and (iv) IBSI (Intrinsic Bond Strength

Index). The 3D structures of both cyclic carbonates with a label of the key atoms are represented in Figure S22 and the key extracted data in Table S1.

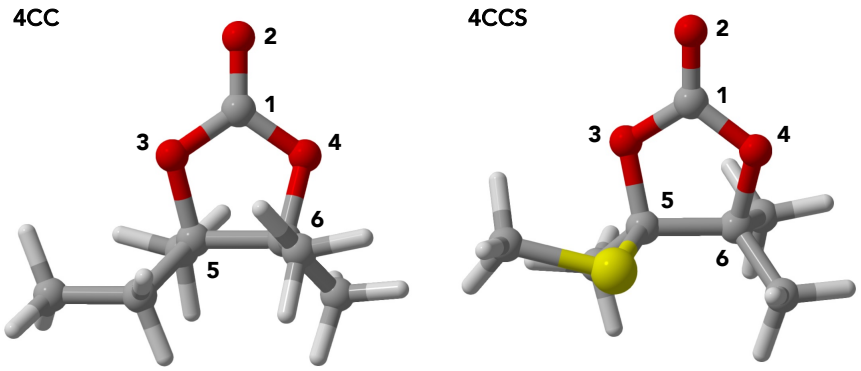

Figure S22 – Optimized 3D structures of **4CC** (left) and **4CCS** (right).

Table S1 – Comparative analysis of **4CC** and **4CCS** through key parameters obtained by DFT optimized structures, AIM and IBSI analyses.

	Atom labels	**4CC**	**4CCS**
Distance (Å)	1-3	1.337	1.347
	1-4	1.338	1.334
	3-5	1.462	1.442
	4-6	1.461	1.458
r	1-3	0.312	0.305
	1-4	0.312	0.314
	3-5	0.226	0.240
	4-6	0.227	0.229
$\nabla^2 r$	1-3	-0.527	-0.540
	1-4	-0.531	-0.520
	3-5	-0.282	-0.344
	4-6	-0.289	-0.300
H	1-3	-0.462	-0.446
	1-4	-0.461	-0.466
	3-5	-0.285	-0.311
	4-6	-0.287	-0.291
IBSI	1-3	1.389	1.347
	1-4	1.388	1.403
	3-5	1.016	1.057
	4-6	1.003	1.033

QTAIM data r , $\nabla^2 r$ and H are in atomic unit. IBSI is dimensionless.

The presence of a bond critical point between a pair of bonded atoms is generally regarded as an indicator of covalent interaction in the AIM (Atoms In Molecules). An interacting pair of atoms is characterized by the presence of a bond path and a bond critical point (bcp) along the bond path. The shared electron density shows a minimum at the bcp. The value of the electron density (r), Laplacian of electron density ($\nabla^2 r$) and Hamiltonian energy density (H) at such bond critical points provides valuable information about the nature of such interaction and sometime correlates with the strength of such interaction. In the case of all bonds, $r >> 0$, $\nabla^2 r << 0$, $H < 0$ at their bcp, meaning that these bonds are polarized covalent bonds.

More interesting are the value of r, $\nabla^2 r$ and H at the bcp of the C(1)-O(3) *vs* C(1)-O(4) and O(3)-C(5) *vs* O(4)-C(6) bonds which are almost identical for **4CC** meaning that the cyclic structure is symmetric in terms of bond strength as also reflected in bond lengths (1.337 Å *vs* 1.338 Å for C(1)-O(3) *vs* C(1)-O(4) and 1.462 Å *vs* 1.461 Å for O(3)-C(5) *vs* O(4)-C(6)). In the same way, the intrinsic bond force index (IBSI), an index allowing to range all two-center chemical bonds by their intrinsic strength in molecular situation, shows very close value between C(1)-O(3) (1.389) and C(1)-O(4) (1.388) as well as between O(3)-C(5) (1.016) and O(4)-C(6) (1.003).

In the case of **4CCS**, the situation is clearly different, since QTAIM descriptors, bond lengths and IBSI show an asymmetry in the cyclic structure with regard to bond strengths. Due to the presence of the thiol group, the C(1)-O(3) bond (1.347 Å) is longer than the C(1)-O(4) bond (1.334 Å) and the IBSI indicates a weaker C(1)-O(3) bond (1.347) than the C(1)-O(4) bond (1.403). In contrast, the O(3)-C(5) bond (1.442 Å) is shorter than the O(4)-C(6) bond (1.458 Å), with a stronger IBSI for the O(3)-C(5) bond (1.057) than for the O(4)-C(6) bond (1.033). The QTAIM descriptors follow exactly the same trends, as detailed in Table S1. It is worth noting that perturbation theory analysis highlighted the presence of stabilizing interactions between the lone pair of the S atom and the antibonding sigma bond C(3)-C(5), and between the lone pair of O(3) and the antibonding sigma bond C-S. Both were non-negligible with stabilizing energies of 11.1 and 11.5 kcal·mol^{-1} respectively.

Based on these various indicators, we can suggest that the reactivity of **4CCS** should be greater than that of **4CC** for the aminolysis reaction and, in particular, should express a significant regioselectivity during the ring-opening step.

5.2 Aminolysis of 4CC

The aminolysis of **4CC** was first studied. This cyclic carbonate bears 4 aliphatic substituents (3 methyl and 1 ethyl groups). It is well-established that five-membered cyclic carbonates can undergo ring-opening aminolysis to provide hydroxy-urethanes. This ring-opening is generally non regioselective, providing two products originating from the two possible C-O bond scissions at the vicinity of the carbonate group. As already described for less substituted cyclic carbonates, this mechanism happens through attack of the amine on the carbonate group, with concomitant C-O bond scission and proton transfer from the amine to the so-formed hydroxyl group.

It must be noted that the approach of the amine onto the carbonate was a two-step process involving the formation of a meta-stable intermediate **int0-Et**. During the amine approach, a transition state **TS0-Et** of rather low energy (around 24 kcal·mol^{-1}) was located, whose imaginary frequency was attributed to the formation of a bond between the electrophilic carbonate carbon atom and the nitrogen atom of the amine. Overcoming this transition state was leading to the intermediate **int0-Et**, with a C-N bond length of 1.68 Å and the carbonyl group in a bended configuration. Despite **TS0-Et** having a higher electronic energy than **int0-Et**, the Gibbs free energy of the TS was found to be lower than that of the intermediate (Figure S23). This intermediate exhibited ambiguous bond orders, but a detailed analysis of this metastable species falls beyond the scope of this work. The energy profile leading to the subsequent transition state **TS1-Et** (higher in energy) suggests that this intermediate is solely on the path leading to **TS1-Et**. The same observation was noted for the path on the other side of the ring (i.e. passing by **TS0-Me** and **TS1-Me**).

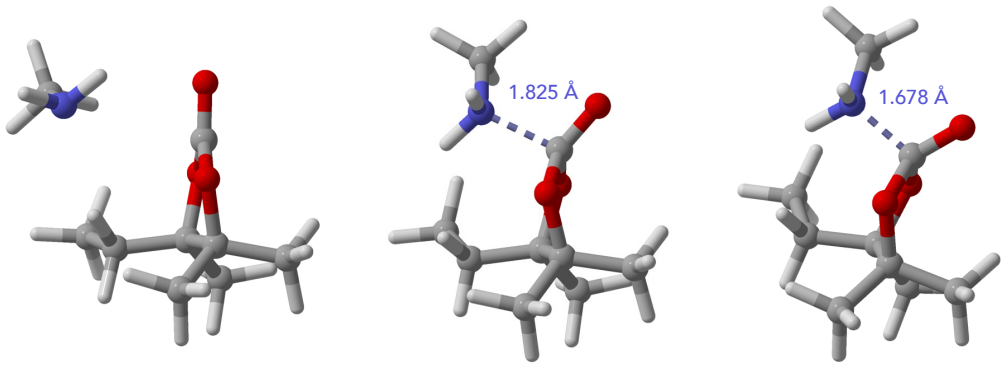

Figure S23 – Electronic energies and Gibbs free energies of pre- and post-reactive intermediates along with their TS (**TS0-Et**).

The bond scission was modelled on both sides of the carbonate, in proximity to the ethyl or the methyl group. Both steps revealed to be rate-determining with energy barriers of 47.1 and 47.3 kcal·mol^{-1} for the ring-opening on the side of the ethyl **TS0-Et** and the methyl groups **TS0-Me** respectively. This small energy difference is expected to provide the two regioisomers with no kinetically defined preference for one pathway. The products of reactions were also of similar energy: 7.0 and 6.6 kcal·mol^{-1}. This destabilization energy is expected to render the reaction thermodynamically unfavorable. In addition to the high energy barriers, these calculations support the experimental finding that no reaction happens in the absence of a catalyst, even at high temperature. The reaction pathway is provided in Figure S24 along with the energetics and structures of transition states and intermediates toward both regioisomers.

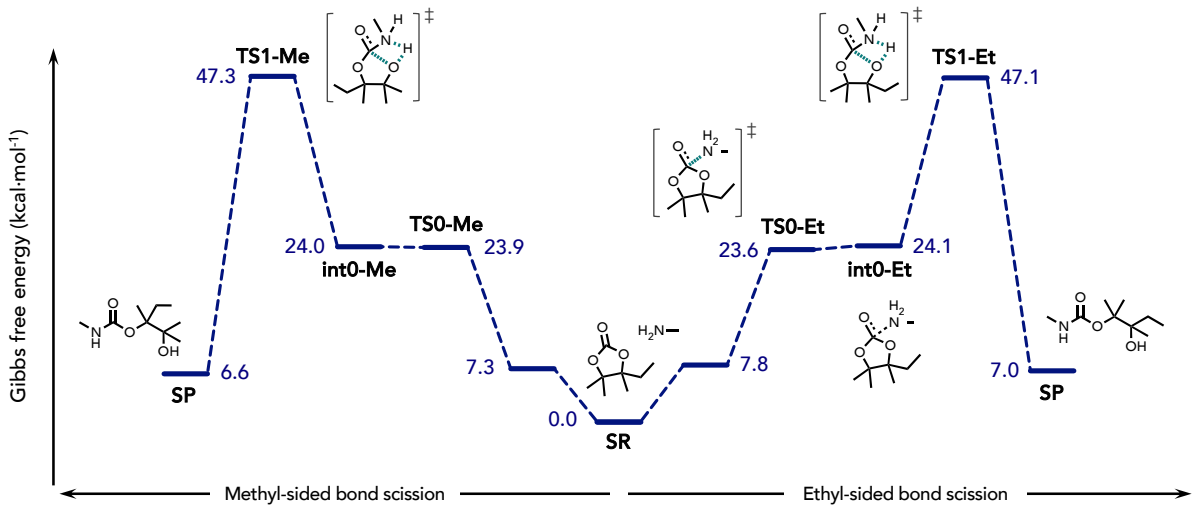

Figure S24 – Gibbs free energy profile for the ring-opening aminolysis of **4CC** with bond scission on both sides of the carbonate function.

5.3 Aminolysis of 4CCS

The aminolysis of **4CCS** was then studied. An important feature of this cyclic carbonate is its experimentally observed regioselective ring-opening. This was supported by DFT calculations through the modelling of ring-opening by both C-O bond scission and a comparison of their respective energetics. A similar mechanism to **4CC** aminolysis was determined, with a simultaneous bond scission and proton transfer to yield a tertiary hydroxyl group. Also, a meta-stable intermediate was observed during the approach of the amine toward the cyclic carbonate in both cases.

We first modelled the ring-opening aminolysis through the C-O bond scission adjacent to the two methyl groups. This pathway is characterized by an energy barrier of 44.3 kcal·mol^{-1} at **TS1-w** (**w** for wrong side), which is only slightly lower than that determined for **4CC**. The product is also destabilized by 5.8 kcal·mol^{-1}, indicating that the reaction is thermodynamically unfavorable.

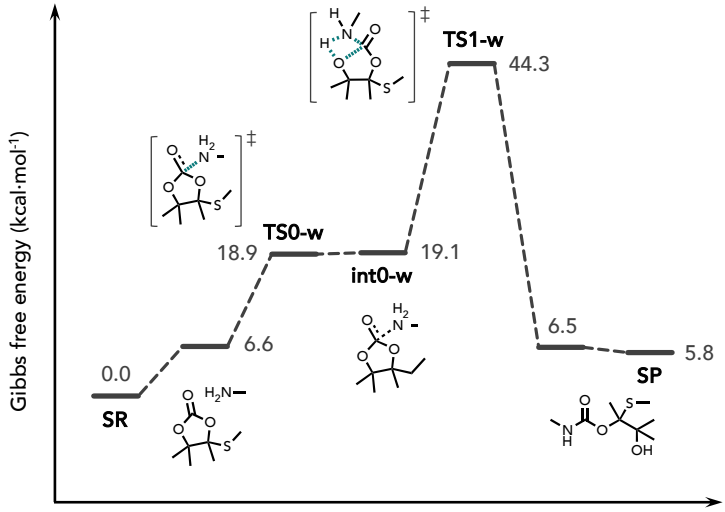

Figure S25 – Gibbs free energy profile for the ring-opening aminolysis of **4CCS** with bond scission on the wrong side of the carbonate function.

When the ring was opened through the C-O scission in vicinity of the sulfur atom (pathway 1), the energy barrier readily decreased to a value of 38.0 kcal·mol^{-1}. The experimental regioselective ring-opening can therefore be explained by a kinetically favorable bond scission on one side of the carbonate group. After aminolysis and proton transfer to form a hydroxyl group, a hemithioacetal intermediate **int1** is formed. These species are known to dissociate into the former ketone and a thiol. This step allows the formation of an oxo-urethane **int2** after proton transfer aided by the -NH- group through an intramolecular 6-membered ring. This step is characterized by an energy barrier of the same order as **TS1** (37.5 kcal·mol^{-1}). The *oxo*-urethane, observed experimentally, can then undergo an intramolecular ring-closure to yield an oxazolidone **1**. This step is aided by the released thiol and possesses a low energy barrier of 27.7 kcal mol^{-1}, supporting why the *oxo*-urethane intermediate is barely observed by NMR during the kinetic experiments. The formation of five-membered oxazolidone is accompanied by a stabilization energy of -11.8 kcal·mol^{-1}, suggesting the reaction to be thermodynamically favorable.

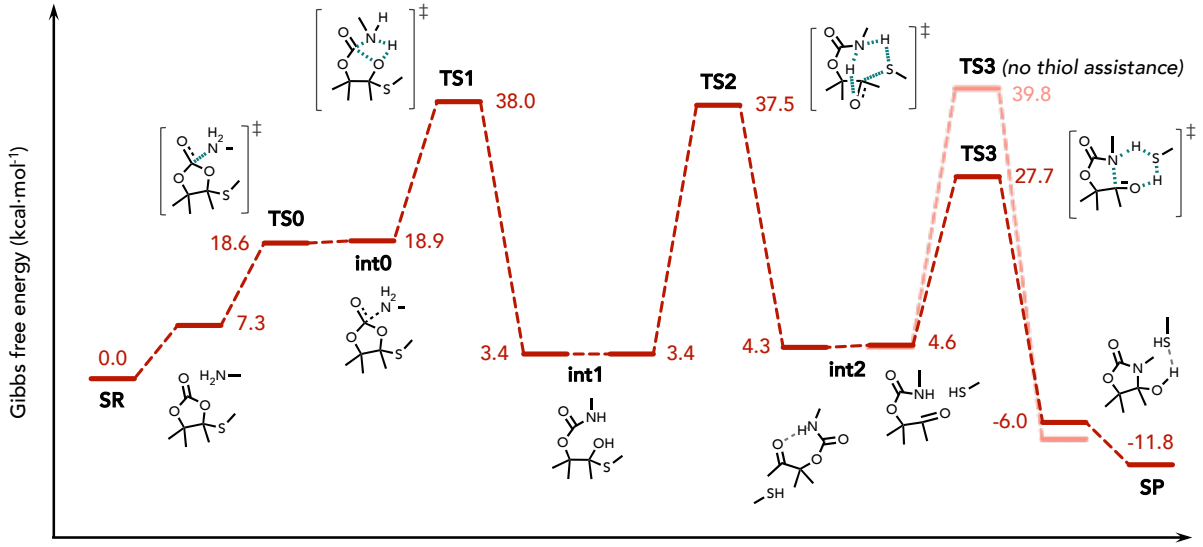

Figure S26 – Gibbs free energy profile for the ring-opening aminolysis of **4CC** with one amine. **TS3** was represented with or without the thiol assistance in lowering the energetics of the TS.

Interestingly, the energy barrier for bond scission during amine attack was greatly influenced by the face of attack. The above-described energy barrier for this step was calculated to be of 38.0 kcal·mol^{-1}. In that scenario, the attack of the thiol was achieved on the same side of the ring as the sulfur atom. When the same transition state was located but on the other side of the ring, a greater energy barrier of 42.7 kcal·mol^{-1} was determined for **TS1-f** (**f** for bad face). This result is even more surprising as the S-containing side of ring is more hindered (Figure S27).

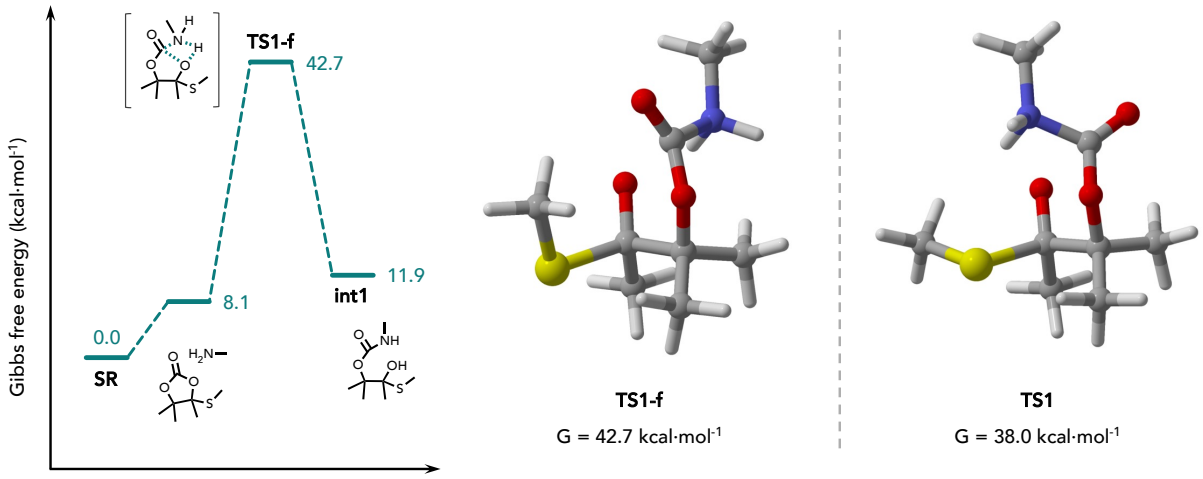

Figure S27 – Gibbs free energy profile for the ring-opening aminolysis of **4CC** with one amine (first step) by attack of the amine on the opposite face of the ring. Both **TS1** (favorable face of

attack) and **TS1-f** (unfavorable face of attack) are represented with the energy barrier associated with each TS.

To shed light on this striking difference, we also had a deeper look at the approach of the amine toward the ring in both cases. Unexpectedly, no meta-stable intermediate **int0-f** could be located in the case of an attack on the oppose side of the ring. Instead, our IRC calculation has shown that the path was directly leading to the separate reactants with no stationary point. However, a loss of inflection was observed at a C-N bond distance of 1.783 Å (Figure S28).

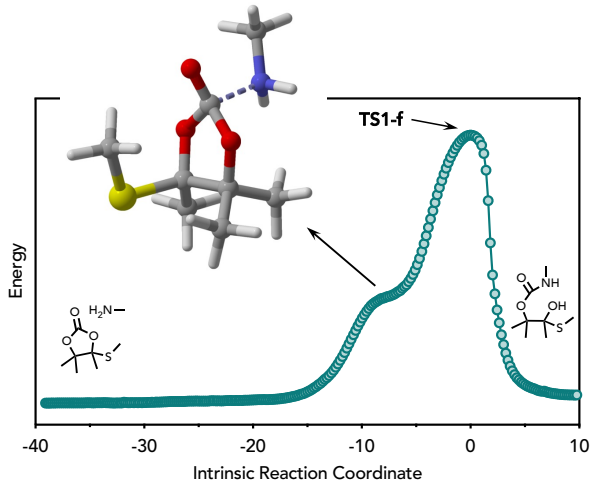

Figure S28 – IRC from **TS1-f** toward pre- and post-reactive complexes.

As already mentioned, the attack of the amine on the right side of the ring proceeded through the meta-stable intermediate as highlighted for the **4CC** aminolysis. As the amine is approaching **4CCS** on the side of the sulfur atom, we noticed some possible favorable orientation of the amine regard the sulfur atom. We performed NBO calculations and analyzed the molecular orbitals interactions through the second order perturbation theory analysis. A stabilizing energy through injection of electron density from the lone pair of the sulfur atom to the antibonding orbital of the N-H bond was found to increase from 0.96 to 7.38 kcal·mol^{-1} along the approach of the amine toward **int0**. We therefore hypothesize this favorable interaction to take part into the favored approach of the amine to this side of the ring. A deeper understanding of this behavior is however out of the scope of this work.

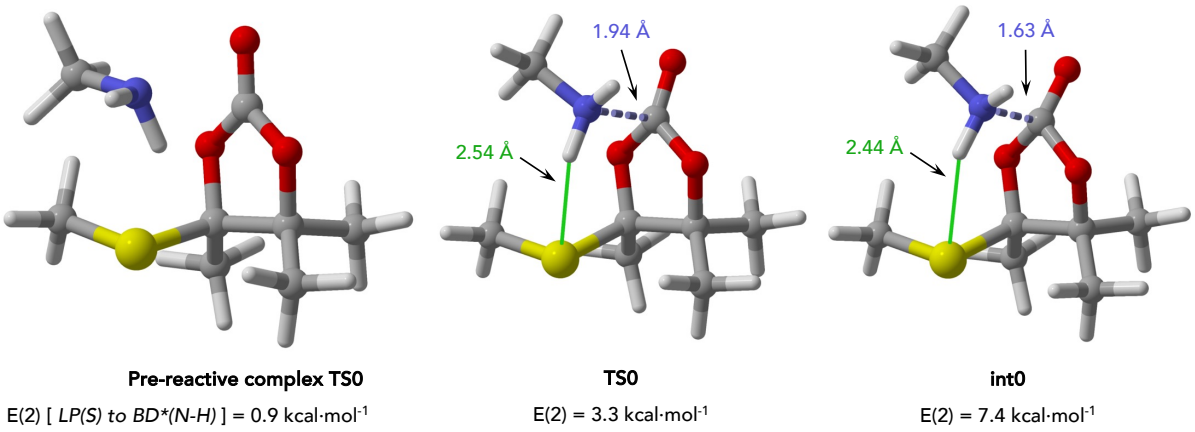

Figure S29 – 3D structures of the pre-reactive complex before **TS0**, **TS0**, and **int0** the post-reactive complex after **TS0**. The interaction between the lone pair of the S atom (*LP(S)*) with the antibonding N-H sigma bond (*BD*(N-H)*) was highlighted and the energy stabilization originating from this interaction attributed to each structure as determined by the perturbation theory.

<u>Alternative pathway 2</u>

An alternative pathway was determined to pathway 1. The approach of the amine toward **4CCS** stays the same with the formation of **int0**. However, the transition state **TS1'** differs from **TS1** as the amine is able to do a concerted proton transfer to the leaving thiol as the C-O bond scission occurs. The *oxo*-urethane **int2** is therefore formed in one step. The last step, involving ring-closure into the oxazolidone, stays the same (Figure S30). The overall energy barrier of this path is 37.4 kcal·mol^{-1}, which is very close to pathway 1. Both mechanisms are therefore likely to happen.

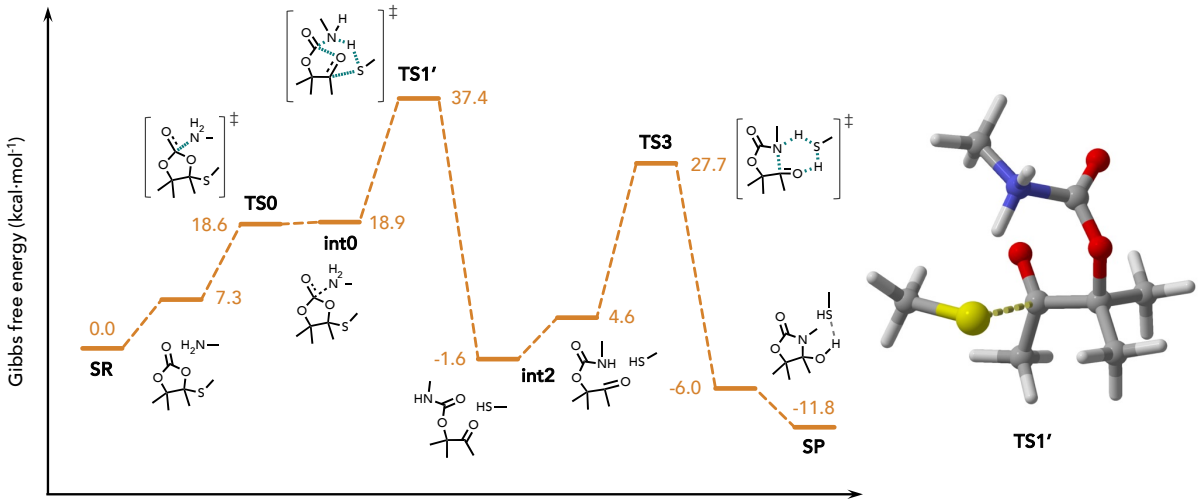

Figure S30 – Gibbs free energy profile for the ring-opening aminolysis of **4CC** with one amine in an alternative favorable pathway where **TS2** is bypassed.

5.4 Aminolysis of 4CCS with 2 amines

It has been determined experimentally that the addition of more equivalents of amine had a great impact on the reaction rate. We therefore hypothesized that several amines might be implied in the reaction mechanism. To this aim, we modelled the reaction of **4CCS** with two amines instead of one.

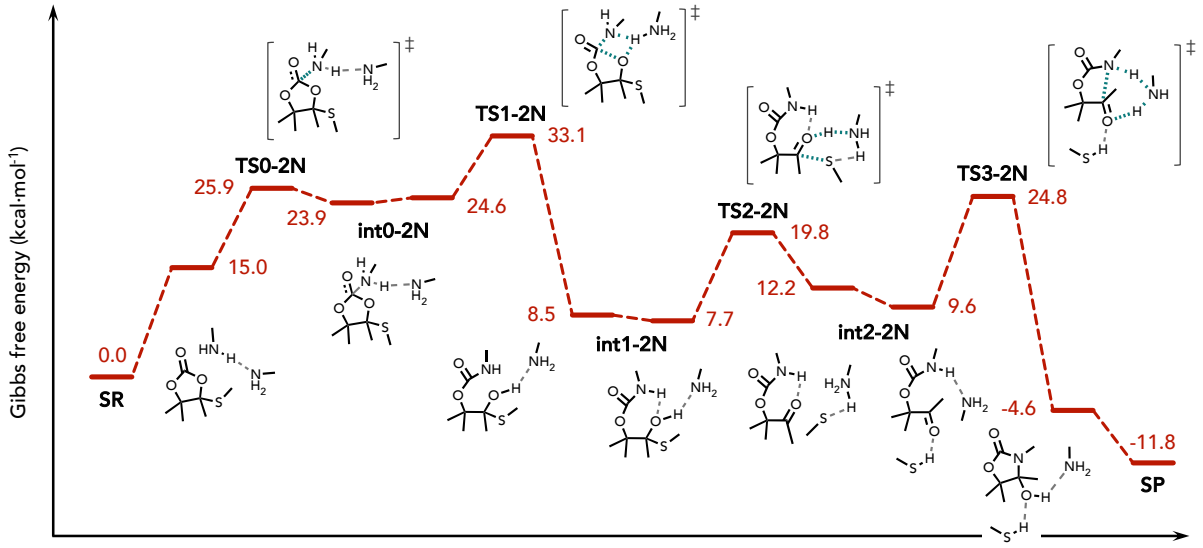

Figure S31 – Gibbs free energy profile for the ring-opening aminolysis of **4CC** with two amines.

The reaction was initiated by the formation of a meta-stable intermediate **int0-2N** (**2N** standing for 2 amines $\underline{N}H_2$-Me). It must be noted that **TS0-2N** was here of higher energy than both pre- and post-reactive complexes unlike **TS0**. After the formation of the complex **int0-2N**, the hemiacetal intermediate **int1-2N** was formed through C-O bond scission and transfer of a proton to the so-formed hydroxyl group. This step was aided by the second amine acting as a proton relay, through the formation of an ammonium which subsequently transfers its acidic proton to the oxygen atom. The complete IRC profile with key structures are provided in Figure S32. The formation of *oxo*-urethane **int2-2N** by thiol ejection from the hemiaminal is hugely influenced by the presence of the second amine, which can here act as a proton relay between the hydroxyl group and the leaving thiol to lower the energy barrier to only 19.8 kcal·mol^{-1} for this step. Finally, the formation of the hydroxyoxazolidone **1** by ring-closure was also favored by the presence of the amine acting as a proton relay and the thiol stabilizing the partial negative charge formed on the carbonyl group of the ketone, lowering the energy barrier to 24.8 kcal·mol^{-1}.

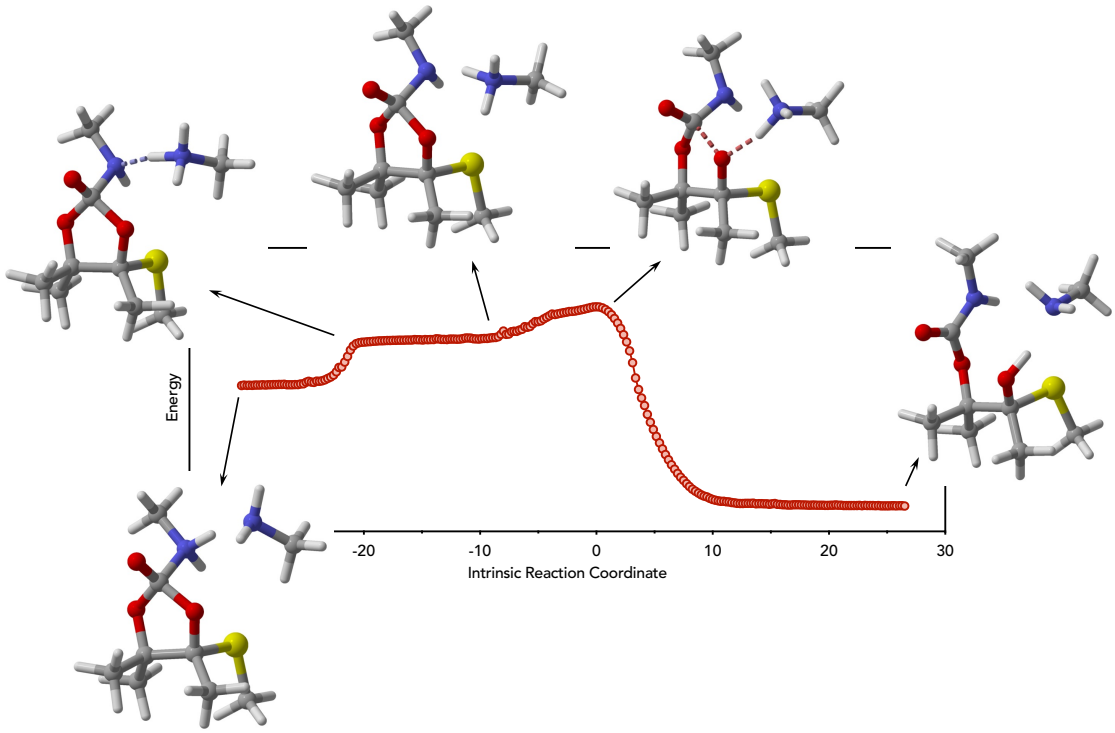

Figure S32 – IRC from **TS1-2N** toward pre- and post-reactive complexes.

Alternative pathway

Interestingly, an alternative pathway bypassing the 2-step addition and elimination process was also found for a system comprising two amines. In a very similar fashion, the complex **int0-2N** between the amine and the cyclic carbonate was formed. The bond scission was then initiated as above with the help of the second amine which can trap the proton released from the attacking amine. In this scenario, the so-formed ammonium does not release the proton to the hydroxyl group but rather keeps in interaction with the thiol as an acid-base complex. The *oxo*-urethane is therefore directly obtained through this step with an energy barrier of 35.7 kcal·mol^{-1}. The following ring-closure into an oxazolidone keeps the same as in the other mechanism involving two amines.

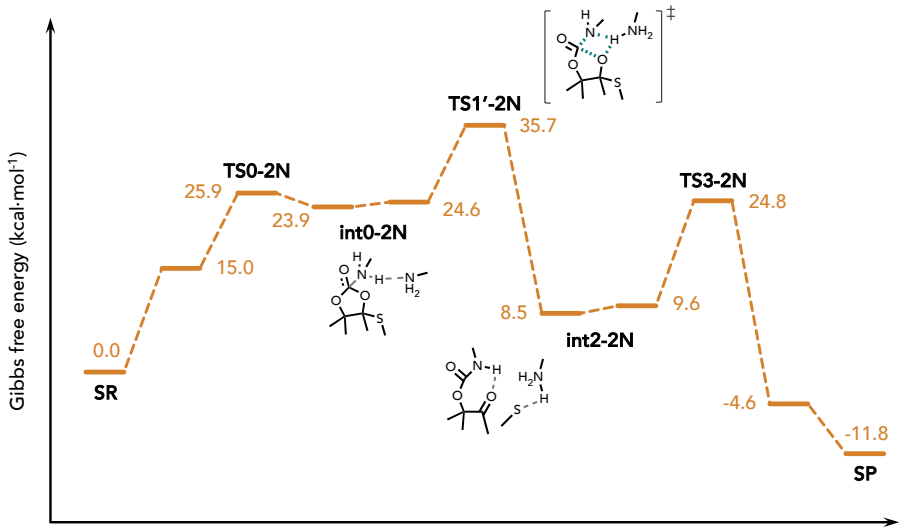

Figure S33 – Gibbs free energy profile for the ring-opening aminolysis of **4CC** with two amines in an alternative favorable pathway where **TS2** is bypassed.

6. Polymer synthesis & characterization

The protocol of synthesis toward poly(cyclic carbonate-co-thioether)s was adapted from a seminal work of some of us[2], and was optimized to reach high molar masses. The objective was to enhance the polymers mechanical properties, strongly dependent on macromolecular chain entanglement.

To reach high molecular weight in step-growth polymerization, the system must be highly concentrated. At temperatures as low as 25 °C, high viscosities are reached even at low molar masses during polymerization. This generally leads to vitrification. To overcome this issue, we opted for a mechanical stirring setup (Figure S34). The temperature during polymerization was regulated through a thermostat immersed in a water bath. As the stirrer rod is rendering the reaction medium not hermetic during rotation, a nitrogen atmosphere inlet was used to avoid contaminations by water or thiol oxidation from the air atmosphere. Although we could perform the reaction under air atmosphere and getting similar molecular weight, precautions were taken for the scale-up to the gram-scale. The same synthesis was performed on a gram-scale with a polymer synthesized with magnetic stirring and SEC chromatograms and molar masses are compared in Figure S37.

A complete characterization of the herein synthesized polymers **P1** and **P2** by NMR, SEC, TGA, DSC is available in Figures S35-41 along with pictures of the as-synthesized and pressed materials.

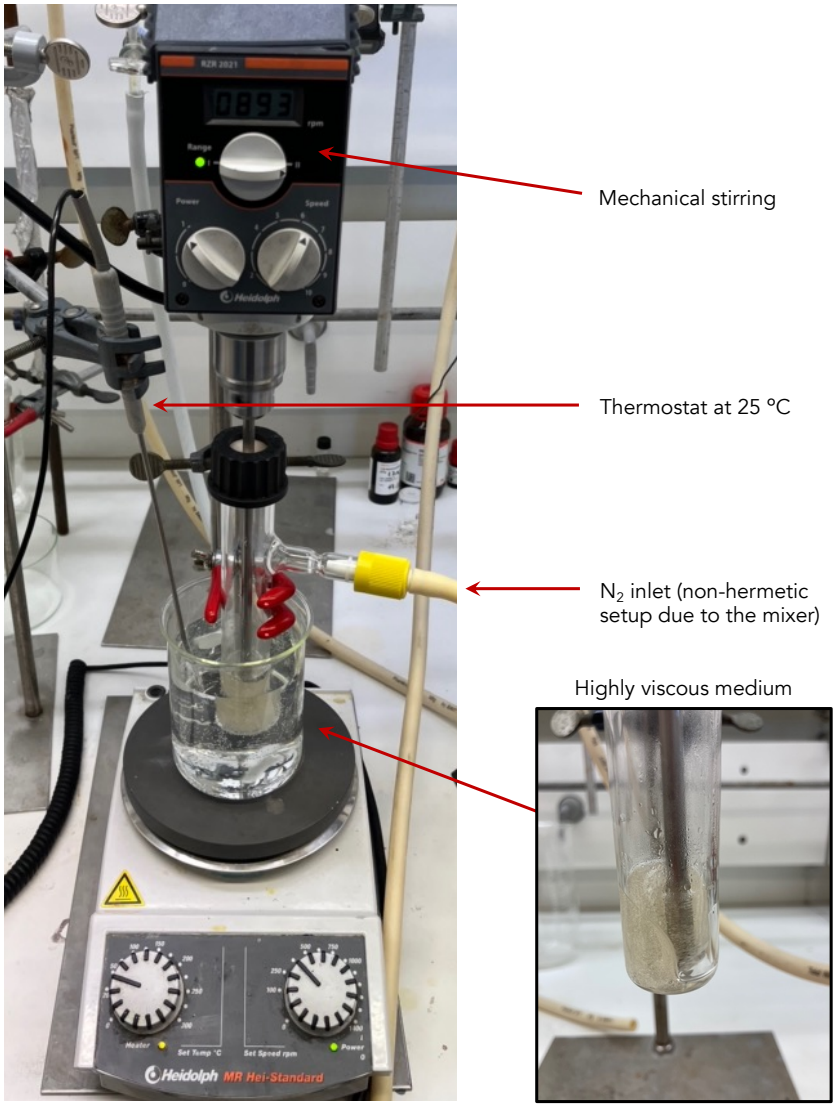

Figure S34 – Polymerization setup including a mechanical stirrer.

Synthesis of **P1**

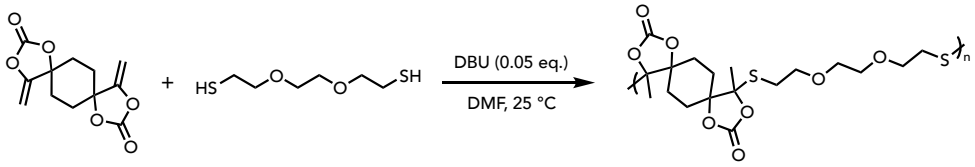

BisαCC (2.52 g, 10 mmol, 1 eq.) was added to a reaction tube with 2,2′-(Ethylenedioxy)diethanethiol (**3a**) (1.82 g, 10 mmol, 1 eq.) and DMF (5 mL). DBU (76 mg, 0.5 mmol, 0.05 eq.) was then added and the reaction mixture was stirred at 25 °C under N_2 atmosphere with a mechanical stirrer. After 24h, acetic acid (200 µL) was added to quench the reaction (by protonation of DBU) and the viscous mixture was diluted with 35 mL of dichloromethane. The polymer was precipitated in 1 L of diethyl ether. The solid was dissolved in 60 mL of dichloromethane and precipitated in diethyl ether (1 L) two times. The remaining white solid was dried under vacuum at 40 °C to yield pure **P1** (4.04 g, isolated yield 93 %).
It must be noted that the stirring speed was continuously decreased during the first hours of reaction due to an increase in viscosity. The reaction was started with a stirring rate of 600 rpm. After 30 min of reaction, the rate was decreased to 150 rpm. After 3 h, the rate was adjusted to 40 rpm until the end of the reaction (24 h).

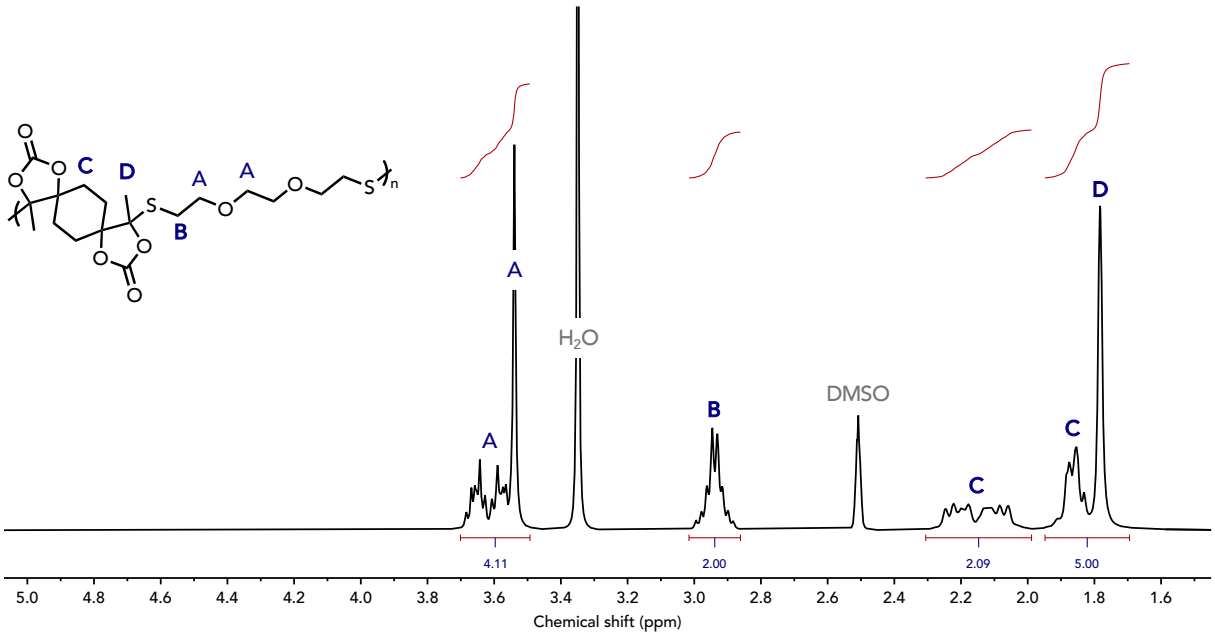

Figure S35 – ^{1}H-NMR spectrum (400 MHz, DMSO-d_6) of **P1**.

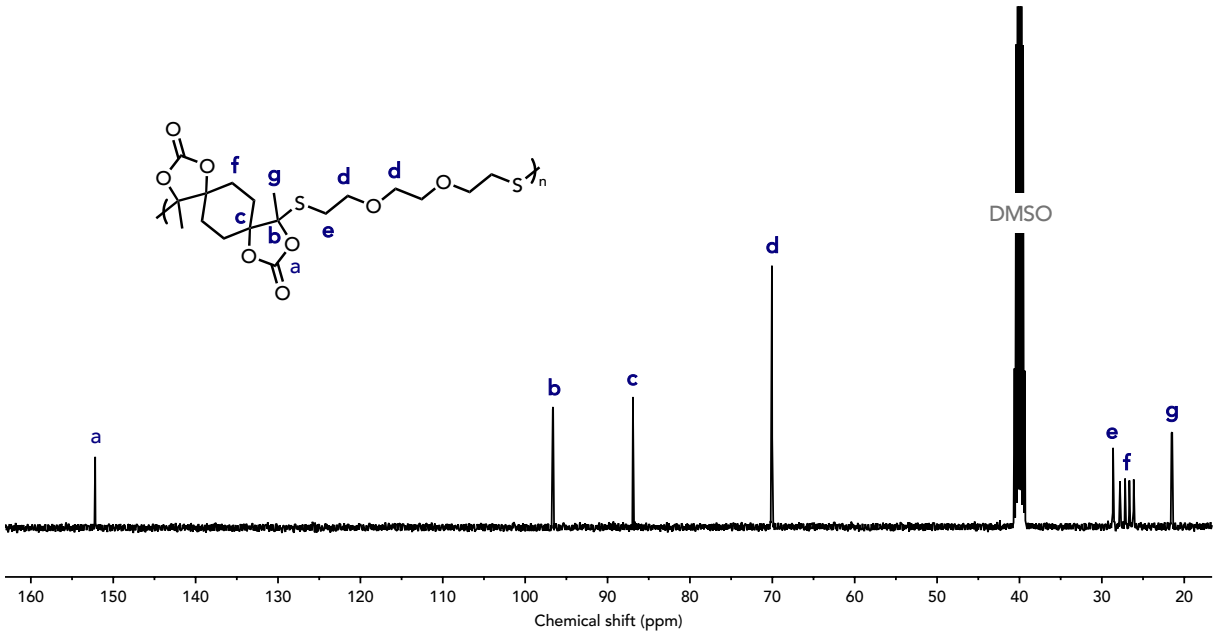

Figure S36 – ^{13}C-NMR spectrum (100 MHz, DMSO-d_6) of **P1**.

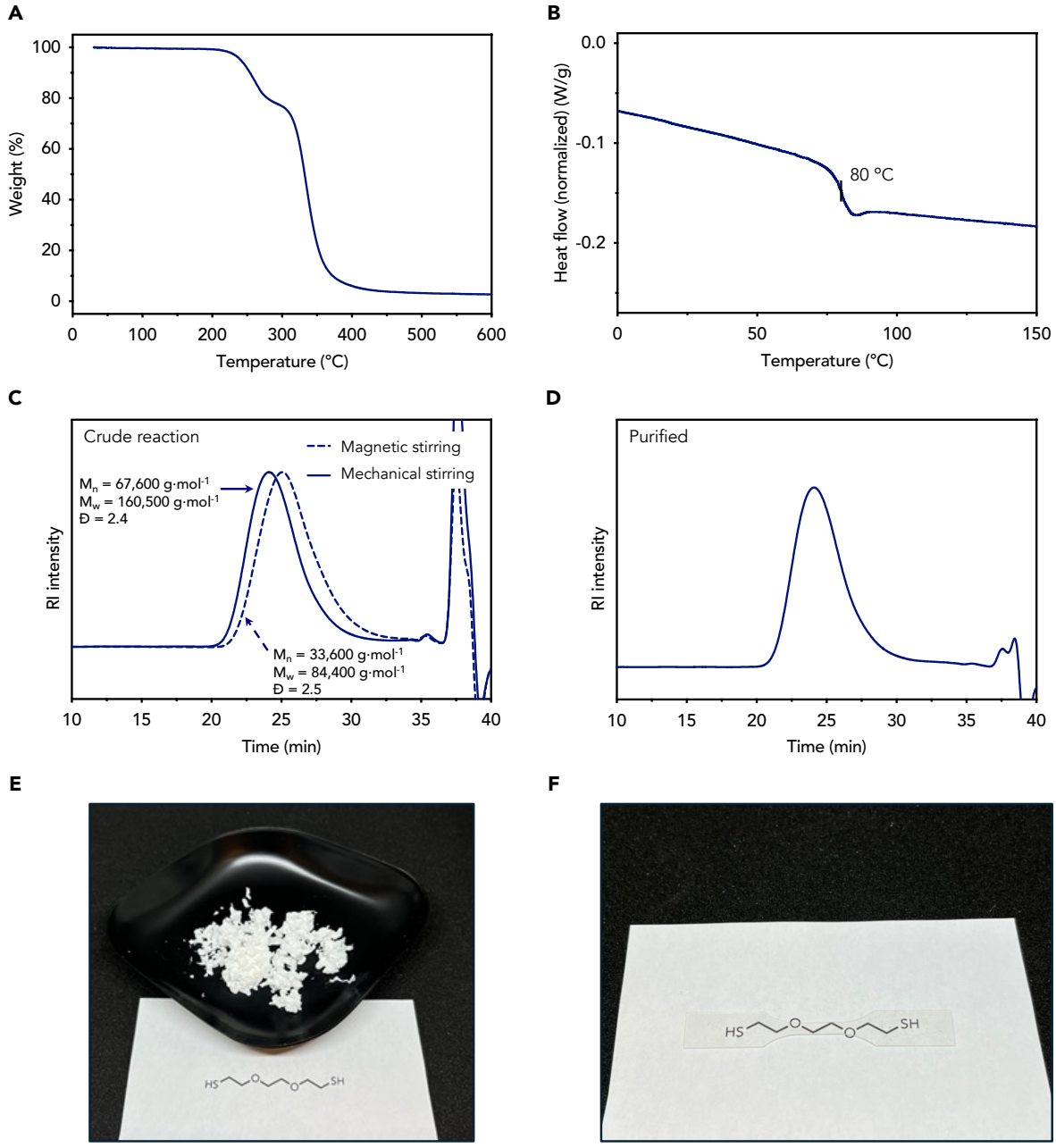

Figure S37 – (A) TGA and (B) DSC curves of **P1**. SEC traces of (C) crude reaction mixture and (D) purified **P1**. (E) Picture of pure **P1** followed by (F) a dogbone specimen following compression molding.

Synthesis of **P2**

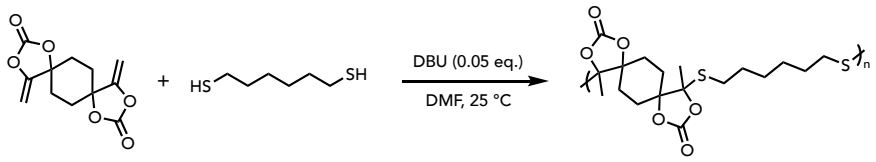

BisαCC (2.52 g, 10 mmol, 1 eq.) was added to a reaction tube with 1,6-Hexanedithiol (**3b**) (1.50 g, 10 mmol, 1 eq.) and DMF (5 mL). DBU (76 mg, 0.5 mmol, 0.05 eq.) was then added and the reaction mixture was stirred at 25 °C under N_2 atmosphere with a mechanical stirrer. After 24h, acetic acid (200 µL) was added to quench the reaction (by protonation of DBU) and the viscous mixture was diluted with 50 mL of dichloromethane. The polymer was precipitated in 1 L of diethyl ether. The solid was dissolved in 70 mL of dichloromethane and precipitated in diethyl ether (1 L). The remaining white solid was dried under vacuum at 40 °C for 24 h and at 50 °C for 2 h to yield pure **P2** (3.62 g, isolated yield 90 %).

It must be noted that the stirring speed was continuously decreased during the first hours of reaction due to an increase in viscosity. The reaction was started with a stirring rate of 1000 rpm. After 1 h 30 of reaction, the rate was decreased to 900 rpm and further decreased after 2 h of reaction to 600 rpm. After 6 h, the rate was adjusted to 150 rpm until the end of the reaction (24 h).

P2 was not soluble in DMSO-d_6 at r.T. and the spectra were therefore recorded in $CDCl_3$. However, for sake of comparison, a diluted sample was recorded in DMSO-d_6 (10 mg of **P2**, 100 µL of $CHCl_3$, and 600 µL of DMSO-d_6).

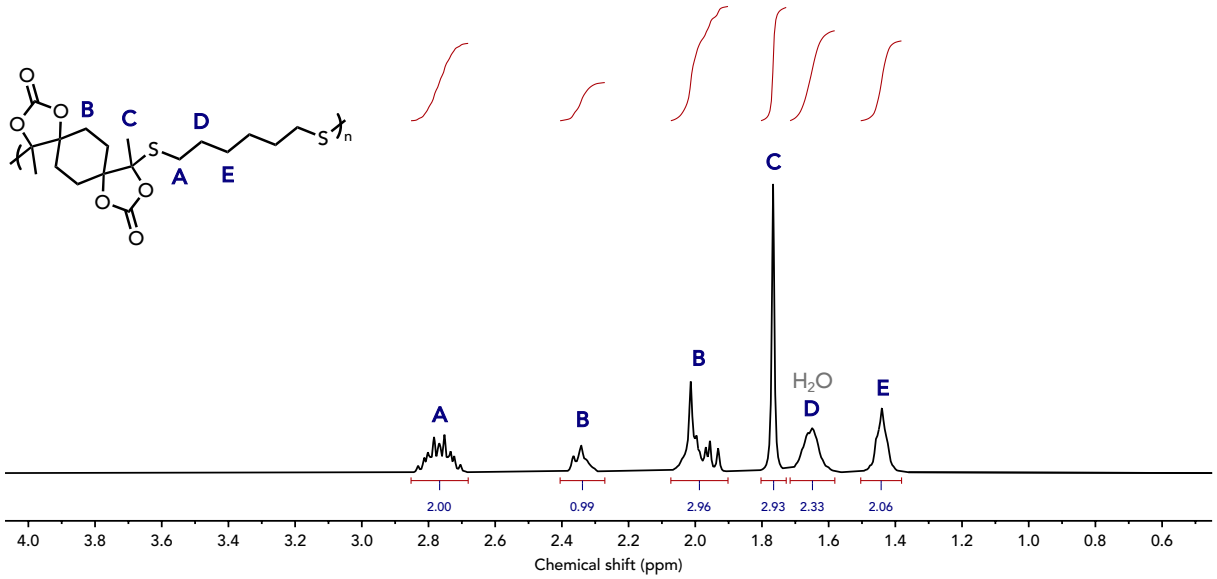

Figure S38 – ^{1}H-NMR spectrum (400 MHz, $CDCl_3$) of **P2**.

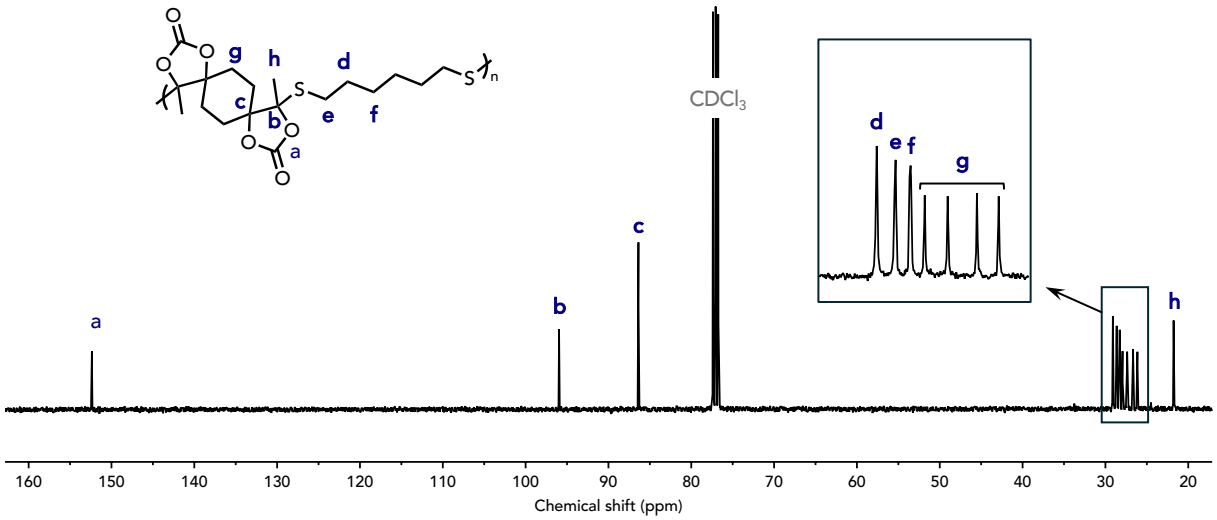

Figure S39 – ^{13}C-NMR spectrum (100 MHz, $CDCl_3$) of **P2**.

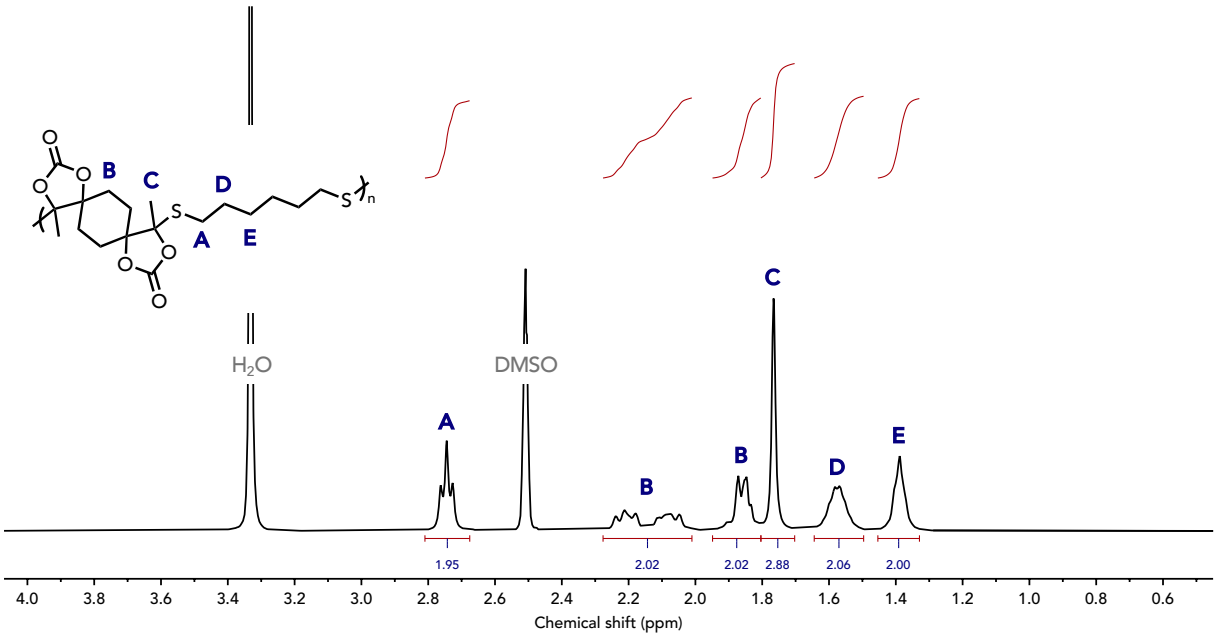

Figure S40 – ^{1}H-NMR spectrum (400 MHz, DMSO-d_6) of **P2**.

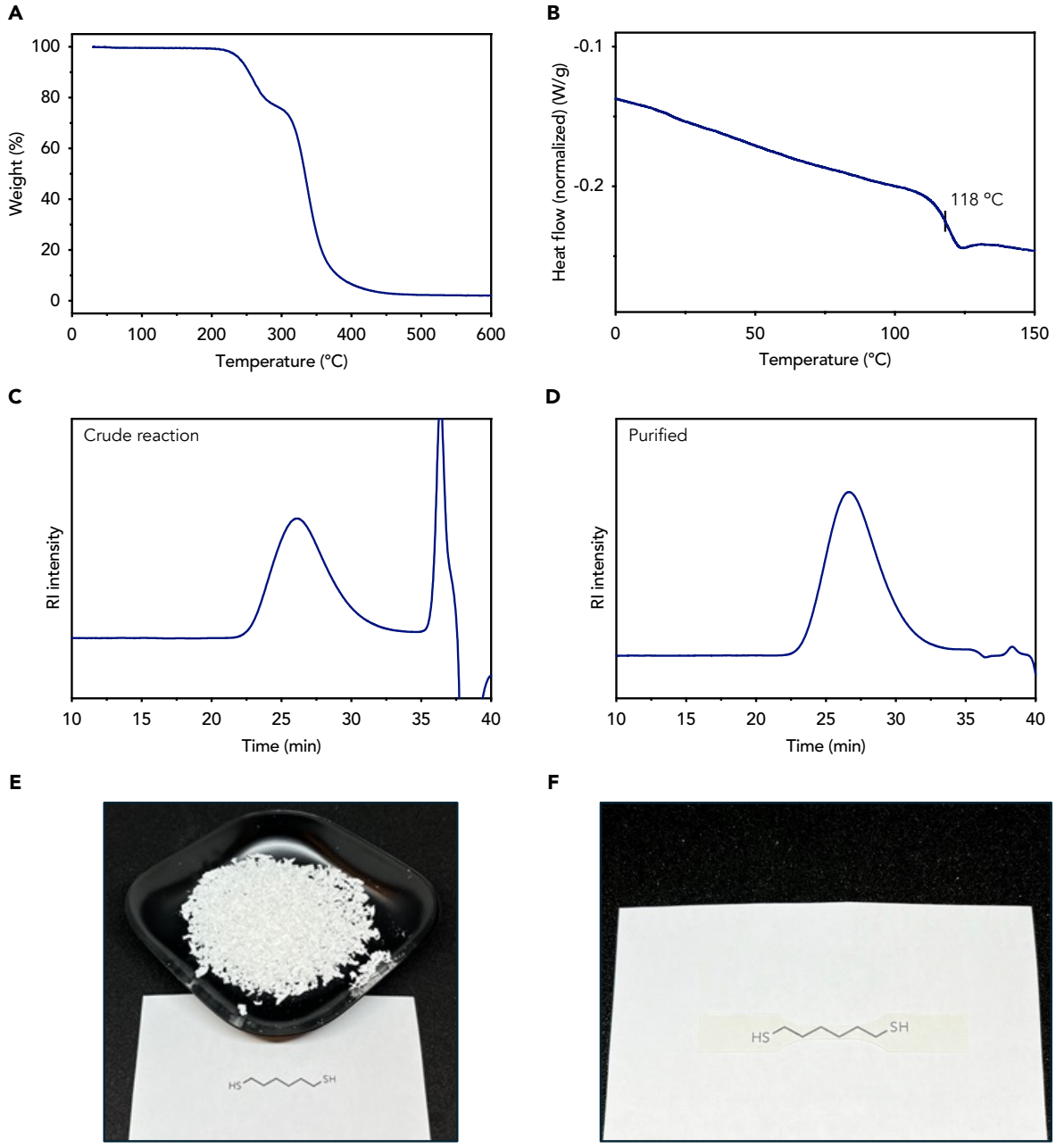

Figure S41 – (A) TGA and (B) DSC curves of **P2**. SEC traces of (C) crude reaction mixture and (D) purified **P2**. (E) Picture of pure **P2** followed by (F) a dogbone specimen following compression molding.

7. Polymer degradation by aminolysis

General procedure

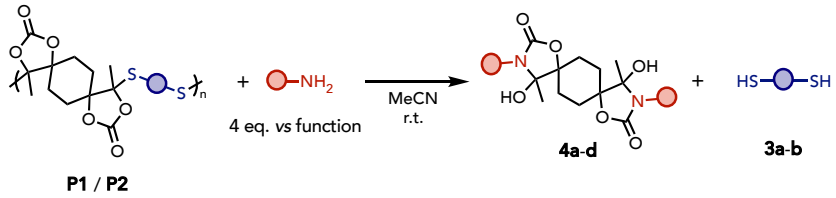

The polymer cut into pieces (434 mg of **P1** or 402 mg of **P2**, 2 mmol of function, 1 eq.) was added to a reaction tube under Ar flush. Acetonitrile (2 mL) and the amine (8 mmol, 2 eq.) were bubbled with argon and were subsequently added to the reaction tube under Ar. The reaction was stirred at r.T for a limited time (30 min to 2h). A small aliquot was sampled out of the crude reaction mixture to ensure complete conversion by ^{1}H-NMR spectroscopy. At the end of the reaction, the viscous solution was diluted with THF (10 mL, bubbled with Ar) and stirred at r.T for 5 to 10 minutes. The solution was then precipitated in cold diethyl ether (300 mL), filtrated, and the solid was washed with 100 mL of cold diethyl ether. The solid was recovered and dried under vacuum to yield pure bis(hydroxyoxazolidone) **4a-d**. The filtrate was concentrated under vacuum and purified by silica gel chromatography (short column is enough, around 10 cm in this study) with diethyl ether / hexane (50/50) as eluent for **3a** and diethyl ether / hexane (10/90) as eluent for **3b**. The dithiol **3a-b** was eluting in the first fractions of the columns, which were concentrated under vacuum to yield the pure dithiol **3a-b**.

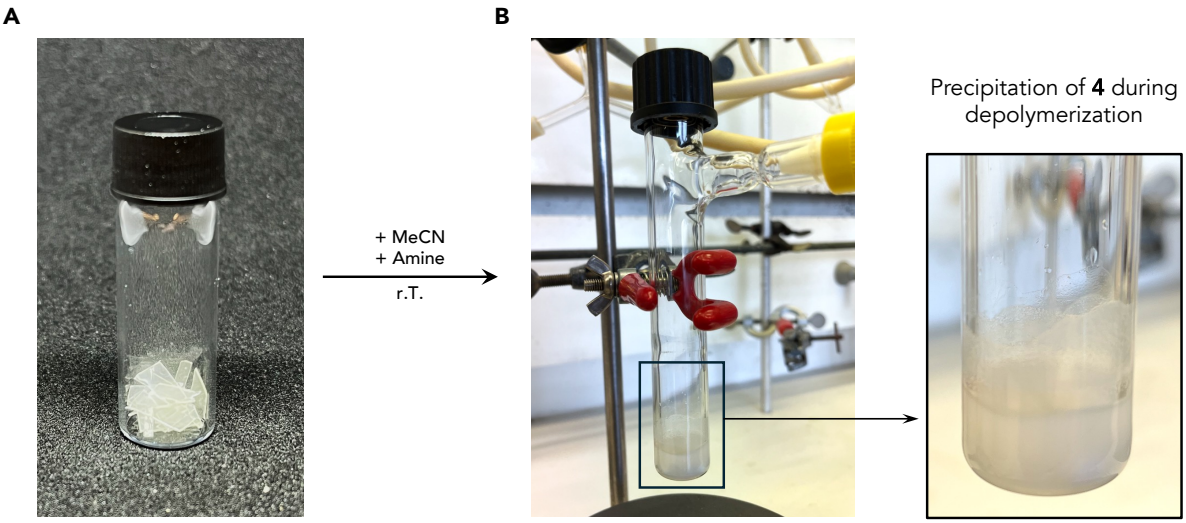

Figure S42 – (A) Shredded **P1**. (B) Depolymerization of **P1** by propylamine.

The end of reaction was assessed by evaluating the disappearance of the signals related to the polymer by ^{1}H-NMR spectroscopy. Stacked spectra of the crude reaction mixture at end of reaction with the starting polymer **P1**/**P2** and the released dithiol **3a**/**3b** were provided for all polymerizations (Figures S43-S50). Spectra of the crude reaction mixture at the end of reaction with the integration of signals corresponding to both **4** and **3** products proved total and selective conversion with an equimolar ratio between them.

It must be noted that integration was not provided for the depolymerization by propanolamine due to overlapping of the dithiol **3a** signals. However, an absorbed disappearance of the polymer's signal suggested total conversion to **4d** and **3a**. The same was noted for the depolymerization of **P2** by propylamine.

Depolymerization of **P1** by propylamine

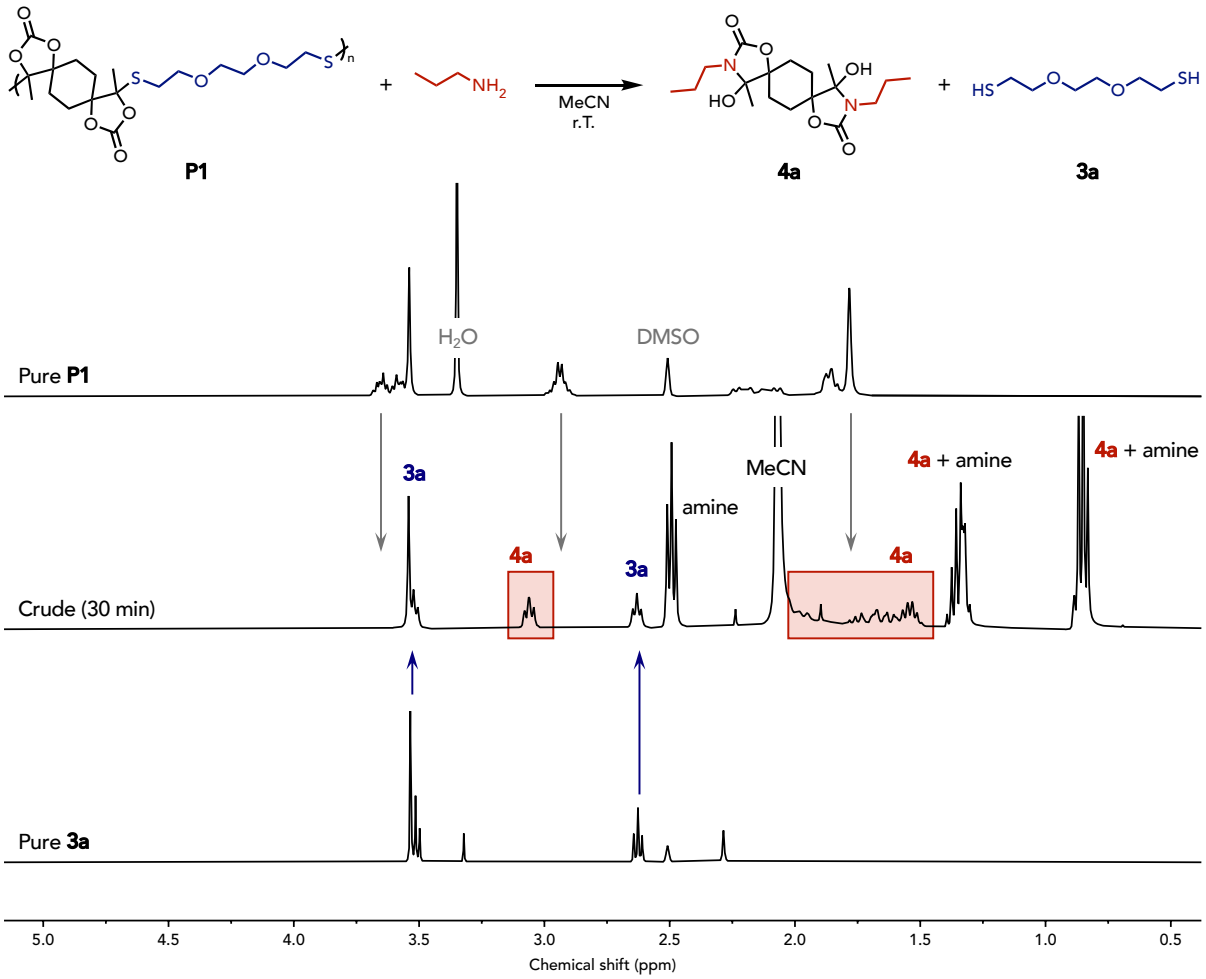

Figure S43 – Stacked ^{1}H-NMR spectra (400 MHz, DMSO-d_6) of pure polymer **P1**, crude reaction mixture after 30 min, and pure dithiol **3a**.

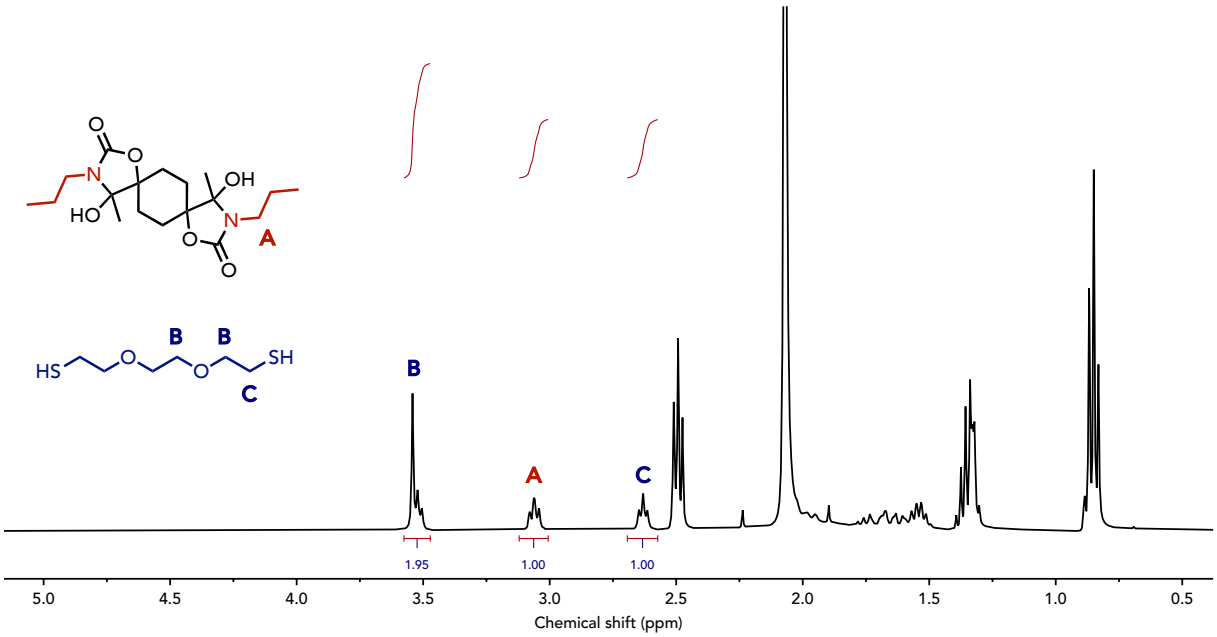

Figure S44 – ^{1}H-NMR spectra (400 MHz, DMSO-d_6) of crude reaction mixture after 30 min with integration for the two degradation products **4a** and **3a**.

Depolymerization of **P1** by heptylamine

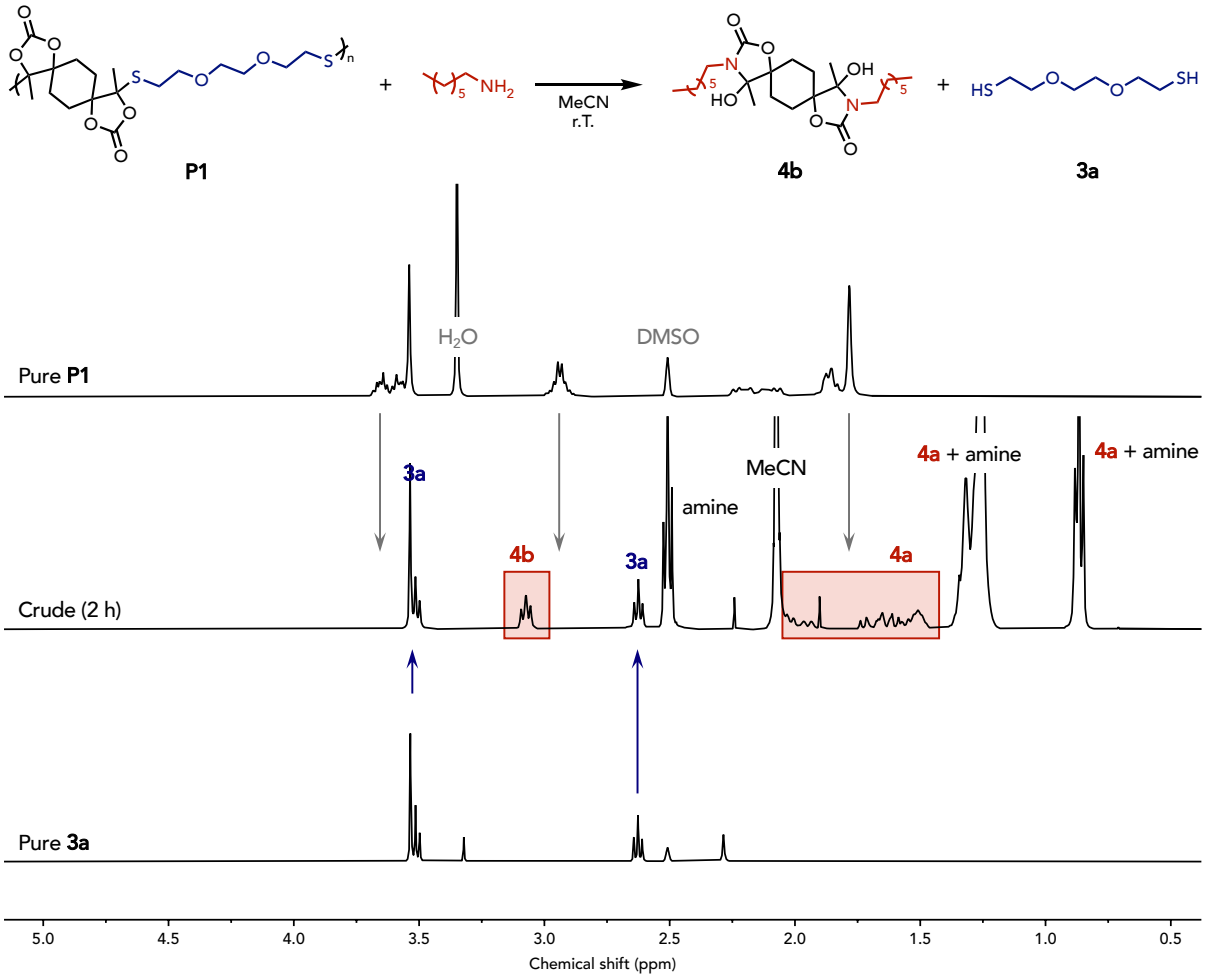

Figure S45 – Stacked ^{1}H-NMR spectra (400 MHz, DMSO-d_6) of pure polymer **P1**, crude reaction mixture after 2 h, and pure dithiol **3a**.

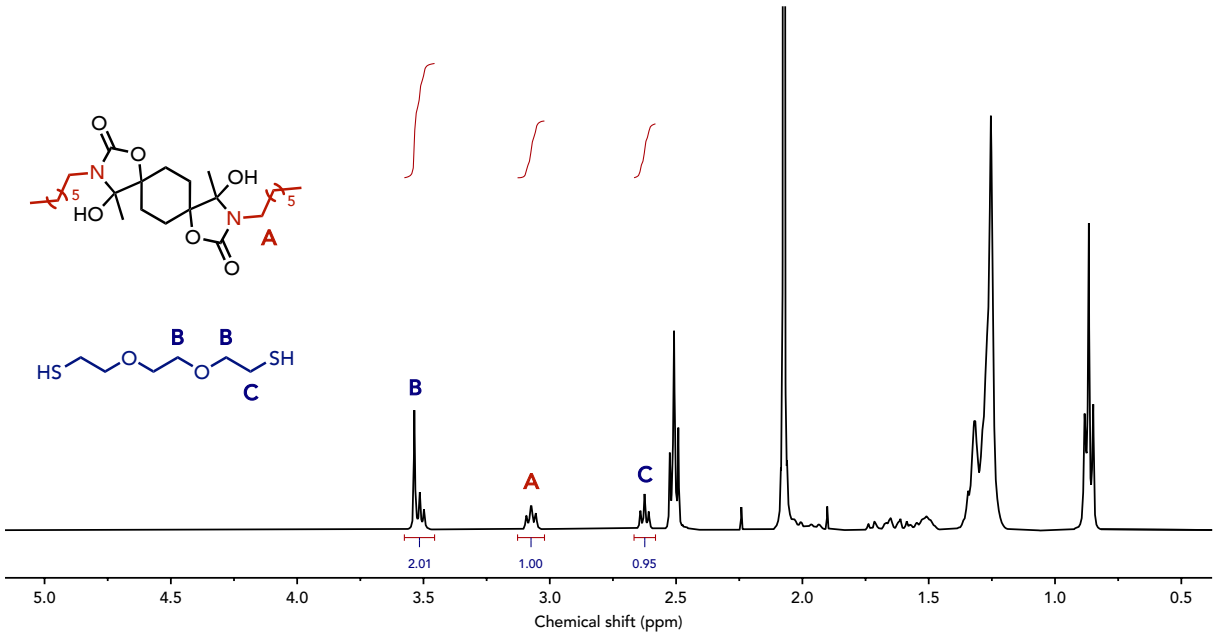

Figure S46 – ^{1}H-NMR spectra (400 MHz, DMSO-d_6) of crude reaction mixture after 2 h with integration for the two degradation products **4b** and **3a**.

Depolymerization of **P1** by 3-methoxpropylyamine

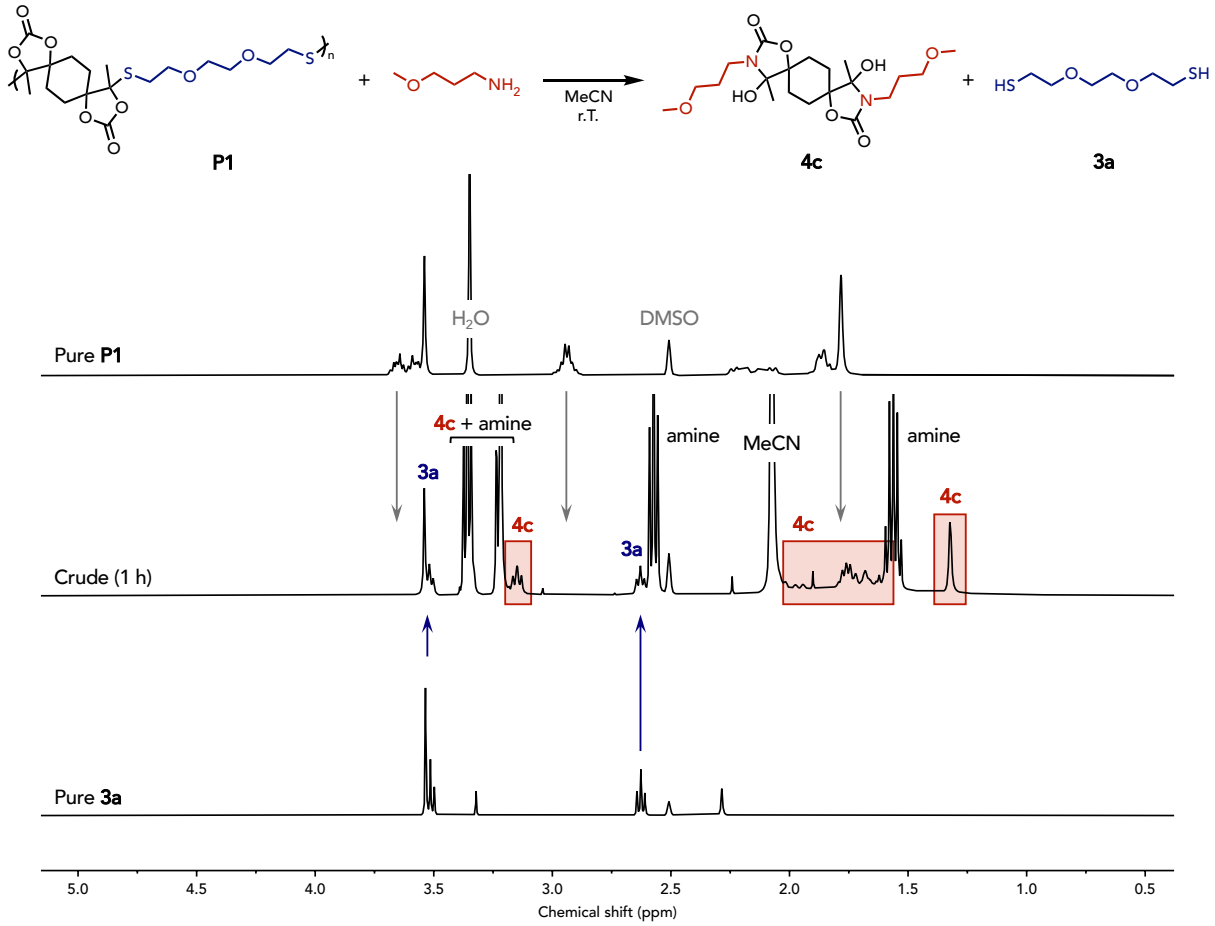

Figure S47 – Stacked ^{1}H-NMR spectra (400 MHz, DMSO-d_6) of pure polymer **P1**, crude reaction mixture after 1 h, and pure dithiol **3a**.

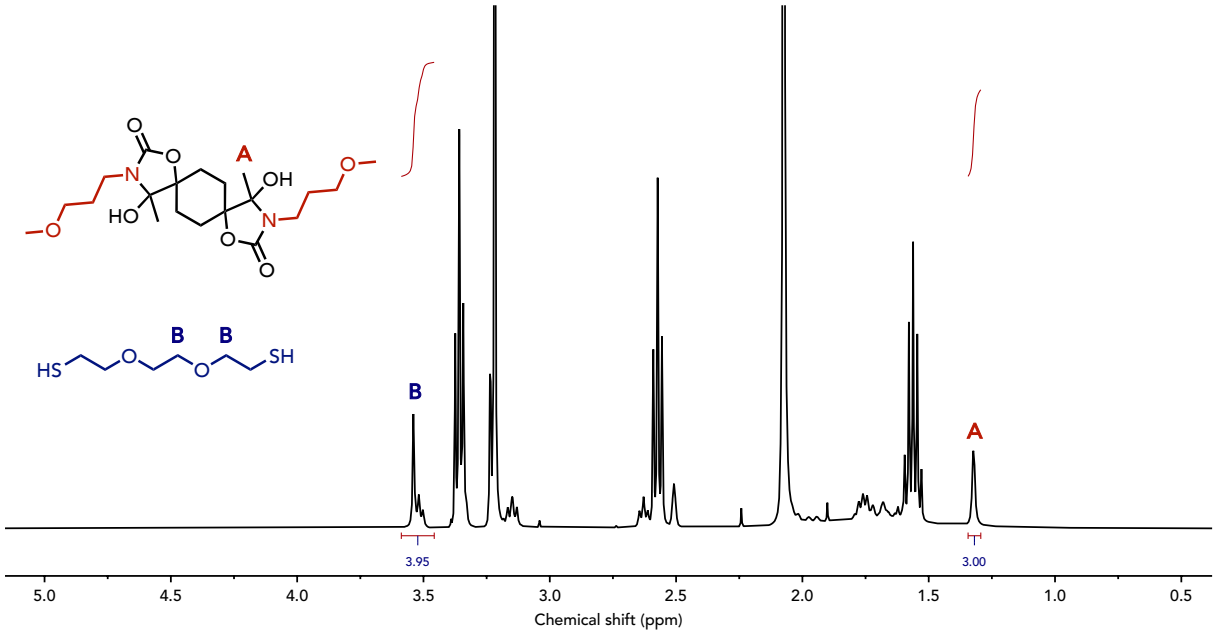

Figure S48 – ^{1}H-NMR spectra (400 MHz, DMSO-d_6) of crude reaction mixture after 1 h with integration for the two degradation products **4c** and **3a**.

Depolymerization of **P1** by propanolamine

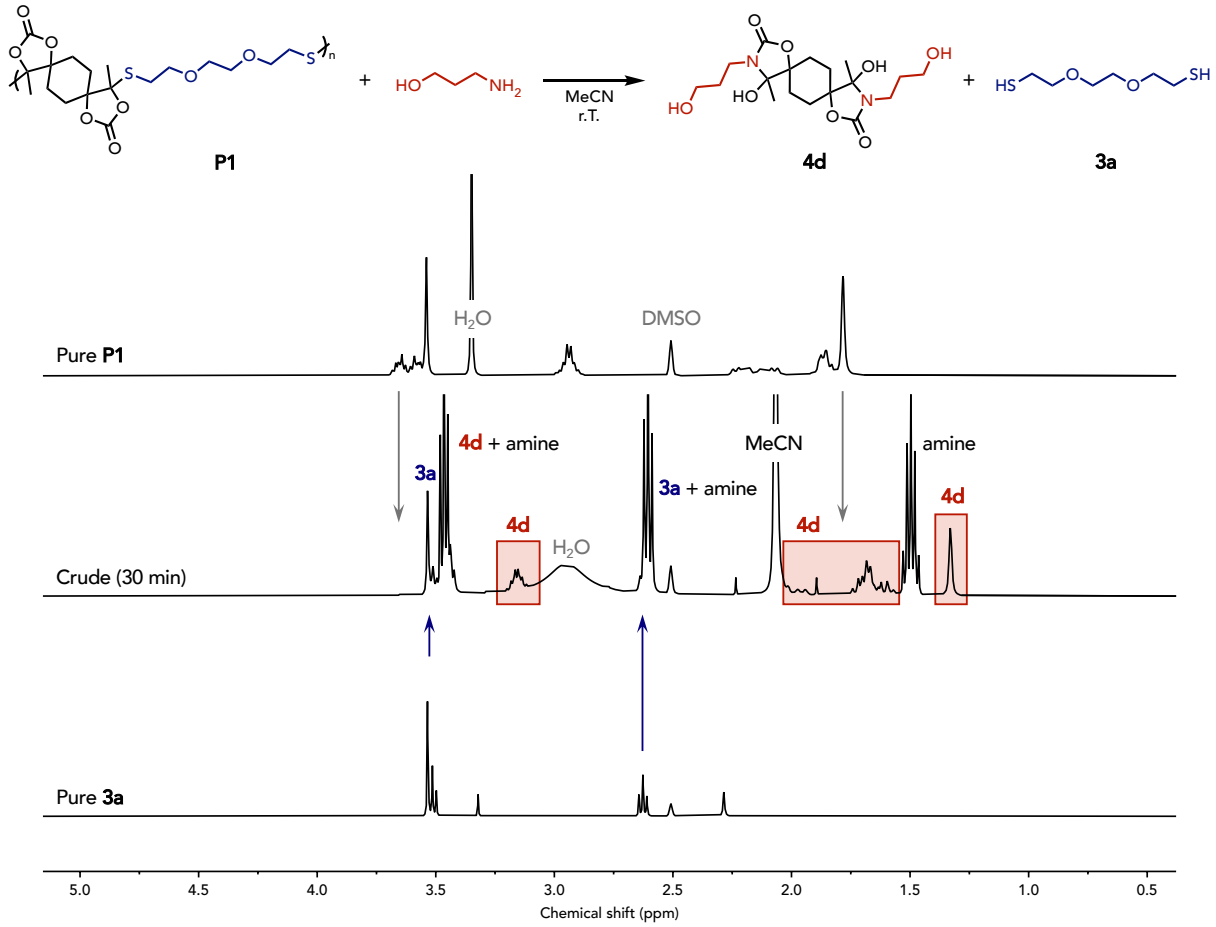

Figure S49 – Stacked ^{1}H-NMR spectra (400 MHz, DMSO-d_6) of pure polymer **P1**, crude reaction mixture after 30 min, and pure dithiol **3a**.

Depolymerization of **P2** by propylamine

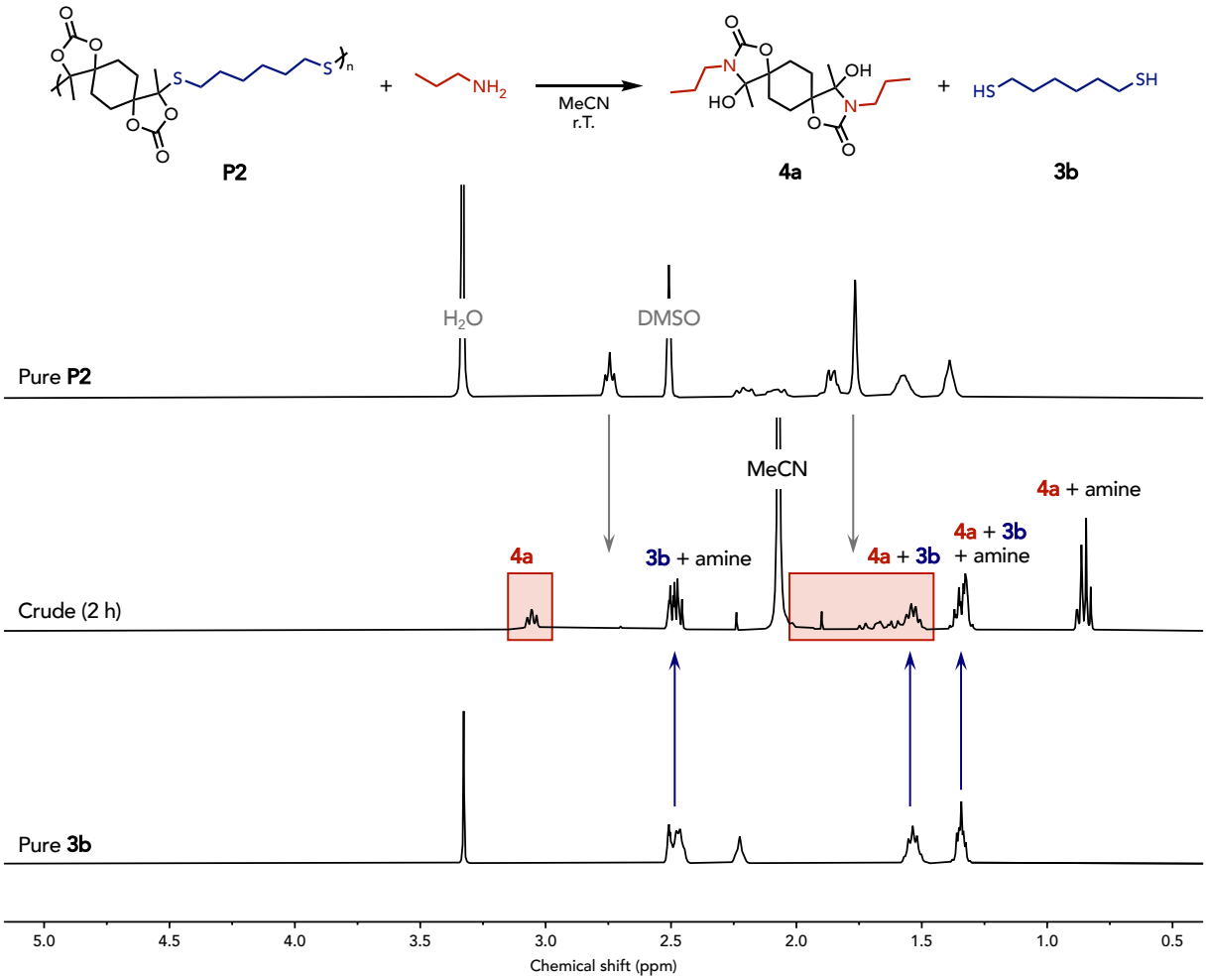

Figure S50 – Stacked ^{1}H-NMR spectra (400 MHz, DMSO-d_6) of pure polymer **P2**, crude reaction mixture after 2 h, and pure dithiol **3b**.

8. Characterization of the pure degradation products

Dithiol **3a**

The dithiol **3a** was recovered after flash column chromatography and has shown to be identical to the commercial compound by ^{1}H- and ^{13}C-NMR spectroscopy.

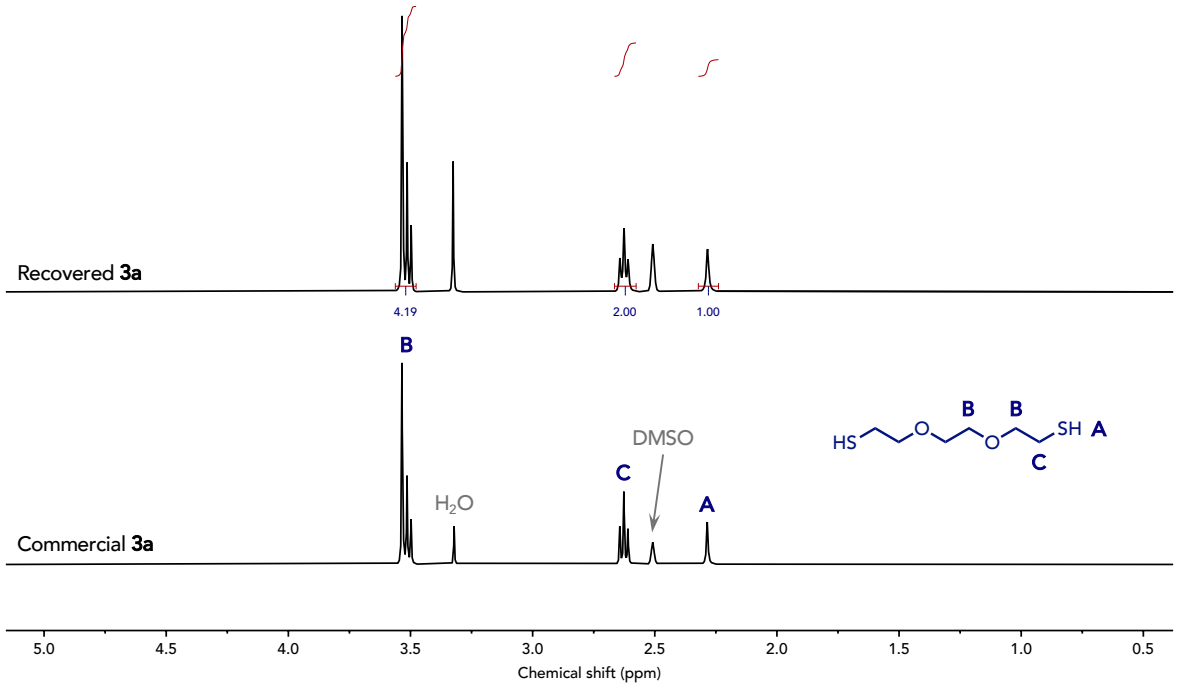

Figure S51 – Stacked ^{1}H-NMR spectra (400 MHz, DMSO-d_6) of the recovered **3a** after polymer degradation and of commercial **3a**.

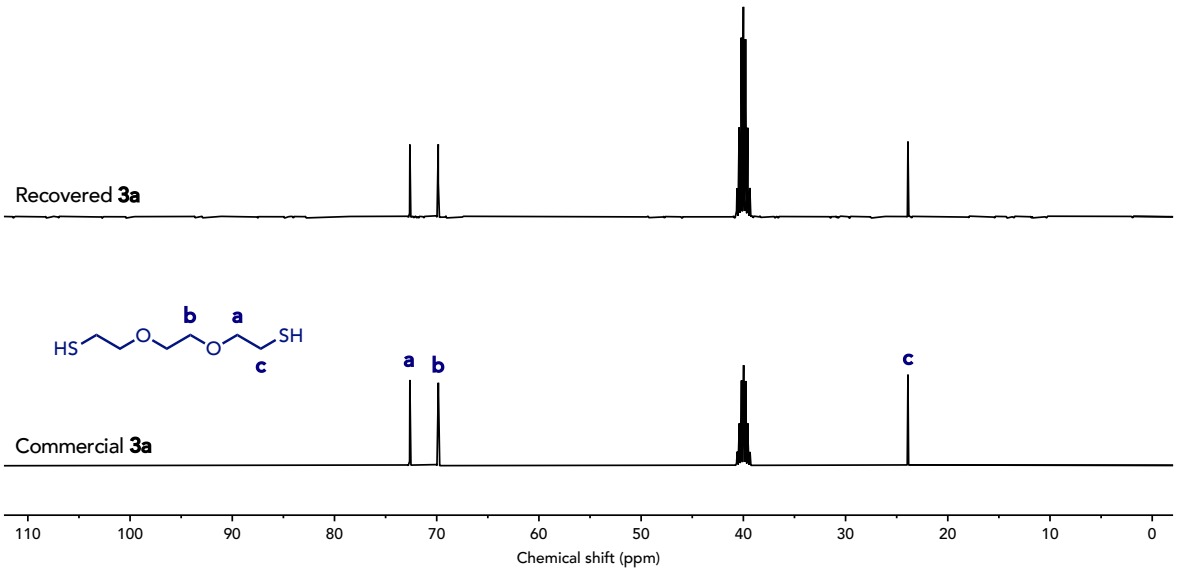

Figure S52 – Stacked ^{13}C-NMR spectra (100 MHz, DMSO-d_6) of the recovered **3a** after polymer degradation and of commercial **3a**.

Dithiol **3b**

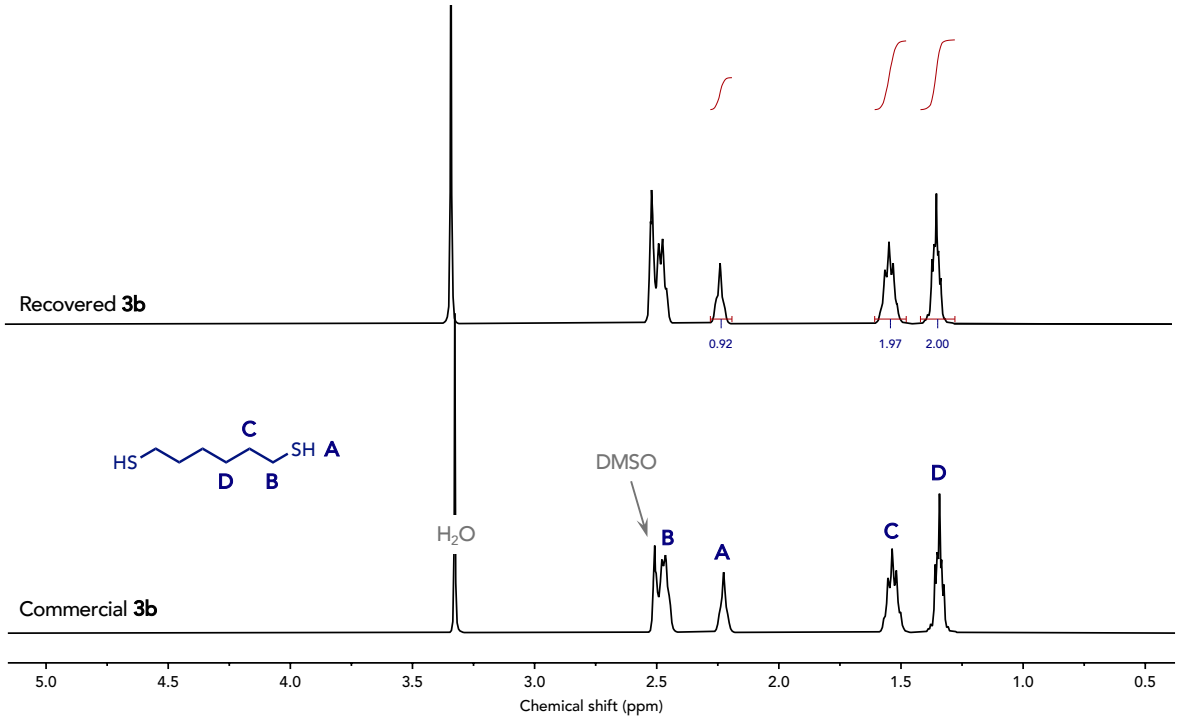

Figure S53 – Stacked ^{1}H-NMR spectra (400 MHz, DMSO-d_6) of the recovered **3b** after polymer degradation and of commercial **3b**.

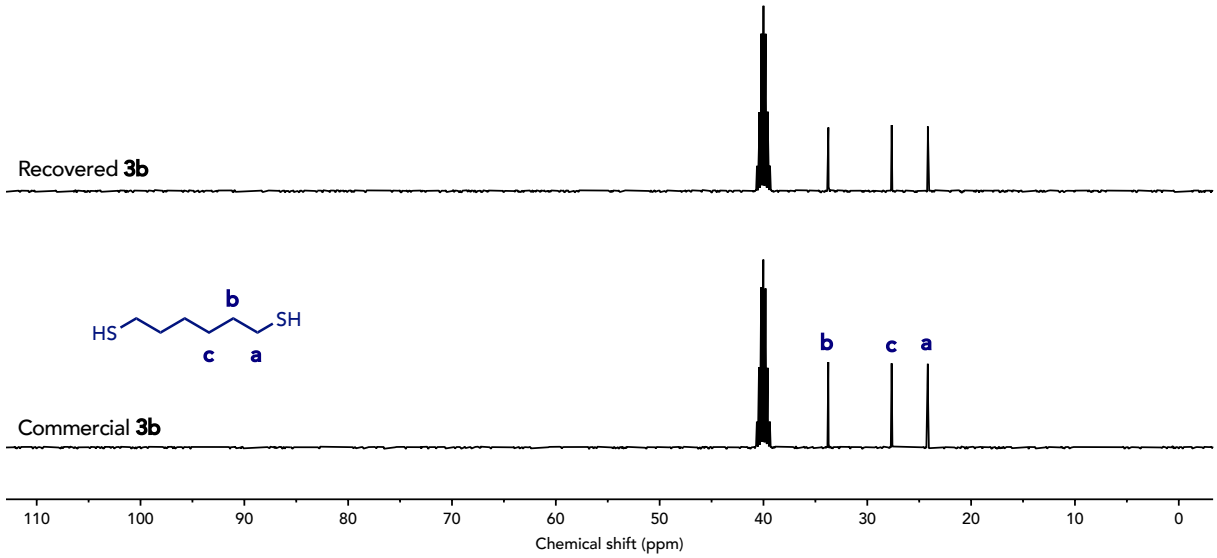

Figure S54 – Stacked ^{13}C-NMR spectra (100 MHz, DMSO-d_6) of the recovered **3b** after polymer degradation and of commercial **3b**.

Bis(hydroxyoxazolidone) **4a**

White solid; **^{1}H NMR** (400 MHz, DMSO-d_6) δ 5.99 (s, 2H), 3.05 (m, 4H), 2.08-1.91 (m, 2H), 1.78-1.46 (m, 10H), 1.32 (s, 6H), 0.86 (t, J = 7.6 Hz, 6H). **^{13}C NMR** (100 MHz, DMSO-d_6) δ 156.7, 89.5, 84.0, 41.5, 28.8, 25.1, 22.8, 21.1, 11.8.

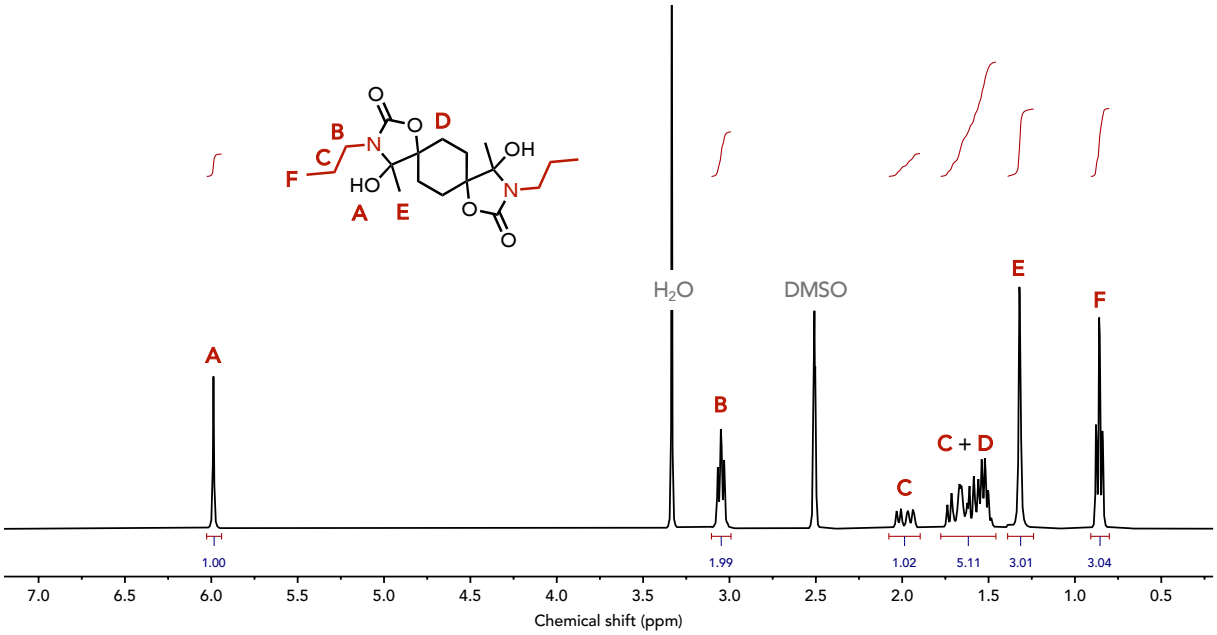

Figure S55 – ^{1}H-NMR spectrum (400 MHz, DMSO-d_6) of **4a**.

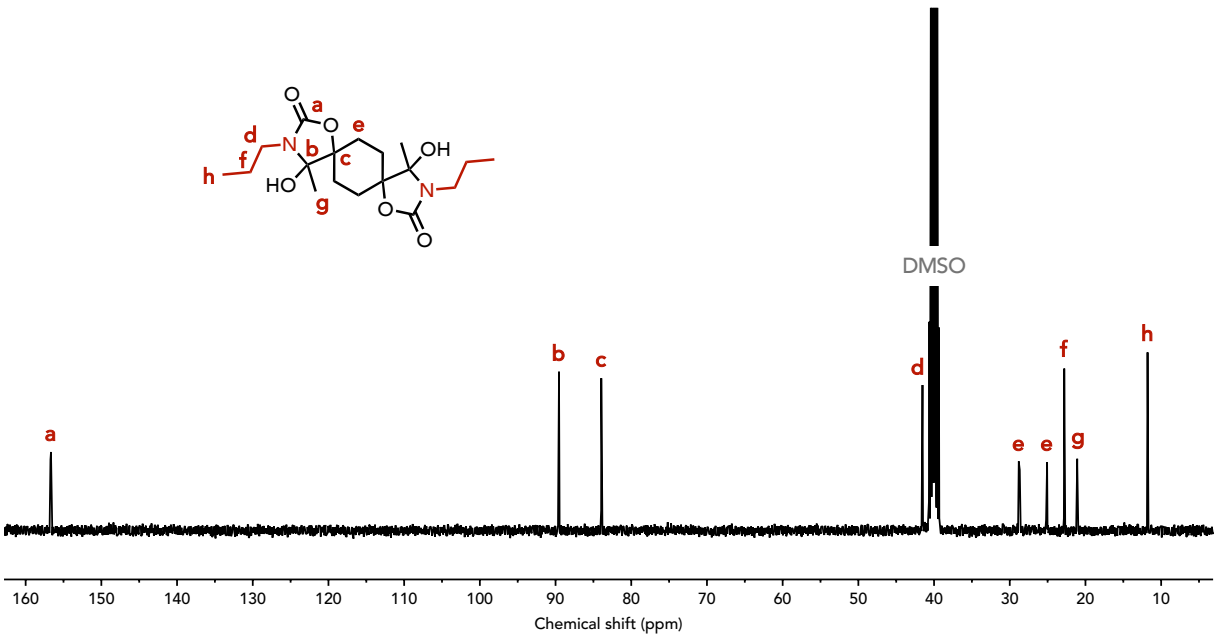

Figure S56 – ^{13}C-NMR spectrum (100 MHz, DMSO-d_6) of **4a**.

Bis(hydroxyoxazolidone) **4b**

White solid; **^{1}H NMR** (400 MHz, DMSO-d_6) δ 5.98 (s, 2H), 3.07 (m, 4H), 2.05-1.89 (m, 2H), 1.77-1.42 (m, 10H), 1.38-1.18 (m, 22H), 0.87 (m, 6H). **^{13}C NMR** (100 MHz, DMSO-d_6) δ 156.6, 89.6, 83.9, 40.7, 31.7, 29.6, 28.9, 28.7, 26.8, 25.2, 22.5, 21.1, 14.4.

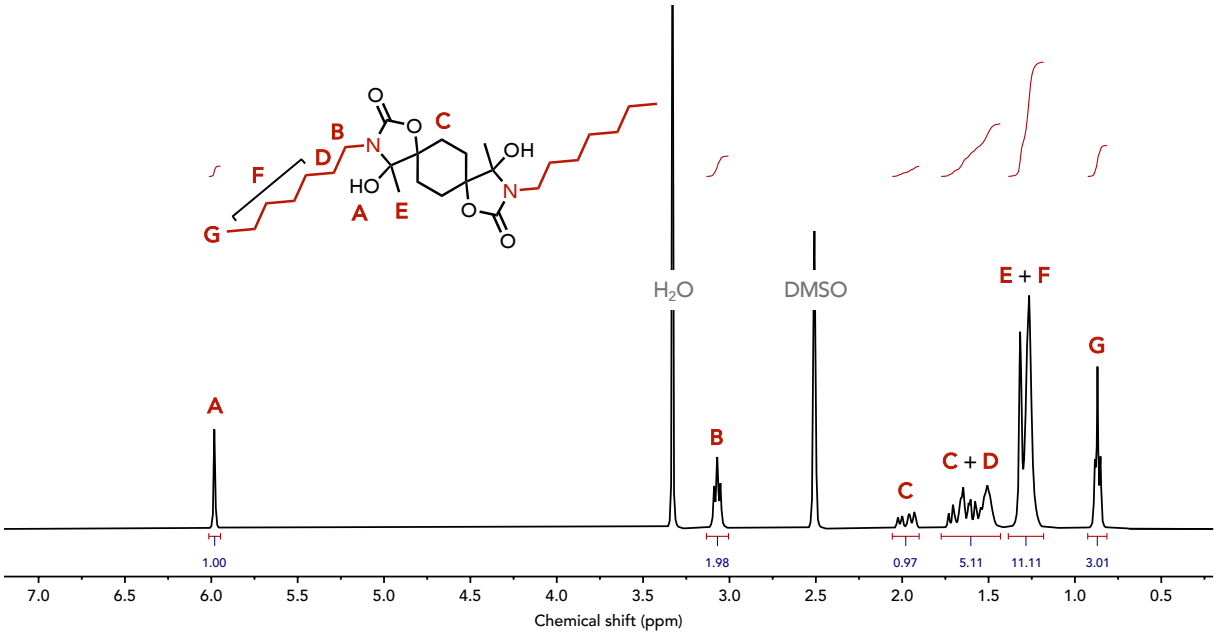

Figure S57 – ^{1}H-NMR spectrum (400 MHz, DMSO-d_6) of **4b**.

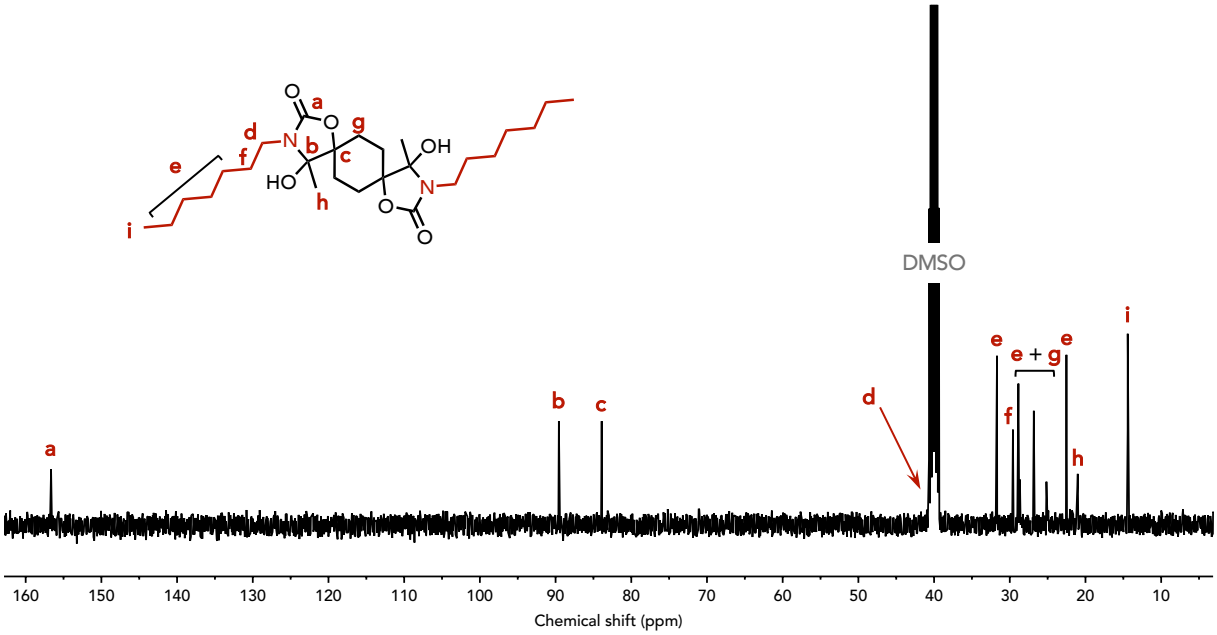

Figure S58 – ^{13}C-NMR spectrum (100 MHz, DMSO-d_6) of **4b**.

Bis(hydroxyoxazolidone) **4c**

White solid; **^{1}H NMR** (400 MHz, DMSO-d_6) δ 6.01 (s, 2H), 3.34 (m, 4H), 3.23 (s, 6H), 3.14 (m, 4H), 2.06-1.89 (m, 2H), 1.80-1.54 (m, 10H), 1.32 (m, 6H). **^{13}C NMR** (100 MHz, DMSO-d_6) δ 156.6, 89.6, 84.1, 70.0, 58.3, 37.3, 29.6, 28.8, 25.1, 20.9.

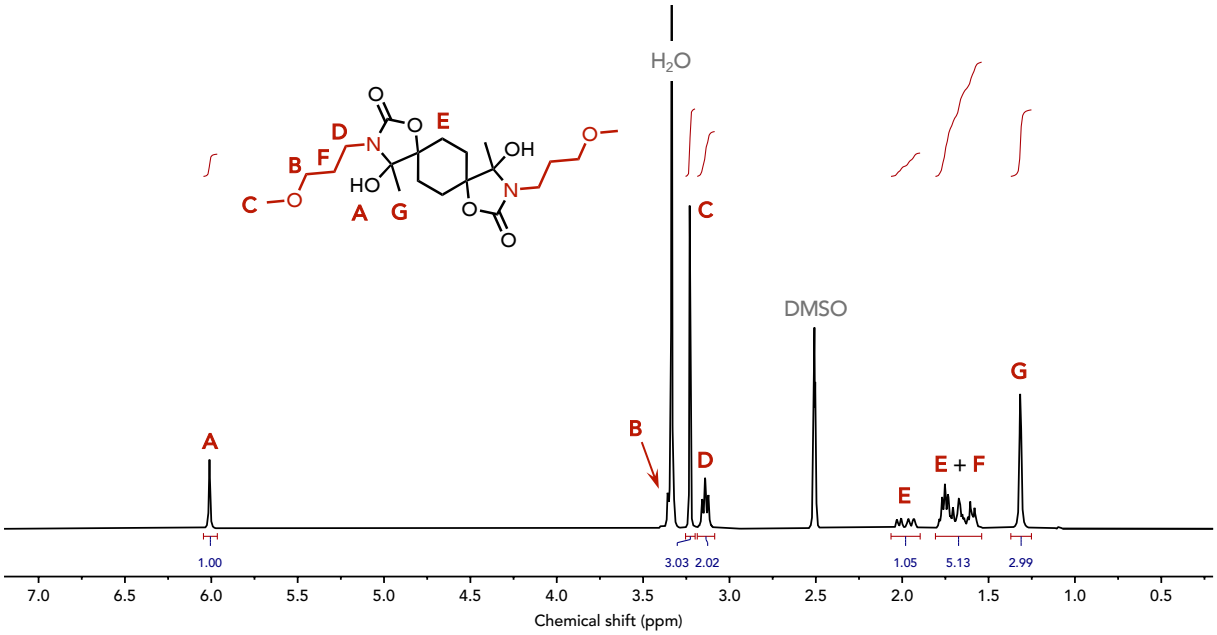

Figure S59 – ^{1}H-NMR spectrum (400 MHz, DMSO-d_6) of **4c**.

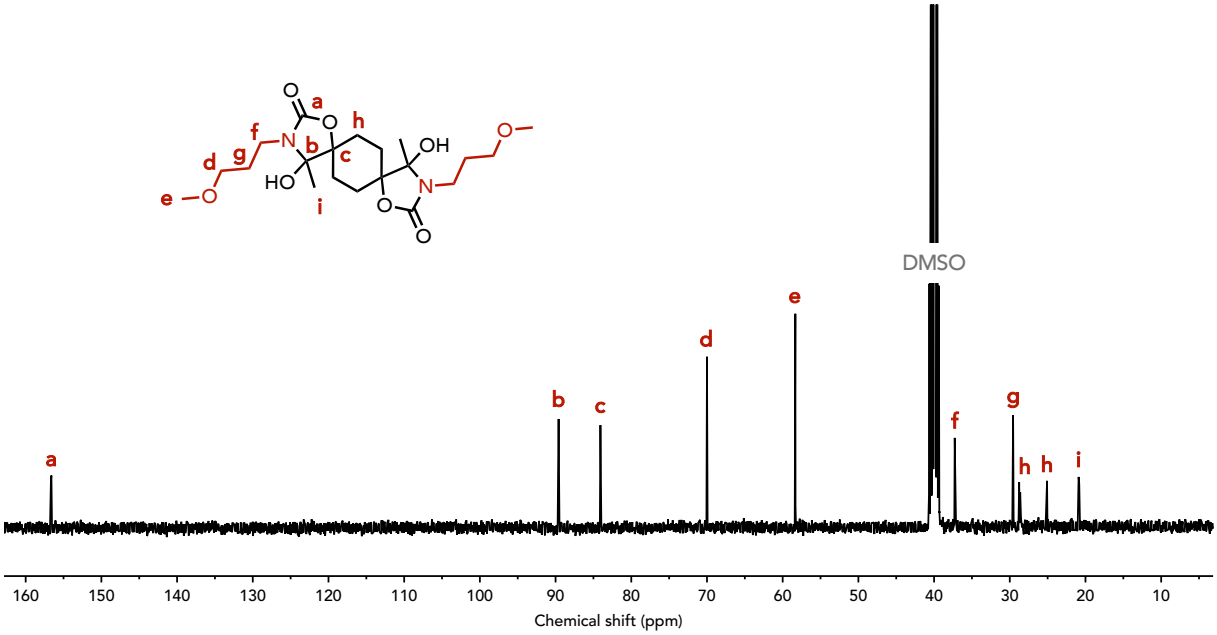

Figure S60 – ^{13}C-NMR spectrum (100 MHz, DMSO-d_6) of **4c**.

Bis(hydroxyoxazolidone) **4d**

White solid; **^{1}H NMR** (400 MHz, DMSO-d_6) δ 6.00 (s, 2H), 4.44 (t, J = 4.8 Hz, 2H), 3.43 (t, J = 5.6 Hz, 4H), 3.15 (m, 4H), 2.06-1.90 (m, 2H), 1.77-1.52 (m, 10H), 1.33 (s, 6H). **^{13}C NMR** (100 MHz, DMSO-d_6) δ 156.7, 89.6, 84.1, 59.0, 37.3, 32.8, 28.8, 25.2, 21.0.

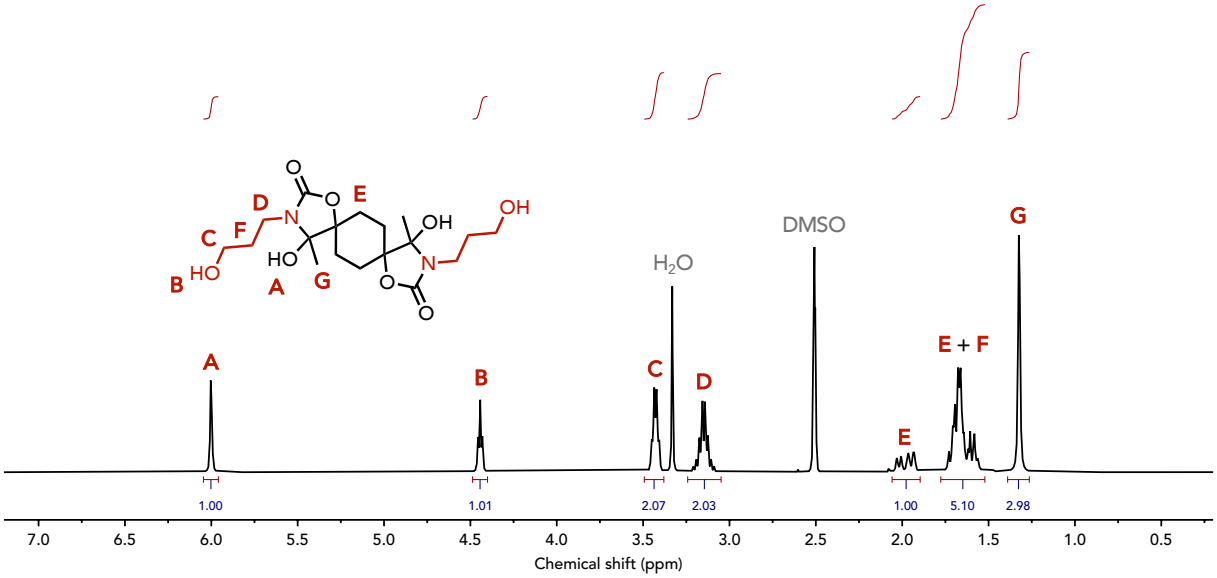

Figure S61 – ^{1}H-NMR spectrum (400 MHz, DMSO-d_6) of **4d**.

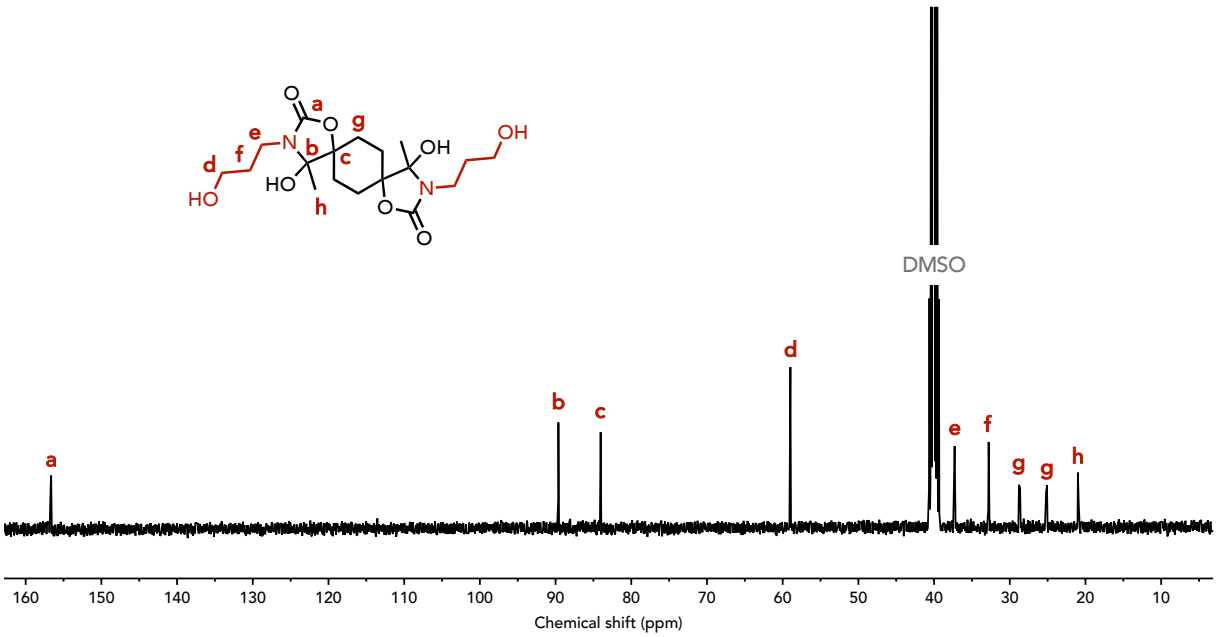

Figure S62 – ^{13}C-NMR spectrum (100 MHz, DMSO-d_6) of **4d**.

9. Valorization of the products of degradation

General procedure for the dehydration of bis(hydroxyoxazolidone)s **4a-c**

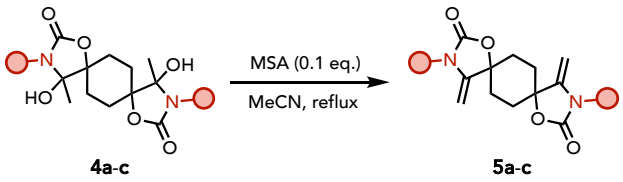

Bis(alkylidene-oxazolidone)s **5** were synthesized according to a reaction setup described in a previous work from our group. The bis(hydroxyoxazolidone) **4** (1 mmol, 1 eq.) was added to a round bottom flask with MSA (0.1 mmol, 0.1 eq.) and acetonitrile (20 mL). An addition funnel containing molecular sieves (3 Å) was added to the round bottom flask together with a condenser (the dehydration setup). The mixture was refluxed overnight and was then quenched by the addition of triethylamine (0.3 mmol, 0.3 eq.). Once cooled to room temperature, dichloromethane (80 mL) was added to dilute the mixture, which was extracted with water (3 x 80 mL). The organic phase was dried over $MgSO_4$, filtered, and dried under vacuum to yield pure **5**.

Bis(alkylidene-oxazolidone) **5a**

White crystals (294 mg, isolated yield 88 %); mp = 226 °C; **^{1}H NMR** (400 MHz, $CDCl_3$) δ 4.17 (d, J = 2.7 Hz, 2H), 4.10 (d, J = 2.7 Hz, 2H), 3.45 (t, J = 7.2 Hz, 4H), 2.18-2.04 (m, 4H), 1.97-1.81 (m, 4H), 1.67 (sx, J = 7.4 Hz, 4H), 0.95 (t, J = 7.4 Hz, 6H). **^{13}C NMR** (100 MHz, $CDCl_3$) δ 155.7, 149.3, 81.8, 80.6, 43.0, 32.4, 19.7, 11.1.

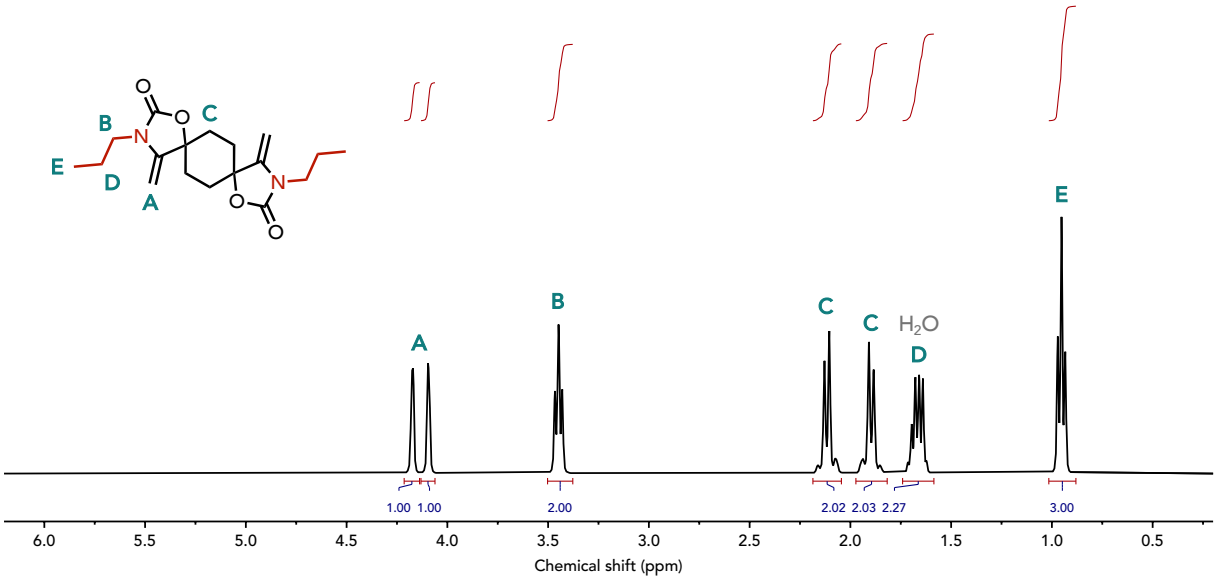

Figure S63 – ^{1}H-NMR spectrum (400 MHz, $CDCl_3$) of **5a**.

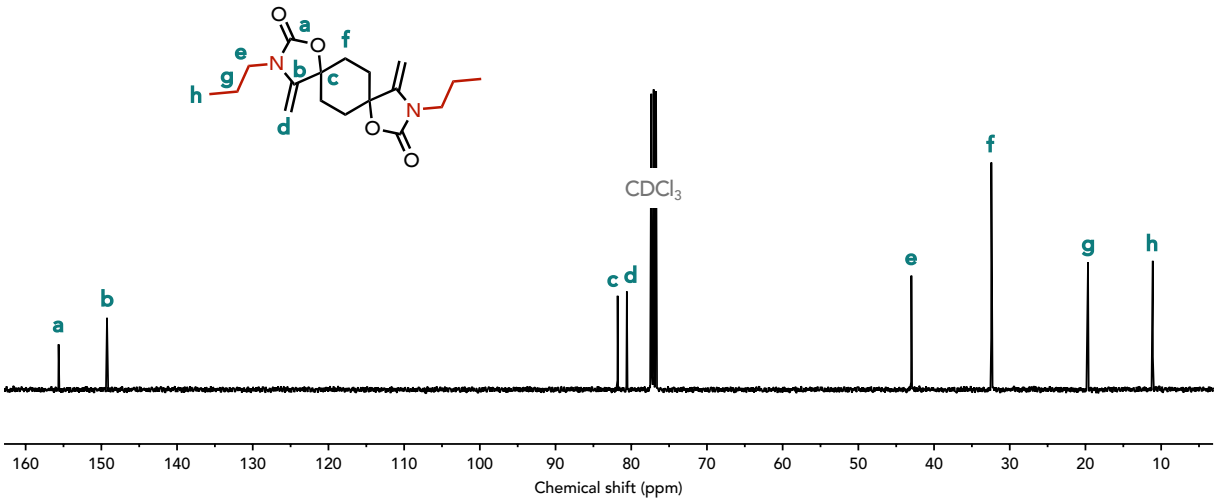

Figure S64 – ^{13}C-NMR spectrum (100 MHz, $CDCl_3$) of **5a**.

Bis(alkylidene-oxazolidone) **5b**

White crystals (415 mg, isolated yield 93 %); mp = 143 °C; **^{1}H NMR** (400 MHz, $CDCl_3$) δ 4.15 (d, J = 3.1 Hz, 2H), 4.08 (d, J = 3.1 Hz, 2H), 3.45 (t, J = 7.6 Hz, 4H), 2.16-2.03 (m, 4H), 1.94-1.80 (m, 4H), 1.67-1.54 (m, 4H), 1.37-1.20 (m, 16H), 0.88 (m, 6H). **^{13}C NMR** (100 MHz, $CDCl_3$) δ 155.6, 149.2, 81.8, 80.6, 41.5, 32.4, 31.7, 28.9, 26.7, 26.3, 22.6, 14.1.

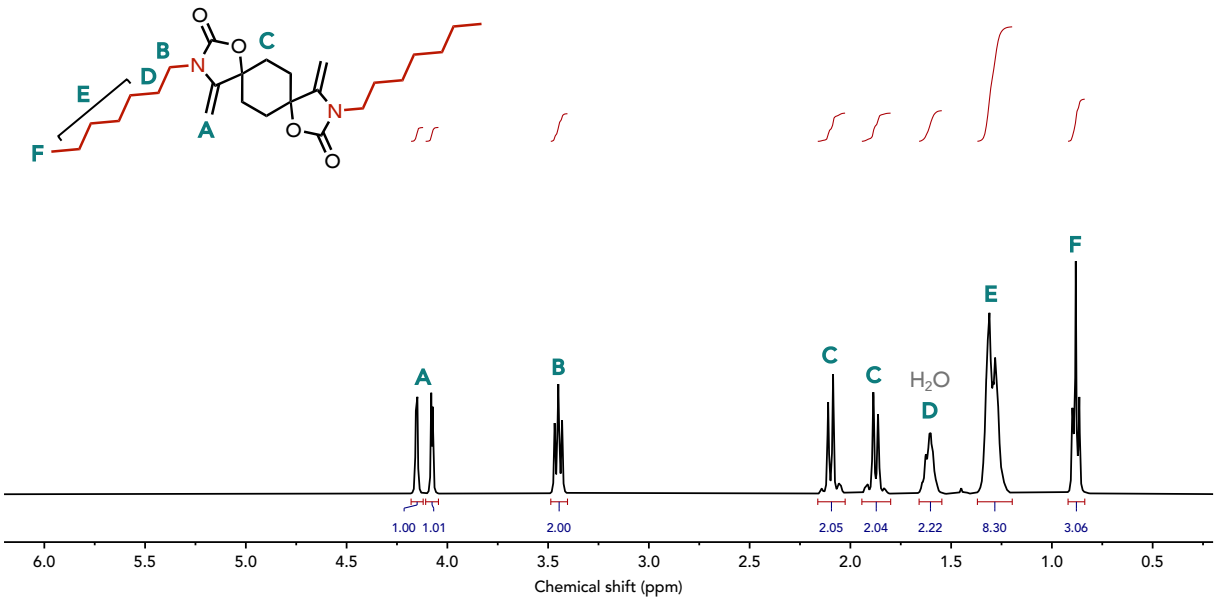

Figure S65 – ^{1}H-NMR spectrum (400 MHz, $CDCl_3$) of **5b**.

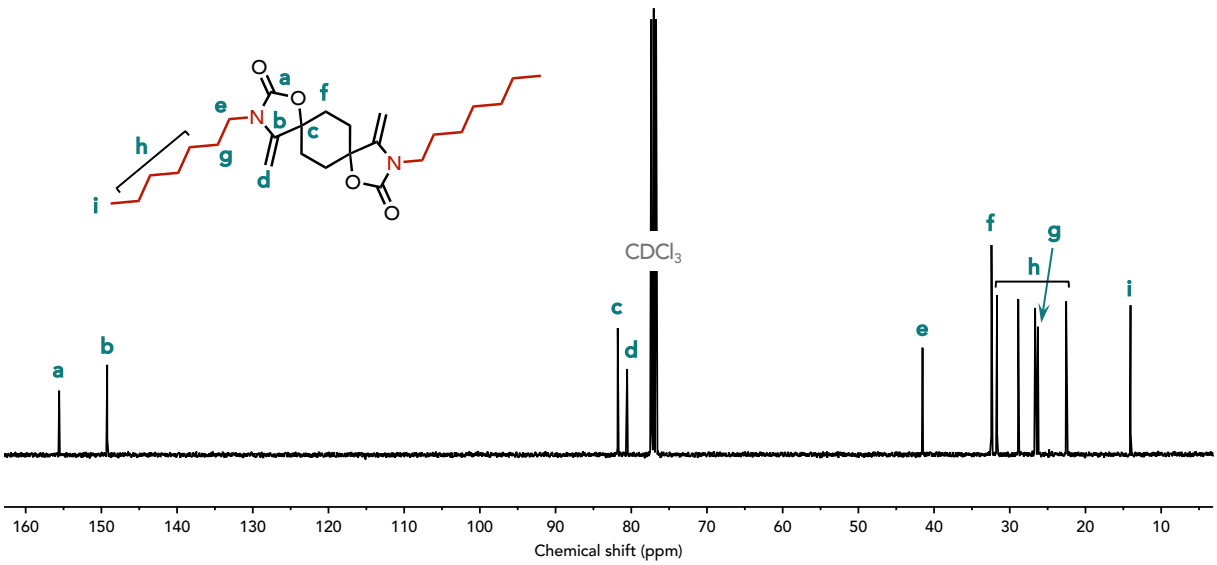

Figure S66 – ^{13}C-NMR spectrum (100 MHz, $CDCl_3$) of **5b**.

Bis(alkylidene-oxazolidone) **5c**

White crystals (351 mg, isolated yield 89 %); mp = 163 °C; **^{1}H NMR** (400 MHz, $CDCl_3$) δ 4.23 (d, J = 3.0 Hz, 2H), 4.09 (d, J = 3.0 Hz, 2H), 3.57 (t, J = 6.8 Hz, 4H), 3.4 (t, J = 5.8 Hz, 4H), 3.32 (s, 6H), 2.17-1.78 (m, 12H). **^{13}C NMR** (100 MHz, $CDCl_3$) δ 155.6, 149.3, 81.9, 80.6, 69.7, 58.7, 38.8, 32.4, 26.8.

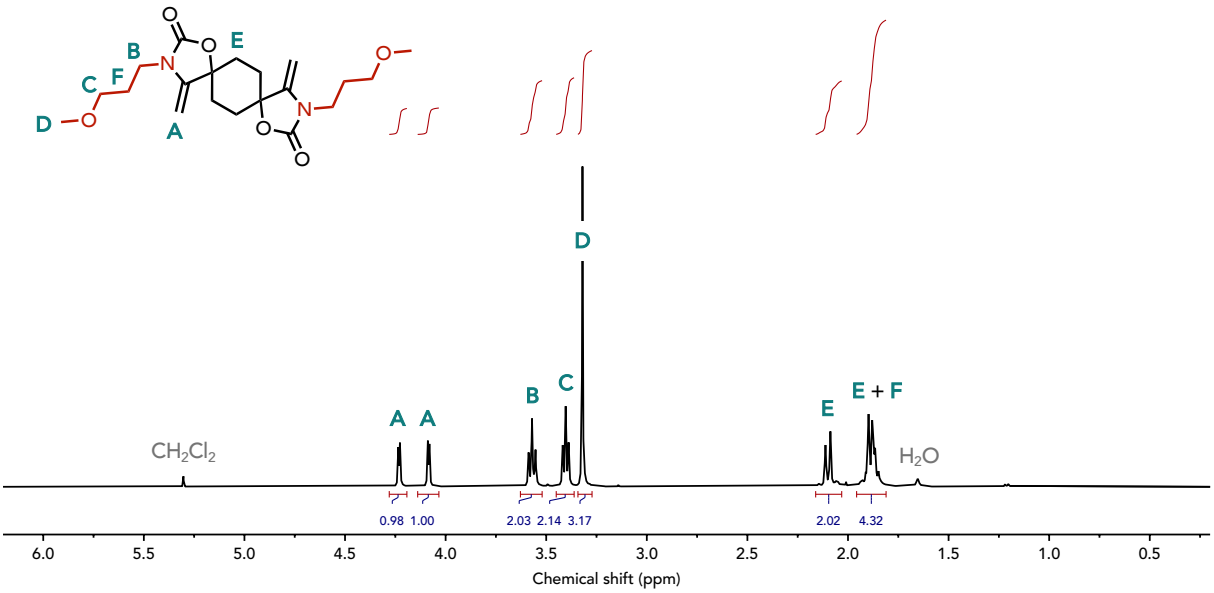

Figure S67 – ^{1}H-NMR spectrum (400 MHz, $CDCl_3$) of **5c**.

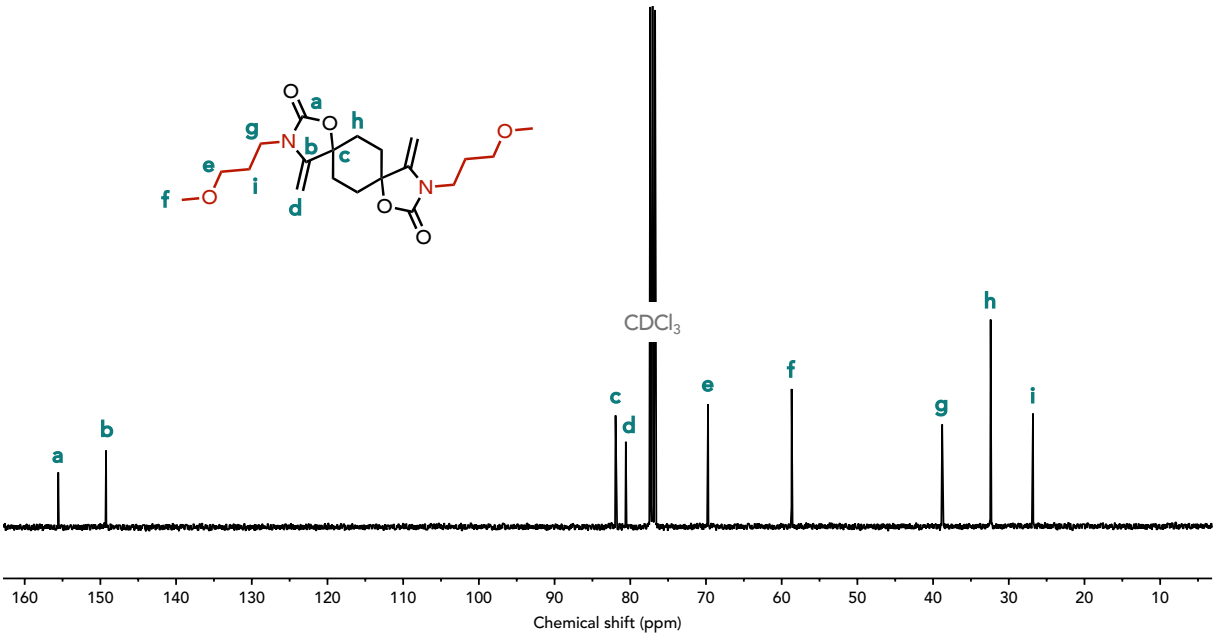

Figure S68 – ^{13}C-NMR spectrum (100 MHz, $CDCl_3$) of **5c**.

Procedure for the dehydration of bis(hydroxyoxazolidone)s **4d** into **6**

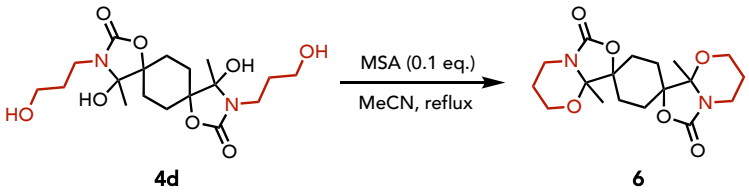

Bis(hydroxyoxazolidone) **4c** (402 mg, 1 mmol, 1 eq.) was added to a round bottom flask with MSA (0.1 mmol, 0.1 eq.) and acetonitrile (20 mL). An addition funnel containing molecular sieves (3 Å) was added to the round bottom flask together with a condenser (the dehydration setup). The mixture was refluxed overnight and was then quenched by the addition of triethylamine (0.3 mmol, 0.3 eq.). Once cooled to room temperature, the suspension was precipitated in diethyl ether (150 mL) and the solid was washed with diethyl ether (100 mL). **6** was obtained as a white fluffy solid (315 mg, isolated yield 86 %); mp = 267 °C; **^{1}H NMR** (400 MHz, $CDCl_3$) δ 4.06 (m, 2H), 3.96-3.80 (m, 4H), 3.24 (m, 2H), 2.30-2.12 (m, 2H), 2.07-1.90 (m, 4H), 1.84-1.64 (m, 4H), 1.52 (s, 6H), 1.46-1.38 (m, 2H). **^{13}C NMR** (100 MHz, $CDCl_3$) δ 157.8, 90.2, 84.5, 61.0, 37.9, 28.0, 24.2, 23.7, 14.2. **HRMS (ESI):** Calculated for $C_{18}H_{27}N_2O_6$ $[M+H]^+$: 367.1869. Found: 367.1855.

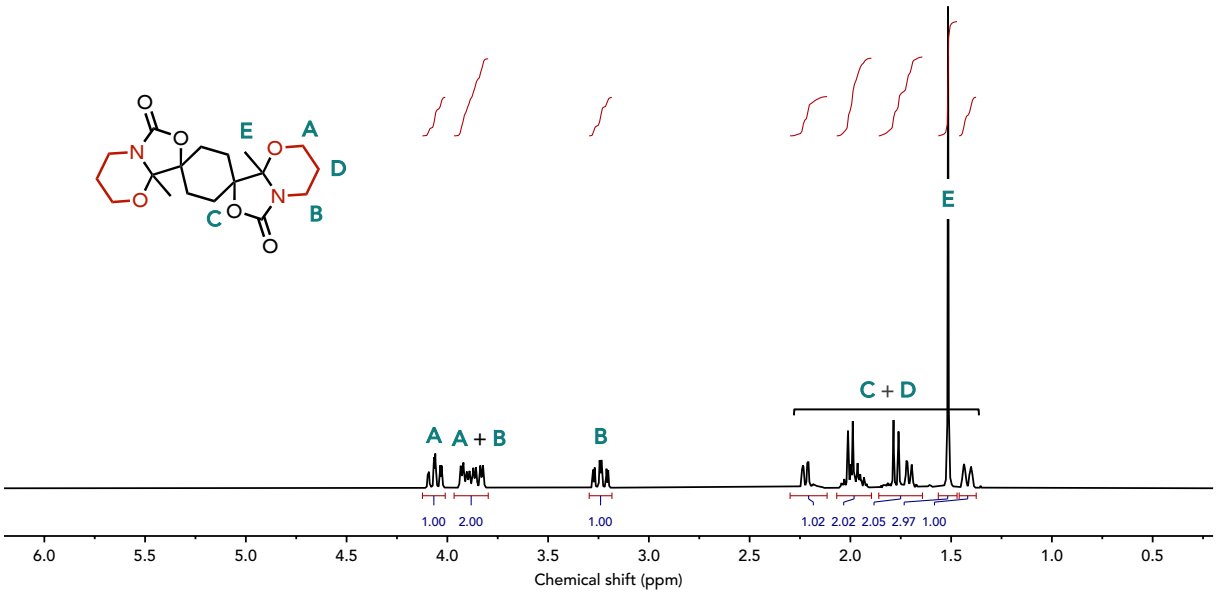

Figure S69 – ^{1}H-NMR spectrum (400 MHz, $CDCl_3$) of **6**.

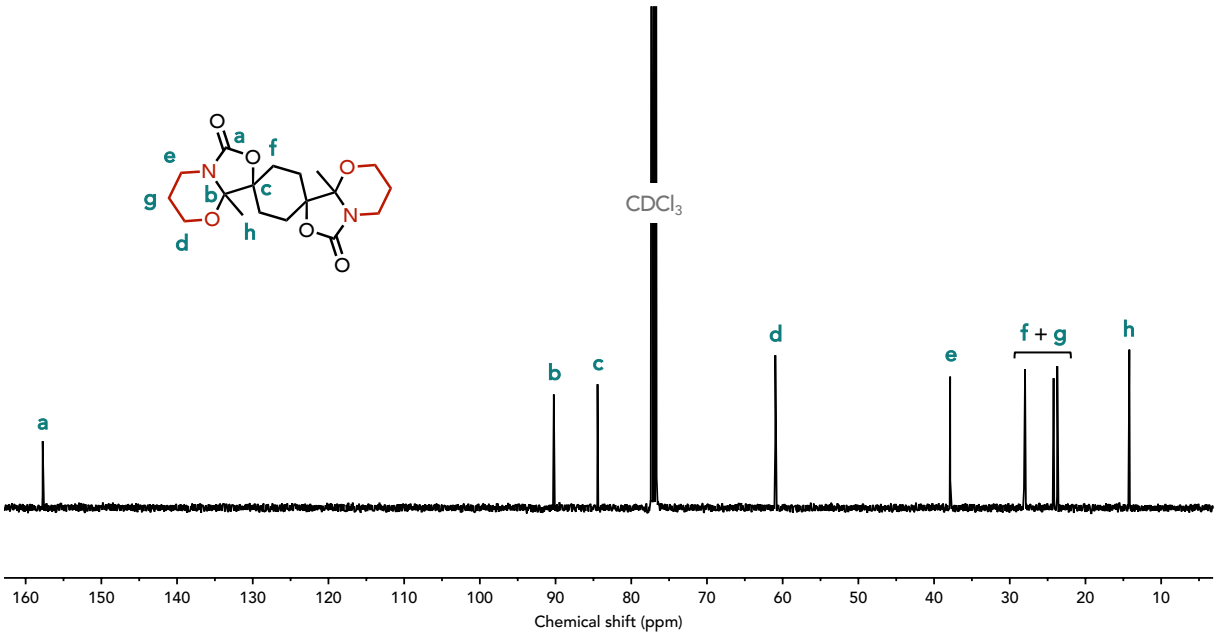

Figure S70 – ^{13}C-NMR spectrum (100 MHz, $CDCl_3$) of **6**.

10. Synthesis and characterization of P3a and P3b

Procedure for the synthesis of **P3b**

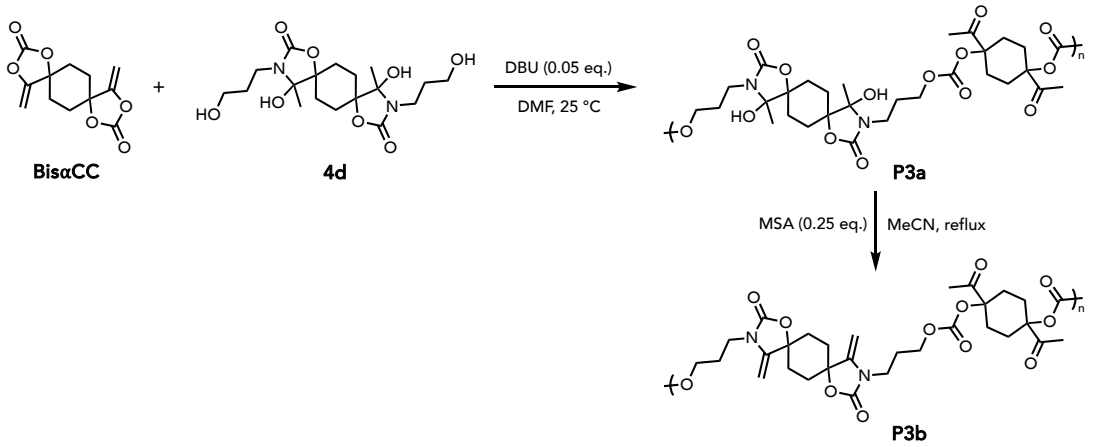

The bis(hydroxyoxazolidone) **4d** (4.04 g, 10 mmol, 1 eq.) was added to a round bottom flask with BisαCC (2.52 g, 10 mmol, 1 eq.) and DMF (13.3 mL). DBU (76 mg, 0.5 mmol, 0.05 eq.) was added to the reaction mixture and the medium was stirred for 24 h at 25 °C. The resulting solid-like gel **P3a** was analyzed through ^{1}H-NMR spectroscopy and SEC chromatography to ensure high monomer conversion before the next step (Figures S71-72). This polymer could however not be isolated due to its insolubility in most organic solvents except DMF and DMSO. To crude **P3a** was added acetonitrile (70 mL) and MSA (240 mg, 2.5 mmol, 0.25 eq.). An addition funnel containing molecular sieves (3 Å) was added to the round bottom flask together with a condenser (the dehydration setup). The mixture was refluxed overnight and was then quenched by the addition of triethylamine (7.5 mmol, 0.75 eq.). Once cooled to room temperature, the polymer was precipitated in diethyl ether (800 mL). The polymer was dissolved in chloroform (70 mL) and a small amount of triethylamine (1 mL) was added to quench residual MSA. The polymer was again precipitated in diethyl ether (80 mL) and the solid was washed with diethyl ether (2 x 200 mL). The solid was dried under vacuum at room temperature and then at 50 °C overnight to yield pure **P3b** as a white powder (5.37 g, isolated yield 87 %). **P3b** could not be characterized by SEC owing to its insolubility in the solvents of our SEC equipment.

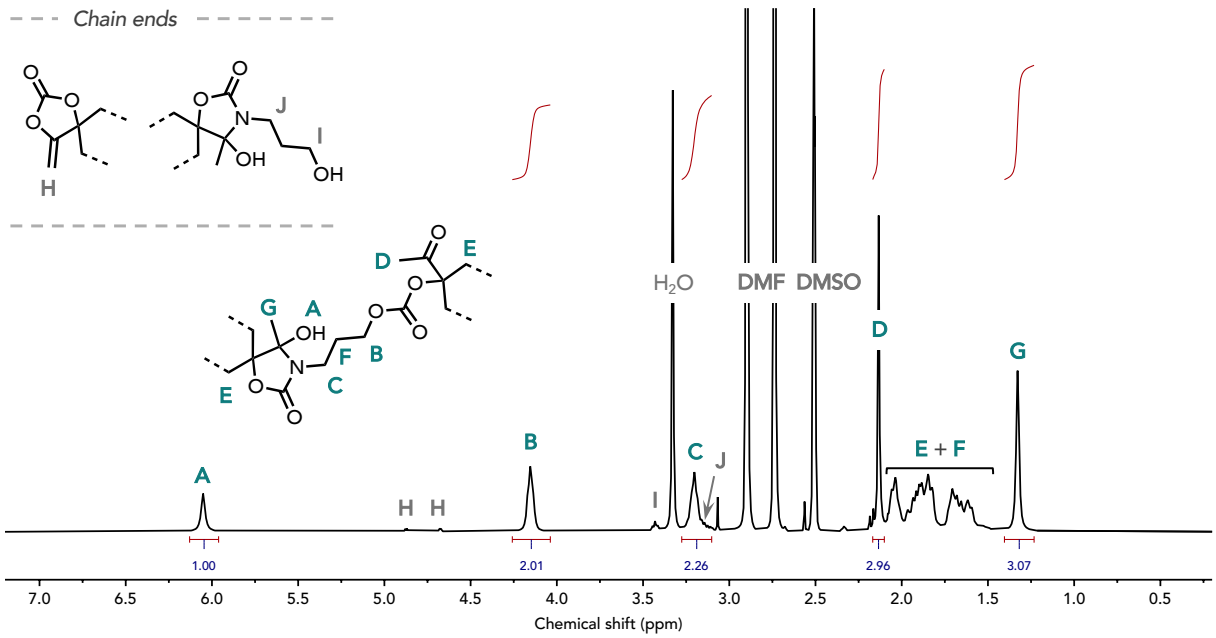

Figure S71 – ^{1}H-NMR spectrum (400 MHz, DMSO-d_6) of crude **P3a**.

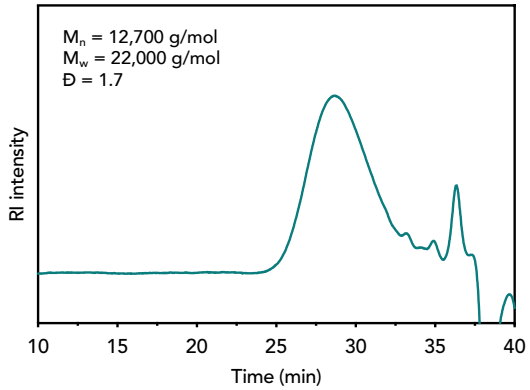

Figure S72 – SEC trace of crude **P3a**.

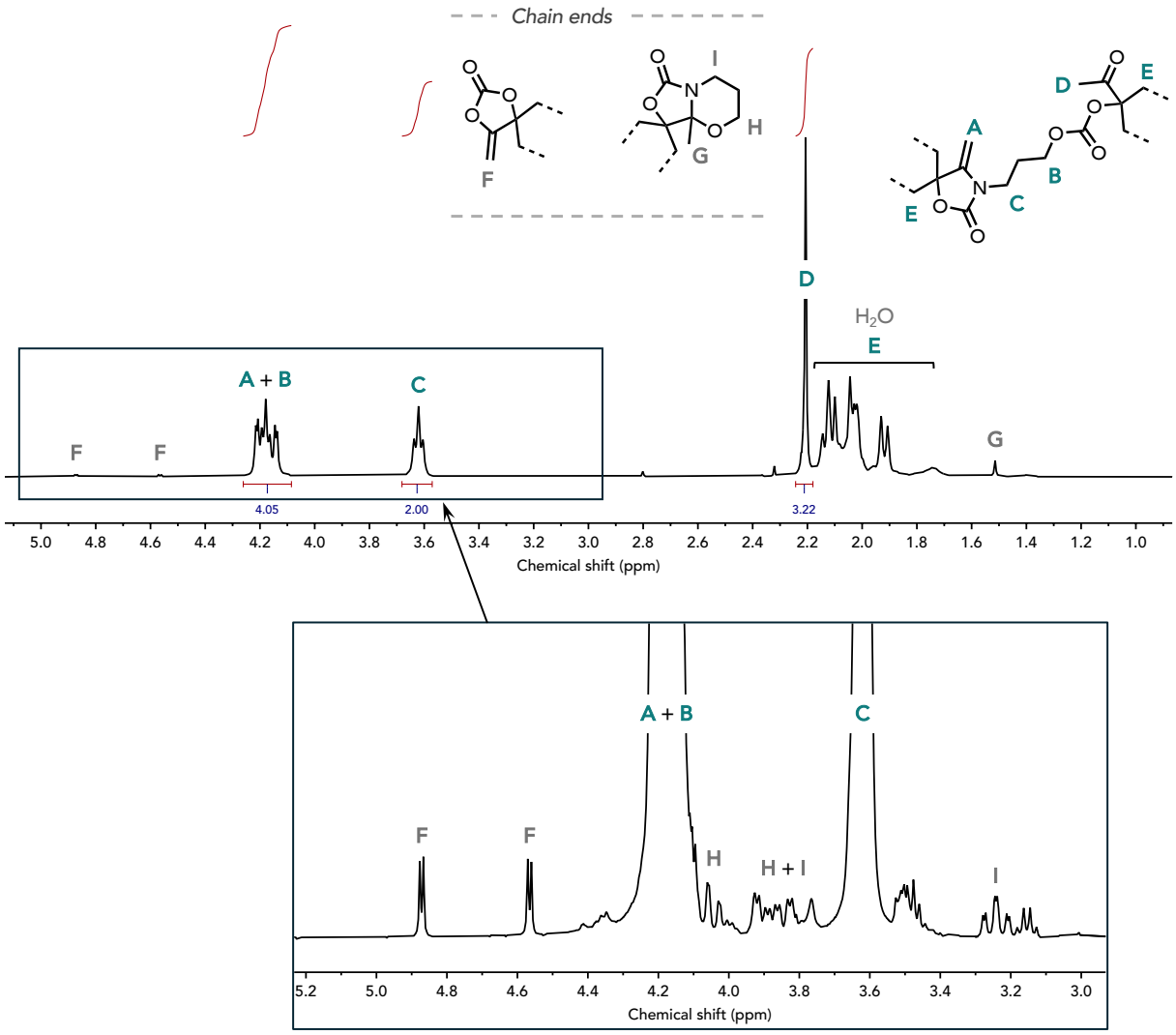

Figure S73 – ^{1}H-NMR spectrum (400 MHz, $CDCl_3$) of **P3b**. The attribution of end-groups was facilitated by the previous synthesis of **6**.

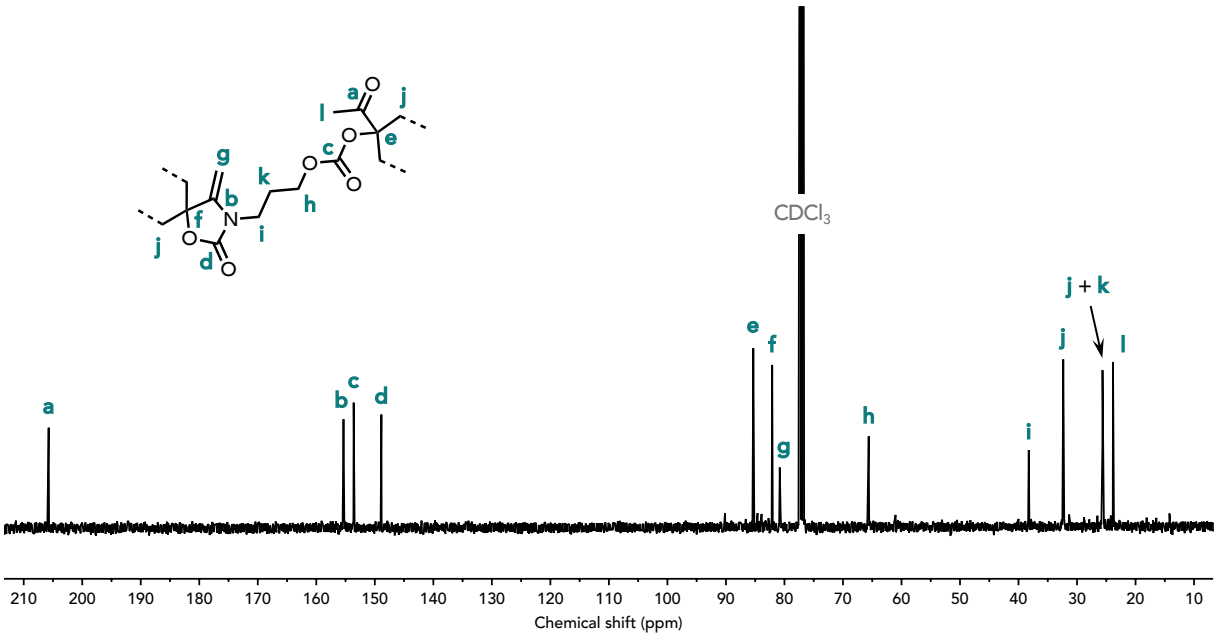

Figure S74 – ^{13}C-NMR spectrum (100 MHz, $CDCl_3$) of **P3b**.

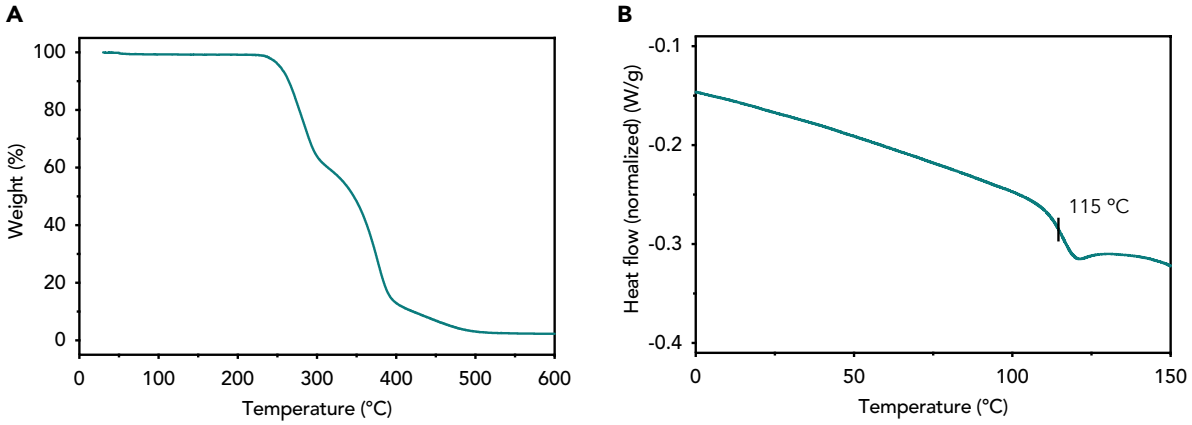

Figure S75 – (A) TGA and (B) DSC curves of **P3b**.

11. Preparation and characterization of a covalent adaptable network P4

Procedure for the synthesis of **P4**

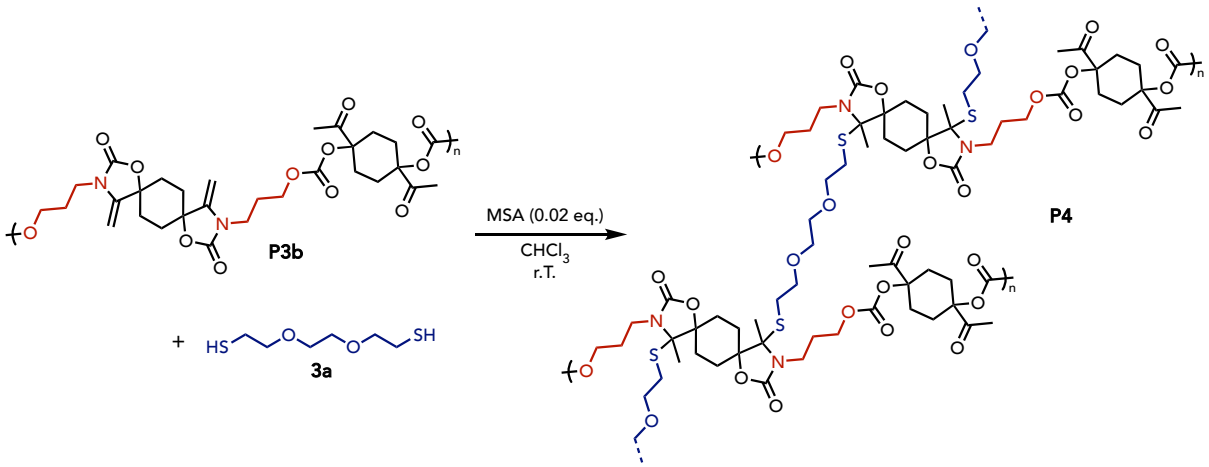

Polymer **P3b** (3.09 g, 10 mmol *in alkylidene functions*, 1 eq.) was added to a plastic beaker with chloroform (20 mL) and was stirred at r.T until solubilization. The dithiol **3b** was added (0.94 g, 5 mmol, 0.5 eq.), followed by MSA (19.2 mg, 0.2 mmol, 0.02 eq.). The mixture was stirred for about 45 minutes until a gel was formed. The gel was easily recovered and dried under vacuum at r.T and then overnight at 70 °C. The solid was grinded and dried under vacuum at 80 °C for 24 h to yield the pure polymer as a yellowish hard solid.

Successful polymerization was confirmed via infrared (ATR-IR) spectroscopy (Figure 4) and high gel content (98.5 ± 0.4%). The swelling ratio in THF was only of 2.5 ± 0.1%. Most alkene functions seemed to be consumed as demonstrated by the spectrum of **P4**, showing only residual alkene function with a shoulder at 1650 cm^{-1}. The carbonyl groups of different nature overlap and are responsible of a large C=O stretching band going from 1830 to 1700 cm^{-1}.

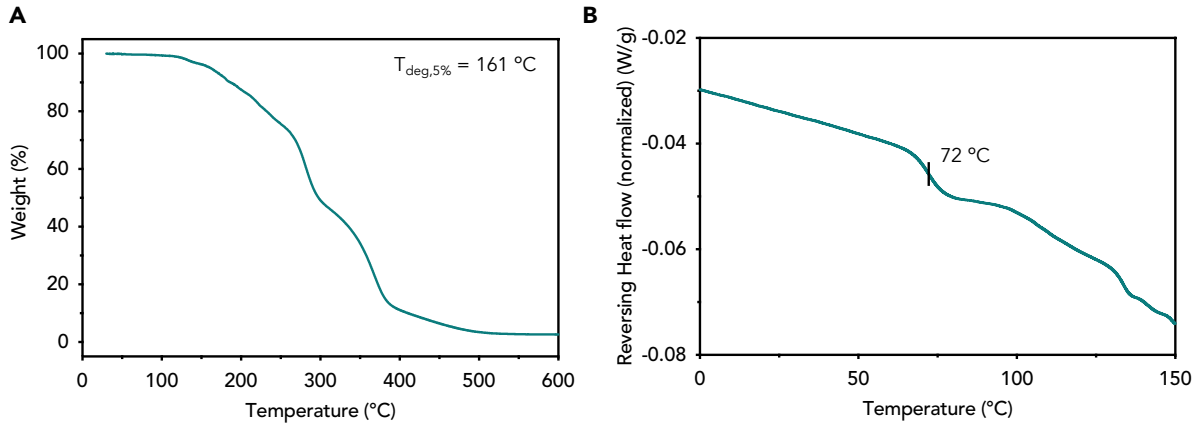

Figure S76 – (A) TGA and (B) mDSC curves of **P4**.

Temperature ramp experiments for **P4**

Temperature experiments were performed to assess the extent of cross-link density along temperature on the network **P4**. DMA was first performed to have an insight into the evolution of the modulus at low temperature starting from 30 °C, well below the T_g of 72 °C (as determined by DSC).

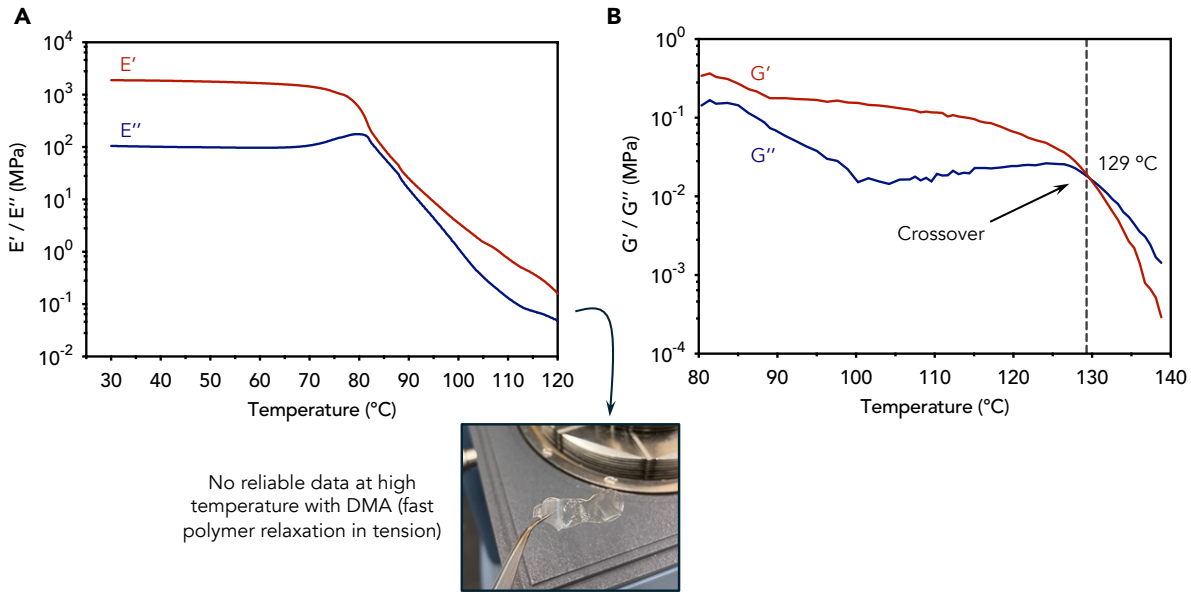

Figure S77 – Temperature ramp analyses by (A) DMA and (B) rheology of **P4**.

Stress relaxation experiments for **P4**

Stress relaxation experiments were achieved to probe the timescale at which the material **P4** can relax an applied stress through dynamic bond reorganization. Figure S78A displays the

raw relaxation data. Expectedly, the initial relaxation modulus G_0 (taken at 10^{-1} s) decreased as a function of temperature. This feature is generally observed for dissociative covalent adaptable networks and supports the experimental findings of the temperature ramp experiments.

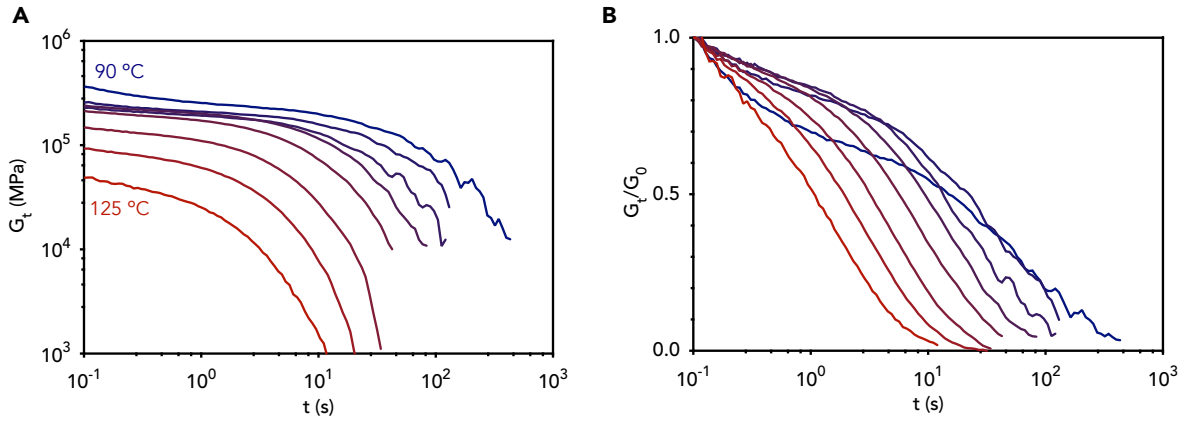

Figure S78 – Stress relaxation experiments on **P4** at different temperatures (90 to 125 °C, step of 5 °C) by rheology. (A) Raw stress relaxation data. (B) Normalized relaxation stress relaxation data.

The data was normalized and plotted in Figure S78B. It is clear from this data that the relaxation behavior is deviating from widely used models such as the single element maxwell model. Therefore, we tried many different models in an effort to well describe the raw relaxation data. We found out that two models were fitting the data with great accuracy as displayed in Figure 5B, where the stress relaxation at 90 °C was used as a representative curve for displaying the fitting accuracy. The three-element Maxwell model was already used in our previous work on *N,S*-acetal oxazolidone networks[14]. We also found that the double stretched exponential model, recently used by Torkelson & coworkers[15], gave an excellent representation of our raw data. Both models have shown to fit the data with R^2 values above 0.99.

Stress relaxation experiments for **P4** – Three-element Maxwell model

The equation for the fit of the experimental data with a three-element Maxwell model was the following:

$$\frac{G(t)}{G_0} = A \times exp\left(-\frac{t}{\tau_1}\right) + B \times exp\left(-\frac{t}{\tau_2}\right) + C \times exp\left(-\frac{t}{\tau_3}\right)$$

Where $G(t)/G_0$ is the normalized modulus, A-C the pre-exponential factors, t the time, and τ the characteristic relaxation time of the element. The fitting curves are all plotted in Figure 5C against the experimental data. Table S2 provides all fitting parameters and the R^2 as descriptor of the fitting quality.

Table S2 – Stress relaxation fitting data using a three-element Maxwell model.

T (°C)	A	τ_1	B	τ_2	C	τ_3	R^2
90	0.4237	0.2498	0.2583	16.44	0.4392	143.0	0.9982
95	0.2614	0.2049	0.2617	11.50	0.5765	85.38	0.9988
100	0.1909	0.2108	0.4166	11.61	0.4661	58.34	0.9992
105	0.1607	0.2039	0.3493	7.567	0.5471	29.38	0.9998
110	0.1670	0.1623	0.3591	4.309	0.5574	17.29	0.9999
115	0.2170	0.1307	0.3816	2.857	0.5319	9.209	0.9999
120	0.2583	0.1064	0.3302	1.391	0.6048	5.097	0.9999
125	0.4184	0.1017	0.4870	1.114	0.4223	3.679	0.9995

From the extracted relaxation times, Arrhenius plot were built and flow energy of activation (E_{flow}) were determined from the slope of a linear fit following the equation:

$$\ln(\tau) = \ln(\tau_0) + \frac{E_{flow}}{RT}$$

All the plots derived from the three characteristic relaxation times are displayed in Figure S79 together with the linear fit accuracy (using R^2 as descriptor) and the determined E_{flow}.

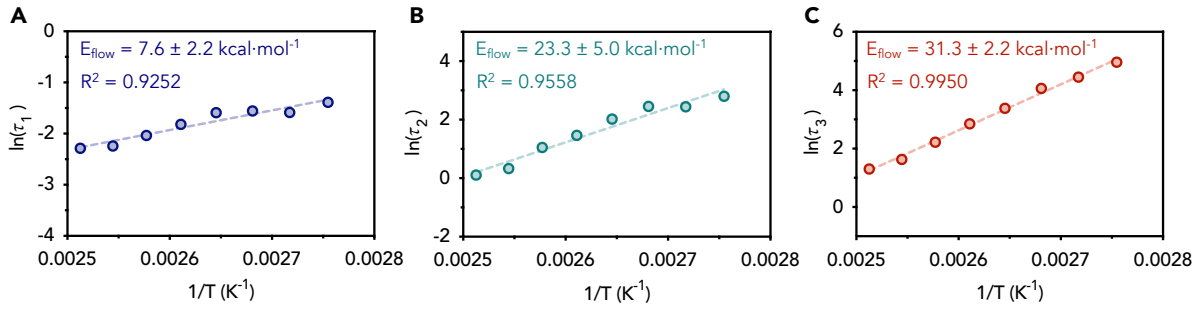

Figure S79 – Arrhenius plots from the three different extracted characteristic relaxation times (A) τ_1, (B) τ_2, and (C) τ_3. A flow energy of activation was determined from the slope of the linear fit.

In contrast to our previous work on *N,S*-acetal oxazolidone networks where only the slowest characteristic relaxation time τ_3 (ln(τ_3) precisely) showed a linear correlation with 1/T, all herein determined times followed a clear trend with temperature.

Stress relaxation experiments for **P4** – Double stretched exponential model

The equation for the fit of the experimental data with a double stretched exponential model was the following:

$$\frac{G(t)}{G_0} = A \times exp\left(-\left(\frac{t}{\tau_1}\right)^{\beta_1}\right) + (1-A) \times exp\left(-\left(\frac{t}{\tau_2}\right)^{\beta_2}\right)$$

Where $G(t)/G_0$ is the normalized modulus, A the pre-exponential factor, t the time, τ the characteristic relaxation time of the element, and β the stretching exponent, expressing the breadth of the relaxation distribution.

The characteristic relaxation times τ were corrected to their average relaxation times $< \tau >$ according to the equation:

$$\langle\tau\rangle_1 = \frac{\tau_1 \Gamma(1/\beta_1)}{\beta_1}$$

Where Γ is the gamma function.

The fitting curves are all plotted in Figure S80 against the experimental data. Table S3 provides all fitting parameters and the R^2 as descriptor of the fitting quality.

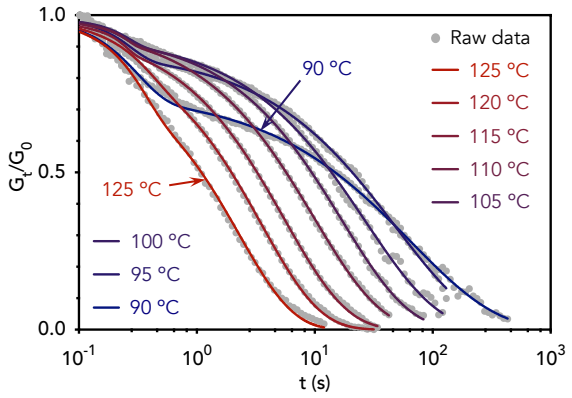

Figure S80 – Normalized stress relaxation data on **P4** from 90 to 125 °C and fitting curve from a double stretched exponential model.

Table S3 – Stress relaxation fitting data using a three-element Maxwell model.

T (°C)	A	τ_1	β_1	τ_2	β_2	$<\tau_1>$	$<\tau_2>$	R^2
90	0.2449	0.3133	1.716	66.11	0.5952	0.2794	100.52	0.9979
95	0.1141	0.2739	2.400	48.82	0.6554	0.2428	66.10	0.9984
100	0.0632	0.2701	2.982	26.92	0.7032	0.2411	33.93	0.9985
105	0.0568	0.2387	3.075	17.07	0.7644	0.2134	20.01	0.9997
110	0.0354	0.2598	5.345	9.91	0.7653	0.2395	11.61	0.9996
115	0.0452	0.2538	5.264	5.537	0.8164	0.2337	6.18	0.9995
120	0.0925	0.3997	2.254	3.554	0.8752	0.3540	3.80	0.9990
125	0.1733	0.3493	2.299	2.278	0.9395	0.3094	2.34	0.9967

From the extracted corrected relaxation times, Arrhenius plot were built and flow energy of activation (E_{flow}) were determined from the slope of a linear fit following the equation:

$$\ln(<\tau>) = \ln(<\tau_0>) + \frac{E_{flow}}{RT}$$

The plots derived from the two corrected characteristic relaxation times are displayed in Figure S81 together with the linear fit accuracy (using R^2 as descriptor) and the determined E_{flow}.

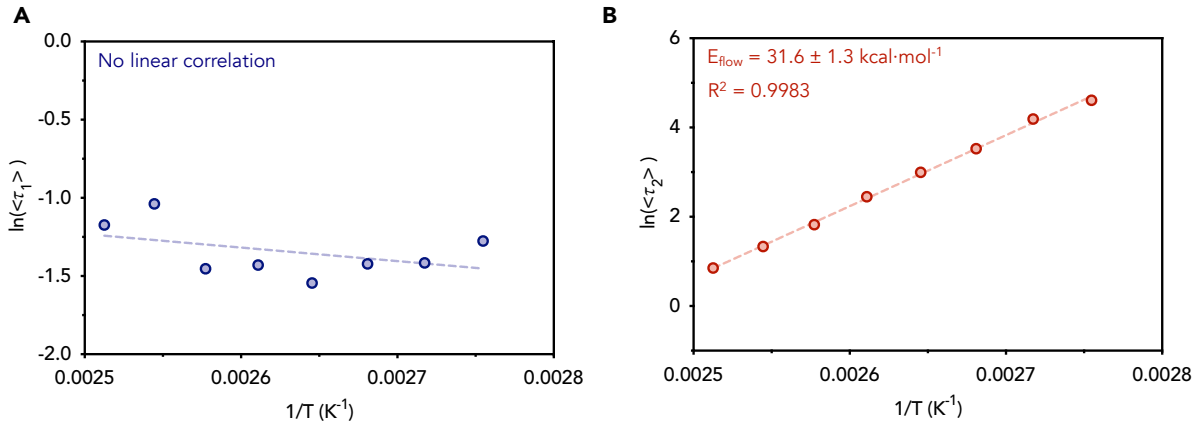

Figure S81 – Arrhenius plots from the two different extracted corrected characteristic relaxation times (A) $<\tau_1>$, and (B) $<\tau_2>$. A flow energy of activation was determined from the slope of the linear fit.

In the case of the double stretched exponential model, no linear correlation was observed for the first element characterized by the small characteristic relaxation times.

12. References

(1) Sopeña, S.; Laserna, V.; Guo, W.; Martin, E.; Escudero-Adán, E. C.; Kleij, A. W. Regioselective Organocatalytic Formation of Carbamates from Substituted Cyclic Carbonates. *Adv Synth Catal* **2016**, *358* (13), 2172–2178. https://doi.org/10.1002/adsc.201600290.

(2) Ouhib, F.; Grignard, B.; Van Den Broeck, E.; Luxen, A.; Robeyns, K.; Van Speybroeck, V.; Jerome, C.; Detrembleur, C. A Switchable Domino Process for the Construction of Novel CO_2-Sourced Sulfur-Containing Building Blocks and Polymers. *Angew. Chem. Int. Ed.* **2019**, *58* (34), 11768–11773. https://doi.org/10.1002/anie.201905969.

(3) Dewar, M. J. S.; Zoebisch, E. G.; Healy, E. F.; Stewart, J. J. P. Development and Use of Quantum Mechanical Molecular Models. 76. AM1: A New General Purpose Quantum Mechanical Molecular Model. *J. Am. Chem. Soc.* **1985**, *107* (13), 3902–3909. https://doi.org/10.1021/ja00299a024.

(4) Řezáč, J.; Hobza, P. Advanced Corrections of Hydrogen Bonding and Dispersion for Semiempirical Quantum Mechanical Methods. *J. Chem. Theory Comput.* **2012**, *8* (1), 141–151. https://doi.org/10.1021/ct200751e.

(5) AMPAC 11, 1992.

(6) Liotard, D. A. Algorithmic Tools in the Study of Semiempirical Potential Surfaces. *Int J of Quantum Chemistry* **1992**, *44* (5), 723–741. https://doi.org/10.1002/qua.560440505.

(7) Frisch, M. J.; Trucks, G. W.; Schlegel, H. B.; Scuseria, G. E.; Robb, M. A.; Cheeseman, J. R.; Scalmani, G.; Barone, V.; Petersson, G. A.; Nakatsuji, H.; Li, X.; Caricato, M.; Marenich, A. V.; Bloino, J.; Janesko, B. G.; Gomperts, R.; Mennucci, B.; Hratchian, H. P.; Ortiz, J. V.; Izmaylov, A. F.; Sonnenberg, J. L.; Williams; Ding, F.; Lipparini, F.; Egidi, F.; Goings, J.; Peng, B.; Petrone, A.; Henderson, T.; Ranasinghe, D.; Zakrzewski, V. G.; Gao, J.; Rega, N.; Zheng, G.; Liang, W.; Hada, M.; Ehara, M.; Toyota, K.; Fukuda, R.; Hasegawa, J.; Ishida, M.; Nakajima, T.; Honda, Y.; Kitao, O.; Nakai, H.; Vreven, T.; Throssell, K.; Montgomery, J. A., Jr; Peralta, J. E.; Ogliaro, F.; Bearpark, M. J.; Heyd, J. J.; Brothers, E. N.; Kudin, K. N.; Staroverov, V. N.; Keith, T. A.; Kobayashi, R.; Normand, J.; Raghavachari, K.; Rendell, A. P.; Burant, J. C.; Iyengar, S. S.; Tomasi, J.; Cossi, M.; Millam, J. M.; Klene, M.; Adamo, C.; Cammi, R.; Ochterski, J. W.; Martin, R. L.; Morokuma, K.; Farkas, O.; Foresman, J. B.; Fox, D. J. Gaussian 16 Rev. C.01, 2016.

(8) Zhao, Y.; Truhlar, D. G. The M06 Suite of Density Functionals for Main Group Thermochemistry, Thermochemical Kinetics, Noncovalent Interactions, Excited States, and Transition Elements: Two New Functionals and Systematic Testing of Four M06-Class Functionals and 12 Other Functionals. *Theor Chem Account* **2008**, *120* (1–3), 215–241. https://doi.org/10.1007/s00214-007-0310-x.

(9) Tomasi, J.; Mennucci, B.; Cammi, R. Quantum Mechanical Continuum Solvation Models. *Chem. Rev.* **2005**, *105* (8), 2999–3094. https://doi.org/10.1021/cr9904009.

(10) Klein, J.; Khartabil, H.; Boisson, J.-C.; Contreras-García, J.; Piquemal, J.-P.; Hénon, E. New Way for Probing Bond Strength. *J. Phys. Chem. A* **2020**, *124* (9), 1850–1860. https://doi.org/10.1021/acs.jpca.9b09845.

(11) Lefebvre, C.; Klein, J.; Khartabil, H.; Boisson, J. -C.; Hénon, E. IGMPlot: A Program to Identify, Characterize, and Quantify Molecular Interactions. *J Comput Chem* **2023**, *44* (20), 1750–1766. https://doi.org/10.1002/jcc.27123.

(12) Bader, R. F. W. *Atoms in Molecules: A Quantum Theory*, Reprinted.; The international series of monographs on chemistry; Clarendon Press: Oxford, 2003.

(13) Kozlowski, D.; Pilmé, J. New Insights in Quantum Chemical Topology Studies Using Numerical Grid-based Analyses. *J Comput Chem* **2011**, *32* (15), 3207–3217. https://doi.org/10.1002/jcc.21903.

(14) Habets, T.; Seychal, G.; Caliari, M.; Raquez, J.-M.; Sardon, H.; Grignard, B.; Detrembleur, C. Covalent Adaptable Networks through Dynamic *N* , *S* -Acetal Chemistry: Toward Recyclable CO_2 -Based Thermosets. *J. Am. Chem. Soc.* **2023**, *145* (46), 25450–25462. https://doi.org/10.1021/jacs.3c10080.

(15) Fenimore, L. M.; Suazo, M. J.; Torkelson, J. M. Covalent Adaptable Networks Made by Reactive Processing of Highly Entangled Polymer: Synthesis-Structure-Thermomechanical Property-Reprocessing Relationship in Covalent Adaptable Networks. *Macromolecules* **2024**, *57* (6), 2756–2772. https://doi.org/10.1021/acs.macromol.3c02515.

In Chapter IV, we demonstrated that high molecular weight poly(cyclic carbonate-co-thioether)s (PCCs) can be synthesized through the step-growth polymerization of bisαCC and dithiols. As previously mentioned, these cyclic functionalities are produced via a domino process involving the rearrangement of *oxo*-thiocarbonates in the presence of DBU. The selectivity could be directed toward PTCs by addition of a fluorinated alcohol (FA) additive, although it remained limited and ranged between 16 and 82 % depending on the starting monomers. The role of FA was not fully elucidated, but we can hypothesize that the acidic nature of these alcohols might interact with the basic site of DBU, thereby altering its activity as an organobase.

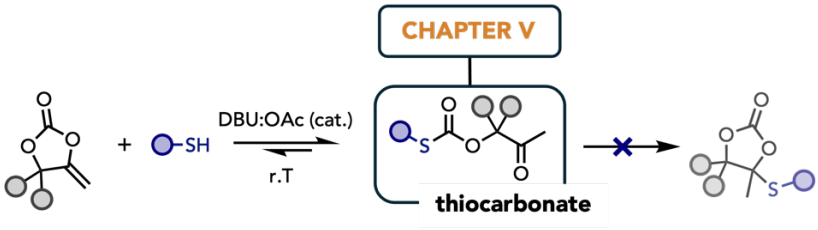

In order to install thiocarbonate linkages with increased selectivity, we tested several mono-component catalysts and an optimal candidate, DBU acetate, provided the best tradeoff in term of selectivity and reaction rate. Previous DFT calculations suggested this reaction to be reversible, which prompted us to evaluate these bonds in covalent adaptable networks. When combined to a lithium salt, the PTCs were also assessed as electrolytes for battery applications.

Chapter V

Facile Access to CO_2-Sourced Polythiocarbonate Dynamic Networks And Their Potential As Solid-State Electrolytes For Lithium Metal Batteries

Thomas Habets, Jorge L. Olmedo-Martínez, Rafael del Olmo, Bruno Grignard, David Mecerreyes, Christophe Detrembleur**

Reference: *ChemSusChem, 2023, 16, e202300225*

Abstract

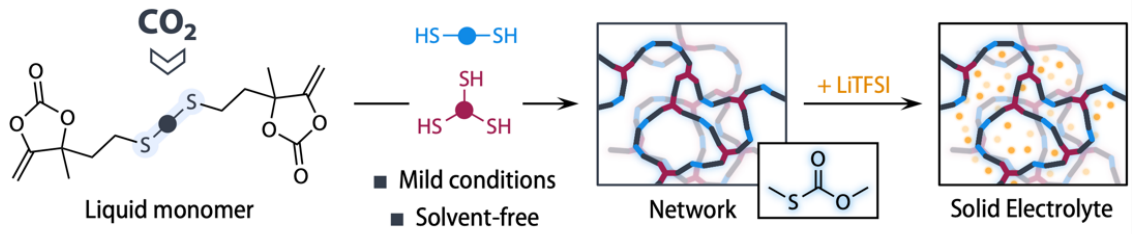

Poly(monothiocarbonate)s are an interesting class of sulfur-containing materials whose application as solid polymer electrolytes was barely studied, certainly due to the elusive production of diversified polymer architectures. Herein, a new liquid CO_2-sourced bis(α-alkylidene cyclic carbonate) monomer was designed at high yield to allow its one-step and solvent-free copolymerization with thiols to produce linear and cross-linked polymers in mild conditions. The influence of the monomer structure on the thermal properties and the ionic conductivity of linear polymers was assessed. The polymer network showed to be thermally re-processable owing to the dynamic nature of the monothiocarbonate bonds. A solid polymer electrolyte was easily obtained from the cross-linked material when combined with LiTFSI salt. The solid polymer electrolyte was characterized by an ionic conductivity reaching 6×10^{-6} $S.cm^{-1}$ at room temperature with a lithium transference number of 0.37 and a wide electrochemical stability window (4.0 V *vs* Li^0/Li^+) valid for lithium cycling. This work thus reports an attractive valorizing approach for carbon dioxide to deliver under mild operating conditions poly(monothiocarbonate)-containing novel covalent adaptable network CAN materials of high potential for energy applications, especially as solid electrolytes for batteries.

Introduction

Sulfur-containing polymers have caught interest of researchers and material manufacturers by virtue of their attractive properties, rendering them particularly suitable for a high diversity of applications such as engineering plastics, optics and optoelectronics, adhesives, or electrolytes[1]. Intensive research in this field is evidenced by the large panel of recently developed polymer scaffolds embedding sulfur atoms in their backbone[2]. Poly(monothiocarbonate)s (PMTCs) is an appealing class of these polymers as the sulfur atom integrated in the carbonate unit thoroughly modifies their chemical and physical properties[3,4] compared to their polycarbonate analogues. The main synthetic pathways relying on the use of harmful reagents and/or the need to eliminate acidic condensate[5–7] have quickly dropped out of sight as researchers focused on a more promising route: the chain-growth copolymerization of epoxides and carbonyl sulfide (COS)[8]. This approach delivers defect-free PMTCs at room temperature with metal-free catalysts from a diversity of commercial epoxides[9]. The main drawback of this polymerization method is the need to carry out the reaction in COS-pressurized autoclaves and in dry conditions, and the range of produced polymers is limited to linear chains.

Recently, some of us pioneered the use of CO_2-sourced bis(α-alkylidene cyclic carbonate)s (bisαCC) monomers to prepare a large palette of new polymers (polycarbonates, polyurethanes, and polythiocarbonates) in unprecedent mild conditions[10,11]. Following studies by us and other research groups have largely expanded the scope of these important families of polymers[12–22]. More specifically, this chemistry allowed to access linear PMTCs through the step-growth copolymerization of bisαCC with dithiols in the presence of a base catalyst under ambient conditions[11]. The versatility of this toolbox was further validated through the one-step synthesis of copolymers containing both urethane and thiocarbonate linkages from the terpolymerization of dithiols and diamines with bisαCC.[23]

Solid polymer electrolytes (SPEs) are materials that have been widely studied with the purpose of replacing liquid electrolytes in lithium batteries, which would make them safer, avoiding the loss of flammable electrolyte by leakage or the growth of lithium dendrites. The most studied polymer for this application is polyethylene oxide (PEO), due to its great capacity to dissolve lithium salts.[24] However, it has certain disadvantages, such as crystallization that restricts ionic conductivity, and a decrease in mechanical properties depending on the concentration of lithium salt in the system.[25] Polycarbonates have been studied as another polymeric matrix in SPEs for lithium batteries[26–28], as they have shown good ionic conductivity, electrochemical stability and a higher transport number than in the case of PEO. The carbonate group shows

weaker coordination with lithium cations compared to the ether groups, which is reflected in increased electrochemical properties.[29]

In the case of polythiocarbonates, Cao, *et al.* reported a first study on PMTCs as SPEs in which they prepared block copolymers from PMTCs and PEO doped with various amounts of LiTFSI to simultaneously increase ionic conductivity and mechanical properties of the resulting electrolyte. Many systems were studied and ionic conductivity values in the order of 10^{-4} $S.cm^{-1}$ at room temperature were obtained. However, the best candidates were containing high amounts of PEO in their chains and the mechanical properties were underperforming other block copolymers scaffolds, e.g. containing polystyrene (PS). Moreover, no further electrochemical studies were performed.[30] This only contribution concerning the use of PMTCs as SPEs in the literature attests for the lack of applicative studies of these polymers compared to conventional polycarbonates, certainly due to their more difficult preparation.

The overall goal of this work is to report the first facile preparation of a poly(monothiocarbonate) network in mild conditions, that presents a covalent adaptable network (CAN) behavior, and to assess its potential as solid electrolyte for Li-Ion batteries. CANs are very interesting materials since they present properties like recyclability, reprocessing and self-healing possibilities which are of great interest for materials applied in batteries.[31] To reach this objective, a novel CO_2-based liquid bisαCC monomer was designed for allowing straightforward one-step and solvent-free synthesis of the cross-linked polymer. The CAN behavior of the cross-linked polymer network was shown and the mechanical properties of the reprocessed material were studied. Various PEO-free PMTCs were prepared and subjected to ionic conductivity tests to evaluate the influence of the polymer structure on the ionic conductivity and the performance of the polymer network as a solid-state battery for Li-ion batteries was assessed.

Experimental section

Synthesis of dione 8,11-dioxa-5,14-dithiaoctadecane-2,17-dione (DO2)

To a mixture of DMDO (28.7 g, 0.15 mol, 1 eq.) and a catalytic amount of DBU (228 mg, 1.5 mmol, 0.01 eq.) in chloroform (125 mL) was added dropwise MVK (25.2 g; 30.4 mL, 0.36 mol, 2.4 eq.) under continuous stirring in an ice bath. The reaction was then driven in air for 30 min at rt. The mixture was diluted with 450 mL of chloroform and extracted with 3 x 600 mL of water. The organic layer was dried over $MgSO_4$ and filtered. The solvent was then removed under vacuum to yield a white solid (46.5g, isolated yield 96%); mp = 30 °C; ^{1}H NMR (400 MHz, DMSO-d_6) δ 3.55 (t, J = 6.4 Hz, 4H), 3.52 (s, 4H), 2.76-2.62 (m, 12H), 2.1 (s, 6H); ^{13}C NMR (100 MHz, DMSO-d_6) δ 207.4, 70.7, 70.0, 43.6, 31.2, 30.2, 26.0. See figures S1 and S2 for ^{1}H- and ^{13}C-NMR spectra, respectively.

Synthesis of bispropargylalcohol 3,18-dimethyl-9,12-dioxa-6,15-dithiaicosa-1,19-diyne-3,18-diol (BPA2)

Ethynylmagnesium bromide solution (800 mL, 0.5 M in THF, 0.4 mol, 3.1 eq.) was added in a two-necked round-bottom flask under nitrogen atmosphere. **DO2** (41.86 g, 0.13 mol, 1 eq.) dissolved in a minimal amount of THF was added dropwise to the solution. After stirring for 24h at room temperature, the reaction was quenched by the addition of a saturated ammonium chloride (NH_4Cl) solution (260 mL). The formed precipitate was removed by centrifugation followed by filtration. Diethylether (300 mL) was added to the filtrate. The aqueous phase was extracted with diethylether (3 x 300 mL). The combined organic phases were dried on $MgSO_4$ and filtered. The solvent was removed under vacuum. The viscous oil was mixed with a small amount of diethylether and purified by flash chromatography onto silica (eluent: diethylether). **BPA2** was collected as a yellow viscous oil after evaporation of the solvent (48.2 g, isolated yield 95%); ^{1}H NMR (400 MHz, DMSO-d_6) δ 5.38 (s, 2H), 3.56 (t, J = 6.8 Hz, 4H), 3.53 (s, 4H), 3.27 (s, 2H), 2.63 (m, 8H), 1.77 (m, 4H), 1.35 (s, 6H); ^{13}C NMR (100 MHz, DMSO-d_6) δ 88.9, 73.5, 70.6, 70.0, 66.2, 44.2, 31.1, 30.2, 27.1. See figures S3 and S4 for ^{1}H- and ^{13}C-NMR spectra, respectively.

Synthesis of bisαCC 4,4'-(6,9-dioxa-3,12-dithiatetradecane-1,14-diyl)bis(4-methyl-5-methylene-1,3-dioxolan-2-one) (M2)

BPA2 (48.2 g, 0.129 mol, 1 equiv.), DBU (0.98 g, 6.45 mmol, 0.05 eq.), CuI (1.23 g, 6.45 mmol, 0.05 eq.) and MeCN (25 mL) were added in a 250 mL high pressure autoclave. The reactor was charged with 40 bar of CO_2 at 25 °C. After 24h, CO_2 was discharged by depressurization of the reactor. The content of the autoclave was dissolved in a minimum amount of CH_2Cl_2 and the mixture was purified by flash chromatography onto silica (eluent: CH_2Cl_2/diethylether 80/20). The solvent was evaporated and the viscous oil was dissolved back in CH_2Cl_2. Chelex resin (200 mg / g of mixture) was added to trap residual copper and the mixture was stirred at rt for 4h. The resin was filtered and stored to be recycled. The solvent was removed under vacuum to yield a yellowish oil **M2** (59.6 g, isolated yield 93 %); ^{1}H NMR (400 MHz, DMSO-d_6) δ 4.87 (d, J = 4 Hz, 2H), 4.69 (d, J = 4 Hz, 2H), 3.56 (t, J = 6.6 Hz, 4H), 3.51 (s, 4H), 2.68 (t, J = 6.6 Hz, 4H), 2.54 (m, 4H), 2.14 (m, 4H), 1.60 (s, 6H) ;^{13}C NMR (100 MHz, DMSO-d_6) δ 156.9, 151.2, 87.3, 86.8, 70.8, 70.0, 39.7, 31.1, 25.9, 25.7. See figures S5 and S6 for ^{1}H- and ^{13}C-NMR spectra, respectively.

General synthetic procedure of the linear polymers P1 and P2

A bisαCC (**M1** or **M2**; 2 mmol; 1 eq.) was added to a reaction tube together with the dithiol DMDO (2 mmol; 1 eq.), DBU:OAc (0.04 mmol; 0.02 eq.) and DMF (1 mL). The tube was stirred at 25°C. After 24h, the mixture was diluted and dialyzed in acetone overnight. The solvent was removed under vacuum and the viscous oil was then dried overnight under vacuum at 60 °C. The molecular characteristics and thermal properties of the polymers are summarized in Table 1.

Synthetic procedure of the linear polymer P3

BisαCC **M2** (2 mmol; 1 eq.) was added to a reaction tube together with the diol TEG (2 mmol; 1 eq.), DBU (0.1 mmol; 0.05 eq.) and DMF (1mL). The tube was stirred at 25°C. After 24h, the mixture was diluted and dialyzed in acetone overnight. The solvent was removed under vacuum and the viscous oil was then dried overnight under vacuum at 60 °C. The molecular characteristics and thermal properties of the polymer are summarized in Table 1.

Preparation of the poly(thiocarbonate) network

BisαCC **M2** (15.68 mmol; 1 eq.), the dithiol DMDO (7.84 mmol; 0.5 eq.), the trithiol trimethylolpropane tris(3-mercaptopropionate) (5.17 mmol; 0.33 eq.) and DBU:OAc (0.78 mmol; 0.05 eq.) were added to a vial and stirred for 30 min under air. The viscous mixture was transferred into a silicon mold and was placed in an oven at 50 °C under air. After 22h, a well-defined film is removed from the mold.

Preparation of the solid polymer electrolytes

The electrolytes were prepared by solvent casting method. **P1**, **P2** and **P3** were dissolved in acetonitrile and 30 wt% LiTFSI were added, then placed in a silicon mold and the solvent was allowed to evaporate at room temperature. Subsequently, the electrolytes were dried under vacuum for 12 h before measurements by EIS and DSC. Data are shown in Figure 1.

In the case of **PN** with 30 wt% LiTFSI, an acetonitrile solution of 30 wt% LiTFSI with respect to the weight of the membrane was prepared and this solution was allowed to adsorb onto the polymer for 12 h. The solvent was then removed under vacuum at 30 °C. EIS and DSC data are shown in Figure 3.

Results and discussion

Monomer design

Although numerous studies were describing the palette of available polymers from bisαCC, only little effort was yet devoted to the synthesis of monomers with higher solubility and lower melting points. The synthesis of these monomers can be achieved by the addition of ethynyl magnesium bromide on a diketone, thus affording a bispropargylalcohol which is further quantitatively reacted with CO_2 to furnish the monomer (Scheme 1a). So far, only two monomers from commercially available diones were synthesized by our group: 1,6-hexanedione[10] and 1,4-cyclohexanedione-based[11] monomers. However, they were characterized by limited solubility and high melting points, avoiding developing solvent-free formulations. Lamb et al. recently developed new bispropargylic alcohols through the addition of solubilizing groups on the double bond[22]. Although these compounds were characterized by T_m ranging from 105 to 200 °C, this approach is an appealing way to potentially access liquid monomers, however total yields starting from the dione were not exceeding 22%. Schaub et al. synthesized monomers starting from 1,4-butynediol and bisepoxides, affording two liquid bisαCCs with overall yields of up to 70%[20]. However, the compounds were unsubstituted αCCs whose relative reactivity is unknown compared to our previous developed monomers and the synthesis was only proposed at the 1 mmol scale.

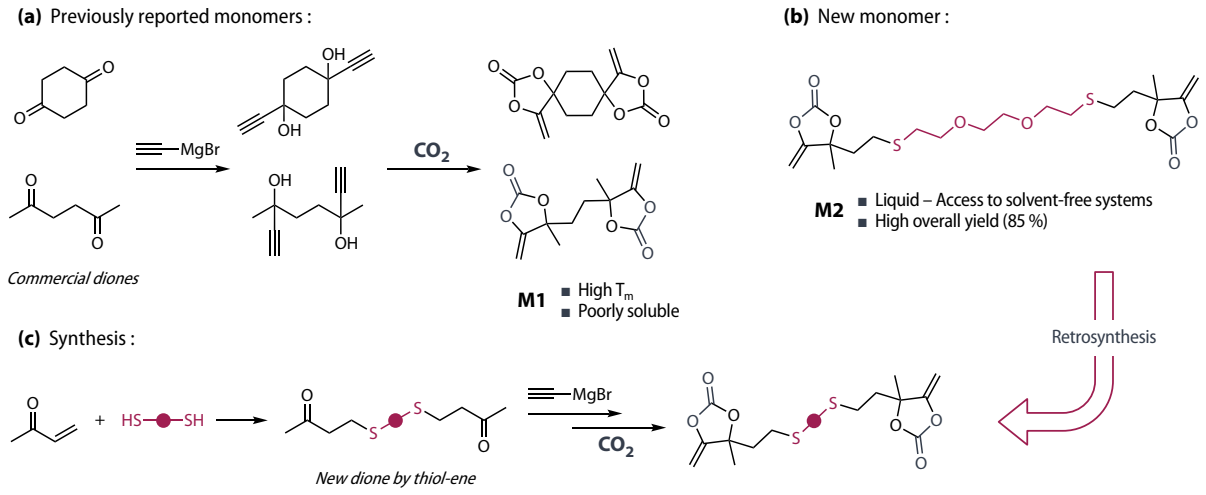

Scheme 1 – Synthetic approach toward bisαCC. (a) Previously reported monomer made from 1,6-hexanedione[10] and 1,4-cyclohexanedione[11]. (b) Structure of the new liquid monomer. (c) Design of a new dione to tune the structure of bisαCC by a retrosynthetic approach.

To tune the structure of the monomer, a retrosynthetic approach has led to design a new dione with a flexible segment (Scheme 1b-c). To do so, methyl vinyl ketone (MVK) is an ideal cheap and available synthon containing a ketone group directly conjugated to a terminal alkene. The electron-attractor nature of the ketone makes the compound very reactive toward thiols through the thia-Michael addition. With the aim to get a novel dione, a dithiol was reacted with MVK in the presence of a low amount of DBU (2 mol%) as base catalyst. To provide flexibility to the backbone, the cheap dithiol 2,2′-(Ethylenedioxy)diethanethiol (DMDO) was selected, affording the new dione in high isolated yield (96 %). The compound was then subjected to the same reactions as the commercial diones (addition of ethynyl magnesium bromide followed by CO_2 coupling), providing a liquid bisαCC **M2** with an overall isolated yield of 85 % (Scheme 1c). The reaction was scaled up to provide nearly 60 g of monomer in one batch. All characterizations (^{1}H-, ^{13}C-NMR and IR) confirmed the chemical structure of the monomer (Figures S5-7).

Synthesis and characterization of PMTCs

We then proceeded to the synthesis of PMTCs by the step-growth copolymerization of bisαCC monomers **M1** and **M2** with the dithiol DMDO to provide **P1** and **P2**. The two monomers **M1** and **M2** were here employed to deliver structurally different PMTCs in order to evaluate the influence of the monomer structure (and thus flexibility) on the ionic conductivity of the polymer material. The syntheses were carried out in DMF at 25°C in the presence of 2 mol% of DBU acetate (DBU:OAc) as base catalyst. As described in a previous work, the thiolysis of bisαCC can lead to two types of linkages: monothiocarbonate and cyclic carbonate-*co*-thioether ones[11]. The selectivity toward both units was tuned through the choice of the catalyst. Here, the use of DBU:OAc provided **P1** and **P2** with a selectivity in monothiocarbonate linkage of 91% and 93%, respectively. The structures of the polymers were confirmed by ^{1}H- and ^{13}C-NMR spectroscopy (Figures S8-12) and the linkage selectivity was determined by integration of characteristic resonance as described in SI.

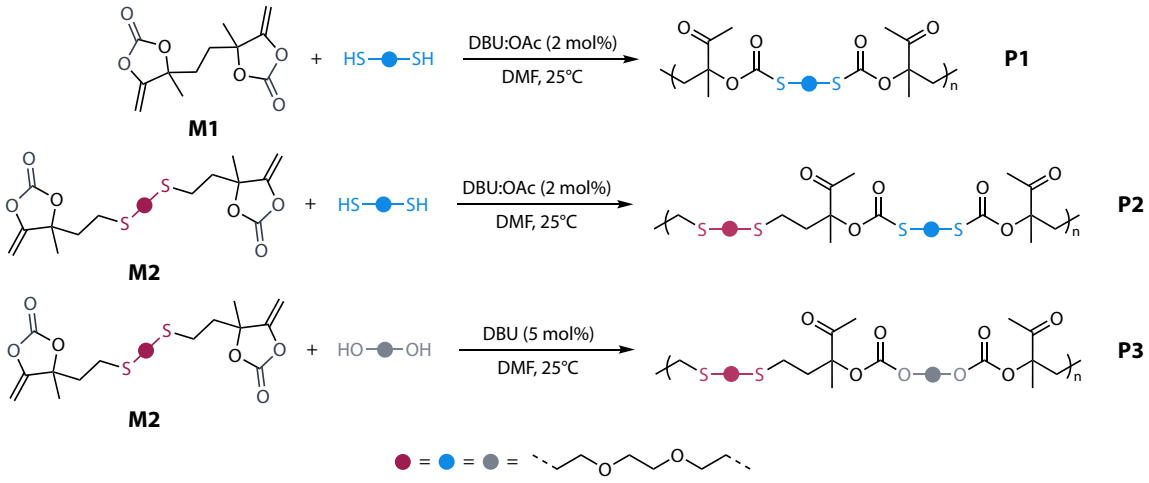

Scheme 2 – Reactions for the polymerization toward **P1**, **P2** and **P3**.

^{1}H-NMR spectra revealed the characteristic ketone methyl of the monothiocarbonate linkage at around 2.14 ppm for both polymers. The cyclic carbonate linkage was evidenced by the resonance of the methylene neighboring the sulfur atom at 2.92 ppm compared to 3.02 ppm for the monothiocarbonate moiety. Both **P1** and **P2** have shown decent molar masses of nearly 20000 g/mol in M_w as determined by SEC (Table 1 & Figure S15).

The thermal properties of the two polymers were determined by differential scanning calorimetry (DSC). As expected, they were both amorphous with T_gs of 8 and -10 °C for **P1** and **P2**, respectively (Table 1). This demonstrates the high impact of the flexible segment within the new monomer **M2**, decreasing the T_g of the polymer of nearly 20 °C compared to the polymer made from **M1**.

As a fair comparison between polythiocarbonates and polycarbonates, **P3** was prepared by the copolymerization of bisαCC **M2** with triethylene glycol (TEG), a diol mimicking the dithiol used in this study. The reaction was carried out in DMF at 25 °C in the presence of 5 mol% of DBU as catalyst. The so-produced polymer was characterized by an even lower T_g of -19 °C (Table 1). It is however not clear if the difference in T_g between **P2** and **P3** is due to the thiocarbonate/carbonate linkage or the presence of a little amount of rigid cyclic linkages in **P2**.

The three synthesized polymers also presented a high thermal stability, with a degradation temperature at 5wt% ($T_{deg,5\%}$) around 240°C for the polythiocarbonate, and around 260°C for the polycarbonate (Table 1).

Table 1 – Molecular and thermal properties of the polymers **P1**, **P2** and **P3** (after purification).

Polymer	M_n (g/mol)	M_w (g/mol)	D	$T_{deg,5\%}$ (°C)	T_g (°C)	Cyclic linkage (%)
P1	8700	19800	2.27	245	8	9
P2	9300	19500	2.09	238	-10	7
P3	16600	32800	1.98	262	-19	0

Evaluation of the ionic conductivity of PMTCs

Encouraged by the drop in T_g induced by **M2**, rich in typical Li conducting groups (ether and thioether bonds)[32–35], the three polymers **P1-3** were evaluated as solid polymer electrolytes (SPEs). For this purpose, the materials were mixed with 30 wt% LiTFSI in acetonitrile prior to solvent removal.

The anhydrous ionic conductivity of the SPEs was measured by electrochemical impedance spectroscopy (EIS) in a temperature range of 25 to 100 °C. As shown in Figure 1a, the installation of additional thioether and ether groups within the polymer backbone is highly favorable for the conductivity of **P2** (1.88×10^{-6} S.cm^{-1}) which is 2.5 times higher at 25 °C than **P1** (7.38×10^{-7} S.cm^{-1}). The ionic conductivity of **P3** (2.09×10^{-6} S.cm^{-1}) was very similar to **P2**, indicating that thiocarbonates or carbonates linkages seem to have only slight impact on the ionic conductivity. The amount of cyclic carbonate linkage in **P1** and **P2** is rather low (< 10 mol%) and is thus expected to benefit to ionic conductivity as already highlighted by our group[36]. Although **P3** was characterized by a lower T_g enabling high motion within the chains, the initial value of -19 °C was readily increased to -2 °C by addition of 30 wt% of LiTFSI. Figure 1b shows the second heating cycle for the polymers as a function of the lithium salt concentration. It is observed that the T_g increases with increasing salt concentration in the electrolyte. This phenomenon is related to a higher concentration of cations and charged ionic agglomerates that limit the movement of the polymer chains[37,38]. Upon addition of the salt, T_gs of **P2** and **P3** become rather similar.

This study highlights that careful tuning of the polymer structure through systematic monomer design allows to reach higher ionic conductivities. Using this strategy by making the monomer **M2** containing flexible groups, decent ionic conductivity could be reached without using long PEO chains which generally induced crystallization. Switching from monothiocarbonate to carbonate linkages did not seem to have major impact on the ionic conductivity of the electrolyte.

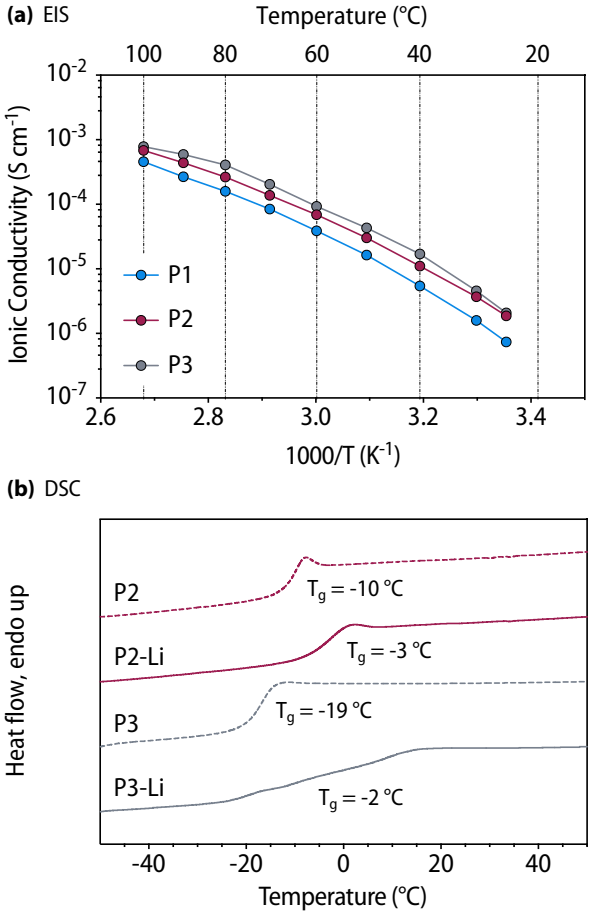

Figure 1 – (a) Ionic conductivity as a function of temperature for the polymers **P1**, **P2** and **P3** with 30 wt% LiTFSI, (b) DSC curves of the second heating for **P2**, **P3**, and **P2-Li** and **P3-Li** containing both 30 wt% of LiTFSI.

Solvent-free synthesis of a PMTC network

Thanks to the highly flexible segment in **M2**, the liquid monomer can be used for solvent-free formulations. After optimization of the conditions, the polymer network **PN** was easily synthesized by mixing **M2**, the dithiol, and a trithiol in a 1 : 0.5 : 0.33 molar ratio (Scheme 3). For a further application as solid-state electrolyte for batteries with enhanced mechanical properties, the network was designed to mimic the reported polymer **P2** while adding sufficient cross-linker to reach desired mechanical properties. The method for producing **PN** is straightforward: the components are mixed together with the catalyst (DBU:OAc) at room temperature and the homogeneous viscous mixture is transferred into a silicon mold. The polymer is then cured at 50 °C for 22h to yield a very flexible self-standing film (Scheme 3). It is noteworthy that the polymerization was performed without any solvent, under air, and in mild

curing temperatures. This method is also scalable and up to 10 g of **PN** was produced in one batch, highlighting the robustness of this chemistry to easily provide PMTC networks.

Although solution polymerizations were carried out at room temperature, no curing was observed in the conditions used for the solvent-free system. It was hypothesized that solvents influenced the reaction. However, a full understanding of these effects is out of the scope of this paper. After optimization, it was found that a slight increase of temperature (25 to 50 °C) was enough to provide curing without affecting the type of polymer linkages.

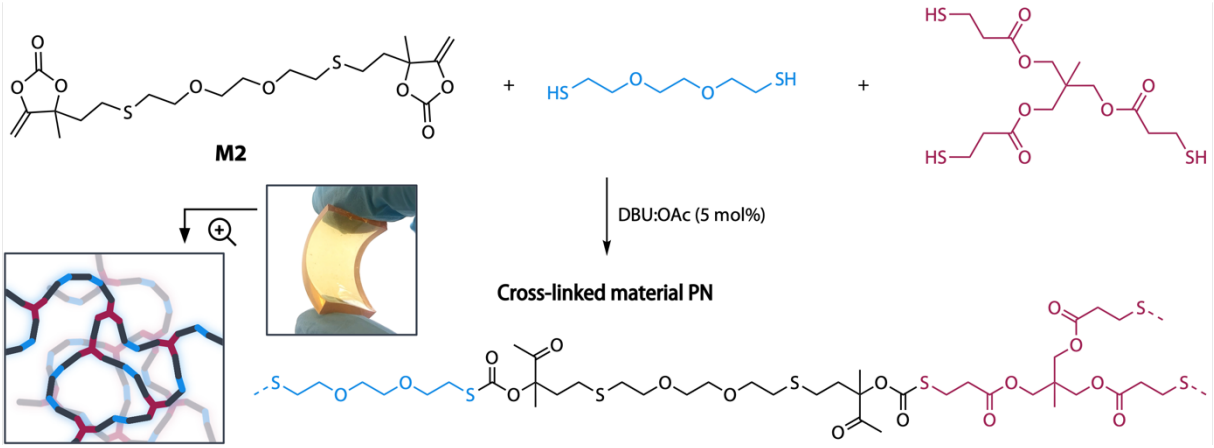

Scheme 3 – Reaction for the polymerization of **M2**, the dithiol, and the trithiol to furnish the cross-linked material **PN**.

The network was characterized by ATR-IR spectroscopy, which showed a nearly complete disappearance of the band at 1815 cm^{-1} which belongs to the monomer **M2** carbonyl stretching (Figure S16), attesting for the almost completeness of the reaction. A moderate gel content of 76 % in THF was measured with a swelling degree of 326 %. DSC analysis of the network showed that it was totally amorphous with a low T_g of -34 °C.

As evidenced in our previous publication, the formation of the thiocarbonate is reversible in the presence of the catalyst[11] (Figure 2a). Although this might be seen as a drawback as it does not allow to provide full conversion and thus high molecular weight linear chains, this particularity can be exploited to design a dissociative covalent adaptable network (CAN)[39]. To assess if the network can be re-processed through its reversible bonds, the dynamic nature of **PN** was studied by dynamic mechanical analysis (DMA) and rheology. First, a temperature ramp DMA analysis was performed and the polymer behaved as expected for dissociative-type CANs, displaying a constant rubber plateau above T_g followed by a drop of the storage modulus starting around 100 °C due to entropically favorable excessive bond dissociation (Figure 2b). Stress relaxations experiments at different temperatures were then performed from 50 to 80 °C. As shown in Figure 2c, **PN** is able to relax following a

Kohlrausch−Williams−Watt (KWW) stretched exponential model[40,41] and relaxation times were extracted out of the data through curve fitting (Table S1 & Figure S17). The material displayed fast relaxation from 4 s at 80 °C to 150 s at 50 °C. An Arrhenius plot was built from the extracted relaxation times at the different temperatures and a linear correlation was observed, rendering possible to calculate a flow energy activation of 111 kJ/mol (Figure 2d).

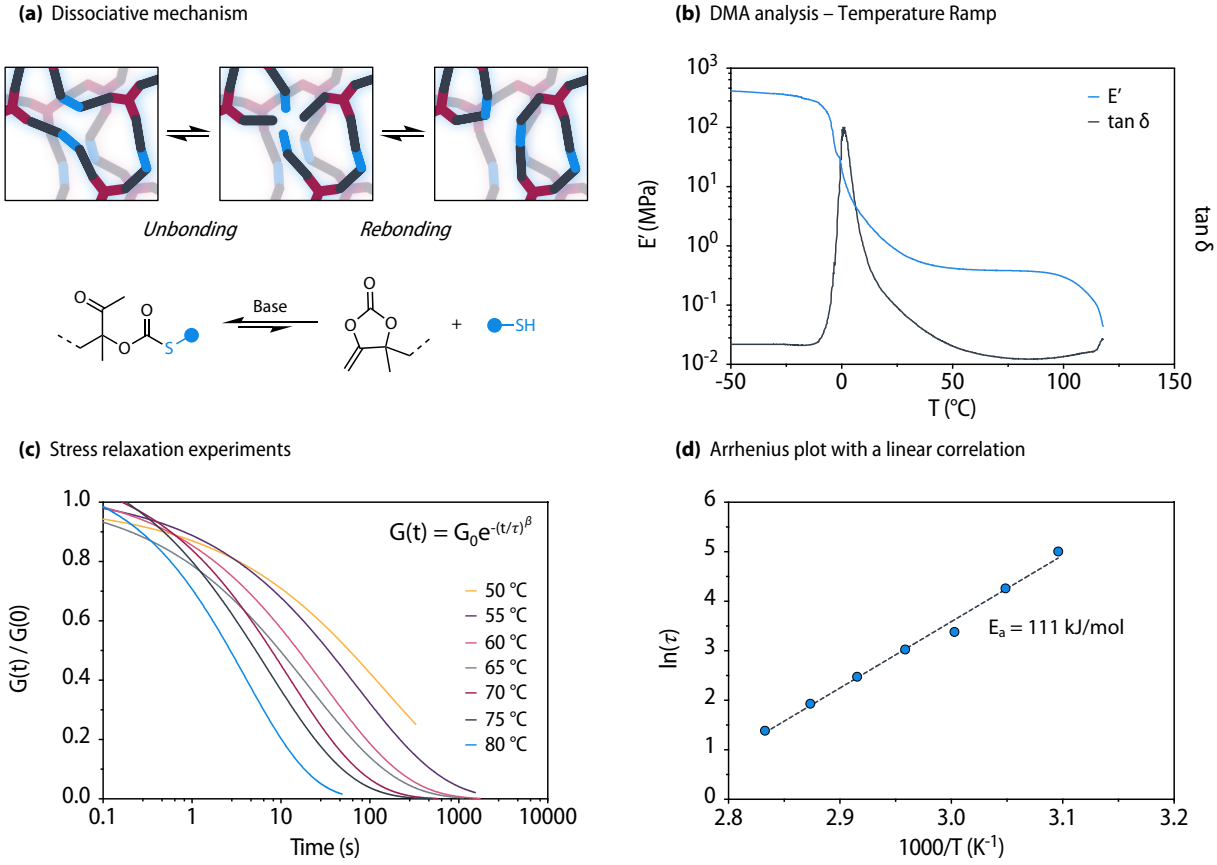

Figure 2 – (a) Dissociative mechanism of the monothiocarbonate linkage in equilibrium with α-alkylidene cyclic carbonate and a thiol, (b) DMA trace of **PN** displaying the tan δ and the modulus along an increasing temperature, (c) Stress relaxation fitted curves using the stretched exponential model at different temperatures, (d) Arrhenius plot from the extracted relaxation times of **PN** showing a linear correlation.

The mechanical properties of **PN** were then evaluated by stress/strain experiments. The material was thus cut in pieces and reprocessed by hot pressing at 70 °C for 15 min. The flat film was cut into rectangular pieces prior DMA analysis. **PN** featured a Young's modulus of 0.51 ± 0.04 MPa, a stress at break of 0.24 ± 0.04 MPa, and a strain at break of 134 ± 16 %, indicating that the polymer is a very flexible material (Figure S18).

Preparation and electrochemical characterization of SPE membranes

As the linear polymers were promising materials for solid-state electrolytes but were lacking decent mechanical properties, the crosslinked material **PN** was evaluated for this application. This **PN** had thus to be loaded by a Li salt, here LiTFSI, in order to impart it ion conductivity. However, adding this salt to the previously described solvent-free formulation inhibited the crosslinking reaction. This was certainly due to strong binding of a high amount of lithium metal to DBU, known to be a good ligand for metal complex catalyzed reactions[42,43]. To solve this issue, we took advantage of the reprocessing ability of **PN** to prepare the SPE membranes through a facile protocol. The polymer was first reprocessed by hot pressing at 70 °C for 10 min to the desired shape and precise thickness. The material was then immersed in a solution of LiTFSI in acetonitrile for 12h prior evaporation of the solvent, yielding a self-standing SPE membrane loaded by 30 wt% of Li salt. For comparison, a membrane was prepared by direct cut out of the raw material after synthesis without reprocessing. However, only a larger material thickness of 1.33 mm could be obtained compared to 0.65 mm for the reprocessed material. For sake of clarity, this material will be named **CPN** (crude **PN**).

Similarly to **P2**, the **PN**-SPE was characterized by EIS and DSC. Following the same trend, the T_g of **PN** increased when introducing LiTFSI in its matrix, passing from -34 to -15 °C. However, this value is lower than the SPE made of **P2**, which was characterized by a T_g of -3 °C. This higher mobility was highlighted by a higher ionic conductivity at room temperature (5.89×10^{-6} S.cm^{-1} for **PN** *vs* 1.88×10^{-6} S.cm^{-1} for **P2**). However, the ionic conductivity of **P2** was similar to the one of **PN** at 60 °C and superior at higher temperatures, certainly due to the restricted mobility of **PN** containing covalent cross-links. **CPN** was characterized by a very similar ionic conductivity compared to **PN**, showing negligible effect of reprocessing (Figure S19).

The electrochemical stability of the electrolyte as a function of the applied potential is an important parameter for the direct application of this material. Figure 3c shows the linear sweep voltammogram (LSV) for the **PN** 30 wt% LiTFSI electrolyte. When scanning toward more anodic values, an increase in current is observed, attributed to the electrolyte decomposition at the interface with the electrode. The electrolyte was stable up to 4 V, enabling its use in standard lithium iron phosphate batteries. Another key parameter for the electrolyte in batteries is the lithium-ion transference number (t_{Li^+}), which is directly related to the fraction of the ionic conductivity that is given by the movement of lithium. Figure S20 shows ac impedance and dc polarization for the lithium-ion transference number measurements for **PN**-Li containing 30 wt% of LiTFSI electrolyte. Using the Bruce-Vincent method[44] a lithium transport number of 0.37 was obtained. The value reported for PEO/LiTFSI systems is around 0.2, although this

value is highly dependent on the LiTFSI concentration and temperature at which the measurement is made. In this case, the increase in the lithium transport number value might be related to the presence of carbonyl groups [45].

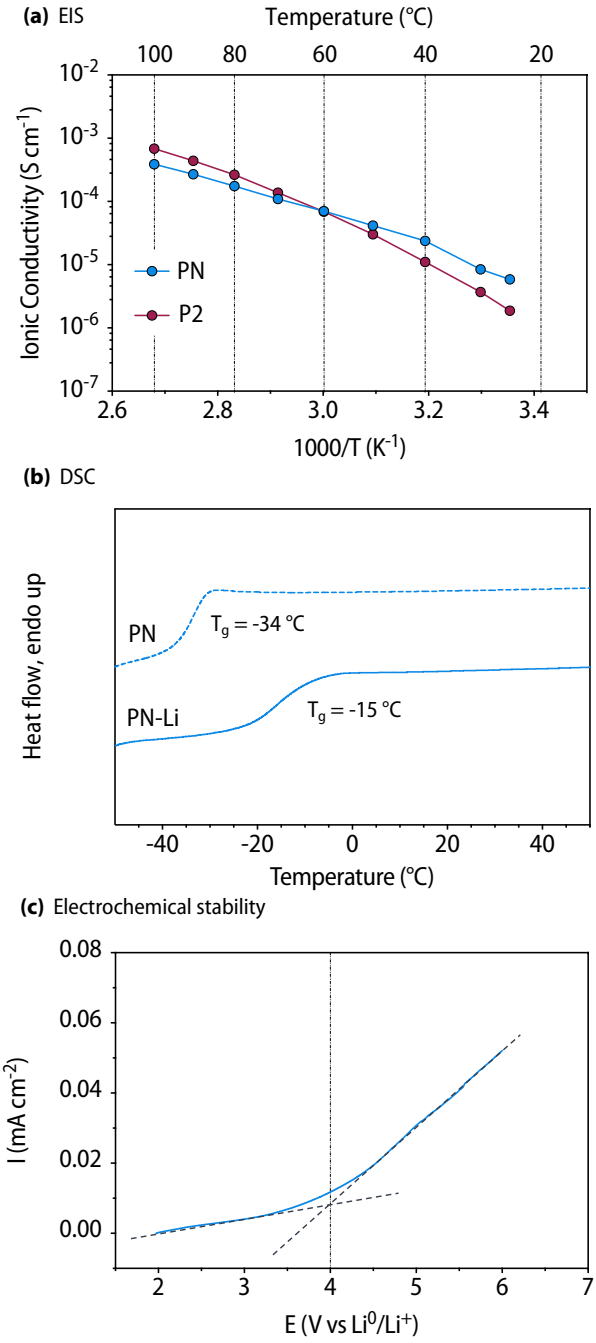

Figure 3 – (a) Ionic conductivity as a function of temperature for the polymers **P2** and **PN-Li** with 30wt% LiTFSI, (b) DSC curves of the second heating for **PN** and **PN-Li** containing 30 wt% of LiTFSI, (c) Electrochemical stability window of **PN**-SPE obtained by CV at scan rate of 10 mV s^{-1}.

The behavior of the polymer electrolyte against lithium is commonly studied by performing plating and stripping tests on a symmetrical lithium cell at different current densities. Figure 4 shows the cell polarization as a function of time for the **PN** and **CPN** electrolytes at 80 °C. For the two studied current densities (0.05 and 0.10 mA cm^{-2}), it was observed that the overpotential in both electrolytes is higher when a higher current density is used. The cells were cycled for 180 h showing a slight increase in the overpotential with time. Interestingly, **PN** has shown drastically lower overpotential as compared to **CPN** though their ionic conductivity was similar (Figure S19). The reduced thickness of the SPE (0.65 mm for **PN** and 1.33 mm for **CPN**) is known to be critical for high battery performance as it imparts the system with reduced internal resistance[46]. The ability to re-process the polymer network into membranes of controlled thickness is thus desirable to reach optimal performances for the electrolyte in lithium batteries. These materials have shown to be stable with lithium metal which opens their application in lithium batteries.

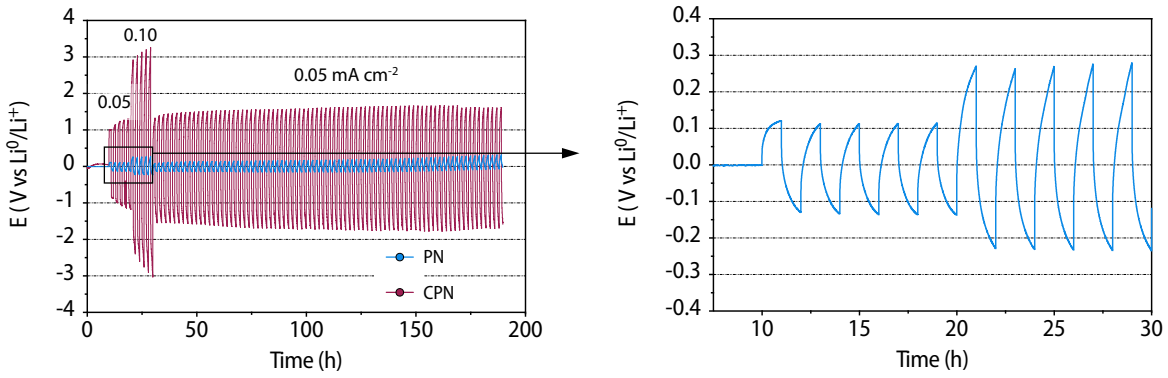

Figure 4 – Potential as a function of time for symmetrical lithium cells from **PN** and **CPN** cycled at 0.05 and 0.1 mA cm^{-2} at 80 °C.

Conclusion

This work described a facile route toward cross-linked CO_2-sourced poly(monothiocarbonate)s and their potential as solid polymer electrolytes for Li-batteries. A new liquid bis(α-alkylidene cyclic carbonate) monomer was designed and easily synthesized in high yields following an up-scalable process by valorizing CO_2 as a carbon feedstock. Linear polymers were first synthesized and characterized to assess the impact on this new monomer on the thermal properties and the ionic conductivity. In contrast to previously reported poorly soluble monomers, the liquid monomer could be used in solvent-free formulation to deliver a cross-

linked material in a simple one-step fashion under mild curing conditions. Owing to the dynamic character of the monothiocarbonate linkages, the covalent adaptable nature of the network was probed and the covalently cross-linked polymer could be re-processed into membranes for solid polymer electrolytes. The SPE was characterized by EIS to measure the ionic conductivity of **PN** reaching 5.89 $\times 10^{-6}$ S.cm^{-1} at room temperature with a t_{Li^+}=0.37. The electrochemical stability of the material (4.0 V vs Li^0/Li^+) was high enough to be applicable in commercial lithium iron phosphate batteries. Finally, the stability against lithium metal was probed with almost 200 h of stable cycling in lithium symmetrical cells at 0.05 mA cm^{-2}. This paper thus describes the first route to poly(monothiocarbonate)s-containing CAN networks under solvent-free and mild conditions that have a potential to be used as solid electrolytes in batteries. Current works are focusing on the optimization of the polymer structure to improve the ion conductivity and on the recycling of the final product by exploiting the dissociative behavior of the material.

References

(1) Kultys, A. Sulfur-Containing Polymers. In *Kirk-Othmer Encyclopedia of Chemical Technology*; John Wiley & Sons, Inc., Ed.; John Wiley & Sons, Inc.: Hoboken, NJ, USA, 2005. https://doi.org/10.1002/0471238961.sulfkult.a01.

(2) Mutlu, H.; Ceper, E. B.; Li, X.; Yang, J.; Dong, W.; Ozmen, M. M.; Theato, P. Sulfur Chemistry in Polymer and Materials Science. *Macromol. Rapid Commun.* **2019**, *40* (1), 1800650. https://doi.org/10.1002/marc.201800650.

(3) Yue, T.-J.; Wang, L.-Y.; Ren, W.-M. The Synthesis of Degradable Sulfur-Containing Polymers: Precise Control of Structure and Stereochemistry. *Polym. Chem.* **2021**, *12* (46), 6650–6666. https://doi.org/10.1039/D1PY01065D.

(4) Marianucci, E.; Berti, C.; Pilati, F.; Manaresi, P.; Guaita, M.; Chiantore, O. Refractive Index of Poly(Thiocarbonate)s and Poly(Dithiocarbonate)s. *Polymer* **1994**, *35* (7), 1564–1566. https://doi.org/10.1016/0032-3861(94)90361-1.

(5) Berti, C.; Marianucci, E.; Pilati, F. Sulfur Containing Polymers: 1. Copolymers of 1,3-Benzeneditiol with Phosgene and Bisphenol-A. *Polymer Bulletin* **1985**, *14* (1), 85–91. https://doi.org/10.1007/BF00254920.

(6) Pilati, F.; Berti, C.; Marianucci, E. Sulfur-Containing Polymers: Thermal Behavior of Copolymers Containing Thiocarbonate Groups. *Polymer Degradation and Stability* **1987**, *18* (1), 63–72. https://doi.org/10.1016/0141-3910(87)90083-8.

(7) Sanda, F.; Kamatani, J.; Endo, T. The First Anionic Ring-Opening Polymerization of Cyclic Monothiocarbonate via Selective Ring-Opening with C−S Bond Cleavage. *Macromolecules* **1999**, *32* (17), 5715–5717. https://doi.org/10.1021/ma9905472.

(8) Zhang, C.-J.; Zhang, X.-H. Recent Progress on COS-Derived Polymers. *Chin J Polym Sci* **2019**, *37* (10), 951–958. https://doi.org/10.1007/s10118-019-2288-y.

(9) Zhang, C.-J.; Wu, H.-L.; Li, Y.; Yang, J.-L.; Zhang, X.-H. Precise Synthesis of Sulfur-Containing Polymers via Cooperative Dual Organocatalysts with High Activity. *Nat Commun* **2018**, *9* (1), 2137. https://doi.org/10.1038/s41467-018-04554-5.

(10) Gennen, S.; Grignard, B.; Tassaing, T.; Jérôme, C.; Detrembleur, C. CO_2-Sourced α-Alkylidene Cyclic Carbonates: A Step Forward in the Quest for Functional Regioregular Poly(Urethane)s and Poly(Carbonate)s. *Angew. Chem. Int. Ed.* **2017**, *56* (35), 10394–10398. https://doi.org/10.1002/anie.201704467.

(11) Ouhib, F.; Grignard, B.; Van Den Broeck, E.; Luxen, A.; Robeyns, K.; Van Speybroeck, V.; Jerome, C.; Detrembleur, C. A Switchable Domino Process for the Construction of Novel CO_2-Sourced Sulfur-Containing Building Blocks and Polymers. *Angew. Chem. Int. Ed.* **2019**, *58* (34), 11768–11773. https://doi.org/10.1002/anie.201905969.

(12) Grignard, B.; Gennen, S.; Jérôme, C.; Kleij, A. W.; Detrembleur, C. Advances in the Use of CO_2 as a Renewable Feedstock for the Synthesis of Polymers. *Chem. Soc. Rev.* **2019**, *48* (16), 4466–4514. https://doi.org/10.1039/C9CS00047J.

(13) Ngassam Tounzoua, C.; Grignard, B.; Detrembleur, C. Exovinylene Cyclic Carbonates: Multifaceted CO_2-Based Building Blocks for Modern Chemistry and Polymer Science. *Angew Chem Int Ed* **2022**, *61* (22), e202116066. https://doi.org/10.1002/anie.202116066.

(14) Siragusa, F.; Van Den Broeck, E.; Ocando, C.; Müller, A. J.; De Smet, G.; Maes, B. U. W.; De Winter, J.; Van Speybroeck, V.; Grignard, B.; Detrembleur, C. Access to Biorenewable and CO_2-Based Polycarbonates from Exovinylene Cyclic Carbonates. *ACS Sustainable Chem. Eng.* **2021**, *9* (4), 1714–1728. https://doi.org/10.1021/acssuschemeng.0c07683.

(15) Habets, T.; Siragusa, F.; Grignard, B.; Detrembleur, C. Advancing the Synthesis of Isocyanate-Free Poly(Oxazolidones)s: Scope and Limitations. *Macromolecules* **2020**, *53* (15), 6396–6408. https://doi.org/10.1021/acs.macromol.0c01231.

(16) Gennen, S.; Grignard, B.; Jérôme, C.; Detrembleur, C. CO_2-Sourced Non-Isocyanate Poly(Urethane)s with pH-Sensitive Imine Linkages. *Adv. Synth. Catal.* **2019**, *361* (2), 355–365. https://doi.org/10.1002/adsc.201801230.

(17) Zhang, Y.-F.; Lai, W.-M.; Xie, S.; Zhou, H.; Lu, X.-B. Facile Synthesis, Structure and Properties of CO_2-Sourced Poly(Thioether-*Co*-Carbonate)s Containing Acetyl Pendants *via* Thio-Ene Click Polymerization. *Polym. Chem.* **2022**, *13* (2), 201–208. https://doi.org/10.1039/D1PY01477C.

(18) Siragusa, F.; Demarteau, J.; Habets, T.; Olazabal, I.; Robeyns, K.; Evano, G.; Mereau, R.; Tassaing, T.; Grignard, B.; Sardon, H.; Detrembleur, C. Unifying Step-Growth Polymerization and On-Demand Cascade Ring-Closure Depolymerization via Polymer Skeletal Editing. *Macromolecules* **2022**, *55* (11), 4637–4646. https://doi.org/10.1021/acs.macromol.2c00696.

(19) Siragusa, F.; Habets, T.; Méreau, R.; Evano, G.; Grignard, B.; Detrembleur, C. Catalyst-Free Approach for the Degradation of Bio- and CO_2-Sourced Polycarbonates: A Step toward a Circular Plastic Economy. *ACS Sustainable Chem. Eng.* **2022**, *10* (27), 8863–8875. https://doi.org/10.1021/acssuschemeng.2c01891.

(20) Dabral, S.; Licht, U.; Rudolf, P.; Bollmann, G.; Hashmi, A. S. K.; Schaub, T. Synthesis and Polymerisation of α-Alkylidene Cyclic Carbonates from Carbon Dioxide, Epoxides and the Primary Propargylic Alcohol 1,4-Butynediol. *Green Chem.* **2020**, *22* (5), 1553–1558. https://doi.org/10.1039/C9GC04320A.

(21) Ouhib, F.; Meabe, L.; Mahmoud, A.; Eshraghi, N.; Grignard, B.; Thomassin, J.-M.; Aqil, A.; Boschini, F.; Jérôme, C.; Mecerreyes, D.; Detrembleur, C. CO_2-Sourced Polycarbonates as

Solid Electrolytes for Room Temperature Operating Lithium Batteries. *J. Mater. Chem. A* **2019**, *7* (16), 9844–9853. https://doi.org/10.1039/C9TA01564G.

(22) Wong, A. R.; Barrera, M.; Pal, A.; Lamb, J. R. Improved Characterization of Polyoxazolidinones by Incorporating Solubilizing Side Chains. *Macromolecules* **2022**, *55* (24), 11006–11012. https://doi.org/10.1021/acs.macromol.2c02104.

(23) Habets, T.; Siragusa, F.; Müller, A. J.; Grossman, Q.; Ruffoni, D.; Grignard, B.; Detrembleur, C. Facile Construction of Functional Poly(Monothiocarbonate) Copolymers under Mild Operating Conditions. *Polym. Chem.* **2022**, *13* (21), 3076–3090. https://doi.org/10.1039/D2PY00307D.

(24) Mindemark, J.; Lacey, M. J.; Bowden, T.; Brandell, D. Beyond PEO—Alternative Host Materials for Li + -Conducting Solid Polymer Electrolytes. *Progress in Polymer Science* **2018**, *81*, 114–143. https://doi.org/10.1016/j.progpolymsci.2017.12.004.

(25) Olmedo-Martínez, J. L.; Porcarelli, L.; Guzmán-González, G.; Calafel, I.; Forsyth, M.; Mecerreyes, D.; Müller, A. J. Ternary Poly(Ethylene Oxide)/Poly(l , l -Lactide) PEO/PLA Blends as High-Temperature Solid Polymer Electrolytes for Lithium Batteries. *ACS Appl. Polym. Mater.* **2021**, *3* (12), 6326–6337. https://doi.org/10.1021/acsapm.1c01093.

(26) Meabe, L.; Huynh, T. V.; Lago, N.; Sardon, H.; Li, C.; O'Dell, L. A.; Armand, M.; Forsyth, M.; Mecerreyes, D. Poly(Ethylene Oxide Carbonates) Solid Polymer Electrolytes for Lithium Batteries. *Electrochimica Acta* **2018**, *264*, 367–375. https://doi.org/10.1016/j.electacta.2018.01.101.

(27) Raj, A.; Panchireddy, S.; Grignard, B.; Detrembleur, C.; Gohy, J. Bio-Based Solid Electrolytes Bearing Cyclic Carbonates for Solid-State Lithium Metal Batteries. *ChemSusChem* **2022**, *15* (18). https://doi.org/10.1002/cssc.202200913.

(28) Boujioui, F.; Zhuge, F.; Damerow, H.; Wehbi, M.; Améduri, B.; Gohy, J.-F. Solid Polymer Electrolytes from a Fluorinated Copolymer Bearing Cyclic Carbonate Pendant Groups. *J. Mater. Chem. A* **2018**, *6* (18), 8514–8522. https://doi.org/10.1039/C8TA01409D.

(29) Sun, B.; Mindemark, J.; Edström, K.; Brandell, D. Polycarbonate-Based Solid Polymer Electrolytes for Li-Ion Batteries. *Solid State Ionics* **2014**, *262*, 738–742. https://doi.org/10.1016/j.ssi.2013.08.014.

(30) Cao, X.; Li, J.; Yang, M.; Yang, J.; Wang, R.; Zhang, X.; Xu, J. Simultaneous Improvement of Ionic Conductivity and Mechanical Strength in Block Copolymer Electrolytes with Double Conductive Nanophases. *Macromol. Rapid Commun.* **2020**, *41* (7), 1900622. https://doi.org/10.1002/marc.201900622.

(31) Elizalde, F.; Amici, J.; Trano, S.; Vozzolo, G.; Aguirresarobe, R.; Versaci, D.; Bodoardo, S.; Mecerreyes, D.; Sardon, H.; Bella, F. Self-Healable Dynamic Poly(Urea-Urethane) Gel

Electrolyte for Lithium Batteries. *J. Mater. Chem. A* **2022**, *10* (23), 12588–12596. https://doi.org/10.1039/D2TA02239G.

(32) Zuo, X.; Cheng, Y.; Xu, L.; Chen, R.; Liu, F.; Zhang, H.; Mai, L. A Novel Thioctic Acid-Functionalized Hybrid Network for Solid-State Batteries. *Energy Storage Materials* **2022**, *46*, 570–576. https://doi.org/10.1016/j.ensm.2022.01.045.

(33) Xuan, C.; Gao, S.; Wang, Y.; You, Q.; Liu, X.; Liu, J.; Xu, R.; Yang, K.; Cheng, S.; Liu, Z.; Guo, Q. In-Situ Generation of High Performance Thiol-Conjugated Solid Polymer Electrolytes via Reliable Thiol-Acrylate Click Chemistry. *Journal of Power Sources* **2020**, *456*, 228024. https://doi.org/10.1016/j.jpowsour.2020.228024.

(34) Sarapas, J. M.; Tew, G. N. Poly(Ether–Thioethers) by Thiol–Ene Click and Their Oxidized Analogues as Lithium Polymer Electrolytes. *Macromolecules* **2016**, *49* (4), 1154–1162. https://doi.org/10.1021/acs.macromol.5b02513.

(35) Zhao, Y.; Wang, L.; Zhou, Y.; Liang, Z.; Tavajohi, N.; Li, B.; Li, T. Solid Polymer Electrolytes with High Conductivity and Transference Number of Li Ions for Li-Based Rechargeable Batteries. *Adv. Sci.* **2021**, *8* (7), 2003675. https://doi.org/10.1002/advs.202003675.

(36) Ouhib, F.; Meabe, L.; Mahmoud, A.; Grignard, B.; Thomassin, J.-M.; Boschini, F.; Zhu, H.; Forsyth, M.; Mecerreyes, D.; Detrembleur, C. Influence of the Cyclic versus Linear Carbonate Segments in the Properties and Performance of CO_2-Sourced Polymer Electrolytes for Lithium Batteries. *ACS Appl. Polym. Mater.* **2020**, *2* (2), 922–931. https://doi.org/10.1021/acsapm.9b01130.

(37) Hekselman; Kalita, M.; Plewa-Marczewska, A.; Żukowska, G. Z.; Sasim, E.; Wieczorek, W.; Siekierski, M. Effect of Calix[6]Pyrrole Anion Receptor Addition on Properties of PEO-Based Solid Polymer Electrolytes Doped with LiTf and LiTfSI Salts. *Electrochimica Acta* **2010**, *55* (4), 1298–1307. https://doi.org/10.1016/j.electacta.2009.06.045.

(38) Edman, L.; Doeff, M. M.; Ferry, A.; Kerr, J.; De Jonghe, L. C. Transport Properties of the Solid Polymer Electrolyte System $P(EO)_n$LiTFSI. *J. Phys. Chem. B* **2000**, *104* (15), 3476–3480. https://doi.org/10.1021/jp993897z.

(39) Winne, J. M.; Leibler, L.; Du Prez, F. E. Dynamic Covalent Chemistry in Polymer Networks: A Mechanistic Perspective. *Polym. Chem.* **2019**, *10* (45), 6091–6108. https://doi.org/10.1039/C9PY01260E.

(40) Zhang, V.; Kang, B.; Accardo, J. V.; Kalow, J. A. Structure–Reactivity–Property Relationships in Covalent Adaptable Networks. *J. Am. Chem. Soc.* **2022**, *144* (49), 22358–22377. https://doi.org/10.1021/jacs.2c08104.

(41) Van Lijsebetten, F.; De Bruycker, K.; Van Ruymbeke, E.; Winne, J. M.; Du Prez, F. E. Characterising Different Molecular Landscapes in Dynamic Covalent Networks. *Chem. Sci.* **2022**, *13* (43), 12865–12875. https://doi.org/10.1039/D2SC05528G.

(42) Kim, S.-T.; Pudasaini, B.; Baik, M.-H. Mechanism of Palladium-Catalyzed C–N Coupling with 1,8-Diazabicyclo[5.4.0]Undec-7-Ene (DBU) as a Base. *ACS Catal.* **2019**, *9* (8), 6851–6856. https://doi.org/10.1021/acscatal.9b02373.

(43) Del Sole, R.; De Luca, A.; Mele, G.; Vasapollo, G. First Evidence of Formation of Stable DBU Zn -Phthalocyanine Complexes: Synthesis and Characterization. *J. Porphyrins Phthalocyanines* **2005**, *09* (07), 519–527. https://doi.org/10.1142/S1088424605000630.

(44) Brissot, C.; Rosso, M.; Chazalviel, J.-N.; Lascaud, S. Dendritic Growth Mechanisms in Lithium/Polymer Cells. *Journal of Power Sources* **1999**, *81–82*, 925–929. https://doi.org/10.1016/S0378-7753(98)00242-0.

(45) Pożyczka, K.; Marzantowicz, M.; Dygas, J. R.; Krok, F. IONIC CONDUCTIVITY AND LITHIUM TRANSFERENCE NUMBER OF POLY(ETHYLENE OXIDE):LiTFSI SYSTEM. *Electrochimica Acta* **2017**, *227*, 127–135. https://doi.org/10.1016/j.electacta.2016.12.172.

(46) Wu, J.; Yuan, L.; Zhang, W.; Li, Z.; Xie, X.; Huang, Y. Reducing the Thickness of Solid-State Electrolyte Membranes for High-Energy Lithium Batteries. *Energy Environ. Sci.* **2021**, *14* (1), 12–36. https://doi.org/10.1039/D0EE02241A.

Supporting Information

1. Materials and Instrumentation

Materials

2,2′-(Ethylenedioxy)diethanethiol (DMDO, 95%), 1,8-Diazabicyclo[5.4.0]undec-7-ene (DBU, 99%), Methyl vinyl ketone (MVK, 99%), Ethynylmagnesium bromide solution (0.5 M in THF), CuI (98%), Triethylene glycol (TEG, 99%), Trimethylolpropane tris(3-mercaptopropionate) (95%) were purchased from Sigma Aldrich. Lithium bis(trifluoromethane) sulfonimide (LiTFSI) (99.9%) salt was purchased from Solvionic. Chelex 100 resin was purchased from Bio-rad. Dialysis membrane Spectra/Por 7 (MWCO 1 kDa) was purchased from Repligen. Formic acid (85%) was purchased from Mobilab. All reagents were used as received without further purification unless otherwise specified.

MVK was purified before used by a single vacuum distillation. Copper iodide was dispersed in glacial acetic acid overnight, filtered, washed with methanol under nitrogen flow, and dried under vacuum. TEG was dried on activated molecular sieves for 48h before use.

4,4-dimethyl-5-methylene-1,3-dioxolan-2-one (**M1**)[1] and DBU acetate (DBU:OAc)[2] were synthesized according to procedures described elsewhere.

Instrumentation

Nuclear magnetic resonance (NMR) spectroscopy. ^{1}H- and ^{13}C-NMR analyses were performed on a Bruker 400 MHz spectrometer at 25 °C in the Fourier transform mode. 16 scans for ^{1}H spectra and 512 scans for ^{13}C spectra were recorded.

Fourier Transform Infrared Spectra (FT-IR). FTIR measurements were carried out on a Nicolet IS5 spectrometer (Thermo Fisher Scientific) equipped with a diamond attenuated transmission reflectance (ATR) device. 32 scans were recorded for each sample over the range 4000-500 cm^{-1} with a normal resolution of 4 cm^{-1}.

Size exclusion chromatography (SEC). Number-average molecular weight (M_n), weight-average molecular weight (M_w) and dispersity (D) of the polymers were determined by size exclusion chromatography (SEC) in dimethylformamide (DMF) containing LiBr (0.025 M) at 55 °C (flow rate: 1 mL/min) with a Waters chromatograph equipped with three columns (PSS gram

1000Å (x2), 30 Å) and a precolumn, a dual absorbance detector (Waters 2487) and a refractive index detector (Waters 2414).

Thermogravimetric analysis (TGA). TGA analysis was performed on a TGA2 instrument from Mettler Toledo. Around 5 of sample was heated at 10 °C/min from 30 to 50 °C and flushed for 10 min at 50 °C. The sample was then heated at 20 °C/min until 600 °C. All the experiment was conducted under nitrogen atmosphere (20 mL/min).

Differential Scanning Calorimetry (DSC). PerkinElmer 8000 DSC equipped with an intracooler II, and calibrated with indium and tin standards was used to determined the thermal transitions of the polymers. Samples were measured in an aluminum standard tray using approximately 5 mg of electrolyte. Samples were heated from 25 to 100 °C at 20 °C min^{-1}, held for 3 min to erase the thermal history, then cooled to −60 °C and subsequent heating at 20 °C min^{-1}.

Dynamic mechanical analysis (DMA). DMA experiments were performed on a DMA Q800 from TA Instruments. Temperature ramp experiment was performed in tension mode with 0.01 N of constant force and a frequency of 1 Hz. The sample was equilibrated at -60 °C and heated with a heating rate of 3 °C/min until 120 °C. Stress strain experiments were performed three times on reprocessed rectangular samples of around 15 x 3 x 0.5 mm at 25 °C with a ramp stress of 0.01 MPa/min until specimen fracture.

Rheology. Rheology experiments were conducted on an ARES G2 rheometer from TA Instruments in shear geometry with a plate diameter of 8 mm. Stress relaxation experiments were performed at a strain of 1 % in the linear viscoelastic region from 50 to 80 °C. The samples were cut out of the synthesized polymer disc using a Boehm hollow puncher and had a thickness of around 2 mm.

Electrochemical Impedance Spectroscopy (EIS). Ionic conductivity was estimated by EIS in an Autolab 302N potentiostat/ galvanostat (Metrohm AG) at different temperatures (95–25 °C), equipped with a temperature controller (Microcell HC station). The sample was placed between two stainless steel electrodes (surface area = 0.5 cm^2). The Nyquist plots were obtained applying a 10 mV perturbation to open circuit in the frequency range of 100 kHz to 1 Hz.

Lithium-ion transference number. t_{Li}^{+} was calculated based on Bruce and Vincent method at 70 °C, using the following equation:

$$t_{Li}^{+} = \frac{I_s(\Delta V - I_0 R_0)}{I_0(\Delta V - I_s R_s)}$$

where R is the resistance, I is the current and ΔV is the potential applied across the cell (10 mV), the subscripts 0 and s, indicate the initial and steady state values respectively. The polymer electrolyte was placed between two lithium electrodes and closed in CR2032. Before the analysis, the cells were left to stabilize at 80 °C for 24 h.

Electrochemical characterization. Linear sweep voltammetry was performed in a two-electrode coin cell with stainless steel/polymer electrolyte/Li^0 configuration. The working electrode was stainless steel, and the lithium metal foils were employed as the counter and reference electrodes. The measurements were performed from OCP conditions ~2 to 6 V versus Li^0/Li^+ at a scan rate of 10 mV s^{-1} at 80 °C.

For Li plating and stripping in symmetrical cells, 0.05 and 0.10 mA cm^{-2} were employed (0.014 and 0.028 mA) with a duration of each process of 1 h. Neware battery cycler was utilized for this purpose. All the electrochemical measurements were carried out at 80 °C after 10h resting.

2. Structural characterization

Dione **DO2**

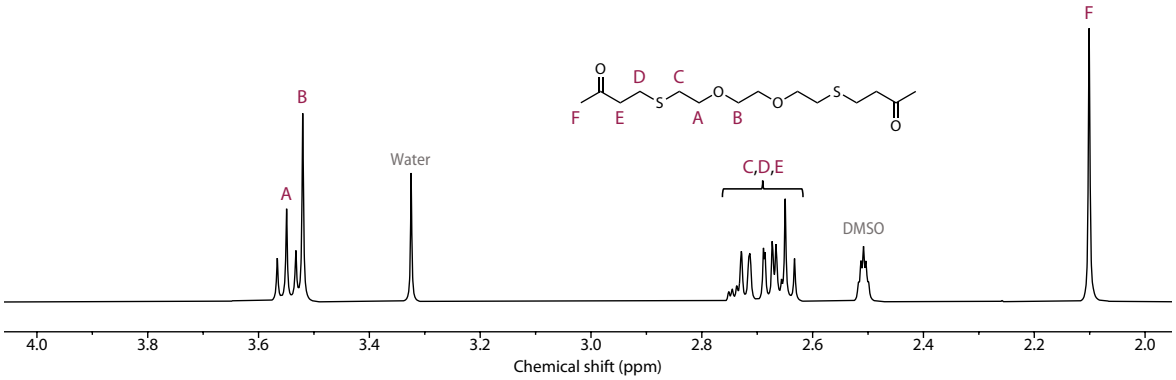

Figure S1 – ^{1}H-NMR spectrum of **DO2** (400 MHz, DMSO-d_6).

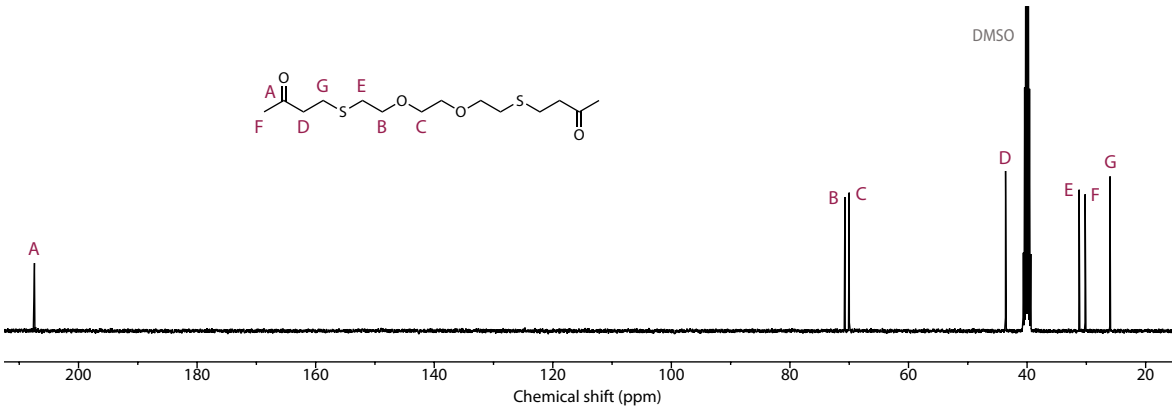

Figure S2 – ^{13}C-NMR spectrum of **DO2** (100 MHz, DMSO-d_6).

Bispropargylalcohol **BPA2**

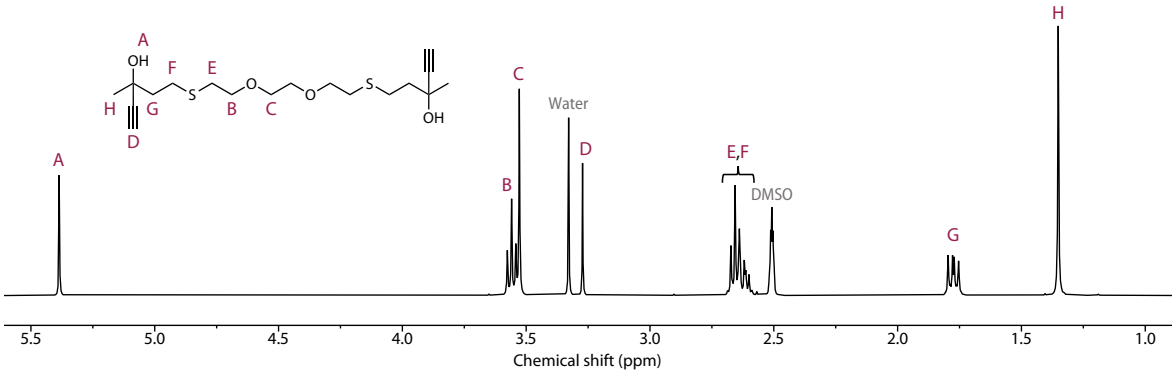

Figure S3 – ^{1}H-NMR spectrum of **BPA2** (400 MHz, DMSO-d_6).

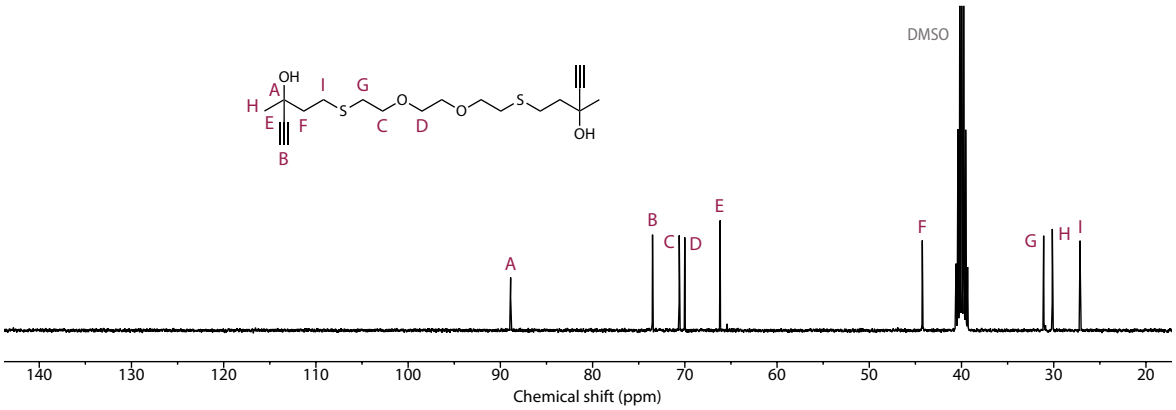

Figure S4 – ^{13}C-NMR spectrum of **BPA2** (100 MHz, DMSO-d_6).

BisαCC **M2**

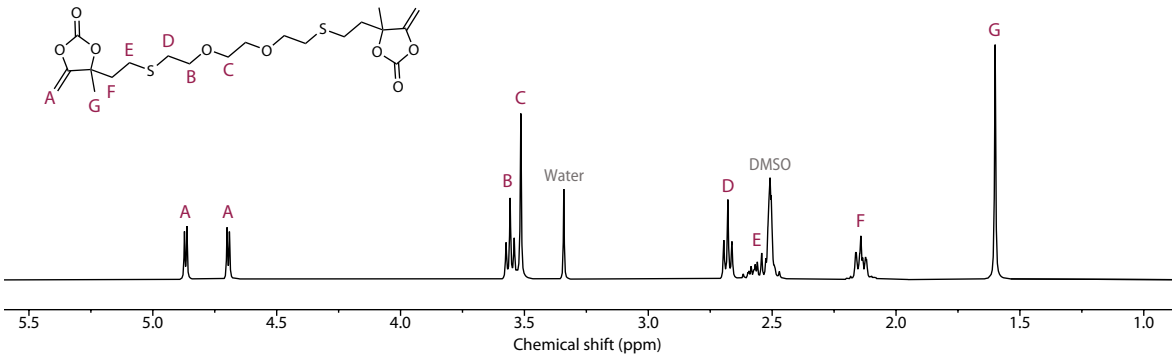

Figure S5 – ^{1}H-NMR spectrum of **M2** (400 MHz, DMSO-d_6).

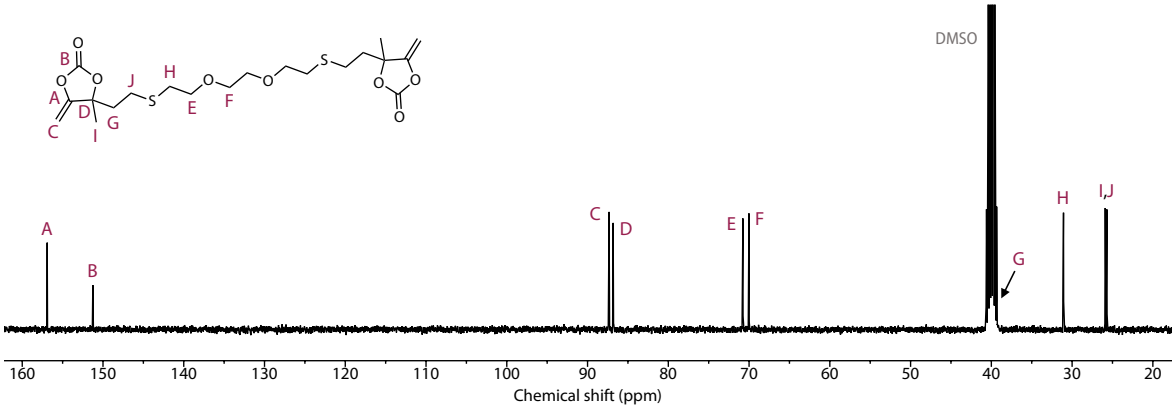

Figure S6 – ^{13}C-NMR spectrum of **M2** (100 MHz, DMSO-d_6).

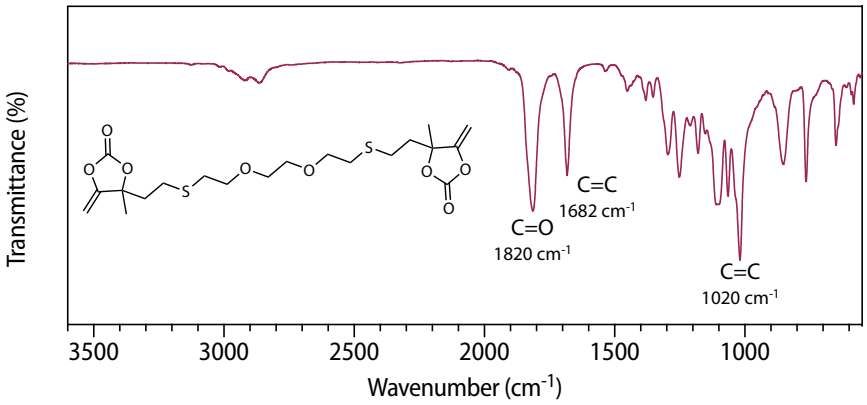

Figure S7 – ATR-IR spectrum of the monomer **M2** with some typical resonances of cyclic carbonate and alkene bonds.

Poly(monothiocarbonate) **P1**

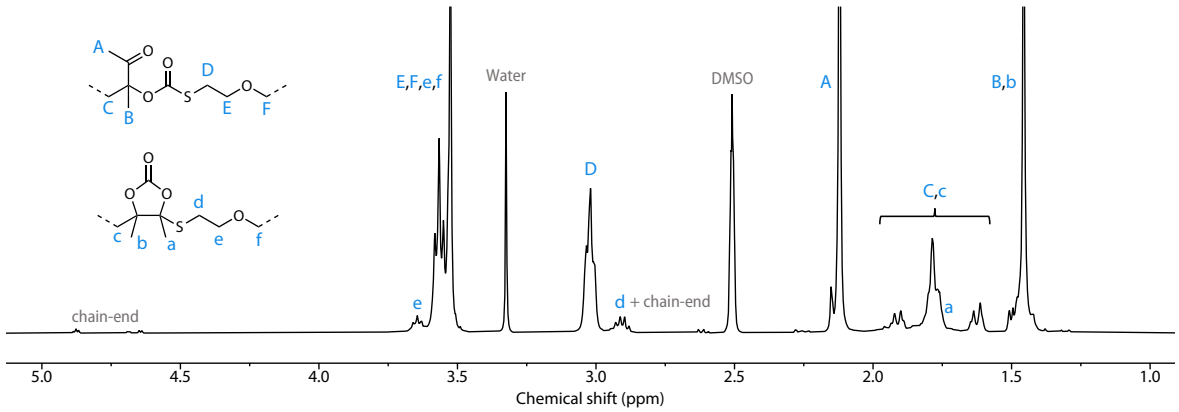

Figure S8 – ^{1}H-NMR spectrum of **P1** (400 MHz, DMSO-d_6).

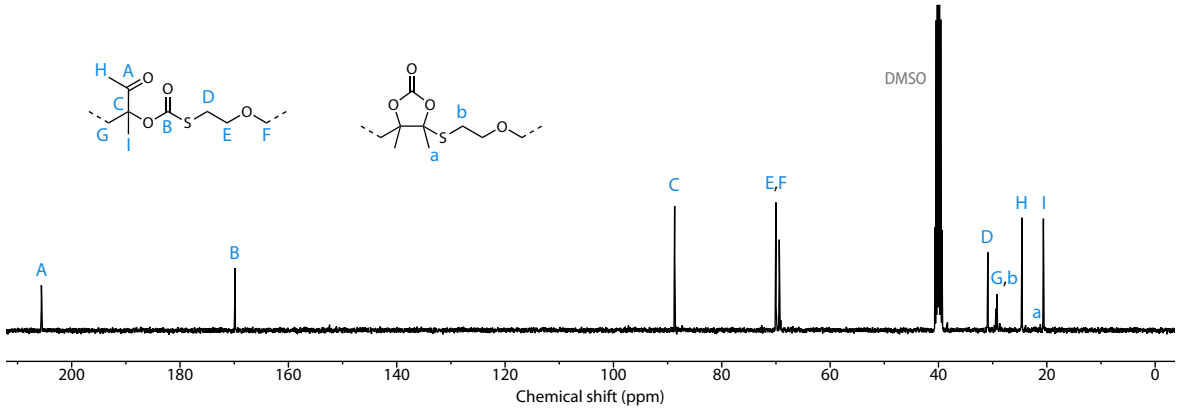

Figure S9 – ^{13}C-NMR spectrum of **P1** (100 MHz, DMSO-d_6).

The linkage selectivity between linear thiocarbonate and cyclic carbonate was determined by integration of the corresponding resonances by NMR. However, spectra in DMSO for **P1** unveiled overlapping peaks. A spectrum was thus recorded in $CDCl_3$ as deuterated solvent (Figure S10). For a full attribution in that solvent, the reader is invited to read our previous publication[3]. The peak at 3.06 ppm accounts for the thiocarbonate and the peak at 2.97 ppm accounts for the cyclic carbonate.

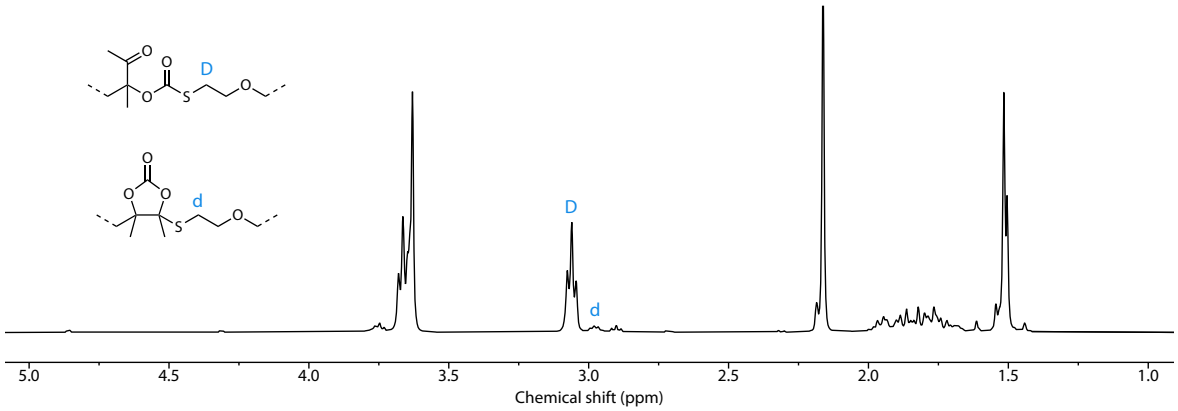

Figure S10 – ^{1}H-NMR spectrum of **P1** (400 MHz, $CDCl_3$).

Poly(monothiocarbonate) **P2**

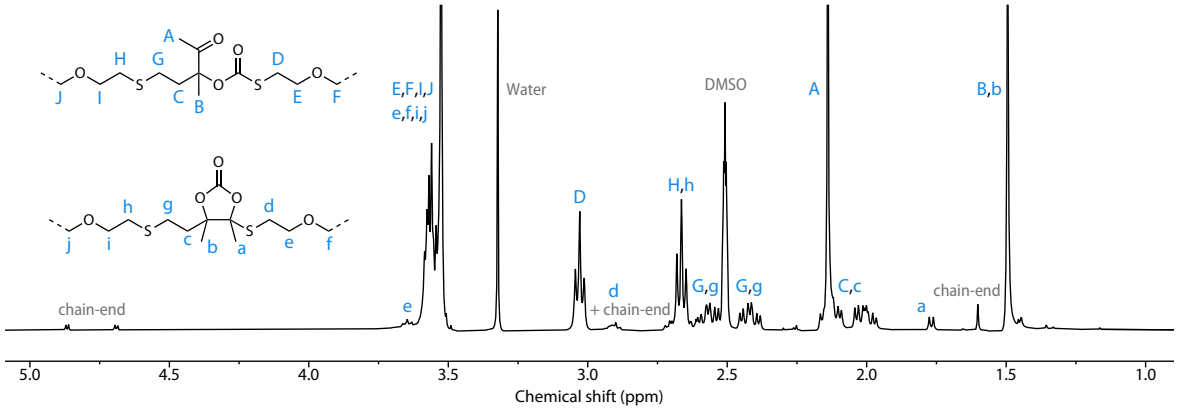

Figure S11 – ^{1}H-NMR spectrum of **P2** (400 MHz, DMSO-d_6).

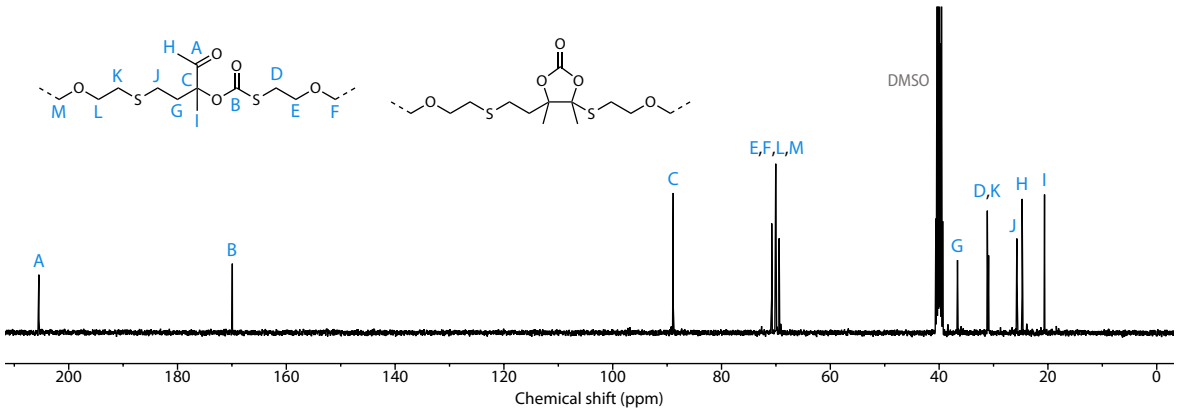

Figure S12 – ^{13}C-NMR spectrum of **P2** (100 MHz, DMSO-d_6).

The linkage selectivity between linear thiocarbonate and cyclic carbonate was determined by integration of the corresponding signals by ^{1}H-NMR. The peak at 3.03 ppm accounts for the thiocarbonate and the peak at 1.77 ppm accounts for the cyclic carbonate.

Poly(carbonate) **P3**

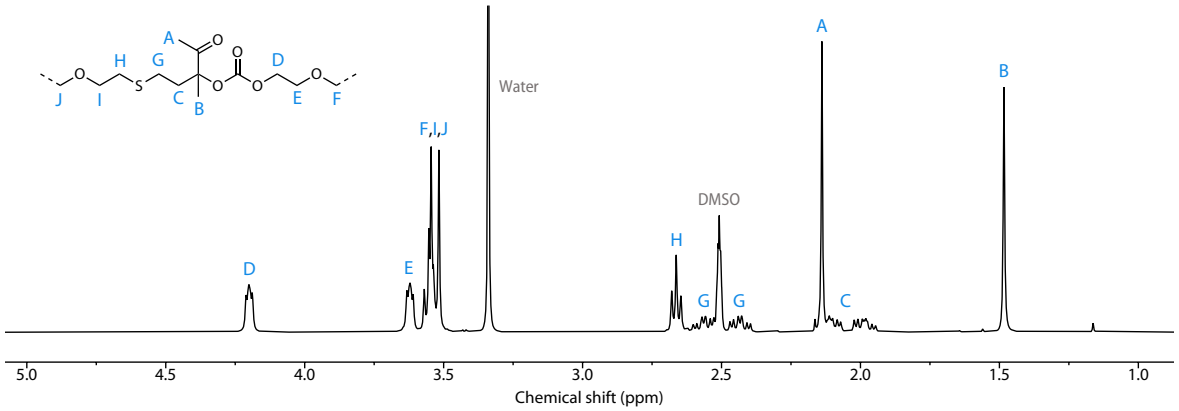

Figure S13 – ^{1}H-NMR spectrum of **P3** (400 MHz, DMSO-d_6).

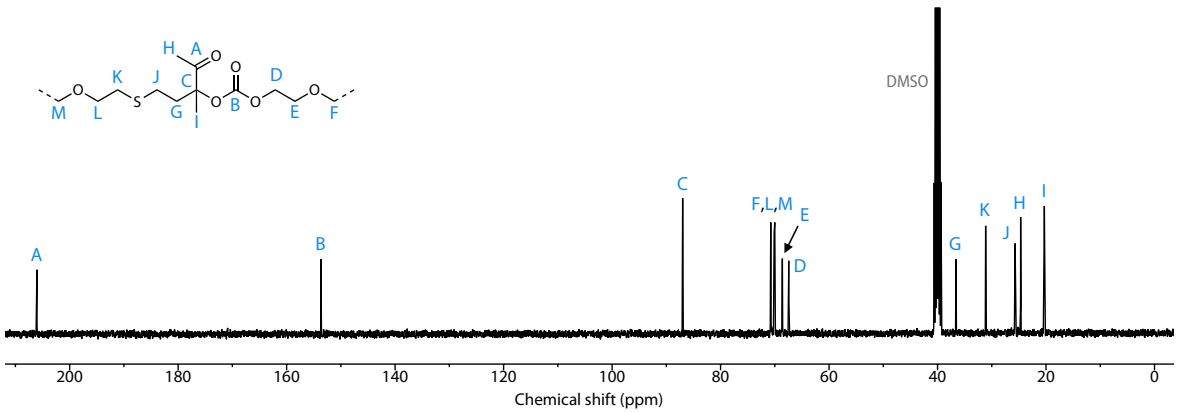

Figure S14 – ^{13}C-NMR spectrum of **P3** (100 MHz, DMSO-d_6).

Size exclusion chromatography (SEC) of the polymers **P1-P3**

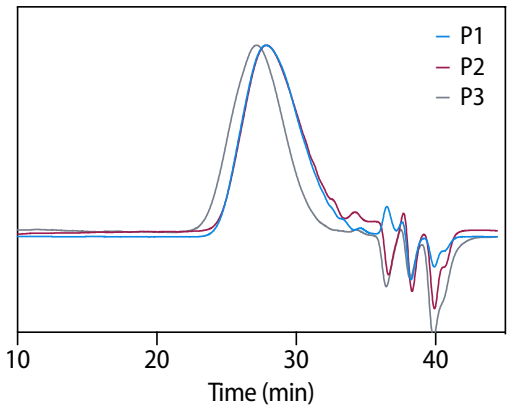

Figure S15 – SEC trace of **P1-3** after purification. M_n, M_w and D values are summarized in Table 1.

Infrared Spectroscopy (ATR-IR) of the polymer network **PN**

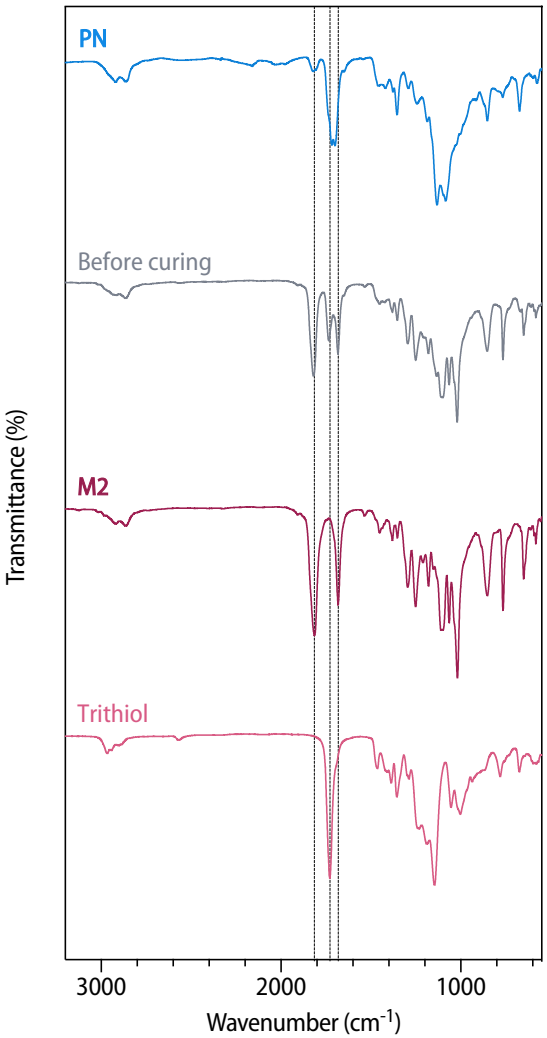

Figure S16 – ATR-IR spectrum of the trithiol, the monomer **M2**, the formulation after 30 minutes of stirring at rt, **PN** after curing for 22h at 50 °C.

3. Gel content and swelling degree of PN

The swelling degree (SD) was determined by immersion of a piece of material **PN** of mass m_i in THF (with 3 drops of formic acid to neutralize the basic catalyst inside the material). After 24h, the swollen sample was weighted as the mass of the gel m_{gel}. The SD was calculated using the following equation.

$$SD\ (\%) = \frac{m_{gel} - m_i}{m_i} \times 100$$

The gel content (GC) was determined by weighting the mass m_f after drying of the swollen sample using the following equation.

$$GC\ (\%) = \frac{m_f}{m_i} \times 100$$

4. Rheology

Stress relaxation experiments were performed on **PN** at different temperatures to obtain the energy of activation of the bond dynamicity within the material. The normalized modulus generally follows a single element Maxwell for most cases encountered in the literature. However, more complex models are often needed to describe the behavior of the sample during these experiments. In this case, the single element Maxwell failed to fit the obtained curves. However, using the stretched exponential model gave excellent fit each time. In this case, the relaxation time is obtained by fitting the curve using the stretched exponential equation (see Equation S1). All fitting parameters can be found in Table S1.

$$G(t) = G_0 e^{-\left(\frac{t}{\tau}\right)^{\beta}} \quad (1)$$

Table S1 – Fitting parameters for the stress relaxation experiments at different temperatures.

	50 °C	55 °C	60 °C	65 °C	70 °C	75 °C	80 °C
R^2	0.9939	0.9981	0.9981	0.9924	0.9988	0.9980	0.9992
τ	149.3	70.9	29.5	20.67	11.93	6.91	3.998
β	0.4024	0.4408	0.4512	0.4356	0.4882	0.4639	0.5747

For sake of clarity, only the fitting curves were represented in the main manuscript (see Figure 2c). The complete plot with all curves and fitted curves is shown in Figure S21.

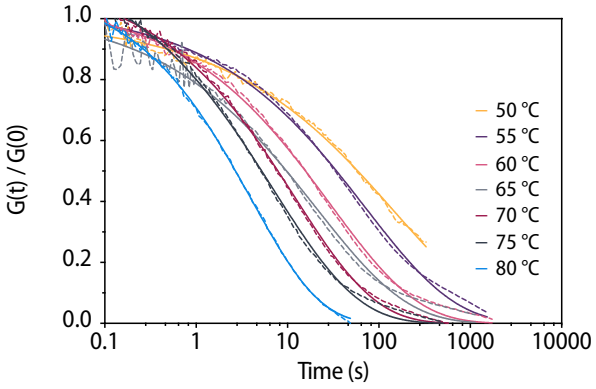

Figure S17 – Stress relaxation curves from raw data (dotted line) and fitted data (plain line).

An Arrhenius plot can thus be built from extracted relaxation times using the linear relationship in Equation S2.

$$\ln(\tau) = \ln(\tau_0) + \frac{E_a}{RT} \qquad (2)$$

5. Mechanical properties

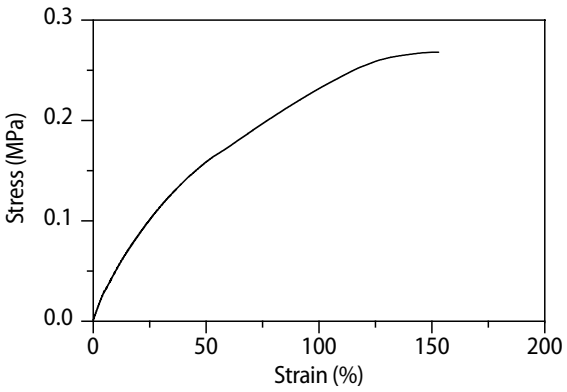

Figure S18 – Representative stress-strain curve obtained by DMA of **PN**.

6. Electrochemical characterization

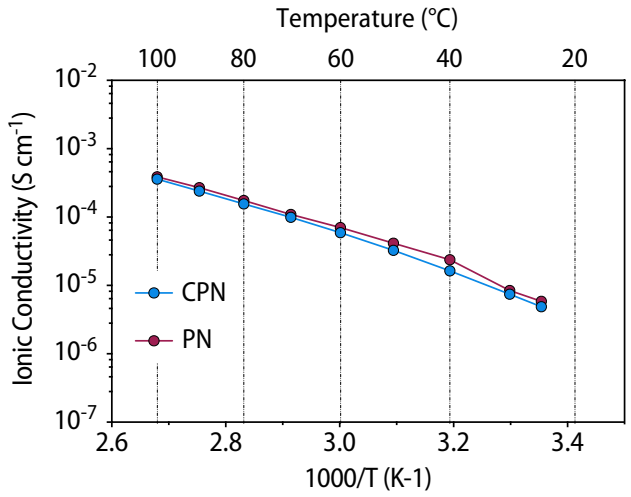

Figure S19 – Ionic conductivity as a function of temperature for the polymers **PN** and **CPN** containing 30 wt% of LiTFSI.

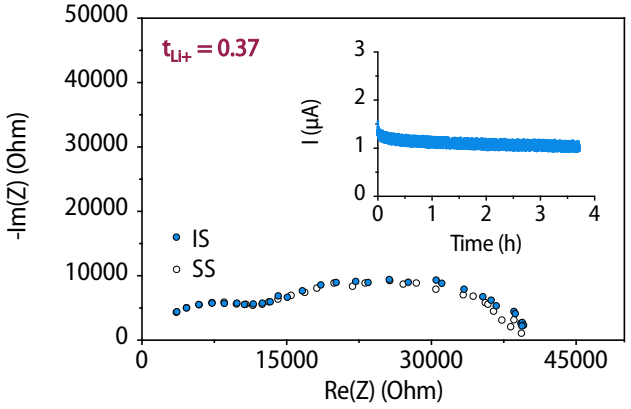

Figure S20 – ac- and dc-measurements for the lithium ion transference number measurements for **PN-Li** containing 30 wt% of LiTFSI electrolyte at 80 °C.

References

[1] S. Gennen, B. Grignard, T. Tassaing, C. Jérôme, C. Detrembleur, *Angew. Chem. Int. Ed.* **2017**, *56*, 10394–10398.

[2] D. J. Coady, K. Fukushima, H. W. Horn, J. E. Rice, J. L. Hedrick, *Chem. Commun.* **2011**, *47*, 3105.

[3] F. Ouhib, B. Grignard, E. Van Den Broeck, A. Luxen, K. Robeyns, V. Van Speybroeck, C. Jerome, C. Detrembleur, *Angew. Chem. Int. Ed.* **2019**, *58*, 11768–11773.

Conclusions

The chemistry of α-alkylidene cyclic carbonate (αCC) has emerged as a promising technology in polymer science, offering a library of novel polymer families under mild conditions and with atom efficiency. Interestingly, this chemistry introduces unique linkages of unknown chemical properties. While the proof-of-concept has been previously validated in the synthesis of unprecedented hetero-atom rich polymers, their characterization was underexplored, especially in the case of poly(oxazolidone)s and the sulfur-containing polymers (i.e. poly(thiocarbonate)s and poly(cyclic carbonate-co-thioether)s) produced by the step growth polymerization of bisαCC and diamines or dithiol, respectively. Similarly, the potential applications of these polymers were not studied when this PhD thesis work started.

The main objective of this PhD thesis was to direct the polymerization of bisαCC with diamines and dithiols with a control on their chemoselective addition and addition rate through organocatalysis. However, findings in Chapter II revealed that chemoselective additions cannot be achieved due to the synergetic catalysis provided by the amine in the system, leading to the concomitant addition of both amines and thiols onto αCC, even in the absence of a additional catalyst. The amine comonomer is indeed basic enough to catalyze the thiolation of αCC. Nevertheless, careful characterization of the chemistry in action, both for the production of the hybrid polyoxazolidones and their further functionalization, allowed us to discover the potential of this chemistry for the design of advanced (recyclable) thermosets.

Chapter I highlighted the so-far developed technologies to synthesize non-isocyanate polyurethanes (NIPUs) at room temperature and key strategies to do so. Among them, αCC proved to be a promising platform for NIPU synthesis due to their fast reactivity at room temperature with primary and secondary amines to provide (a)cyclic carbamate linkages.

In Chapter II, the terpolymerization of bisαCC with diamines and dithiols was investigated. Initial model reactions confirmed the compatibility of both chemistries with no noticeable side reactions. Although a possible control of the thiol addition was anticipated as this reaction typically requires the presence of a strong organobase, it was found that the diamine comonomer catalyzed the reaction. This drawback for the project was exploited in our advantage for the successful catalyst-free synthesis of polymers from mixtures of diamines and dithiols with bisαCC, achieving hybrid poly(oxazolidone)s with M_w values of up to 16,300 $g \cdot mol^{-1}$ (Scheme 1A). The structure and basicity of the amine both significantly influenced the

catalysis effectiveness and consequently the resulting polymer molecular weight. For less efficient amines, additional DBU was used as an organobase to accelerate the reaction and provided polymers of higher molar mass (M_w up to 24,500 g·mol^{-1}). DBU has also shown to promote the formation of the cyclic carbonate-*co*-thioether (CCS) linkages. The increased solubility of the hybrid polymers compared to previously studied poly(oxazolidone)s facilitated an in-depth characterization of their thermal properties, revealing two T_gs, with respective values of 50-85 °C and 95-130 °C, depending on the comonomers. Based on these results, a controlled thermal dehydration procedure of the polymers at the dried state was developed, enabling the facile production of (exovinylene oxazolidone)-containing polymers in only 2 h without the need of any further purification (Scheme 1A). The exovinylene linkages were further functionalized via a cationic thiol-ene reaction affording *N,S*-acetal oxazolidones linkages. A proof-of-concept application as adhesives demonstrated the beneficial role of the hydroxyl functions in hydroxy-oxazolidones for substrate adhesion compared to dehydrated polymer analogs.

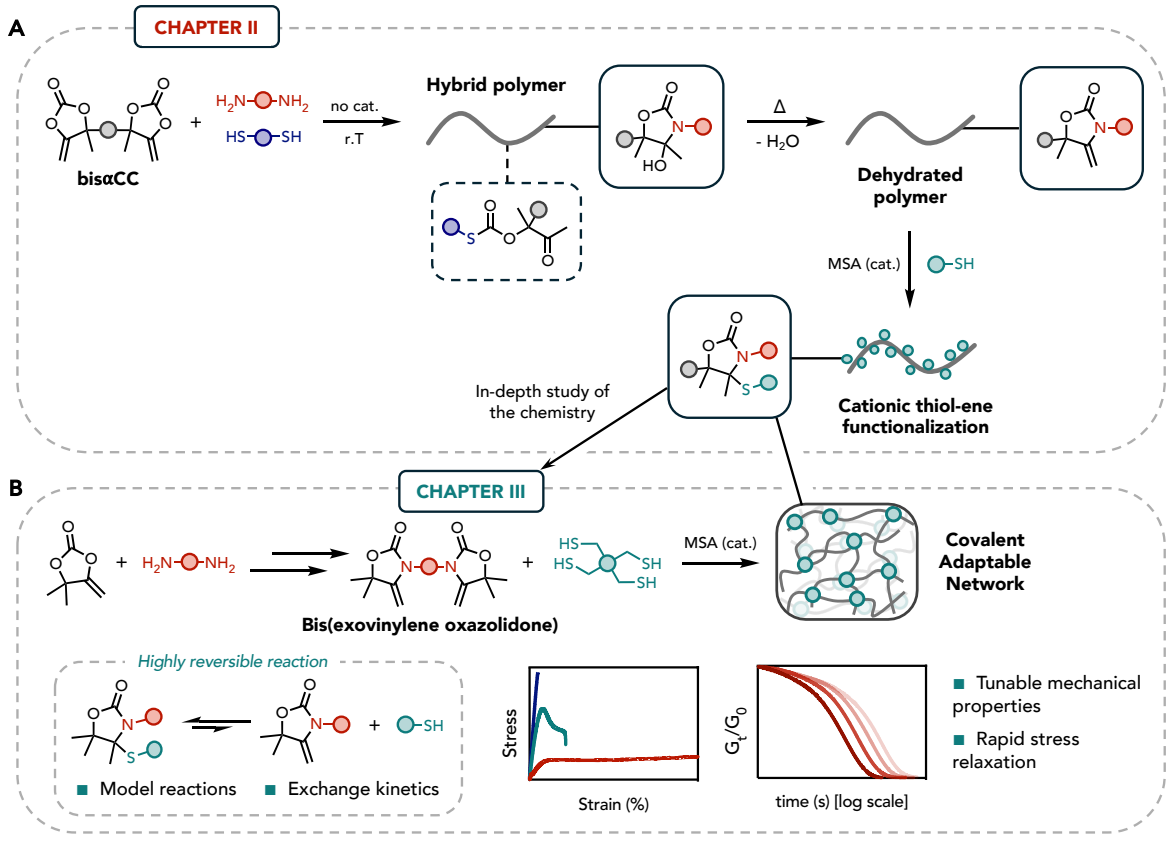

Scheme 1 – (A) Chapter II disclosing the terpolymerization of bisαCC with diamines and dithiols toward hybrid polymers. The polymers were further post-functionalized. (B) Chapter III arose from the cationic thiol ene reaction explored in Chapter II. The reversible reaction was studied and applied to the synthesis of recyclable thermosets.

In Chapter III, the cationic thiol-ene applied to exovinylene oxazolidone discovered in Chapter II was studied in depth. This study, initiated on model compounds, revealed fast reactions in the presence of a Bronsted acid (methanesulfonic acid, MSA) at r.T, quickly providing *N,S*-acetal oxazolidones (Scheme 1B). These functions exhibited high reversibility and rapid exchange at low temperature (7-50 °C), which prompted us to evaluate this chemistry in covalent adaptable networks. New bis(exovinylene oxazolidone)s were synthesized from αCC using an optimized protocol on > 20 g scales. Reaction with a tetrafunctional thiol produced thermosets, with T_gs varying from 8 to 62 °C (Scheme 1B). Remarkably, the polymers displayed highly tunable and attractive mechanical properties comparable to those of some commodity thermoplastics such as PDMS or PS. The dynamic nature of the bonds within the thermoset was exploited for reprocessability, and rheological studies highlighted fast relaxation times under stress, with very low viscosities at moderate temperature (70-90 °C). Fast reprocessing of these thermosets was achieved using techniques typically reserved for thermoplastics, such as extrusion or injection molding. Other end-of-life scenarios were also explored, such as the upcycling of divergent materials into a new one, or the chemical deconstruction into the constitutive monomers. This technology was also applied to the production and recycling of composites.

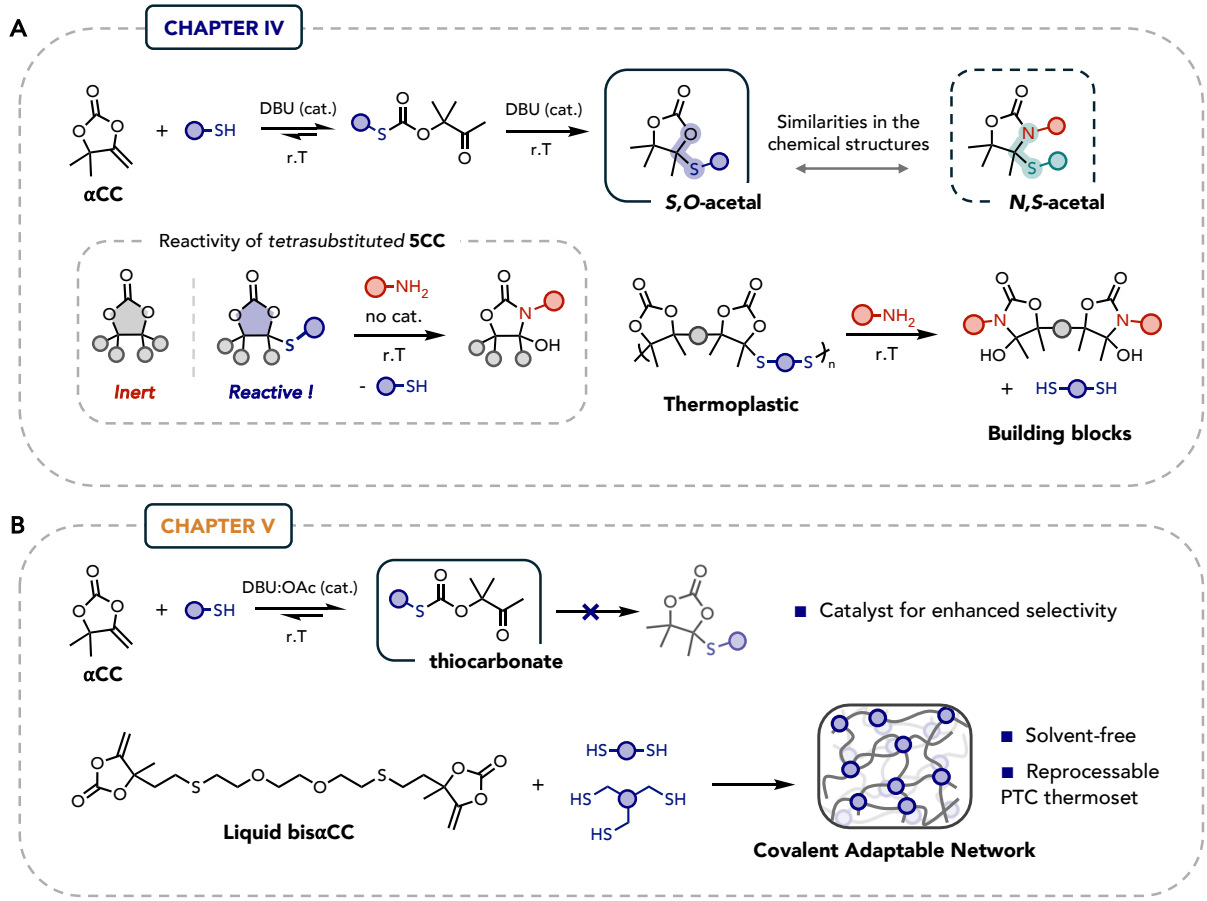

Scheme 2 – (A) Chapter IV exploring the reactivity of *S,O*-acetal cyclic carbonates of similar structure to *N,S*-acetals studied in Chapter III. (B) Chapter V focusing on the selective preparation of thiocarbonates from αCC and thiols, further applied to the solvent-free preparation of recyclable thermosets from the novel liquid bisαCC monomer.

In Chapter IV, we explored the reactivity of another type of cyclic acetal, the *S,O*-acetal cyclic carbonates (CCSs) produced by the thiol addition onto αCC. Although the reversibility of the thiol addition was not observed as with *N,S*-acetal oxazolidones studied in Chapter III, these moieties underwent facile aminolysis. Notably, tetrasubstituted five-membered cyclic carbonates are traditionally challenging to ring-open by aminolysis, even in harsh conditions and in the presence of catalysts. When one of the four alkyl substituents of the tetrasubstituted cyclic carbonate is replaced by a thioether bond, the reactivity gets unlocked and aminolysis was complete in only 2 h at r.T without any catalyst. This marked a significant milestone in the field of densely substituted five-membered cyclic carbonates. This exacerbated aminolysis of the tetrasubstituted, thioether functionalized cyclic carbonates was exploited for the facile, fast deconstruction of poly(cyclic carbonate-*co*-thioether)s (PCCs) obtained via the r.T DBU-catalyzed step-growth polymerization of bisαCC with dithiols. These PCCs, characterized by a rather high molar mass, displayed high transparency and attractive mechanical properties

comparable to commodity polyolefins, highlighting their potential as high-performance thermoplastics. Their facile aminolysis was complete in short time (maximum 2 h) under catalyst-free conditions, providing bis(hydroxy-oxazolidone)s and the former dithiols at high yield. Both degradation products were re-valorized for the preparation of novel recyclable thermosets embedding dynamic *N,S*-acetal oxazolidone cross-link nodes.

In Chapter V, the step-growth polymerization of bisαCC with dithiols was directed to the selective formation of poly(thiocarbonate)s (PTCs) for the first time by the choice of a new catalyst. We have also prepare a new liquid bisαCC that enabled us to prepare solvent-free formulations with polythiols for the facile production of PTCs networks. The reversible character of the thiocarbonate bonds was leveraged to reprocess the thermoset. Finally, the PTCs were evaluated as solid electrolytes for Li-ion batteries applications.

Perspectives

This PhD thesis demonstrates that αCCs are expanding the CO_2-based monomers toolbox for the production of unprecedented functional heteroatom-rich polymers with unique, still largely unexplored properties. Having explored new chemistries and developed new building blocks overcoming previous critical roadblocks to the wider employment of αCCs, there is now space to expand the range of obtainable materials and explore new applications.

BisαCC monomers are exceptional building blocks for the construction of a large library of polymers embedding numerous linkages. Their reaction with different nucleophiles is quick in ambient conditions, giving birth to poly(hydroxy-oxazolidone)s, poly(oxo-urethane)s, poly(oxo-carbonate)s, poly(oxo-thiocarbonate)s, and poly(cyclic carbonate-co-thioether)s. In this thesis, a liquid bisαCC monomer was developed and served for the PTC thermoset synthesis from a solvent-free multicomponent resin containing the bisαCC, polythiols, and a catalyst. Previous monomers developed in our group were solids of low solubility (Scheme 3), rendering the synthesis of thermosets challenging, even when using solvents.

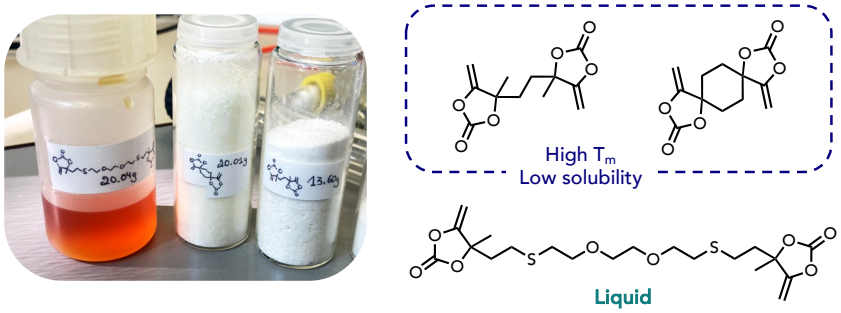

Scheme 3 – Picture of the liquid monomer next to the previously developed solid BisαCC monomers and their respective chemical structures.

This advancement has paved the way for many research projects in the group, addressing the limitations posed by the physical properties of our previous monomers. Notably, the liquid bisαCC is central to the development of new solvent-free resins toward PUs or PCs thermosets, targeting coating and adhesive applications (“NIPU-EJD” and “D-Carbonize” Marie-Curie projects funded by EU). This technology is particularly well-suited for consumer-grade applications, such as 2K (2 components) formulations commonly used in epoxy resins or polyurethanes, enabling easy application and curing without the need of specialized equipment (Scheme 4).

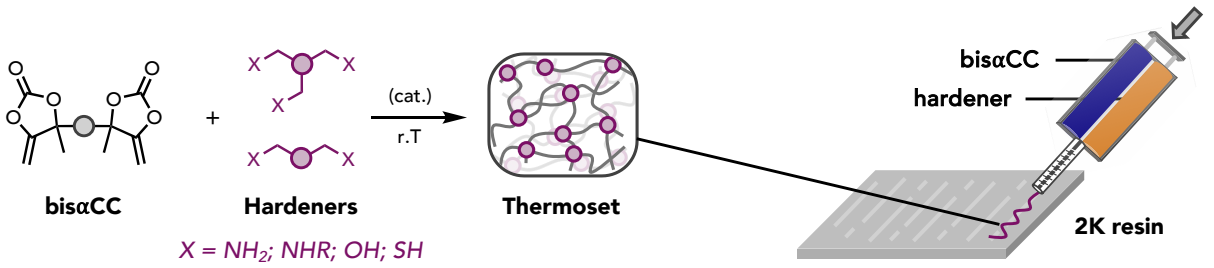

Scheme 4 – Polymer thermosets might easily be prepared in solvent-free conditions from the liquid BisαCC monomer and hardeners of different functionality (primary or secondary amines, alcohol, thiol) to target different polymer families. A typical consumer application is the 2K resin where both components are mixed and applied on a surface, typically as coating or adhesive.

Additionally, the liquid bisαCC has been applied in continuous flow chemistry to efficiently produce poly(oxazolidone)s within short residence time[1] (maximum 35 min) ("CO_2Fluidics" project funded by ULiege). The liquid nature of the monomer ensures easy handling in flow reactors and results in soluble polymers, preventing reactor clogging issues. By connecting multiple reactors in sequence, the synthesis of poly(oxazolidone)s with different functionalities (i.e. hydroxy-oxazolidone, alkylidene oxazolidone, *N,S*-acetal oxazolidone) can be achieved seamlessly without the need of isolating intermediates (Scheme 5). The user can then select the starting monomers and the flow setup of his choice to deliver polymers with targeted structure and functionalities. Current efforts are focused on other polymer classes, such as poly(*oxo*-carbonate)s or poly(*oxo*-thiocarbonate)s.

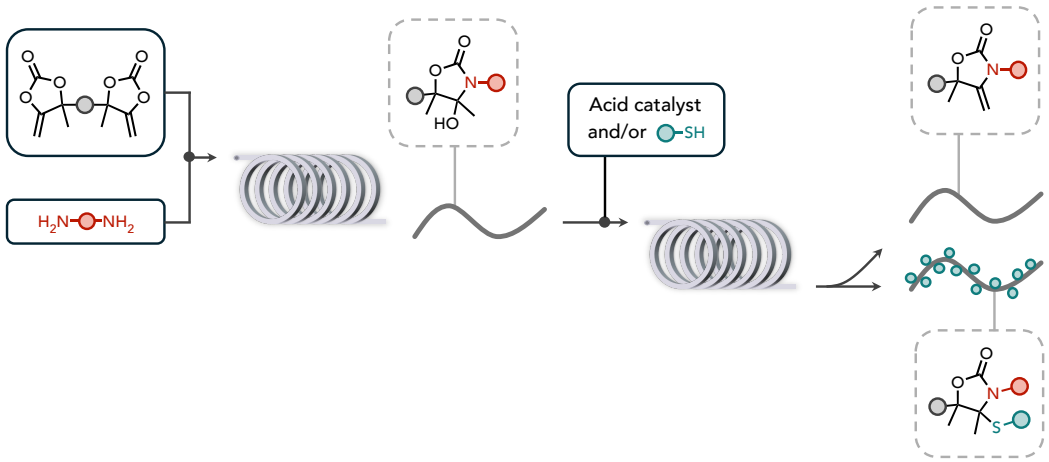

Scheme 5 – Step-growth polymerization of liquid BisαCC monomer and diamines in flow. A poly(hydroxy-oxazolidone) is obtained after the first reactor. A second reactor can be connected to the first with an input of acid catalyst and/or thiol to target alkylidene oxazolidone or *N,S*-acetal oxazolidone linkages respectively, without the need of purifying intermediates.

Overall, this liquid monomer technology has opened many doors for synthesizing polymers under innovative conditions, ranging from solvent-free 2K resins for thermosets to the use of flow reactors for targeted linear polymers production.

Nevertheless, the widespread adoption of BisαCC is currently hindered by its relatively expensive and unscalable synthesis process. The synthesis involves multiple steps using nasty reagents (e.g. Grignard reagents, metal catalysts) and requires chromatography for purifying both intermediates and the final monomer, limiting our synthesis to 60 grams per batch scale (Scheme 6). There is an important gap in research toward a more sustainable and scalable syntheses of these monomers that must be addressed in the near future.

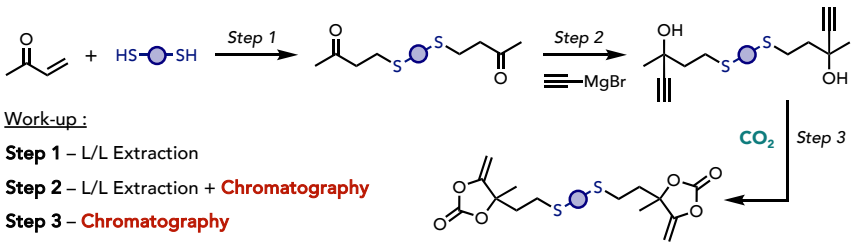

Scheme 6 – Stepwise synthesis of the liquid monomer. Each step is followed by a work-up toward the pure product.

In contrast to bisαCC monomers, the bis(exovinylene oxazolidone)s that serve for the production of *N,S*-acetal oxazolidone thermosets are simpler and cheaper to synthesize and scale-up, without the need of chromatography at any step. Although the synthesis was achieved to a scale of up to 50 grams, we expect this facile process to be scaled up significantly.

The rapid and efficient reaction of exovinylene oxazolidones with thiols produces attractive *N,S*-acetal recyclable materials. These materials are compatible with multiple processing techniques thanks to the highly dissociative nature of their bonds, reaching low viscosities at elevated temperatures. Additive manufacturing has gathered significant attention in the last years for its ability to precisely build customized complex structures. Employing this trending processing technique with this chemistry might be achieved by either fused deposition modeling (FDM, corresponding to the extrusion of the melted material) (Scheme 7A), or by photopolymerization of a resin involving a photoacid generator to activate the reaction while the resin is being deposited (Vat photopolymerization) (Scheme 7B). This approach would allow for the construction of objects benefiting from the advantages of additive manufacturing, without compromising the end-of-life(s) of the material. Hybrid photo-crosslinked materials

based on the *N,S*-acetal chemistry are for that purpose of high interest and are currently being studied by some of us (NIPU-EJD Marie-Curie project funded by EU).

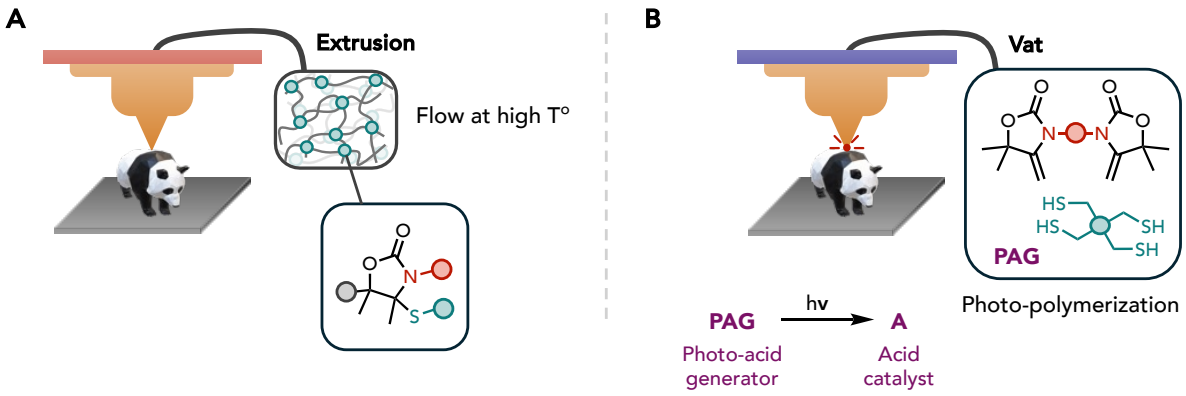

Scheme 7 – Additive manufacturing of a poly(oxazolidone) by the *N,S*-acetal oxazolidone chemistry by (A) fused deposition modeling (FDM), or (B) Vat photopolymerization of the monomers with a photoacid generator, releasing the acid catalyst upon irradiation.

Additionally, *N,S*-acetal oxazolidone thermosets have been effectively combined with flax to produce composite materials. Composites are everywhere in our daily life with many applications, some of them being used the automotive and aerospace industries, wind turbine blades, sports equipment, and in construction. Unlike lone polymers, its combination with a matrix allows to significantly enhance mechanical properties while benefiting from low weight, yielding materials of long durability and high tunability. A nowadays challenge in the field of composites is their recyclability, hampered by the difficult separation of the resin from the fiber matrix. For instance, massive wind turbine blades typically end up in landfills at their end of service because other recycling or upcycling options are often too costly for industries. A potential solution to address this problem, explored in the Chapter III of this thesis, involves using highly dissociative thermosets to facilitate the easy separation and recovery of both components of the composite material. Although the proof-of-concept was demonstrated, there is still space to fabricate a multitude of novel materials from diverse polymers and fibers, such as glass fibers, carbon fiber, or Kevlar (Scheme 8). This diversity would allow to target many specific applications that exploit the benefits of both the resin and the fiber.

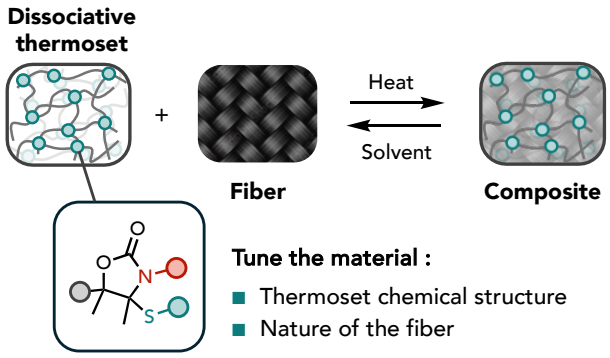

Scheme 8 – Usage of a *N,S*-acetal oxazolidone thermoset as polymeric matrix to impregnate the fiber. The resulting composite material can be recycled by dissolution of the polymer.

In this thesis, a solvent-selective polymer dissolution was proposed to recover the components of *N,S*-acetal oxazolidone composites. Although this approach has proven effective in recovering the products, a large amount of chloroform was required to dissolve the resin. Therefore, other recycling strategies should be explored to improve the sustainability of the process.

References

(1) Siragusa, F.; Crane, L.; Stiernet, P.; Habets, T.; Grignard, B.; Monbaliu, J.-C. M.; Detrembleur, C. Continuous Flow Synthesis of Functional Isocyanate-Free Poly(Oxazolidone)s by Step-Growth Polymerization. ACS Macro Lett. 2024, 13 (5), 644–650.

List of publications

(1) Habets, T.; Siragusa, F.; Grignard, B.; Detrembleur, C. Advancing the Synthesis of Isocyanate-Free Poly(Oxazolidones)s: Scope and Limitations. *Macromolecules* **2020**, *53* (15), 6396–6408. https://doi.org/10.1021/acs.macromol.0c01231.

(2) Habets, T.; Siragusa, F.; Müller, A. J.; Grossman, Q.; Ruffoni, D.; Grignard, B.; Detrembleur, C. Facile Construction of Functional Poly(Monothiocarbonate) Copolymers under Mild Operating Conditions. *Polym. Chem.* **2022**, *13* (21), 3076–3090. https://doi.org/10.1039/D2PY00307D.

(3) Siragusa, F.; Demarteau, J.; Habets, T.; Olazabal, I.; Robeyns, K.; Evano, G.; Mereau, R.; Tassaing, T.; Grignard, B.; Sardon, H.; Detrembleur, C. Unifying Step-Growth Polymerization and On-Demand Cascade Ring-Closure Depolymerization via Polymer Skeletal Editing. *Macromolecules* **2022**, *55* (11), 4637–4646. https://doi.org/10.1021/acs.macromol.2c00696.

(4) Siragusa, F.; Habets, T.; Méreau, R.; Evano, G.; Grignard, B.; Detrembleur, C. Catalyst-Free Approach for the Degradation of Bio- and CO_2-Sourced Polycarbonates: A Step toward a Circular Plastic Economy. *ACS Sustainable Chem. Eng.* **2022**, *10* (27), 8863–8875. https://doi.org/10.1021/acssuschemeng.2c01891.

(5) Habets, T.; Olmedo-Martínez, J. L.; Del Olmo, R.; Grignard, B.; Mecerreyes, D.; Detrembleur, C. Facile Access to CO_2-Sourced Polythiocarbonate Dynamic Networks And Their Potential As Solid-State Electrolytes For Lithium Metal Batteries. *ChemSusChem* **2023**, *16* (14), e202300225. https://doi.org/10.1002/cssc.202300225.

(6) Habets, T.; Seychal, G.; Caliari, M.; Raquez, J.-M.; Sardon, H.; Grignard, B.; Detrembleur, C. Covalent Adaptable Networks through Dynamic *N* , *S* -Acetal Chemistry: Toward Recyclable CO_2-Based Thermosets. *J. Am. Chem. Soc.* **2023**, *145* (46), 25450–25462. https://doi.org/10.1021/jacs.3c10080.

(7) Razavi-Esfali, M.; Habets, T.; Siragusa, F.; Grignard, B.; Sardon, H.; Detrembleur, C. Design of Functional Isocyanate-Free Poly(Oxazolidone)s under Mild Conditions. *Polym. Chem.* **2024**, *15* (19), 1962–1974. https://doi.org/10.1039/D4PY00101J.

(8) Maes, S.‡; Habets, T.‡; Fischer, S. M.; Grignard, B.; Detrembleur, C.; Du Prez, F. E. Unprecedented Associative Exchange in CO_2-Sourced Cyclic *S* , *O* -Acetal-Based Covalent Adaptable Networks. *Polym. Chem.* **2024**, *15* (22), 2296–2307. https://doi.org/10.1039/D4PY00359D.

(9) Siragusa, F.; Crane, L.; Stiernet, P.; Habets, T.; Grignard, B.; Monbaliu, J.-C. M.; Detrembleur, C. Continuous Flow Synthesis of Functional Isocyanate-Free Poly(Oxazolidone)s by Step-Growth Polymerization. *ACS Macro Lett.* **2024**, *13* (5), 644–650.